DR. 1056

CONF-791228

EBT RING PHYSICS

290
4/16/80

proceedings of the workshop

DECEMBER 3-5, 1979
OAK RIDGE, TENNESSEE

SPONSORED BY
FUSION ENERGY DIVISION
OAK RIDGE NATIONAL LABORATORY
Operated by Union Carbide Corporation
For the Department of Energy

DISTRIBUTION OF THIS DOCUMENT IS UNLIMITED

Conf-791228
Dist. Category UC-20 a, d, f, g

Proceedings of the Workshop on

EBT RING PHYSICS

December 3-5, 1979 Oak Ridge, Tennessee

N. A. Uckan
Chairman and Editor

Date Published: April 1980

DISCLAIMER

This report was prepared as an account of work sponsored by an agency of the United States Government. Neither the United States Government nor any agency thereof, nor any of their employees, makes any warranty, express or implied, or assumes any legal liability or responsibility for the accuracy, completeness, or usefulness of any information, apparatus, product, or process disclosed, or represents that its use would not infringe privately owned rights. Reference herein to any specific commercial product, process, or service by trade name, trademark, manufacturer, or otherwise, does not necessarily constitute or imply its endorsement, recommendation, or favoring by the United States Government or any agency thereof. The views and opinions of authors expressed herein do not necessarily state or reflect those of the United States Government or any agency thereof.

Sponsored by
FUSION ENERGY DIVISION
of the
OAK RIDGE NATIONAL LABORATORY
operated by
UNION CARBIDE CORPORATION
for the
DEPARTMENT OF ENERGY

PREFACE

The workshop on EBT Ring Physics was held at Oak Ridge, Tennessee, on December 3-5, 1979, under the sponsorship of the Oak Ridge National Laboratory (ORNL), Fusion Energy Division (FED). About 70 U.S. and Japanese participants attended the workshop. They represented various U.S. industries, universities, national laboratories, and the Department of Energy. Also attending were representatives of the Japan Ministry of Education (MOE) and Nagoya University.

The workshop organizing committee members were:

N. A. Uckan, Chairman, ORNL
W. B. Ard, McDonnell-Douglas Research Laboratories
R. A. Dandl, Consultant
A. Favale, Grumman Aerospace Corporation
G. E. Guest, General Atomic Company
G. R. Haste, ORNL
C. L. Hedrick, ORNL
H. Ikegami, Nagoya University, Japan
Caila Cox, Secretary, ORNL

The purposes of the workshop were (i) to evaluate the status of the current experimental and theoretical understanding of hot electron ring properties; (ii) to identify the dominant physical processes that influence ring formation, scaling, and their optimal behavior; and (iii) to determine critical areas for near-term research.

The first part of the workshop was devoted to the oral presentations of more than two dozen (5 experimental, 20 theoretical) technical papers or reviews accompanied by technical discussions. The second part of the workshop was devoted to open forum discussions (i) instabilities in hot electron plasmas, (ii) EBT/NBT ring diagnostics, and (iii) ring power balance implications for a reactor. Summary talks by the chairmen of the sessions, six in all, concluded the workshop.

In addition to the workshop, the attendees were able to participate in a tour of the ORNL FED.

These proceedings include (i) workshop summaries prepared by session chairmen; (ii) 24 full-length manuscripts that were submitted within one month of the close of the workshop, along with the technical discussions that took place; and (iii) open forum discussions (accompanied by 3 papers) and summaries.

This workshop could not have been successful without the efforts of many dedicated individuals — the Workshop Organizing Committee, session chairmen, authors, participants, ORNL-EBT staff members, and last but not least all of the Japan-NBT staff members who were able to travel thousands of miles just for this purpose.

The chairman wishes to acknowledge a special appreciation to a delightful coworker: Caila Cox, the workshop secretary, who handled the administrative details and many aspects of the workshop before, during, and after the workshop in an efficient, complete, and professional manner. Caila's help in the preparation of many of the drafts and handwritten or incomplete manuscripts submitted by some of the authors is also appreciated. Thanks are also due to the staff of the ORNL FED Reports Office who handled the collection of the abstracts (distributed during the workshop) and the coodination and assembly of these proceedings.

Nermin A. Uckan
Oak Ridge, Tennessee
February, 1980

CONTENTS

OPENING REMARKS — L. A. Berry and N. A. Uckan vii

1. SUMMARY OF THE WORKSHOP — N. A. Uckan, W. B. Ard, C. L. Hedrick, G. R. Haste, A. Favale, G. E. Guest, H. Ikegami, and R. A. Dandl 1

2. OVERVIEW 29

REVIEW OF RING EXPERIMENTS — R. A. Dandl 31

CHARACTERISTICS OF HOT ELECTRONS IN A SIMPLE MAGNETIC MIRROR FIELD — H. Ikegami and M. Hosokawa 59

REVIEW OF EBT ELECTRON RING STABILITY — D. A. Spong 75

A BRIEF REVIEW OF ELMO RING STABILITY THEORY — G. E. Guest 97

3. EXPERIMENTS 121

THE RING FORMATION IN NAGOYA BUMPY TORUS — M. Fujiwara, M. Hosokawa, H. Iguchi, T. Shoji, M. Tanaka, and H. Ikegami 123

DIAMAGNETIC MEASUREMENTS FOR EXPERIMENTAL DETERMINATION OF EBT RING PARAMETERS — K. H. Carpenter 143

COMPARISONS OF ENERGETIC ELECTRON FORMATION IN EBT AND IN MINIMUM-B CONFIGURATIONS — G. R. Haste 163

4. RING/CORE MODELING 173

HOT ELECTRON RING EQUILIBRIA AND EFFECTS ON EBT TRANSPORT — L. W. Owen, C. L. Hedrick, and E. F. Jaeger 175

NUMERICAL CALCULATION OF THE ELECTRON DISTRIBUTION FUNCTION FOR EBT RING ELECTRONS — J. Tolliver, E. F. Jaeger, and C. L. Hedrick 193

A MODEL KINETIC EQUATION FOR ELECTRON CYCLOTRON HEATING OF EBT RINGS — D. C. Baxter and I. B. Bernstein 221

A MODEL FOR ELECTRON RING FORMATION IN EBT — S. Hamasaki, H. H. Klein, N. A. Krall, J. B. McBride, and J. L. Sperling 233

ANISOTROPY OF THE EBT RING ELECTRONS — A. H. Boozer 253

5. MICROWAVE HEATING AND RADIATION 259

MICROWAVE HEATING OF THE ANNULUS IN EBT — D. B. Batchelor 261

MICROWAVE INTERACTION WITH HOT ELECTRON PLASMAS — M. Tanaka, M. Fujiwara, and H. Ikegami 289

SYNCHROTRON RADIATION FROM THE RING AND NONLINEAR EFFECTS IN MICROWAVE HEATING OF EBT — V. K. Tripathi, E. Ott, and C. S. Liu 305

6. POWER BALANCE 317

RING POWER BALANCE — S. K. Borowski, N. A. Uckan, E. F. Jaeger, and T. Kammash 319

ANNULUS POWER LOSSES IN EBT — R. J. Kashuba and W. B. Ard 333

OPTIMIZATION OF EBT ANNULUS POWER DRAIN WITH RESPECT TO CORE PROPERTIES — M. C. Vella 349

STEADY-STATE MICROWAVE POWER REQUIREMENTS FOR EBTR ELECTRON RINGS — A. Andrade, R. A. Krakowski, and C. G. Bathke 363

7. STABILITY 381

FLUTE-INTERCHANGE STABILITY IN A HOT ELECTRON PLASMA — R. R. Dominguez 383

MACROSCOPIC STABILITY OF THE HOT ELECTRON ANNULUS IN EBT — R. L. Miller, R. R. Dominguez, G. E. Guest, and T. Okhawa 409

A TWO-POINT MODEL FOR ELECTRON TRANSPORT IN EBT — S. C. Chiu and G. E. Guest 437

STABILITY OF A TOROIDAL PLASMA BY HOT ELECTRON ANNULUS IN A BUMPY TORUS — H. Sanuki and M. Fujiwara 453

STABILITY ANALYSIS OF A HOT ELECTRON EBT PLASMA — J. W. Van Dam and Y. C. Lee 471

8. OPEN SESSION DISCUSSIONS 491

8.1 INSTABILITIES IN HOT ELECTRON PLASMAS 493

SUMMARY OF THE OPEN SESSION — M. C. Vella 495

INSTABILITIES IN MIRROR CONFINED HOT ELECTRON PLASMAS — W. B. Ard 499

8.2 POWER BALANCE IMPLICATIONS FOR A REACTOR 503

SUMMARY OF THE OPEN SESSION — W. B. Ard 505

RING POWER BALANCE IMPLICATIONS FOR A REACTOR — N. A. Uckan 507

8.3 DIAGNOSTICS 525

SUMMARY OF THE OPEN SESSION — G. R. Haste 527

MEASUREMENTS OF THE STORED RING ENERGY IN EBT-I — R. J. Colchin 529

AUTHOR INDEX 533

ATTENDANCE LIST 535

AGENDA 539

OPENING REMARKS

L. A. Berry and N. A. Uckan

Good morning. It is a great pleasure for us to welcome you to Oak Ridge once again. Many of you throughout the month of November have participated in extensive discussion sessions held at ORNL to establish the goals and schedule of the ultimate "proposed reference design" for EBT-P. One of the primary physics objectives of EBT-P is the study of the hot electron rings.

During the past twenty years, experiments at Oak Ridge National Laboratory (ORNL) and at other institutions have shown that electron cyclotron heating (ECH) is an efficient and reliable technique for creating and sustaining hot electron plasmas. Oak Ridge ECH experiments were conducted in both simple (PTF and ELMO) and minimum-B (INTEREM and IMP) mirror geometries. The minimum-B experiments were directed toward providing a target plasma of sufficient quality (n_e/n_0) for effective neutral injection, while the simple mirror experiments were directed toward gaining a general understanding of the heating, equilibrium, and stability of hot electron plasmas. In 1967 it was shown by R. A. Dandl and coworkers that the plasma in ELMO was in the form of an annulus composed of very energetic electrons ($\sim$0.5-1.0 MeV) with beta values approaching unity. These rings were a few Larmor radii thick and were found to be macroscopically stable for sufficiently high filling pressures. Also during this period, more refined energy balance calculations made it clear that even with classical behavior, it would be very difficult to produce net power in a standard mirror configuration. Thus, it was highly desirable to utilize in some way the high-beta annulus in a toroidal configuration.

In 1967 R. A. Dandl conjectured that the high-beta electron rings that were observed in ELMO could be formed in a bumpy torus and that the local magnetic well that these rings create would stabilize the toroidal plasmas. The first step in advancing this concept was to establish that the relativistic electron rings could be formed in a nonaxisymmetric

mirror with the coils oriented at an appropriate angle with respect to each other ($\sim$10-20° for a reasonable number of sectors). This was demonstrated on the canted mirror experiment in 1971. This led to approval of EBT-I, and its construction was completed in late 1973.

Very early experiments in EBT-I showed that the high-beta rings did indeed stabilize the toroidal core. Increasingly detailed measurements over the last five years, coupled with the theoretical studies, have resulted in a deeper understanding of the fundamental confinement processes in EBT-I, which led to the advancement of this concept to the proof-of-principle level (EBT-P). The progress in EBT experiments owes much to the pioneering efforts of Dandl.

The existence of a stable equilibrium for the hot electron rings and the ability to maintain them with sufficiently low amounts of microwave power are central to the successful operation of EBT-P and to the viability of the EBT reactor concept.

We hope that this workshop will help refine our understanding with respect to these critical issues.

1. SUMMARY OF THE WORKSHOP

N. A. Uckan, W. B. Ard, C. L. Hedrick, G. R. Haste,
A. Favale, G. E. Guest, H. Ikegami, and R. A. Dandl

1. INTRODUCTION

The first workshop on ELMO Bumpy Torus (EBT) Ring Physics was held at Oak Ridge, Tennessee, December 3-5, 1979. Attending were approximately 70 people, including essentially all of the EBT staff from the United States and the Nagoya Bumpy Torus (NBT) staff from Japan and representatives from all major laboratories, universities, and industries having extensive programs or interests in the field.

The purposes of the workshop were (i) to evaluate the status of the current experimental and theoretical understanding of the hot electron ring properties, (ii) to identify the dominant physical processes that influence ring formation and scaling and their optimal behavior, and (iii) to determine critical areas for near-term research.

The first part of the workshop was devoted to the presentation of more than two dozen technical papers or reviews followed by full discussion. The second part of the workshop was devoted to an enthusiastic open forum discussion of (i) instabilities in hot electron plasmas and (ii) ring power balance implications for reactors. Summary talks by the chairmen of the respective sessions concluded the workshop.

It is convenient to review the workshop under the subject headings chosen for the sessions.

2. OVERVIEW (CHAIRMAN: N. A. UCKAN)

In what proved to be one of the liveliest sessions of the workshop, the past two decades of experimental and theoretical investigation of hot electron ring properties were reviewed. Results from the early hot

electron ECH experiments were covered by Dandl and Ikegami. The theoretical aspects of stability were summarized in the very clear and convincing presentations of Spong and Guest.

In EBT a steady-state plasma is sustained and heated by ECH. The key element of this concept, derived from the ELMO mirror experiments, is a high-beta, hot electron ring (annulus) formed in each sector of the torus. By forming a magnetic well of sufficient depth at the plasma edge, these rings provide stabilization against flute and interchange modes, and at higher toroidal core betas they enhance stability against ballooning modes. Both EBT and NBT have demonstrated that the plasma currents produced by microwave heated, hot electron rings can provide macroscopically stable plasma confinement in a bumpy torus.

The stability of hot electron rings is essential to the overall stability of the system. In the EBT and NBT experiments the rings are operationally stabilized by providing adequate amounts of gas and microwave power to create a significant flux of cold plasma. For given microwave power and machine characteristics, the amount of ambient gas pressure distinguishes the operating modes (i.e., the C-, T-, and M-modes) of EBT/NBT. The conditions under which the electron rings themselves are stable have not yet been adequately established, even though it has been frequently conjectured that the important transition from the quiescent T-mode (toroidally connected sectors) to the turbulent M-mode (disconnected, mirror-like sectors) in EBT/NBT marks the threshold for the onset of ring instability.

Because the behavior of the hot electron plasma in a bumpy torus is anticipated to be very similar to that in a simple mirror, and thus

possibly relevant to the T-M transition in EBT/NBT, and because most ring physics experiments in mirrors were performed in the 19[illegible] and early 1970s, experimental data and observations from the PTF and ELMO experiments at Oak Ridge National Laboratory (ORNL) and the TPM experiment at Nagoya were reviewed.

In these experiments the hot electron plasma was produced by ECH. Investigations of hot electron plasma were first carried out in PTF in the mid-60s with up to 4 kW of ECH power at 10.6 GHz. These investigations showed the presence of several electron energy groups with evidence of peaked hot electron energy density near the outer edge of the plasma. However, strong ring formation was first observed in ELMO, a variable-mirror-ratio mirror experiment with up to 2 kW of 8-mm (35-GHz) continuous wave microwave power. The mirror ratio for optimum operation of ELMO was observed to be ∿2-2.2. Electron energies were in the ∿MeV region with a high energy tail truncation near ∿3-4 MeV. The ELMO data indicated that the plasma was in the form of an annulus located at a radius of ∿10 cm, with a radial width of ∿3-4 cm (a few electron gyroradii) and an axial length of ∿10 cm.

The equilibrium of the ELMO rings was observed to be instability-limited at low pressure and consequently at low cold plasma density. At low heating power levels, narrow band instabilities near the half harmonic of the microwave heating frequency were observed; these are accompanied by only a fractional decrease of perpendicular energy and are reasoned to be of the Timofeev half-harmonic variety (for electrons). The half-harmonic instability was essentially suppressed when upper off-resonant heating (UORH @ 5 mm) was added. Theoretically, the stabilizing effect

of UORH was shown to be due to the reduction in temperature anisotropy of the hot electrons and the relativistic broadening of the particle cyclotron spectrum. The hot electron ring energy and density were an increasing function of UORH power with "calculated" hot electron betas of ∿50-100%. On the other hand, lower off-resonant heating (LORH @ 3 cm) had a very deleterious effect on ring formation, although the details have not been thoroughly investigated. (LORH is known to increase $v_{\parallel}$ rather than $v_{\perp}$.)

In TPM, hot electron plasma was produced by a microwave pulse of 200-ms duration at 6.4 GHz and powers up to 5 kW. Again, the plasma was observed to have three components: hot electrons, cold electrons, and cold ions. However, hot electrons were observed to take a so-called ring shape or shell structure with an M-shape radial profile that was formed at a radius determined by the location of the second-harmonic ($\omega \sim 2\omega_{ce}$) resonance (typically ∿10 cm in diameter) with an axial length of ∿10 cm. The significance of second-harmonic heating in ECH experiments was first pointed out by Ikegami in the late 60s. Although the formation of the ring is possible both at fundamental ($\omega \sim \omega_{ce}$) and second-harmonic ($\omega \sim 2\omega_{ce}$) resonance, generation at $\omega \sim \omega_{ce}$ may be susceptible to instabilities, probably due to large temperature anisotropies (i.e., large $T_{\perp}/T_{\parallel}$). In TPM, an average ring kinetic energy was typically a few hundred keV with $T_{\perp}/T_{\parallel} \sim 5$-10, and several tens of milliseconds were needed to establish the ring at a sufficient density ($\sim 10^{10}$ cm^{-3}) and temperature (>100 keV). From the measured electron energy distribution, saturation in the high energy tail (<1 MeV) was

observed; this may be attributed to several factors including relativistic mass effect, loss of adiabaticity, a decrease in heating rate at $\omega \sim 2\omega_{ce}$ with the increasing energy, and an electromagnetic Whistler instability (high energy hot electrons are stable against this mode).

During the heating period the loss of hot electrons was observed to be enhanced by microwave heating itself. Many of the instabilities occurring during the heating were similar to those that occurred during the transient state just after the removal of microwave power. A few of these modes were studied in TPM by external triggering. Strong electromagnetic instabilities at one-third harmonic ($\sim$2.1 GHz) of the fundamental were observed to dump a significant fraction of stored energy within several microseconds. The instability was a characteristic of the sudden loss of hot electrons (due to strong microwave bursts) but not of cold electrons. The high energy component of the hot electrons (>100 keV) appears unaffected by the instability; this was identified to be the Whistler mode. This instability was artificially triggered by either pulsed microwave power (electromagnetic triggering) or the extraction of cold electrons (electrostatic triggering). Associated with the extraction, a flute-like low frequency instability was detected in addition to the Whistler instability. The mechanism responsible for stabilization of hot electron plasma against flute modes, although not so clearly identified, appears to be correlated with the presence of cold electrons in TPM as well as in ELMO.

There was no satisfactory experimental confirmation of MHD instabilities. This was due, in part, to the difficulties associated with the susceptibility of the low energy component (<100 keV) of the ring to

the electromagnetic instability before any MHD activity. Another possibility is that in the related experiments, the ions may not have been hot enough to be subject to MHD instability.

Experimental results from EBT and NBT indicate many similarities to simple mirror results, and much of this is discussed in the next section. Detailed experimental study of the T-M transition and M-mode operation has not yet been possible in EBT because of the experimental difficulties encountered during unstable operation. These difficulties are associated with wall sputtering, deterioration of subsequent machine performance caused by aluminum impurities, and deposition of aluminum on diagnostics, as well as to the assigned priorities for the investigation of other phenomena, e.g., transport. However, many of the instabilities observed in the mirrors were not present in the current bumpy torus experiments. For example, the half-harmonic microwave emission common in ELMO was not present in the M-mode. M-mode instabilities are believed to be electromagnetic, but there has been no supporting experimental confirmation.

The hot electron ring and toroidal core plasma stability requirements are closely coupled in EBT/NBT. From both the kinetic theory models and the experiments, it appears that the relative density of cold plasma (provided by the toroidal core) is a critical factor in ring stability. However, the stability of the toroidal plasma requires a magnetic well [e.g., $U' < 0$, where $U = \oint d\ell/B$ (provided by the rings)], near the edge of the plasma to support a pressure gradient there. The limits of this stabilization were reviewed; these can be classified into two categories, rigid ring models and interacting ring models. The rigid ring approximation typically assumes that the only effect of the ring is to produce

a local minimum in the magnetic field and that there is no coupling between ring and core plasmas on the MHD time scales. Within this approximation, an ideal MHD model indicates stable confinement of the toroidal core plasma with $\beta_{core} \lesssim \beta_{hot}$, if the ring beta exceeds the critical value required to produce a local magnetic well. This critical value of $(\beta_{hot})_{crit} \sim 10\%$ agrees with experimental observation of the C-T transition.

The stable β_{core} limits from interacting ring stability models in highly idealized "bumpless torus" geometry differ significantly from those obtained in the rigid ring models. To reconcile the differences, further work will be needed in more realistic "bumpy" torus geometry with ring kinetic effects and source effects of the background plasma. However, one significant feature of the results of the interacting ring slab model is that the ring-plasma interaction is of importance in predicting the actual limiting values of β_{core} and in modeling the confinement characteristics of EBT.

As has been seen experimentally, the rings themselves may be subject to various macroscopic and microscopic instabilities. In addition to cold plasma stabilization, certain features intrinsic to the rings (e.g., finite gyroradius, large guiding center drift frequency, finite length) can influence the stability boundaries of macroscopic modes. Microinstabilities, which are due to anisotropic distributions, may be stabilized in the experiment through the use of off-resonant heating (ORH), as demonstrated in ELMO. This mechanism builds up the energetic tail and increases $T_{\parallel}/T_{\perp}$ by spatially spreading out the electron cyclotron resonant heating (ECRH) surfaces. One such microinstability is the

Whistler instability, which is an electromagnetic mode driven by anisotropy and seen in TPM and NBT at the T-M transition. Investigations of this instability for hot electron distributions with an energetic tail indicated that a relativistic spread in the electron cyclotron frequency led to resonant particles in the tail that contribute to damping rather than growth. Such instabilities could be suppressed simply by building up the tail of the hot electron distribution to a certain critical density.

In summary, many possibilities were believed to be responsible for the T-M transition. These include the manifestation of macroscopic modes of hot electrons, an electromagnetic Whistler instability, or just a transport phenomenon affected by wall conditioning. But in all fairness, the dominant processes responsible for the T-M transition, the main modes of instability, and the critical plasma parameters at which the threshold value is reached have not yet been fully established experimentally and theoretically.

3. EXPERIMENTS (CHAIRMAN: W. B. ARD)

The three papers presented in this session dealt primarily with two topics: (i) ring formation and experimental measurements in NBT and EBT and (ii) an attempt to resolve (or to indicate) the apparent discrepancy between EBT and minimum-B mirrors.

The NBT, discussed by Fujiwara et al., is a 24-sector torus with dimensions similar to EBT-I (i.e., a throat radius of ∿12.5 cm and a major radius of 160 cm). However, the magnetic field is capable of supporting a bulk resonance frequency of only ∿8.5 GHz, half of the

EBT-I heating frequency of 18 GHz. Also, NBT has two straight mirror sections 80 cm long in what can be called a "bumpy race track" configuration. Behavior in the C-, T-, and M-modes was observed. The C-T transition occurred at an ambient gas pressure of 1-2 x 10^{-5} torr, and the T-M transition occurred at 5-7 x 10^{-6} torr. The pressure at both transitions increases as the microwave input power is increased.

The ring temperature is measured to be about 100 keV and is almost constant with changing pressure and power. On the other hand, the stored energy and beta value of the hot electron ring β_{hot} increase with increasing microwave heating power until saturation is reached (for input powers over $\sim$30 kW). A remarkable increase in β_{hot} was observed when 10.5 GHz of microwave power was added in addition to the fixed 8.5-GHz power. Because the ring temperature remains almost constant, the increase in β_{hot} corresponds to the increase in hot electron density, and the saturation of β_{hot} may be attributed to the increased drag losses of ring electrons and/or to instability limitations. As the pressure is decreased, beta increases and the electrostatic potential difference between the ring locations and the axis of the toroidal plasma also increases until the M-mode is reached. After the M-mode is reached, the electrostatic potential at the ring location continues to increase, but the potential well present in the T-mode vanishes.

The location of the ring has been determined by an ionization chamber probe inserted from both the inside and outside of the torus. Three peaks are observed. The position of the outside peak is located at the second-harmonic resonance ($\omega \sim 2\omega_{ce}$) and changes position as expected when the magnetic field is changed. The inside peak associated

with the ring also changes location with the magnetic field, but its position is shifted from second-harmonic resonance. A third peak, which is located inside of the inside peak, is associated with circulating (passing) hot electrons. The location of this peak is near the center of the drift surfaces for $v_{\parallel}/v = 1$ particles and is independent of magnetic field.

The explanation given of the inward shift of the ring is that the electrons heated at the second harmonic follow a drift surface and that the positions of the inside and outside peaks correspond to the location of the drift surface for particles with $W_{\perp}/W \cong 0.75$. From this information the axial extent of the ring can be determined; this is comparable to the radius of the ring. Apparently, the ring extends to the first-harmonic resonance zone in NBT. The NBT mirror ratio is 1.9, and it was pointed out that for larger mirror ratios ($\gtrsim 2$), the expected axial length of the hot electron ring will be shorter than that of NBT.

As reported by K. H. Carpenter, one experimental approach for obtaining information about the hot electron ring in EBT is the measurement of the ring diamagnetic flux that couples to the pickup coils. The magnetic field measurements are interpreted in terms of the equivalent surface current on the inside and the outside of the ring and the gradB drift current in the ring volume. Calculations of the expected coil voltages as a function of ring thickness and radius indicate that the measured signals should depend on the total stored energy but would be insensitive to the exact shape of the rings. The diamagnetic measurements show that the stored energy of the ring is almost constant around the torus.

The measurements made on ECH plasmas in the INTEREM device at ORNL were reviewed by G. R. Haste. INTEREM was a mirror-quadrupole magnetic well device that was operated in the early 1970s. In his paper Haste made two important points. One was that high energy electrons can be formed in a geometry in which second-harmonic resonance is not possible; the second was that the processes of ECH cause considerable anisotropy in the resulting electron distribution. The main results concerned measurements of the pitch angle distribution of the hot electrons. At low power levels (or at high pressures), the electron temperatures and stored energy were low in the plasma, and most of the confined electrons had turning points near the resonance heating zone. As the power was raised (or the pressure decreased), a population of very energetic electrons was produced that was confined very near the midplane. These electrons were heated completely nonresonantly because the midplane magnetic field, the lowest field in the minimum-B mirror, was too high for the second-harmonic resonance, which appears to locate the high beta rings formed in simple mirrors.

To summarize, INTEREM results indicated some features of ECH that appear to be at variance with observations in EBT and NBT. In EBT and NBT, as is well known, the location of the rings is determined by the position of electron cyclotron resonance for second harmonics, whereas the energetic electron distributions seen in INTEREM were obtained without second-harmonic resonance. Furthermore, increased power and increased heating in INTEREM led to plasmas that were more closely confined to the midplane. Some preliminary results of EBT and NBT seem to indicate that as the heating is increased, the axial

length of the energetic electron rings increases. Although there was no resolution of the apparent discrepancies between minimum-B mirrors and EBT (as well as simple mirrors), the effects of the intrinsic physical differences between these geometries have not been isolated.

4. RING/CORE MODELING (CHAIRMAN: C. L. HEDRICK)

In modeling classical and neoclassical processes, as in analyzing stabilities, it is ultimately necessary to treat the coupling of the hot electron ring and toroidal core plasmas. The papers given in this session treated this coupling in different ways and emphasized various facets.

Changes in the magnetic field produced by the hot electron rings can now be taken into account in the 1-D transport calculations for the toroidal core plasma. Flux-surface averaging in 1-D transport calculations introduces two geometric form factors that were discussed by Owen and coworkers. These form factors were examined for various tensor pressure magnetic equilibria, and their sensitivity to various ring parameters (i.e., axial length, radial width, mean radius, ring beta) was studied. The behavior of the geometric form factors was shown to be dominated by mod-B in the midplane. The comparison was made with previous approximations that omitted these form factors. Although overall power balance was unaffected, the averaging introduces an additional term that is convective in nature. This term tends to retard losses at the outer edge of the core plasma where gradB is positive and to decrease density and temperature gradients where gradB is negative.

The remaining papers were concerned with kinetic treatments of ring and core plasmas. Clear progress has been made in these models, all of which are in the early development stage. Early results from some of the models indicate tentative agreement with experimental observations. Two of the papers (Baxter et al. and Boozer) were pure velocity space models (energy and pitch angle). The papers by Tolliver et al. and Hamasaki et al. combined spatial and velocity coordinates (radius and energy). The two approaches are regarded as complementary aspects of the longer term goal of achieving a model involving four coordinates (2 space + 2 velocity). This goal is based upon the observation that the hot electron rings are a spatially localized tail on the electron distribution. The rings are localized in pitch angle because ECH tends to increase perpendicular energy faster than it does parallel energy and because the losses are higher for high energy passing (circulating) electrons than for high energy trapped electrons. A possible method for treating poloidal variations induced by toroidal curvature was indicated by Tolliver et al. and is analogous to approximations used in calculating neoclassical transport coefficients.

Hamasaki et al. calculated the line-averaged heating rate from quasi-linear formalism by comparing the heating rate with the classical electron energy loss rate. They then estimated the radial extent of the electron rings and the steady-state ring temperature. Microwave heating distribution in phase space was considered in a paper by Baxter et al. This is important because heat and particle deposition in the phase space can control the velocity and spatial profiles of the rings and the core; these in turn play an important role in stability.

These kinetic modeling calculations will provide a focal point for understanding the hot electron ring properties (i.e., heating, formation, power balance, etc.) and will have much the same significance for the rings that the 1-D (1-1/2-D) calculations presently have for the toroidal core plasma. It was recognized that this is a complex field requiring long term efforts with high importance for understanding future experimental observations.

5. MICROWAVE HEATING AND RADIATION (CHAIRMAN: G. R. HASTE)

The first paper, presented by Batchelor, dealt with the characteristics of the microwave field likely to occur in an ECH plasma and with the effects that can enhance the heating at the second harmonic.

The ordinary mode is very weakly damped in EBT-I (except possibly at the annulus). The extraordinary mode is heavily damped when propagating from the high field side, but it cannot propagate to the resonance because of the right-hand cutoff.

The dominant heating mechanism for the core plasma appears to be the conversion of ordinary mode energy into the extraordinary mode in the high field resonance by the depolarization that occurs at a wall reflection. Since it is expected that several wall reflections occur, the resultant microwave field should be a random superposition of rays with a coherent wave near the waveguide opening.

The resonant interaction is highly dependent on pitch angle. A small group of particles with $v_{\parallel}/v \approx 0$ can stay in resonance for many wave periods. The energy gain per bounce for these particles can be comparable to the initial energy of the particles. It was suggested

that this might be a mechanism by which some cold particles could gain significant energy and thereby large values of $k\rho$, for which the linear cyclotron interaction is effective.

In the paper presented by Tanaka et al., ray tracing techniques were used to determine the path taken by the injected microwave power. The absorbed power was determined from the imaginary part of k along that path. However, the simple treatment of the ray trajectory leads to an unphysical result – that the group velocity can exceed the velocity of light in the region of cyclotron resonance.

The propagation properties of radiation in a plasma with bi-Maxwellian distribution ($T_\perp$, $T_\parallel$) were investigated. Due to the presence of hot electrons with anisotropic temperature, a new resonance was found whose frequency depended on the values of the parallel and perpendicular temperatures. This new resonance (and cutoff) may give rise to new diagnostics to estimate the plasma beta value.

Some experimental observations in the interferometry measurement of plasma density in NBT were presented. The phase shifts determined from interferometers at 35 GHz and 55 GHz were compared as a function of the neutral gas pressure. At high pressure (in the C-mode) there was an agreement between the two, but at lower pressures (in the T-mode) the lower frequency gave a higher phase shift. Because hot electrons were present in the T-mode but not in the C-mode, it is felt that these electrons are the source of the discrepancy. Depending on the frequency, interferometric measurement may lead to an erroneous result if it does not use proper calibration.

Synchrotron radiation from the hot electron ring was considered as a diagnostic tool in the paper by Tripathi and coworkers. By treating the high harmonics ($n \sim 10$), one avoids the heating frequency and cold plasma contribution. The energetic electrons have harmonic radiation that overlaps strongly. At 90°, the ordinary mode is much weaker than the extraordinary mode, but its intensity varies with the width of the pitch angle distribution, whereas the extraordinary mode is independent.

The paper by Pipkins treated the effects of magnetic field variation, relativistic changes, finite k, and finite Larmor radius in a slab model. The requirement for the second-harmonic instability was that the field amplitude be larger than a collisionality parameter. When this instability occurs, the dominant detuning effects arise from magnetic field variations across the field and from the relativistic change in the resonant frequency. Appropriate values of k can offset these detuning effects. However, even when the detuning effects are cancelled, the heating is limited by finite Larmor radius effects [i.e., when the argument of the Bessel function is such that $J_n(k\rho) = 0$].

6. POWER BALANCE (CHAIRMAN: A. FAVALE)

Because, as previously indicated, electron rings play an important role in the confinement characteristics and performance of EBT, the microwave power required to sustain the rings during steady-state operation represents an important question for future devices, especially in scaling the EBT to a reactor. Four papers concerning the ring power balance were presented in this session.

While disagreement is seen in details, the models developed by Borowski et al. and Kashuba et al. are in qualitative agreement, predicting the dominant power loss mechanisms to be drag cooling, scattering, and synchrotron radiation. Drag losses dominate a significant range of the ring energy and are large for small energies. At high ring energies (>1 MeV), accelerated ring cooling occurs due to the synchrotron radiation. Because the drag and scattering losses decrease with increasing energy, the resulting total loss rate has a broad minimum that is bounded by these loss mechanisms. The parameters important for the total power loss are ring beta β_{hot}, the ratio of cold to hot plasma density $f_R = n_{cold}/n_{hot}$ required for the ring stability, the magnetic field strength near the vicinity of the rings B, and the ring volume V_R. Agreement is found between these two models (within 10-20%) for the range of interest of typical ring parameters. The microwave power required to sustain the rings in EBT-I/S is modest and reasonably well estimated by these models.

Borowski and coworkers showed that applying stability considerations of both ring and toroidal core plasma narrows the parameter space in which one can conduct meaningful power calculations. Specifically, the ring beta was limited to $\sim 0.1 < \beta_{hot} < \sim 0.5$, the lower limit being necessary for core stability corresponding roughly to C-T transition and the upper limit being determined by the onset of ring instabilities corresponding roughly to T-M transition. For this range of ring beta in the T-mode, the stability of the hot electron ring itself requires the presence of an appreciable cold electron density component. Stability requirements were used in the paper for determining minimum values of f_R.

It was pointed out that the major uncertainty in the power analysis was the specification of ring volume. Present understanding of ring physics, both theoretical and experimental, is not sufficiently broad to allow credible straightforward extrapolation of ring geometry.

Power requirements from these analyses are quite severe for a reactor if one assumes the core-to-ring volume ratio V_C/V_R to be similar to EBT-I and NBT (i.e., $V_C/V_R \sim 10$). For $V_C/V_R \sim 10$, the Q of the reactor would be too low for economic viability. However, most of the projections, all of which seem to fit past and present experiments, find that if ring volume scales with magnetic field, core plasma radius, magnetic field gradients, etc., the ratio V_C/V_R for reactor scale plasmas would be expected to be much larger than that of EBT-I. The use of ion rings and/or alternate heating schemes has been proposed for increasing volume ratio and reducing power requirements.

The use of ion rings to reduce the power requirements has been investigated by Kashuba et al., who have derived an expression for power losses from the ion rings. Charge exchange is found to be the dominant energy loss mechanism. For ions, all the loss mechanisms decrease with ion temperature. The limit on maximum temperature is shown to be set by the size of the Larmor orbits. It is stated that ion rings should be possible and should show a reduction in power loss by a factor of at least three over electron rings. No discussion of ion ring formation and their stability properties was presented.

An optimization of the ring power losses with respect to core plasma parameters has been investigated by Vella. A substantial reduction in the importance of ring power losses compared to core power

production for overdense operation was pointed out. His analysis indicated that any heating technique that would permit an increase in the core density with respect to cutoff could reduce the recirculating power fraction in the reactor regime. Development of either beam plasma electron heating or ion cyclotron core heating was suggested.

Andrade et al. have investigated the power losses for an EBT reactor. Reactor Q values are determined parametrically for a large range of machine parameters. The motivation of the study was to deduce target values of f_R, V_C/V_R, and β_{hot} for specified reactor performance, assuming that self-consistency has been maintained by other means. It was also shown that drag losses are relatively insensitive to the details of the hot electron distribution. When relativistic expressions are used, power losses of up to an order of magnitude larger are found. This model and the two previously discussed models that also use the relativistic formalisms are in substantial disagreement.

As pointed out in the open session, future research in this area should be directed toward a better understanding of rings, in particular the geometry. Independent control of the rings could be possible; this may lead to improvement in performance and optimization in ring economics.

7. STABILITY (CHAIRMAN: G. E. GUEST)

The stability requirements of hot electron rings and toroidal core plasma are closely coupled, and the papers given in this session investigated both.

Because of the qualitative character of the instabilities observed in earlier ECH experiments using simple mirror devices, it has been

customary to discuss ring stability in terms of two major destabilizing properties of ECH plasmas: the anisotropy of the hot electron pressure $p_\perp \gg p_\parallel$, and the unfavorable curvature of the magnetic lines of force in the region occupied by the rings. The anisotropy can drive both electrostatic and electromagnetic plasma waves unstable, and the magnetic configuration is inherently unstable to flute-like modes. Conditions for stabilization of the modes driven by pressure anisotropy appear to relate to properties of the ECH process, particularly the effective (mirror) ratio between the resonant magnetic field and the minimum field strength on the same magnetic lines of force: if $B_{res}/B_{min} \gtrsim 1.2$, the plasma is relatively free of anisotropy-driven instabilities. The mechanisms responsible for stabilization of flutes, although not so clearly identified, appear correlated with the relative density of the colder plasma component. Because ECH typically leads to a two-component plasma if the microwave power density is high enough and other conditions are suitably chosen, this aspect of flute-mode stabilization suggests a possible role for these instabilities in the T-M transition.

The anisotropic guiding center fluid model can be used to compute high beta equilibria that emulate many features of the rings, particularly the geometrical shape and continuous pressure gradients and thus the actual magnetic configuration resulting from diamagnetic plasma currents and vacuum magnetic field. This model has been developed extensively and applied to EBT. Recent results from a variational study that combines the earlier equilibrium models with the new stability techniques developed in tokamak programs (i.e., PEST, ERATO, GATO) were reported by Miller et al. The fluid nature of this model rules out the important

stabilizing effect of the finite-sized gyroradius of the plasma ions and the relativistic electrons. In actual practice, the radial thickness of the rings is only a few hot-electron gyrodiameters, and the perpendicular wavelength of the flute modes can be comparable for relatively low poloidal mode numbers.

A more microscopic kinetic theory approach, which accounts for the finite gyroradius effect but at the expense of geometric realism, is presented by Dominguez. Due to the complexity of the problem, most studies have used the idealized geometry of a simple slab model; the effect of the curvature is simulated by an artificial gravity. Almost all studies to date have made the assumption that unstable modes were highly localized, which, as was clear from the guiding center fluid model, neglects a strong stabilizing effect associated with the finite radial extent of the unstable perturbations. This artificial localization can be somewhat mitigated by modeling the ring as a hollow cylinder, but the radial boundaries must then be assumed to be mathematically sharp: n = constant, $r_{inner} \leq r \leq r_{outer}$; and $n = 0$, otherwise. Thus, the kinetic theory model is complementary to the guiding center fluid model in several important respects, and both models predict that rings would generally be unstable in the absence of some additional stabilizing mechanisms. One such potential mechanism, background cold plasma, is included in the kinetic model. Results reported by Dominguez from a kinetic theory, sharp-boundary cylindrical model indicate that cold plasma can stabilize hot electron flute modes if critical threshold values of $f_R = n_{cold}/n_{hot}$ are exceeded. The critical cold electron concentration is a monotonically decreasing function of the hot electron

precessional frequency. Nonmonotonic behavior that was observed in localized theory when the precessional frequency was larger than or comparable to ion cyclotron frequency was not present in this nonlocal theory, and it was observed that the predicted critical f_R can be significantly less than that predicted by the localized theory. It should be noted that in all these cases, finite length effects have not been analyzed using a fully electromagnetic dispersion relation.

From the kinetic theory model and earlier experiments, it appears that the relative density of the cold plasma surrounding the ring is a critical factor in ring stability. The cold plasma den , in turn, is controlled by the microwave power applied to the plasma and by the ambient neutral gas pressure at the surface of the plasma. The paper by Chiu et al. summarized a model calculation for determining the relation between cold plasma parameters and the power and pressure.

In this approach, the plasma is modeled as two contiguous regions within which all local values of plasma parameters are replaced by their average values. The edge plasma is assumed to be turbulent; the central core plasma is assumed to be quiescent, as in T-mode, and subject to neoclassical transport. The profound differences between the toroidal and open-ended simple mirror configuration were presented.

Two papers, by Sanuki et al. and Van Dam and Lee, reconsidered the stabilizing effect of the hot electron rings on the toroidal plasma. The rings are predicted to stabilize low beta plasmas in EBT devices if the ring beta exceeds the value required to produce a local average magnetic well (i.e., the value above which $\oint d\ell/B$ becomes a nonmonotone function of the minor radius). It has also been predicted that if these

minimum conditions were exceeded, the toroidal core plasma would be stable up to values of core-plasma beta comparable to the ring beta. Above these limiting values of the core-plasma beta, unstable ballooning modes are expected to enhance radial transport of the toroidal plasma.

The analytical results presented by Sanuki and coworkers support Nelson and Hedrick's prediction of stable confinement of a core plasma with beta $\gtrsim$ 50% if the ring beta exceeds 20-40%. These results assumed that the rings are unaffected by low frequency perturbations of the core plasma; this is the so-called rigid-ring assumption.

Van Dam and Lee reached a very different conclusion, namely, that the rings respond significantly to low frequency fluctuations in the (parallel) magnetic field, leading to destabilization if the core beta exceeds a very low critical value. They used a highly idealized "bumpless torus" model, that is, an ideal solenoid in which the magnetic field strength is constant along field lines. Because only flute-like ($k_{\parallel} = 0$) modes have been considered, the ring electrons exhibit adiabatic, 2-D behavior and follow distorted drift trajectories in response to low frequency fluctuations in the magnetic field. The result is a significant compressional effect in which the magnetic field perturbation is greatly enhanced by the hot electron response and the core plasma supports unstable flute-like modes at very low beta values.

It is possible that this enhanced compressional effect is an artifact of the bumpless torus model and may not occur in an actual bumpy torus. In a bumpy torus, the adiabatic response of the hot electrons would be mainly a change of pitch angle that would preserve total energy ε, magnetic moment μ, and action invariant $J = \oint v_{\parallel} d\ell$ during the slow

change in B. The change in perpendicular pressure resulting from a low frequency variation in the magnetic field strength [$\delta p_\perp \sim (\partial p_\perp/\partial B)\delta B$] could be small because of the possibility of expansion and contraction along the magnetic field lines in a more realistic "bumpy" model of EBT. However, further research will be needed to reconcile the differences.

8. OPEN SESSION — POWER BALANCE IMPLICATIONS FOR A REACTOR (MONITORS: N. A. UCKAN AND W. B. ARD)

The consensus from the open session discussions on ring power balance was that the identified energy loss processes (drag, scattering, and synchrotron radiation) and the estimates of energy loss as a function of hot electron temperature, magnetic field, and plasma parameters are probably correct. The microwave power required to sustain the rings in EBT-I, NBT, and recently in EBT-S is modest and reasonably well estimated by the theoretical models. There was, however, a considerable amount of discussion about how the total power to sustain the rings would scale to a reactor.

The question here was how the ring volume will scale with magnetic field, core plasma radius, magnetic field gradients, etc. The modest parameter range accessible in the past mirror and EBT/NBT experiments, which all had similar device and plasma parameters, is not sufficiently broad to make a credible extrapolation to future larger devices, especially to a reactor. When scaled up from EBT-I/S, the ring power requirements for a reactor can become favorable or unfavorable depending on the scaling assumptions made for the volume as well as the completeness and/or self-consistency of the models used (i.e., stability, ring-core

interaction, etc.). There was also concern that rings sufficiently thin to allow a favorable power balance in a reactor would require the radial density gradients in the core plasma to be unrealistically steep. However, transport models predict rather steep density profiles. Of course the validity of the models requires that the scale lengths of the density gradients be at least several gyroradii. Because the ring electrons and core ions near the surface have comparable gyroradii (i.e., relativistic electron gyroradius $\sim$ ion gyroradius near the rings), minimum ring thickness (of a few gyrodiameters) and minimum core density scale lengths are not incompatible.

Another possible limitation on the thinness of the ring could result from stability requirements on the ring or on the minimum ring dimensions required for core stability. Stability calculations are presently under way to determine the limits of the ring thickness. On the other hand, a number of ring instabilities (Whistlers, mirror modes, etc.) are avoided through isotropization. Since the ring length is related to the size of $T_{\parallel}/T_{\perp}$, such requirements may lead to a lower bound on the finite ring length.

NOTE: Since the time of the workshop, EBT-S has become operational. The scale up in magnetic field and microwave frequency from EBT-I (28 GHz, resonant field $B_r \cong 1.0$ T) has resulted in significantly improved ring parameters and performance. In EBT-S the ring temperatures ($\sim$500 keV) are about three times higher than in EBT-I ($\sim$150 keV) for comparable ring plasma densities ($\sim$2-3 x 10^{11} cm^{-3}), and stable T-mode operation extends to lower pressure and

has a broader range than observed in EBT-1. EBT-S presently operates ∿50 kW of cw 28 GHz and is expected to reach power levels of ∿100 kW in the near future.

2. OVERVIEW

N. A. Uckan, Session Chairman

REVIEW OF RING EXPERIMENTS

R. A. Dandl

The flow of high beta ECH plasma information has been erratic and slow over a period spanning the 1960s to the present time. First, because these plasmas were initially considered not fusion plasma relevant, and secondly, because support (both fiscal and scientific) corresponded to fusion plasma community interest.

Because of EBT and other fusion device ECH applications, interest in high beta ring plasma has recently increased considerably. However, most of the ring physics experiments were performed in the 1960s so that much of the data that I present will be quite dated.

I would like to start by showing early and late experimental manifestations of hot electron ring plasmas in PTF in the 1960s and in EBT in 1973, followed by more detailed ring data from the ELMO experiments in the late 1960s. These data include ring temperature density and stored energy measurements as a function of combinations of heating frequencies (i.e., upper and lower off-resonance heating as well as varied resonant frequencies), unfolded high beta equilibria, some instability signatures and parameter variations with heating power frequency and pressure.

Finally, some ring profile information from the EBT experiment, including skimmer profile measurements and pressure-ring parameter measurements.

CHRONOLOGY OF ECH RING EXPERIMENTS

1960

FIRST ECH PLASMAS
DIAGNOSTIC TOOL DEVELOPMENT

1964

HEATING THEORY – MODELING
STABILITY STUDIES

1967

HIGH BETA RING EQUILIBRIA (STUDIES)
HEATING AND STABILITY EXPERIMENTS

1970

HIGH BETA EQUILIBRIUM IN NONAXISYMMETRIC GEOMETRY

1974

REDUCED RING STUDY ACTIVITY

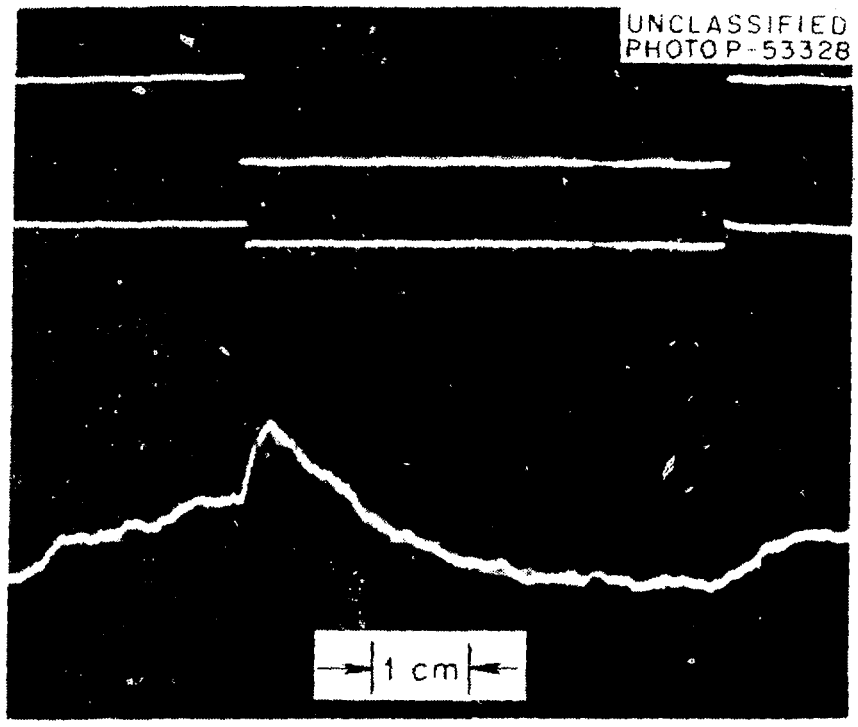

GAS PRESSURE: 3.1×10^{-6} mm Hg
SWEEP SPEED: 25 ms/cm
HEATING FREQUENCY: 2250 Mc
NOISE RECEIVER TUNED TO 2500 Mc

Decay of Electron Cyclotron Radiation.

This is one of the first measurements in PTF of a hot electron population produced by ECH. It shows the decay of electron cyclotron radiation after turnoff of the microwave heating power.

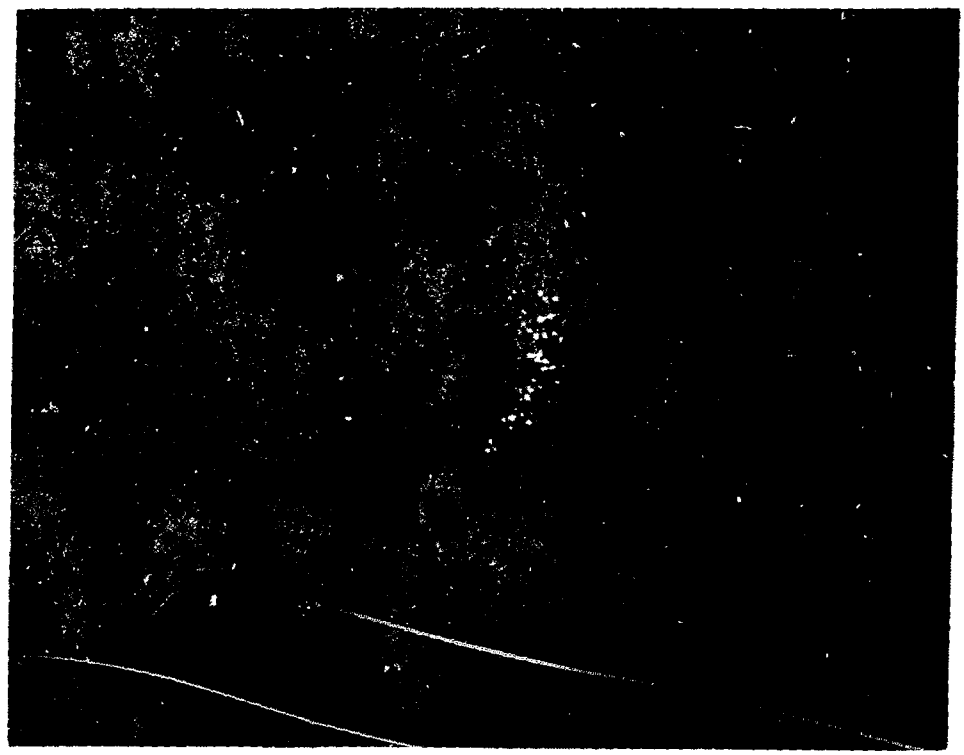

This ring is a photograph of incandescent moly powder dropped into the PTF plasma while heating at fundamental frequency on nonaxis crossing resonant mod-B surfaces.

ORNL DWG 70-1091

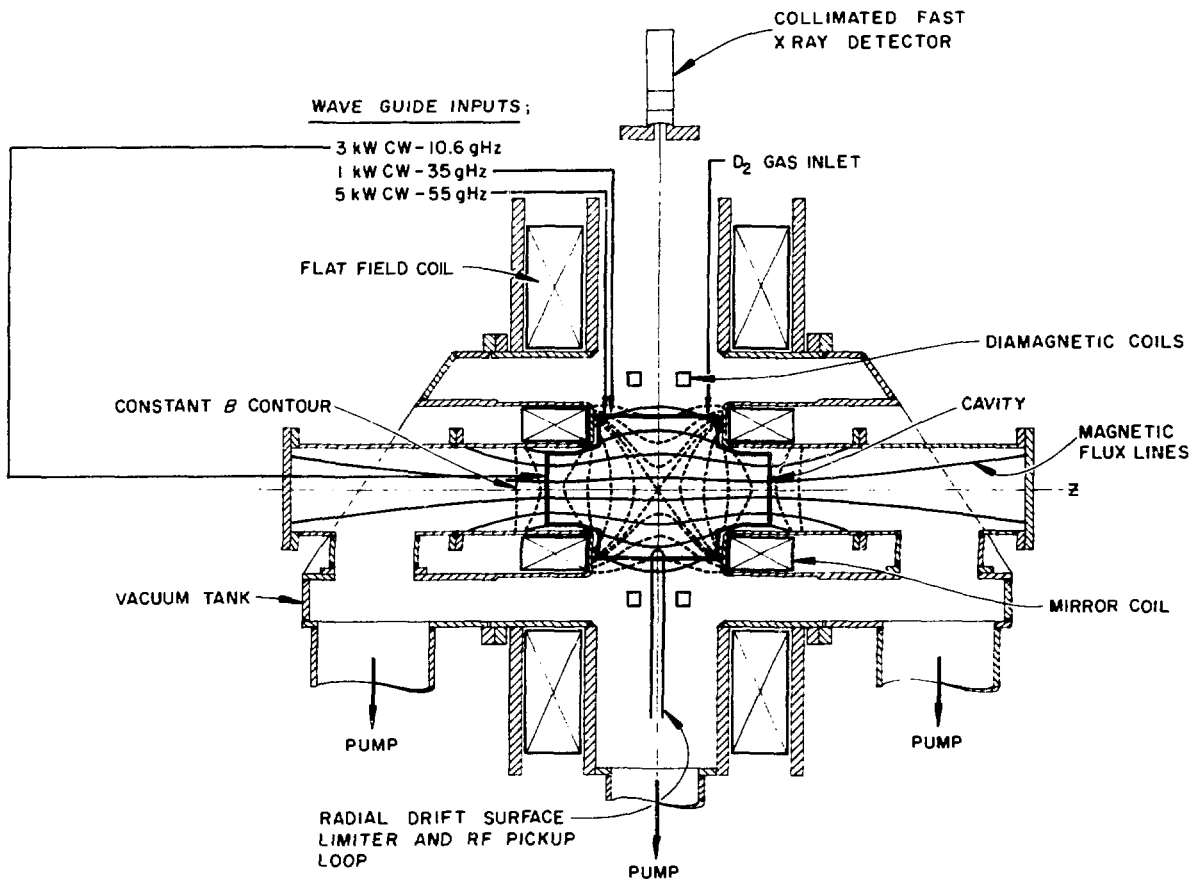

This is a cross section of the ELMO device, showing flux lines and mod-B's and the positioning of some diagnostics and microwave hardware.

ELMO, JUNE 23, 1965

ORNL-DWG 65-10302

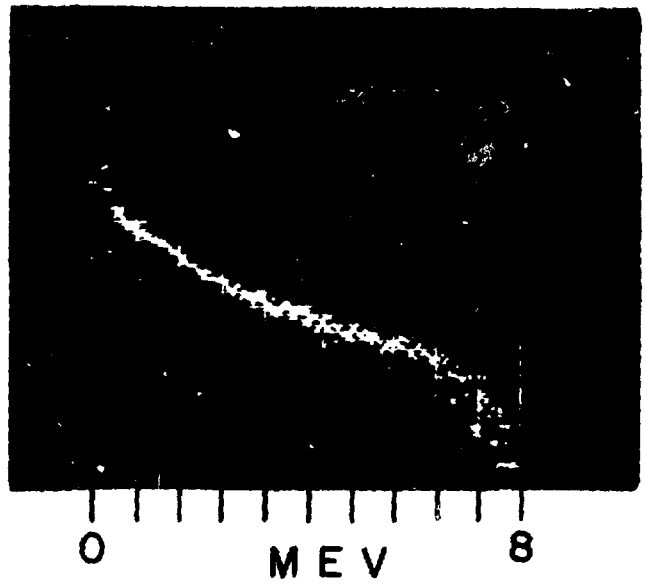

X-RAY SPECTRUM

10 MIN. COUNT.
1 ½ IN. OF LEAD IN PATH AS LOW ENERGY ABSORBER.
MR = 2.3, Boo = 7.6, Z = 5.4
1 KW POWER AT 8 mm.
PRESSURE = 2.3×10^{-5} TORR.

A free-free (hard x-ray) bremsstrahlung spectrum from an ELMO 8-mm plasma showing the temperature to be in the MeV region.

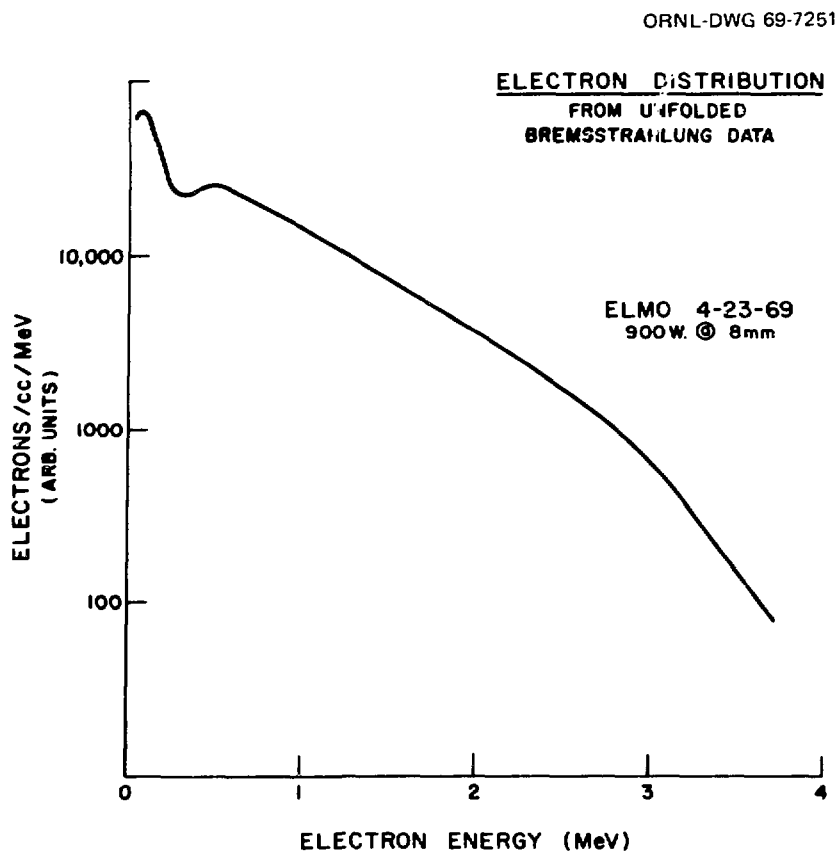

An unfolded ELMO bremsstrahlung spectrum showing a high energy tail truncation and high average electron energy.

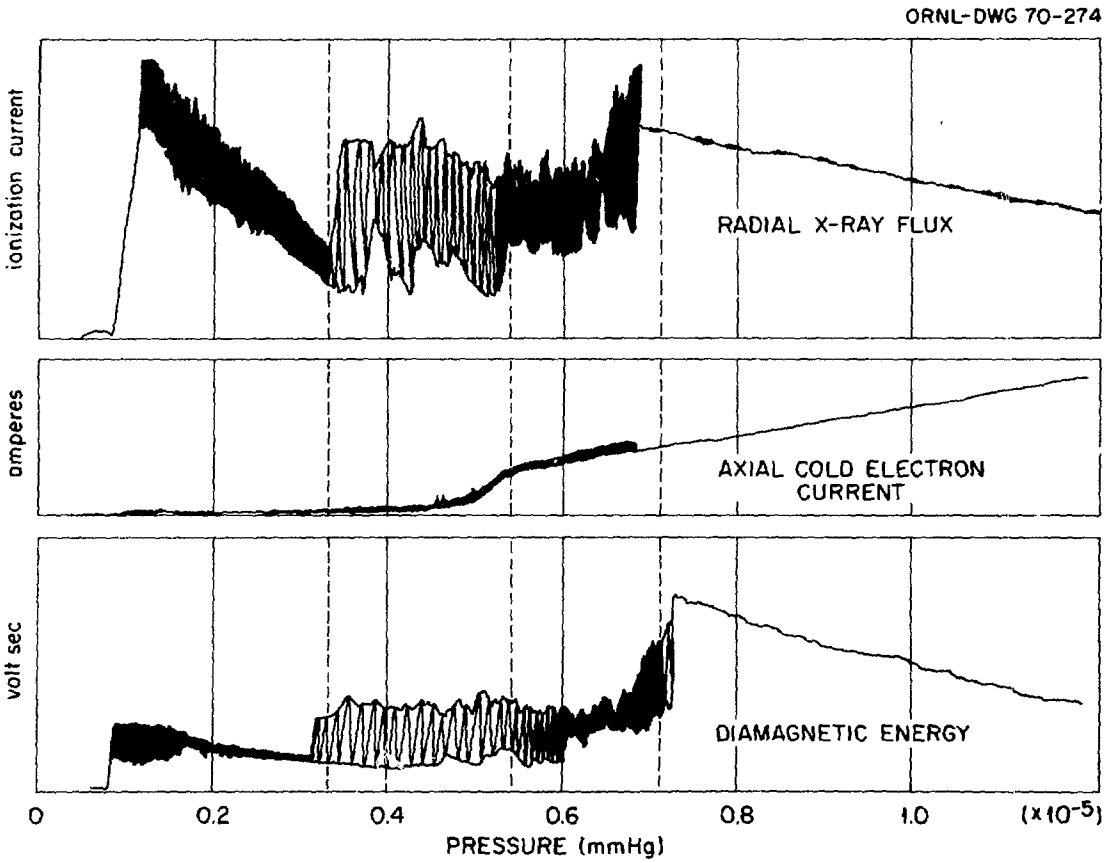

STABILITY REGIONS VS PRESSURE
ELMO 1969

A pressure scan of ELMO parameters showing $W_\perp$ (the ring energy) to be instability limited at low pressure and low cold plasma density.

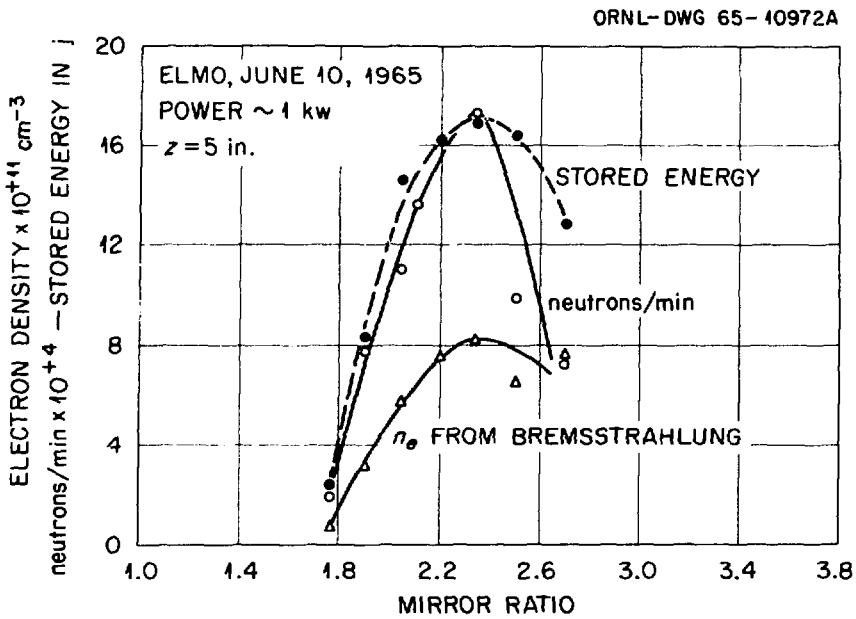

A scan in ELMO of energetic plasma parameters as a function of mirror ratio, showing the optimum (for this cavity configuration) at $M_R \cong 2:1$.

ORNL-DWG 67-9217AR1

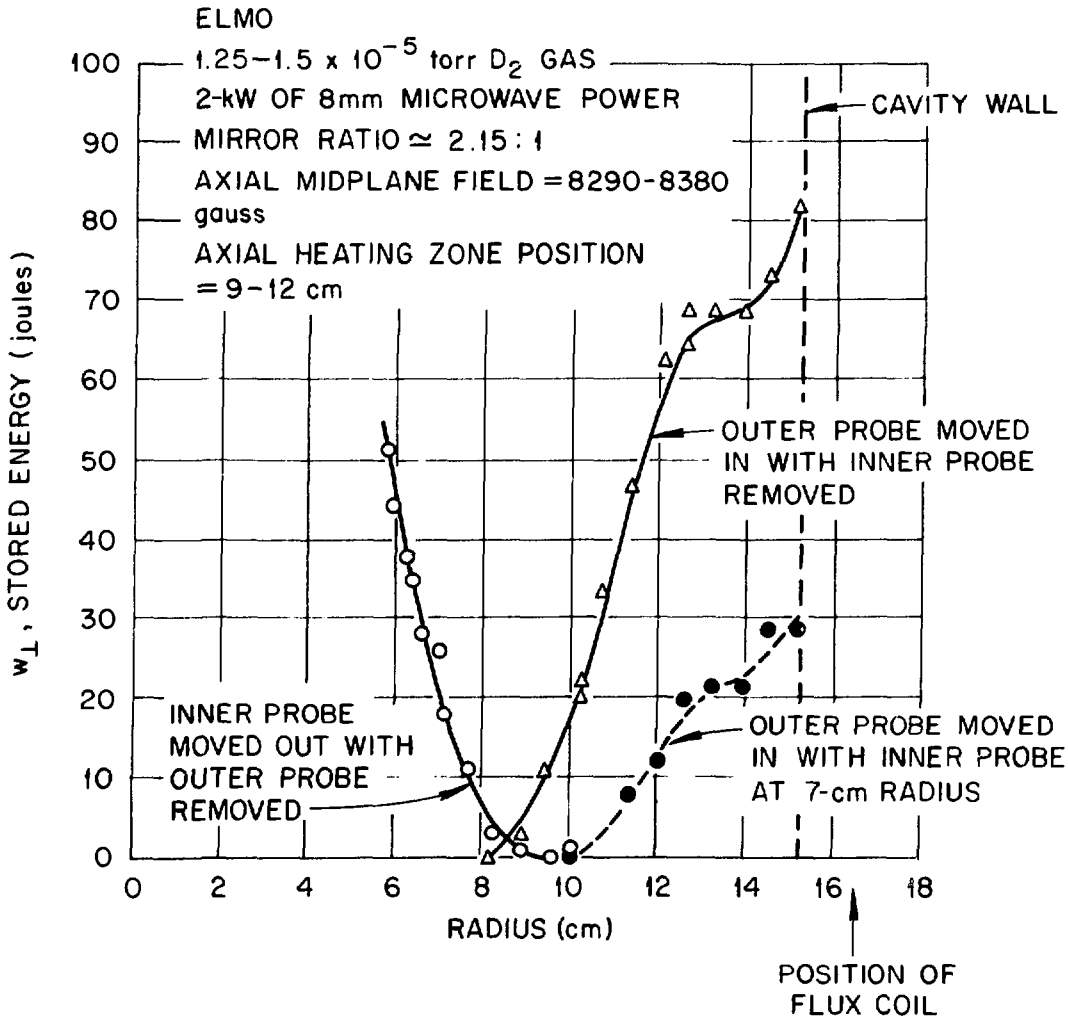

This is a skimmer probe (i.e., drift surface skimmer) profile of perpendicular energy of an 8-mm ELMO plasma, showing the dominant features of the ring structure. The skimming was performed from both the outside in and from the axis out, and combinations of these to delineate the ring structure.

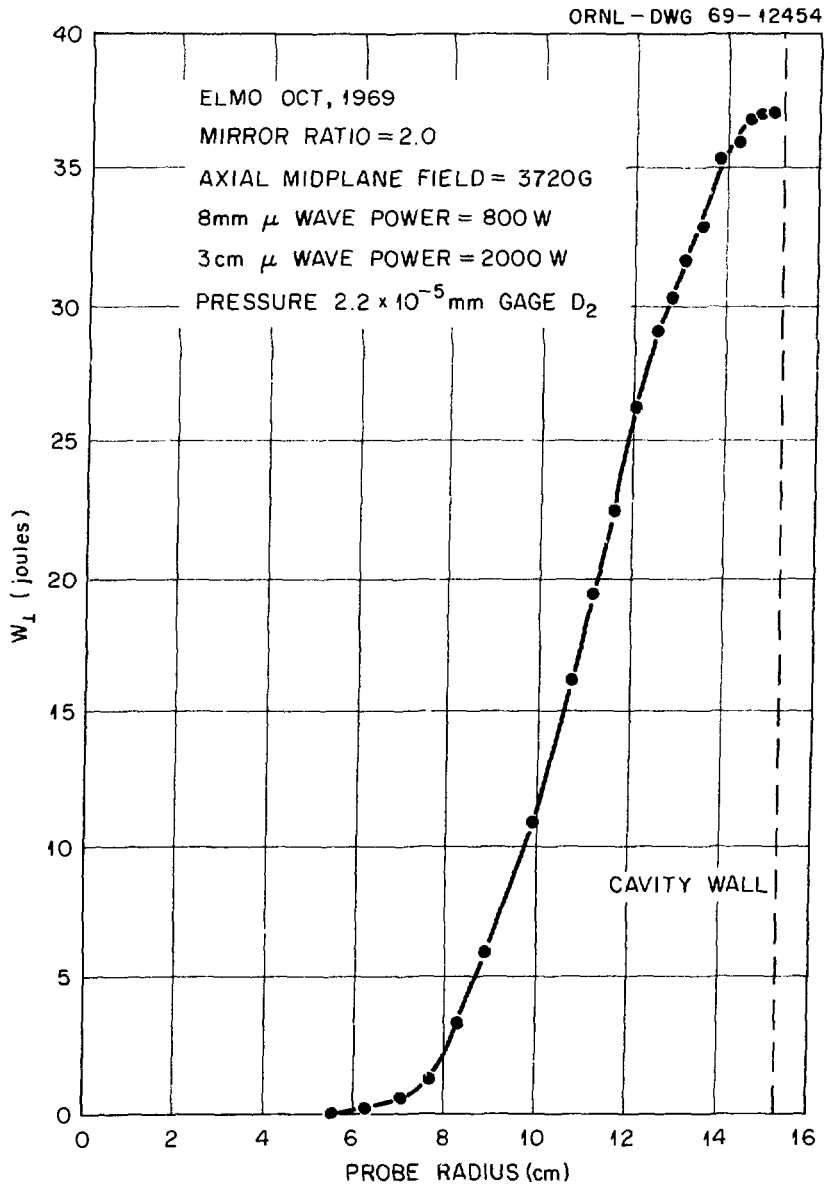

Another skimmer profile of a 3-cm ELMO plasma showing an almost identical plasma pressure profile to that obtained with 35-GHz heating frequency.

ORNL-DWG 67-4416

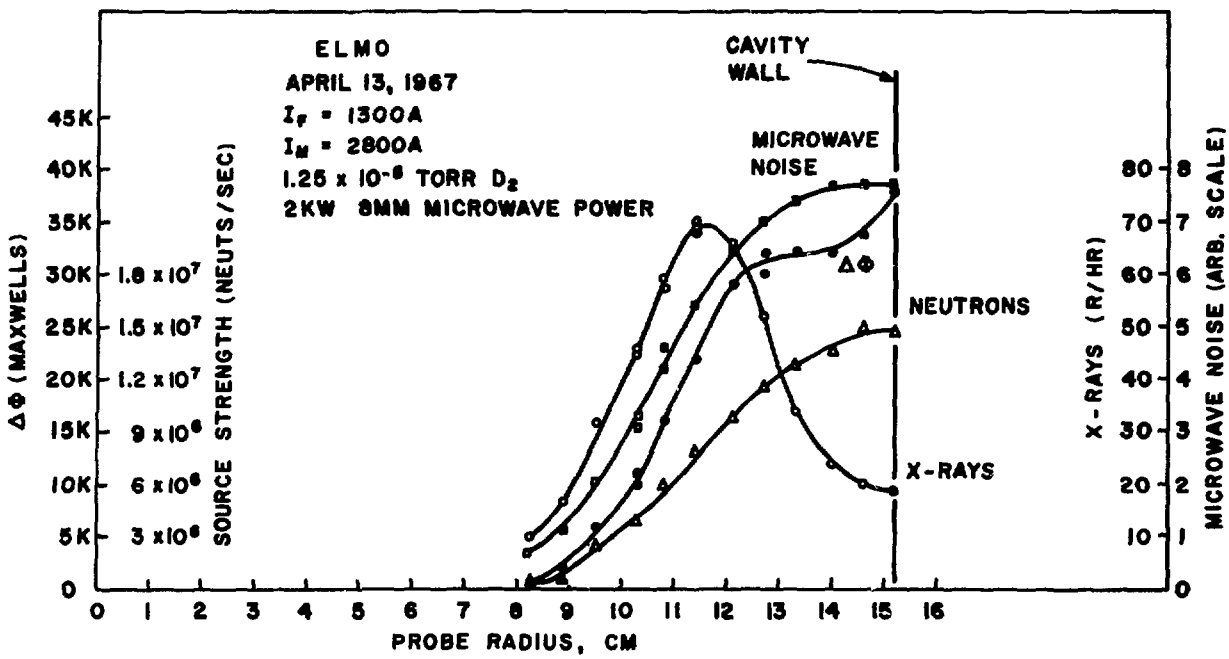

A skimmer profile showing the corresponding change of all of the energetic ring parameters including: neutrons from electron dissociation of deuterium, synchrotron radiation, and $\Delta\phi$ on $W_\perp$ from a diamagnetic flux integrator. The x-ray signal is a measure of hot electron flux on the skimmer probe as it is inserted into the plasma.

ORNL-DWG 68-13159

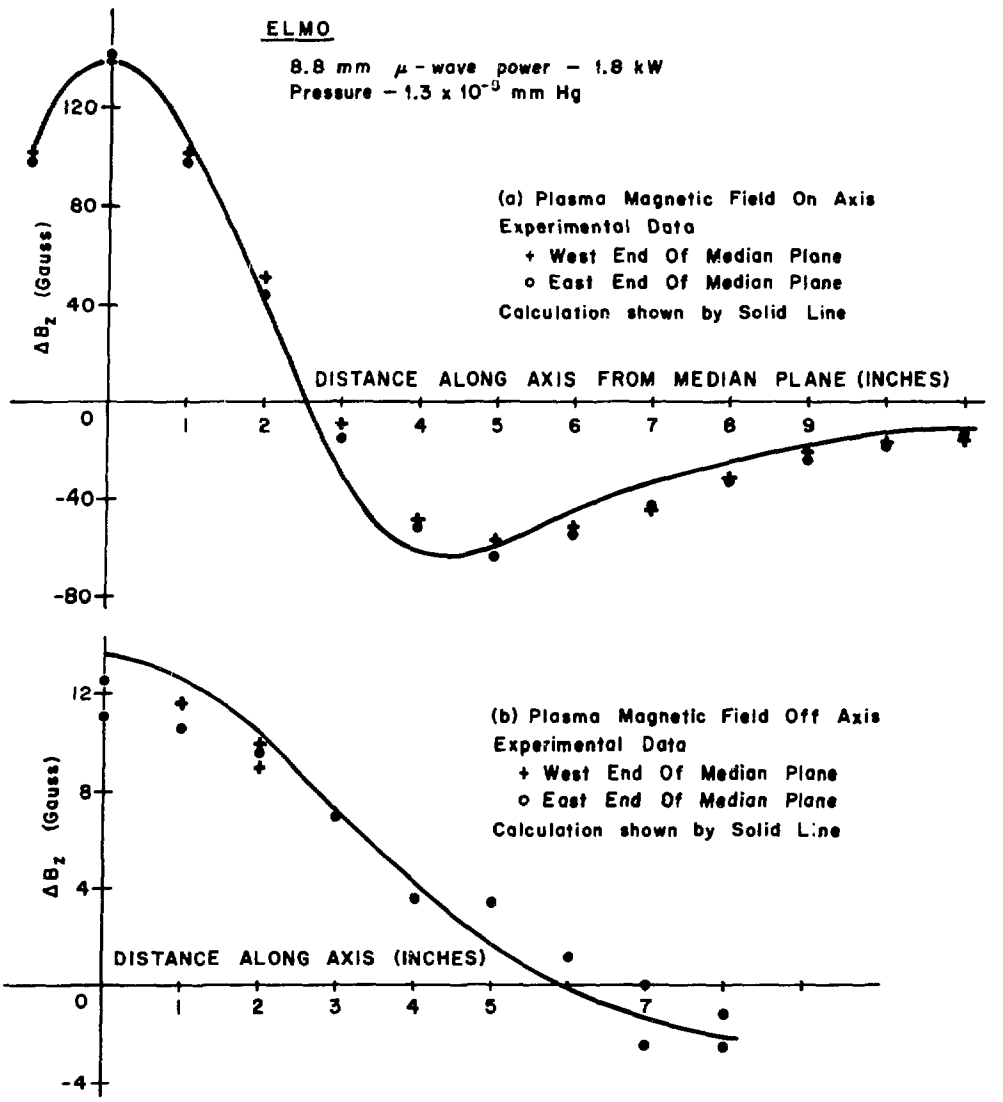

Axial plot of the diamagnetic $\Delta\phi$ of an ELMO ring, obtained from movable Hall probes.

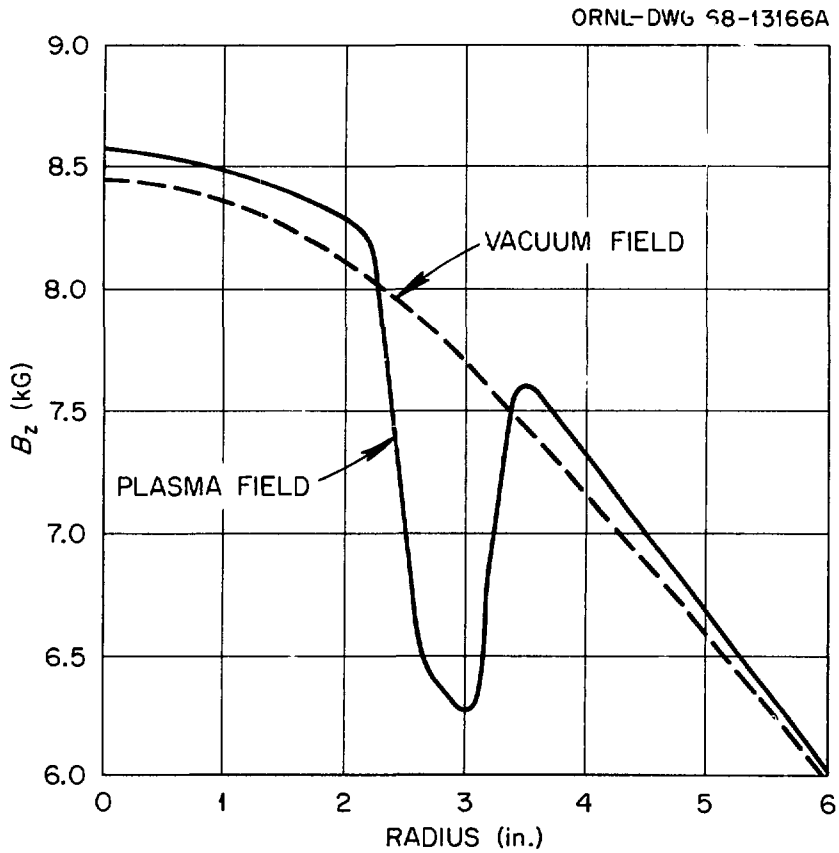

An unfolded radial ring pressure profile.

ORNL-DWG 70-199

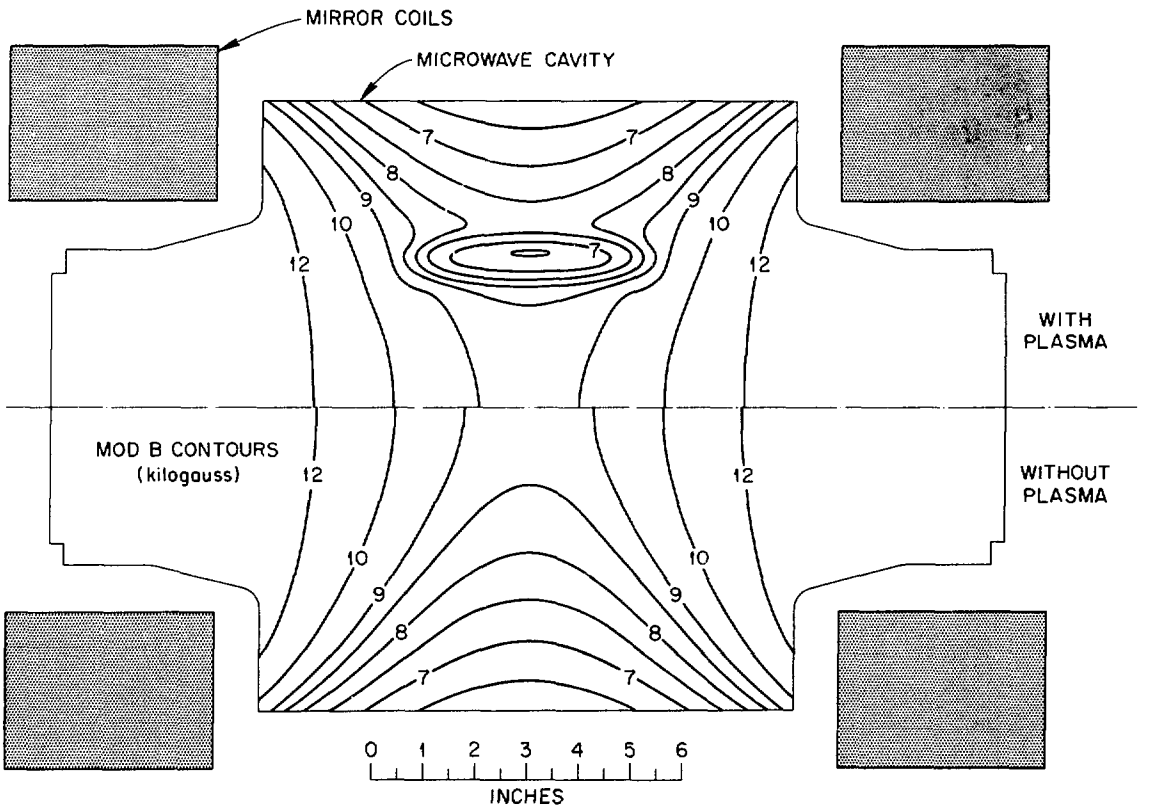

Mod B Contours for ELMO System with Plasma Profile Derived from Diamagnetic Data.

A ring-magnetic field plot from an unfolding which used axial and radial $\Delta\phi$ profiles along with skimmer profile information.

ORNL-DWG 68-6434

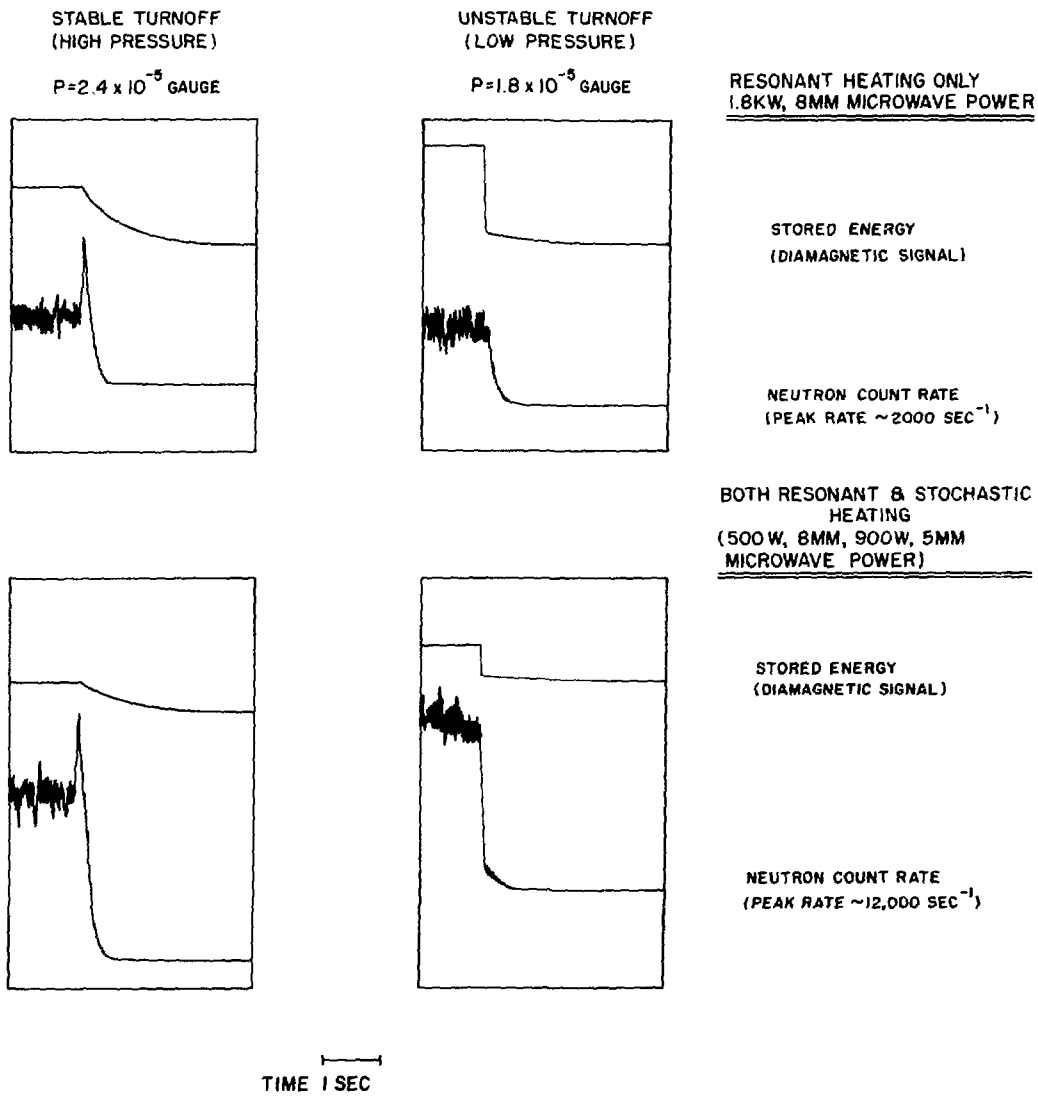

Stable and unstable ring decays after turnoff of microwave power for a resonant only and a resonant and upper off-resonant heating cases. The pressure was so adjusted for these cases to allow a stable decay and then lowered to allow a ring instability or plasma dump during decay.

ORNL-DWG 68-9802

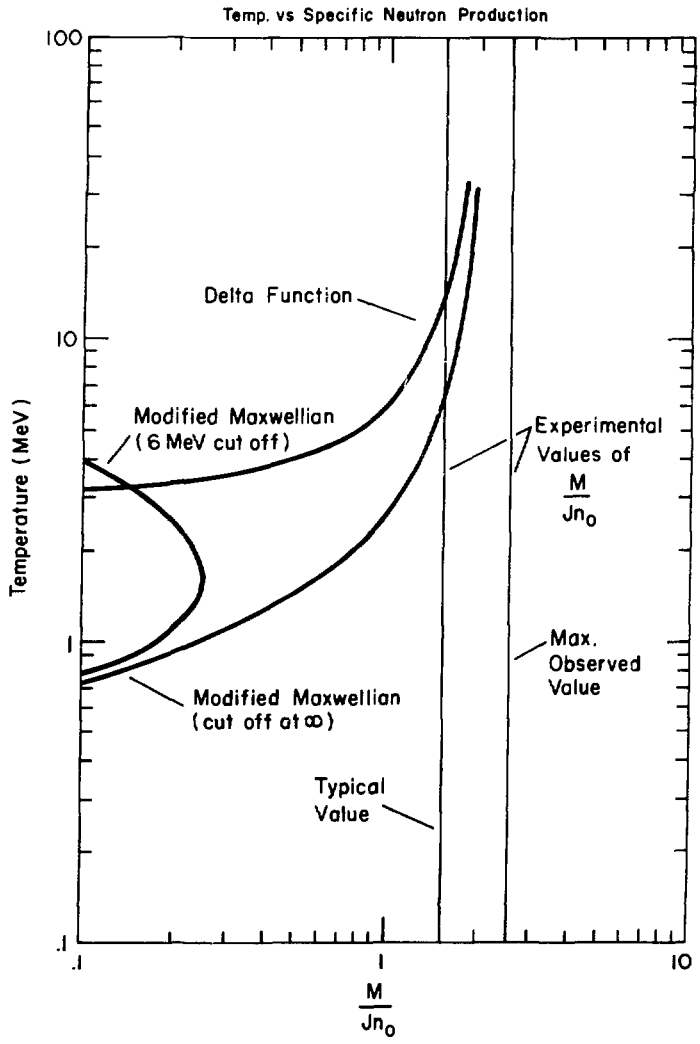

A calculation of neutron production from electron disassociation of deuterium was performed by measuring the total ring energy, J, the neutron source strength, M, and the nucleon target density, n_0. When integrating the neutron production as a function of cross section over the different electron energy distributions, the average electron energy function is essentially independent of plasma volume and shape and is simply a function of the ratio, $\frac{M}{Jn_0}$. The highest observed plasma parameters (i.e., $\frac{M}{Jn_0} \approx 2$) fall well above the 6-MeV cutoff distribution reasoned to be in the experiment.

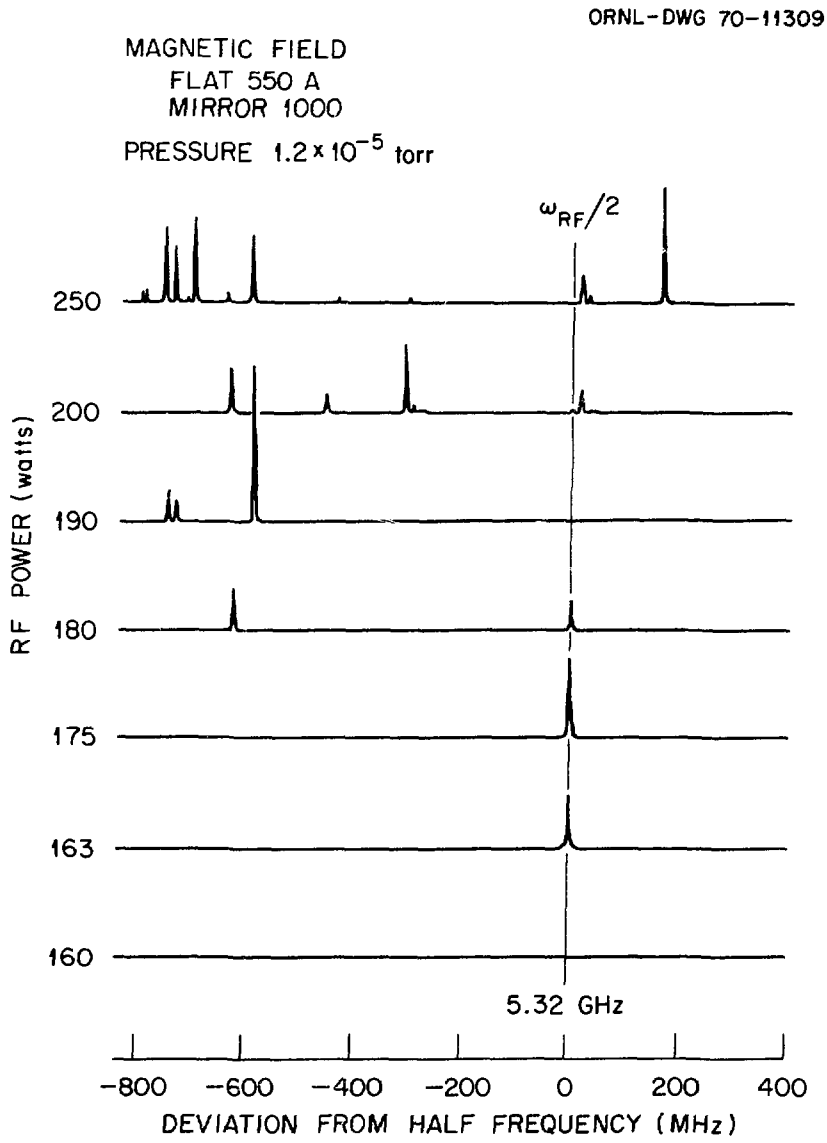

An observation of instability threshold microwave radiation at 1/2 the microwave (ECH) heating frequency in ELMO experiments. This instability is assumed to be of the Timofeev half harmonic variety (for electrons) as elucidated by Sigmar and Guest in publications circa 1970-1971.

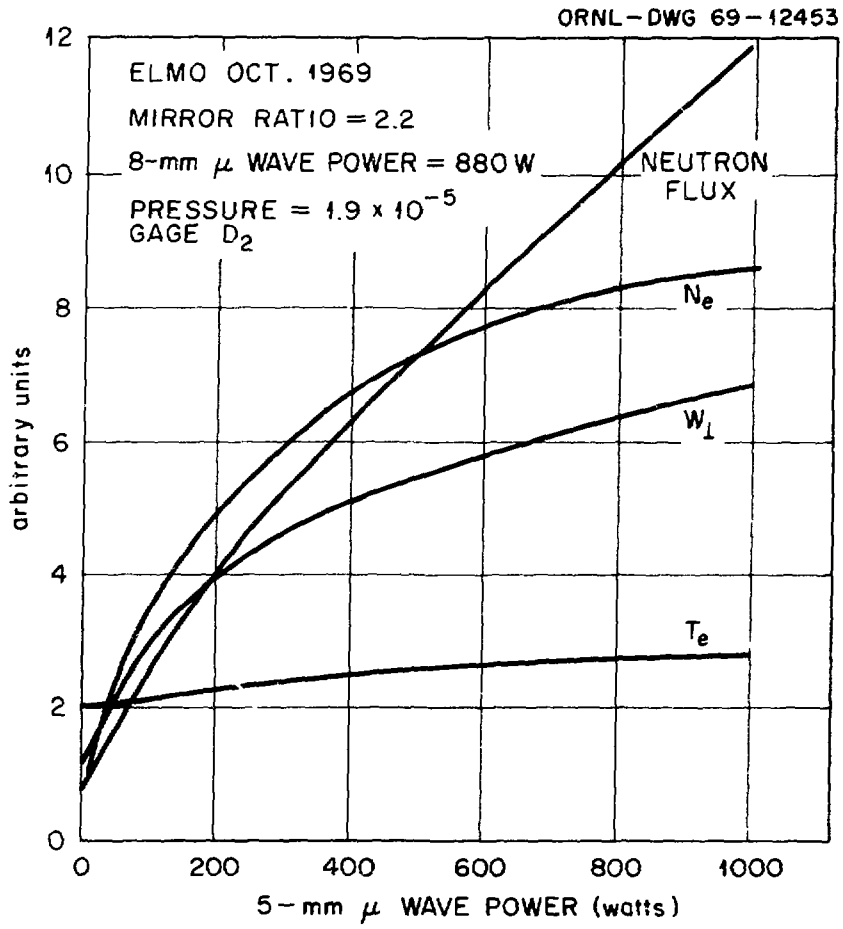

When upper off-resonant heating is employed, the half harmonic instability is essentially surpressed (i.e., the anisotropy is reduced) and the hot electron ring energy and density are increased with UORH power.

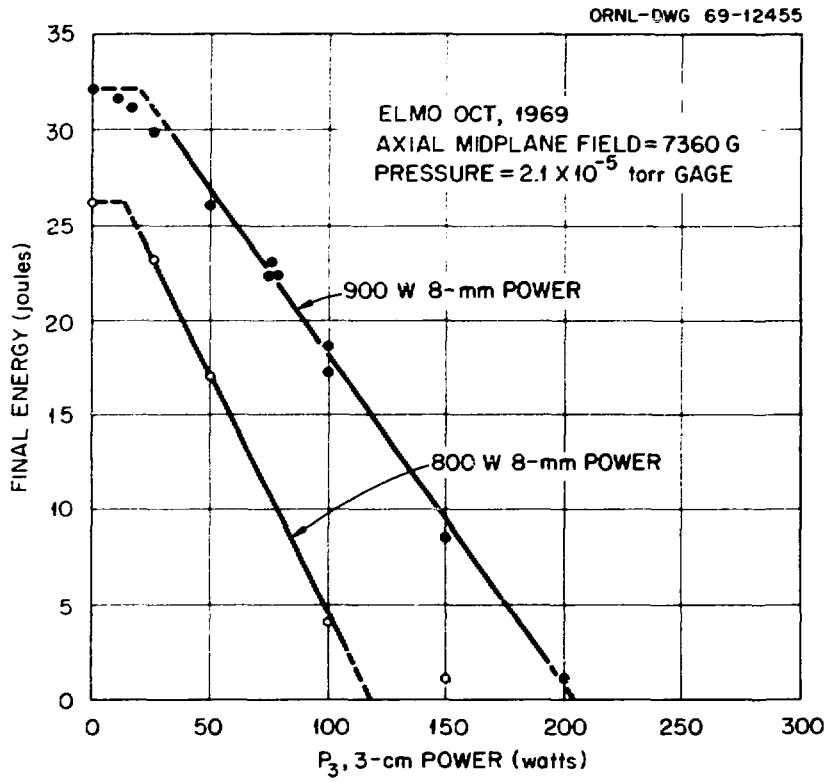

Lower off-resonant heating (LORH) has a very deleterious effect on ring formation, although the details have not been thoroughly investigated.

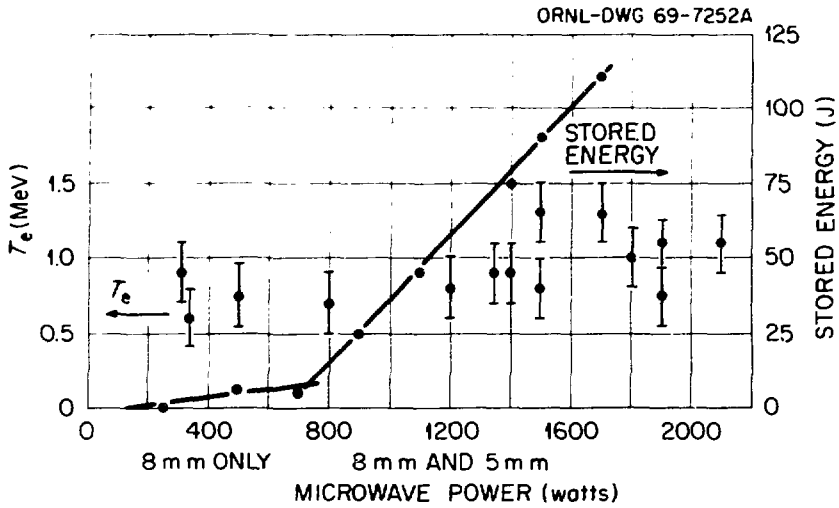

This is a plot of ring temperature (bars) (from bremsstrahlung measurements) and ring energy diamagnetic $W_\perp$ versus resonant (8 mm) heating power and then when applying UORH (5 mm) heating power. Note slight increase in temperature with large increases in $W_\perp$ and hot electron density.

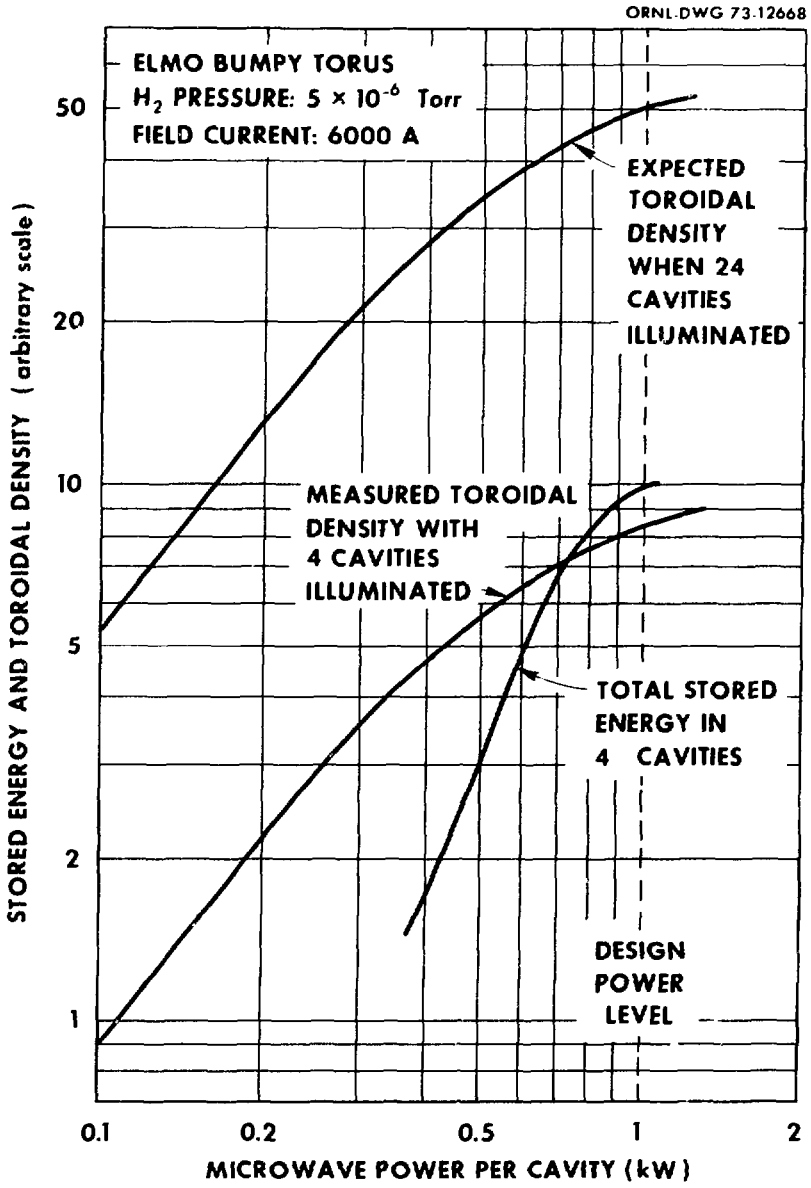

Very early EBT data showing ring formation ($W_\perp$) versus microwave power.

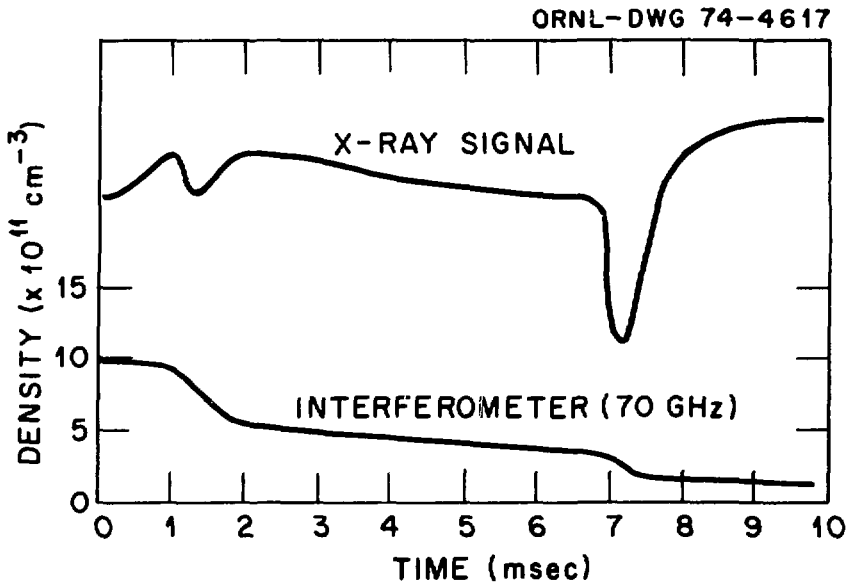

This time decay of density in EBT is an early piece of data showing loss of toroidal plasma with both a prompt and later-on ring instability resulting in a loss of the high beta region.

ORNL-DWG 75-10570

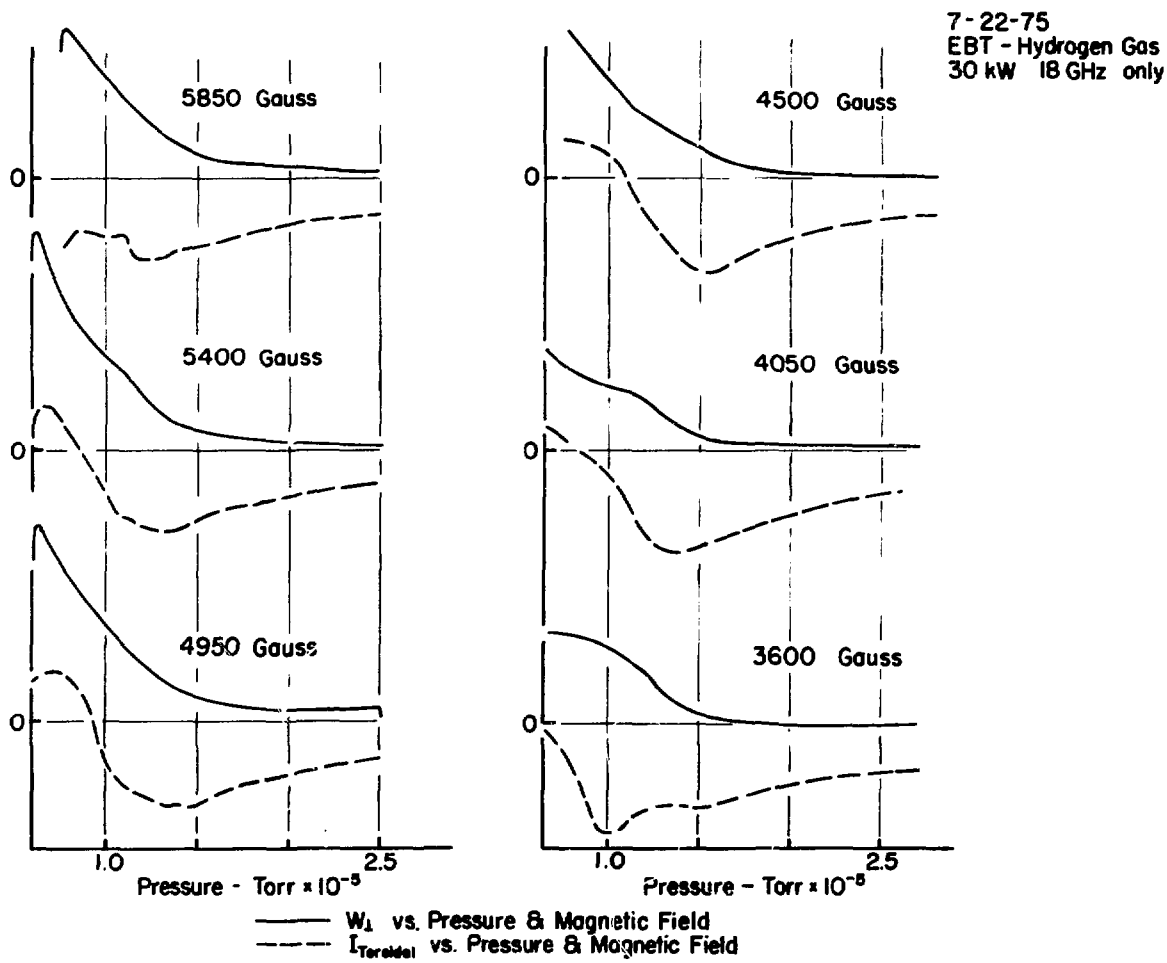

Plots of $W_{\perp}$ and toroidal current versus pressure in EBT for magnetic field values corresponding to rings positioned near axis to values for rings positioned near radial cavity wall. The optimum magnetic field is around 5000 gauss but the optimum value probably includes toroidal behavior as well.

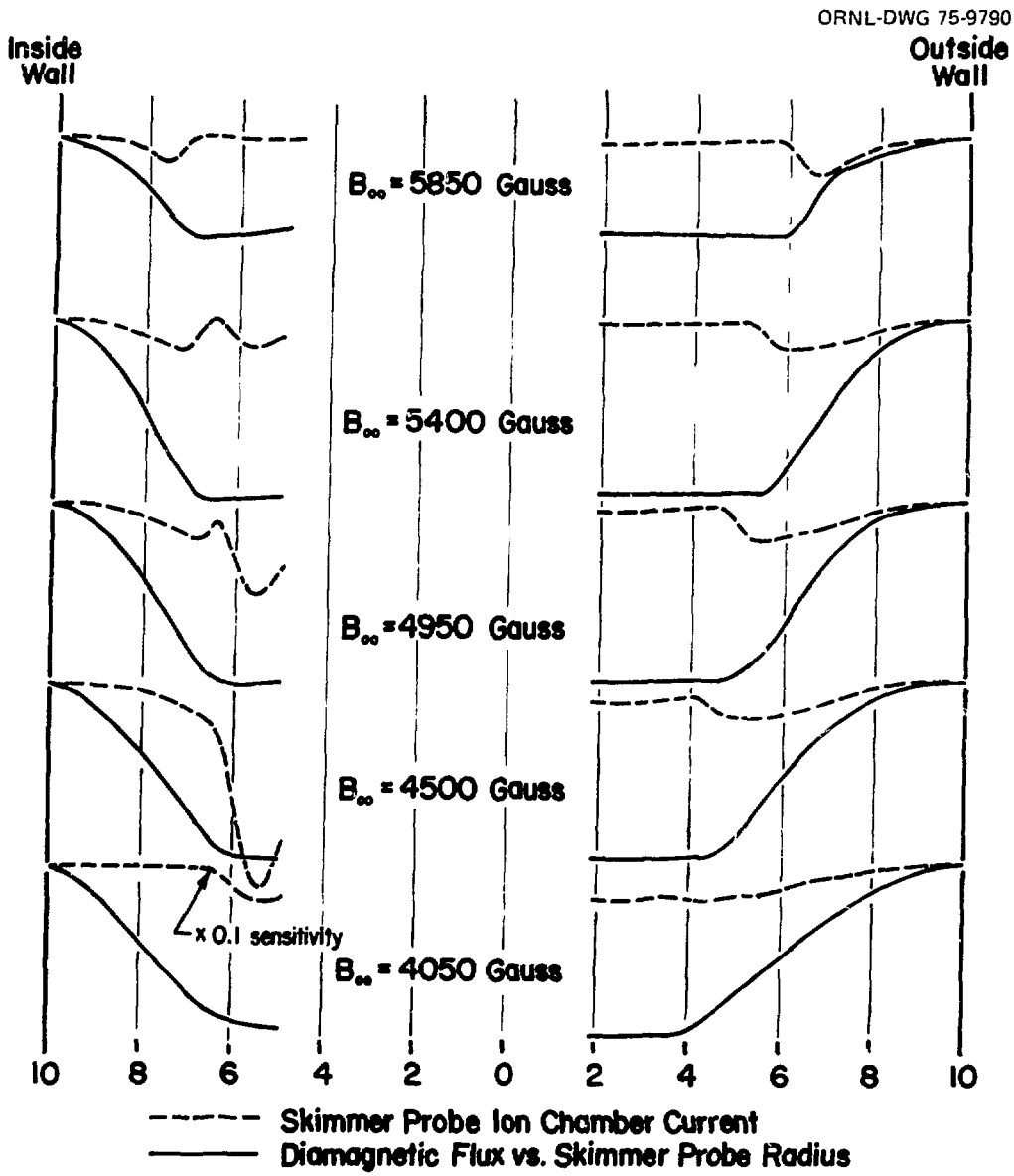

A series of skimmer probe profiles from EBT as a function of ring position, i.e., the position of the second harmonic ECH resonance. These profiles include skimming from inside the torus and from the outside, both in the equatorial plane.

I would like to conclude by showing my list of important ring physics work for the near future.

A PARTIAL LIST OF UNFINISHED RING STUDIES

1. CONFINEMENT-RELATED ISSUES

   A. DETAILED MEASUREMENTS OF SYNCHROTRON-RADIATION AND DRAG-COOLING LOSSES

   B. MEASUREMENT OF MICROINSTABILITY-INDUCED LOSSES

2. HEATING-RELATED ISSUES

   A. DETAILED COUPLING MECHANISMS (TO MAXIMIZE DESIRABLE HEATING PROPERTIES)

   B. SELF-CONSISTENT HIGH BETA HEATING MODELS

3. STABILITY-RELATED ISSUES

   A. MHD STABILITY LIMITS VERSUS COLD PLASMA PARAMETERS

   B. MICROSTABILITY VERSUS HEATING GEOMETRY

4. MEASUREMENT-RELATED ISSUES

   A. MORE DETAILED, MORE ACCURATE EQUILIBRIUM MEASUREMENTS

   B. MORE DETAILED STABILITY STUDIES

   C. MORE ACCURATE LOSS MECHANISM MEASUREMENT STUDIES

DISCUSSION

H. IKEGAMI: When you skimmed off the hot electron ring, did you observe the cold plasma get unstable?

R. A. DANDL: At lower pressure case, yes. It was hard to tell anything about microinstabilities, but some MHD activity was observed.

M. FUJIWARA: What is the energy of the transit (circulating) hot electrons?

R. A. DANDL: It is not well known since it was measured from thick target bremsstrahlung, but it is ~200 keV region.

S. TAMOR: The ring can reside on a field line which does or does not intersect wall. Are there any systematic differences between these two configurations?

R. A. DANDL: In ELMO, at high mirror ratio, the fundamental resonance and second harmoic resonance mod B's are on flux lines decoupled by the corner of the cavity throat section.

J. PIPKINS: Could you hold the position of the resonance absorption constant and vary the mirror ratio?

R. A. DANDL: Yes.

G. D. TSAKIRIS: At what frequency with respect to the microwave heating frequency have you measured the synchrotron radiation?

R. A. DANDL: Synchrotron radiation was monitored in the mirror experiments by simply reading a microwave crystal connected to the cavity through a wave guide having a cutoff frequency about three times the heating frequency.

A. KADISH: How do you distinguish between instabilities and oscillations when you examine your data? The viewgraphs you exhibited often show what I would call an oscillatory situation, especially when the amplitudes appear to be small. However, you always refer to these as evidence of instabilities.

R. A. DANDL: The oscillations are usually characterized as instabilities when corroborating plasma losses are synchronously present.

Characteristics of Hot Electrons in a Simple Magnetic Mirror Field

M. Hosokawa and H. Ikegami
Institute of Plasma Physics, Nagoya University,
Nagoya 464, Japan

1. INTRODUCTION

It has been known for a long time that the hot electron plasma generated by microwaves in a magnetic mirror configuration takes a ring shape.

Because of high beta property of the hot electron ring, its application to magnetic fusion devices has attracted great interests. For example, poloidal Heliotron ring or Dawson ring could be replaced by the hot electron ring which has no support losses nor anomalous scattering at the stagnation points. Since the stabilization effect due to minimum average B with the use of poloidal ring currents has been well studied experimentally, the stabilization and physics of the hot electron ring is subject to further investigation.

In the bumpy torus concept where hot electron rings play a crucial role for stabilization, the behavior of the hot electron plasma is anticipated to have a great similarity to that in a simple mirror.

In the following section, general description is given to microwave generated plasmas in a simple magnetic mirror machine, TPM, at the Institute of Plasma Physics, Nagoya University. Spatial structure or the density profile of the hot electron plasma is discussed in section 3. Experimental studies on the evolution of energy distribution function of the hot electrons are made in section 4. In the last section, several instabilities are investigated by triggering them artificially with their effects on the density profile and energy distribution of the hot electrons.

2. GENERAL DESCRIPTION OF THE TPM MIRROR MACHINE

The hot-electron plasma was generated by the microwave discharge in a

simple mirror field with a mirror ratio R = 3.4 by means of the electron cyclotron heating and is contained in a cylindrical cavity 40 cm long and 30 cm in diameter. The discharge is produced by a microwave pulse at 6.4 GHz with 20 msec duration and powers variable up to 5 kW. The microwave power is introduced radially through two opposite pairs of waveguide ports in the cavity wall. The schematic diagram of the device is shown in Fig.1.

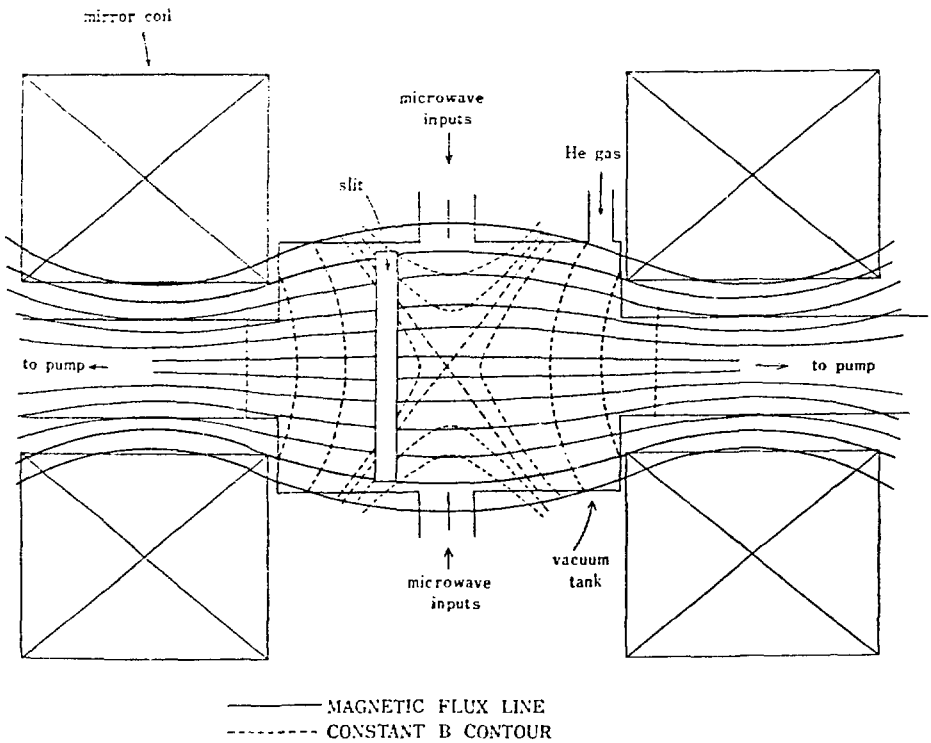

Fig.1. Schematic diagram of TPM machine. The bold hyperbola-like lines across the flux lines indicate the fundamental cyclotron resonance region.

The plasma produced at various power levels are very similar both in the electron temperature and the electron density. For the most part, the microwave was pulsed and afterglow plasma was studied.

In summary, various diagnostic techniques revealed the following properties of the plasma in TPM mirror machine:

i) the plasma consists of three components: hot electrons, cold electrons and helium ions;

ii) plasma density is composed of about 10^9-10^{10} hot electrons/cm^3 and 10^{11}-10^{12} cold electrons/cm^3;

iii) the average energy is typically 100 keV for hot electrons and approximately 20 eV for the cold electrons;

iv) temperature of ions is about 7-10 eV;

v) the hot electrons take a density profile of shell structure with 10 cm diameter;

vi) plasma density decay time is about several tens of msec, which does not deppend on the heating microwave power.

3. STRUCTURE OF HOT ELECTRON PLASMA

In order to determine the density and temperature of the hot electrons, X-ray photons are taken through a 0.1 mm-thick Mylar window onto a 3" dia. x 3" long NaI scintillator being collimated by an X-ray telescope. The solid angle subtended by the crystal through the collimator is about 10^{-5} sr and it collects photons from a cylindrical volume of plasma approximately 10 cm long with a cross section of 2 cm^2. The collimation system excludes any reception from the chamber walls. When the X-ray telescope is moved along the vertical slit (see Fig.1), it is possible to calculate the radial distribution of X-ray emission by using Abel's transformation. This distribution is directly proportional to that of the hot electron density. The hot electrons are thus observed to be bunched in a shell structure throughout the microwave discharge and the afterglow of the plasma as shown in Fig.2. The radial density distribution of the cold electrons has the shape of a bell centered on the axis of the machine, while after the power has been removed, the top of the bell is depleted to form a shell. The fact assures that the cold electrons present in the plasma during the afterglow are those produced by ionization of neutral atoms by the hot electrons present

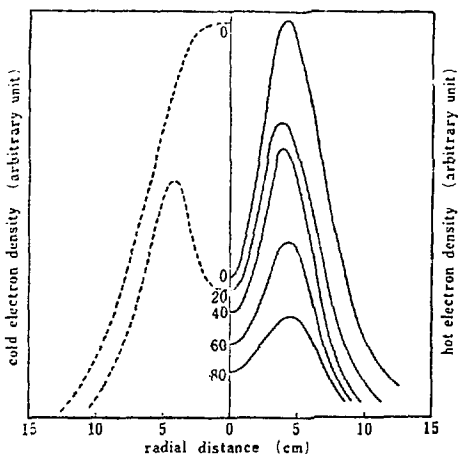

Fig.2. Plot of the radial density distribution of the electrons, after Abel's transformation. The dashed curves in the left half are related to the cold electrons and solid curves in the right half to the hot electrons. Parameters are the times (msec) after the front of the heating microwave pulse, of 20-msec duration. Each observation is made for 20 msec.

in the shell. The decay of this new cold electron distribution is determined now by the longer lifetime (30-100 msec) of the hot electrons.

It has been confirmed that the location of the hot-electron shell corresponds to the throat of the single-lobe hyperboloidlike surface of constant magnetic field intensity, which provides the second harmonic resonance for the heating microwave at 6.4 GHz. As the magnetic field increases, the radius of the throat increases and the radius of the hot-electron shell is observed to follow this growth. In other words, the hot-electrons are generated within the mirror always at the zone of constant magnetic field intensity which provides the electron cyclotron frequency at 3.2 GHz.

Structure of the hot electron ring along the magnetic lines of force is studied by measuring the perturbed magnetic field intensity due to the presence of the hot electron ring. A Hall element is fit at the tip of stainless steel pipe which is movable along the axial magnetic lines of force without much perturbation on the hot electrons. The results are shown in Fig.3, where paramagnetic perturbation is observed over 10 cm at the midplane when the hot electron ring is established after 10 msec of heating. Away from the ring, the perturbation is observed to be diamagnetic.

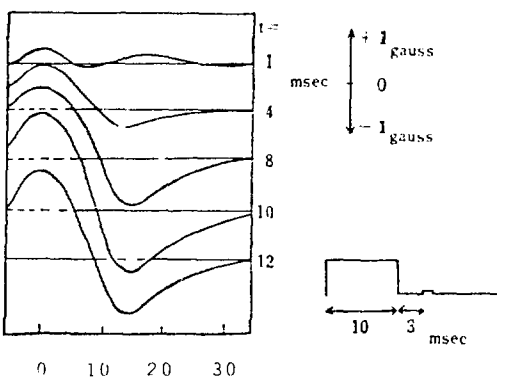

Fig.3. Perturbation of axial magnetic field on the axis with a time of heating as a parameter.

The structure of the hot electron plasma thus observed to be a tubing of approximately 10 cm in diameter and 10 cm in length rather than a thin ring. The location is determined by the constant |B| surface in the midplane that satisfies the second cyclotron harmonic resonance to the applied microwave frequency. The length is obviously a function of pitch angles, so that it will strongly depends on the field shape as well as the microwave power density.

One may interested in production of hot electrons at the fundamental

cyclotron resonance. The ratio of the heating rate due to the second harmonic resonance, Γ_2, to that for the fundamental resonance, Γ_1, may be given by

$$\frac{\Gamma_2}{\Gamma_1} \sim \frac{J_1^2(k\rho)}{J_1^2(k\rho)} ,$$

where k is the wavenumber and ρ is the Larmor radius of the electron. The condition, $\Gamma_2/\Gamma_1 > 1$, requires $k_\rho \gtrsim 1.5$, which is satisfied for the electron with the energy greater than 200 keV under the experimental condition: B = 1150 G and k = 1.28 cm^{-1}. The main reason why the second harmonic resonance observed to be so effective in generating the hot electrons is due to the fact that in the present mirror field the electrons trapped in the midplane with large pitch angles turn out to interact only with the second harmonic resonance.

4. ENERGY DISTRIBUTION OF HOT ELECTRONS

Spectral distribution of the X-ray bremsstrahlung is normally used to determine the hot electron temperature, for which a typical spectral distribution is shown in Fig.4. If we assume the hot electrons to have the Maxwellian energy distribution and adopt the quasi-classical approximation (Weiche-Näherrung formula) for the total cross-section for the emission of a photon with energy k, the photon number $\eta(k)$ within the energy interval $(k, k + \Delta k)$ is given by

$$\eta(k) = 3.38 \times 10^{-15} Z^2 N n T^{-1/2} k^{-1} \exp(-k/T) \qquad (1)$$

(photons/sec·cm^3keV)

where N is the density of atoms with the atomic number Z, n is the hot-electron density, and T is the hot-electron temperature in keV. The electron temperature can be roughly estimated from the slope of log $k\eta(k)$ vs. k. However, the quasi-classical approximation valid only for the condition $2\pi Ze^2/hv \gg 1$, to which corresponding critical energy of the electron in hydrogen atoms is as low as 700 eV. For the hot electron plasma in the present experiment, Born's approximation is preferable, whose applicability is based on the condition $2\pi Ze^2/hv \ll 1$. With the Born approximation, we get

$$\eta(k) = 1.69 \times 10^{-15} Z^2 N n T^{-1/2} k^{-1} \exp(-k/2T) K_0(k/2T) \tag{2}$$

(photons/sec·cm^{3}keV)

where $K_0(Z)$ is the modified Bessel function.

Such behavior of so-called temperature in time presents us only limited information. The energy distribution function is calculated from the Volterra's integral equation given by

$$\eta(k) = \frac{16}{3} \phi \mu N k^{-1} \int_k^{\infty} \sqrt{2E/m}\, G(E, k) E^{-1} f(E) dE \tag{3}$$

where $\phi = Z^2 r_0^2/137$, $\mu = mc^2$, $f(E)$ is the energy distribution function of the electron, and

$$G(E, k) = \ln\{(\sqrt{E} + \sqrt{E - k})^2/k\} \tag{4}$$

is the energy dependent part of the total cross-section for the bremsstrahlung of photon with energy k by the electron with energy E. If f(E) is assumed to be Maxwellian, Eq.(3) is reduced to Eq.(2).

In order to find f(E) from the raw data as shown in Fig.4 with the use of Eq.(3), it is necessary to smooth the scattered distribution of $\eta(k)$ vs. k, which is obtained in a punched, paper tape from a pulse height analyzer. Then, those measured points $(\eta(k), k)$ are simulated by an elastic string where each point is connected by a proper spring. Fairing is carried out by using a computer in such a way that the elastic energy of the system becomes minimum. Let assume a smooth, elastic string $g(k_i)$ which has flexure rigidity EI, and a spring constant K, then the elastic energy of the system is given by

$$U = \frac{1}{2} K \sum_i \{g(k_i) - \eta(k_i)\}^2 + \frac{1}{2} EI \sum_i g''(k_i)^2 \tag{5}$$

A smooth curve g(k) which best represents the measured points is determined by an elastic string resulting the minimum value of U. Such a fairing technique may more or less depend upon the subjective expectation of those who engage in the problem, and arbitrarinesses could be introduced through the determination of K and EI. An example of the energy distribution function determined from Eq.(3) after the fairing process described above is

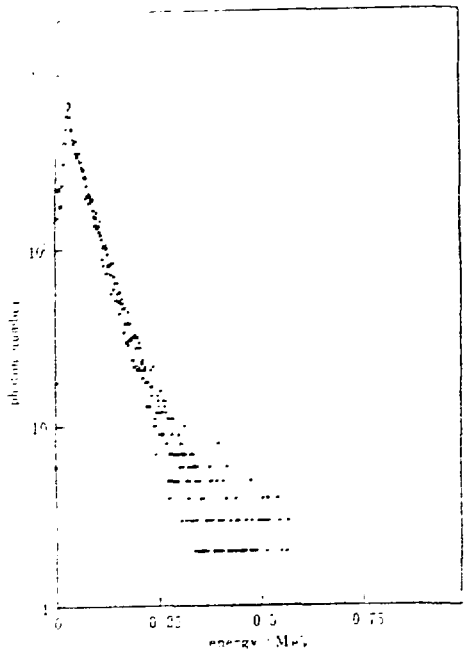

Fig.4. Typical energy spectrum of the X-ray bremsstrahlung. The ordinate is the photon number obtained with the use of a 4096 channel pulse height analyzer

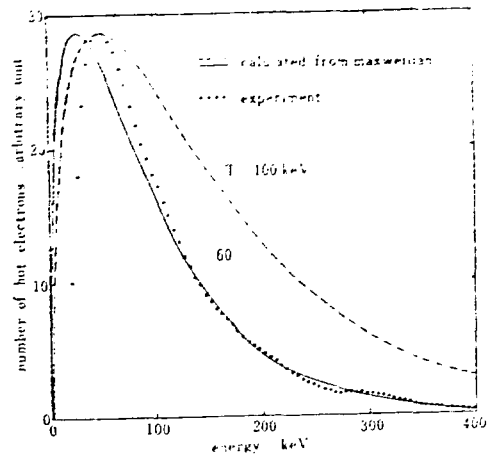

Fig.5. Energy distribution function of the hot electron calculated from the raw data in Fig.4.

shown in Fig.5, for which the raw data shown in Fig.4 is examined.

The energy distribution resembles a Maxwellian distribution with the temperature 60 keV, but its peak does not locate at 30 keV, but at 50 keV. One may find that the calculated distribution function reflects the feature of a loss-cone distribution, except a slight bump in the high energy tail.

Energy distribution determined from the X-ray spectrum tends to smooth bumps and hollows. Direct measurements of the distribution functions with the use of a solid state detector are made simultaneously. The detector is located in the mirror end by 70 cm behind the mirror point, and in order to protect the detector from bombardment and burning by a copious amount of hot-electrons, the detector is mounted behind a 1 mm-thick lead disk with a hole of 0.1 mm in diameter. Therefore, the solid state detector accepts those hot electrons being lost into the loss cone, and for those electrons to reach onto the detector, their pitch angle in terms of $v_\perp/v_\parallel$ must be at least smaller than 0.1 at the point of detection. However, this does not bring about any serious modification of the energy distribution function, since the detector is located outside the mirror trap on the longitudinal axis of the magnetic field.

Some examples of thus measured energy distribution functions are shown

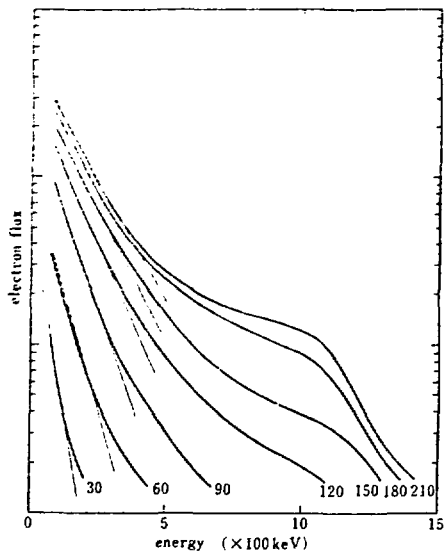

Fig.6. Electron energy bistribution measured by silicon surface barrier detectors. The ordinate is the electron flux in logarithmic scale. Input microwave pulse is of 200-msec duration at the peak power 4 kW. Gas is helium at 10^{-5} torr.

in Fig.6 where the energy distribution is measured for each successive 30 msec during the heating period of 200 msec. For the first 90 msec from the introduction of the microwave power, the so-called hot-electron temperature determined from the slope increases and thereafter tends to saturate. However, the average kinetic energy keeps on increasing by producing a plateau in the high energy tail of the distribution. Two reasons may account for the formation of the plateau in the high energy tail of the hot-electron energy distribution function. One is attributed to the fact that in a mirror trap, lower energy electrons are rapidly lost into the loss cone by the Coulomb scattering and that the ultimate kinetic energy of the electron is proportional to the lifetime in the stochastic heating process. High energy electrons are not only contained for a longer time in the mirror trap, but also they experience more heating because of that prolonged lifetime. The other reason is the experimental fact, which will be shown later, that higher energy electrons are stable against the whistler instability, which is the most dangerous among many coexisting instabilities in hot electron plasmas.

5. INSTABILITY OF HOT ELECTRON PLASMA

Electromagnetic triggering

In the present device, the instability can be triggered by introducing an additional small microwave pulse of about 100 W at the same frequency as the heating microwave pulse from 1-50 msec after the end of the main pulse. For some conditions at pressures lower than the critical value of 10^{-4} torr, the plasma is spontaneously unstable. However, no physical difference is observed between the triggered instability and the spontaneous ones. When

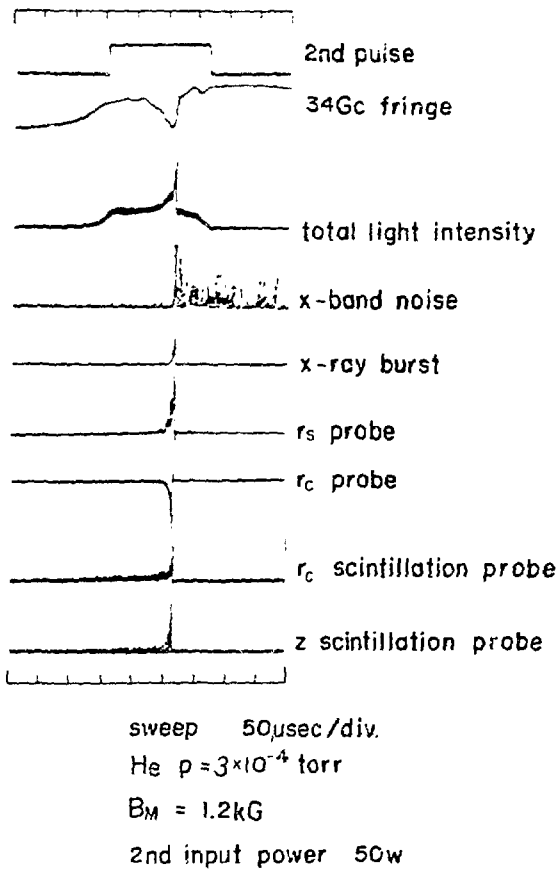

Fig.7. Signals accompanied with the instability triggered by the second microwave pulse (500 W). The onset of the instability is seen about 70 μsec after the pulse front. Helium (2×10^{-4} torr) is admitted in steady flow operation. In the 6th and 7th traces, r_s denotes a radially inserted Langmuir probe situated close to one end-walls of the cavity and r_c that at the center of the cylindrical cavity wall. Both probes are 10 cm apart on the same magnetic lines of force.

the pressure is above 8×10^{-4}, no instability could be triggered.

Some details of the triggered instability are shown in Fig.7. The instability is characterized by the sudden loss of hot electrons from the mirror bottle, but not of the cold electrons, and by the strong burst of microwave emission. The signals related to the hot electrons, like X-ray signal, microwave noise, scintillator output and diamagnetic signals, disappear within several microseconds. However, those related to the cold electrons, like Langmuir probe signal, light intensity and plasma density, decay at a slower time constant of about 200 μsec.

The strong microwave burst accompanied by the instability characterizes the nature of the instability. The microwave emission is composed of harmonics of 2.1 GHz for the typical mirror field (4000 G - 1200 G - 4000 G). The lower-frequency harmonics (2.1, 4.2 and 6.3 GHz) are collected by a loop antenna, while the higher-frequency emission (8.4, 10.5, 12.6 and the frequency region up to 18.9 GHz) are collected by X-band waveguides.

Although the magnetic field is varied around the optimum field intensity (4000 G - 1200 G - 4000 G), the variation of the microwave frequency (2.1 GHz) with the magnetic field at the mirror center is insensitive. This is quite reasonable, since the hot electrons are produced in a shell which touches the throat of the singlelobe hyperboloid-like surface of the constant magnetic field intensity, which provide the electron cyclotron frequency at 3.2 GHz. Since the frequency 6.4 GHz of the heating microwaves is fixed, the magnetic field intensity which give rise to the second harmonic resonance is also fixed. This fact implies that most hot electrons stay always around the region of 1140 gauss, corresponding to the second harmonic resonance, as far as the mirror remains around the optimum field intensity. When the field is changed drastically to give the production and heating at the center of the mirror at the fundamental cyclotron resonance, the frequency of the microwave radiation is doubled and becomes 4.2 GHz. The main contribution to the total power emission comes from the fundamental component and the power collected by the probe is found to be several 10 W within a bandwidth of 5 MHz. The amplitude of the burst increases with the growth rate of about 0.1 μsec, and reaches its maximum at about 1 μsec after the initiation of the instability.

Furthermore the radiation is detected by using a pair of two loop antennas inserted into the cavity each through the opposite end arms, one is fixed and the other is movable along the axis of the machine. The microwave emission accompanied with the instability is found to be standing electromagnetic waves with the wavelength of 19 cm for 2.1 GHz. The mode of the wave is likely to be determined by the diameter of the cylindrical side arms of the vacuum chamber as a circular waveguide with TE_{11} mode. It will be also interesting to note that the instability destroys the hollow structure of the hot electron plasma. Experimental detection with the use of a Hall element is shown in Fig.8, where longitudinal magnetic perturbations are compared in two cases of stable and unstable decay. In case of unstable decay, either the hot electrons fill the hole, or the peaked edge disappears.

At the onset of the instability, the burst of end loss electrons, which escaped out of the magnetic mirror, was led onto an aluminum foil of six different thicknesses. The energetic electrons passed through the foil impinge into a plastic scintillator mounted on a photomultiplier. The resulting signal of the photon pulse-height is a function of the absorber

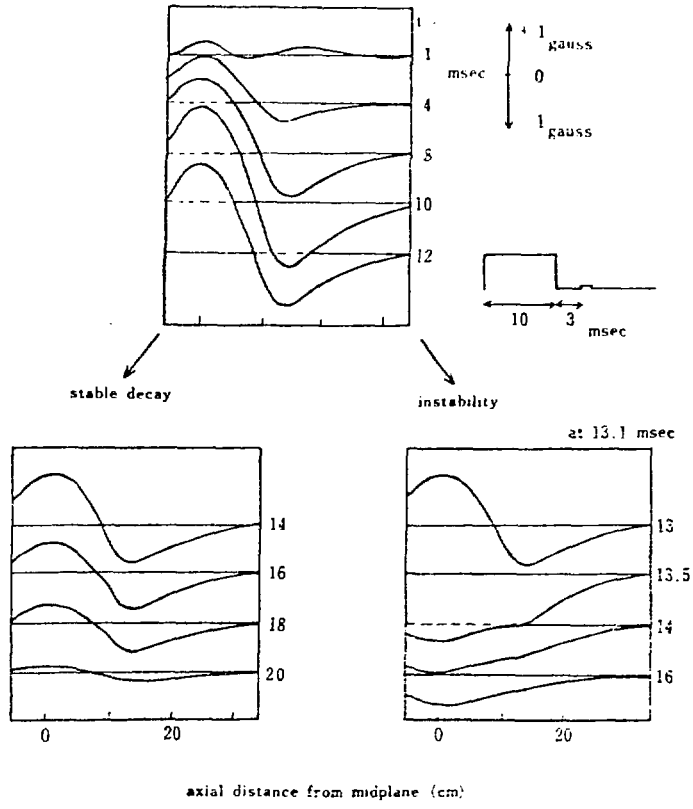

Fig.8. Plasma magnetic field along the axis of the machine. The parameters are the time in msec from the heating pulse front. When the instability is triggered at 13 msec, the anti-diamagnetic field disappears and larger diamagnetic fields are observed, which tells us that the shell structure has been carried away by the instability.

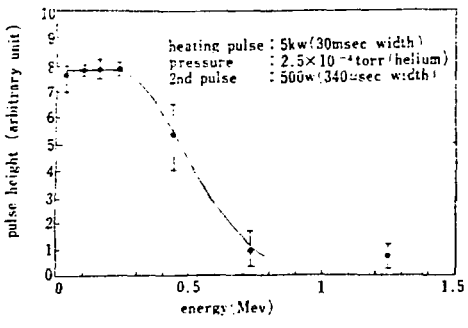

Fig. 9. Number of electrons escaped from the mirrors at the triggered instability, vs. their energy measured by the scintillator probe on the z-axis. The 2nd microwave pulse was applied 20 msec after the main pulse turnoff.

thickness. The pulse height at the instability is shown in Fig.9, where the thickness has been related to the energy of the electrons from the range-energy curve. The electrons that escaped from the mirror during the quiet decay is observed to have a Boltzmann distribution with the temperature of about 150 keV.

Spontaneous instability

Transient state just after the removal of the microwave power have been observed to support various kinds of instability: interchange modes in simple mirror traps, electrostatic velocity space mode, and electromagnetic, whistler mode. During the heating period with the microwave power input, the stability aspect of the plasma is similar to that during the transient state, and the life time of the hot electron is supposed to be much shorter than it is during the stable, late afterglow. The fact is not only attributed to those instabilities, but also to the stochastic heating process itself in the sense that the diffusion in velocity space inevitably accompanies that in the coodinate space. During the heating period, a copious amount of X-ray emission is detected, which is obviously radiated by numbers of hot electrons colliding with the cylindrical wall of the vacuum chamber.

Spontaneous instabilities are typical of the hot electron plasma especially operated in a lower pressure regime. Effect of the instabilities on the energy distribution of the hot electrons are shown in Fig.10, where striking feature lies in the repetitive sudden decrease in the number of low energy electrons. These wild fluctuations are observed to correspond with spontaneous instabilities appearing regularly during the heating period. These instabilities have been studied in a detail and identified to be the whistler instability. Driving whistler waves, resonant electrons consume their energy component perpendicular to the magnetic field and fall into the loss cone. From Fig.10 we see that those resonant electrons have energy below or approximately 50 keV. More important fact is that the electrons with higher energy are found not to participate with the instabilities. The fact implies that the cloud of high energy electrons be stable against the whistler instability, which is the most dangerous, absolute instability among many coexisting electrostatic and electromagnetic instabilities. This character will be in the favor of producing self-minimum B configuration with the use

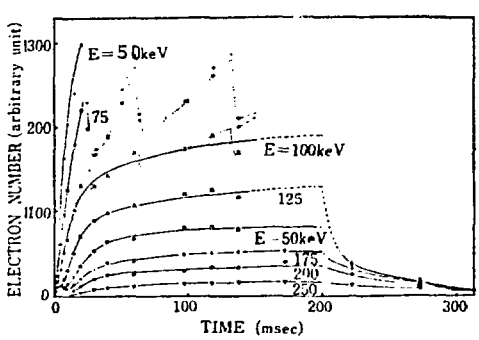

Fig.10. Relative change in the number of electrons with specified energy E. The heating microwave pulse is turned off at 200 msec.

of a collection of high energy electrons.

Electrostatic triggering

The reason why the hot electron plasmas are stable against flute instabilities during afterglow, especially, is understood as being due to the presence of the cold electrons; the stabilization is attributed to a linetying effect caused by 'volume' short-circuiting cold electrons, which are continuously generated by the hot electrons ionizing residual helium atoms during the late afterglow plasma.

By controlling the cold electrons, one can artificially trigger hydrodynamical instabilities, as well as microscopic ones.

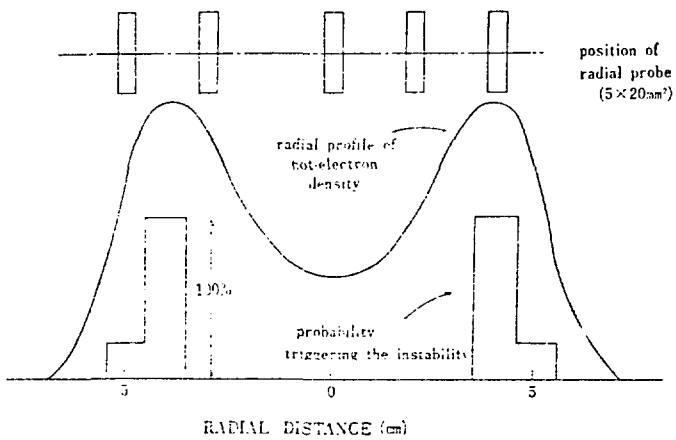

Fig.11. Probability of triggering the instability by radial probes ($P_1 \sim P_5$); probes P_4 and P_5 can trigger the instability.

In order to check the stabilization mechanism in detail, a disturbance is introduced by extracting the cold-electron component from the plasma by means of a pulsed Langmuir probe. Several probes are located at different radial positions and a pulse of positive voltage is applied to them against the plasma. As shown in Fig.11, probability of triggering instabilities are observed to be maximum when the positive voltage is applied to the end probe, located on the magnetic lines of force which pass through the region of maximum hot-electron density. It is important to recollect that the hot electrons from a shell-structure, which is a peculiar feature of ECH hot electrons in a magnetic mirror trap. By varying the height and width of the pulse applied to the probe, the triggering probability is plotted as a function of the cold-electron number deprived by the pulsed Langmuir probe. As shown in Fig.12 the minimum number of electrons extracted to provoke the instability at 100 % is estimated to be 10^{12}, which corresponds to average 5 % depletion of local electron densities. Being associated with the extraction, a whistler instability is detected, as well as a flute-like, low frequency instability.

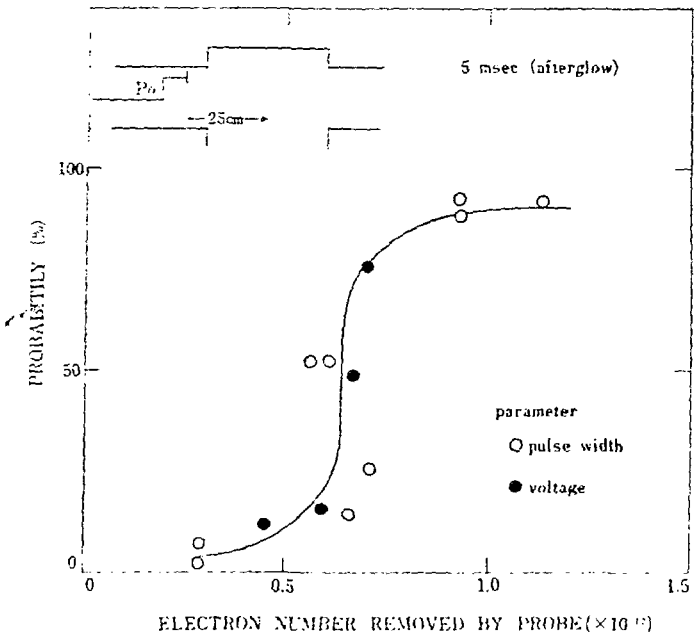

Fig.12. Probability of triggering instabilities by the probe P_0. Extracted electron number was estimated by time integration of the probe current.

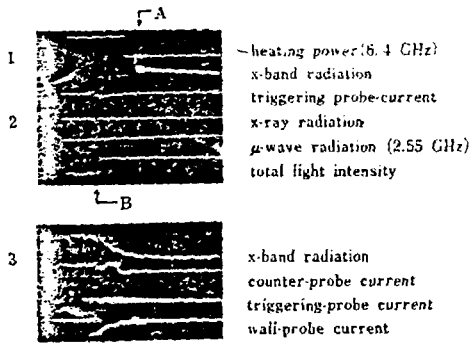

1 : 5 ms/div ; 2 : A expanded to 0.2ms/div
3 : B expanded to 20 μs/div

Fig.13. Instability is triggered in 3.5 msec after the heating power turned off.

The detailed process of the triggering is shown in Fig.13. About 8 μsec after the pulse current of cold-electron evulsion, flute-like instability, propagating azimuthally in the diamagnetic direction, is observed to grow and successively a whistler instability is detected in the similar way as described in the previous section of electromagnetic triggering.

In the present ECH plasma, the hot-electron energy is so high that the electromagnetic instability can easily compete with electrostatic ones. It should be noticed that hot electron plasmas are almost always electromagnetically unstable, since the condition $T_\perp/T_\parallel > 1$ is inevitable.

Experimentally a critical ambient, neutral gas pressure is observed below which the hot electron plasma carries various instabilities. The pressure is higher for higher microwave input power. The stable and unstable boundary with the input power of 5 kW is shown in Fig.14, where quasi-stable region is determined by the electrostatic triggering.

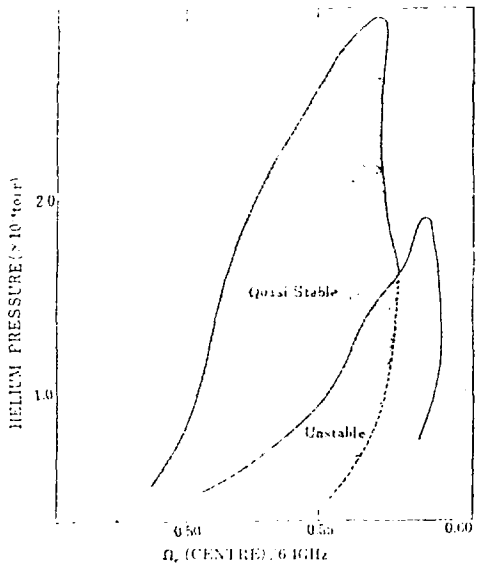

Fig.14. Region of the stable and unstable state. In the quasi-stable region, the instability can be triggered artificially.

Acknowledgement

The authors like to express appreciations to those who participated in the experiments of TPM mirror program in the past ten years for their collaboration, especially to Professor S. Tanaka of Kyoto University, Professor S. Aihara of University of Campinas, and Dr. H. Ikezi of Bell Laboratories.

DISCUSSION

B. H. QUON: Do you observe low frequency fluctuation associated with ring? e.g., at $\sim\omega_{ci}$ (ion cyclotron frequency)?

H. IKEGAMI: Electromagnetic instability with a growth rate of microseconds is a dominant one and no low frequency instabilities are observed, nor are spontaneous low frequency fluctuations detected. The electromagnetic instability is so violent that it destroys the plasma completely. Ion cyclotron frequencies are typical of plasmas with high temperature ions, which is not in this case.

J. T. WOO: What is the interpretation for the reduction in the probability to trigger instability after 10 ms? Is there any data to suggest that this time constant is related to the time for establishing the ring?

H. IKEGAMI: No experimental verification has been made, but I can think of several possibilities:

(1) Density of cold plasma just after the turnoff of microwaves is lower. Usually it first decreases, then increases again due to the ionization by hot electrons, which are decaying slowly.

(2) Anisotropy in hot electron temperature $T_{\perp}/T_{\parallel}$ is still large, say >5.

The time of 10 ms has nothing to do with the time of establishing rings. Some interesting data may be found in a *Nuclear Fusion* article by H. Ikegami et al. (1973).

REVIEW OF EBT ELECTRON RING STABILITY*

D. A. Spong
Oak Ridge National Laboratory
Oak Ridge, Tennessee 37830

ABSTRACT

High beta electron rings are an essential ingredient in maintaining the stability of the EBT toroidal core plasma. By forming a magnetic well of sufficient depth at the plasma edge, the rings provide stabilization against flute and interchange, and at higher toroidal core betas they enhance stability against ballooning modes. In defining stable operating regimes for the toroidal plasma, it is therefore necessary to understand the ring stability boundaries. Due to the simultaneous importance of kinetic, finite geometry, and profile effects, the general problem of ring stability is complex and has been examined in the past only with certain simplified models. In this paper, previous work in this area will be reviewed.

*Research sponsored by the Office of Fusion Energy, U.S. Department of Energy, under contract W-7405-eng-26 with the Union Carbide Corporation.

1. INTRODUCTION

Energetic electron rings are an essential ingredient in maintaining the stability of the EBT toroidal core plasma. As was shown in early work by Kadomtsev,[1] a closed-line torus with isotropic pressure and monotonically increasing $\oint d\ell/B$ is always unstable to simple interchange modes. For annular betas in excess of ~15%, the diamagnetic current associated with the hot electron annuli transforms the bumpy torus into an average minimum-B configuration, in which such modes are stabilized.

Because the rings themselves may be subject to various instabilities, it is important to understand their stability boundaries in defining stable operating regimes for the toroidal plasma. Ring stability depends on an interaction between the ring and core plasma (i.e., cold plasma stabilization) as well as on certain features intrinsic to the rings (e.g., finite gyroradius, large guiding center drift frequency). In addition, geometric parameters of the rings such as length can influence stability boundaries.

Besides macroscopic instabilities, the rings may also be subject to microinstabilities. Such instabilities would adversely affect ring power balance. Experimentally, it has been observed that nearly classical ring energy losses are obtained if off-resonant heating is used.

In this paper, work in the area of hot electron ring stability will be reviewed. First, the anisotropic equilibrium characteristic of the bumpy torus will be examined, followed by a discussion of the ring requirements necessary for toroidal plasma stability. Next, the possible

macroscopic instabilities of the ring will be mentioned. In closing, a brief discussion of ring microinstabilities will be given.

2. TENSOR PRESSURE EQUILIBRIA

The anisotropic nature of electron cyclotron resonance heating in the hot electron ring is an important consideration in developing a model for EBT equilibria. Other features that must be incorporated into a realistic EBT equilibrium model are localized high-β regions, closed magnetic field lines, and mirror symmetry. The basic equations for equilibrium are the tensor pressure force balance and Maxwell's equations as given below:[2]

$$(\vec{J}_R + \vec{J}_P) \times \vec{B} = \vec{\nabla} \cdot \overleftrightarrow{P} , \tag{1}$$

$$\vec{\nabla} \times \vec{B} = \vec{J}_R + \vec{J}_P , \tag{2}$$

and

$$\vec{\nabla} \cdot \vec{B} = 0 , \tag{3}$$

where $\vec{J}_R$ is the current in the hot electron ring, $\vec{J}_P$ is the current in the isotropic core plasma, and $\overleftrightarrow{P}$ is the anisotropic ring pressure distribution plus the isotropic core plasma pressure.

The form that is typically used for the pressure tensor is the double adiabatic model as given below:

$$\vec{\nabla} \cdot \overleftrightarrow{P} = \vec{\nabla} p_\perp + \hat{b} \frac{\partial}{\partial \ell} (p_\parallel - p_\perp) + (p_\parallel - p_\perp) \left(- \frac{1}{B} \frac{\partial B}{\partial \ell} \hat{b} + \vec{K} \right) , \tag{4}$$

where $\vec{K}$ = curvature = $\frac{1}{B}\vec{\nabla}_\perp B$; $\hat{b} = \vec{B}/B$; and $p_\parallel$, $p_\perp$ = pressure parallel and perpendicular to the $\vec{B}$ field.

The component of Eq. (1) parallel to the magnetic field line results in the following constraint condition on the B-field dependence of $p_\parallel$ and $p_\perp$:

$$\frac{\partial p_\parallel}{\partial B} - \frac{(p_\parallel - p_\perp)}{B} = 0 \ , \tag{5}$$

$$B = |\vec{B}| \ .$$

The component of Eq. (1) perpendicular to the field line results in the partial differential equation given below, which is solved to obtain the equilibrium fields and pressure distributions:

$$[\vec{\nabla} \times (\sigma\vec{B})] \times \vec{B} = \vec{\nabla}_\perp p_\parallel - (p_\parallel - p_\perp)\vec{K} \ , \tag{6}$$

$$\sigma = 1 + \frac{p_\perp - p_\parallel}{B^2} \ .$$

Numerical solutions of this equation have been carried out in both two and three dimensions using underrelaxation methods. For stability analyses, only 2-D solutions have been employed to date. In this case, axisymmetry is generally assumed (i.e., uniformity in the poloidal direction) and $j_\parallel$ is taken as zero. The magnetic field can then be written in a Clebsch representation:

$$\vec{B} = \vec{\nabla}\psi \times \vec{\nabla}\theta \ ,$$

where $\psi = rA_\theta$ = flux function. The equilibrium equation becomes:

$$\Delta^*\psi + \frac{1}{\sigma}\vec{\nabla}\sigma \cdot \vec{\nabla}\psi = -\frac{r^2}{\sigma}\frac{\partial p_\parallel}{\partial\psi} \ , \tag{7}$$

where $\Delta^*\psi = \left(\frac{\partial^2}{\partial r^2} - \frac{1}{r}\frac{\partial}{\partial r} + \frac{\partial^2}{\partial z^2}\right)\psi$.

Two conditions must be satisfied in order for solutions of Eq. (7) to exist. These are the mirror [Eq. (8)] and firehose [Eq. (9)] instability limits:

$$\tau = 1 + \frac{1}{B}\frac{\partial p_\perp}{\partial B} \geqslant 0 \ , \tag{8}$$

and

$$\sigma = 1 + \frac{p_\perp - p_\parallel}{B^2} \geqslant 0 \ . \tag{9}$$

The mirror instability limit is necessary in order for Eq. (7) to remain elliptical. If this is exceeded, then steady-state solutions do not exist. The firehose limit must be satisfied in order to avoid singularities in Eq. (7). As will be discussed further in Sect. 4, phenomena that were identified as mirror instabilities have been experimentally observed in electron cyclotron heated plasmas.[2]

The form of EBT pressure distribution often used in Eq. (7) is:

$$p_{\parallel} = \hat{p}_{\parallel}(B)\ g(\psi) + p(\psi)\ ,$$

$$p_{\perp} = \hat{p}_{\perp}(B)\ g(\psi) + p(\psi)\ .$$

The first term in these expressions describes the hot electrons; the second one describes the bulk plasma. The function $g(\psi)$ is peaked near the edge of the plasma to simulate the radial structure in the hot electron pressure profile. The functional form for $\hat{p}_{\parallel}$ and $\hat{p}_{\perp}$ is usually that introduced by Taylor:[3]

$$\hat{p}_{\perp}(B) = mCB^2(B_c - B)^{m-1} \quad \text{for} \quad B \leqslant B_c\ , \tag{10}$$

$$\hat{p}_{\parallel}(B) = CB(B_c - B)^{m} \quad \text{for} \quad B \leqslant B_c\ , \tag{11}$$

and

$$p_{\perp}(B),\ \hat{p}_{\parallel}(B) = 0 \quad \text{for } B \geqslant B_c\ ,$$

where m = an integer, C = a constant, and B_c is a constant that controls the longitudinal extent of the hot electron plasma.

A typical 2-D bumpy cylinder equilibrium[4] is shown in Fig. 1 including a β = 0.5 electron annulus. In Fig. 2 typical 3-D equilibria[5] are displayed both with and without a high-β annulus; here again the annulus β is 50%. As may be seen, the main effect of the annulus is to produce a localized magnetic well (solid lines are mod-B contours). The magnetic gradients are increased in the vicinity of the annulus, but the curvature (dashed lines are magnetic field lines) is changed little if at all.

ORNL/DWG/FED/ - 77947R

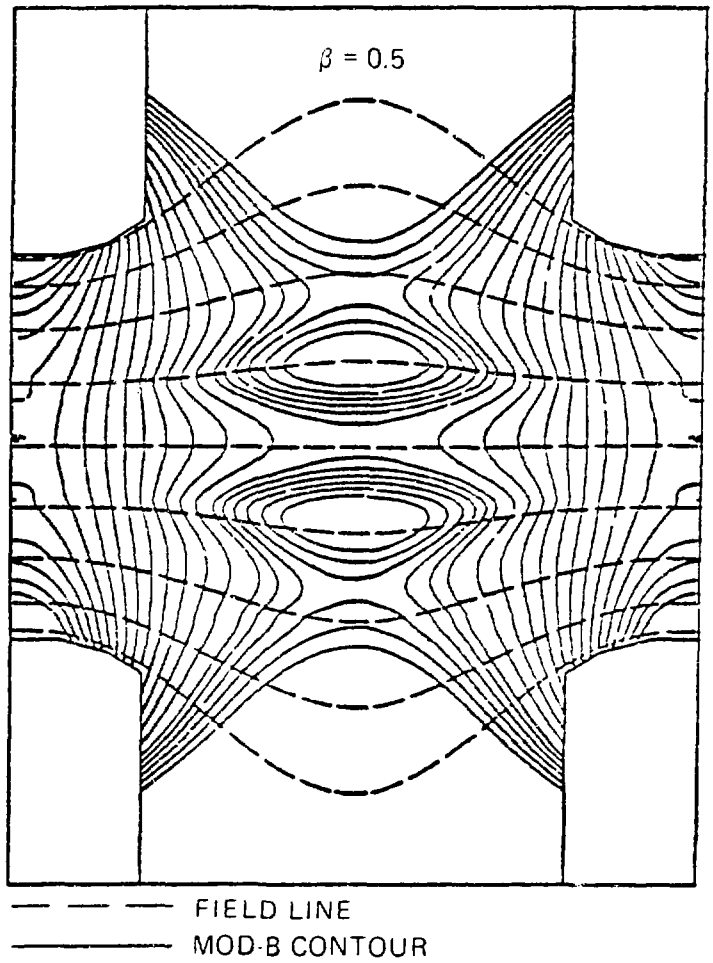

Fig. 1. 2-D bumpy cylinder equilibrium with a $\beta = 0.5$ annulus region. Magnetic field lines are indicated by dashed lines and $|B|$ contours by solid lines.

ORNL-DWG 76-18487R

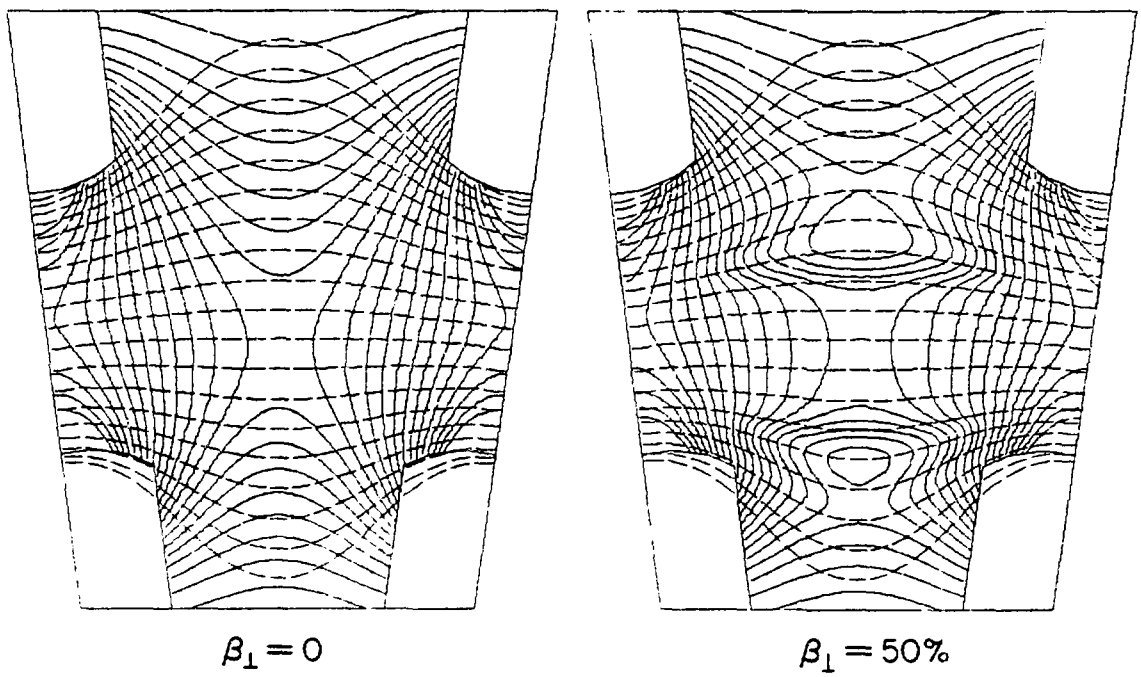

Fig. 2. 3-D bumpy torus equilibrium without and with a β = 0.5 annulus region. Magnetic field lines are indicated by dashed lines and $|\beta|$ contours by solid lines.

3. INFLUENCE OF ELECTRON RINGS ON TOROIDAL PLASMA STABILITY

The role of high-β electron rings in maintaining the stability of the toroidal plasma against flute and interchange modes may be seen from Fig. 3 and the simple stability criterion given below:

$$\left(p' + \gamma p \frac{U'}{U}\right)\left(U' - p' \oint \frac{d\ell}{B^3}\right) > 0 \ , \tag{12}$$

where $U = \oint d\ell/B$, $' = \frac{d}{d\psi}$. This was derived in Ref. 4 from a modified energy principle appropriate to an isotropic core plasma with high-β annular electron rings. For stability, Eq. (12) must be satisfied on each flux surface. In Fig. 3, typical profiles of $\oint d\ell/B$, B, and $\beta_\perp$ are given as a function of the radius at the midplane. Equation (12) indicates that in the central plasma region, stability is attained if either $p' = 0$ or $U' > 0$ and $p'U' > -\gamma pU'$; i.e., pressure gradients may be stably supported up to some critical slope. At the inside of the plasma edge region, where U' is positive and increasing, a somewhat larger pressure gradient may be tolerated. Finally, at the outer edge where $p \to 0$, $p' < 0$, and $U' < 0$, stability is possible if $|p'| < |U'|/\oint d\ell/B^3$. Thus, the electron annulus modifies the B field and $\oint d\ell/B$ in such a way as to stably support plasma pressure gradients in the regions in which they are largest.

The stability threshold is then related to the critical value of annulus β required to make $U' < 0$ at the outer edge of the plasma, since this is necessary to support a pressure gradient there. The value for U' may be written as follows:

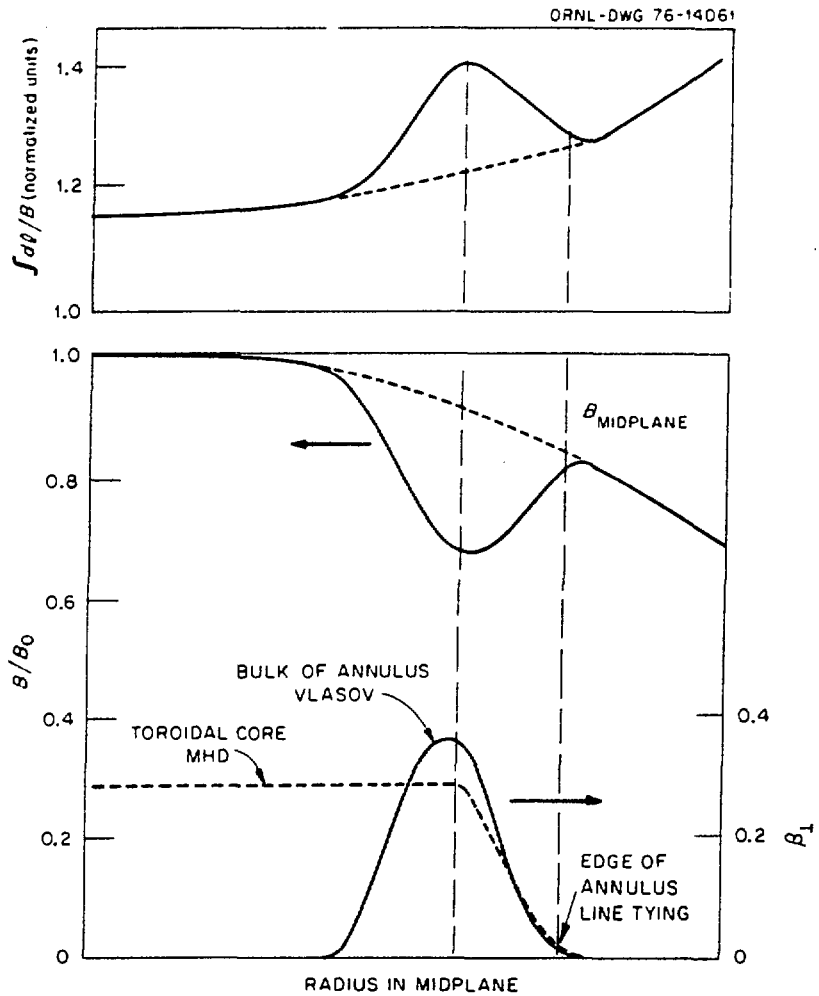

Fig. 3. Effect of hot electron annuli on B and $U \equiv \oint d\ell/B$.

$$U' = -\oint \frac{d\lambda}{B^2}\left(\frac{K}{r} + \frac{\partial B}{\partial \psi}\right) < 0 \tag{13}$$

for stability. As indicated in Fig. 4, the field line curvature K is negative in the midplane and positive in the mirror throat. Since the

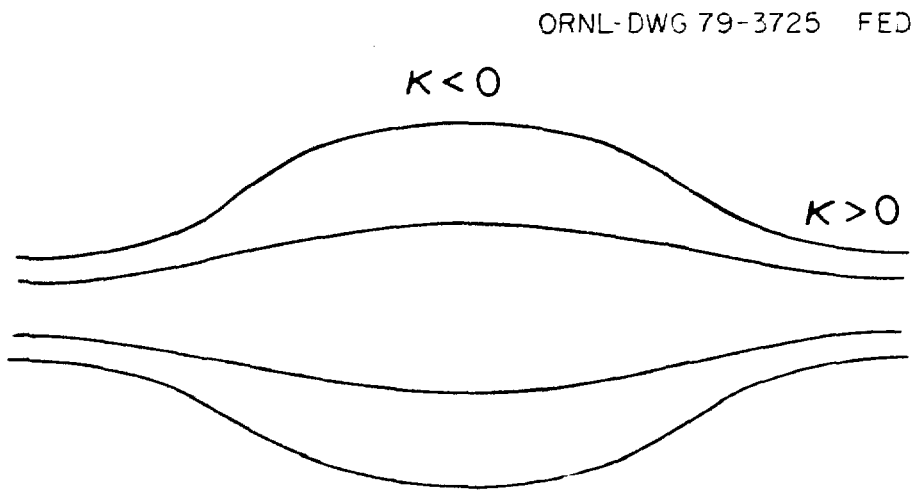

Fig. 4. Regions of positive and negative curvature for magnetic field lines in a single mirror sector.

factor of $1/rB^2$ tends to weight the midplane contribution more heavily than that from the throat,[4] the field line integral of the curvature term in Eq. (13) will be negative. To counteract this, $\partial B/\partial\psi$ must be $\geqslant 0$. The annulus β required to make $\partial B/\partial\psi$ just positive may be estimated from the equilibrium condition given below:

$$\vec{\nabla}_\perp\left(p_\perp + \frac{B^2}{2}\right) = \sigma B^2 \vec{K} \ . \tag{14}$$

Replacing gradients by scale lengths, one then finds that $\partial B/\partial\psi = 0$ when[4]

$$\frac{p_\perp}{r_a} \cong \frac{B^2}{R_c} ,$$

where r_a = annulus thickness and R_c = magnetic radius of curvature. In terms of annulus β_η, this becomes[4]

$$\beta_\eta \cong 2 \frac{r_a}{R_c} = 10\text{-}20\% .$$

Such approximate estimates of the critical β_η for stability are in reasonable agreement with more elaborate calculations[4,6] that take into account geometric and profile effects.

Studies of core stability limitations in the bumpy torus may be classified in two categories: rigid ring models and interacting ring models. The rigid ring approximation[4,6] typically assumes that the only effect of the ring is to produce a local minimum in the magnetic field and that there is no coupling between ring and core plasmas on the MHD time scale. In Ref. 4 a modified energy principle was developed that included the hot electron diamagnetic current and tensor pressure equilibrium. A sufficient condition for stability was then obtained that could be related to positive eigenvalues of an integrodifferential equation along each field line. Stability limits were calculated for a variety of plasma and ring 2-D equilibrium models with both flat and peaked pressure profiles and with short and long annulus models. Typical results are presented in Fig. 5 for the maximum stable core beta possible at a given annulus β for the long and short annulus models. Stable regions are located below these curves and instability is present above them. As may be seen, stability is generally attained for core betas

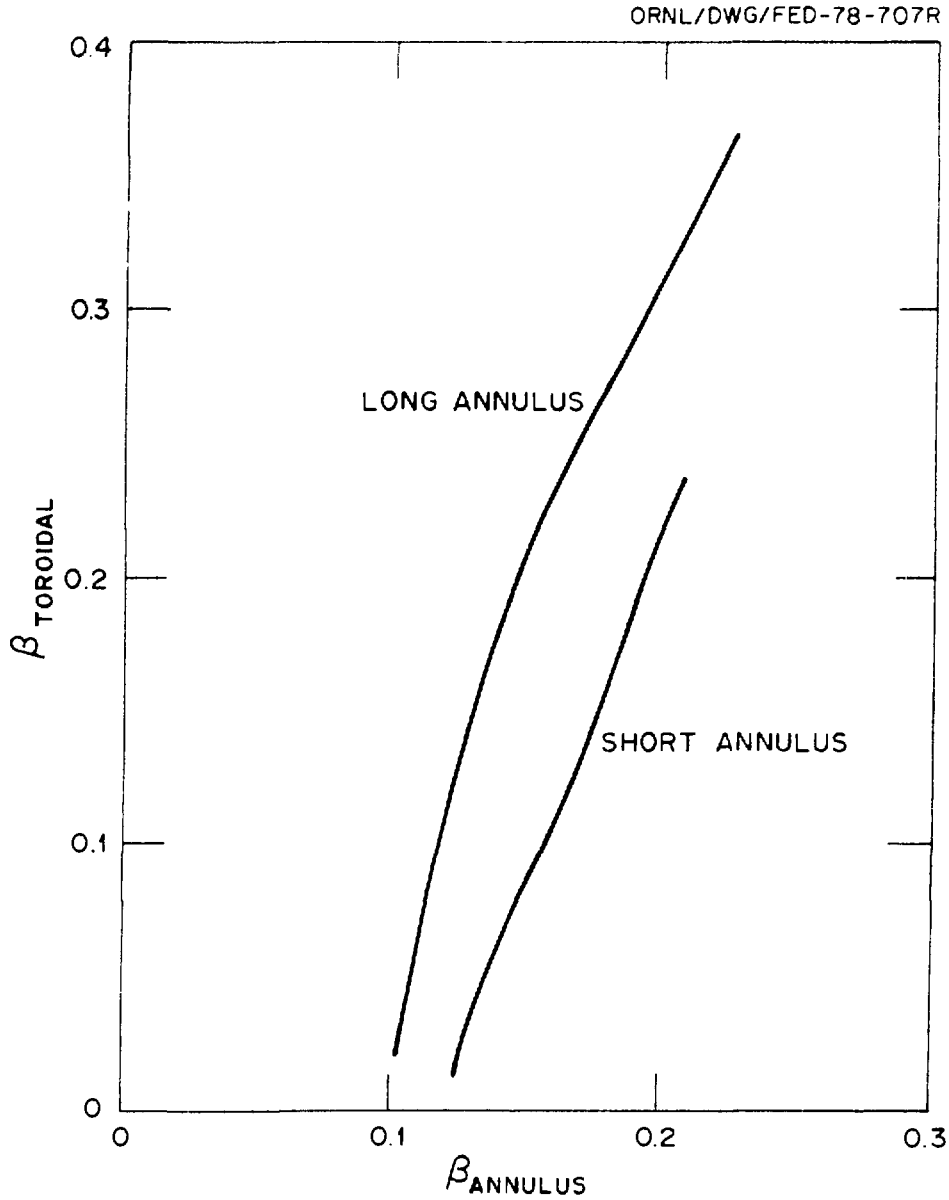

Fig. 5. Rigid ring model maximum stable toroidal beta as a function of $\beta_{annulus}$, using Taylor's form for the hot electron pressure, with m = 2 and B_c = 1.6 for the long annulus, B_c = 1.2 for the short annulus.

less than the annulus β above the stability threshold ($\beta_h \cong 10$-20%). Similar results have also been obtained in Ref. 6, in which a rigid ring model was developed using fluid equations. These resulted in normal mode equations of the Mathieu type, which were solved for the stability boundaries.

Interacting ring stability models[7,8] differ from the above-mentioned calculations in that the hot electron response to perturbed fields is taken into account. So far this has been carried out only in simple slab models that incorporate gradient scale lengths typical of the outer reversed gradient region of the ring where $U' < 0$. A three-species (cold ion, cold electron, hot electron) Vlasov-Maxwell model is typically used, with artificial gravity added to simulate the effects of field line curvature. The results of the most recent work[8] of this type indicate that the ring-core interaction is an important factor (related to enhanced compression of the core by the ring) that necessarily must be included in core stability studies. The simple slab model results[7,8] indicate that the stability threshold is in about the same range of values of β_h as was obtained with the rigid ring model; however, at higher values of β_h, the linear improvement in attainable β_p values with β_h (observed in the rigid ring results[4,6]) is not present. Instead the plasma beta is limited to values no larger than about 10%, independent of β_h. There also exists a second stability regime at large β_p ($\cong 30$-80%), but it is not clear how this could be accessed. Qualitatively similar results have been recently obtained at Oak Ridge National Laboratory using an improved version of the dispersion relation given in Ref. 7. In assessing the meaning of these results, it should be kept in mind

that they are based on a slab model with parameters characteristic of the midplane at the outer edge of the ring. This is the location of the worst magnetic curvature from the viewpoint of stability; also, no radial coupling with the inner regions of the ring and core plasma is taken into account. Probably the most significant feature of the results of interacting ring slab model calculations is the conclusion that the ring-plasma interaction is of importance rather than the actual limiting values of β_p predicted. More accurate estimates of the limiting core plasma beta will have to come from models that more realistically take into account the geometry and profile effects.

4. RING MACROSCOPIC STABILITY

The hot electron rings in EBT are themselves subject to many of the same macroscopic instabilities as the toroidal core plasma (i.e., interchange, ballooning modes, etc.). The major experimental manifestation of these modes is expected to be near the T-M transition; however, the threshold for this transition may be related to transport phenomena rather than ring stability limits.

One of the most primitive hot electron ring stability limits is the mirror mode instability, mentioned in Sect. 2 and related to a loss of equilibrium. For an infinite medium, this limit may be written[9] as

$$2\beta\left(\frac{T_\perp}{T_\parallel} - 1\right) < 1 , \qquad (15)$$

for stability. A phenomenon attributed to the mirror instability was observed[9] in studies on the PTF device. Hot electron distributions

sufficiently anisotropic to excite the instability were produced by varying the ratio of the electron cyclotron resonant magnetic field to the midplane magnetic field (B_{res}/B_{mid}). Since only those electrons with turning points at fields greater than B_{res} are heated by the microwaves, the relationship given below exists between $T_\perp/T_\parallel$ and B_{res}/B_{mid} in an electron cyclotron heated simple mirror:

$$\frac{T_\perp}{T_\parallel} = \frac{1}{(B_{res}/B_{mid} - 1)} \ . \tag{16}$$

Lowering B_{res}/B_{mid} will at some point make $T_\perp/T_\parallel$ large enough to exceed the condition of Eq. (15).

In addition to the mirror mode, a class of MHD instabilities occurs at fairly low values of beta; these are the interchanges, or line-preserving displacements. In this case the perturbed magnetic field is parallel everywhere to the equilibrium magnetic field. These are equivalent to the electrostatic flute modes contained in Vlasov-Maxwell kinetic models. They were first analyzed[10] for the EBT hot electron rings using guiding center plasma theory; this resulted in the stability criterion given below (this must be satisfied on each field line):

$$\left\langle \frac{K}{rB}\frac{\partial p_\parallel}{\partial \psi} + \frac{\partial/nB}{\partial \psi}\frac{\partial p_\perp}{\partial \psi} \right\rangle + \frac{\langle \partial p_\perp^2/\partial \psi \rangle}{\langle \tau B^2 \rangle} \leq 0 \ . \tag{17}$$

When this criterion was applied to typical EBT equilibria, it was concluded that the self-dug well of the annulus could stabilize interchanges over most of the ring region, provided the annulus β exceeded $\sim$15%. However,

at the outer edge, it was predicted that some degree of line-tying would be necessary if the plasma pressure extended beyond the edge of the well.

Flute modes in hot electron plasmas were also analyzed in Ref. 11, where a slab model was used with cold electrons, ions treated in the fluid approximation, and hot electrons with the Vlasov equation. The precessional drift frequency of the hot electrons was allowed to be comparable to or larger than the ion cyclotron frequency. (Such an ordering is typical of EBT hot electrons and cannot be taken into account in the MHD approximation.) The conclusion of this analysis was that flutes could readily be stabilized by a sufficient cold plasma density without relying on line-tying. The required cold plasma to hot plasma density ratio for stability is given below:[11]

$$\frac{n_c}{n_h} > 2\left[\frac{1}{q} + \left(\frac{1}{q^2} + \frac{1}{q}\right)^{1/2}\right] \tag{18}$$

An additional stabilizing factor for flute modes is the finite length effect.[12,13] As was shown in Ref. 12, a charge density fluctuation that is flutelike in infinite medium theory could, in a finite length plasma, give rise to fluctuating axial electric fields near the end regions. If a sufficient density of cold plasma was present at the ends, then the large response of the cold electrons to the fluctuating fields could exert a stabilizing influence on the mode.

The annulus β in EBT is sufficiently high for pressure-driven ballooning modes also to become energetically possible. In contrast to the line-preserving interchange modes discussed above, these distort and

stretch the magnetic field lines. Such modes again were first analyzed for EBT using the guiding center fluid model; this resulted in the following stability criterion:[14]

$$\left\langle \frac{K}{rB} \left(\tau^{-1}\sigma \frac{\partial p_\perp}{\partial \psi} + \frac{\partial p_\parallel}{\partial \psi} \right) \right\rangle \leq 0 \tag{19}$$

for stability. Since Eq. (19) involves only curvature, which is not appreciably modified by finite beta, it is much more difficult to satisfy than the criterion in Eq. (17) for interchange modes, which involved both curvature and ∇B. In using Eq. (19) with typical EBT finite beta equilibria, it was found that only a very careful tailoring of the equilibrium pressure profile coupled with line-tying at the edge could result in stability.

This discrepancy with the experimental observation that the annuli are stable over a range of conditions led to the recognition of the inadequacy of the guiding center fluid model for treating ballooning mode stability in the hot electron rings. A kinetic model for such modes was given in Ref. 15, where a Vlasov slab model was used. It was found that the high drift frequency of the hot electrons (comparable to the ion cyclotron frequency) permitted stabilization of ballooning modes. In later work[16] a cold plasma component was included, and it was found that the presence of cold plasma density also had a significant stabilizing effect. Stability was possible even when the hot electron drift frequency was somewhat less than the ion cyclotron frequency, provided sufficient cold plasma was present. This feature may be indicative of the T-M transition where the ring becomes unstable below a certain plasma density.

5. RING MICROINSTABILITIES

The hot electron rings in EBT are subject to several microinstabilities as a result of their anisotropic distributions. All of these apparently may be stabilized in the experiment through the use of off-resonant heating, which builds up the energetic tail and increases $T_{\parallel}/T_{\perp}$ by spatially spreading out the electron cyclotron resonant heating surfaces.

One such mode is the whistler instability, which is an electromagnetic mode driven by anisotropies. Investigations of this instability for distributions with energetic tails were given in Ref. 17. The result was that a relativistic spread in the electron cyclotron frequency led to resonant particles in the tail that contributed to damping rather than growth. It was concluded that such instabilities could be suppressed simply by building up the tail of the electron distribution to a certain critical density. Whistlers were also examined in Ref. 18 for electron cyclotron resonance heated plasmas and found to be stabilized, provided that $T_{\parallel}/T_{\perp} \gtrsim \sqrt{\beta_{\perp}/2}$.

A second microinstability considered[18] for EBT is the anisotropy-driven Timofeev mode. These are electrostatic modes that occur at the half harmonics of the ion cyclotron frequency, $\omega \cong (n + 1/2)\omega_{ci}$. They are expected to be stabilized if $T_{\parallel}/T_{\perp} \gtrsim 1/6$. Apparently this can be attained in the experiment by the use of off-resonant heating.

6. SUMMARY

As has been indicated, the electron ring and toroidal plasma stability requirements are closely coupled. The rings require cold plasma (provided by the toroidal core) for stability, whereas the toroidal plasma requires a magnetic well ($U' < 0$) near the edge (provided by the rings). In addition, the rings require some degree of off-resonant heating (leading to finite $T_{\parallel}/T_{\perp}$ and ring length) to prevent several possible microinstabilities.

Because the requirements for ring stability generally involve characteristics (finite $T_{\parallel}/T_{\perp}$, high energy, high background plasma density) that have an unfavorable influence on ring energy losses, it is of importance to closely couple ring stability considerations with power balance estimates for future devices. The stability requirements will impose a lower bound on ring losses. Better estimates of this minimum will depend on improvements in ring stability models in conjunction with more refined experimental observations of ring stability phenomena.

REFERENCES

1. B. B. Kadomtsev, *Plasma Physics and the Problem of Controlled Thermonuclear Reactions*, Vol. 4, p. 17 (1960).
2. C. L. Hedrick, G. E. Guest, and D. B. Nelson, Oak Ridge National Laboratory Report ORNL-TM/4076, Oak Ridge, Tennessee (March 1973).
3. J. B. Taylor, Phys. Fluids 6, 1529 (1963).
4. D. B. Nelson and C. L. Hedrick, Nucl. Fusion 19, 283 (1979).
5. L. W. Owen and C. L. Hedrick, Bull. Am. Phys. Soc. 20, Abstract 8D5 (1975).

6. H. Sanuki and M. Fujiwara, IPPJ-426 (December 1979).

7. D. B. Nelson, Oak Ridge National Laboratory Report ORNL/TM-6824, Oak Ridge, Tennessee (June 1979).

8. J. W. Van Dam and Y. C. Lee, "Stability Analysis of a Hot Electron EBT Plasma," paper presented at the EBT Ring Physics Workshop, Oak Ridge, Tennessee, December 4, 1979.

9. W. B. Ard, R. A. Dandl, and R. F. Stetson, Phys. Fluids 9, 1498 (1966).

10. G. E. Guest, C. L. Hedrick, and D. B. Nelson, Oak Ridge National Laboratory Report ORNL/TM-4077, Oak Ridge, Tennessee (December 1972).

11. H. L. Berk, Phys. Fluids 19, 1255 (1976).

12. G. E. Guest and C. O. Beasley, Jr., Phys. Fluids 9, 1798 (1966).

13. G. E. Guest and E. G. Harris, Phys. Rev. Lett. 27, 1500 (1971).

14. D. B. Nelson, C. L. Hedrick, and G. O. Spies, Oak Ridge National Laboratory Report ORNL/TM-4109, Oak Ridge, Tennessee (March 1973).

15. G. E. Guest, C. L. Hedrick, and D. B. Nelson, Phys. Fluids 18, 871 (1975).

16. R. R. Dominguez and H. L. Berk, Phys. Fluids 21, 827 (1978).

17. *Thermonuclear Division Annual Progress Report for Period Ending December 31, 1970*, Oak Ridge National Laboratory Report ORNL-4688, Oak Ridge, Tennessee (August 1971).

18. G. E. Guest and D. J. Sigmar, Nucl. Fusion 11, 151 (1971).

DISCUSSION

V. K. TRIPATHI: (1) Has anybody attempted nonlocal theory of Whistler instability? (2) Are the existing theories of this instability based on guiding center approximations?

D. A. SPONG: The only sense in which nonlocal theory has been done is in the axial direction. Convective and absolute boundaries were calculated for ELMO in ORNL/TM-3143 by Hedrick [also the Fusion Energy Division Annual Report and Guest and Sigmar, Nucl. Fusion, p. 151 (1971)].

I am not aware of any treatment which is nonlocal in the radial coordinate. However, since so much work in space physics has been done on Whistlers, some such treatment may have been given there.

A. KADISH: Are the guiding center and isotropic MHD ($\int d\ell/B$) stability criteria qualitatively the same for the special case $p_\perp = p_\parallel$? In particular, is the radial variation of $\int d\ell/B$ in the same way always the desirable thing to try to achieve according to both theories?

C. L. HEDRICK: Qualitatively, tensor (guiding center plasma) and scalar pressure were observed to be similar numerically. Except for a term which is analagous to the γ_p term in MHD, the two theories go smoothly into each other. It is hard to calculate the term corresponding to γ_p in scalar pressure, but the scalar pressure theory forms a lower bound for this term. Except for 10-20% effects, $\oint d\ell/B$ is adequate for estimating effects which should really be calculated with the more elaborate theory.

A BRIEF REVIEW OF ELMO RING STABILITY THEORY

G. E. Guest

General Atomic Company
San Diego, California 92138

I. INTRODUCTION

The stabilization of a toroidally-confined plasma in the ELMO Bumpy Torus is observed[1] to depend on the high-beta, hot-electron "ELMO" rings, annular regions occupied by relativistic, mirror-confined electrons. This stabilizing effect on the isotropic, scalar-pressure plasma confined in the bumpy torus can be interpreted using the interchange theory originally developed by Kadomtsev.[2] The limits of this stabilization have been examined more recently in studies of ballooning modes,[3] expected to place more stringent limitations on beta as the core plasma pressure increases, as discussed at this workshop. Nonetheless, the conditions under which the ELMO rings themselves are stable have not yet been adequately established, even though it has been conjectured frequently that the important transition from the quiescent T-mode (toroidally-connected sectors) to the turbulent M-mode (disconnected, mirror-like sectors) in EBT marks the threshold for onset of instability of the rings. Still, the dominant processes responsible for the transition, the main modes of instability and the critical plasma parameter whose threshold value is reached when the ambient gas pressure and microwave power approach the limiting values for T-mode operation have not yet been established experimentally or theoretically. It would be very advantageous to be able to extend T-mode operation to lower pressures and higher microwave powers in order to achieve higher temperature and longer confinement times. It is thus important to investigate theoretically the conditions which are necessary for the stability of the ELMO rings, and to seek confirmation from available experiments with ECH plasmas. Investigations of exactly this sort were presented at the workshop and are summarized here, together with some additional material not discussed at the workshop.

Because of the qualitative character of instabilities observed in earlier ECH experiments in simple mirror devices,[4] it has been customary to discuss ELMO ring stability in terms of two major destabilizing properties of ECH plasmas: the anisotropy of the hot-electron pressure, $P_\perp >> P_\parallel$; and the unfavorable curvature of the magnetic lines of force in the region occupied by the rings. The anisotropy can drive both electrostatic and electromagnetic plasma waves unstable;[5] and the magnetic configuration is inherently unstable to flute-like modes.[6] Conditions for stabilization of the modes driven by pressure anisotropy appear to relate to properties of the ECH process, particularly the effective (mirror) ratio between the resonant magnetic field and the minimum field strength on the same magnetic lines of force: both in theory and experiment, if $B_{res}/B_{min} \geqslant 1.2$, the plasma is relatively free of anisotropy-driven instabilities. The mechanisms responsible for stabilization of flutes, although not so clearly identified, appear correlated with the relative density of the colder plasma component.[7] Since electron cyclotron heating typically leads to a two-component plasma if the microwave power density is high enough and other conditions are suitably chosen, this aspect of flute-mode stabilization suggests a possible role for these instabilities in the T-to-M mode transition. With that motivation we shall begin the present brief review with a discussion of the status of our understanding of flute modes.

In Section 2, we summarize the recent results from a variational study of an anisotropic, guiding-center fluid model, reported in the paper by R. L. Miller *et al.*[8] presented at this workshop. This model can be used to analyze equilibria which closely resemble the actual geometrical configuration of the experimental ELMO rings. But the fluid nature of this model rules out the important stabilizing effect of the finite-size gyroradius of the plasma ions and the relativistic electrons. In actual practice, the radial thickness of the ELMO rings is only a few hot-electron gyrodiameters; and the perpendicular wavelength of the flute modes can be comparable for relatively low poloidal mode numbers.

A more microscopic, kinetic theory approach, which accounts for the finite gyroradius effect but at the expense of geometric realism, is then summarized in Section 3, using results presented by R. R. Dominguez.[9]

Both theoretical models predict that the ELMO rings would generally be unstable in the absence of some additional stabilizing mechanisms. One such potential mechanism, background cold plasma, is included in the kinetic model; and threshold values of the relative cold-plasma concentration are given.

In Section 4, we summarize the work presented by Chiu and Guest[10] relating the relative cold-plasma density in the rings to ambient gas pressure and microwave power. These three papers thus establish the basic framework with which the theory and experiment can be compared. Unfortunately, one particularly sensitive ambiguity remains in the theory which makes that comparison uncertain; viz., the effect on cold-plasma stabilization of the finite length of the ELMO rings along the magnetic field lines.

We conclude in Section 5 with a summary of two papers by Sanuki and Fujiwara[11] and Van Dam and Lee,[12] which reconsider the stabilizing effect of the ELMO rings on the toroidal plasma. The paper by Sanuki and Fujiwara confirms the earlier work of Nelson and Hedrick,[3] while the paper by Van Dam and Lee finds a weaker stabilizing effect. The differences in the models used in these two papers are identified, although further work will be needed to reconcile the differences in conclusions reached through the two approaches.

II. STABILITY OF THE ELMO RINGS IN THE ANISOTROPIC GUIDING-CENTER MODEL

The anisotropic, guiding-center fluid model can be used to compute high-beta equilibria which emulate many features of the ELMO rings, particularly the geometrical shape and continuous pressure gradients, and thus the actual magnetic configuration resulting from diamagnetic plasma currents and vacuum magnetic fields. This model was developed extensively by Kruskal and Oberman,[13] Taylor and Hastie,[14] Grad,[15] and then applied to EBT by Guest, Hedrick, and Nelson.[16] At that time it was not mathematically feasible to carry out a full stability analysis using the variational techniques developed by the early workers. But new techniques have become available as the result of the world-wide tokamak program through such codes as PEST, ERATO, and GATO. Miller has combined the earlier equilibrium models and these new stability techniques to provide a transparent stability analysis of plausible single-component models of the ELMO rings. We shall first summarize the results and then discuss the physical phenomena missing in this model and their possible impact on the unstable modes.

The equilibria studied by Miller *et al.*[8] use the functional forms of Guest, Hedrick, and Nelson.[16]

$$\left.\begin{aligned} 2\mu_0 P_\perp &= s\, g(\psi)\, (B_c^2 - B^2) \\ 2\mu_0 P_\parallel &= s\, g(\psi)\, (B_c - B)^2 \end{aligned}\right\} B \leqslant B_c$$

$$P_\parallel = P_\perp = 0 \text{ if } B \geqslant B_c \ .$$

The radial pressure profile, specified through $g(\psi)$, is assumed to be symmetrical and parabolic. The model does not include any background plasma components, such as a cold plasma component or a scalar pressure toroidal plasma. The equilibria examined in these studies were typically 6 cm thick and roughly 10 cm long; and the plasma pressure was varied over a range thought to be typical of EBT-I experimental operation: $\beta_\perp \lesssim 0.5$.

The stability analysis uses a finite-element technique in χ and ψ with Fourier analysis in the (ignorable) θ-direction to evaluate the second variation in the energy (analagous to the usual δW). A conducting shell is assumed at the edge of the plasma to prevent perturbation of the boundary. Even with this stabilizing assumption all equilibria examined to date are found to be unstable for all poloidal mode numbers. The unstable modes have the following characteristics:[8]

(1) growth rates increase rapidly with beta and with poloidal mode number, as shown in Fig. 1.

(2) the modes are interchanges at low values of beta, but show a strong ballooning effect at higher beta, as shown in Fig. 2.

(3) the mode amplitude is large in the outer regions where ∇p and the curvature are in the same direction, and small in the inner regions where they have opposite directions, as shown in Fig. 3.

(4) the unstable waves produce radial and azimuthal flow patterns with a clear vortex natures, as shown in Fig. 3.

In the limit of very large poloidal mode numbers, e.g., $\ell = 100$ (where the waves depend on θ through $\exp i\ell\theta$), the modes are strongly localized in the unfavorable regions and have growth rates which extrapolate to the usual value[7] at low beta, provided finite gyroradius effects are neglected. From elementary electrostatic kinetic-theory models, the unstable modes correspond to zeros of the perpendicular dielectric constant.

$$\kappa_\perp = 0 \ , \quad \text{or} \quad 1 = \frac{\Omega_i}{k_\perp R_p}\left(\frac{1}{\omega - \omega_{ge}} - \frac{1}{\omega - \omega_{gi}}\right)$$

where

$$\omega_{gj} = k_\perp v_{gj} = \frac{\ell}{r}\frac{T_j}{q_j\ B\ R_c(r)}$$

For hot-electron, cold-ion plasmas, this dispersion relation predicts growth rates

$$\gamma^2 \cong \frac{\omega_{ge}\Omega_i}{k_\perp R_p}\left(1 + \frac{\omega_{ge}}{4}\frac{k_\perp R_p}{\Omega_i}\right) ,$$

or

$$\frac{\gamma^2}{\omega_A^2} \cong \frac{-\beta L^2}{2R_p R_c(r)}\left[1 - \frac{\ell^2}{8}\frac{M}{m}\frac{R_p}{r}\frac{\rho_e^2}{r R_c(r)}\right]$$

In EBT-I, the geometry is such that

$$\left.\frac{L^2}{2R_p R_c(r)}\right]_{r = 12\ \mathrm{cm}} \cong 21$$

From the guiding-center model, the growth rate of the $\ell = 100$ modes extrapolates at low values of $\beta_\perp$ to a limit given by

$$\lim_{\beta \to 0}\left|\frac{1}{\beta_\perp}\frac{\gamma^2}{\omega_A^2}\right| \cong 22 ,$$

in very good agreement with the leading term of the electrostatic growth rate expression.

To get some idea of the relative importance of the finite gyroradius effect, which is not accounted for in the guiding-center fluid model, we can estimate the maximum poloidal mode number predicted to be unstable in EBT-I:

$$\ell_{max} \cong \sqrt{8\frac{m}{M}\frac{r}{R_p}\frac{r R_c(r)}{\rho_e^2}} \sim 6 .$$

Similarly, the $\ell = 5$ mode could have its growth rate reduced by nearly 40% by this type of finite gyroradius effect; and we are therefore strongly motivated to investigate the more microscopic, kinetic-theory models.

III. STABILITY OF THE ELMO RINGS IN THE KINETIC THEORY MODEL

The kinetic theory model developed originally by Rosenbluth, Krall, and Rostoker,[17] and reviewed at length by Krall[18] and others provides a framework for dealing with the short-wavelength catastrophe revealed by the guiding center fluid model and for including several distinct plasma species, such as hot electrons, cold electrons, and cold ions. This model can therefore account for important stabilizing effects such as (electrostatic) cold-plasma stabilization in plasmas which are either finite in length or which extend indefinitely along the magnetic lines of force, as well as the finite gyroradius effects referred to earlier. The models can be electrostatic ($\vec{E} = -\vec{\nabla}\phi$), or fully electromagnetic ($\vec{E} = -\vec{\nabla}\phi - \partial\vec{A}/\partial t$). Unfortunately, in order to gain the added realism associated with these microscopic and multispecies effects, it is apparently necessary to idealize the geometry to that of a simple slab in which the magnetic lines of force are straight, and the effect of curvature is emulated by an artificial gravity. Almost all studies to date have made the assumption that unstable modes were highly localized, which, as was clear from the guiding-center fluid model, neglects a strong stabilizing effect associated with the finite radial extent of the unstable perturbations. This artificial localization can be somewhat mitigated by modeling the ELMO ring as a hollow cylinder; but the radial boundaries must then be assumed to be mathematically sharp: n = constant, $r_{inner} \leqslant r \leqslant r_{outer}$; and $n = 0$, otherwise. Thus, the kinetic theory model is complementary to the guiding-center fluid model in several important respects.

In his paper, R. R. Dominguez[9] used the kinetic-theory model to calculate the relative cold-plasma concentration required to stabilize modes of specified azimuthal mode number in a sharp-boundary cylindrical model of the ELMO rings. The results are shown in Fig. 4, where the critical value of cold-electron density (relative to the hot-electron density), N_c/N_h, is plotted against the grad B-drift frequency relative to the ion gyrofrequency,

$$q = \frac{\ell T_h}{M_i \Omega_i^2 r_c} = \ell q_0$$

Note that more cold plasma is required to stabilize the long-wavelength modes, $\ell = 1$; but in all cases $N_c/N_h > 1$ is needed for stability. Even so, the "non-local" theory permitted by the sharp-boundary model leads to more optimistic predictions than the local theory, as indicated in Fig. 5. In this figure, the local and sharp-boundary model results are compared for a case in which $\ell = 10$, $\beta_h = 0.1$, and $R_c/R_p = 20$, a somewhat extreme choice for the pressure gradient. Note that, although $(N_c/N_h)_{crit}$ depends on the hot-plasma beta, the critical value of N_c/N_h in the local model can be very large for $q_0 \sim 1$.

Dominguez concludes that cold plasma can stabilize hot-electron flute modes if $N_c/N_h \gtrsim 2 - 10$, and that the critical relative concentration predicted by the non-local theory is significantly less than that predicted by the localized theory. Keep in mind that in all these cases, the ELMO ring is modeled by an infinitely-long cylinder or slab; finite-length effects have not been analyzed using the fully electromagnetic dispersion relation.

The empirical result that flute-like modes are often absent in simple magnetic mirror plasmas has traditionally been attributed to phenomena associated with the finite length of the mirror-confined plasma. Field lines that pass through the plasma in such devices may intersect conducting walls, effectively tying the magnetic field lines (and the plasma potential) at that point. Several theoretical models of finite-length stabilization of flute modes have been developed,[19] and some experimental support can be found for each of the different models. But experimental attempts to validate any of these models have remained ambiguous due to the fundamental difficulties of controlling and measuring the parameters critical to the theories. A relatively recent experiment on cold-plasma stabilization[20] discusses these difficulties and tentatively concludes that bulk stabilization by cold plasma[21] is more compatible with the observations than the theoretical finite-length effects.

IV. CONTROL OF THE COLD-PLASMA CONCENTRATION

From the kinetic-theory model and from earlier experiments, it appears that the relative density of cold plasma surrounding the ELMO ring is a critical factor in ring stability. The cold-plasma density, in turn, is controlled by the microwave power applied to the plasma and by the ambient neutral gas pressure at the surface of the plasma. The paper by Chiu and Guest[10] summarized a model calculation for determining the relation between cold-plasma parameters and the power and pressure.

In Chiu's approach, the plasma is modeled as two contiguous regions within which all local values of plasma parameters are replaced by their average values, analagous to "water-bag" models used for many years in stability analyses. The edge plasma, in which the unstable outer edge of the ELMO ring is located, is assumed to be weakly turbulent, so that Bohm transport is expected for the cold plasma there. The central plasma is assumed to be quiescent, as in T-mode operation, and subject to neoclassical transport. The source of particles is an incident flux of neutral atoms, a small part of which is trapped directly in the (thin) edge region, but most of which enters the central (core) region, is ionized, and eventually diffuses out into the edge region. The object of this calculation is to determine the dependence of the steady-state edge-plasma parameters on power and pressure.

The profound difference between the toroidal case and the open-ended, simple-mirror configuration has been illustrated in Ref. 10. For the simple-mirror case, no steady-state solutions are possible below a critical neutral-atom density. This is a consequence of the fact that only the direct ionization of neutral gas can provide a cold-plasma source for the simple mirrors, since end losses prevent a significant perpendicular diffusion from the central to the edge regions.

But in the fully toroidal case (which assumes that the edge is not mirror confined), the results are more complex and take the form of scaling predictions in general, or numerical predictions for specific cases. This added complexity arises from the non-linear nature of the underlying transport equations. The scaling relations obtained in the paper are, in the edge region,

$$T_c \propto \frac{P_\mu}{n_0}$$

$$n_c \propto \frac{n_0^2}{P_\mu} ,$$

where n_0 is the ambient neutral-atom density and P_μ is the microwave power absorbed by the plasma. Numerical solutions of the transport equations are shown in Fig. 6, where n_0 is varied at constant P_μ, and Fig. 7, where P_μ is varied at constant n_0.

One concludes from these studies that if a constant value of cold-electron density, n_c, is needed for stability of the ELMO rings, the critical levels of microwave power and ambient gas pressure should satisfy a relation of the form[10]

$$P_\mu < P_{\mu,crit} \propto n_0^2$$

or, alternatively,

$$n_0 > n_{0\ crit} \propto P_\mu^{1/2} .$$

V. LIMITS ON BUMPY TORUS STABILIZATION BY ELMO RINGS

The ELMO rings are predicted to stabilize low-beta plasmas in EBT devices if the ring beta exceeds the value required to produce a local average magnetic well (i.e., the value above which $\oint d\ell/B$ becomes a non-monotone function of the minor radius). It has also been predicted that when these minimum conditions are exceeded, the toroidal core plasma would be stable up to values of (core-plasma) beta comparable to the ELMO ring beta. Above these limiting values of the core-plasma beta, unstable ballooning modes are expected to enhance radial transport of the toroidal plasma.

Nelson and Hedrick[3] have given numerical estimates of this core-plasma beta limit for a few specific sets of ELMO ring parameters; and in the paper by Sanuki and Fujiwara[11] supporting analytical results are presented, indicating stable confinement of a core plasma with beta $\gtrsim$50% if the ring beta exceeds to 20 to 40%. These results assume the rings to be unaffected by low-frequency perturbations of the core plasma, the so-called rigid-ring assumption, which was also made by Nelson and Hedrick.[3] Nelson[22] has investigated the validity of the rigid-ring assumption and concluded that supporting evidence existed. Representative results of these recent studies are shown, together with the Nelson and Hedrick[3] and Sanuki and Fujiwara[11] rigid-ring results in Fig. 8 of Ref. 11.

In the paper by Van Dam and Lee,[12] a very different conclusion is reached; namely, that the rings respond significantly to low-frequency fluctuations in the (parallel) magnetic field, leading to de-stabilization if the core beta exceeds a very low critical value. Van Dam and Lee use a highly-idealized, "bumpyless torus" model; that is, an ideal, toroidal solenoid in which the magnetic field strength is constant along field lines. Since they consider only flute-like ($k_{\parallel} = 0$) modes in this model, the ELMO ring electrons exhibit adiabatic, two-dimensional behavior and follow distorted drift trajectories in response to low-frequency fluctuations in the magnetic field. The result is a significant compressional effect in which the magnetic field perturbation is

greatly enhanced by the hot-electron response; and the core plasma supports unstable flute-like modes at very low beta values.

It is possible that this enhanced compressional effect is an artifact of the bumpyless torus model, and may not occur in an actual bumpy torus. In a bumpy torus, the adiabatic response of the hot-electrons would be mainly a change of pitch angle so as to preserve ε, μ, and J during the slow change in B. Here μ is the magnetic moment, ε is the total energy of the ring electron, and J is its action invariant, $\oint v_{\parallel} d\ell$. The change in perpendicular pressure resulting from a low-frequency variation in the magnetic field strength would have the form

$$\delta p_{\perp} \sim \frac{\partial p_{\perp}}{\partial B} \delta B \sim \delta B \frac{\partial}{\partial B} \left[\int_0^{\infty} d\varepsilon \int_0^{\varepsilon/B} d\mu \; f_0(\varepsilon,\mu) \; B\left(\frac{\mu B}{\varepsilon - \mu B}\right)^{1/2} \right].$$

This change in perpendicular pressure can be quite small because of the possiblity of expansion or contraction along the magnetic field lines in a more realistic "bumpy" model of the EBT. Note in particular that it depends on the distribution in pitch angle of the hot electrons, which has been determined experimentally in the Canted-Mirror Experiment.[23]

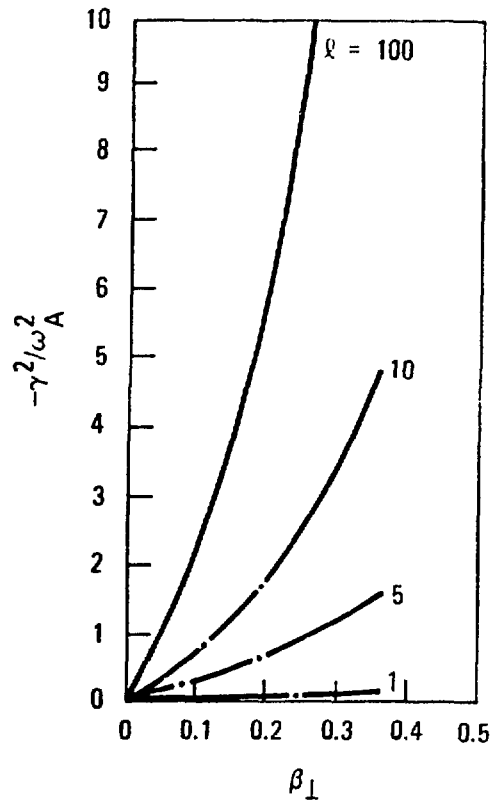

1. The dependence of growth rate, here expressed through γ^2/ω_A^2, on perpendicular pressure, $\beta_\perp$, for poloidal mode numbers 1, 5, 10, and 100. [Reference 8]

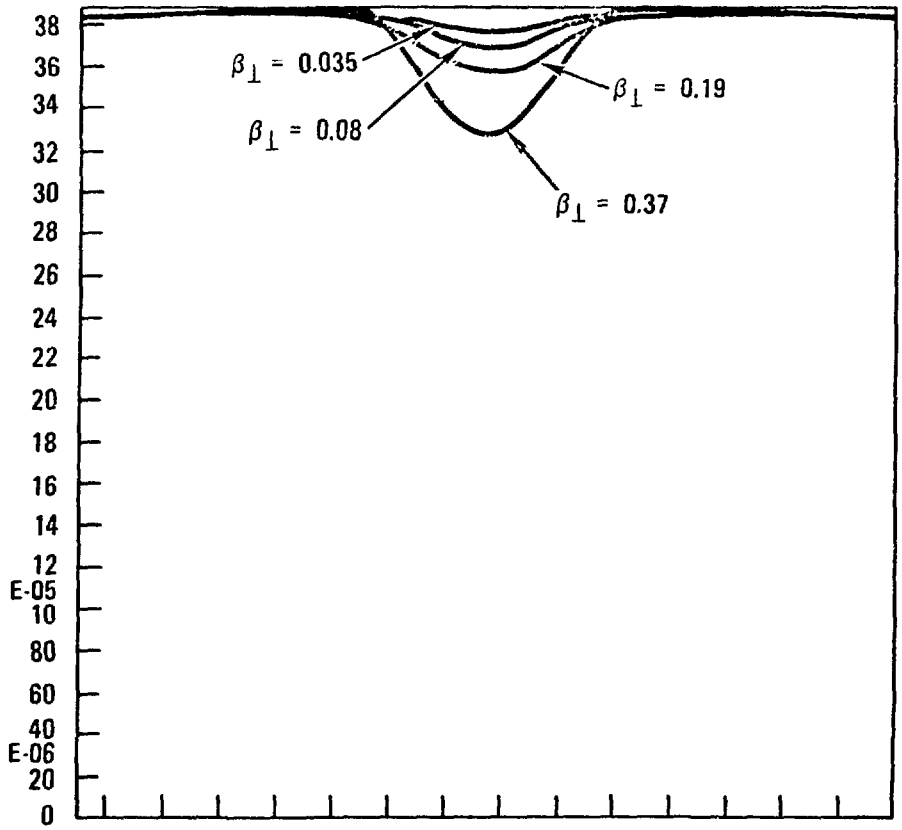

2. The variation of the perpendicular displacement along the unperturbed magnetic line of force. [Reference 8]

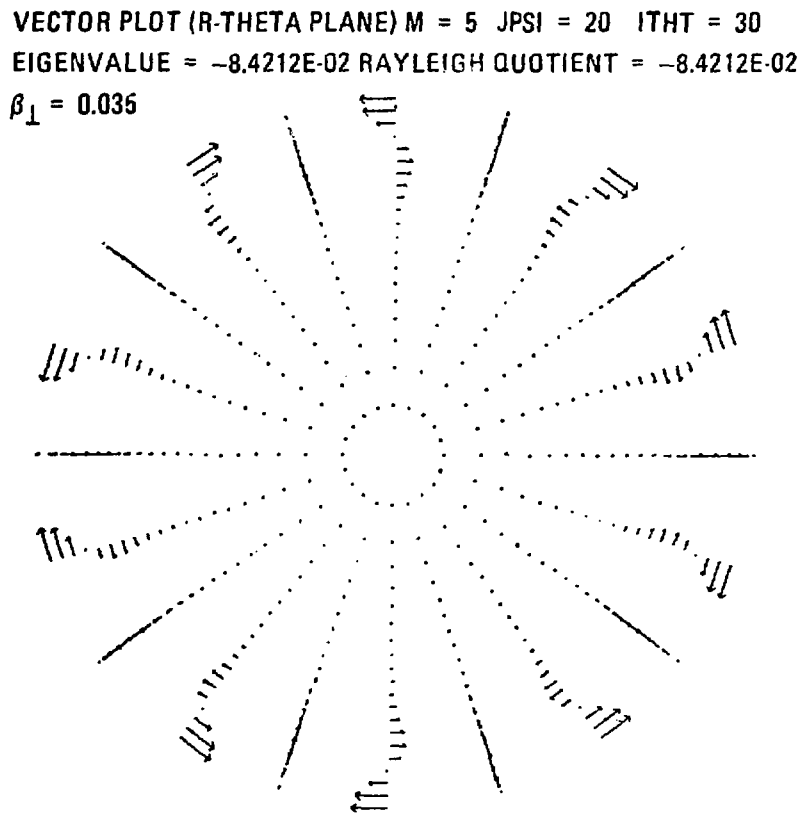

3. An end-on view of the perturbation field (in the r-θ plane). [Reference 8]

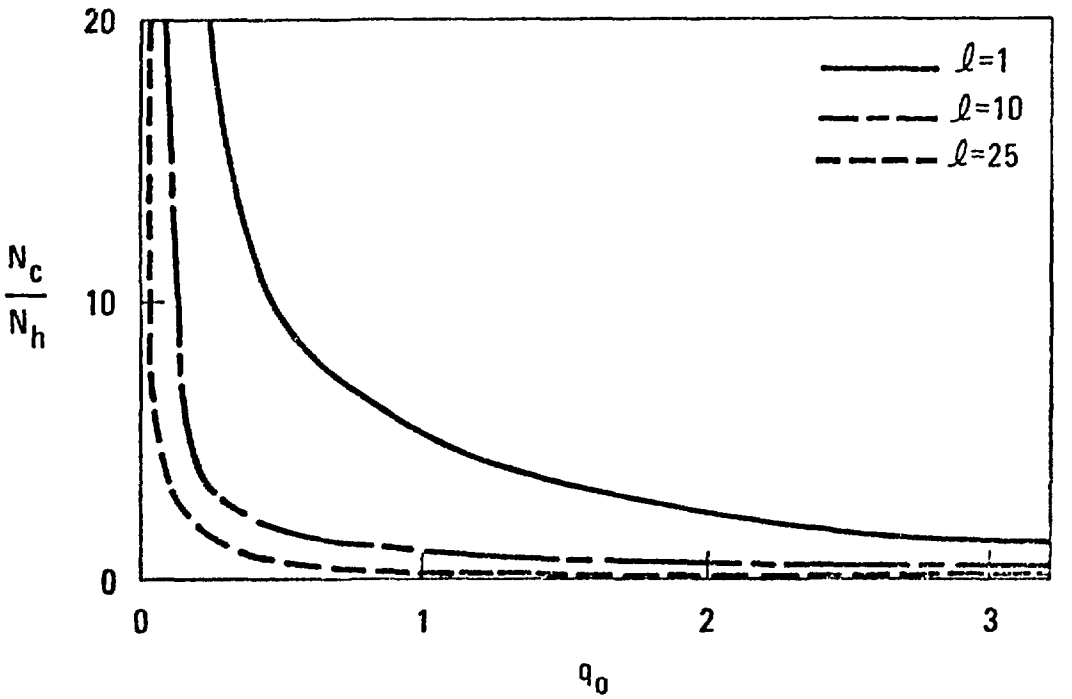

4. The critical relative cold-electron concentration for varying drift frequencies in the sharp-boundary model: ℓ = 1, 10, and 25. [Reference 9]

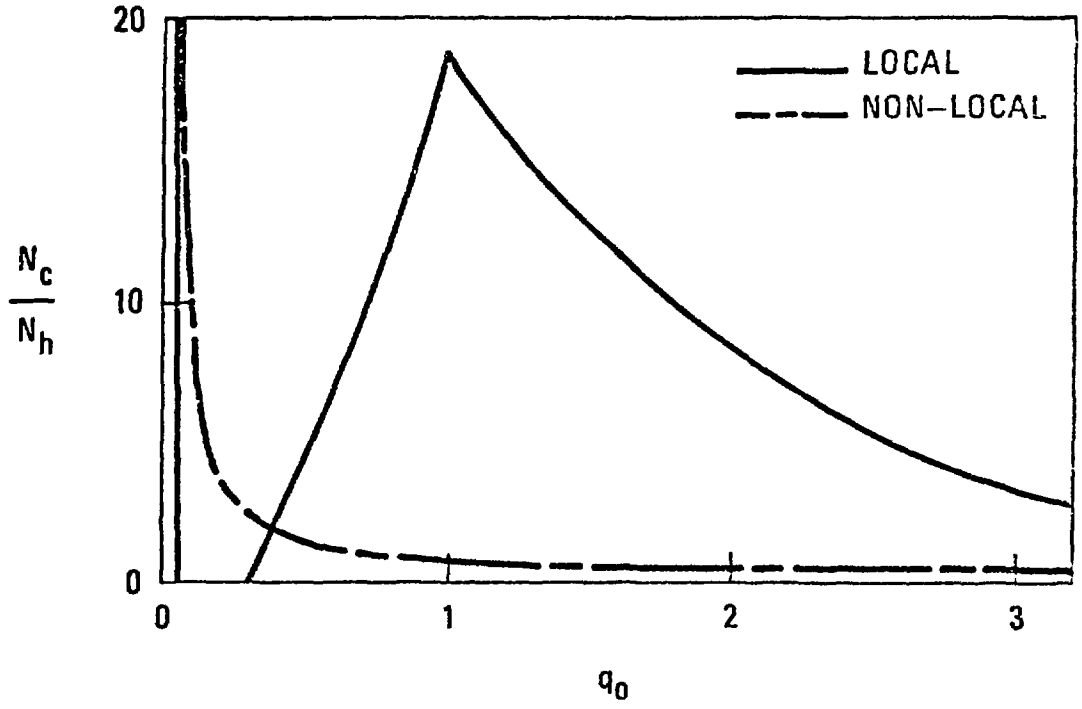

5. Comparison of critical cold-electron concentrations in the non-local (sharp boundary) and local model. [Reference 9]

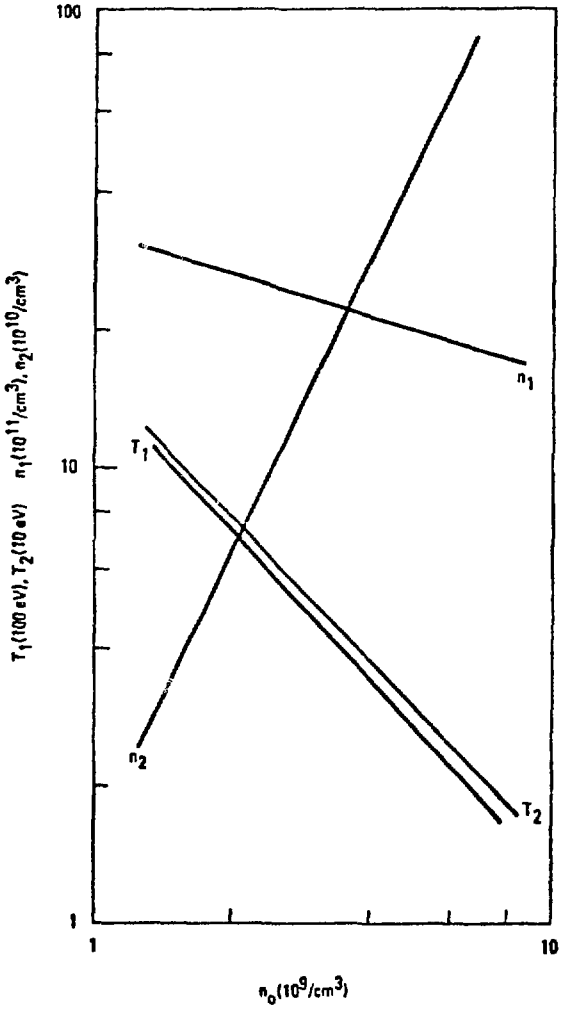

6. Equilibrium parameters for varying neutral gas density but constant microwave power. [Reference 10]

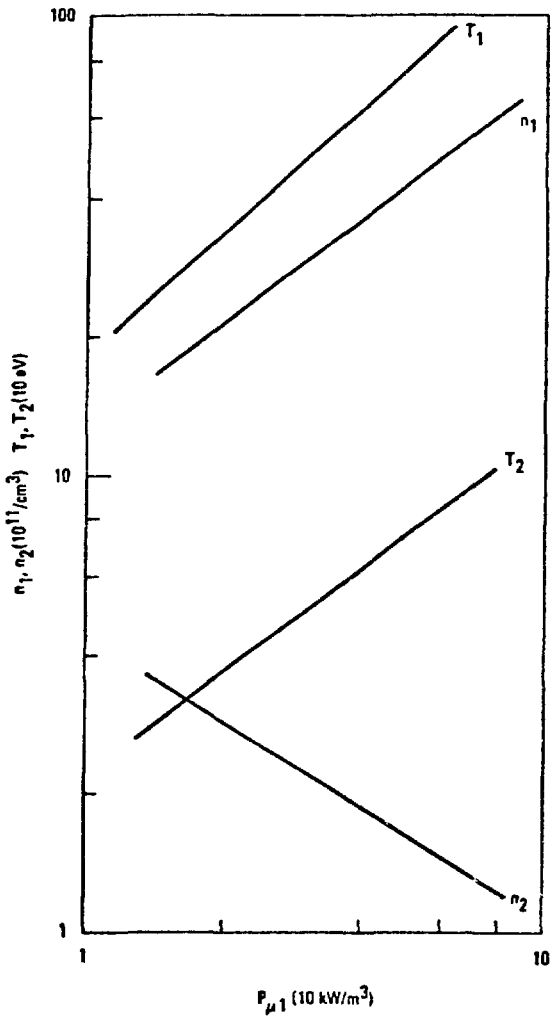

7. Equilibrium parameters for varying microwave power but fixed ambient gas density. [Reference 10]

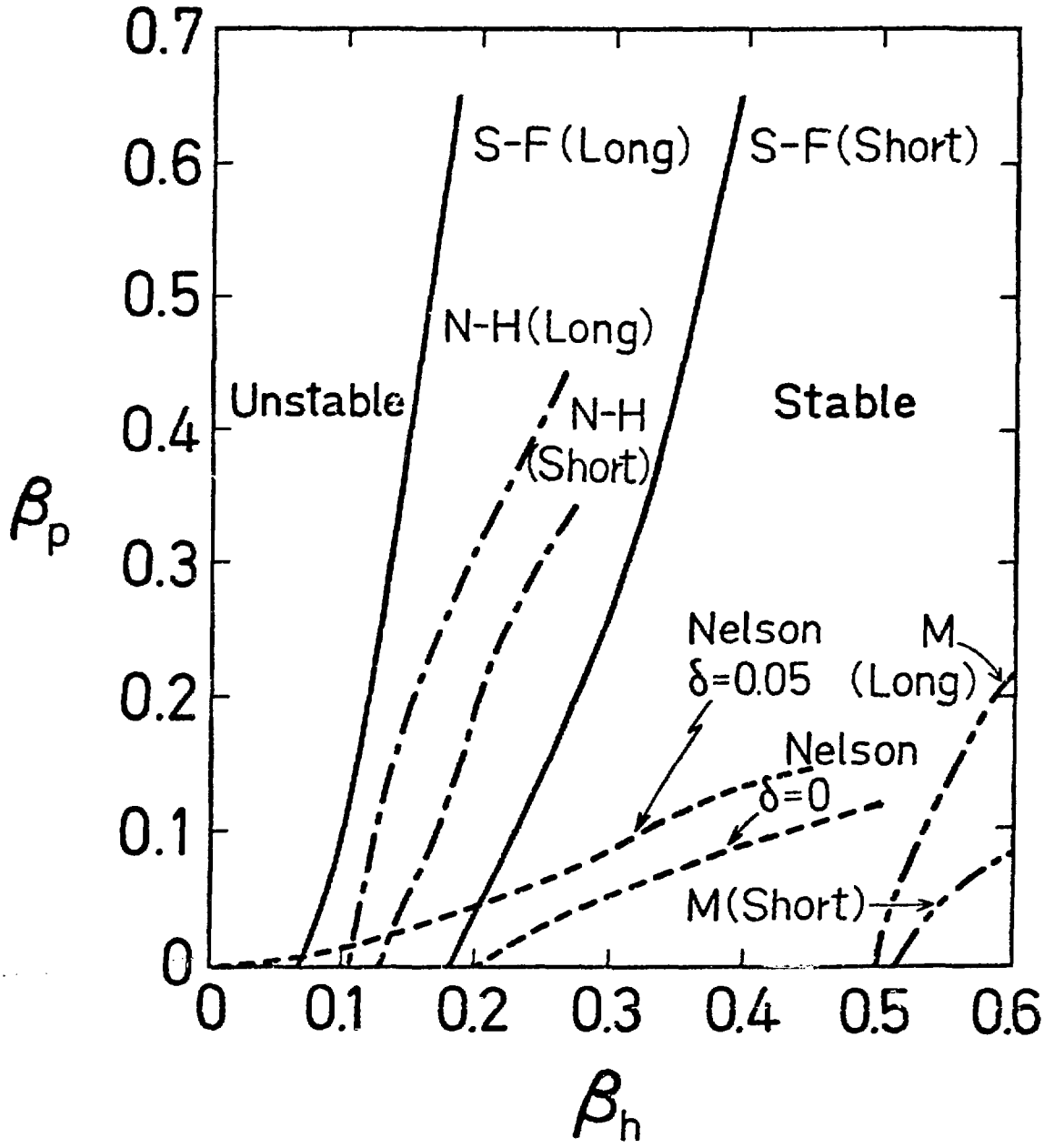

8. The maximum stable values of core-plasma beta, β_p, versus the hot-electron, ELMO ring beta, β_h. [Reference 11]

REFERENCES

1. R. A. Dandl *et al.*, in Plasma Physics and Controlled Nuclear Fusion Research (Proc. Conf. Tokyo, 1974) Vol. II, IAEA, Vienna (1975) 141.
2. B. B. Kadomtsev, "Plasma Physics and the Problem of Controlled Thermonuclear Reactions," M. A. Leontovich, Editor, Vol. IV, p. 450 (Pergamon, 1960).
3. D. B. Nelson and C. L. Hedrick, Nucl. Fusion *19*, 283 (1979).
4. R. A. Dandl, A. C. England, W. B. Ard, H. O. Eason, M. C. Becker, and G. M. Haas, Nucl. Fusion *4*, 344 (1964); see also W. B. Ard, R. A. Dandl, and R. F. Stetson, Phys. Fluids *9*, 1498 (1966).
5. G. E. Guest and D. J. Sigmar, Nucl. Fusion *11*, 151 (1971).
6. M. N. Rosenbluth and C. L. Longmire, Annals of Physics *1*, 120 (1957).
7. See G. E. Guest and C. O. Beasley, Jr., Phys. Fluids *9*, 1798 (1966) and references cited there.
8. R. L. Miller *et al.*, "Macroscopic Stability of the Hot Electron Annulus in EBT," in these proceedings.
9. R. R. Dominguez, "Interchange Stability of Hot Electron Rings in a Warm Plasma," in these proceedings.
10. S. C. Chiu and G. E. Guest, "A Two-Point Model for EBT Transport," in these proceedings.
11. H. Sanuki and M. Fujiwara, "Stability of a Toroidal Plasma by Hot Electron Annulus in a Bumpy Torus," in these proceedings.
12. J. W. Van Dam and Y. C. Lee, "Stability Analysis of a Hot Electron EBT Plasma," in these proceedings.
13. M. D. Kruskal and C. R. Oberman, Phys. Fluids *1*, 275 (1958).
14. J. B. Taylor and R. J. Hastie, Phys. Fluids *8*, 323 (1965).
15. H. Grad, Phys. Fluids *9*, 225 (1966).
16. See the following unpublished technical memos: ORNL-TM-3943, "Elements of the Stability Theory of the Guiding-Center Plasma;" ORNL-TM-4077, "On the Interchange Stability of a Guiding-Center Plasma in an Axisymmetric Magnetic Trap;" and ORNL-TM-4076, "Some Techniques for Determining Fusor Pressure Equilibria."
17. M. N. Rosenbluth, N. A. Krall, and N. Rostoker, Nucl. Fusion Suppl. Pt. 1, 143 (1962).

18. N. A. Krall, in "Advances in Plasma Physics," edited by A. Simon and W. B. Thompson (Interscience, New York, 1968) Vol. I, p. 153.
19. See, for example, G. E. Guest and E. G. Harris, Phys. Rev. Lett. *27*, 1500 (1971) and references cited there.
20. I. G. Brown, A. J. Lichtenberg, M. A. Lieberman, and N. C. Wyeth, Phys. Fluids *19*, 1203 (1976).
21. H. L. Berk, Phys. Fluids *19*, 1255 (1976).
22. D. B. Nelson, "Effect of Hot Electrons on Magnetohydrodynamic Modes in EBT," (Oak Ridge National Laboratory Report ORNL/TM-6824, June 1979).
23. G. E. Guest, C. L. Hedrick, and J. T. Hogan, Phys. Fluids *15*, 1159 (1972).

DISCUSSION

A. KADISH: In general, anisotropic theories admit to more instabilities than those with an isotropic constraint. The anisotropic theory will sometimes yield slower growth rates for an isotropic instability. What is your feeling regarding the implications of the larger Pandora's box for EBT?

G. E. GUEST: It is clear now that, although anisotropy ($p_\perp >> p_\parallel$) may inhibit certain modes such as interchange modes, it permits new modes to occur and may lower thresholds or increase growth rates for others. The ballooning mode calculations by R. L. Miller illustrate the destabilization by $\beta_\perp$ for global modes, while the theory of Whistler modes illustrates the destabilization of high-frequency modes by anisotropy.

3. EXPERIMENTS

W. B. Ard, Session Chairman

The Ring Formation in Nagoya Bumpy Torus

M. Fujiwara, M. Hosokawa, H. Iguchi, T. Shoji,
M. Tanaka, H. Sanuki and H. Ikegami
Institute of Plasma Physics, Nagoya University,
Nagoya 464, Japan

1. INTRODUCTION

Nagoya Bumpy Torus (NBT) is the toroidal confinement device in which the plasma is produced, heated and stabilized by the electron cyclotron heating at four microwave frequencies of 18 GHz, 10.5 GHz, 8.5 GHz (main microwave power source) and 6.4 GHz. The size is very similar to EBT-1 device and the magnetic field strength is 1/2 of EBT-1 but it is possible to feed the maximum input power level up to 155 kW. One of the main objects of NBT is to study and obtain the scaling law of the plasma confinement by comparing the NBT (8.5 GHz, 3 kG) data with the result of EBT-1 (18 GHz, 6 kG) and EBT-s (28 GHz, 10 kG). The other purpose is to study the basic physics of bumpy torus plasma, that is to say, the mechanism of ring formation, the build up of plasma potential well and the physical process of the steady toroidal current generation. In this paper the global behavior of the plasma is described briefly in section 2 and the experimental results are reported about the details of hot electron in section 3. In section 4 is illustrated the numerical result for drift surface.

2. MACROSCOPIC BEHAVIOR OF THE PLASMA IN NBT DEVICE

Nagoya Bumpy Torus consists of 24 toroidally connected mirrors with a 1.9 : 1 mirror ratio on the magnetic axis, which is shown in Fig.1. The major radius is 160 cm and the minor radius at the midplane is approximately 20 cm. It is possible to convert from circular torus to a race track configuration by the use of two 80 cm long straight mirror sections. The following are typical NBT machine parameters:

Magnetic field (maximum):	4 kG (midplane) - 8 kG (mirror)
Magnetic field power:	4 MW
Plasma volume:	500 liters

Major radius:	160 cm
Average aspect ratio:	10 : 1
Microwave power sources:	20 kW cw maximum at 18 GHz 30 kW cw maximum at 10.5 GHz 100 kW cw maximum at 8.5 GHz 30 kW cw maximum at 6.4 GHz

The microwave power is divided into 24 equal parts and fed to each mirror section. The mode at the injection ports is ordinary mode rather than extraordinary one.

Magnetic field lines and constant $|B|$ lines in a plane of the median horizontal cut are shown in Fig.1. The hatched regions correspond to the 1st and 2nd cyclotron resonance zone for 8.5 GHz: plasmas are produced and heated at the fundamental resonance and the energetic electrons are generated at the second harmonic resonance to form a hot electron ring in the midplane.

At the present stage, the main diagnostics are listed in the following: (1) Single channel, 8 mm, 6 mm, 4 mm microwave interferometers to determine the average electron density. (2) Scintillator (NaI)-Photomultiplier-Pulse height analyzer system and X-band microwave radiometer to measure the energy and density of the hot electron rings. (3) Diamagnetic coils and Hall elements to estimate the magnetic field produced by diamagnetic currents of the hot electron rings. (4) Visible spectrometer to measure the intensity of H_α line. (5) Movable Langmuir probe for the radial distribution of the density and plasma space potential. (6) Li beam probing instrument to determine the local electron density. (7) Toroidal loops (Hall elements) to measure the total (the spatial distribution of toroidal) currents.

The bumpy torus plasma is supposed to be stably confined by means of the average minimum magnetic field owing to the high β hot electron ring encircling the plasma surface. This mode of operation is called T-mode. In the higher pressure regime X-ray intensity is weak (the intensity is plotted in the logarithmic scale) and the radial magnetic field B_r produced by hot electron rings is not detectable. The plasma is produced and isolated within each simple mirror section with rather poor confinement: C-mode operation which stands for cold plasma. With decreasing the gas pressure, X-ray and microwave radiation are enhanced indicating the formation of hot electron rings. In this region, the plasmas are quiescent

($\tilde{n}\ell/n\ell$ is less than 5 %) than those in C mode ($\tilde{n}\ell/n\ell$ is 20 %). The value of $\int n_e d\ell$ is almost constant, while the intensity of H_α line, i.e., $\int n_e n_o \langle\sigma v\rangle_{ex} d\ell$ decreases with the gas pressure. These facts mean that the plasma is stably confined by means of average of minimum magnetic field owing to the high β hot electron ring (T-mode). When the gas pressure is further decreased, strong and spontaneous X-ray bursts are observed and the plasma becomes unstable macroscopically (M-mode). The dependence of the transition between C, T and M modes on the microwave input power and the ambient gas pressure is shown in Fig.2.

In Fig.3 are the dependence of the beta value of hot electron ring β_{hot} and X band microwave radiation on the microwave input power. The β_{hot} is estimated from the diamagnetic signal assuming the reasonable shape of the hot electron ring as is described in the later section. As is shown in Fig.3, at the region of the high microwave input power, the β_{hot} is saturated. If 10.5 GHz microwave power is fed additionally with fixed 8.5 GHz power, the β_{hot} increases remarkably. These results are shown in Fig.4. In the case of 1.6 kA, the β_{hot} is not increased because there is no second harmonic resonance for 10.5 GHz. Figure 5 indicates the increase of hot electron density n_h and β_{hot} ($\propto n_h T_h$) with the input power, where n_h and T_h are evaluated from the photon number measurement and the pulse height analysis by NaI scintillator. The spatial distribution is determined from the result measured by the movable ionization chamber. It is found from the energy analysis of hard X-ray that the temperature of the hot electron does not depend so much on the input power ($T_{hot} \simeq 100$ keV).

3. DETAILED MEASUREMENT OF THE HOT ELECTRON RING'S STRUCTURE

It is very important to know the structure or the spatial distribution of hot electron rings from the view point of the equilibrium of ring itself and the MHD stability of the toroidal plasma. It is well known that the hot electron ring is produced at the second harmonic cyclotron resonance region, but the radial distribution or the axial length of the hot electrons is not clarified. The energy of the hot electrons is estimated to be 100 keV from the NaI scintillator measurement, so such a high energy particle moves due to the grad-B and curvature drifts of the vacuum magnetic field of the bumpy torus configuration without the effect of plasma potential (E x B drift motion) which is the order of a hundred volt. Strictly speaking,

the effects of modification of vacuum magnetic field due to high β hot electrons should be considered, however, we now neglect these effects. In Figs.6-9 are shown the magnetic field line and the mod-B contours in NBT. This figure shows that the mirror ratio at the magnetic axis is 1.9, which is a little smaller than that in EBT-1. The distribution of hot electrons is measured by inserting an ionization chamber from the inside and the outside of torus along the radial direction. The typical case is shown in Fig.7. In such a way, the distribution of hot electrons can be determined within the error of the order of $2\rho_{HL}$. We should note that the signal of the ionization chamber from the outside shows the single peak, on the other hand, the double peaks are observed by the signal from the inside. The diagnostic system of radiometer of X-band microwaves and the diamagnetic loop are laid on at the same cavity. Figure 7 shows that P_{rad} decreases gradually as the ionization probe scrapes off hot electrons. Little changes are measured in P_{rad} and the diamagnetic signal at the inside second peak. In Fig.10 are shown the dependence of B field on the location of peak for ionization probe signal, and the characteristic positions, where P_{rad} and diamagnetic signal start to decrease. In this case, the second peak moves little, and locates near X = -12.5 cm. This position is in agreement with the axis of drift surface for particles with $v_{\parallel}/v = 1$ obtained by the calculation of drift surface and tracing of electron beam. When the microwave source, which are fed to the cavity and the neighboring cavities, are taken off, the second peak is only measured. Then, this second peak depends essentially on the toroidal transit hot electrons. Let us consider the other peaks. Since P_{rad} and the diamagnetic loop signal decrease when the ionization probe locates at the positions of these peaks, particles associated with the peaks contribute to the formation of hot ring. The position of the outside peak locates at $\omega \sim 2\omega_c$, however, the inside peak shifts from this location ($\omega \sim 2\omega_c$).

The present results are summarized as follows:

i) If this position coinsides exactly with that of hot ring, the pitch angle can be obtained from the drift surface corresponding to the inside and outside peaks using the results calculated in section 4. Since this drift surface is given by the normalized pitch angle, and $W_{\perp}/W$ is $\mu B_{axis}/W$, then at the position of hot ring, $W_{\perp} = \mu B_{ring}$, and the value of $W_{\perp}/W$ becomes a little smaller. The distance for electrons making hot ring to spread along the z-axis is expressed by the dotted region in Figs.6-9.

ii) If this measurement contains an error for position of the order of $2\rho_{HL}$, the shape is still remained but the location of the hot electron ring shifts toward $\omega \sim 2\omega_c$ region.

Finally we may conclude that the axial length of hot electron ring is comparable to the radius of hot electron ring. This is justified by the universal situation for several values of radius of the diamagnetic loop, r = 20 cm, 25 cm and 50 cm.

4. THE MOTION OF CHARGED PARTICLES IN THE BUMPY TORUS

The guiding center drift motion of charged particles is studied numerically for the bumpy torus configuration. The drift surface is closed by the poloidal drift motion due to the field gradient and the curvature of the magnetic field line, because the magnetic field lines do not have the rotational transform in the bumpy torus. In an infinite bumpy cylinder the drift surfaces are concentric circles for particles with any pitch angle. The drift surface in the toroidal bumpy field, however, is affected greatly by the toroidal effect, especially the axis of the drift surface is shifted towards the major axis by large amount for passing particles whose poloidal drift motion is cancelled almost all during the passage through the successive good and bad curvature region of liked mirrors. Generally the motion of the guiding center in a vacuum magnetic field is described by the following quantity if the longitudinal motion is periodic,

$$J = \oint m v_{\parallel} d\ell \tag{1}$$

where m and $v_{\parallel}$ are the mass and the velocity along the field line, respectively. The effective drift distance is given by

$$\langle\delta\rangle = \frac{m}{eB} \nabla J \times B \tag{2}$$

where e, B and b are the charge, magnetic field strength and unit vector along the field line. The equation (2) means that the particle moves along the constant J surface. Figure 1 shows the constant J surfaces at the midplane of the mirror computed for the particles with various pitch angle. Figure 11(a) is the drift surface (J = constant surface) of $v_{\perp}/v = 1$ particles, which move along the constant B surface according to the conser-

vation of the first invariant $\mu = v_\perp^2/B \approx v^2/B$. It is shown in Fig.11(e) that the particle with $v_\parallel^2/v^2 = 1/2$ which started from the position near the minor axis can go around the torus, but the particle with the same pitch angle, whose starting position is far away from the minor axis, is trapped in the single mirror. In this case, passing particles drift vertically due to the toroidal effect and go into the region where the mirror ratio is larger than that at the minor axis. Finally the parallel velocity $v_\parallel$ is nearly equal to zero and the particle spends an excessive amount of time at the mirror throat, where the particle drifts along the constant B surface, and forms the closed drift surface. On the other hand the particle trapped in the single mirror drift into the region where the mirror is shallow and also stays for long time near the mirror throat. The drift surface is approximately given by the constant B surface, which is located very closely to the outer boundary of the untrapped drift surface. The fact above described is completely different from the result calculated by Hedrick et al.. Figure 12 shows the effective figure of merit F for the confinement of charged particles in a standard bumpy torus. The quantity F is defined as the ratio A_c/A_L and A_c are the area surrounded by the shadow of the discharge chamber wall of the mirror throat projected to the midplane along the magnetic field line, which means the limiter and the area of the largest contour which does not intercept the shadow of the limiter. The mirror ratio of the NBT device at the minor axis is 1.9 and the boundary between trapped and untrapped region is $v_\parallel/v = 0.745$. The axis of the drift surface does not shift so much for the particles deeply trapped in the single mirror. The quantity F is a decreasing function of $v_\parallel/v$, because the poloidal drift velocity decreases with $v_\parallel/v$. F is nearly equal to zero at the transition layer of trapped to untrapped region, where the drift motion is dominated by the toroidal drift and the trajectory of the particle drift is not closed. The strong peak of F at $v_\parallel/v \approx 0.75$ corresponds to the well confined passing particle due to the new fact as is mentioned above.

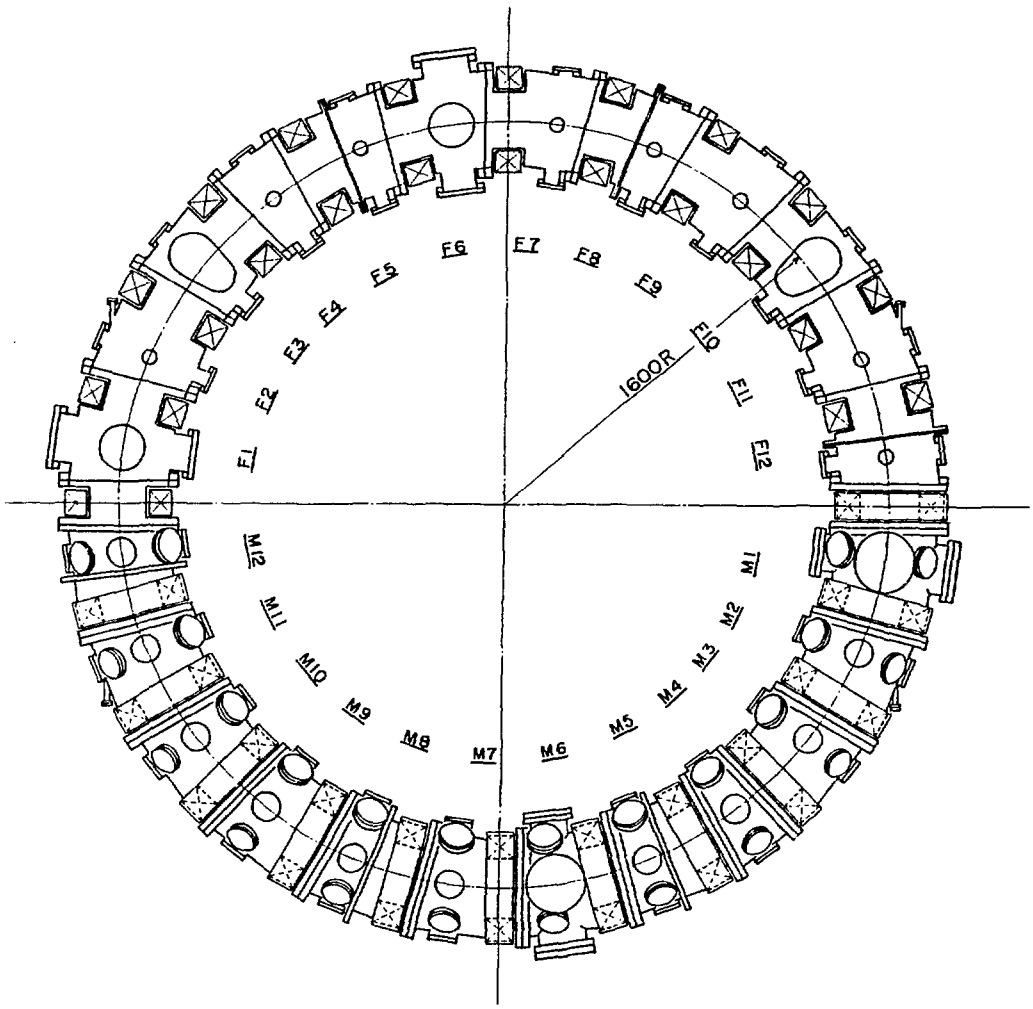

Fig.1. A schematic view of Nagoya Bumpy Torus.

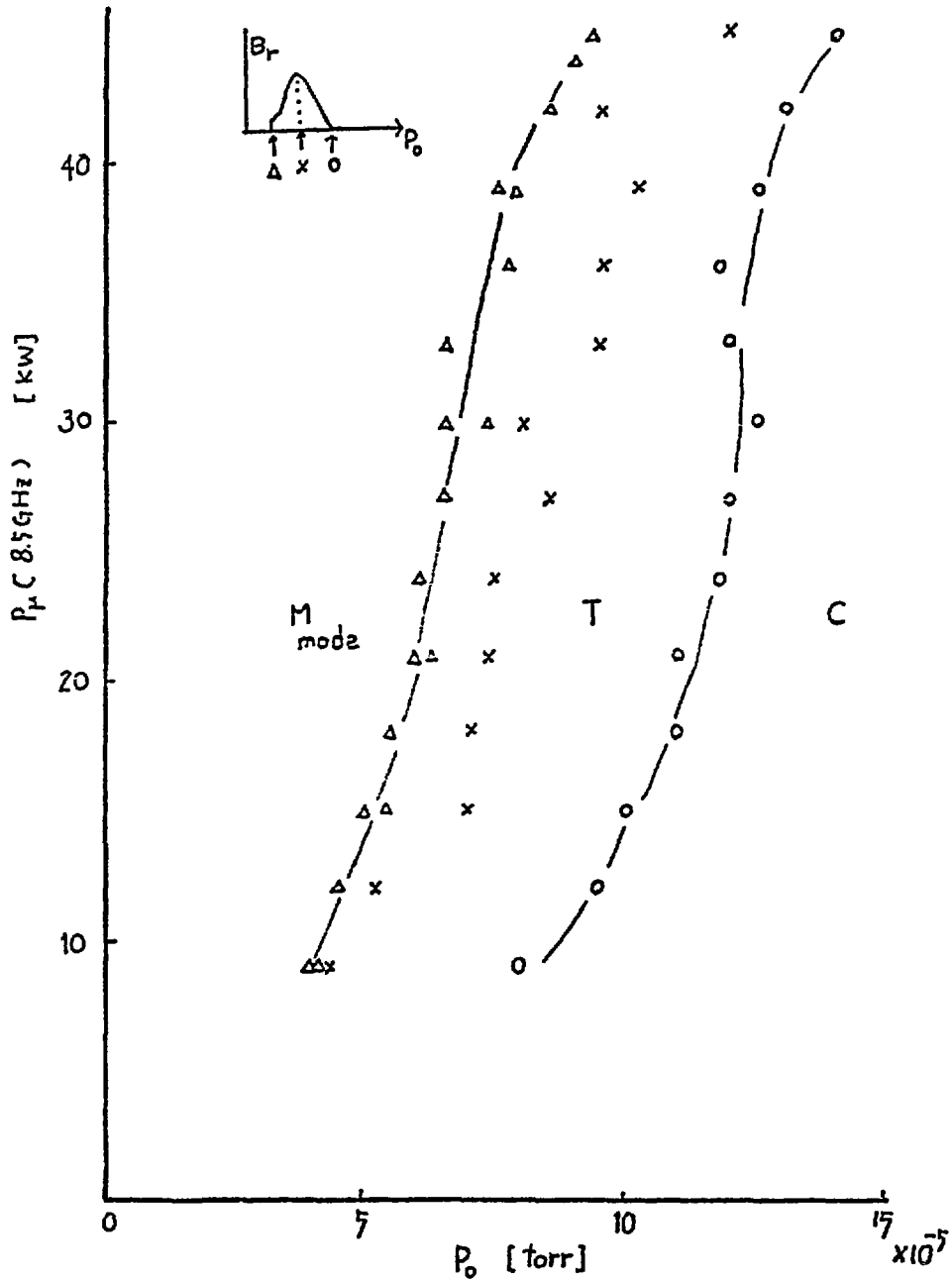

Fig.2. Dependence of the transition between C, T and M modes on the microwave input power and the ambient gas pressure.

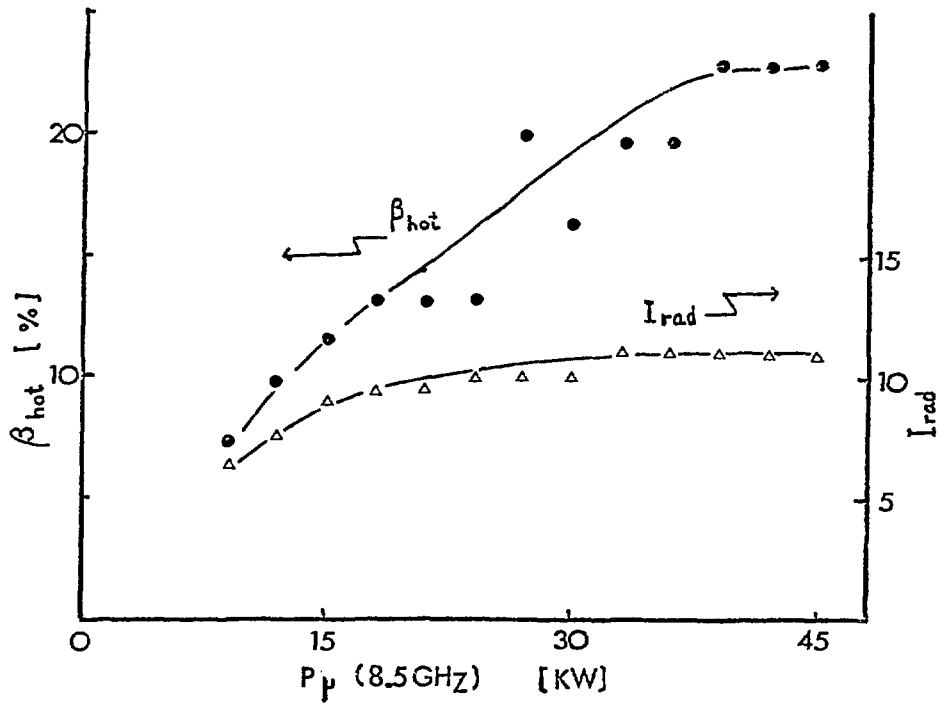

Fig.3. Intensity of X band microwave radiation, diamagnetic signal and radial magnetic field produced by hot electron annulus vs. microwave input power.

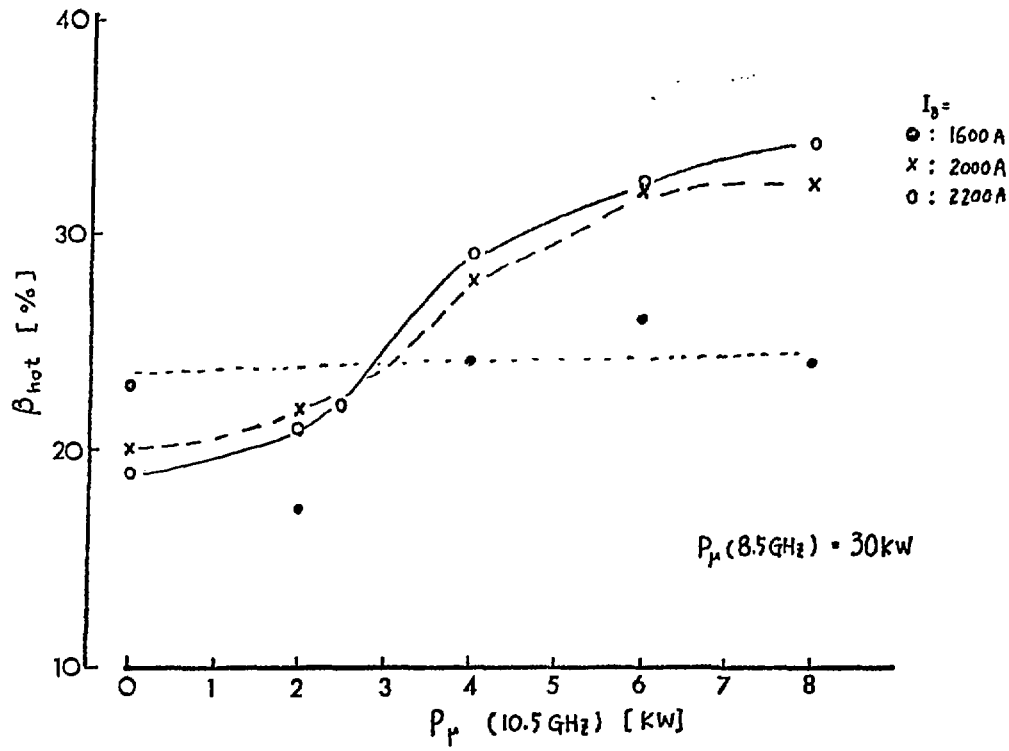

Fig.4. The β value of hot electrons (estimated from diamagnetic measurement) vs. the microwave input power at 10.5 GHz in addition to the input power of 30 kW at 8.5 GHz.

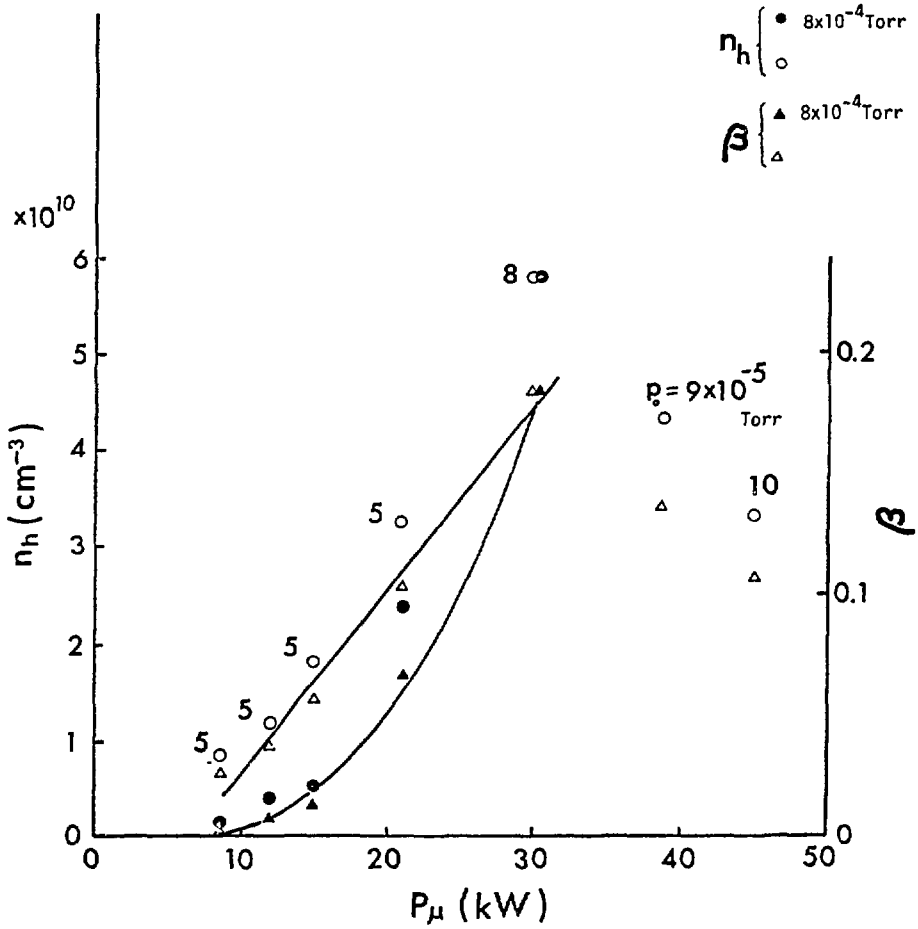

Fig.5. The density and the β value of hot electrons obtained from the hard X-ray measurement.

FIG.6

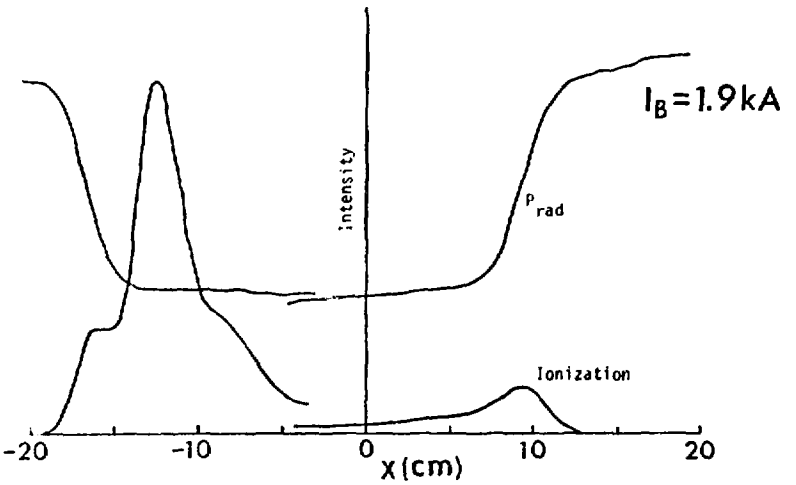

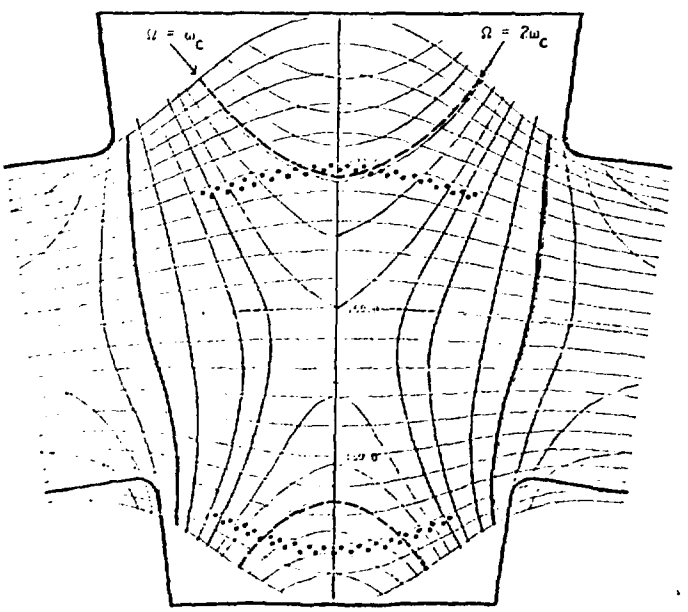

Figs.6-9. Median horizontal cut view of a single sector of NBT showing the contour of const. |B| and the magnetic field lines. The position of hot electron ring is denoted by the dotted region. P_{rad} and the ionization chamber signal are also shown in figures.

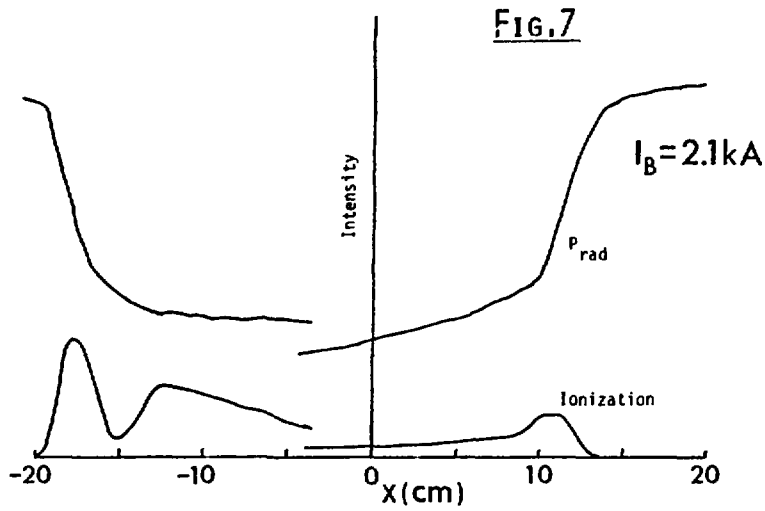
FIG.7
I_B=2.1kA
Intensity
P_{rad}
Ionization
-20
-10
0
10
20
X(cm)

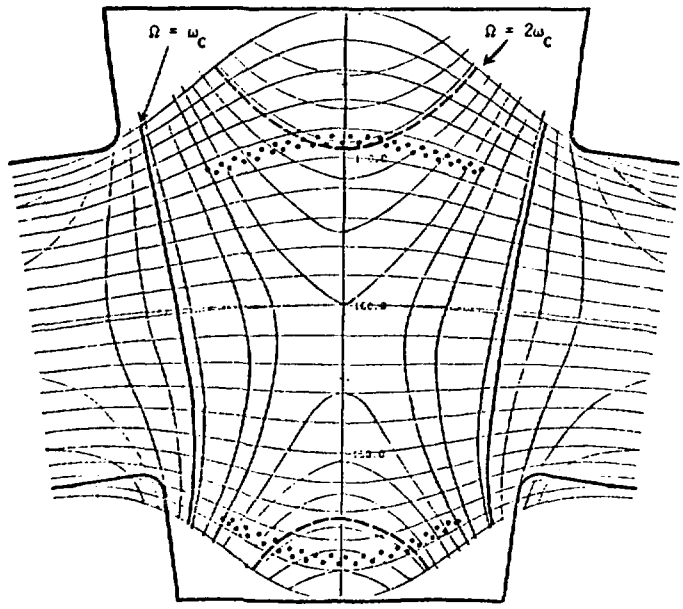
$\Omega = \omega_c$
$\Omega = 2\omega_c$

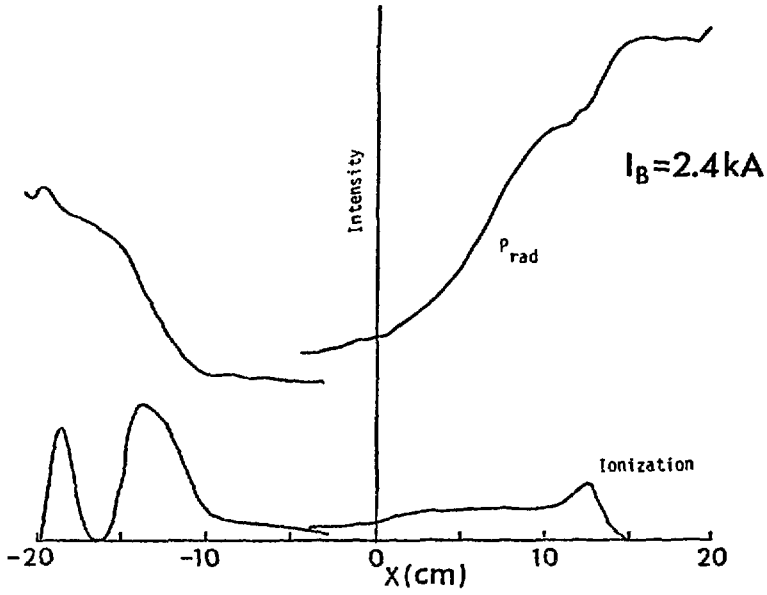
Intensity
I_B=2.4kA
P_{rad}
Ionization
-20
-10
0
10
20
X(cm)

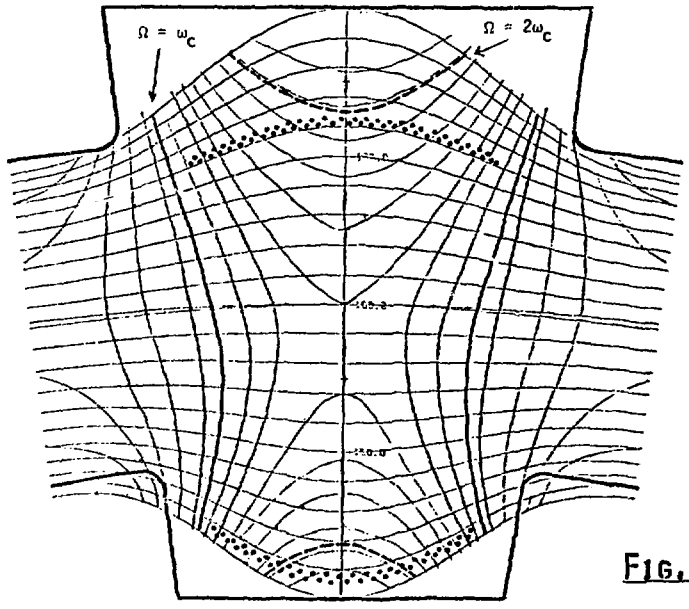
$\Omega = \omega_c$
$\Omega = 2\omega_c$

FIG.8

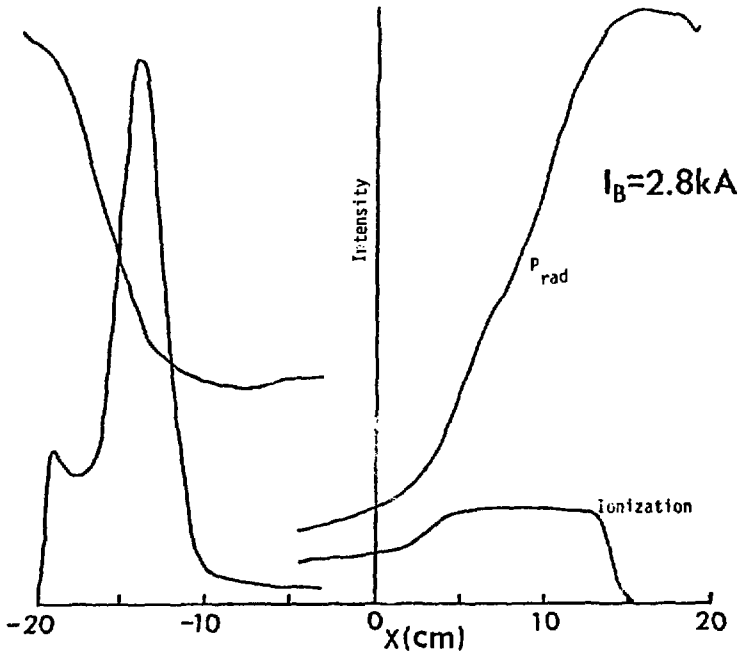
Intensity
I_B=2.8kA
P_{rad}
ionization
-20
-10
0
10
20
X(cm)

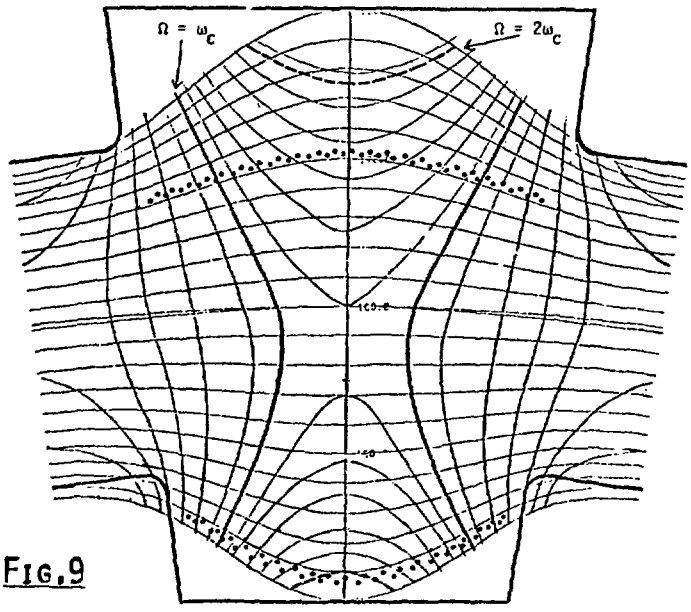
$\Omega = \omega_c$
$\Omega = 2\omega_c$

FIG.9

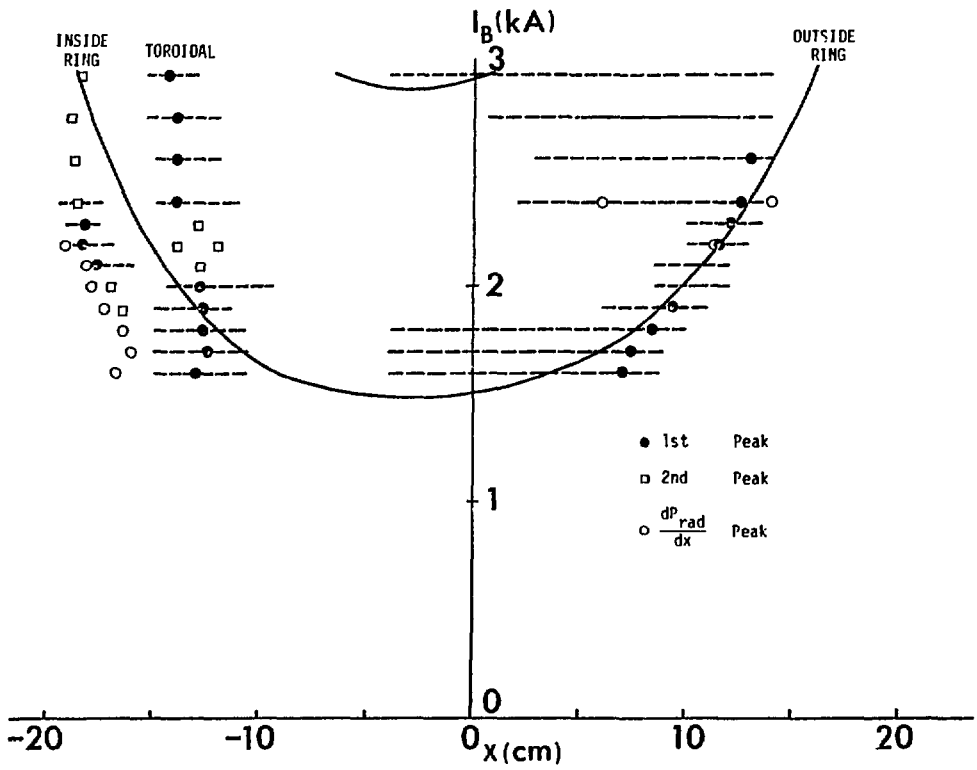

Fig.10. The relationship between the magnetic field strength and the radial positions where the intensity of the ionization chamber signal is peaked and the X band microwave radiation disppears.

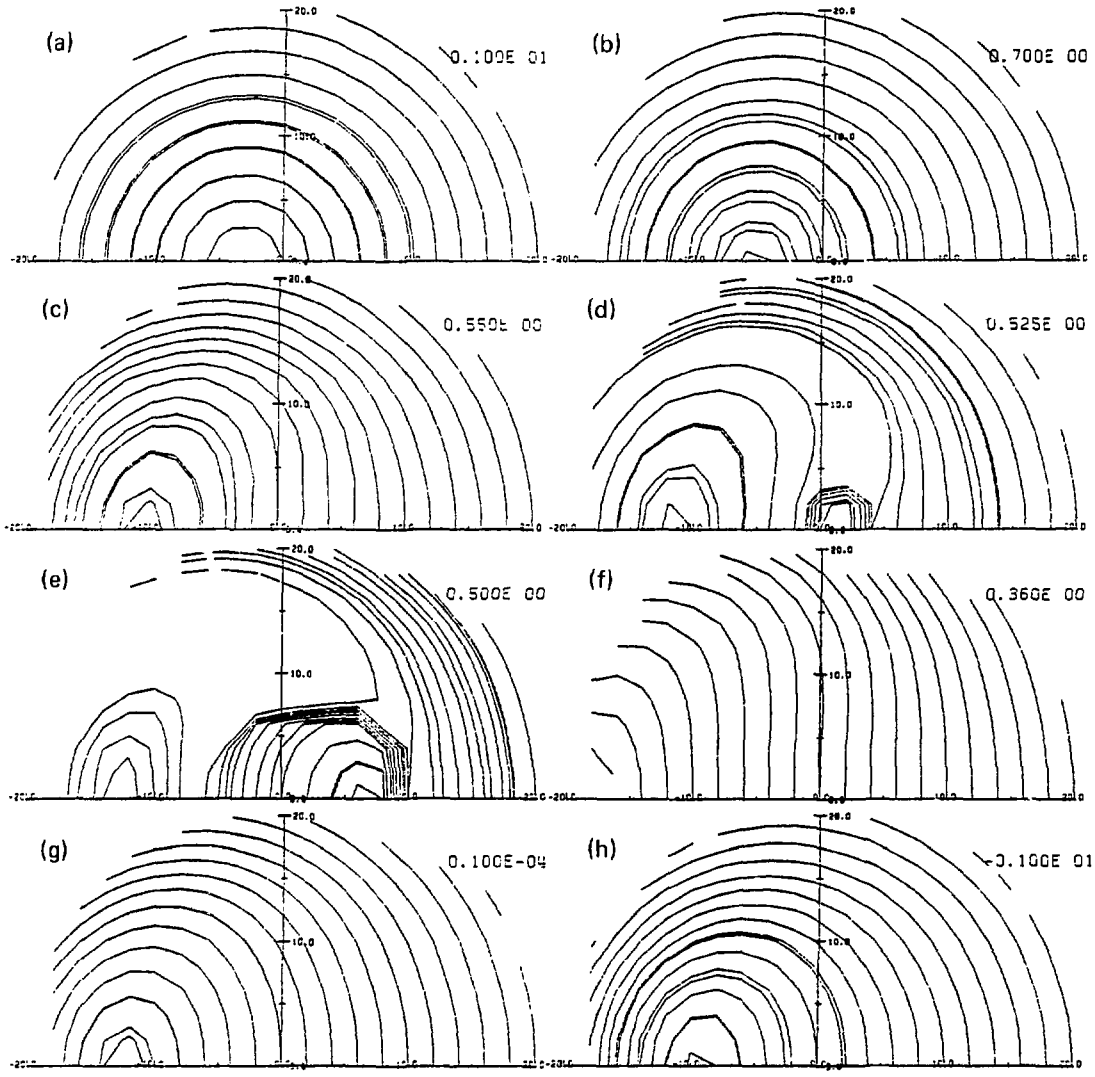

Fig.11(a)-(g). Drift surfaces for particles with several values of $W_\perp/W$, where $W_\perp$ is given as μB_{axis}.

Fig.11(h). The contour of the constant U defined by $\oint d\ell/B$.

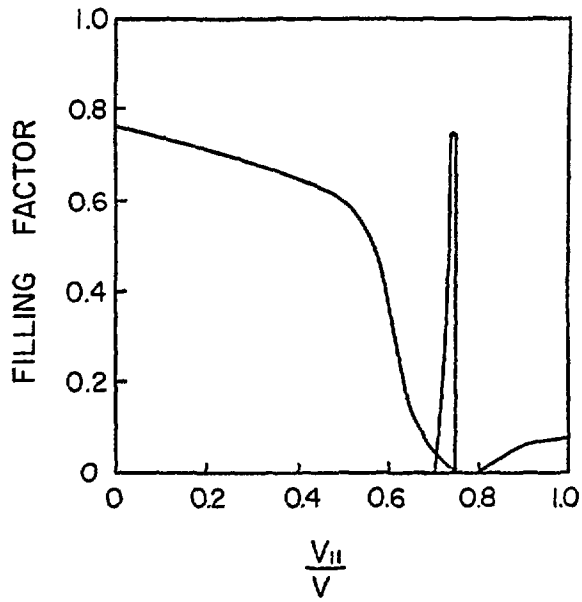

Fig.12. *The filling factor is plotted as a function of* $v_{\parallel}/v$ *in the* bumpy torus.

DISCUSSION

G. HASTE: When the ionization chamber probe is inserted from the outside, the current shows a peak and then a slow decrease. Could you comment on this behavior?

M. FUJIWARA: The variation of the drift surfaces with pitch angle is such that $v_{\parallel}/v = 0$ particles describe a circle. As the pitch angle increases, the particles drift on surfaces that are tangent to the $v_{\parallel}/v$ surface on the inner side, but they are displaced inward on the outer portion. The ionization chamber thus encounters a radial variation in the hot electron density, which is due to the variation in pitch angles.

J. PIPKINS: Can the ring location being not located exactly at the $2\,\omega_{ce}$ value of the magnetic field be due to $kv_{\parallel}$ Doppler shift?

M. FUJIWARA: No.

V. K. TRIPATHI: Why is the change in β_{hot} due to additional microwave source not linear with the power?

H. IKEGAMI: It may be linear/nonlinear depending on the size of the error bars.

DIAMAGNETIC MEASUREMENTS FOR EXPERIMENTAL DETERMINATION OF EBT RING PARAMETERS

Kenneth H. Carpenter
Dept. of EE, University of Missouri - Rolla

Introduction

One of the experimental approaches to obtaining information about the hot electron annuli in Elmo Bumpy Torus (EBT) is through measurement of the annulus diamagnetic flux that couples to pickup coils. (The coils' induced voltages when the microwave plasma heating is turned off are integrated to give signals proportional to flux.) Use of large diameter pickup loops gives a total diamagnetic flux measurement, while use of small diameter coils gives a measurement of a flux density vector component. These measured values can then be related to the parameters of a mathematical model for the annulus to obtain physically interesting quantities such as stored energy, energy density (β), and length along the toroidal direction. Unfortunately, the constraints that pickup coils must be in physically accessible locations and outside the plasma itself yet near enough to the annulus to allow detection of more than the far field of a dipole - all with useable signal to noise ratio - limits the information that can be obtained from diamagnetic measurements quite severely. Fortunately, it is possible to obtain diamagnetic measurements of annulus "perpendicular" energy, which should be close to total stored energy. The length of the annulus in the toroidal direction also seems diamagnetically observable, and it may be possible with better mechanical access (e.g., through split mirror coils) and the aid of theoretical constraints on the annulus model to determine the other parameters as well.

Annulus mathematical model

Figure 1 shows the presumed location of the annulus for a typical EBT plasma. Although the detailed electron distribution function would be quite complicated, a model for the distribution having a minimum of free parameters has been

adopted for calculational purposes as a first approximation. This model consists of a uniform dipole moment density M, due to electrons, everywhere between two concentric circular cylindrical surfaces of length L having the inner surface with radius R1 and the outer with radius R2. The (dia)magnetic effect of this distribution is entirely represented by a surface current density $j_s = M$, azimuthally directed about the cylindrical surfaces with inner and outer currents in opposite directions. The effect of drift currents is represented by adding a drift component to the surface currents, yielding unequal inner and outer current densities. The cylinders are centered in the EBT cavities with axes tangent to the midplane vacuum field - but the cylinder axis is offset from the geometrical cavity center to the center of single particle, high pitch angle, drift orbits. The parameters of the model are then L, R1, R2, and the current densities, j1 and j2. The number of free parameters can be reduced by theoretical constraints such as relating drift current to dipole current and field gradient, or forcing the mean radius $RR = \frac{1}{2}(R1 + R2)$ to be at the heating resonance position. This model has been used for energy and length observations as will be discussed below.

Energy measurement

The diamagnetic measurement of annulus perpendicular energy is discussed elsewhere (see: K.H.Carpenter, R.A.Dandl, M.W.McGuffin, Calibration of a Diamagnetic Diagnostic for Stored Energy of High Temperature Electron Annuli in Elmo Bumpy Torus (EBT), ORNL/TM, to be published) and only an outline will be given here. Two large flux detecting loops are placed about each cavity at the location shown in Fig. 1. The signal from these loops is integrated by a carefully balanced analog circuit which has compensation for the fluctuations of the vacuum toroidal field. The output from the integrators is recorded both on analog charts and digitally. The resulting output trace for one cavity for a typical plasma is shown in Fig. 2.

To get the value of stored energy from these flux values requires the following equations. First the kinetic energy of a single electron in a magnetic field B is given by

$$K.E. = \mu B \frac{(v_\perp^2 + v_\parallel^2)}{v_\perp^2} \left[1 + \frac{1}{1 + (m_o c^2/\frac{1}{2}K.E.)} \right] \tag{1}$$

where μ is the electron's orbital magnetic moment, $v_\perp$ and $v_\parallel$ are the velocity compenents and m_o is the rest mass. The factor μB is the "perpendicular" energy of the electron, and for the cyclotron resonance heated annulus of EBT one presumes that the pitch angle factor and relativistic factors are near unity. The dipole moment density of the model is simply $M = n_e \mu$ so that the total annulus perpendicular energy in the model is

$$W_\perp = \int \underset{\sim}{M} \cdot \underset{\sim}{B} \, dv \approx j_s B_R L R_T 2\pi R_R \tag{2}$$

where B_R is the field at heating resonance and $R_T = R2 - R1$.

The drift current can be taken into account by noting that for a single electron with $v_\perp >> v_\parallel$,

$$v_d = \tfrac{1}{2} v_\perp r_c \frac{|\nabla B|}{B} \tag{3}$$

One can represent the combined total drift of all the electrons as another surface current density

$$j_d = R_T e n_e v_d \tag{4}$$

which can be ratioed to j_s to give

$$\frac{jd}{js} = R_T \frac{|\nabla B|}{B} = \frac{\Delta B}{B} \tag{5}$$

where ΔB is the change in B over the thickness of the model annulus. (If ∇B is not constant, as for finite β cases, this represents the average drift current - which should be all that matters for the diamagnetic signal.)

In the model we set $j1 = j_s - \frac{1}{2} j_d$ and $j2 = j_s + \frac{1}{2} j_d$ to include the drift effect for energy measurements.

The basic formulas for coupling the current sheets to the pickup loops are simple in principle but complicated in practice

and require double numerical integration. The two integrals are found in the expression of vector potential of a cylindrical current sheet:

$$A_\phi(\rho,z) = \frac{\mu_o j_s}{\pi}\left(\frac{a}{\rho}\right)^{\frac{1}{2}} \int_{u=z-\frac{1}{2}}^{z+\frac{1}{2}} k^{-1}\,[(1-\tfrac{1}{2}k^2)K - E]\,du$$

$$k^2 = \frac{4a\rho}{[(a+\rho)^2 + u^2]}\,, \qquad (6)$$

and the flux linkage of a loop: (see first reference for details)

$$\Phi = 2b \int_0^\pi \rho_A^{-1}\, A_\phi(\rho_A, z_A)(x_b \cos\alpha + b\cos\alpha)\,d\alpha$$

$$\rho_A^2 = (x_b + b\cos\theta\cos\alpha)^2 + (b\sin\alpha)^2$$

$$z_A = z_b - b\sin\theta\cos\alpha\,. \qquad (7)$$

In one sense, a triple numerical integration must be performed, if one includes the elliptic integrals K and E.

For each set of annulus parameters the model "calibration factor" between integrator output voltage and annulus energy must be obtained by calculating and combining six of these numerical double integrations - for the inner and outer current sheets in the EBT cavity having the pickup loops and also for the cavities on either side, since significant signals are present from the neighboring annuli. A code has been written to carry out this calculation on the PDP-10 computer. In this code the free parameters are L and R_T with RR calculated as the resonant radius, and j_d/j_s taken as outlined above using ΔB of the vacuum field in the midplane. Plots of the resulting calibration factor versus these parameters are shown in Figs. 3 and 4. The lack of sensitivity to actual choice of R_T and L is a highly desirable result in the absense of reliable measurements of these parameters. This calibration factor can then be applied to the raw data from a plasma turn off to obtain a plot of perpendicular energy versus annulus as shown in Fig. 5 for a typical case.

Geometrical parameter measurements

The difficulty in determing the geometrical parameters of the annulus model from diamagnetic measurements is that at a distance, to first order, any current distribution looks like a magnetic dipole. Since pickup coils must be outside the plasma being measured this requires sufficient sensitivity and noise immunity to observe higher multipole moments. In an attempt to observe the annulus length on EBT a probe consisting of five 2 x 1 cm relay coils in a water cooled, L-shaped tube was inserted near the outside of the annulus as shown in Fig. 6. For a given distance from the cavity wall this gave a means of measuring the toroidal component of the diamagnetic B field at five points in space.

The drift and noise problems encountered with the integrators and this relay coil probe were substantial since the flux linkage was down by almost two orders of magnitude from that of the large flux loops encircling the cavity, in spite of the relay coils having thousands of turns. A reasonably usable set of data was obtained for one plasma condition with maximum microwave power while using three positions for the probe - at 1.5, 3.3, and 5.0 cm from the cavity wall. Only four of the relay signals were integrated at the time the data was taken, giving 12 values of the toroidal components of B. Eleven of these values were ratioed to the twelfth to eliminate absolute calibration problems, and these eleven values were then fitted to various combinations of the four model parameters, L, R1, R2, and (j1/j2), using a least squares procedure in conjunction with numerical field calculations in a computer code. Needless to say, the results were ambiguous. There are many sets of the four parameters that reproduce the observed data to the accuracy imposed by the noise and drift on the integrator outputs. In spite of this ambiguity in fitting the parameters, the length parameter L had nearly the same value for almost all the fits obtained that had physically reasonable values for the other parameters.

To further explore the reason for the results of this data fitting and to search for possible probe locations that would resolve the ambiguity, a computer code was written which would simulate a model annulus field (and include the effect of fields of neighboring annuli) and plot it in space. Figures 7 and 8 show plots produced by this code for two different sets of model parameters that fit the data. Note that the B vectors on the plots are nearly identical at the locations of the relay coil probe used for taking the data, and also note that the B vectors are also identical at all locations external to the EBT vacuum cavity and toroidal field coils. There is a hope, however, of eliminating the ambiguity by additional diamagnetic observations if a split mirror coil configuration is implemented which would give access for a pickup coil in the mirror throat. At that location different annulus parameters cause large changes in B.

The model annuli of Figs. 7 and 8 have nearly equal values of L. Figure 9 shows the result when the parameters of Fig. 8 are retained except that L is halved. Although the B vectors stay nearly the same at the two outer probe positions, at the innermost probe position (5 cm from the inside of the wall to the coil centers) the B vectors have measureable differences between the cases. This is the basis for determing the annulus length diamagnetically.

General observations and recommendations

Diamagnetic measurements on the EBT electron annuli are not without problems and limitations but do provide a means of determing annulus energy, and, to a limited degree, information on annulus toroidal length. The calibration of the energy measurement involves theoretical constraints for annulus mean radius and drift current effects, although the flux pickup loops used to measure energy, being in the approximate form of Helmholtz coils, are not particularly sensitive to the annulus geometry.

The observation of annulus toroidal length with the relay coil probe appears to be successful provided the probe is inserted close enough to the annulus. However, we note that for the position nearest the annulus (5 cm from the wall) used to obtain the sample set of data, the probe was already inserted far enough to be "skimming" the plasma of the actual (not the model) annulus. (See: R.A.Dandl, et.al.,Summary of EBT-I Experimental Results, ORNL/TM-6457, Oct. 1978, Sec. 2.2, p12.)

The code which best fit the model parameters to the relay coil probe data was written two years before the code carrying out the energy calibration calculation, and no provision was made in the former to include theoretical constraints between the parameters, such as the drift current - thickness relation. With proper theoretical constraints it may be possible to obtain unambiguous results for model parameters with diamagnetic probes in non-disturbing locations. In any event, there remains considerable work to be done in the area in each of theory, experiment, and data analysis.

Acknowledgements

The author wishes to thank R.A.Dandl and the entire staff of the EBT experimental group for the help, suggestions, and guidance given to this work, which was carried out while he was at Oak Ridge National Laboratory with the Computer Sciences Division.

ORNL-DWG 74-2066A-R2

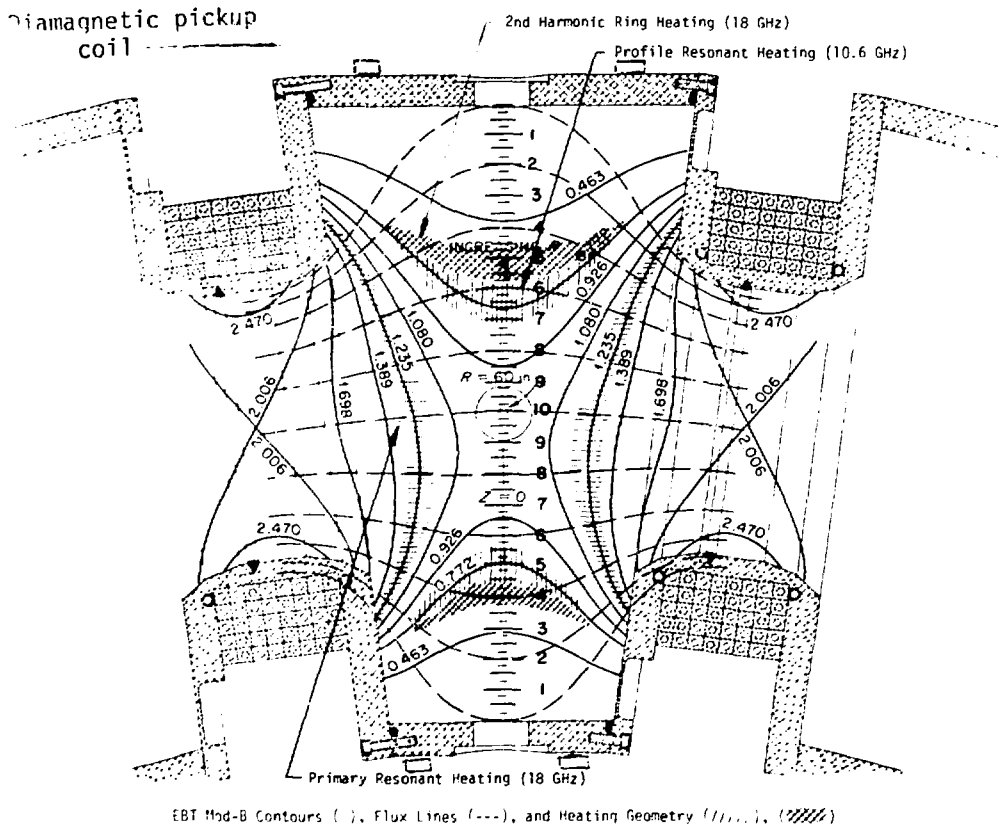

Figure 1. Section through EBT-I in the horizontal midplane. Solid lines indicate surfaces of constant B , and dotted lines indicate flux lines. Shaded areas are regions of cyclotron resonance for electrons when B_0 = 4.55 kG.

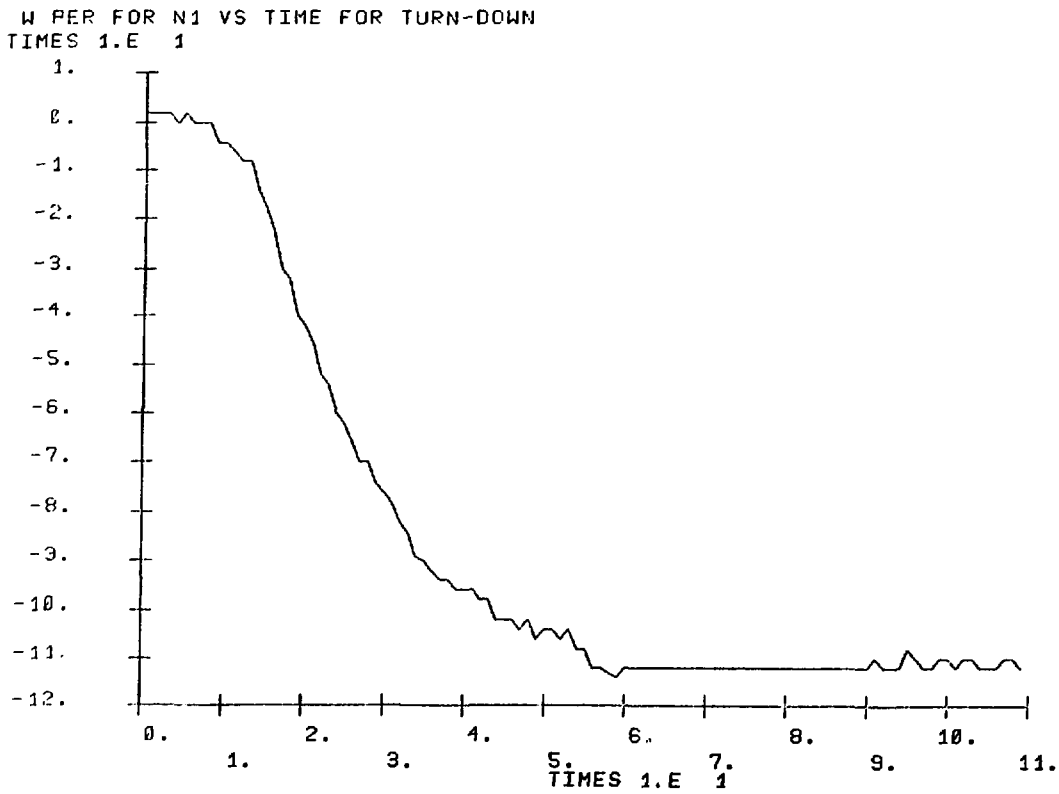

Figure 2. Output of flux loop integrator as digitally recorded on plasma turn-off

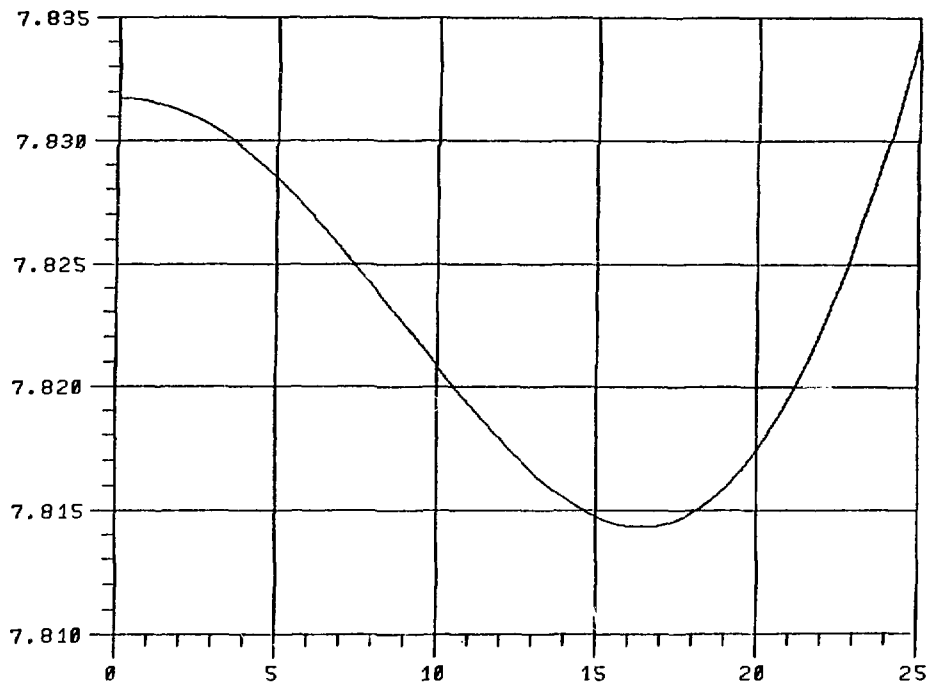

Figure 3. Implied annulus perpendicular energy (in Joules) vs annulus length in toroidal direction (in cm) for the current sheet model annulus with an assumed pickup coil signal of 1 millivolt-sec per turn, 5000 gauss midplane central field and 9-GHz heating resonance.

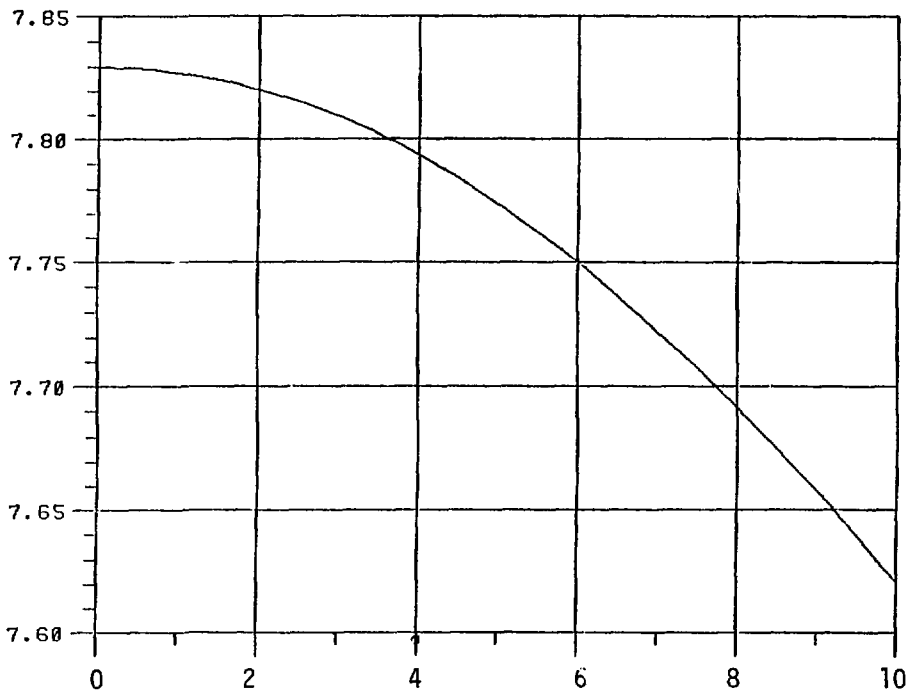

Figure 4. Implied annulus perpendicular energy (in Joules) vs annulus thickness (in cm) for the condition of Fig. 3.

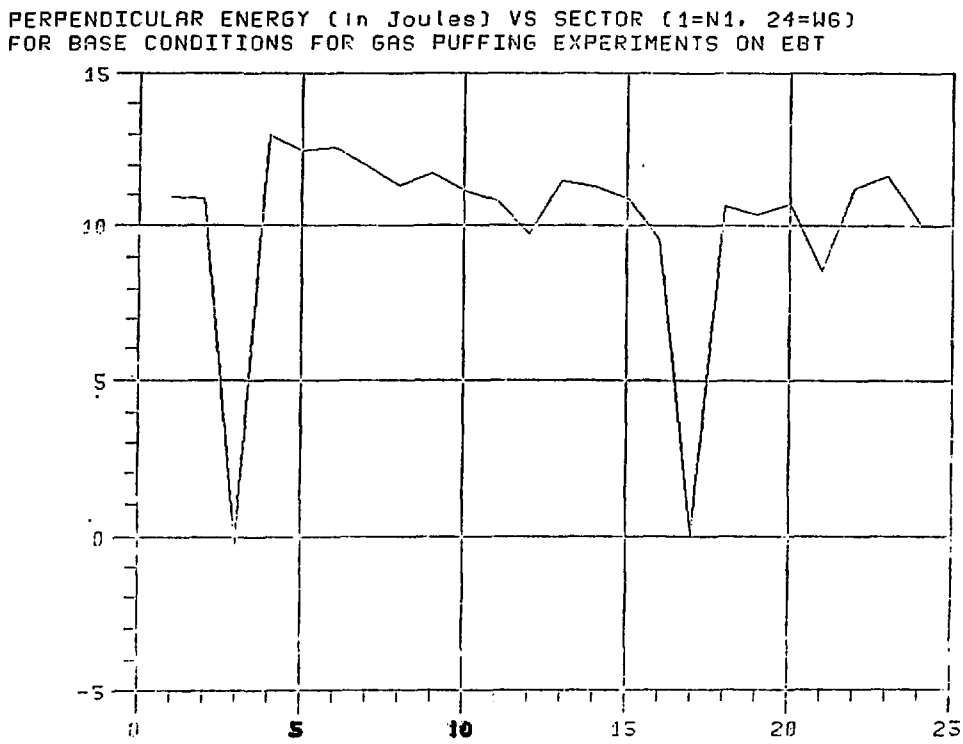

Figure 5. Computer generated, calibrated plot of perpendicular energy for all 24 EBT sectors for a typical condition (integrators not connected for sectors 3 and 17).

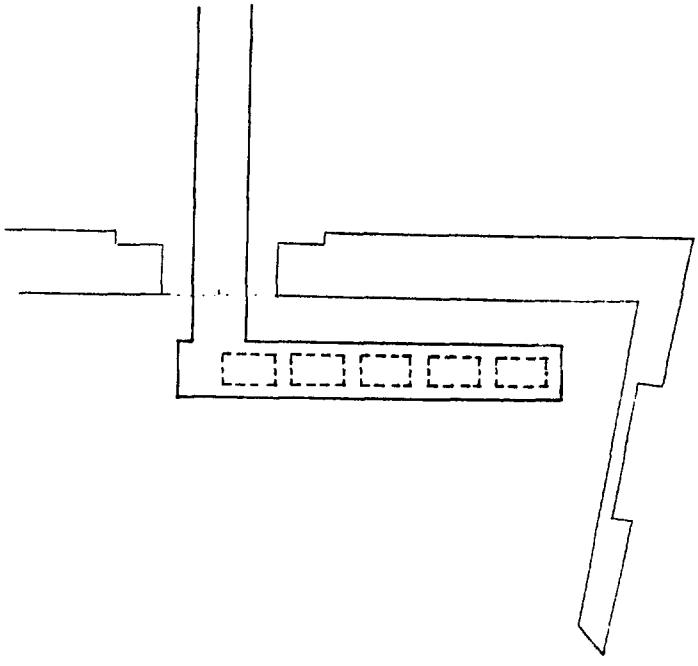

Figure 6. Relay coil diamagnetic probe in typical location near the outside of one cavity in EBT.

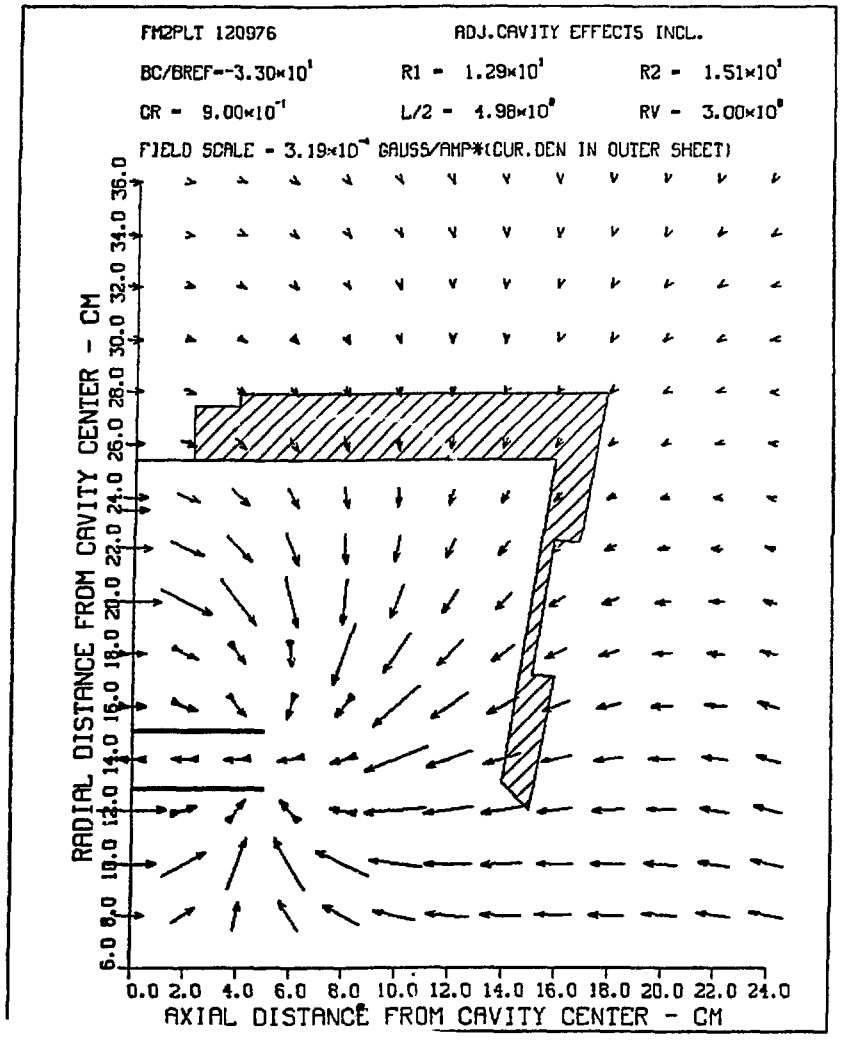

Figure 7. Magnetic field vectors due to a model annulus. (Length of single-ended arrows is proportional to local B. Double-ended arrows show direction of B only.)

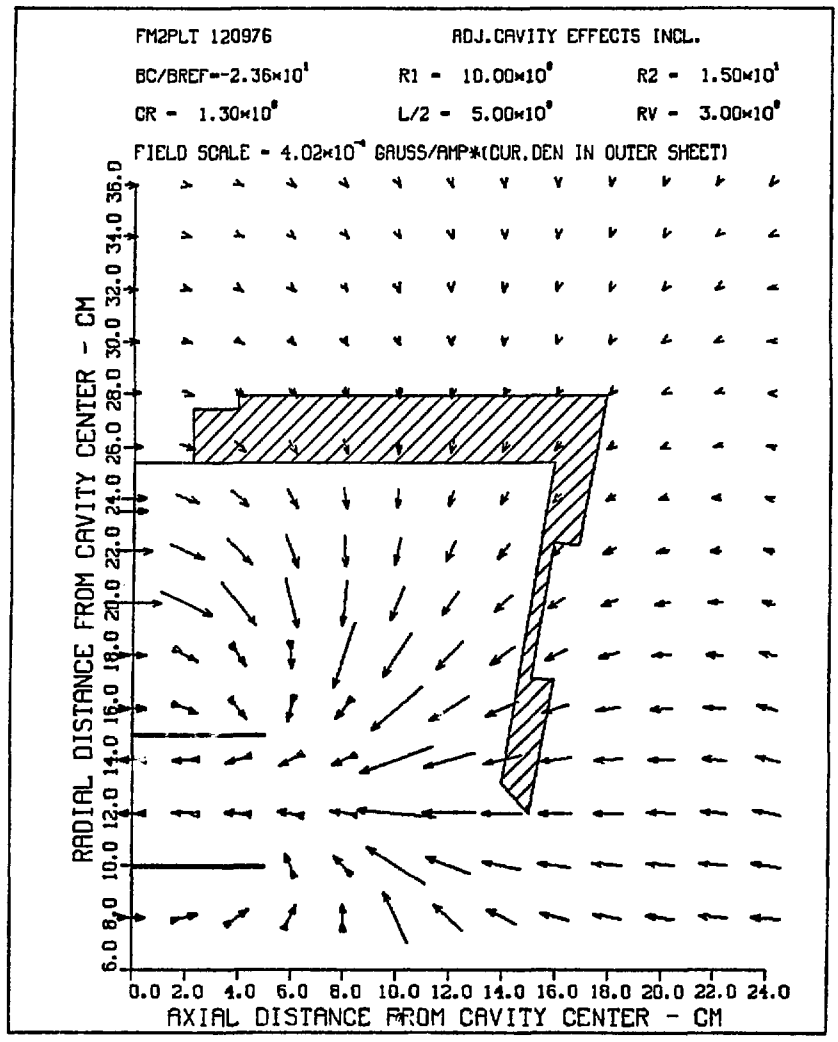

Figure 8. Magnetic field vectors as in Fig. 7 but for a different set of model annulus parameters.

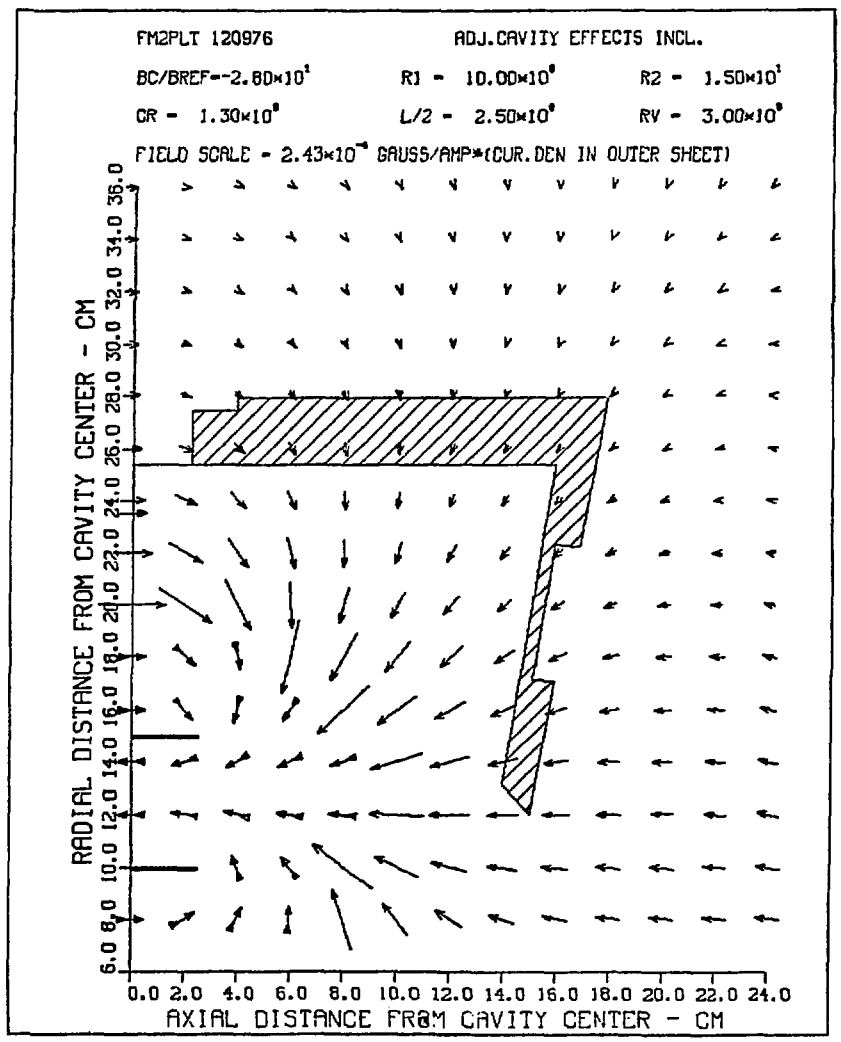

Figure 9. Field vectors as in Fig. 8, but with model annulus length reduced to one-half the value for Fig. 8.

DISCUSSION

H. IKEGAMI: Does nonequality of two opposite currents that constitute the hot electron ring change your results completely? Could you say the effect is within say, 30% or so in estimating size or energy?

K. CARPENTER: Nonequality due to drift currents does affect the energy value significantly. This is why its value is included by the theoretical j_d/j_s ratio. Nonequality due to a nonuniform radial distribution fraction would have a minimal effect on energy value due to lack of sensitivity to actual dipole locations in space.

T. SHOJI: What will be the change in β_h if you adopt a different current model (flowing in the inner side and outer side of the hot ring) and if you suppose the radial distribution of the hot electrons to be an M-shape (shell structure) rather than a ring, i.e.,

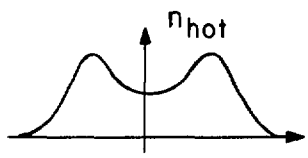

instead of

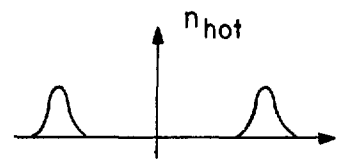

What do you think about the real distribution of $j_\perp$ in z direction?

K. CARPENTER: The method outlined here does not give a value for β_h. Additional information on geometry is essential to obtain β_h or distribution function details beyond this simple model annulus.

F. M. BIENIOSEK: How much is the coupling of diamagnetic signal from the neighboring rings compared to the ring you are looking at?

K. CARPENTER: A significant amount — in the figure of $W_\perp$ vs L, the rise for L > 15 cm is due to the adjacent annulus. I can't recall the exact figure, but the effect is about 20-30%.

J. PIPKINS: Could you get some information by turning off the microwave in adjacent cavities and observing the change in the field measurements?

K. CARPENTER: Yes, provided one is able to assume that the annulus in the primary cavity is not affected by the change in the adjacent one — which is probably not the case.

A. BOOZER: The total perpendicular current in a plasma is given by $\vec{\nabla} \times \overleftrightarrow{P} = \vec{j} \times \vec{B}$, with $\overleftrightarrow{P}$ the $p_{\parallel}$, $p_{\perp}$ pressure tensor. This result is essentially independent of the distribution function.

K. CARPENTER: The simple cylindrical model was chosen for ease of calculation. Results for energy calibration using this model show independence of the model parameters, which in turn imply independence from the distribution function.

R. A. DANDL: The uncertainties in ring modelling make the calibration of your ring energy ordinate (plot of $W_{\perp}$ vs pressure) somewhat questionable. In the dipole model calculation of ring energy, the values of $W_{\perp}$ are considerably larger. Also the nonzero net poloidal current further complicates the calculation. At low pressures where the toroidal plasma $n\ell$ starts to drop, $W_{\perp}$ is still increasing but the rings are now much noisier.

K. H. CARPENTER: The model used to calculate $W_{\perp}$ is that of two current sheets. The radial extent and the length of these current sheets can be varied at will in the computer code, down to arbitrarily small (dipole-like) lengths. However $W_{\perp}$ is relatively invariant as the length of these sheets is changed by a factor of 100 (from 0.1 to 10 cm), varying by less than 1%. A much bigger error (50%) is incurred by neglecting rings in neighboring cavities.

The net poloidal current in the annulus is represented in the model by making the outer current sheet of greater magnitude than the inner. In order to produce a flux cancellation effect that would cause the perpendicular energy implied by the model to be significantly too low, a source of net poloidal current would have to exist with a direction opposite to that of the drift current due to high pitch angle particles in the midplane. In addition, the magnitude of this "reverse drift"

current would have to be in the range of 5 to 20% of the annulus equivalent surface current to produce significant flux cancellation. We have no basis for postulating such a source. The model itself may be inadequate to represent the rings, but in so far as it is adequate, the values for $W_\perp$ follow in a straightforward manner.

C. L. HEDRICK: 2-D magnetic equilibrium code can be used to explore the ring-β question. This was done in the past with R. A. Dandl and Clint Sprott for the Canted Mirror Facility to supplement calculations similar to those done by Carpenter on EBT.

COMPARISONS OF ENERGETIC ELECTRON FORMATION IN EBT AND IN MINIMUM-B CONFIGURATIONS*

G. R. Haste

Oak Ridge National Laboratory
Oak Ridge, Tennessee 37830

Abstract

The energetic electrons in EBT are observed to form an annulus at the position where the applied microwave frequency is twice the local (cold) electron cyclotron frequency. The axial extent of these rings is not accurately known, but there are indications that they lengthen as the stored energy increases. By contrast, in an open-ended minimum-B geometry the energetic electrons were observed to form in a region in which there was no possibility of second harmonic resonance. The axial extent of the energetic electron population was observed to decrease as the stored energy increased.

*Research sponsored by the Office of Fusion Energy, U. S. Department of Energy, under Contract W-7405-eng-26 with the Union Carbide Corporation.

This paper is concerned with some experimental data which is quite old. In fact, this was reported in Physics of Fluids, May 1973, in an article by Haste and Lazar. This is data taken in a minimum-B geometry with electron cyclotron heating. Hopefully, these results are not so much specific to the minimum-B geometry, but are generally representative of electron cyclotron heating processes. The purpose of the paper is to make two points. One is that high energy electrons can be formed in a geometry in which second harmonic resonance is not possible, and two that the processes of electron cyclotron heating result in considerable anisotropy in the resulting electron distribution.

Figure 1 illustrates the experiment. These experiments were carried out in INTEREM, which was a mirror quadrupole magnetic field. As such, the minimum-B was generated by the quadrupole or Ioffe windings and the resulting magnetic field is illustrated in the figure. The characteristic shape of the flux lines are shown in that figure; that is, they are quite narrow at one end and fan out in the other. Naturally, in the plane at 90° to this one, the arrangement of the flux lines are simply reversed; that is, they are narrow at the opposite end and fan out where these are narrow. Since it is a minimum-B configuration, the surfaces of constant magnetic field are closed and one of these surfaces is illustrated on this figure in the dotted lines. This surface can, for example, be the resonant surface for the electron cyclotron heating.

An array of collimated sodium iodide detectors is arranged to view the plasma with the detectors displaced in the axial direction. Each detector then views a small volume of the plasma and the resulting signals can be used to determine axial distribution of the X-ray emission. The X-ray spectra in turn can be used to determine the spectrum of the energetic electrons confined in the device. The X-ray spectra for the five detectors are shown on this same figure. You can see that at larger values of Z the X-ray spectrum is both less intense and is colder. Those observations will be made more quantitative later.

The first observation which should be made, however, concerns the role of second harmonic heating. In a minimum-B geometry such as this, the well depth is limited. In the case of INTEREM, the maximum well depth was 1.3. This means that when heating on one of the larger resonant surfaces the lowest magnetic field in the device was only 30% lower than the resonant value. Thus, there was no region in which the magnetic field was half of the resonant field and, therefore, there was no possibility of second harmonic heating. Nonetheless, energetic electrons were formed in this device. The point then is that second harmonic resonance is not an essential feature in the creation of energetic electron populations.

The second point has to do with the anisotropy produced by electron cyclotron heating. Figure 2 shows the density distributions obtained for three different values of the magnetic field strength. Since the microwave frequency was fixed, variation of the magnetic field resulted in variation of the length of the resonant surface. There are a number of features shown in this figure. The points shown are the densities determined from the bremsstrahlung distributions. The dotted lines are assumed distributions in pitch angle; that is, the positions at which the energetic electrons have their turning points. The solid lines then are the densities determined from that assumed distribution in turning points. The criteria for choosing a particular turning point distribution was that the resulting density distribution should match the experimentally determined points. In this figure, we see that the turning point distribution is peaked in the vicinity of, but not exactly at, the resonant position. The resonant position is indicated schematically by the hatched region.

Figure 3 shows the variation in these quantities as the microwave power is increased. For all the cases shown in this figure, the maximum extent of the resonant surface was at roughly 20 cm. At the low power level, that is in the 100-watt case, the pitch angle distribution is peaked near but inside the resonant position and the resulting density distribution shows a peak at larger Z; that is, a higher density at large Z than near zero. As the power is increased, this tendency no

longer remains true. At the highest power, that is, the 800-watt case in this figure, the density is peaked on the midplane and the turning point distribution is peaked well inside the resonant surface. This illustrates the point that the process of electron cyclotron heating tends to make the plasma narrower; that is, it is concentrated near the midplane.

A summary of the energy information obtained in the various spectra is shown in Fig. 4. In this figure, the mean energy of the electron distribution is shown as a function of position for the various power levels. At the lowest power level the mean energy is low and the distribution in Z is relatively flat. At the highest power levels, the maximum mean energy reaches 600 keV and is peaked near the midplane. These two figures together illustrate the effect of electron cyclotron heating on the anisotropy. Namely, that as the power is increased, the heating becomes more intense and the particles are confined more closely to the midplane. In fact, the most energetic particles are confined closest to the midplane, so that the effect of electron cyclotron heating is to concentrate those particles which are most heated most closely near the midplane.

To summarize, these results indicate some features of electron cyclotron heating which appear to be at variance with some preliminary observations in the EBT. These energetic electron distributions were obtained without second harmonic resonance. In EBT, as is well known, the position of the rings is determined by the position of electron cyclotron resonance for second harmonics. Secondly, the result of increased power on the increased heating leads to plasmas which are more closely confined near the midplane. Some preliminary results on EBT, and on NBT as well, seem to show that as the heating is increased the length of the energetic electron rings increases. The resolution of this apparent discrepancy will be very interesting.

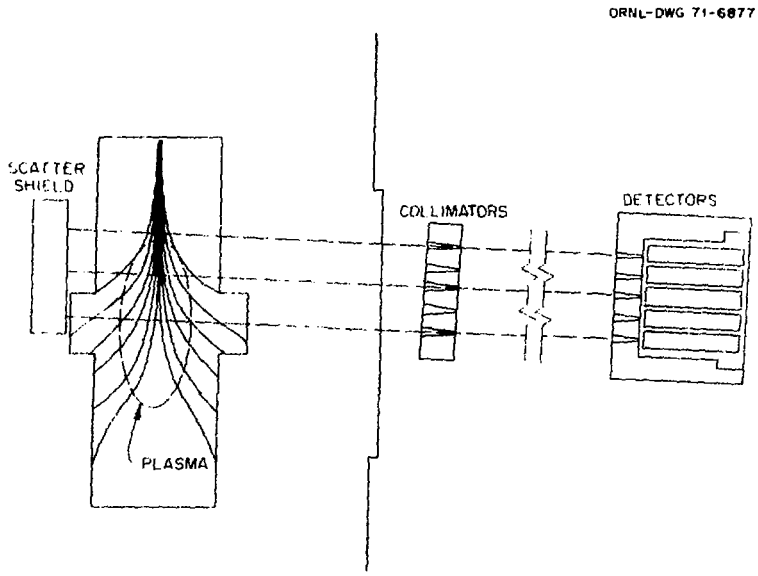

Fig. 1.a. View of bremsstrahlung detector array in horizontal plane.

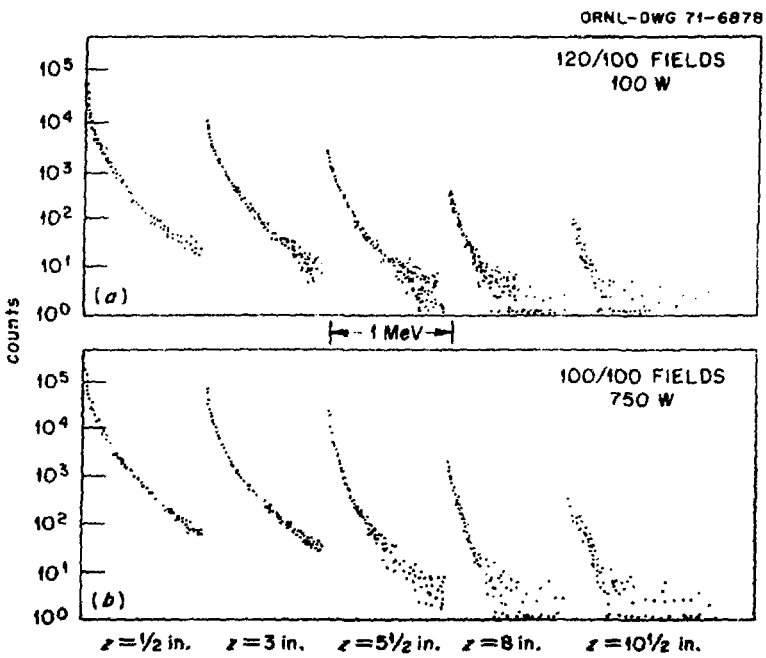

Fig. 1.b. Count rate spectra at various z locations for (a) B_0 = 3000 G and (b) B_0 = 3600 G.

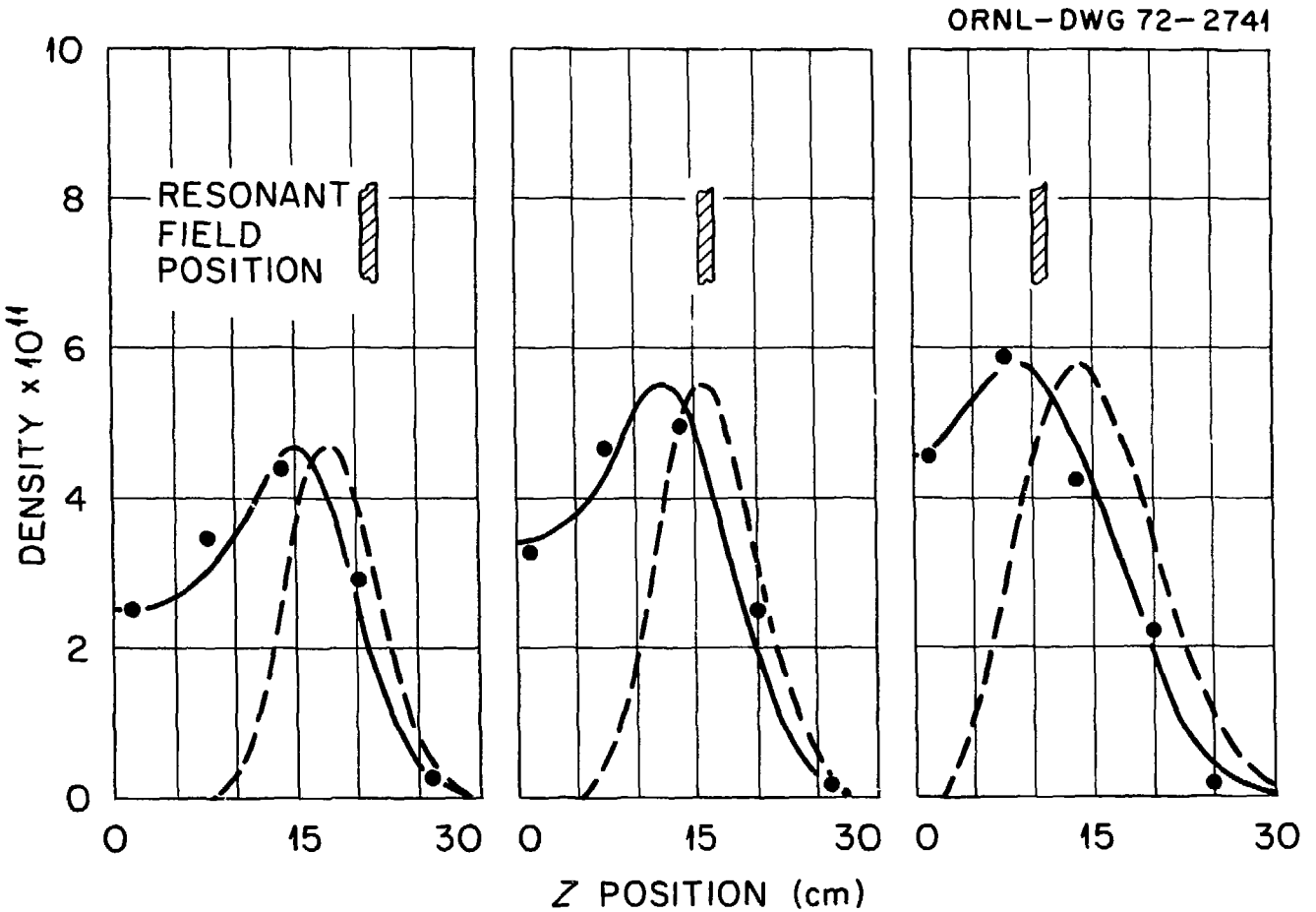

Fig. 2 Density and turning point profiles for various mirror field strengths. Pressure = 3×10^{-6} torr. The turning point profile is the dotted curve. In each case the turning point profile is normalized to the same amplitude as the density profile.

a) B_0 = 3000 g, 800 W
b) B_0 = 3300 g, 400 W
c) B_0 = 3600 g, 200 W

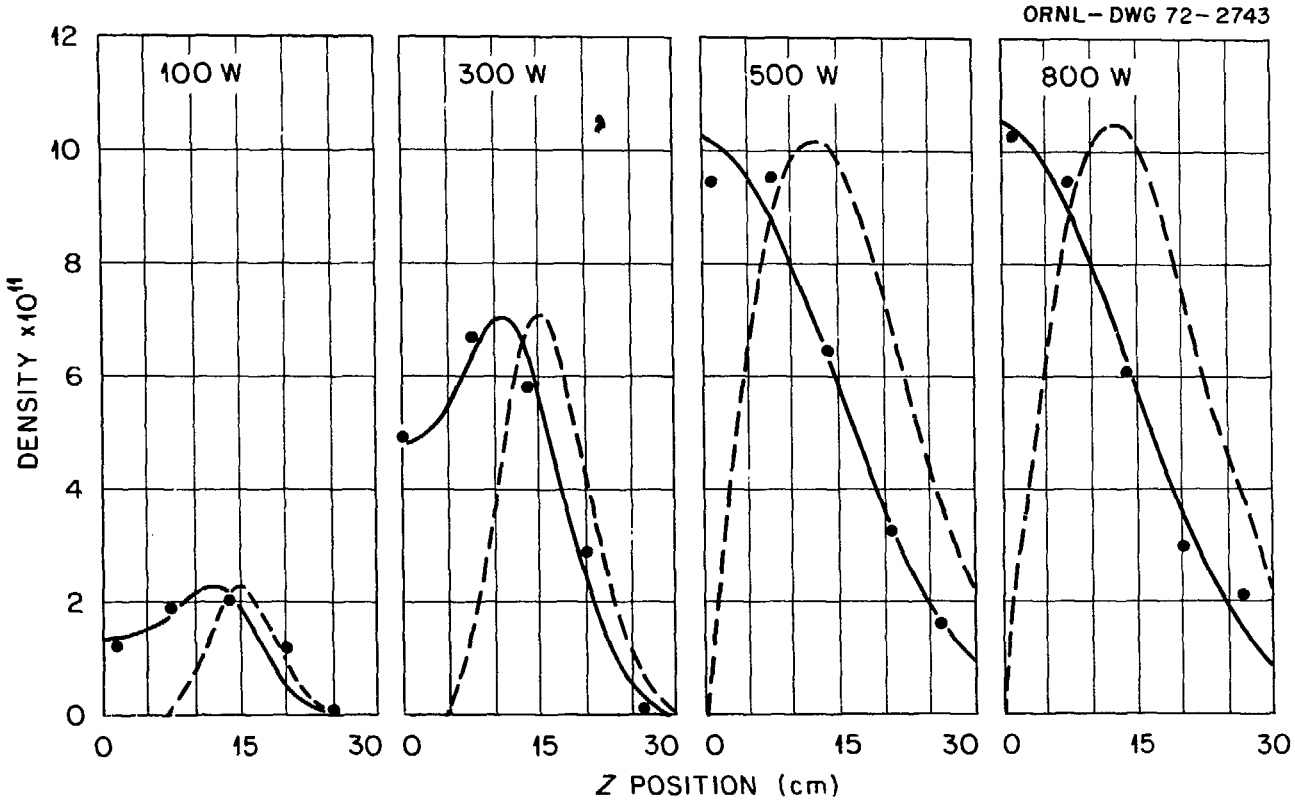

Fig. 3 Density and turning point profiles for various power levels. B_0 = 3000 g, 4 x 10^{-7} torr. The turning point profile is the dotted curve. In each case the turning point profile is normalized to the same amplitude as the density profile.

a) 100 W
b) 300 W
c) 500 W
d) 800 W

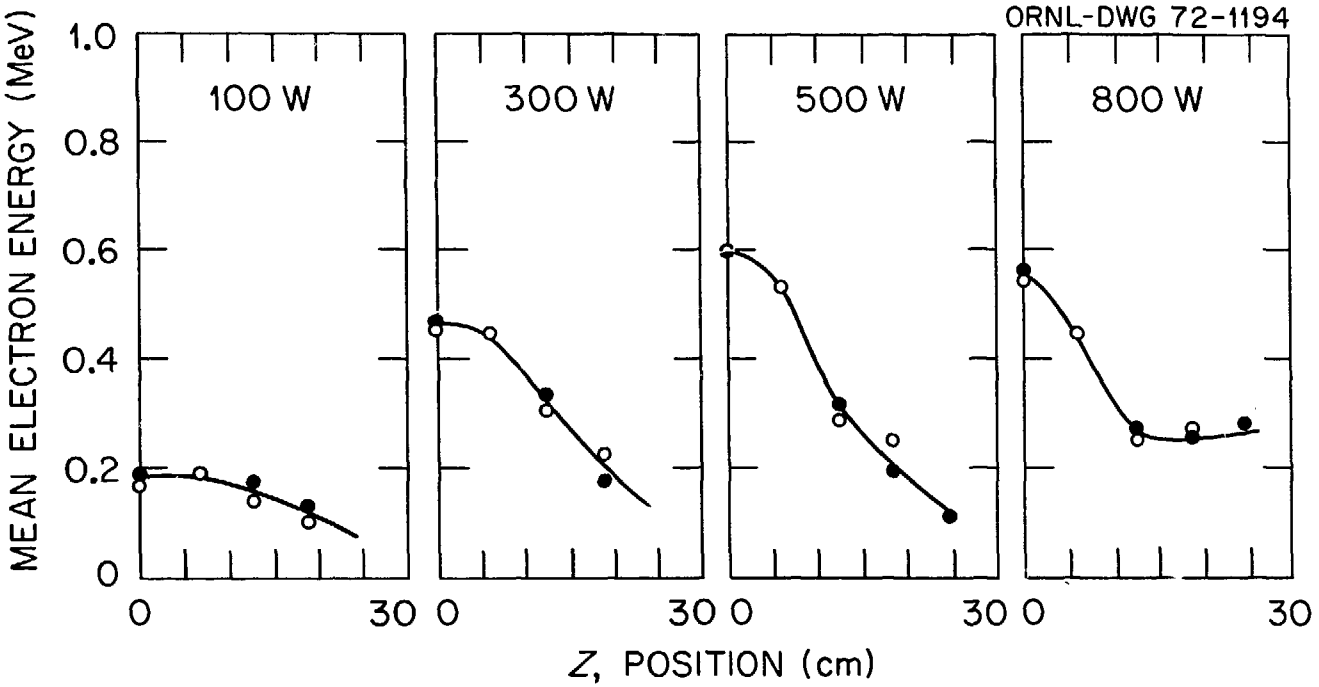

Fig. 4 Profiles of mean energy for various power levels. B_0 = 3000 g, 4×10^{-7} torr.
a) 100 W
b) 300 W
c) 500 W
d) 800 W

DISCUSSION

R. A. DANDL: What was the maximum average energy observed when heating with fundamental frequency coupling?

G. HASTE: The maximum shown in this data was 600 keV, but temperatures as high as 1 MeV were observed.

R. A. DANDL: This is different from the observations in simple mirrors. Microinstabilities in that case limited the hot electron temperature to lower values.

H. IKEGAMI: At the fundamental resonance heating, what was the radial structure?

G. HASTE: The structure within the resonant surface was not known.

W. ARD: The density was effectively zero outside the resonance surface in those experiments.

M. RENSINK: Was there any relation between the axial length of the plasma and the axial extent of the resonant surface?

G. HASTE: Yes, the maximum length of the plasma is determined by the length of the resonant surface.

J. PIPKINS: Why doesn't the ∇B reversal generate drifts in the opposite direction to cause a region of high shear in the drift velocity to cause an unstable situation?

G. HASTE: There was no reversal of ∇B in this experiment. The magnetic well resulted in a field which increased from the center.

G. GUEST: What evidence was there from IMP regarding instabilities and enhanced losses associated with the anisotropic heating where magnetic field lines were tangent to the resonant $|B|$-surface?

G. HASTE: A skimmer probe was used to interrupt the flux lines near their point of tangency to the resonant surface. The result was a reduction in the rf noise, which presumably means that the plasma was more stable. The effects on the plasma losses were not as apparent.

M. VELLA: Is there any experimental observation of MHD instability?

H. IKEGAMI: I believe that MHD instabilities, although it depends very much on the definition, have never been confirmed. On the other hand, in experiments, instabilities are so nonlinear that plasmas are driven out in microseconds and disappear. There are no beautifully oscillating instabilities, unless purposely generated.

G. GUEST: The flute-like instabilities are not fully described in either the MHD <u>or</u> the kinetic theories. The observed modes have azimuthal phase velocities near the diamagnetic speed — a finite-gyroradius phenomenon; but the kinetic theory is not well suited to analyzing their nonlocal character.

4. RING/CORE MODELING

C. L. Hedrick, Session Chairman

HOT ELECTRON RING EQUILIBRIA AND EFFECTS ON EBT TRANSPORT*

L. W. Owen, E. F. Jaeger, and C. L. Hedrick

Oak Ridge National Laboratory
Oak Ridge, Tennessee

Abstract

Averaging the EBT transport equations along magnetic field lines introduces geometric form factors into the 1-D equations. These form factors are modified by changes in the magnetic field produced by the hot electron rings. On the basis of a small number of numerically determined 2-D magnetic equilibria, we tentatively conclude that overall the form factors do appear to be important in determining the core density and temperature profiles in the region occupied by the hot electron rings. For example, the form factors introduce a term proportional to midplane values of dB/dr into the transport equations. The sense of this type of additional term is to retard losses at the outer edge of the core plasma where dB/dr is positive and decrease gradients of density and temperatures at smaller radii where dB/dr is negative. Further numerical calculation of magnetic equilibria is in progress to determine the sensitivity of these geometric form factors to the hot electron ring parameters.

*Research sponsored by the Office of Fusion Energy, U.S. Department of Energy, under contract W-7405-eng-26 with Union Carbide Corporation.

OUTLINE

- Derivation of field line averaged 1-D transport equations for EBT.

- 2-D magnetic equilibrium calculations and dependence of the geometric form factors that result from field line averaging on the pressure distribution model and spatial parameters of the hot electron rings.

- Qualitative estimates of the effects of field line averaging on overall power balance and on core density and temperature profiles in the region occupied by the rings.

The EBT transport equations (3-D) are

$$\frac{\partial n}{\partial t} + \nabla\cdot\vec{\Gamma} = n_o \langle\sigma v\rangle_i \, n$$

$$\frac{3}{2}\frac{\partial P_e}{\partial t} + \nabla\cdot\vec{Q}_e = P_\mu - Q_{ei} - e\vec{\Gamma}_e \cdot \vec{E}$$

$$\frac{3}{2}\frac{\partial P_i}{\partial t} + \nabla\cdot\vec{Q}_i = P_i + Q_{ei} + e\vec{\Gamma}_e \cdot \vec{E} - Q_{cx}$$

$$\nabla \cdot (\vec{\Gamma}_e - \vec{\Gamma}_i) = 0$$

where $\vec{\Gamma}$ and $\vec{Q}$ are particle and energy fluxes, respectively.

We wish to average the transport equations along magnetic field lines: hence, $\nabla\cdot\vec{\Gamma}$ and $\nabla\cdot\vec{Q}$ must be averaged over a flux surface. The flux surface may be characterized by:

(i) the flux function, ψ,

(ii) the volume within the surface, V,

(iii) the radius in the midplane, ρ.

If θ is the symmetry direction ($\partial/\partial\theta = 0$) in bumpy cylinder geometry, then the magnetic field can be written in the Clebsch representation as

$$\vec{B} = \nabla\psi \times \nabla\theta = \nabla\psi \times \hat{e}_\theta/r$$

so that in the midplane

$$\frac{\partial\psi}{\partial r} = rB \quad \text{or} \quad \frac{\partial\psi}{\partial\rho} = \rho B_{MID},$$

where B_{MID} is the magnetic field in the midplane of a sector.

In terms of ψ, B, and arc length along a field line ℓ, the volume is given by

$$V = 2\pi \int_0^{\psi} d\psi' \oint \frac{d\ell}{B}$$

and $\frac{\partial V}{\partial\psi} = 2\pi \oint \frac{d\ell}{B}$

Define the field line average of a quantity f by

$$\langle f \rangle = \frac{1}{\oint \frac{d\ell}{B}} \oint \frac{d\ell}{B} f.$$

We note that since the neoclassical transport coefficients are presently based on an isotropic core distribution function, the density, n, temperature, T, and transport coefficients are constant along magnetic field lines. Thus, for brevity considering just the ∇n term of the particle flux equation, •

$$\vec{\Gamma} = -D_n \nabla n = -D_n \frac{\partial n}{\partial\rho} \frac{\partial\rho}{\partial\psi} \nabla\psi$$

or $\vec{\Gamma} = \Gamma^* \dfrac{\nabla\psi}{\rho B_{MID}}$.

Now form the field line average of $\nabla\cdot\vec{\Gamma}$. From Gauss' Theorem

$$\langle\nabla\cdot\vec{\Gamma}\rangle = \frac{\partial}{\partial V}\langle\vec{\Gamma}\cdot\nabla V\rangle.$$

Using

$$\nabla V = \frac{\partial V}{\partial\psi}\,\partial\psi = 2\pi \oint \frac{d\ell}{B}\,\nabla\psi$$

we can write

$$\langle\vec{\Gamma}\cdot\nabla\rangle = \frac{2\pi\Gamma^*}{\rho B_{MID}} \oint d\ell\; r^2 B.$$

In terms of radius in the midplane,

$$\frac{\partial}{\partial V} = \frac{1}{2\pi\rho B_{MID} \oint \frac{d\ell}{B}}\,\frac{\partial}{\partial\rho}$$

and $$\langle\nabla\cdot\vec{\Gamma}\rangle = \frac{1}{\frac{B_{MID}}{L}\oint\frac{d\ell}{B}}\,\frac{1}{\rho}\,\frac{\partial}{\partial\rho}\left\{\rho\Gamma^*\oint\frac{d\ell}{L}\,\frac{r^2B}{\rho^2 B_{MID}}\right\}.$$

Define two geometric form factors:

$$U_1 = \frac{1}{\frac{B_{MID}}{L} \oint \frac{d\ell}{B}}$$

and

$$U_2 = \oint \frac{d\ell}{L} \frac{r^2 B}{\rho^2 B_{MID}},$$

then

$$\langle \nabla \cdot \vec{\Gamma} \rangle = U_1 U_2 \left\{ \frac{1}{\rho} \frac{\partial}{\partial \rho} (\rho \Gamma^*) + \Gamma^* \frac{\partial \log U_2}{\partial \rho} \right\}$$

This may be compared with the corresponding expression which neglects variation along field lines:

$$\langle \nabla \cdot \vec{\Gamma} \rangle = \frac{1}{\rho} \frac{\partial}{\partial \rho} (\rho \Gamma^*).$$

Hence, field line averaging results in an additional term proportional to $\partial \log U_2 / \partial \rho$.

The dependence of the geometric form factors U_1 and U_2 on the parameters of the relativistic electron rings is illustrated with a number of numerically determined 2-D magnetic equilibria. The radial position and extent, axial extent, beta, and anisotropic pressure model of the rings are varied.

Comparison is made between two anisotropic pressure distributions: with $X = B/B_c$

(i) n = 3 Taylor distribution

$$P_{\parallel} = \hat{P}_{\parallel}(B)\, g(\psi) = \frac{2}{3} s B_c^2\, X(1 - X)^3 g(\psi), \qquad B < B_c$$

$$P_{\perp} = \hat{P}_{\perp}(B)\, g(\psi) = 2 s B_c^2\, X^2 (1 - X)^2 g(\psi), \qquad B < B_c$$

$$P_{\parallel} = P_{\perp} = 0, \qquad B > B_c$$

and

(ii) Constant - τ distribution

$$P_{\parallel} = \frac{1}{2} s B_c^2\, (1 - X)^2\, g(\psi), \qquad B < B_c$$

$$P_{\perp} = \frac{1}{2} s B_c^2\, (1 - X^2)\, g(\psi), \qquad B < B_c$$

$$P_{\parallel} = P_{\perp} = 0, \qquad B > B_c$$

$\hat{P}_{\perp}$ for these two anisotropic pressure models is shown in Fig. 1. The curves are normalized at the peak of the N = 3 Taylor distribution.

Mod-B contours and magnetic field lines in the equatorial plane of a sector are illustrated in Fig.2 for a typical high-β bumpy cylinder equilibrium. The spatial position and extent of the annulus is shown, as is the field line curvature as the lines converge in the coil throat region.

The radial dependence of U_1, U_2, $\beta_{\perp}$ and mod-B in the midplane are illustrated in Figs. 3,4, and 5. It is readily seen that the behavior of U_1 and U_2 is dominated by B_{MID}. In particular,

$$U_2 = \frac{1}{B_{MID}},$$

$$\frac{\partial \log U_2}{\partial \rho} = -\frac{\partial \log B_{MID}}{\partial \rho},$$

and $$\langle \nabla \cdot \vec{\Gamma} \rangle = U_1 U_2 \left[\frac{1}{\rho} \frac{\partial}{\partial \rho} (\rho \Gamma^*) - \Gamma^* \frac{\partial \log B_{MID}}{\partial \rho} \right].$$

Therefore, the additional term in $\langle \nabla \cdot \vec{\Gamma} \rangle$ (and $\langle \nabla \cdot \vec{Q} \rangle$) arising from field line averaging is proportional to $-\Gamma^* \partial \log B_{MID}/\partial \rho$.

Since Γ^* is positive, the additional term acts as a convective term inward for reversed gradients in B ($\partial \log B_{MID}/\partial \rho > 0$) and convects outward for the normal gradient region ($\partial \log B_{MID}/\partial \rho < 0$). One hypothesizes that this will reduce density and temperature gradients for normal ∇B_{MID} and increase them for reversed ∇B_{MID}. This is illustrated by the dashed portion of the $n(\rho)$ curve in Fig. 6.

Because U_1 and U_2 can be a number of order 2, one might expect a discrepancy in gross power balance. This, however, neglects the fact that taking account of curved field lines reduces the volume. Indeed one expects that U_1 and $U_2 > 1$ occur because of sharper gradients in the region of high magnetic field. Counterbalance occurs by virtue of the smaller cross sectional area in the high field region. (See Fig. 2)

To make these arguments more concrete, consider power balance:

$$\text{Power Loss/Volume} = \langle \nabla \cdot \vec{Q} \rangle$$

$$= U_1 \frac{1}{\rho} \frac{\partial}{\partial \rho} (\rho Q^* U_2)$$

and $$\text{Total Power Loss} = \int dV \; U_1 \frac{1}{\rho} \frac{\partial}{\partial \rho} (\rho Q^* U_2)$$

$$= 2\pi a \; Q^* \; U_2 L.$$

To get a rough estimate of the difference produced by U_1, $U_2 \neq 1$, assume that Q is unchanged. Then the power loss is simply increased by the factor U_2, since the total power loss neglecting field line curvature in just $2\pi a Q^* L$. However, the input power is

$$P = \int dV \; \hat{P}$$

$$= 2\pi L \int_0^a d\rho \; \rho \; \hat{P}/U_1,$$

where $\hat{P}$ is the input power per unit plasma volume. If $\hat{P}$ is independent of ρ,

$$\frac{P^{new}}{P^{old}} = U_2 \frac{2}{a^2} \int_0^a \frac{\rho \, d\rho}{U_1} = U_2 \int_0^1 \frac{d(\rho^2/a^2)}{U_1}.$$

Then, estimating crudely

$$\frac{P^{new}}{P^{old}} \approx (1.3)(0.64) = 0.83.$$

Thus, including field line averaging is seen to result in a modest improvement in power balance.

SUMMARY

- Averaging the EBT transport equations along magnetic field lines introduces an additional term into the 1-D particle and heat flux equations. The sense of the term is to retard losses at the outer edge of the core plasma where dB/dr is negative.

- Overall power balance is relatively unaffected by the geometric form factors that result from flux surface averaging. Crude estimates indicate that by virtue of the smaller volume obtained when field line curvature is included, the ratio P(with field line averaging)/P(without) < 1.

- For realistic annulus anisotropy, the behavior of the geometric form factors U_1 and U_2 is dominated by mod-B in the midplane.

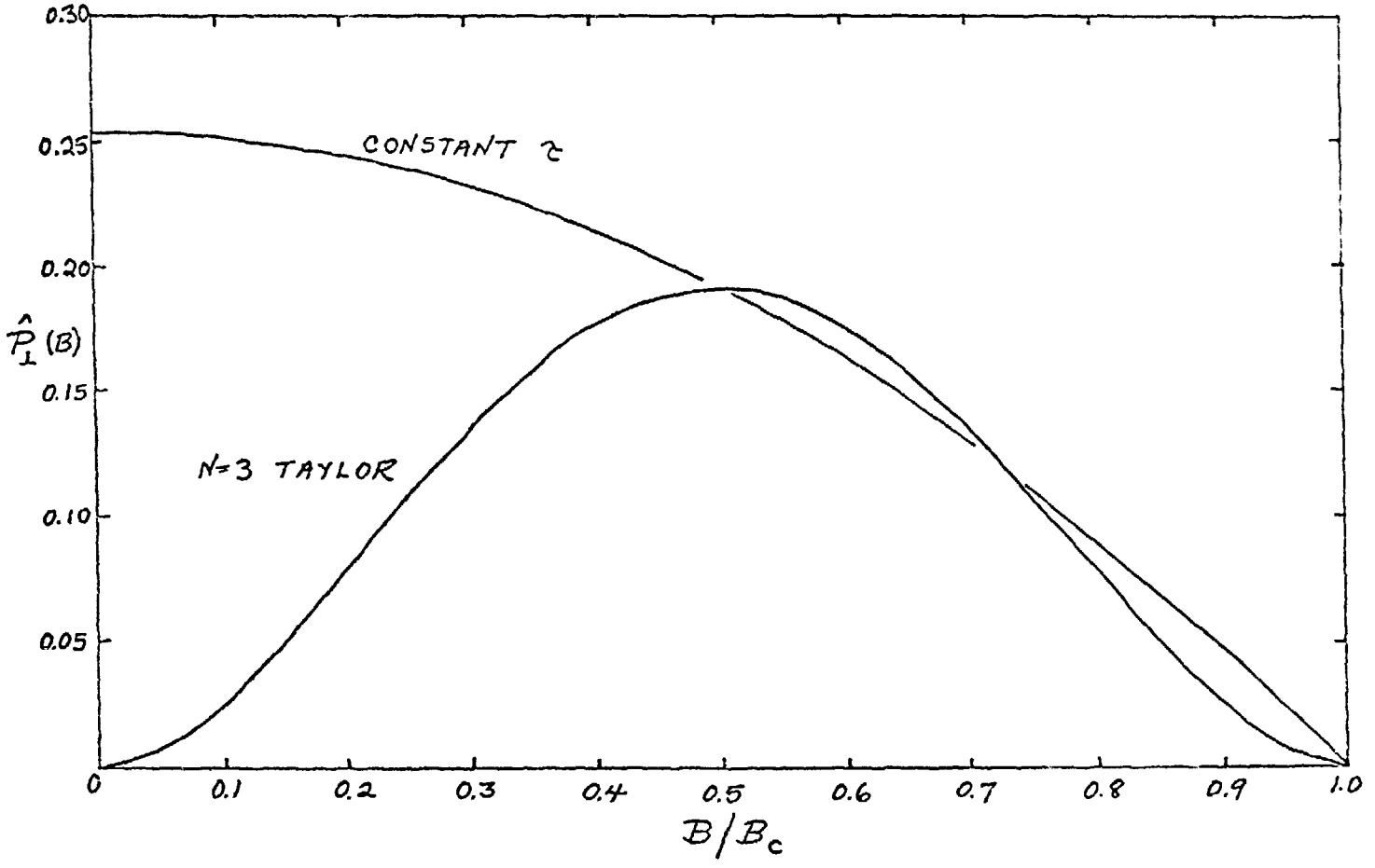

MODEL PRESSURE DISTRIBUTIONS
USED IN 2-D EQUILIBRIUM CALCULATIONS

FIGURE 1

ORNL/DWG/FED-77947

BUMPY CYLINDER EQUILIBRIUM

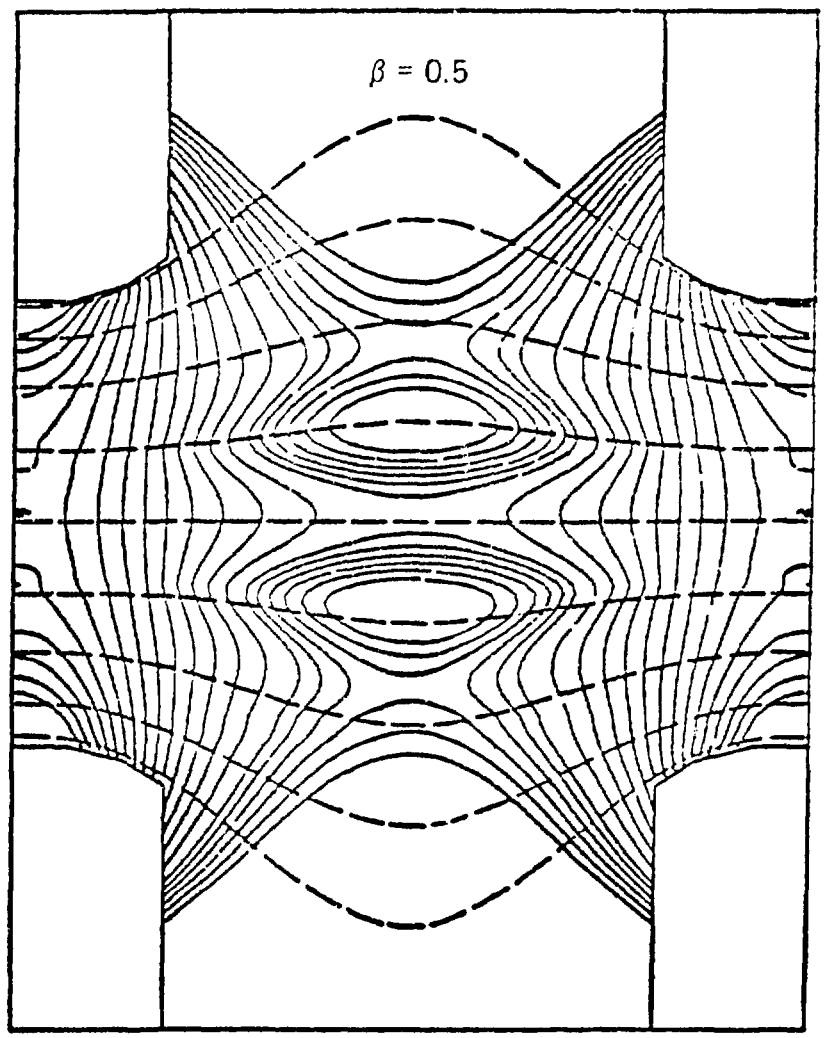

— — — FIELD LINE

——— MOD-B CONTOUR

FIGURE 2

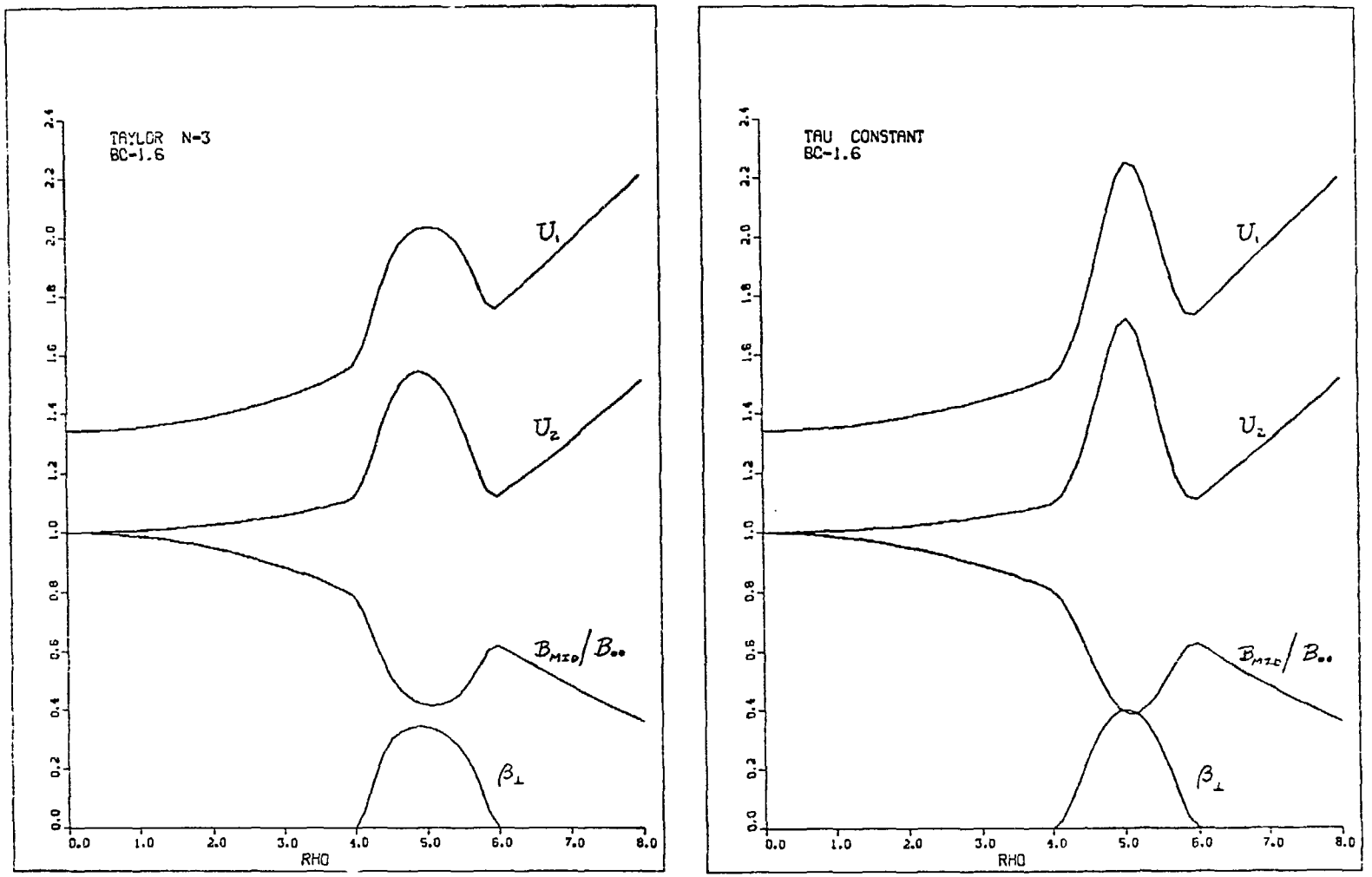

COMPARISON OF THE GEOMETRIC FORM FACTORS U_1 AND U_2, MOD-B IN THE MIDPLANE, AND $\beta_\perp$ FOR TWO ANISTROPIC PRESSURE MODELS.

FIGURE 3

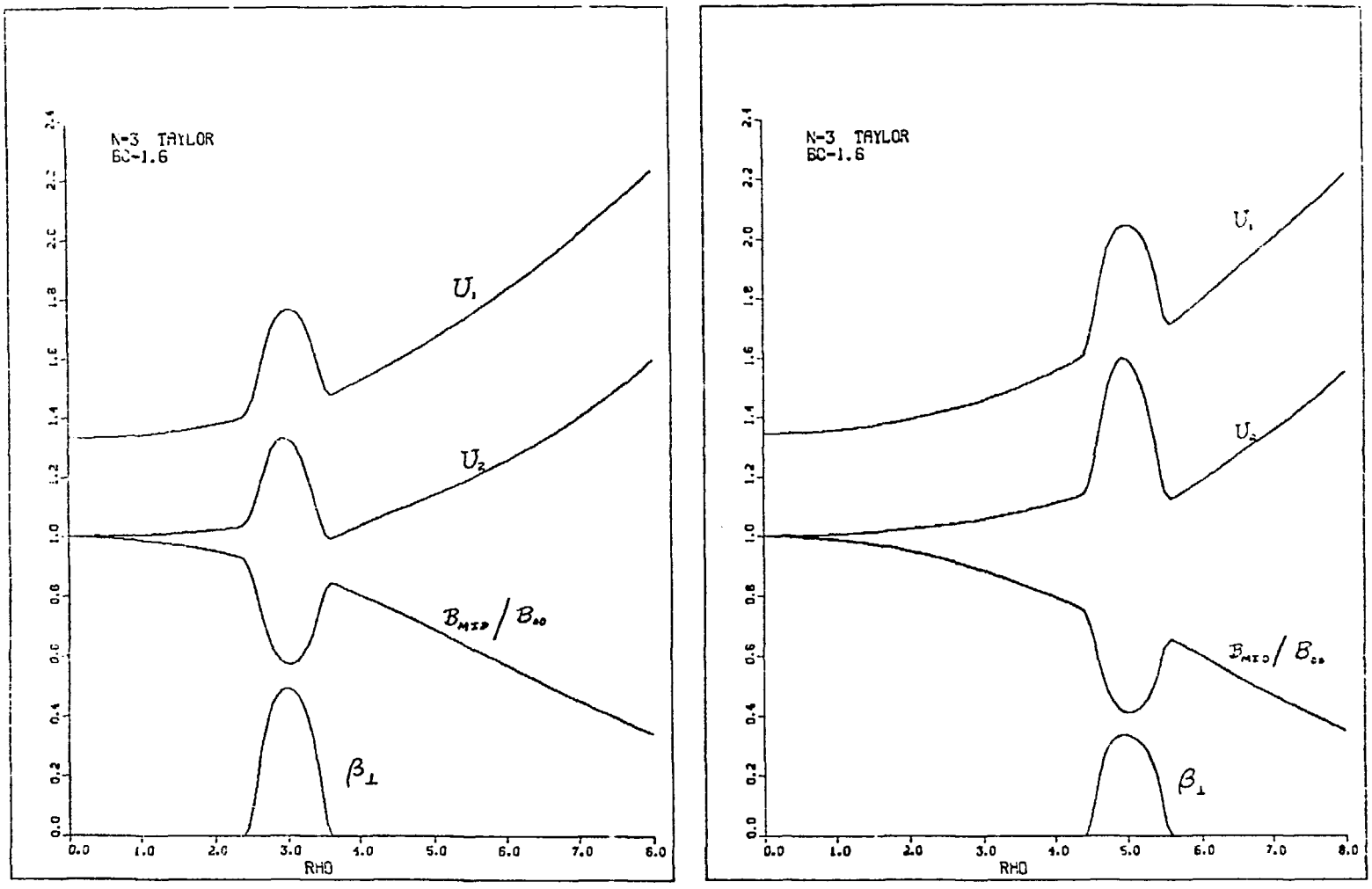

DEPENDENCE OF THE GEOMETRIC FORM FACTORS U_1 AND U_2, MOD-B IN THE MIDPLANE, AND $\beta_\perp$ ON THE RADIAL POSITION OF THE ANNULUS.

FIGURE 4

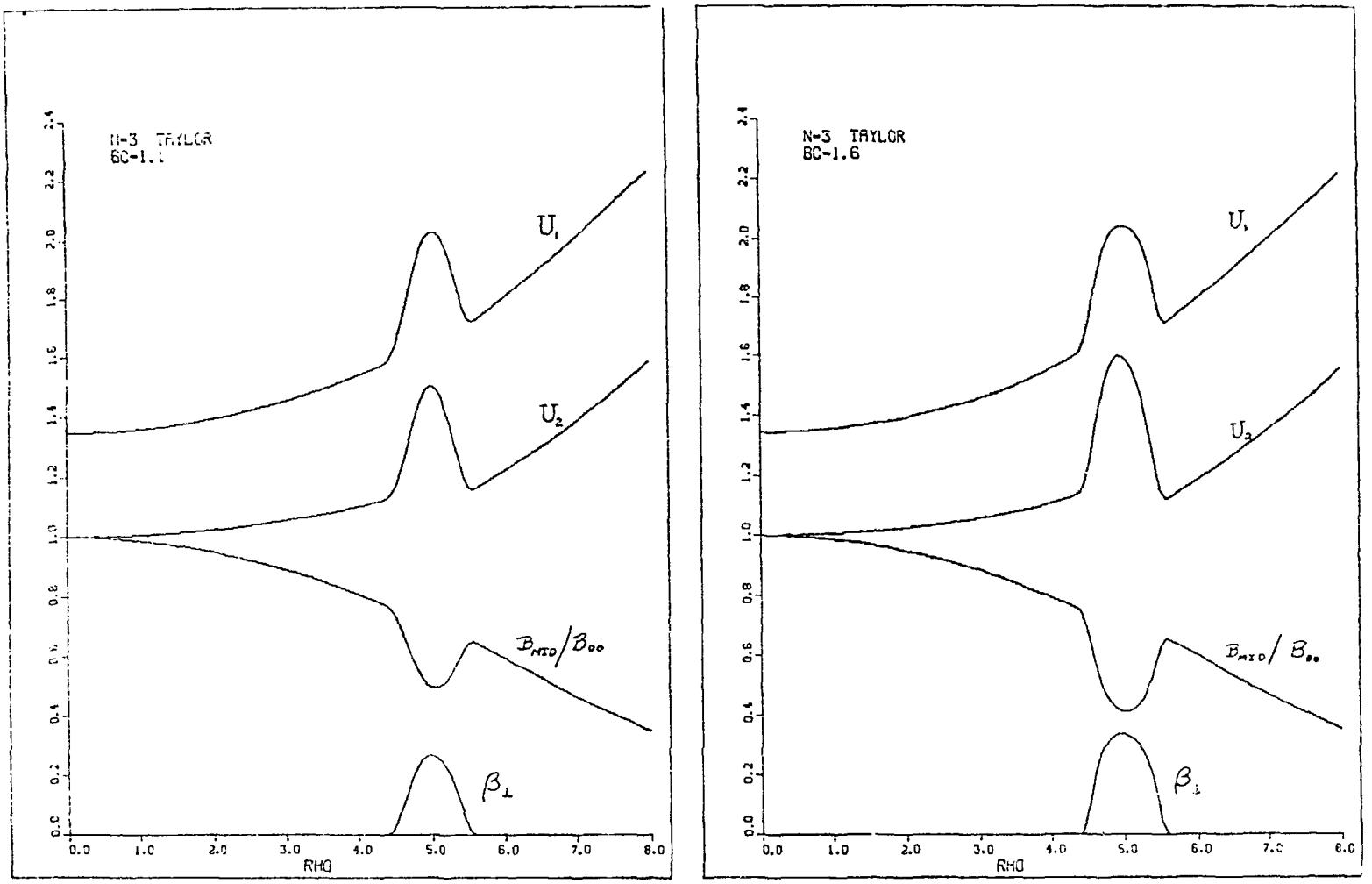

DEPENDENCE OF THE GEOMETRIC FORM FACTORS U_1 AND U_2, MOD-B IN THE MIDPLANE, AND $\beta_\perp$ ON THE AXIAL EXTENT (LENGTH) OF THE ANNULUS.

FIGURE 5

ORNL-DWG 80-2129 FED

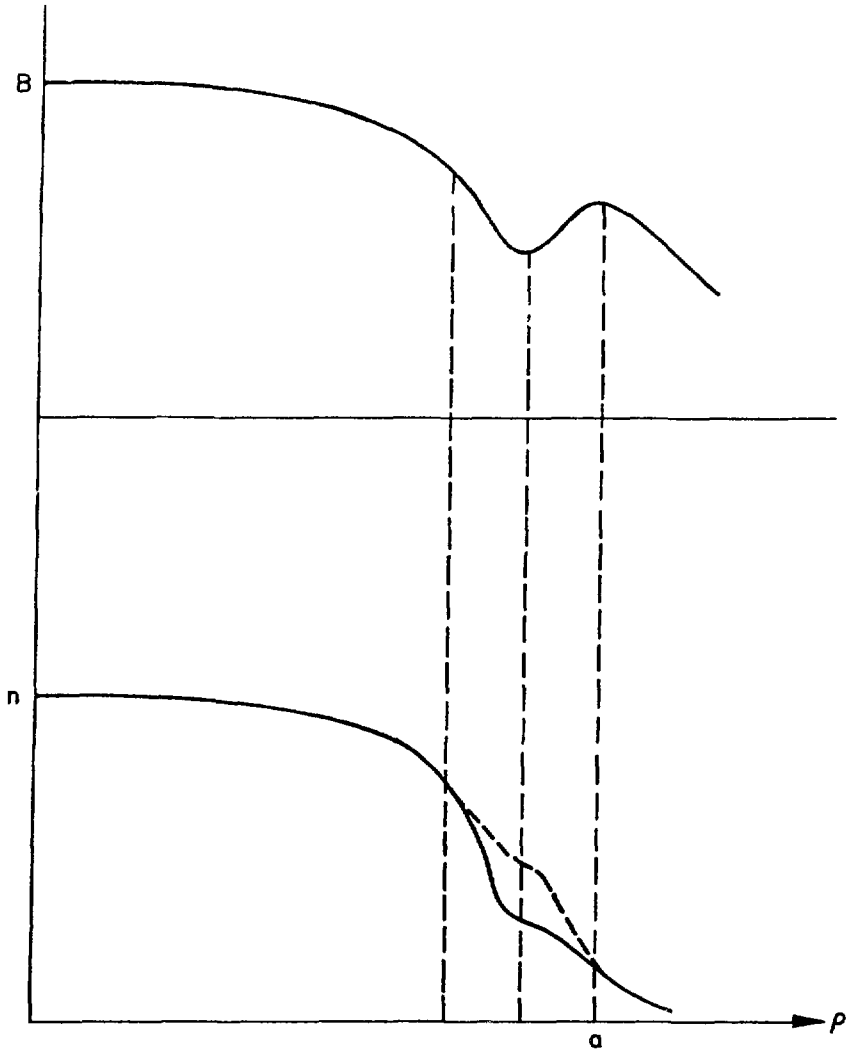

EFFECT OF FIELD LINE AVERAGING ON RADIAL PROFILES IN THE REGION OF THE HOT ELECTRON RINGS IS INDICATED BY THE DASHED $n(\rho)$ CURVE.

FIGURE 6

NUMERICAL CALCULATION OF THE ELECTRON DISTRIBUTION FUNCTION FOR EBT ELECTRON ANNULI*

J. S. Tolliver, E. F. Jaeger, and C. L. Hedrick

Oak Ridge National Laboratory
Oak Ridge, Tennessee 37830

ABSTRACT

In the ELMO Bumpy Torus (EBT), high beta relativistic electron annuli in each mirror sector provide the average minimum-B configuration necessary for stability of the toroidal plasma. Using a nonrelativistic bounce-averaged kinetic equation, we solve for the electron distribution function, which is assumed to be isotropic in velocity space. The equation is solved in time and two dimensions and includes both velocity and radial derivatives. The Fokker-Planck collision operator includes Coulomb collisions and first- and second-harmonic microwave heating terms. Ionization of cold neutrals (assuming a cylindrical neutral transport model) provides a source of cold electrons. Under the influence of microwave heating, these electrons diffuse upward in velocity space, and a high energy tail corresponding to the hot electron annulus is observed to form on the electron distribution function. A simulated pitch angle scattering term provides a sink of hot electrons from the high energy tail. As the neutral density is increased, the annulus pressure decreases, as observed experimentally.

*Research sponsored by the Office of Fusion Energy, U.S. Department of Energy, under contract W-7405-eng-26 with the Union Carbide Corporation.

1. INTRODUCTION

In the ELMO Bumpy Torus (EBT), high beta relativistic electron rings, or annuli, in each mirror sector produce diamagnetic plasma currents that provide the average minimum-B configuration necessary for MHD stability of the core plasma in the toroidal, or T-, mode of operation. The importance of these electron rings is evident from the transition from the T-mode to the unstable cold, or C-, mode of operation, when the annulus beta is so low that the minimum in the magnetic field is not sufficient to prevent MHD instability through interchange modes. On the other hand, at high annulus beta the EBT device operates in the M-mode, in which the toroidal plasma has low density and large-amplitude fluctuations and is unsuitable for use as a fusion plasma. Because of the recognized importance of the electron rings, we have undertaken to solve a kinetic model for the electron distribution function in EBT. This paper describes a numerical solution of the bounce-averaged drift kinetic equation. Because this is a first approximation, relativistic effects are ignored. In order to reduce the problem to one that can be solved with current computing capabilities, the distribution function is assumed to be isotropic in pitch angle and is calculated as a function of radius and speed on a two-dimensional finite difference mesh.

In Sect. 2, we derive the nonlinear partial differential equation used with a Fokker-Planck collision operator to model the time evolution of an isotropic electron distribution function in an EBT device having a large aspect ratio. The equation includes an ad hoc radial diffusion coefficient chosen to simulate pitch angle scattering. The Fokker-Planck collision operator includes Coulomb collisions, ionization of cold neutral particles, and first- and second-harmonic microwave heating. The problem is solved numerically with an alternating-direction-implicit (ADI) scheme, as discussed in Sect. 3.

Results are discussed in Sect. 4. A high energy tail, corresponding to the high energy electron ring, is observed to form on the electron distribution function near the plasma edge under the influence of microwave heating and against the action of Coulomb drag. In addition, the annulus pressure is observed to fall with increases in the edge neutral

density, as observed experimentally in the T-C transition. Low neutral pressures lead to the presence of a large high energy tail everywhere in radius, suggestive of the experimentally observed M-mode. Section 5 presents our conclusions and plans for the future.

2. DERIVATION OF THE KINETIC MODEL

2.1 THE DRIFT KINETIC EQUATION FOR A LARGE-ASPECT-RATIO EBT DEVICE

We start with the nonrelativistic bounce-averaged drift kinetic equation[1]

$$\frac{\partial f}{\partial t} + \vec{v}_D \cdot \nabla f + \frac{e}{mv} \vec{v}_D \cdot \vec{E} \frac{\partial f}{\partial v} + \frac{\tan \alpha}{2} \vec{v}_D \cdot \left(\frac{\nabla B}{B} - \frac{2e\vec{E}}{mv^2} \right) \frac{\partial f}{\partial \alpha} = C(f) \ , \tag{1}$$

where $f = f(r,\theta,v,\alpha,t)$ is the distribution function of guiding centers; v is the speed, $\vec{v}_D$ is the bounce-averaged guiding center drift velocity; e and m are the particle charge and mass; and $\alpha \equiv \tan^{-1} (v_\perp / v_\parallel)$ is the pitch angle, where $v_\perp$ and $v_\parallel$ are the components of velocity perpendicular to and parallel to the magnetic field B. The collision operator is represented by $C(f)$. Using the toroidal coordinate system shown in Fig. 1 and following Jaeger et al.,[2] Eq. (1) may be simplified for large aspect ratios by assuming that f is isotropic in pitch angle, with the result

$$\frac{\partial f}{\partial t} + v_{Dy} \sin \theta \frac{\partial f}{\partial r} + \left(\Omega_o - \frac{E}{B_o R_T} \cos \theta + \frac{v_{Dy}}{r} \cos \theta \right) \frac{\partial f}{\partial \theta} + \frac{e E v_{Dy}}{mv} \sin \theta \frac{\partial f}{\partial \theta} = C(f) \ , \tag{2}$$

where $\vec{v}_D$ has been written in terms of a vertical drift v_{Dy} owing to toroidal curvature and a poloidal drift frequency

$$\Omega = \Omega_o - \frac{E}{B_o R_T} \cos \theta \ , \tag{3a}$$

where

$$\Omega_o = \Omega_{\nabla B} - \frac{E}{rB_o} . \tag{3b}$$

Here, E is a purely radial electric field; B is assumed to be a purely axial magnetic field with toroidal correction $B = B_z = B_o/h$, where $h = 1 + r/R_T \cos\theta$, R_T is the major radius of the torus, and B_o is the magnitude of the magnetic field on axis. The vertical and poloidal drifts are chosen to have the form

$$v_{Dy} = - \frac{mv^2}{3eB_oR_T} \tag{4a}$$

and

$$\Omega_{\nabla B} = - \frac{mv^2}{3eB_oR_cr} , \tag{4b}$$

where R_c is the average radius of curvature for N_s mirror sectors approximated as[3]

$$\frac{1}{R_cr} = \frac{1}{4}\left(\frac{N_s}{R_T}\right)^2 . \tag{5}$$

A Fokker-Planck collision operator is written as

$$C(f) = a(f) \frac{\partial^2 f}{\partial v^2} + b(f) \frac{\partial f}{\partial v} + c(f)f + S(f) , \tag{6}$$

where a, b, c, and S are linear functions of f. For a large-aspect-ratio torus, the distribution function may be Fourier expanded in θ,

$$f = f_o + f_c \cos\theta + f_s \sin\theta + \ldots , \tag{7}$$

and the higher order terms dropped. Substituting Eq. (7) into Eqs. (2) and (6) results in three coupled nonlinear partial differential equations for f_o, f_c, and f_s:

$$\frac{\partial f_o}{\partial t} + \frac{1}{2}\left[v_{Dy}\left(\frac{\partial f_s}{\partial r} + \frac{f_s}{r}\right) - \frac{Ef_s}{B_o R_T}\right] + \frac{1}{2}\frac{eEv_{Dy}}{mv}\frac{\partial f_s}{\partial v} = C_o(f_o) + \frac{1}{2}\left[C_c(f_c) + C_s(f_s)\right] , \tag{8a}$$

$$\frac{\partial f_c}{\partial t} + \Omega_o f_s = C_o(f_c) + C_c(f_o) , \tag{8b}$$

and

$$\frac{\partial f_s}{\partial t} - \Omega_o f_c + v_{Dy}\frac{\partial f_o}{\partial r} + \frac{eEv_{Dy}}{mv}\frac{\partial f_o}{\partial v} = C_o(f_s) + C_s(f_o) , \tag{8c}$$

where we have used the notation

$$C_\alpha(f_\beta) = a(f_\alpha)\frac{\partial^2 f_\beta}{\partial v^2} + b(f_\alpha)\frac{\partial f_\beta}{\partial v} + c(f_\alpha)f_\beta + S(f_\alpha) . \tag{9}$$

By integrating over velocity and averaging over θ, it may be shown that the model contained in these three equations conserves particles. Similarly, energy conservation may be demonstrated by first multiplying by $1/2\ mv^2$ and then integrating over velocity and averaging over θ.

By using the nonconservative form of the Krook collision operator[4]

$$C(f) \approx \nu(f_E - f) \ , \tag{10a}$$

where ν is the collision frequency and f_E is some equilibrium distribution function, we may solve Eqs. (8b) and (8c) in steady state for f_c and f_s by taking $f_E = f_o$. Then the collision operator becomes

$$C(f) \approx \nu(f_o - f) = -\nu f_c \cos\theta - \nu f_s \sin\theta \ , \tag{10b}$$

resulting in

$$f_c = -\frac{\Omega_o}{\nu} f_s \tag{11a}$$

and

$$f_s = -\frac{\nu v_{Dy}}{\nu^2 + \Omega_o^2}\left(\frac{\partial f_o}{\partial r} + \frac{eE}{mv}\frac{\partial f_o}{\partial v}\right) \tag{11b}$$

These then are substituted into Eq. (8a) for f_o. The electric field is assumed to be zero to simplify the calculation. After discarding the second-order $C_c(f_c)$ and $C_s(f_s)$ terms, we obtain

$$\frac{\partial f_o}{\partial t} - \frac{1}{2}\frac{\nu v_{Dy}^2}{\nu^2 + \Omega_o^2}\left(\frac{\partial^2 f_o}{\partial r^2} + \frac{1}{r}\frac{\partial f_o}{\partial r}\right) = a(f_o)\frac{\partial^2 f_o}{\partial v^2} + b(f_o)\frac{\partial f_o}{\partial v} + c(f_o)f_o + S(f_o) \ , \tag{12}$$

which may be written as

$$\frac{\partial f_o}{\partial t} = a \frac{\partial^2 f_o}{\partial v^2} + b \frac{\partial f_o}{\partial v} + c f_o + S + D\left(\frac{\partial^2 f_o}{\partial r^2} + \frac{1}{r}\frac{\partial f_o}{\partial r}\right) , \tag{13}$$

where

$$D = \frac{1}{2} \frac{\nu v_{Dy}^2}{\nu^2 + \Omega_o^2} . \tag{14a}$$

To simulate pitch angle scattering, we assume a velocity-dependent collision frequency $\nu \sim 1/v^3$. For simplicity, we assume collisionless transport at all velocities and take

$$D = \frac{D'}{(v_{TH}^2 + v^2)^{3/2}} , \tag{14b}$$

where v_{TH} is the thermal velocity and D' is a constant chosen to give the core particles a 10-ms diffusion time. The full effects of this diffusion coefficient are being studied, and work is under way to choose a more realistic form for D.

2.2 THE COLLISION OPERATOR

2.2.1 Coulomb Collisions

The Fokker-Planck collision operator for Coulomb collisions may be written as[5]

$$C_\nu(f_k) = a_\nu(f_k) \frac{\partial^2 f_k}{\partial v^2} + b_\nu(f_k) \frac{\partial f_k}{\partial v} + c_\nu(f_k) f_k , \tag{15}$$

where k indicates the kth species and for $v > 0$

$$a_\nu(f_k) = \pi^{3/2}\gamma_k \sum_j \left(\frac{1}{3} \int_0^v dv' \frac{v'^4}{v^3} f_j + \frac{1}{3} \int_v^\infty dv' \, v' f_j \right) , \tag{16a}$$

$$b_\nu(f_k) = \pi^{3/2}\gamma_k \sum_j \left[\int_0^v dv' \left(\frac{m_k}{m_j} - \frac{v'^2}{3v^2} \right) \frac{v'^2}{v^2} f_j + \frac{2}{3} \int_v^\infty dv' \frac{v'}{v} f_j \right] , \tag{16b}$$

and

$$c_\nu(f_k) = \pi^{3/2}\gamma_k \sum_j \frac{m_k}{m_j} f_j , \tag{16c}$$

with

$$\gamma_k = \frac{e_k^4 \, \ell n \, \Lambda}{\pi^{3/2}\varepsilon_o^2 m_k^2} ,$$

$$\Lambda = \frac{12\pi(\varepsilon_o \kappa T/e^2)^{3/2}}{n^{1/2}} ,$$

and the sum over j being a sum over species. As $v \to 0$, Eq. (15) may still be used with the coefficients expressed as

$$a_\nu(f_k) = \pi^{3/2}\gamma_k \sum_j \int_v^\infty dv' \, v' f_j , \tag{17a}$$

$$b_\nu(f_k) = 0 , \tag{17b}$$

and

$$c_\nu(f_k) = \pi^{3/2}\gamma_k \sum_j \frac{m_k}{m_j} f_j \ , \tag{17c}$$

where a boundary condition of $\partial f_k/\partial v = 0$ at $v = 0$ has been used. As a simplifying assumption, we consider only electron-electron collisions, and the summations consist of only one term, $j = k$. These Coulomb collisions conserve both particles and energy.

2.2.2 Ionizing Collisions

We assume that particles created by the ionization of cold neutrals are born with a Maxwellian velocity distribution at the temperature of the neutrals T_o. That is,

$$S_i(f) = \nu_i \frac{n}{\pi^{3/2}\ \alpha_o^3} e^{-v^2/\alpha_o^2} \ , \tag{18}$$

where S_i denotes the contribution to the collision operator owing to ionization; $\alpha_o^2 = 2kT_o/m$; and ν_i is the ionization rate $n_o\langle\sigma v\rangle_i$ where n_o is the neutral density and $\langle\sigma v\rangle_i$ is the cross section for ionization. Integration of $S_i(f)$ over velocity yields

$$\int S_i(f)\ d^3\vec{v} = \nu_i n$$

and

$$\int S_i(f)\ \frac{1}{2}\ mv^2\ d^3\vec{v} = \nu_i\left(\frac{3}{2}\ kT_o\right)$$

so that ionization conserves neither particles nor energy.

2.2.3 Microwave Collisions

We include the effects of microwave heating by electron cyclotron resonance with the microwave field in the collision operator $C_\mu(f)$, which models quasi-linear diffusion in velocity space:[6]

$$C_\mu(f) = \nabla_v \cdot (D_\mu \nabla_v f) \ , \tag{19}$$

where D_μ is the velocity space diffusion coefficient. In spherical coordinates, this operator may be expressed as

$$C_\mu(f) = a_\mu(f) \frac{\partial^2 f}{\partial v^2} + b_\mu(f) \frac{\partial f}{\partial v} + c_\mu(f) f \ , \tag{20}$$

where for $v > 0$

$$a_\mu(f) = D_\mu \ , \tag{21a}$$

$$b_\mu(f) = \frac{\partial D_\mu}{\partial v} + 2 \frac{D_\mu}{v} \ , \tag{21b}$$

and

$$c_\mu(f) = 0 \ . \tag{21c}$$

In the limit as $v \to 0$, Eq. (20) is still used with the coefficients redefined as

$$a_\mu(f) = 3D_\mu \ , \tag{22a}$$

$$b_\mu(f) = 0 \ , \tag{22b}$$

and

$$c_\mu(f) = 0 \ . \tag{22c}$$

By integrating over velocity space, it is easy to show that this microwave collision operator conserves particles. That is,

$$\int C_\mu(f)\ d^3\vec{v} = 0\ . \tag{23a}$$

The second moment $P_\mu \equiv \int C_\mu(f)\ \frac{1}{2}\ mv^2\ d^3\vec{v}$ can be approximated by assuming D_μ to be independent of velocity, resulting in

$$P_\mu = 3mr^{\cdot}\ . \tag{23b}$$

Thus, the microwave operator with velocity-independent D_μ provides a power density of $3mnD_\mu$ W/m^3 to the electrons. For a velocity-dependent microwave diffusion coefficient, the power density may be written as

$$P_\mu = -4\pi m \int_0^\infty dv\ v^3 D_\mu \frac{\partial f}{\partial v}\ . \tag{24}$$

When integrated over volume, this becomes the total input microwave power

$$P_{\mu TOT} = -16\pi^3 R_T m \int_0^a r\ dr \int_0^\infty dv\ v^3 D_\mu \frac{\partial f}{\partial v}\ , \tag{25}$$

which depends on the radial and velocity dependencies of D_μ and $\partial f/\partial v$. To ensure a constant microwave power deposition, the coefficient D_μ is normalized whenever necessary so that the integral in Eq. (25) is constant for all time.

Assuming random phase between wave and particle, we choose an effective velocity space diffusion coefficient as given by Eldridge:[7]

$$D_\mu = \frac{1}{4} \frac{d\langle v_\perp^2\rangle}{dt}\ ,$$

where

$$\frac{d\langle v_\perp^2\rangle}{dt} = 2\pi\left(\frac{e}{m}\right)^2 \sum_{\text{modes}} |E_\perp|^2 \sum_{n=-\infty}^{+\infty} J_{n-1}^2\left(\frac{k_\perp v_\perp}{\Omega_e}\right) \delta(\omega - n\Omega_e - k_\parallel v_\parallel) \ . \tag{26}$$

The variable $E_\perp$ is the complex microwave electric field perpendicular to B, Ω_e is the electron cyclotron frequency, ω is the microwave frequency, and k is the wave number. Averaging Eq. (26) over a field line using $|E_\perp|^2 \approx \frac{2}{3}|E_\mu|^2$ and assuming $v_\perp \gg v_\parallel$ and one mode with $k_\perp \approx \omega/c$ and $k_\parallel = 0$, we obtain

$$D_\mu = N[b_1 J_0^2(v/c) + b_2 J_1^2(2v/c) + \ . \ . \ .] \ , \tag{27}$$

where N is the normalization factor mentioned above,

$$b_1 = \frac{2\pi}{3}\left[\left|\frac{eE_\mu}{m}\right|^2 \frac{n(s)/\bar{n}}{L(d\Omega/ds)}\right]_{\omega=\Omega_e} \ , \tag{28a}$$

and

$$b_2 = \frac{2\pi}{6}\left[\left|\frac{eE_\mu}{m}\right|^2 \frac{n(s)/\bar{n}}{L(d\Omega/ds)}\right]_{\omega=2\Omega_e} \ , \tag{28b}$$

where $\bar{n}$ is the field-averaged plasma density and L is the separation in z between resonance zones. These coefficients b_1 and b_2 are to be evaluated at the position s along the field line such that $\omega = \Omega_e(s)$, $2\Omega_e(s)$, and so on. Since many of the quantities in Eq. (28) are not well known, we have not explicitly calculated b_1 and b_2 from these equations. Instead, b_1 and b_2 have initially been chosen on an ad hoc basis, with b_1 chosen to be uniform in radius. Coefficient b_2, corresponding to second-harmonic resonance heating, is chosen to be

either zero — in order to study the problem with no second-harmonic heating — or zero everywhere except at the resonance zone (about 9.5-11 cm) where b_2 is arbitrarily assigned a value 100 times greater than the first-harmonic heating coefficient b_1. The reason for this second choice is that $d\Omega/ds$ in the denominator of Eq. (28b) approaches zero at the second-harmonic resonance zone, thus making b_2 very large.

2.3 BOUNDARY CONDITIONS

Owing to assumed symmetry about the plasma center $r = 0$, we take a boundary condition of

$$\frac{\partial f}{\partial r} = 0 \quad \text{at} \quad r = 0 \ . \tag{29}$$

For the velocity dimension, we require that

$$\frac{\partial f}{\partial v} = 0 \quad \text{at} \quad v = 0 \ . \tag{30}$$

At the plasma edge $r = a$, we choose a Milne-type boundary condition:

$$\frac{\partial f}{\partial r} = -\frac{1}{\lambda_t} f \quad \text{at} \quad r = a \ . \tag{31}$$

This is tantamount to requiring that the distribution function become zero linearly at some small distance λ_t outside of the region under consideration, $r = 0$ to $r = a$, while still allowing f to have some value at the edge. The distance λ_t is chosen to be the smallest resolvable distance in the code, one mesh width.

At the maximum of the velocity mesh, the boundary condition is more complicated. We have chosen a nonlinear boundary condition such that the distribution has the form of a local Maxwellian at $v = v_{max}$. Thus,

$$f = Ae^{-v^2/b^2} \ , \tag{32a}$$

where

$$A = f_{j-1} e^{v_{j-1}^2/b^2} , \tag{32b}$$

$$b^2 = \frac{v_{j-1}^2 - v_{j-2}^2}{\ln(f_{j-2}/f_{j-1})} , \tag{32c}$$

and the subscripts j-1 and j-2 refer to the values at the two mesh points immediately preceding v_{max}. The full effects of this boundary condition are currently under study. We have observed that the local temperature of the high energy tail of the calculated distribution function increases when the point v_{max} is increased. This is possibly due to the boundary condition Eq. (32). Work is under way to investigate this effect and to improve the boundary condition if necessary.

3. NUMERICAL METHODS

The partial differential Eq. (13) has been written in finite difference form using the collision operator terms developed in Sect. 2.2. The resulting difference equation has been set up on a finite difference mesh of 20 radial points by 100 velocity points. The equation is nonlinear since the coefficients a, b, and c, and the source term S depend on the value of f_o. In principle, the diffusion coefficient D may also depend on f_o, although the results presented here are calculated using D as defined in Eq. (14b), which is independent of f_o. We use an alternating-direction-implicit (ADI) scheme attributable to Douglas and Rachford,[8] which is accurate to order $(\Delta t)^2$, where Δt is the time step, and requires only the solution of M + N tridiagonal matrix equations to advance one time step, where M and N are the mesh sizes. For our 20 × 100 mesh, this means 120 tridiagonal solutions, a much faster method than the solution of a large matrix equation for a completely implicit two-dimensional Crank-Nicholson method. Since the equation is nonlinear, we assume an initial form for the distribution function and calculate the values of a, b, c, S, and D over the entire mesh for this value of f_o. These coefficients and the source term then are held constant while a purely linear problem is solved in time with the ADI method. When the linear problem has converged or after some fixed number of time steps (nominally 100), whichever occurs first, the coefficients and source term are reevaluated using the latest value of f_o. Again, the linear problem is stepped in time using the new values of a, b, c, S, and D. This process continues until steady state is reached — that is, the linear form of the equation has converged, and the coefficients are no longer changing. The computer code is designed to run on the NMFECC CRAY-1 computer and requires 5000-15,000 time steps and 5-10 min. of computer time to reach steady state.

4. RESULTS

We assume typical EBT-I parameters with $N_s = 24$ mirror sectors, a major radius of $R_T = 150$ cm, a plasma radius of $a = 12$ cm, and a magnetic field of $B_o = 0.65$ T on axis. The electron distribution function f_o is initially chosen to be a Maxwellian with parabolic density and temperature profiles

$$n_e(r) = (n_{ce} - n_{we})(1 - r^2/a^2) + n_{we} \tag{33a}$$

and

$$T_e(r) = (T_{ce} - T_{we})(1 - r^2/a^2) + T_{we} , \tag{33b}$$

where n_{ce} and n_{we} are the central ($r = 0$) and edge ($r = a$) densities and T_{ce} and T_{we} are the central and edge temperatures. The initial densities and temperatures are chosen as $n_{ce} = 2 \times 10^{12}$ cm^{-3}, $n_{we} = 2 \times 10^{11}$ cm^{-3}, $kT_{ce} = 300$ eV, and $kT_{we} = 40$ eV. The ion distribution function is chosen as a Maxwellian with the same parabolic density profile as the electron distribution function and a parabolic temperature profile with central and edge temperatures of $kT_{ci} = 40$ eV and $kT_{wi} = 13.5$ eV. The ion distribution function does not change and no electron-ion collisions are accounted for; this function is needed, however, in the calculation of neutral particle transport.

Typical steady-state results are shown in Figs. 2a and 2b. Both show a plot of $\ln f_0$ vs energy and radius for a high edge neutral density of $n_o = 3 \times 10^{10}$ cm^{-3}. Figure 2a is for the case of first-harmonic heating only — that is, $b_2 = 0$ in Eq. (27); Fig. 2b shows the result when second-harmonic heating is applied in addition to first-harmonic heating. In both figures, we note the appearance of a high energy tail on f_o more localized near the plasma edge. This peak in f_o corresponds to the hot electron ring. (We should point out that in Fig. 2b f_o is not negative near the plasma center, as it might appear. The figure shows the logarithm of f_o, rather than f_o itself, and the base line,

which is merely an arbitrary choice, does not correspond to $f_o = 0$.) Local Maxwellians fitted to the high energy tails of Figs. 2a and 2b correspond to temperatures of about 2.5 keV for the case of no second-harmonic heating and about 5.5 keV with second-harmonic heating.

Three important observations about these results are in order. First is the occurrence of a hot electron ring in Fig. 2a in the absence of second-harmonic heating. This is believed to be due to the effects of little Coulomb drag at the plasma edge and a large amount of drag at the center. Figure 3 shows the contribution of the various Fokker-Planck collision terms and the radial diffusion coefficient as a function of radius for the high energy tail of Fig. 2a. In this figure, we note that the contribution of Coulomb collisions is greater at the plasma center, where the plasma density is highest.

A second observation is that the ring temperatures are one to two orders of magnitude below experimental observations; a third is that the width of the peak in f_o is much greater than the experimentally conjectured ring width of 2-3 cm. Both of these deficiencies are possibly due to the finite choice for v_{max}. For the results shown here, v_{max} has been chosen to correspond to a maximum energy of 20 keV. It has already been mentioned that increasing the value v_{max} results in increased local temperature of the high energy tail. We also note that the radial diffusion term, which is roughly proportional to $1/v^3$, will decrease rapidly as v_{max} is increased. Lower radial diffusion at higher energies will limit the radial spread of the peak in f_o. Unfortunately, diffusion is our only source of particle loss; with much lower diffusion at high energies, it will take much longer to reach steady state, and thus much more computer time will be required. At higher energies it is also important to include radiation losses and relativistic effects. Plans are being developed to upgrade the model to include all these effects and to allow a much higher maximum energy.

When the edge neutral density is decreased to $n_o = 2 \times 10^{10}$ cm^{-3}, the high energy tail becomes larger. This relationship is shown in Figs. 4a and 4b, which correspond to first-harmonic heating only and first- and second-harmonic heating, respectively. Experimentally, when

the neutral pressure is lowered sufficiently, the EBT plasma changes from the stable T-mode of operation to the unstable M-mode, characterized by large, energetic electron rings. The large high energy component of f_o in Figs. 4a and 4b is suggestive of moving toward this mode of operation.

These results are summarized in Fig. 5, which shows the pressure of the high energy tail of f_o as a function of radius for three edge neutral densities from 1×10^{10} cm^{-3} to 3×10^{10} cm^{-3} when both first- and second-harmonic heating are applied. We note that at low neutral density the high energy tail is strong and large, occupying the entire plasma radius, whereas at high neutral density the high energy tail is weaker and more localized in radius. This latter condition is suggestive of moving toward the experimentally observed cold, or C-, mode of operation, where the annulus beta falls so low that the minimum in the magnetic field owing to diamagnetic ring currents is no longer sufficient to prevent MHD instability of the core plasma.

5. CONCLUSIONS

The model presented here is only preliminary and has much room for improvement. However, our results show that, within the limitations of our assumptions and computing ability, an electron distribution function can be numerically calculated that contains a high energy tail localized near the plasma edge heated by second-harmonic electron cyclotron resonance. The behavior of this high energy tail simulates some of the experimentally observed features as the edge neutral density is varied.

Work now under way and plans for the future call for improvement of the radial diffusion term and the microwave heating model to accompany the use of higher maximum energies. We also plan to include radiation losses and relativistic effects and the use of a nonzero electric field.

ACKNOWLEDGMENT

The authors wish to thank D. B. Batchelor and D. A. Spong for their many helpful discussions as this model was developed.

REFERENCES

1. R. D. Hazeltine, Plasma Phys. 15, 77 (1973).
2. E. F. Jaeger, C. L. Hedrick, and J. S. Tolliver, *A Kinetic Transport Model for the ELMO Bumpy Torus*, Oak Ridge National Laboratory report ORNL/TM-6313, Oak Ridge National Laboratory, Oak Ridge, Tennessee (1978).
3. D. A. Spong, E. G. Harris, and C. L. Hedrick, "Neoclassical Ion Transport Coefficients for the ELMO Bumpy Torus Device," paper presented at the 18th Annual Meeting, Division of Plasma Physics of the American Physical Society, San Francisco, California, November 15-19, 1976; Bull. Am. Phys. Soc. 21, 1069 (1976), paper 3C-4.
4. N. A. Krall and A. W. Trivelpiece, *Principles of Plasma Physics*, p. 316, McGraw-Hill, New York, 1973.
5. D. C. Montgomery and D. A. Tidman, *Plasma Kinetic Theory*, p. 34, McGraw-Hill, New York, 1964.
6. C. F. Kennel and F. Engelmann, Phys. Fluids 9, 2377 (1966).
7. O. Eldridge, Phys. Fluids 15, 676 (1972).
8. J. Douglas and H. Rachford, Trans. Am. Math. Soc. 82, 421-39 (1956).

ORNL-DWG 77-12491R

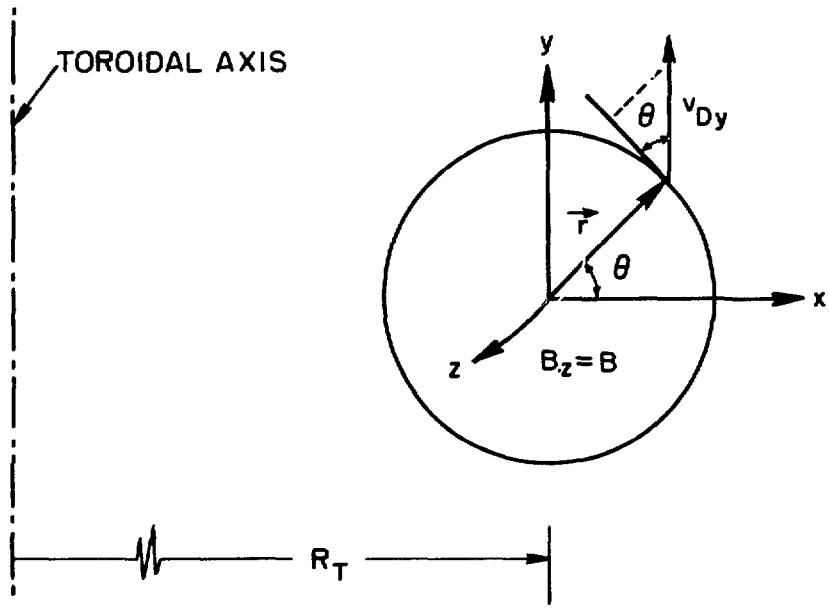

Fig. 1. Toroidal coordinate system.

ORNL-DWG 80-2025 FED

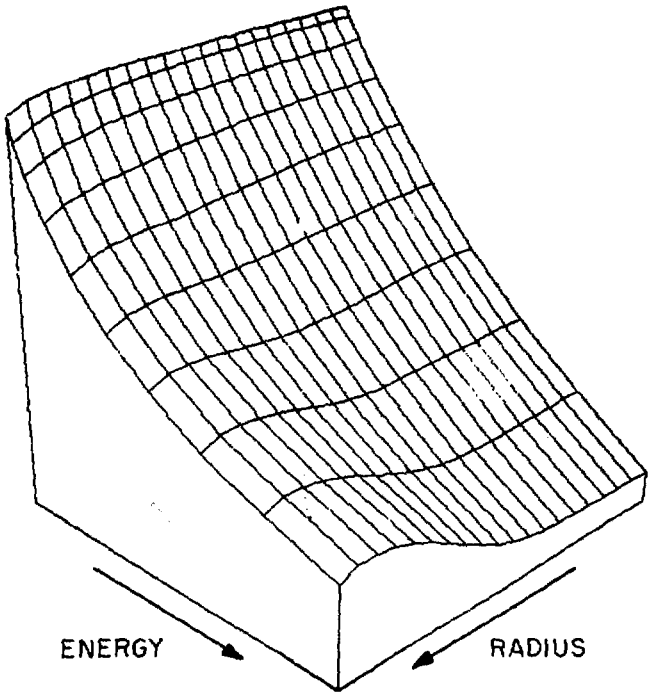

(a)

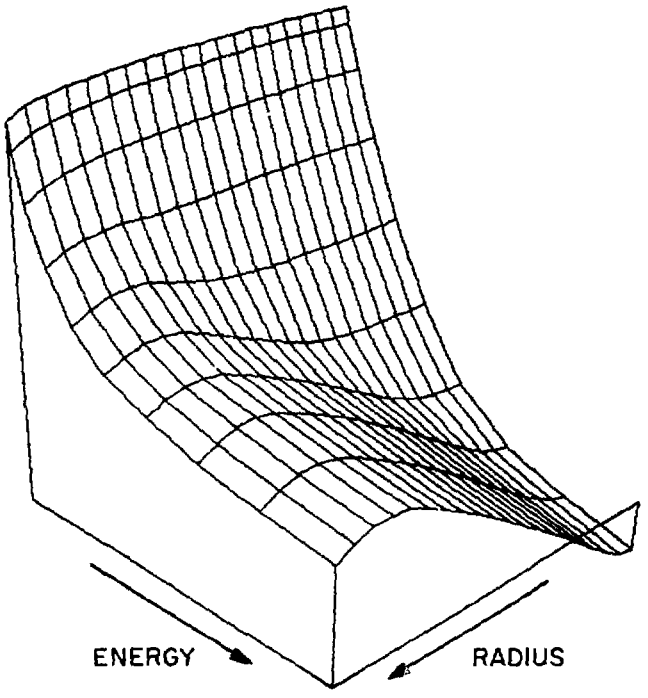

(b)

Fig. 2. Plot of $\ln f_o$ vs energy and radius for an edge neutral density of $n_o = 3 \times 10^{10}$ cm^{-3} (a) with first-harmonic microwave heating only and (b) with first- and second-harmonic microwave heating.

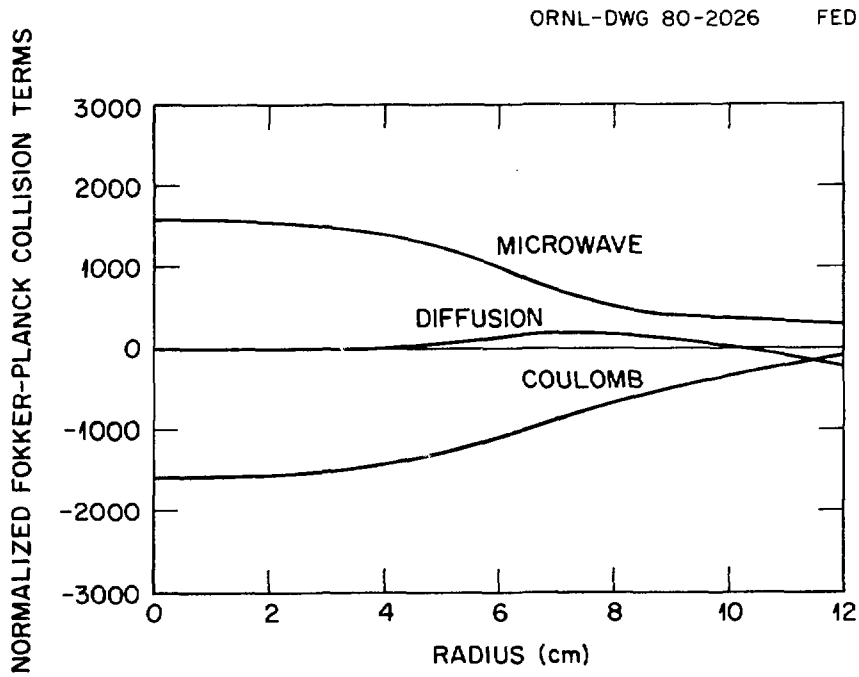

Fig. 3. Normalized Fokker-Planck collision operator terms for $n_o = 3 \times 10^{10}$ cm^{-3} and first-harmonic microwave heating only.

ORNL-DWG 80-2027 FED

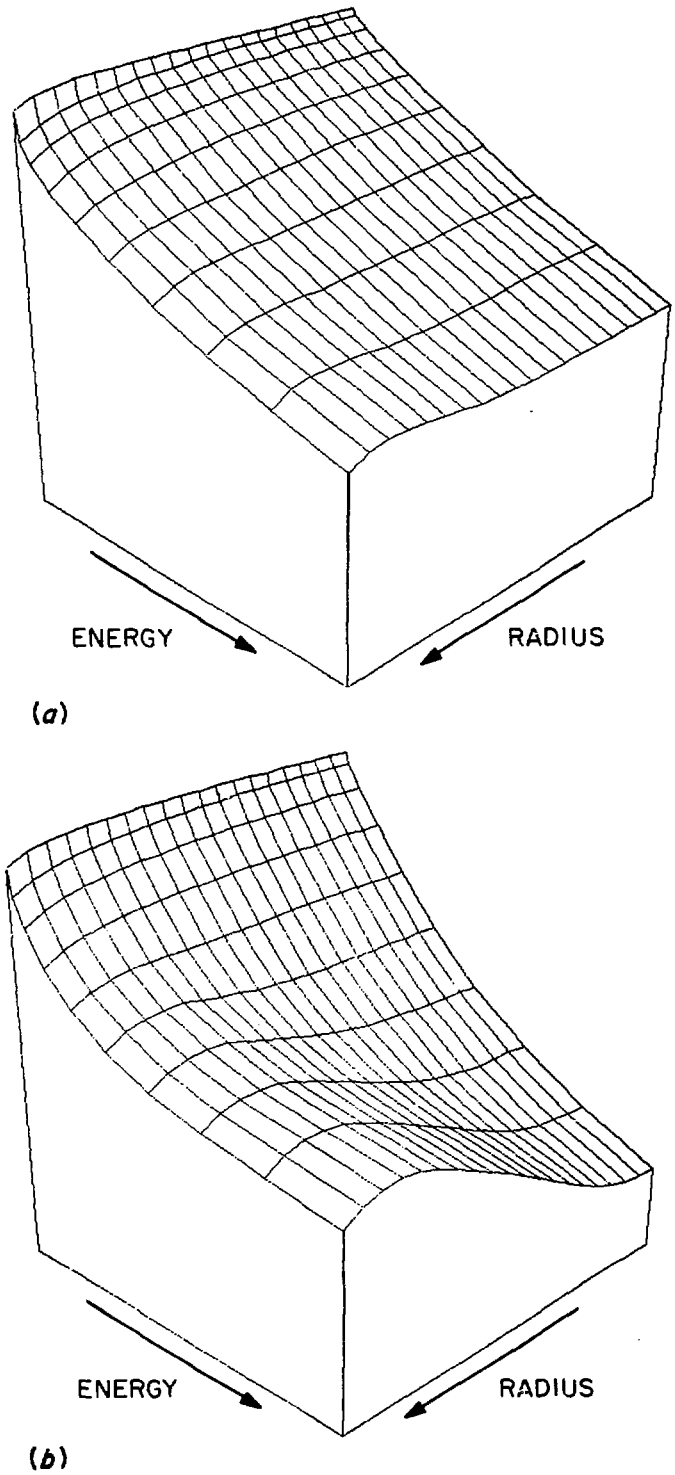

Fig. 4. Plot of $\ell n\ f_o$ vs energy and radius for $n_o = 2 \times 10^{10}\ cm^{-3}$ (a) with first-harmonic microwave heating only and (b) with first- and second-harmonic microwave heating.

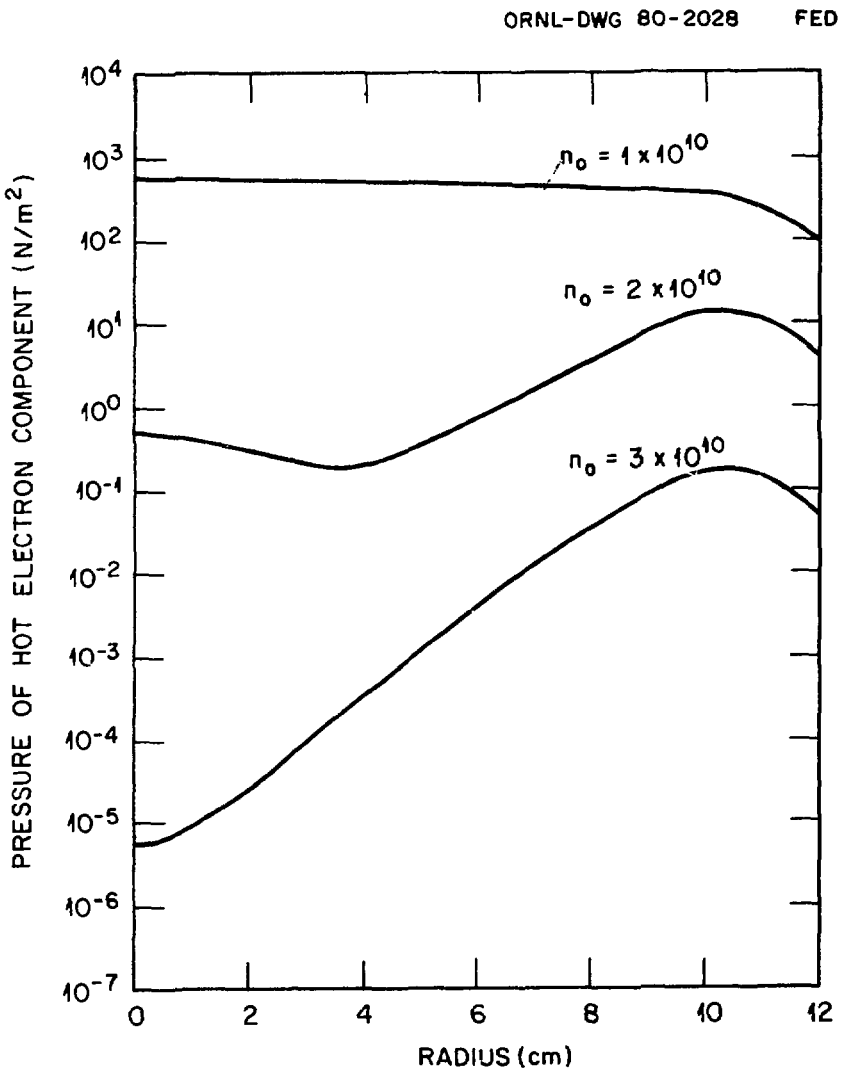

Fig. 5. Plasma pressure of high energy tail of the electron distribution function for three values of the edge neutral density n_o. First- and second-harmonic microwave heating has been applied in each case.

DISCUSSION

M. FUJIWARA: How do you determine the radial distribution of microwave field intensity?

J. TOLLIVER: Radial profiles of the first and second harmonic heating coefficients b_1 and b_2 are chosen on an ad hoc basis. Coefficient b_1 is chosen to be uniform in radius. When second harmonic heating is used, coefficient b_2 is given a "square-wave" profile being zero at all radial points except where the second harmonic resonance occurs (at 10-11 cm) where b_2 is arbitrarily chosen to be 100 times the uniform value of b_1. This choice is made because b_2 contains $d\Omega/ds$ in the denominator which approaches zero at the second harmonic resonance. The microwave power is distributed between the b_1 and b_2 profiles such as to give a total microwave power input of 25 kW for EBT-I parameters.

V. K. TRIPATHI: Is the velocity space diffusion coefficient the same as encountered in the quasilinear theory?

J. TOLLIVER: Essentially the same.

W. H. MINER: Would you estimate the increase in cost to run this code if you go out to relativistic velocities?

J. TOLLIVER: Unknown at this time. The code currently requires 5-10 minutes of Cray computer time, depending on the problem, to calculate one complete distribution function f as a function of radius and speed. We have ideas of how to speed up the solution at higher energies, because radius becomes less important. This high energy solution will then be connected to the low energy solution.

A MODEL KINETIC EQUATION FOR ELECTRON CYCLOTRON HEATING OF EBT RINGS

D. C. Baxter
Science Applications, Inc.
La Jolla, CA

I. B. Bernstein
Yale University
New Haven, CT

I. INTRODUCTION

Calculations of single particle orbits have produced estimates of single particle heating rates for electrons which transit a region where the microwave radiation frequency equals the local electron cyclotron frequency (e.g. 1, 2, 3). We derive a Fokker-Plank equation to describe the evolution of an electron distribution function which is anistropic in velocity space. Finite element numerical techniques may be used to find steady state solutions. These solutions will yield information about steady state microwave power requirements, parallel and perpendicular pressure of the ring and its longitudinal spatial distribution.

In addition to the ECR effects, we include collisions with a cold background plasma, self-collisions and the effective drag from cyclotron radiation.

II. BASIC EQUATIONS

Consider a fully ionized plasma in which the electrons are relativistic, described by the Fokker-Plank equation:

$$\frac{\partial f}{\partial t} + \frac{\vec{v}}{\gamma} \cdot \vec{\nabla} f + \vec{\nabla}_v \cdot \left[- \frac{e}{m} \left(\vec{E} + \frac{\vec{v} \times \vec{B}}{\gamma c} \right) f + \vec{\Gamma}_c + \vec{\Gamma}_R \right] = 0 \qquad (1)$$

$\vec{v} = \vec{p}/m$ momentum per unit rest mass

$\gamma = (1 + v^2/c^2)^{\frac{1}{2}}$

$\vec{E} = \vec{E}_0 (\vec{r},t) + R_e \left[\vec{h} (r,t) \exp (-i\omega t) \right]$

$\vec{B} = \vec{B}_0 (\vec{r},t) + R_e \left[- i (c/\omega) (\vec{\nabla} \times \vec{h}) \exp (- i\omega t) \right]$

$\vec{\Gamma}_c$ and $\vec{\Gamma}_R$ are particle currents in velocity space due to collisions and cyclotron radiation reaction respectively. For collisions with a cold background

$$\vec{\Gamma}_c = - \nu_c \left[(v^2 \vec{I} - \vec{v}\vec{v}) \cdot \vec{\nabla}_v f + \gamma \vec{v} \left(f + \frac{\gamma T}{mv^2} \vec{v} \cdot \vec{\nabla} f \right) \right], \qquad (2)$$

T = background temperature,

$$\nu_c = 4\pi NC \left(\frac{e^2}{mc^2} \right)^2 \left| \frac{\gamma}{(\gamma^2 - 1)^{3/2}} \right| \ln(\Lambda),$$

$$\Lambda = 4\pi N \left(T/4\pi Ne^2 \right)^{3/2}$$

N = background density.

An appropriate (non-linear) operator is substituted to include self-collisions.

Separating f into a rapidly varying part, f_1, and slowly varying part, f_o, from equation (1) we obtain

$$f_o = \left\langle f \right\rangle = \frac{\omega}{2\pi} \int_{t-\pi/\omega}^{t+\pi/\omega} f \, dt \quad ,$$

$$f_1 = f - f_o \quad ,$$

and

$$\frac{\partial f_o}{\partial t} + \frac{\vec{v}}{\gamma} \cdot \vec{\nabla} f_o + \vec{\nabla}_v \cdot \left[- \frac{e}{m} \left(\vec{E}_o + \frac{\vec{v} \times \vec{B}_o}{\gamma c} \right) f_o + \left\langle \vec{\Gamma} \right\rangle \right] = 0 \quad (3)$$

where:

$$\left\langle \vec{\Gamma} \right\rangle = - \frac{e}{m} \left\langle \left(\vec{E}_1 + \frac{\vec{v} \times \vec{B}_1}{\gamma c} \right) f_1 \right\rangle$$

$$+ \left\langle \vec{\Gamma}_c \right\rangle$$

$$+ \left\langle \vec{\Gamma}_R \right\rangle \quad .$$

and the angle brackets indicate a time average over the microwave radiation period.

Phase space coordinates are transformed to the usual (α, β, s, ε, μ, ϕ) coordinates. Then Equation (3) is averaged over ϕ and integrated over a bounce orbit to obtain

$$\frac{\partial}{\partial t}(\tau_b G_o) + \frac{\partial}{\partial \alpha}\Gamma_\alpha + \frac{\partial}{\partial \beta}\Gamma_\beta + \frac{\partial}{\partial \mu}\Gamma_\mu + \frac{\partial}{\partial \varepsilon}\Gamma_\varepsilon = 0$$

$$\left(\text{non relativistically } \frac{\partial \Gamma_\alpha}{\partial \alpha}, \frac{\partial \Gamma_\beta}{\partial \beta} = 0\right)$$

$$\Gamma_\mu = \oint ds \left| \frac{m\gamma}{u\mu} \left\langle\left\langle \vec{w}_o \cdot \vec{\Gamma}_o \right\rangle\right\rangle - \frac{\gamma\mu}{u} \frac{\partial \ln B_o}{\partial t} G_o \right|$$

$$\Gamma_\varepsilon = \oint ds \left| \left\langle\left\langle m\dot{b} \cdot \vec{\Gamma}_o \right\rangle\right\rangle + \frac{m}{u} \left\langle\left\langle \vec{w} \cdot \vec{\Gamma}_o \right\rangle\right\rangle - \frac{\gamma}{u}\left(\frac{\partial e\Phi}{\partial t}\right) G_o \right| \quad (4)$$

where

$$\tau_b = \oint \frac{ds}{(u/\gamma)} \sim 10^{-9} \text{ s}$$

$$F_o = G_o + G_1 + \ldots$$

$$\frac{\partial G_o}{\partial s} = 0$$

The double angle brackets indicate both fast time averaging and phase angle averaging.

The quasi-linear contributions to Γ_ε, Γ_μ is zero except in the region of ε, μ space where the resonant interaction occurs, as shown in the hatched region of Figure 1. The curves c and d correspond to boundaries where trapped particles resonate at their turning points and passing particle resonate at the throat respectively. Curve b separates passing particles from trapped particles. No particles exist below curve a.

a) $(\varepsilon/mc^2)^2 = 1 + 2\mu\, B_{min}/mc^2$

b) $(\varepsilon/mc^2)^2 = 1 + 2\mu\, B_{max}/mc^2$

c) $(\varepsilon/mc^2)^2 = 1 + (\varepsilon/mc^2)\, 2\mu\, B_{res}/mc^2$

$$\frac{e\, B_{res}}{mc} = \omega$$

d) $(\varepsilon/mc^2) = B_{max}/B_{res}$ (5)

The trajectory integral for f_1 reduces to a sum over resonant passages, following relativistic guiding center orbits and then becomes a sum of Bessel functions.

$$f_1 \propto \sum_{\substack{\text{resonant}\\ \text{passages}}} \sum_{n=-\infty}^{n=+\infty} \exp(i\chi_j)\, \tau_{eff} \Big\{ J_n(k_\perp\rho)(\vec{h}\cdot\hat{b}\, u/\gamma) m \frac{\partial f_o}{\partial \varepsilon}$$

$$+ \frac{1}{2}\left[J_{n-1}(k_\perp\rho)(\hat{e}_1 - i\hat{e}_2) + J_{n+1}(k_\perp\rho)(\hat{e}_1 + i\hat{e}_2)\right] \qquad (6)$$

$$\cdot \left[\vec{h}\left(\frac{m}{\gamma}\frac{\partial f_o}{\partial \varepsilon} + \frac{m}{B_o}\frac{\partial f_o}{\partial \mu}\right) + \frac{mu\hat{b}\times(\vec{k}\times\vec{h})}{\omega\gamma B_o}\frac{\partial f_o}{\partial \mu}\right] w \Big\} \; .$$

where, at resonance

χ_j = phase difference between microwave radiation and cyclotron gyration

$$\frac{d\chi}{dt} = n\frac{\Omega}{\gamma} - \omega + \frac{\hat{b} \cdot \vec{k}u}{\gamma} + \vec{k} \cdot \vec{V}_p = 0$$

$$\tau_{eff} = \left[\frac{d^2\chi}{dt^2}\right]^{-1/2} \cong \left|\frac{u}{\gamma} n \frac{d\Omega}{ds}\right|^{-1/2} \sim [\tau_b/n\Omega]^{1/2}$$

III. SIMPLE LIMIT CASE

A simple limiting case illustrates the type of results which may have to be considered. Consider the extraordinary mode, with small Larmon radius at the fundamental resonance. Ignoring any effect of loss cone.

$$\vec{\Gamma}_Q = -D(\overleftrightarrow{I} - \hat{b}\hat{b}) \cdot \vec{\nabla}_v f$$

$$\vec{\Gamma}_c = -\nu_c \left[(V^2\overleftrightarrow{I} - \vec{v}\vec{v}) \cdot \vec{\nabla}_v f + \gamma\vec{v}\left(f + \frac{\gamma T}{mv^2}\,\vec{v} \cdot \vec{\nabla}_v f\right)\right] \tag{7}$$

where

$$D = \left|\frac{eE}{m}\right|^2 \tau_{eff}^2/\tau_b >> \nu_c v$$

Using $v_\parallel$, $v_\perp$ coordinates appropriate to a "square-well" approximation and considering the limit that $\vec{\Gamma}$ is adequately described by $\vec{\Gamma}_Q$ in the resonant region and $\vec{\Gamma}_c$ in the non-resonant (deeply trapped) region.

In steady state

$$\frac{\partial f}{\partial t} = -\vec{\nabla}_v \cdot \vec{\Gamma} = 0 \tag{8}$$

So in the resonant region

$$\vec{\nabla} \cdot \vec{\Gamma}_Q = \frac{1}{v_\perp}\frac{\partial}{\partial v_\perp}\left(v_\perp\, D\, \frac{\partial f}{\partial v_\perp}\right) = 0 \tag{9}$$

and $v_\perp D \frac{\partial f}{\partial v_\perp}$ is a function of $v_\parallel$ only and must be zero because $v_\perp = 0$ is included in this region.

Therefore

$$f = Q\,(v_\parallel) \quad \text{(independent of } v_\perp\text{)} \tag{10}$$

and

$$\vec{\Gamma}_Q = 0. \tag{11}$$

In steady state

$$-\int \vec{\nabla}\cdot\vec{\Gamma}\varepsilon d^3v = +\int \frac{m\vec{v}}{\gamma}\cdot\vec{\Gamma} d^3v = 0, \tag{12}$$

so the contribution from $\vec{\Gamma}_Q$ to local heating is zero in those regions of velocity space where $\vec{\Gamma}_Q = 0$, (i.e. everywhere except near the boundary between resonant and non-resonant particles.) Even in this simple limiting case, the actual steady state solution will require an appropriate treatment of the boundary. A complete solution of equation (4) even in steady state for non-trivial geometries and including all modes and harmonics will be even more complicated.

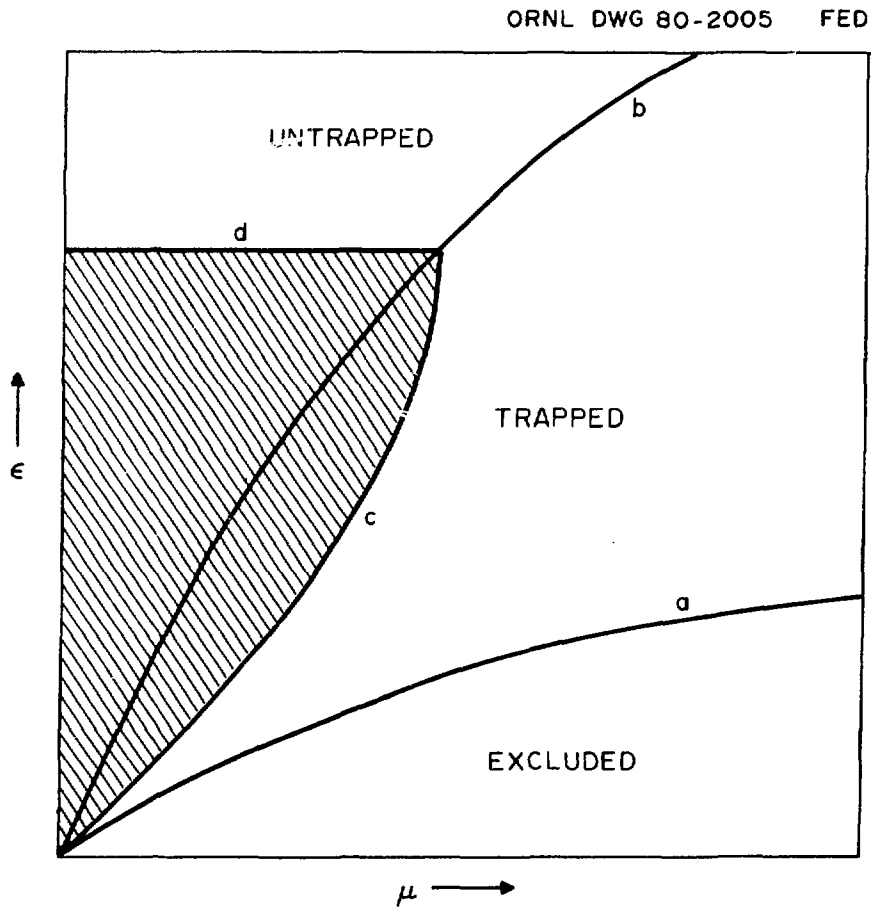

FIGURE 1

The electrons in the shaded region of ε, μ space experience ECRH. Curves a, b, c, d are explained in text.

REFERENCES

1. H. Grawe Plasma Physics, II, p. 151-162, 1969
2. O. Eldridge, Phys. Fluids, 15, p. 676-682, 1972.
3. D. Batchelor, ORNL/TM 6320, 1978.

DISCUSSION

V. K. TRIPATHI: The electric field of the microwave in the quasilinear diffusion coefficient is taken to be uniform — how far is this justified?

D. BAXTER: We did not mean to assume uniform electric field. We take applied field to be an externally given parameter of unspecified spatial dependence. We have not yet attempted to solve the self-consistent propagation problem.

J. PIPKINS: The distribution function f being independent of $v_\perp$ implies it is most applicable as a connection formula for low $v_\perp$ and high $v_\perp$ where collisions or collective effects become important.

D. BAXTER: Yes, the statement $\partial f/\partial v_\perp = 0$ is a consequence of neglecting any effects except the perpendicular quasilinear velocity diffusion. At best, this is appropriate in a finite range of velocity.

A MODEL FOR ELECTRON RING FORMATION IN EBT

S. Hamasaki, H. H. Klein, N. A. Krall,
J. B. McBride and J. L. Sperling

JAYCOR
1401 Camino Del Mar
Del Mar, CA 92014

In this paper we discuss a model for electron ring formation in EBT using a relativistically correct heating rate, based on the quasilinear interaction of the electrons with the microwave electric fields. The steady state ring temperature, the radial extent of the rings, and thus the power required to sustain the rings are determined by balancing the line averaged heating rate against existing expressions for the classical energy loss processes of the ring electrons. We emphasize the role of second harmonic heating in the formation of the rings and the role of relativistic effects in determining the steady state ring temperature.

Paper contributed to Workshop on EBT Ring Physics, Oak Ridge, Tennessee, December 3-5, 1979.

I. INTRODUCTION

In this paper we formulate a simple model of the high energy electron rings in EBT. Using this model we can calculate the radial extent of the rings, their steady state temperature and the power required to sustain them. Earlier work[1-3] on EBT rings has concentrated on the classical energy loss processes of the ring electrons in order to determine the power required to sustain the rings against such losses. In these treatments no specific model for the microwave power deposition was considered, and in this sense no attempt at self consistency was made. Here we attempt to extend the earlier work by formulating a relativistically correct microwave heating rate based on the quasilinear interaction of the ring electrons with the microwave electric fields. By balancing this expression for power input against the existing expressions for the classical energy loss processes, a self consistent determination of many of the ring properties is made possible. In Section II we formulate the ring heating model. Section III contains a brief review of the cold plasma dispersion characteristics and cutoff regions for the microwave modes in EBT. We then discuss ring calculations for EBT-1 parameters in Section IV. Section V contains our conclusions to date and indicates directions for future work.

II. HEATING MODEL

The approach we adopt to calculate the heating of the ring electrons is based on the quasilinear interaction of these ring electrons with the microwave fields. Such an approach has been employed in a different but analogous situation by Stix[4] to treat ion cyclotron heating in tokamaks. Since the ring particles reach quite high energies, a relativistic description of the heating process will be necessary. We proceed by comparing the relativistic Vlasov equation

$$\frac{\partial f}{\partial t} + \underset{\sim}{v} \cdot \frac{\partial f}{\partial \underset{\sim}{x}} - e\left(\underset{\sim}{E} + \frac{\underset{\sim}{v} \times \underset{\sim}{B}}{c}\right) \cdot \frac{\partial f}{\partial \underset{\sim}{p}} = 0 \qquad (1)$$

with its usual nonrelativistic analog. In Eq. (1) the momentum $\underset{\sim}{p}$ and velocity $\underset{\sim}{v}$ are related by

$$\underset{\sim}{p} = \gamma\, m_o\, \underset{\sim}{v}$$

where $\gamma = (1 + p^2/m_o^2c^2)^{\frac{1}{2}}$ is a constant of the motion (the electron energy in units of their rest energy) and m_o is the electron rest mass. The familiar results of nonrelativistic quasilinear theory[5] can be generalized in a straightforward way to treat relativistic energies by making the following replacements

$$\underset{\sim}{k} \longrightarrow \underset{\sim}{k}/m_o\,\gamma$$

$$\underset{\sim}{v} \longrightarrow \underset{\sim}{p}$$

$$\Omega_o \equiv eB_o/m_oc \longrightarrow \Omega = \Omega_o/\gamma$$

$$e \longrightarrow em \quad .$$

The result is

$$\frac{\partial F}{\partial t} = i\left(\frac{e}{2\omega}\right)^2 \sum_k \sum_n \left[\frac{1}{p_\perp}\frac{\partial}{\partial p_\perp} n\Omega + \frac{\partial}{\partial p_z}\frac{k_z}{m_o\gamma}\right] \frac{|\theta|^2}{\omega - n\Omega - k_z p_z/m_o\gamma}$$

$$\cdot \left[\frac{n\Omega}{p_\perp}\frac{\partial f_o}{\partial p_\perp} + \frac{k_z}{m_o\gamma}\frac{\partial f_o}{\partial p_z}\right] \qquad (2)$$

where

$$\theta \equiv p_\perp E^- J_{n-1}(b)\, e^{i\psi} + p_\perp E^+ J_{n+1}(b)\, e^{-i\psi} + 2\, p_z E_z J_n(b)$$

$$\underset{\sim}{k} = \hat{e}_x k_\perp \cos\psi + \hat{e}_y k_\perp \sin\psi + \hat{e}_z k_z$$

$$b \equiv k_\perp p_\perp/m_o\,\Omega_o$$

and f_o is the solution to the (zeroth order) Vlasov equation. The symbol $\perp$ means perpendicular to the magnetic field, $\underset{\sim}{B}$, and the z- direction is chosen to lie along $\underset{\sim}{B}$.

Here we will not be concerned with changes in the distribution function directly, but assume that we can sensibly attribute a temperature to the ring electron distribution. Thus we define the heating rate of the ring electrons as

$$\frac{3}{2}\frac{\partial(n_A T_A)}{\partial t} \equiv \int d^3p\, m_0\, c^2\, (\gamma - 1)\, \frac{\partial F}{\partial t} = \frac{\partial}{\partial t}\int d^3p\, \gamma\, m_0 c^2\, F\, d^3p$$

The resonant heating specialized to a Maxwellian zeroth order distribution of ring electrons, f_0, is then described by

$$\frac{3}{2}\frac{\partial(n_A T_A)}{\partial t} = \frac{\pi\omega_{pA}^2}{8T_A m_0} \sum_k \sum_n |E^-|^2 \int_0^\infty dp_\perp \int dp_z$$

$$\cdot\ \delta\left(\omega - \frac{n\Omega_0}{\gamma} - \frac{k_z p_z}{m_0\gamma}\right) \cdot \frac{p_\perp^3}{\gamma^3} J_{n-1}^2\,(b)\, f_0\,(p) \qquad (3)$$

where the subscript A denotes ring (annulus) quantities, and we retain only the electron interaction with the right circularly polarized component of the microwave electric field, E^-. Several points deserve comment:

1) The resonant condition

$$\omega - n\Omega_0/\gamma - k_z p_z/m_0\gamma = 0$$

determines p_z as a function of $p_\perp$.

2) The presence of the relativistic mass shift in the resonance condition changes the location of the usual vacuum cyclotron resonance at high energies, and is a principal effect of relativity in the ring heating process.

3) Higher harmonic contributions to the heating can be important at relativistic energies since $b \sim O(1)$, and thus a small argument expansion of the Bessel functions is not correct; i.e., if $\omega/ck \sim O(1)$ then $b \equiv kp_\perp/m_0\Omega_0 \sim O(v_\perp/c) \sim O(1)$ at relativistic energies.

In order to calculate the steady state ring properties, we balance $\frac{3}{2}\,\partial(n_A T_A)/\partial t$ given by Eq. (3) against existing expressions for the classical energy losses of the ring electrons as given in Borowski, et al.[1] Specifically, we write

$$\frac{3}{2}\frac{\partial(n_A T_A)}{\partial t} = (P_{synch} + P_{brems} + P_{scatt} + P_{drag})/\text{Volume} \tag{4}$$

where the terms on the right hand side of Eq. (4) are the powers per unit volume lost from the ring due to synchrotron radiation, bremsstrahlung, scattering and drag on the background plasma. These terms are given in Eq. 4.2 of Ref. 1 by $P_{\mu A}/NV_A$, except that the drag term is replaced by the more general form in Eq. 3.1.1 of Ref. 1 as $n_A \frac{dE}{dt}$.

In the calculations presented further on, we model the ring equilibrium distribution by the relativistic Maxwellian

$$f_o(p) = \frac{1}{4\pi T_A m_o^2 c\, K_2\left(\frac{m_o c^2}{T_A}\right)} \exp\left[-\frac{m_o c^2}{T_A}\sqrt{1 + \frac{p^2}{m_o^2 c^2}}\right] \tag{5}$$

where K_2 is a modified Bessel function of the second kind. Thus, our model situation is one in which the background plasma has its own given density and temperature n_p and T_p, and the ring is chosen to be a Maxwellian with a different (in general) given density n_A and temperature T_A, calculated from Eq. (4).

III. CUTOFF REGIONS IN EBT

We assume that the propagation characteristics of the microwaves in EBT are determined by the cold background plasma rather than by the ring itself. The cold plasma dispersion relation in the electron-cyclotron frequency range, $\omega \sim \Omega_e >> \Omega_i, \omega_{pi}$, is expressed as[6]

$$n^2 = 1 - \frac{2\alpha\,(1-\alpha)}{2(1-\alpha) - \beta \sin^2\theta \pm \Gamma} \tag{6}$$

where

$$\alpha = \frac{\omega_{pe}^2}{\omega^2}, \quad \beta = \frac{\Omega_e^2}{\omega^2}, \quad n = \frac{ck}{\omega}$$

$$\Gamma = \left[\beta^2 \sin^4\theta + 4\beta\,(1-\alpha)^2 \cos^2\theta\right]^{1/2}$$

$$\theta = \cos^{-1}\left(\underset{\sim}{k} \cdot \underset{\sim}{B}/|\underset{\sim}{k}|\,|\underset{\sim}{B}|\right)$$

and the +(-) signs refer to ordinary (extraordinary) mode propagation.

As described in Batchelor and Goldfinger's paper[7], the dispersion relation of Eq. (6) gives the cutoff (n= 0) condition

$$\omega_{pe}^2 = \omega^2 \tag{7}$$

for the ordinary mode propagation, and

$$\omega_{pe}^2 = \omega^2 \ (1 - \Omega_e/\omega) \tag{8}$$

for the extraordinary mode propagation. We note that a resonance ($n \to \infty$) occurs in the extraordinary mode at

$$\omega_{pe}^2 = \omega^2 \ (1 - \Omega_e^2(1 - \alpha \cos^2 \theta)/\omega^2) \quad . \tag{9}$$

However, an extraordinary wave propagating from a low magnetic field and low density region will encounter the right-hand cutoff [the condition of Eq. (8)], and hence be reflected before reaching this resonance [the condition of Eq. (9)].

Also, the right-hand cutoff condition of Eq. (8) indicates that an extraordinary wave propagating from the low magnetic field and low density region will not even reach the first harmonic heating resonance, $\omega = \Omega_e$, for a finite (non-zero) density plasma. This implies that heating by an extraordinary wave propagating from outside in EBT may only be possible for higher harmonics than the first harmonic resonance. Usually the heating by an ordinary wave is weak when the plasma is cold [see Eq. (2), the term in E_z]. Thus we conclude from cold plasma theory that second harmonic heating by an extraordinary wave may be dominant in the formation of electron rings in EBT. Based on this, we emphasize discussion of the second harmonic heating by extraordinary waves in the remainder of this paper. Figure 1, taken from Ref. 7, contains a sketch of the resonance and cutoff regions in EBT.

IV. RING CALCULATIONS FOR EBT

We now describe some calculations using the heating formula given by Eq. (3) for second harmonic heating, $\omega = 2\Omega_0$, for parameters in the EBT-1 range of operation. In all calculations presented in this section, the microwave field is a given constant and we simply take $\omega/k_\perp = c$ and $k_\parallel = 0.2\ k_\perp$. Figure 2 shows the heating rate normalized to the square of the microwave field amplitude at an assumed ring temperature of 5 keV versus the magnetic field normalized to the resonant value, taken to be $B_0 = 6.5$ kG. This figure illustrates the localized nature of the heating process in the radial direction for low ring energies. Figure 3 shows a similar curve at a ring temperature of 150 keV. The curve labeled "total" is the sum of the first 3 terms in the Bessel function series in Eq. (3). Note that at these high energies, the heating rate is much less localized, and that off resonant terms make a sizeable contribution to the total heating rate. For comparison, we have plotted the nonrelativistic ($c \to \infty$) result which indicates that the relativistic effect is to decrease the heating rate in the vacuum resonance region and to shift the maximum to larger magnetic fields.

Figures 5-7 summarize the results of more meaningful calculations in which the heating rate was field line averaged. We assumed a model magnetic field of the form

$$B = B(r)\ (1 + z^2/L^2)$$

with L chosen to be 10 cm, and calculated

$$\langle d(n_A T_A)/dt \rangle \equiv \frac{1}{1.4L} \int_{-0.7L}^{+0.7L} dz\ d(n_A T_A)/dt \qquad (10)$$

In order to understand the labeling in Figures 5-7, we refer to Figure 4, which sketches the magnetic geometry in the region of the ring second harmonic resonance. The field line labeled S_0 intersects the second harmonic resonance surface at the tanget point r_0 where the midplane magnetic field is exactly at resonance, $B(r_0)/B_0 = 1$. The field line labeled S_1 intersects the resonant surface away from the midplane, but the field line labeled S_{-1}

does not intersect resonance at all. The midplane radius on field lines S_1 and S_{-1} are denoted r_1 and r_{-1}, respectively. In Figure 5 we have plotted the line averaged heating rate of Eq. (5) normalized to the square of the microwave electric field vs. annulus temperature for three values of $B(r)/B_0$ corresponding to the field lines S_0, $S_{\pm 1}$ of Figure 4. The background plasma density and temperature were chosen as $n_p = 1 \times 10^{12}$ cm^{-3} and $T_p = 200$ eV, and the ring density was chosen as $n_A = 1 \times 10^{11}$ cm^{-3}. We have also plotted the classical loss processes for two choices of microwave electric field, E = 100 V/cm and 200 V/cm. We assume that the ring does not begin to form unless the heating exceeds the losses at $T_A = T_p$. The radial extent of the ring is thus determined in the model by the range of $B(r)/B_0$ for which the heating exceeds the energy losses at $T_A = T_p$. Saturation of the ring temperature occurs at high energies when the heating rate eventually drops and the heating equals the power losses. Figure 6 shows the effect of different background plasma density assumptions, and indicates that lower background density leads to radially thicker rings for a given microwave field amplitude. Figure 7 shows the effect of different assumptions on the background plasma temperature and indicates that preheat to higher temperatures by a mechanism other than second harmonic heating by the extraordinary mode allows formation of more radially extended ring structures due to second harmonic heating. Note that for low background temperatures, ring startup is not possible at all with second harmonic heating alone. We note that the ring localization depends on the microwave electric field strength, the background plasma density and temperature, and for these calculations is typically $\delta B/B_0 \simeq 0.1$, which corresponds to 1-2 cm for the EBT-1 geometry, and that the saturated temperature is $T_A \sim 500$ keV.

For comparison we plot in Figure 8 results for direct first harmonic ring heating to illustrate the affects associated with first harmonic penetration to the ring resonance region, should the cold plasma cutoff discussion of Section III prove to be misleading. A salient feature of these results is that broader rings can form for lower assumed values of the microwave electric fields. The heating due to first harmonic interaction is much more efficient at low energies than that due to second harmonic interaction, and thus could more easily lead to ring startup even for cold background temperatures, if the waves in fact penetrate to the ring resonance region.

V. CONCLUSIONS AND DIRECTIONS FOR FUTURE WORK

The results of our study of ring heating and formation to date can be summarized by the following conclusions:

(1) Second harmonic heating alone appears insufficient to startup the rings from low temperatures (< 100 eV), unless the microwave field amplitude is much larger than ~100 V/cm.

(2) However, localized rings are predicted to form for EBT-1 parameters by second harmonic interaction with the electrons providing another mechanism is invoked to preheat the plasma to $\gtrsim$ 100 eV.

(3) First harmonic heating is adequate to startup the rings from low temperatures, but penetration is questionable from the standpoint of conventional cold plasma dispersion theory.

(4) The first harmonic calculations lead to more radially extended ring structures at more modest microwave electric fields than for second harmonic heating.

(5) Within our model, second harmonic heating leads to radial ring thicknesses of 1~2 cm and steady state ring temperatures of ~500 keV in the range of EBT-1 plasma parameters, and assumed microwave electric field strengths ~100 V/cm.

We emphasize that much more attention to details of the physics and thus much more work will be necessary to produce a ring model to realistically compare with experiment and to use for scaling predictions. What we have done here is to take a step towards that goal by beginning to look from first principles at the heating process. Future work aimed at improving our theoretical understanding of the heating description should focus on:

(1) Inclusion of more realistic magnetic field models and averaging procedures for better modelling of actual EBT magnetic geometry.

(2) More realistic description of wave propagation characteristics. Here we considered only spatially constant microwave electric fields, and simply took $\omega/k = c$ and $k_{\parallel} = 0.2\ k_{\perp}$.

(3) Understanding the role of first harmonic heating (can these modes penetrate by a mechanism that renders cold plasma predictions of cutoff misleading, e.g., by warm plasma effects).

(4) Understanding the role of ordinary wave heating. Here we treated only the resonant extraordinary wave heating.

(5) Determination of the distribution function. Here we simply assumed an isotropic Maxwellian with time varying temperature. As a first step in this direction we could test the sensitivity of the results to other model choices of f_0, e.g., a two temperature Maxwellian.

In addition to the many improvements required in treating the ring heating processes, an adequate model for ring formation and power balance will also require improved treatments of the ring energy loss mechanisms, e.g., a correct Fokker-Planck description of the electron drag on the background plasma.

REFERENCES

1. S. K. Borowski, N. A. Uckan, E. F. Jaeger and T. Kammash, Oak Ridge National Laboratory Report #ORNL/TM-6910 (1979).

2. A. Andrade and R. A. Krakowski, Draft Report dated Sept. 10, 1979, communicated to us on a recent visit to JAYCOR by R. A. Krakowski.

3. W. B. Ard and R. J. Kashuba, contained in McDonnell Douglas Corporation Report #MDC E2160 (Oct. 29, 1979).

4. T. H. Stix, Nuclear Fusion 15, 737 (1975).

5. C. F. Kennel and F. Engelmann, Phys. Fluids 9, 2377 (1976).

6. T. H. Stix, "The Theory of Plasma Waves," McGraw Hill, New York (1962).

7. D. B. Batchelor and R. C. Goldfinger, Oak Ridge National Laboratory Report #ORNL/TM-6992 (Sept. 1979).

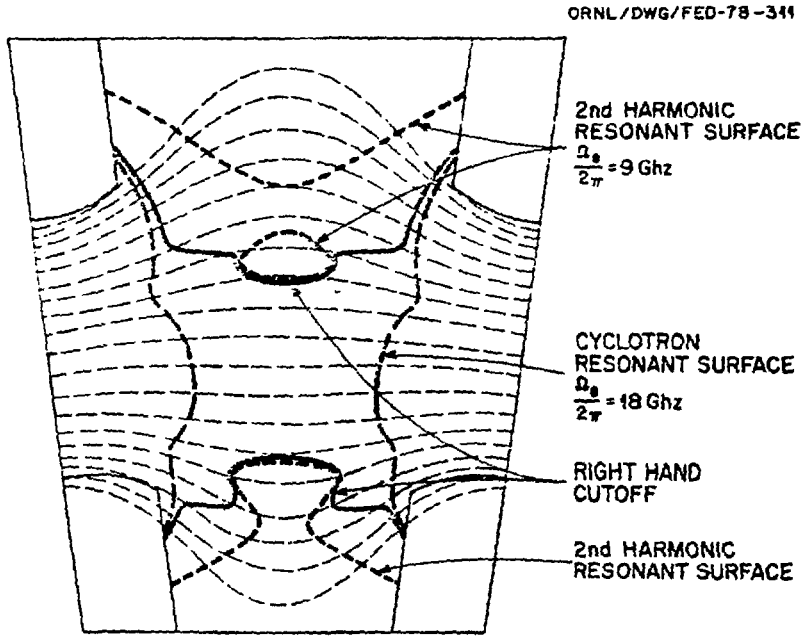

Figure 1. Sketch of the cyclotron resonance and cutoff regions in EBT. This figure is taken from Ref. 7.

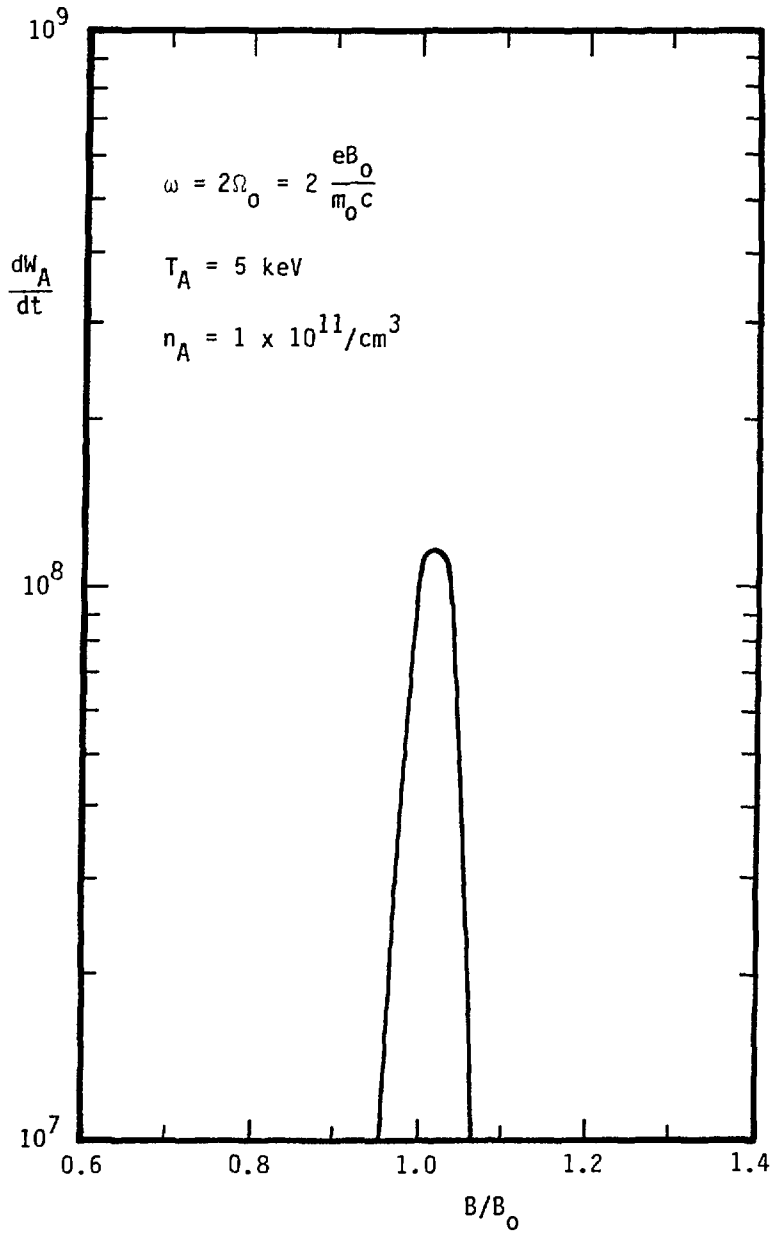

Figure 2. Plot of second harmonic heating rate normalized to $|E^-|^2$ vs. magnetic field normalized to the resonant magnetic field, B_o, for T_A = 5 keV. Here and in succeeding figures B_o = 6.5 kG as in EBT-1 and $\frac{dW_A}{dt} = \frac{3}{2}\frac{d}{dt}(n_A T_A)/|E^-|^2$.

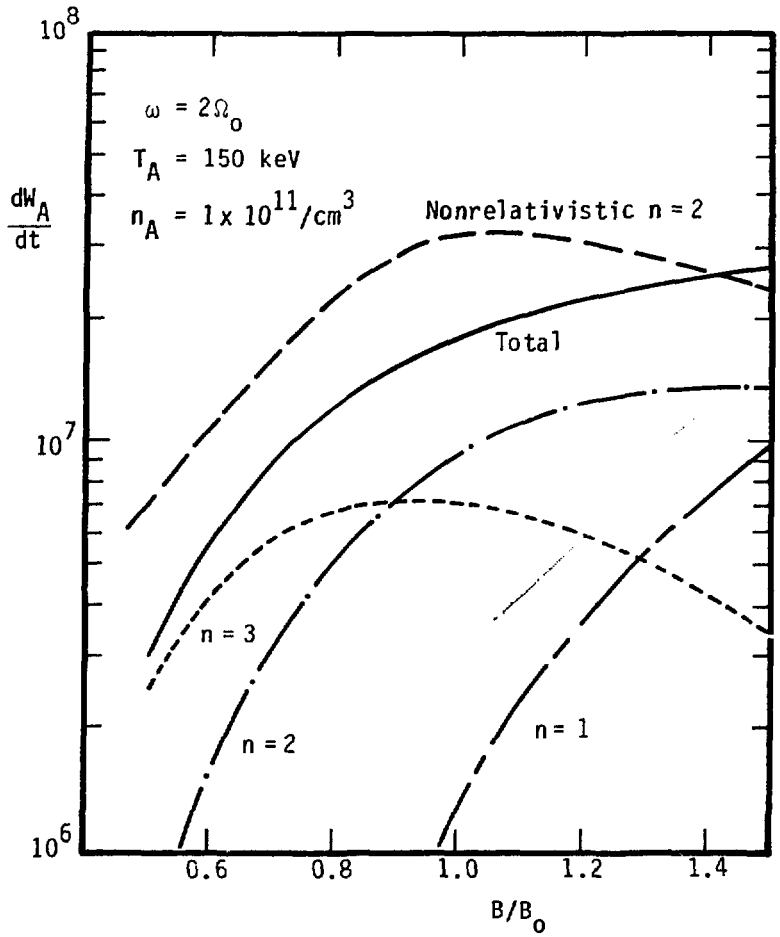

Figure 3. Same as Figure 2 but for T_A = 150 keV. We have plotted separately the contributions from the n = 1,2,3 terms in the Bessel series summation as well as their sum. Also we give the nonrelativistic result for n = 2 for comparison.

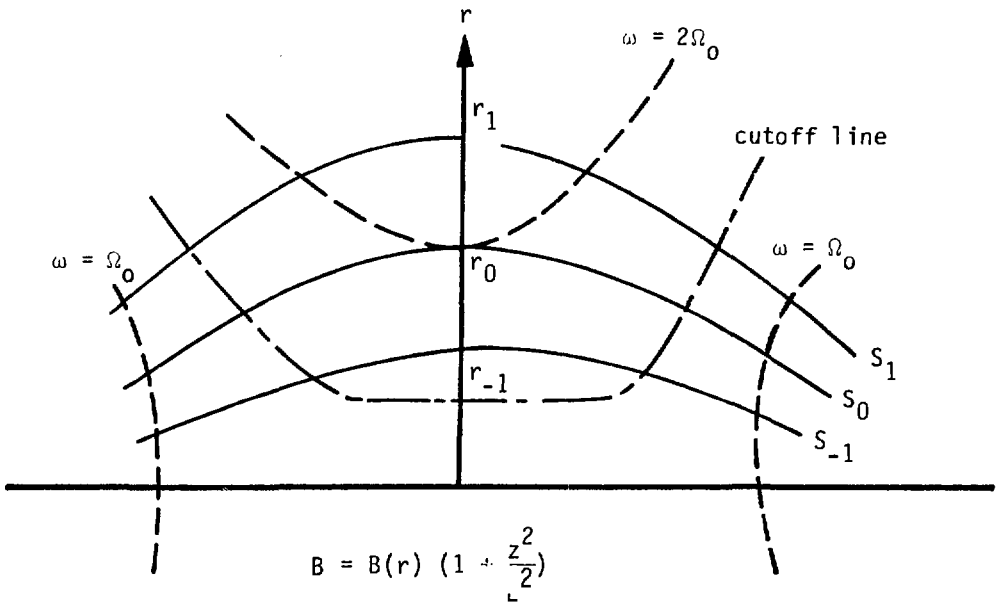

Figure 4. Sketch of EBT magnetic field lines, resonant and cutoff surfaces appropriate to second harmonic heating by extraordinary waves. The letter S labels a field line, and r the radial location of a field line at the midplane.

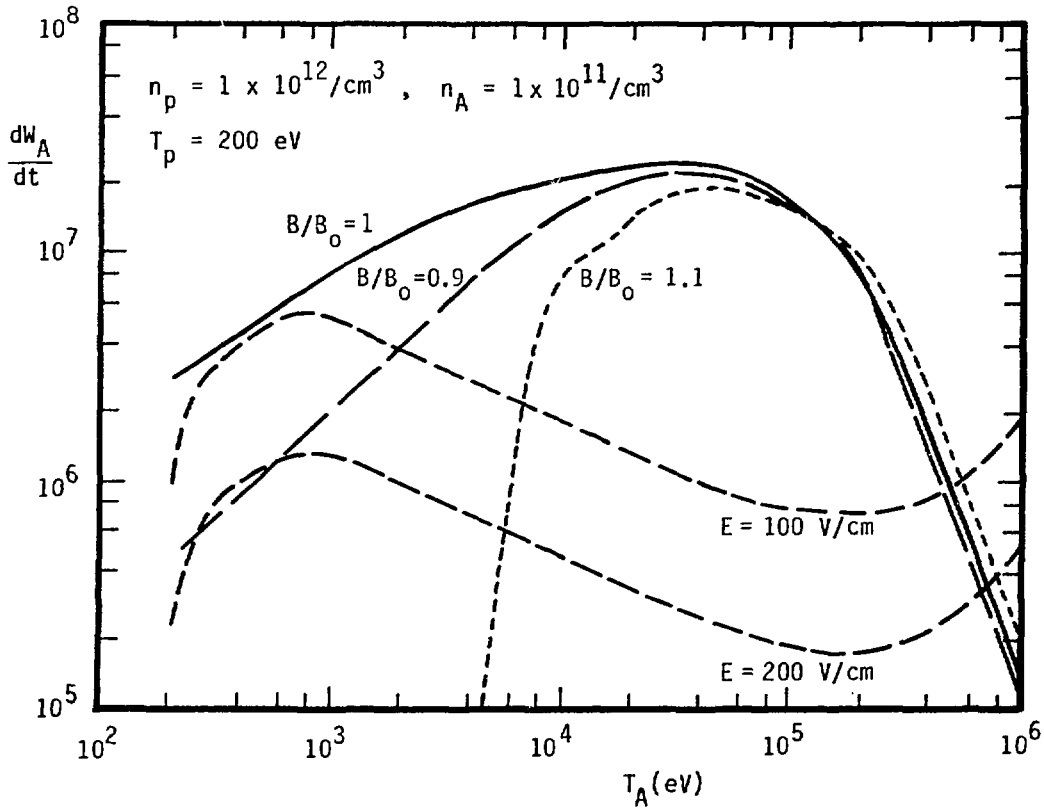

Figure 5. Plot of the line averaged second harmonic heating rate normalized to $|E^-|^2$ vs. ring temperature for given background plasma parameters and ring density for three different field lines corresponding to S_0, $S_{\pm 1}$ of Figure 4. The ratio $B/B_0 \equiv B(r)/B(r_0)$ at the midplane. Also plotted are the classical power losses per unit volume normalized to $|E^-|^2$ for two values of the extraordinary mode field amplitude.

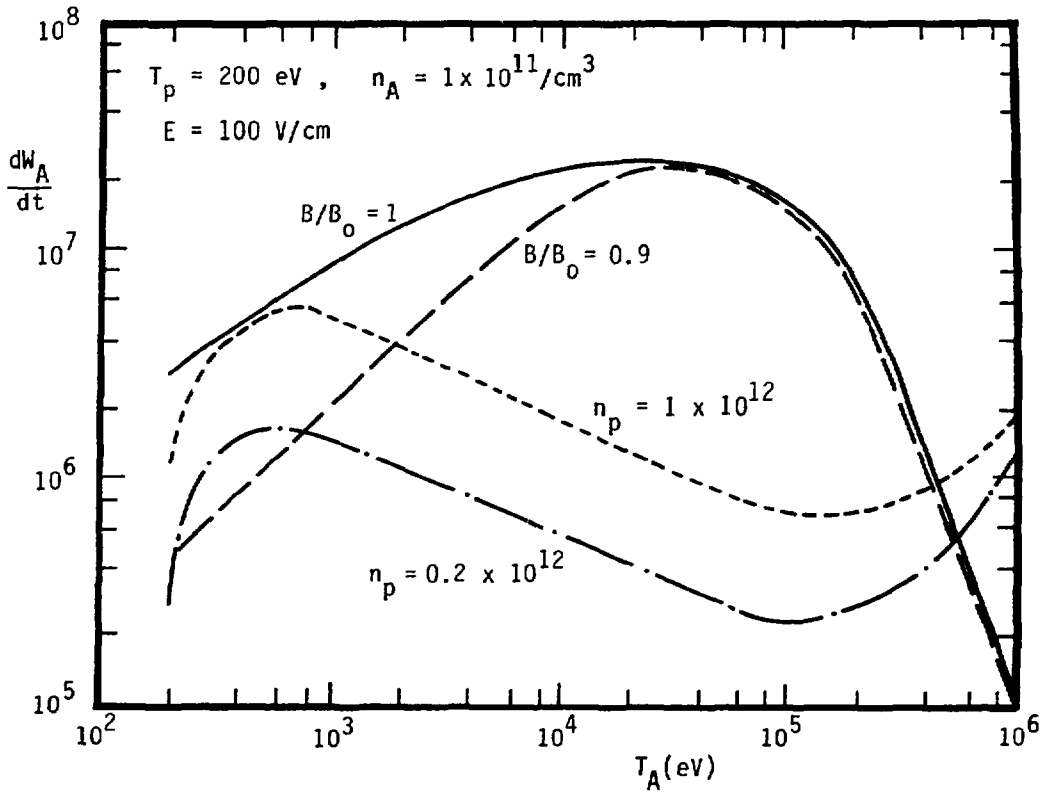

Figure 6. Similar to Figure 5 but for a single fixed value of the microwave electric field but now for two different choices of background plasma density.

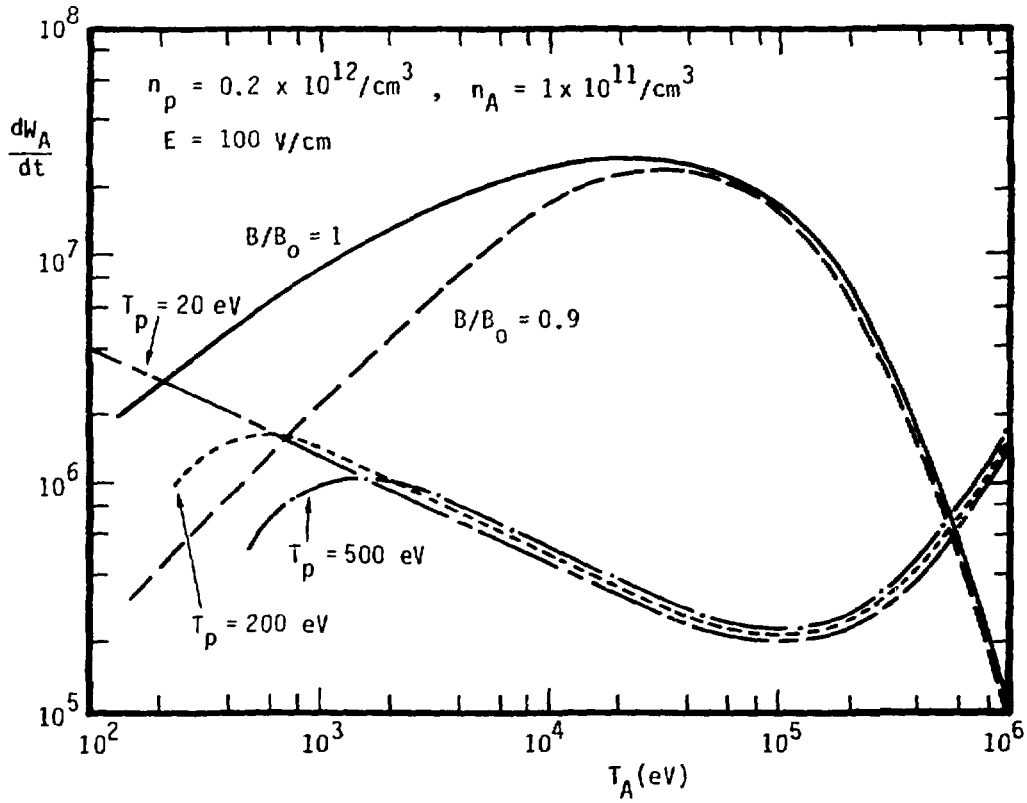

Figure 7. Similar to Figure 5 but for several choices of background plasma temperature and a single microwave electric field strength.

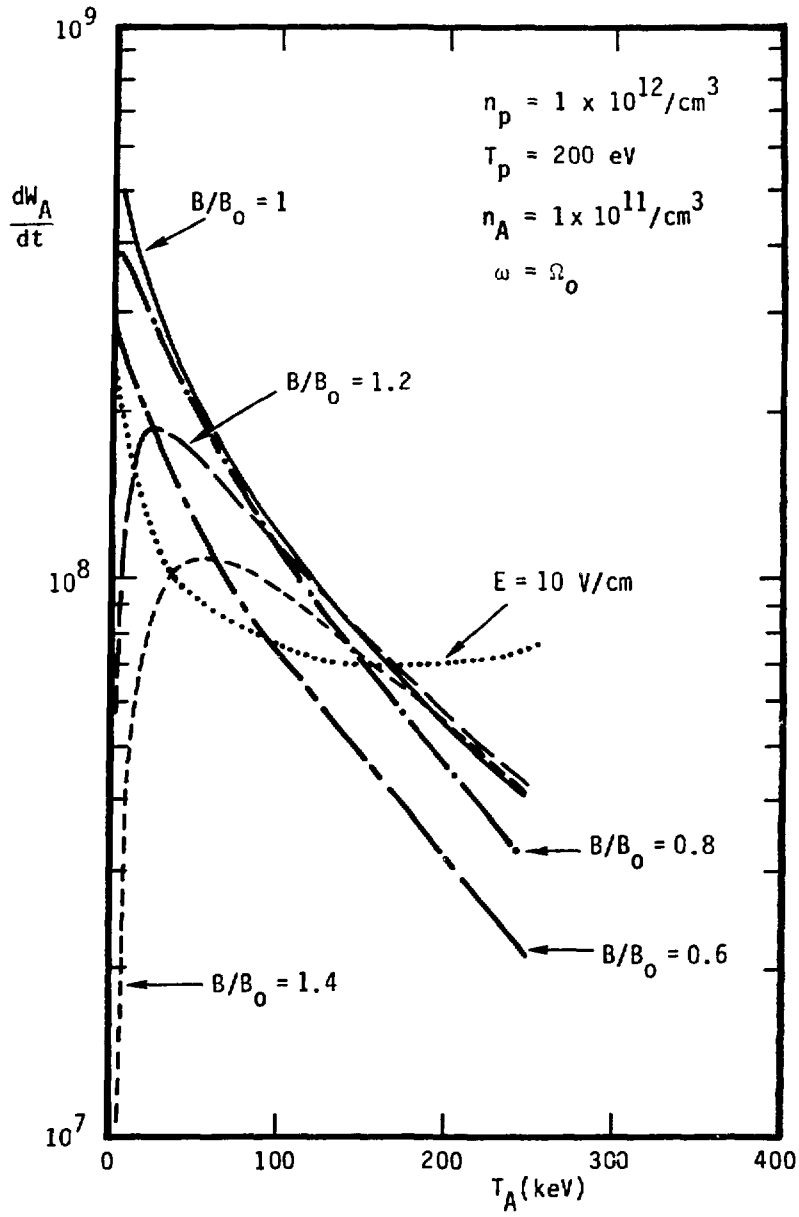

Figure 8. Plot of the line averaged first harmonic heating rate normalized to $|E^-|^2$ vs. ring temperature for fixed background plasma parameters. Also plotted is the classical power loss per unit volume normalized to $|E^-|^2$ for a given value of the microwave field amplitude.

DISCUSSION

G. HASTE: It appears that the heating rate calculated for second harmonic heating for $B/B_0 = 0.9$ is equivalent to that for $B/B_0 = 1.0$ at $T = 10^5$ eV. It then appears that you would expect 100-keV rings outside the second harmonic resonant position. Could you explain how the ring position is determined to be at the second harmonic position?

S. HAMASAKI: The ring size is determined by the region where the microwave heating term can overcome the plasma drag heat loss term in starting up the ring. The second harmonic heating rate is larger than plasma drag term at the starting-up stage only at the region just outside of $B/B_0 = 1$.

V. K. TRIPATHI: Does $dW_\perp/dt$ decrease with increasing E_0 or something else?

S. HAMASAKI: In the quasilinear formalism, the heating rate dW/dt is proportional to $|E_0|^2$. Another explicit proportional quantity is the annular density n_A.

H. IKEGAMI: For energetic electrons, the interaction time at the local resonance becomes too small to have one cyclotron period. For proper treatment of the hot electron heating and generation in a nonuniform field, this point must be carefully taken into consideration.

S. HAMASAKI: If the nonuniformity of field is too strong, we have to be careful. In fact, quasilinear approach itself may not be valid. However, when magnetic field variation is weak, the quasilinear approach may be valid regardless of the interaction time as long as the electrons pass through successively the resonant layer, each time getting kicked in velocity space with enough random phases. [cf. T. H. Stix, Nucl. Fusion 15, 737 (1975)].

ANISOTROPY OF THE EBT RING ELECTRONS*

Allen H. Boozer

Princeton Plasma Physics Laboratory
Princeton, New Jersey

ABSTRACT

In this calculation we show that the hot electron pressure of the EBT rings tends to be close to isotropic and the hot electron density essentially constant along the field lines. In the analysis a square well model of the magnetic field is used. Let $\psi(v,\lambda)$ be the net power gained by electrons of velocity v and pitch $\lambda = v_{\parallel}/v$, then the square well model kinetic equation is

$$C(f) = \frac{1}{v^2}\frac{\partial}{\partial v}\left(\frac{2v}{m}\psi\right)$$

with C(f) the Fokker-Planck collision operator. This kinetic equation is solved by using a variety of forms for ψ with the assumption that the cold background electrons dominate the collisional effects due to their higher density.

*Work supported by SAI and by the U.S. DOE Contract #EY-76-C-02-3073.

It has become customary to assume the EBT electron rings are quite localized along magnetic field lines due to their anisotropy. If all the drift orbits which cross a magnetic field line are confined, large anisotropies are not easily maintained. To study the anisotropy question we assume microwave power is fed into the electrons as a known function of the electron's velocity v and pitch $\lambda = v_{\parallel}/v$. As a further simplification the magnetic field along the drift orbit is assumed to have an average value close to its minimum value B_0. This approximation, the square well model, has been used in mirror work where it is found to give accurate results. Under these assumptions the microwave power $P_\mu(v,\lambda)$ must be balanced by Coulomb collisions. The hot annulus electrons primarily scatter and slow down on the cold background plasma. Then collision operation can be written

$$\begin{aligned} C &= \nu_\Omega \frac{\partial}{\partial\lambda}(1-\lambda^2)\frac{\partial f}{\partial\lambda} + \frac{1}{v^2}\frac{\partial}{\partial v}(v^2\nu_s v f) \\ &= \nu_s\left[(1+Z)\frac{\partial}{\partial\lambda}(1-\lambda^2)\frac{\partial f}{\partial\lambda} + v\frac{\partial f}{\partial v}\right] \end{aligned} \tag{1}$$

where we have used the $1/v^3$ dependence of the collision frequencies and the relation $\nu_\Omega/\nu_s = 1 + Z$ with Z the charge of the ions. The equation to be solved is

$$P_\mu(v,\lambda) = -\frac{1}{2}mv^2C(f) \tag{2}$$

This equation can be solved by expanding P_μ and f in Legendre polynomials

$$\begin{aligned} P_\mu(v,\lambda) &= \sum_\ell P_\mu^{(\ell)}(v)\, P_\ell(v) \\ f(v,\lambda) &= \sum_\ell f(v) P_\ell(\lambda) \end{aligned} \tag{3}$$

and let

$$\psi(v,\lambda) = \frac{1}{\nu_s v} \frac{1}{\frac{1}{2} mv^2} \int_v^\infty P_\mu(v,\lambda)dv \tag{4}$$

then one can show the isotropic part of the distribution function $f_0(v)$ is just

$$f_0(v) = \psi_0(v)$$

with ψ_0 the zero order term in the Legendre expansion of ψ. It is, of course, this term which determines the energy distribution of the annulus electrons. One can also show that

$$f_\ell(v) = - \int_v^\infty \left(\frac{v}{u}\right)^{(1+Z)\ell(\ell+1)} \frac{d\psi_\ell}{du} du \tag{5}$$

Once we have the distribution function $f(v,\lambda)$ at the field minimum B_0, the distribution can be found at other values of B using magnetic moment conservation. The density, parallel, and perpendicular pressures can then be given as a function of field strength B. Let

$$n_\ell = \int_0^\infty f_\ell(v)4\pi v^2 c$$

$$p_\ell = \int_0^\infty \frac{1}{3} mv^2 f_\ell(v)4\pi v^2 dv \tag{6}$$

then one can show

$$n(B) = n_0 + n_2 \left[1 - \frac{B_0}{B}\right] + n_4 \left[1 - \frac{10}{3}\frac{B_0}{B} + \frac{7}{3}\left(\frac{B_0}{B}\right)^2\right] + \ldots$$

$$p_\parallel = p_0 + p_2\left[1 - \frac{3}{5}\frac{B_0}{B}\right] + p_4\left[1 - 2\frac{B_0}{B} + \left(\frac{B_0}{B}\right)^2\right] + \ldots \tag{7}$$

The quantity $p_\perp(B)$ can be found using the relation

$$dp_\parallel(B)/dB = (p_\parallel - p_\perp)/B \ . \tag{8}$$

One model of the microwave power is that all the heating takes place on particles which have turning points at $B = B_R$. Then one has

$$P_\mu(v,\lambda) = P_\mu^{(0)}(v)\ \delta(\lambda \pm \lambda_R),\ \lambda_R^2 = 1 - \frac{B_0}{B_R} \tag{9}$$

with this model one finds

$$\begin{aligned} n_\ell &= \frac{3(2\ell + 1)}{3 + (1 + Z)\ell(\ell + 1)}\ P_\ell(\lambda_R)n_0 \\ p_\ell &= \frac{5(2\ell + 1)}{5 + (1 + Z)\ell(\ell + 1)}\ P_\ell(\lambda_R)p_0 \end{aligned} \tag{10}$$

If the resonant field B_R is chosen as the minimum field B_0 — that is only the most deeply trapped electrons are heated — one finds the variation in hot electron density from $B = B_0$ to $B = 2B_0$ is $n(2B_0) = 0.77\ n(B_0)$. The pressure anisotropy at $B = B_0$ is $p_\parallel/p_\perp = 0.62$. These anisotropies are significantly reduced if the resonant field B_R is chosen to be moderately larger than B_0. In fact $p_\parallel/p_\perp$ becomes greater than one at $B = B_0$ for $B_R > 3B_0/2$.

DISCUSSION

J. PIPKINS: The reason for not getting the usual runaway distribution is the treatment of the microwave absorption as a diffusion term as opposed to dn $\overline{F} \times \overline{\nabla}_v$ term?

A. BOOZER: One obtains a runaway distribution unless the power from the microwaves goes to zero as the electron energy goes to infinity. Relativistic detuning of the electrons gives such an effect.

D. BATCHELOR: Your results are very counter-intuitive since the heating rate $dW/dt \propto J_1^2(k_\perp v_\perp/\Omega) \propto v_\perp^2$ whereas the collision terms go like $1/v^3$. It certainly seems that the solution should be anisotropic at high energy.

A. BOOZER: The point is the microwave heating is balanced by the Coulomb drag. Therefore a typical hot electron remains at high energy in a drag time, during which time it scatters widely in pitch angle.

H. IKEGAMI: Experimentally, it seems to be that pitch angles and maximum energy are essentially determined by the plasma confinement time rather than radiative cooling and collisional energy transfer.

A. BOOZER: In the calculation, I assumed all the electron drift orbits were confined. If particles of given energy and pitch are unconfined they can be included in the theory by taking the boundary condition that the distribution function is zero for that energy and pitch. The effect on the isotropy of the distribution function would be large.

M. RENSINK: Your expression for the heating involved only derivatives with respect to total velocity and not pitch angle; doesn't this imply isotropic heating?

A. BOOZER: No. The power into the electron was assumed to have an arbitrary but known pitch dependence.

G. HASTE: It appears that the magnetic field distribution chosen is such that the probability of reaching a resonant surface is independent of pitch angle.

A. BOOZER: No, the variation in magnetic field is slow compared with ion or electron characteristic scale lengths.

5. MICROWAVE HEATING AND RADIATION

G. R. Haste, Session Chairman

MICROWAVE HEATING OF THE ANNULUS IN EBT*

D. B. Batchelor

Oak Ridge National Laboratory
Oak Ridge, Tennessee 37830

*Research sponsored by the Office of Fusion Energy, U.S. Department of Energy, under contract W-7405-eng-26 with the Union Carbide Corporation.

ABSTRACT

Our current understanding of electron cyclotron heating in the ELMO Bumpy Torus (EBT) is reviewed and the propagation characteristics of the different modes are described for EBT geometry. Wave absorption processes near the second harmonic resonance (where the annulus is observed to form in EBT) are discussed. Calculations of single particle energy gain are presented for finite wavelength waves propagating in a magnetic mirror geometry. It is shown that the heating is highly pitch angle-dependent and the relativistic effects are quite important even at moderate energies. Calculations are presented which suggest that coherent, wave-particle interactions may be important in producing the annulus from a population of particles having small initial perpendicular energies.

1. INTRODUCTION

In this talk I want to address two topics which are to some extent independent. First, I would like to review our current understanding of electron cyclotron heating in EBT devices and outline the dominant processes involved in the heating of the core plasma in EBT-I. A more detailed discussion is offered in Ref. 1. Second, I intend to address the question of what role the second harmonic resonance plays in the formation of the annulus. The annulus is experimentally observed to form at the location of the second harmonic resonance. However, for a low temperature plasma such as that in the surface region of EBT-I ($T_e \sim 10$-20 eV), the strength of second harmonic wave-particle interaction is reduced by a factor $k_\perp^2 \rho_e^2 \sim 10^{-4}$ from that of the fundamental resonance. Preliminary results of single particle orbit calculations are presented that suggest a possible mechanism for enhancement of second harmonic heating for low energy particles.

2. A BRIEF OVERVIEW OF MICROWAVE PROPAGATION AND HEATING IN EBT

Figure 1 shows a cross section in the equatorial plane of a sector of EBT-I with a finite beta ($\beta \cong 40\%$) magnetic field configuration calculated using the Oak Ridge 3-D equilibrium code. An ad hoc density profile model was used for the low beta core plasma component, in which the density is constant along field lines, decreases slowly out to the vicinity of the annulus, and then drops rapidly to a constant value outside the annulus. Also shown in Fig. 1 are the fundamental cyclotron resonance surface [$\Omega_e(\underset{\sim}{x})/2\pi = 18$ GHz], the second harmonic resonance surface [$\Omega_e(\underset{\sim}{x})/2\pi = 9$ GHz], and the extraordinary mode right-hand cutoff surface, $\omega = \Omega_e/2 + (\Omega_e^2/4 + \omega_{pe}^2)^{1/2}$. At the right-hand cutoff, the extraordinary mode does not propagate at any angle. Therefore, the extraordinary mode energy launched near the mirror midplane is reflected before reaching the cutoff surface and in particular before reaching the fundamental resonance. The topology of the cutoff surface depends upon the peak plasma density. Figure 1 is plotted such that $\omega_{pe}^2 = \omega^2/2$ (i.e., $n_e = 2 \times 10^{12}/\text{cm}^3$) at the second harmonic resonance, the maximum density for which the entire second harmonic resonance is accessible for the extraordinary mode. The entire plasma is accessible to the ordinary mode since $\omega_{pe} < \omega$ everywhere.

The degree of cyclotron absorption that a wave experiences depends upon the plasma density and temperature and depends very sensitively upon the angle θ between $\underset{\sim}{k}$ and B at resonance and the angle between $\underset{\sim}{v}_g$ and the normal to the resonant surface. After the introduction of $k_r = |\text{Re}\{\underset{\sim}{k}\}|$, $k_i = |\text{Im}\{\underset{\sim}{k}\}|$, where $\underset{\sim}{k}$ is the complex wave vector, the cyclotron absorption of extraordinary and ordinary mode can be summarized as follows.

Near the first harmonic ($\Omega_e \cong \omega$):

the X-mode

is heavily damped, $k_i/k_r \sim 1$ for $\theta \sim 0$,
decreases as θ increases,
decreases as ω_{pe}^2/ω^2 increases, and
increases as v_e increases;

the O-mode

is weakly damped, $k_i/k_r \sim T_e/mc^2$ for $\theta \sim \pi/2$,
increases as θ increases,
increases as ω_{pe}^2/ω^2 increases, and
increases as v_e increases.

Near the second harmonic ($\Omega_e \cong \omega/2$):

the X-mode

is weakly damped, $k_i/k_r \sim T_e/mc^2$ for $\theta \sim \pi/2$,
increases as θ increases,
increases as ω_{pe}^2/ω^2 increases, and
increases as v_e increases;

the O-mode

is extremely weakly damped, $k_i/k_r \sim (T_e/mc^2)^2$ for $\theta \sim \pi/2$,
peaks for $0 < \theta < \pi/2$,
increases as ω_{pe}^2/ω^2 increases, and
increases as v_e increases.

For the complicated geometry of EBT, details of the wave propagation and absorption must be determined by ray tracing.

We now present cyclotron damping calculations for nonstratified plasma geometry representative of the actual EBT configuration. In particular, we consider a bumpy cylinder magnetic field, $\underset{\sim}{B}(\underset{\sim}{x}) = B_z(r,z)\hat{z} + B_r(r,z)\hat{r}$, given analytically as the field due to a set of coaxial current loops spaced uniformly along the z axis. A non-self-consistent density model for the low beta core plasma was adopted in which $n_e(\underset{\sim}{x})$ is constant along magnetic field lines and is an explicit function of the toroidal magnetic flux $\psi(r,z)$,

$$n_e(x) = n_0 \frac{1 - \tanh\,[\psi(\underset{\sim}{x}) - \psi(r_0, z = 0)/\delta^2]}{1 + \tanh\,[\psi(r_0, z = 0)/\delta^2]}, \tag{1}$$

where

$$\psi(r,z) = \int_0^r dr'\, r' B_z(r',z) \ .$$

Here r_0 plays the role of a plasma radius (typically r_0 = 10 cm, which is approximately the radius of the annulus) and δ is a gradient scale length (typically $\delta \sim 3$ cm).

The ray paths are traced using the Hamiltonian form of the geometrical optics equations,

$$\frac{d\underset{\sim}{x}}{ds} = \frac{1}{|\underset{\sim}{v}_g|}\frac{d\underset{\sim}{x}}{dt} = -\mathrm{sgn}\left(\frac{\partial D}{\partial \omega}\right)\frac{\partial D/\partial \underset{\sim}{k}}{|\partial D/\partial \underset{\sim}{k}|} , \tag{2}$$

$$\frac{d\underset{\sim}{k}}{ds} = \frac{1}{|\underset{\sim}{v}_g|}\frac{d\underset{\sim}{k}}{dt} = \mathrm{sgn}\left(\frac{\partial D}{\partial \omega}\right)\frac{\partial D/\partial \underset{\sim}{x}}{|\partial D/\partial \underset{\sim}{k}|} , \tag{3}$$

and using the Appleton-Hartree dispersion relation $D[\underset{\sim}{k},\omega_{pe}(\underset{\sim}{x}),\Omega_e(\underset{\sim}{x})] = 0$. The parameter s is the arc length along the ray. The ray equations, Eqs. (2) and (3), and the wave damping equation are integrated numerically from given initial conditions $\underset{\sim}{x}_0$, $\underset{\sim}{k}_0$.

Figure 2 shows the results of injecting extraordinary mode rays into the bumpy cylinder equilibrium at varying angles from two points located in the equatorial plane (y = 0). The plasma parameters were chosen to be representative of EBT-I: $\omega/2\pi$ = 18 GHz, $(\omega_{pe}/\omega)_{max} = 0.4$, and $v_e/c = 0.034$. Also shown in Fig. 2 are the magnetic field lines and equatorial cross sections of the first and second harmonic resonant surfaces and the right-hand cutoff. The fraction of power absorbed in passing through resonance is indicated by each ray. A group of rays was injected from the low field region at the mirror midplane (z = 0) and outside the core plasma (x = -18 cm). It can be seen that these rays do not penetrate to the cyclotron resonant surface but are reflected at the right-hand cutoff. Absorption at the second harmonic resonance, which is accessible, is negligible (<2% for the most heavily damped ray).

It is of interest to examine the fate of an extraordinary mode ray originating near the mirror throat, which, for example, might arise from depolarization of an ordinary mode ray on reflection. Figure 2 also shows ray paths and wave vectors for extraordinary mode rays injected at varying angles from a point near the mirror coil. On this side, the cyclotron resonance zone is accessible. It can be seen that the rays approach the cyclotron resonance layer with $\underset{\sim}{v}_g$ nearly perpendicular to $\underset{\sim}{B}$ and $\underset{\sim}{k}$ nearly parallel to $\underset{\sim}{B}$. This is characteristic of parallel-stratified media in the cold plasma model. The rays are terminated at the point at which 99% of the wave power has been absorbed. For the EBT-I parameters used in the calculation, the waves are completely damped well before reaching the resonant layer.

The situation is much less complicated for the ordinary mode. As long as the microwave frequency is higher than the plasma frequency, the entire plasma is accessible to the ordinary mode. Figure 3 shows ordinary mode rays for the same equilibrium and injection geometry as shown in Fig. 2. The rays are virtually straight, with slight curvature due to density gradients. For the EBT-I parameters used, only rays within a narrow cone have more than 1% of the wave energy absorbed in passing through the fundamental cyclotron resonance. Absorption of the ordinary mode at the second harmonic resonance is entirely negligible ($f \leqslant 10^{-4}$).

Similar calculations have been performed for plasmas having parameters characteristic of the projected values for EBT-II: $\omega/2\pi = 120$ GHz, $(\omega_{pe}/\omega)_{max} = 0.4$, and $v_e/c = 0.09$. In this case there is significant absorption ($f \sim 60\%$) at the second harmonic resonance from the rays injected near the midplane. The rays injected from the high field side are again completely absorbed. At this density and temperature the ordinary mode is heavily absorbed by the core plasma ($f \lesssim 80\%$). Absorption of the ordinary mode at the second harmonic resonance is again quite small ($f \lesssim 2\%$).

Despite the overall complexity of wave propagation and absorption in EBT, a number of general statements can be made.

- The density and temperature of the core plasma in EBT-I are sufficiently small that heating of the core plasma by the ordinary mode is negligible at both fundamental and second harmonic resonance.
- Heating of the core plasma by the extraordinary mode is negligible at the second harmonic resonance.
- Because of strong gradients in $|\underset{\sim}{B}|$ along field lines, any extraordinary mode energy propagating from the high field side (mirror throat region) is totally absorbed at the fundamental resonance. This is true even for the low density surface plasma.
- Both ordinary and extraordinary modes are absorbed by the hot electron annuli. Experimental measurements of the annulus lifetime indicate that one-fourth to one-third of the total injected power is absorbed by the annuli.
- Plasma resonance occurs at the upper hybrid frequency only for perpendicularly stratified plasmas. Because of the geometry of EBT, the upper hybrid resonance plays no role.

Since the core plasma in EBT-I is observed to be strongly heated, some mechanism must exist whereby extraordinary mode energy reaches the high magnetic field region, from which it can be efficiently absorbed at the fundamental cyclotron resonance. A number of mechanisms have been considered in this regard, including Budden tunnelling, destruction of the cutoff by finite temperature effects, and depolarization of ordinary mode energy into extraordinary mode in the high field region upon wall reflection. Of these, the dominant process appears to be conversion of ordinary mode energy to extraordinary mode in the high field region. In considering a low density, magnetized plasma having parameters characteristic of the surface plasma in EBT-I in contact with a perfectly conducting wall, it is found that a fraction of ordinary mode power approaching 100% is converted to extraordinary mode for certain angles of incidence on the wall. Averaging over a uniform distribution in angle of incidence gives average conversion efficiencies in the range of 10-50% for parameters characteristic of the mirror throat region in EBT-I.

The core heating of EBT-I can be summarized as follows. Extraordinary mode energy injected at the midplane is partially absorbed by the annulus, partially depolarized into ordinary mode upon wall reflection, and weakly absorbed and transmitted to the high field region by Budden tunnelling. Aside from these sinks, extraordinary mode energy is trapped in the region outside the right-hand cutoff. Ordinary mode energy launched from the midplane is partially absorbed by the annulus and partially depolarized into extraordinary mode at all wall surfaces. Because the production of extraordinary mode energy in the high field region is such an indirect process, it is quite difficult to calculate the radial distribution of extraordinary mode power flux into the fundamental resonance surface. However, if one makes the reasonable assumption that this power flux is uniform across the resonance surface, then the power deposited directly into the core plasma as opposed to the surface plasma is just proportional to the fraction of surface area of the resonant zone which lies in the surface plasma. A simple geometric model embodying these ideas indicates that in EBT-I, $\sim$30% of the microwave power is deposited in the plasma, $\sim$20% is deposited in the core, and $\sim$50% is deposited in the surface plasma.

In scaling the EBT concept to a proof-of-principle device, the plasma parameters change in such a way as to modify this view of heating. Increasing density, temperature, scale lengths, and microwave frequency all tend to increase local cyclotron absorption rates. In particular, assuming $n_e \cong 1.5 \times 10^{13}$, $T_e \cong 2.5$ keV, $\omega/2\pi = 60$ GHz, and a plasma radius at the midplane of 20 cm, one obtains fractional absorption rates of 50% to 80% at the fundamental resonance for ordinary mode waves launched near the midplane. This is advantageous because the ordinary mode is preferentially absorbed in the hot, dense core plasma rather than the surface plasma. In addition, direct absorption of the ordinary mode reduces the production of extraordinary mode energy in the high field region, which tends to be equally partitioned between core and surface plasma. Ordinary mode absorption at the second harmonic resonance is still small (fractional absorption $\lesssim$ 3%).

Because of the increased annulus density and temperature, the extraordinary mode is quite heavily damped at the second harmonic

resonance. Indeed, the annulus should be virtually opaque to extraordinary mode radiation propagating perpendicular to the field lines.

3. SINGLE PARTICLE ORBITS NEAR THE SECOND HARMONIC RESONANCE

The last part of the talk concerns the motion of charged particles in an equilibrium mirror magnetic field and a single propagating electromagnetic wave. The relativistically correct equations of motion can be written

$$\frac{d}{dt}(\gamma \underset{\sim}{v}) = \frac{e}{m}\left(\underset{\sim}{E} + \frac{1}{c}\underset{\sim}{v} \times \underset{\sim}{B}\right)$$

$$\frac{d\gamma}{dt} = \frac{e}{mc^2}\underset{\sim}{E} \cdot \underset{\sim}{v}\ , \tag{4}$$

where $\gamma = (1 - v^2/c^2)^{-1/2}$ and the other symbols have their conventional meanings. For analytic simplicity, we initially restrict consideration to a nonrelativistic particle and assume that the equilibrium magnetic field $\underset{\sim}{B}^0(\underset{\sim}{x})$ is aligned along the z axis and is a function only of z, $\underset{\sim}{B}^0(\underset{\sim}{x}) = [0,0,B_0(z)]$. In this case the equations of motion reduce to

$$\dot{v}_\pm \pm i\Omega(z)v_\pm = \frac{e}{m}E_\pm$$

$$\dot{v}_z = \frac{e}{m}E_z - \frac{\mu}{m}\frac{\partial B_0}{\partial z} \tag{5}$$

where $v_\pm = v_x \pm iv_y$, $E_\pm = E_x \pm iE_y$, $\Omega(z) = eB_0(z)/mc$, and $\mu = mv_\perp^2/2B$.

We proceed along the lines of quasi-linear theory[2,3] by assuming the wave-particle interaction to be sufficiently weak that on the time scales of interest the orbit does not deviate significantly from the unperturbed orbit [i.e., $\underset{\sim}{E}(\underset{\sim}{x},t) \to 0$]. The unperturbed solution to Eq. (5) can be written

$$x(t) = x_0 + v_\perp \int_0^t d\tau \cos\left\{\int_0^\tau d\tau'\Omega[z(\tau')] - \phi\right\}, \tag{6}$$

where z(t) satisfies

$$\ddot{z} + \frac{\mu}{m'}\frac{\partial B_0}{\partial z} = 0 \ . \tag{7}$$

Assuming a plane propagating electromagnetic wave with ky = 0,

$$\underset{\sim}{E}(\underset{\sim}{x},t) = \underset{\sim}{E} \exp\,[i(\underset{\sim}{k} \cdot \underset{\sim}{x} - \omega t)] \ ,$$

the field seen by the particle on its unperturbed orbit, is

$$\underset{\sim}{E}(t) = \underset{\sim}{E} \exp\,[i\Phi(t)] \ , \tag{8}$$

where

$$\Phi(t) = k_x x_0 + k_x v_\perp \int_0^t d\tau \cos\left\{\int_0^\tau d\tau' \Omega[z(\tau')] - \phi\right\} + k_z z(t) - \omega t \ , \tag{9}$$

and the solution to the perturbed equation is

$$v_\pm(t) = v_\perp^0 \exp\left\{\pm i \int_0^t d\tau\, \Omega[z(\tau)] \pm i\phi\right\}$$

$$+ \frac{eE_\pm^0}{m} \exp\left\{\pm i \int_0^t d\tau\, \Omega[z(\tau)]\right\} \int_0^t d\tau \exp\left[i\Phi(\tau) \pm i \int_0^\tau d\tau' \Omega(\tau')\right] . \tag{10}$$

The energy gained by the particle is

$$\Delta W = \frac{1}{2} \int_0^t d\tau\, \mathrm{Re}\{e\underset{\sim}{E}^* \cdot \underset{\sim}{v}\} \ . \tag{11}$$

In order to calculate an average heating rate, we adopt a simple stochastic model[3] according to which the resonant interaction is assumed to take place in a thin zone along z, and the angle ϕ between the particle gyrophase and the wave phase is assumed uncorrelated on successive transits of the particle through the resonant zone. This amounts to a Fokker-Planck treatment in which the energy gain averaged over ϕ represents a step size and the mirror bounce frequency is the collision frequency. For simplicity we assume a circularly polarized wave ($E_+ \neq 0$, $E_- = E_z = 0$) and assume the resonant zone to be sufficiently thin that v_z = constant within the zone. In this case the unperturbed orbit is just $z(t) = v_z t$ and the average (over ϕ) energy gain per transit through resonance reduces to

$$\langle \Delta W \rangle = \frac{e^2 |E_+|^2}{2m} \mathrm{Re} \left\{ \int_{-\infty}^{\infty} dt \exp\left[-i\psi(t)\right] \int_{-\infty}^{t} d\tau \exp\left[i\psi(\tau)\right] \right\}, \quad (12)$$

where

$$\psi(t) = \int_0^t d\tau\, \Omega(\tau) + (k_z v_z - \omega)t + k_x v_\perp \int_0^t d\tau \cos\left[\int_0^\tau d\tau'\, \Omega(\tau')\right].$$

Using the generating functions for Bessel functions we can express

$$\exp i\psi(t) = \sum_\ell J_\ell\left(\frac{k_\perp v_\perp}{\Omega_0}\right) \exp iG(t) , \quad (14)$$

where

$$G(t) = (\ell + 1)\left[\Omega_0 t + \Omega_0 \int_0^t d\tau\, f(\tau)\right] + (k_z v_z - \omega)t$$

$$- k_\perp v_\perp \int_0^t d\tau \cos\left[\Omega_0 \tau + \Omega_0 \int_0^t d\tau' f(\tau')\right] f(\tau) ,$$

$\Omega_0 = \Omega(z)$ evaluated at $z = 0$, and $\Omega_0 f(t)$ = deviation of $\Omega(t)$ from Ω_0. The average energy gain is of the form

$$\langle\Delta W\rangle = \frac{e|E_+|^2}{2m} \sum_{\ell,m} J_\ell\left(\frac{k_\perp v_\perp}{\Omega_0}\right) J_m\left(\frac{k_\perp v_\perp}{\Omega_0}\right)$$

$$\times \operatorname{Re}\left\{\int_{-\infty}^{\infty} dt \exp\,[-iG(t)] \int_{-\infty}^{t} d\tau \exp\,[iG(\tau)]\right\}. \quad (15)$$

We now consider the equilibrium field to be a parabolic magnetic mirror, $B_0(z) = B_0(1 + \kappa z^2)$. Then taking $z(t) = v_z t$ near the midplane, we have $\Omega(t) = \Omega_0(1 + \kappa v_z^2 t^2)$ and $f(t) = \kappa v_z^2 t^2$. We assume the midplane to be the wave resonant point,

$$(\ell + 1)\Omega_0 + k_z v_z - \omega = 0 .$$

The integrals in Eq. (15) can now be approximated using a stationary phase argument. The stationary phase point is $t = 0$, for which $G(0) = 0$, $G'(0) = 0$, $G''(0) = 0$, and $G'''(0) = 2\kappa v_z^2(\ell + 1)\Omega_0$ so that

$$\operatorname{Re}\left\{\int_{-\infty}^{0} d\tau \exp\,[iG(\tau)]\right\} \cong \operatorname{Re}\left\{\int_{-\infty}^{0} d\tau \exp\,[i(G'''/3!)\tau^3]\right\}$$

$$= \pi\left(\frac{2}{G'''}\right)^{1/2} \mathrm{Ai}(0) ,$$

where $\mathrm{Ai}(x)$ is the Airy integral. At last we obtain for $\langle\Delta W\rangle$

$$\langle\Delta W\rangle = A\,\frac{\pi e^2|E_+|^2}{m}\,\frac{J_\ell^2\left(\frac{k_x v_\perp}{\Omega_0}\right)}{[(\ell + 1)\Omega_0\kappa v_z^2]^{2/3}} , \quad (16)$$

where $A = \pi A_1^2(0) \cong 0.4$. It is convenient to introduce a characteristic magnetic field scale length L such that

$$\kappa = \frac{1}{B}\frac{d^2B}{dz^2}\bigg|_{z=0} \equiv \frac{1}{L^2} .$$

Using the fact that the bounce frequency in a parabolic magnetic well is of the form $\omega_B = v_\perp\sqrt{\kappa} = v_\perp/L$, the heating rate can be expressed as

$$\frac{\langle\Delta W\rangle}{\Delta Z} = \frac{\langle\Delta W\rangle}{2\pi/\omega_B} = \frac{A}{2\pi(\ell + 1)^{2/3}}\frac{\pi e^2|E_+|^2}{m\Omega_0} J_\ell^2(k_\perp\rho_e)\left(\frac{v_\perp}{v_z}\right)^{4/3}\left(\frac{L}{\rho_e}\right)^{1/3} , \quad (17)$$

where $\rho_e = v_\perp/\Omega_e$. The two dominant features of this expression are the strong pitch angle dependence $(v_\perp/v_z)^{4/3}$ and the Bessel function, which for low energy particles is a very small factor.

Consider now an application of these results to EBT-I. We assume a low temperature plasma, $T_e \sim 20$ eV ($v_e/c \sim 0.01$) such as might be expected initially at the outside of EBT-I. We take the wave to be propagating perpendicularly with $n_\perp \sim 1$ and take the wave frequency as $\omega/2\pi = 18$ GHz, the cyclotron frequency as $\Omega_0/2\pi = 9$ GHz (i.e., $\rho_e = 5 \times 10^{-3}$ cm), and the magnetic field scale length as L = 20 cm. The microwave power flux S is taken as $S = 100$ W/cm^2 ($E_+ \sim 200$ V/cm), which is reasonable for the second harmonic surface directly in front of the waveguide opening. These assumptions give

$$\frac{e^2|E_+|^2}{m\Omega_e^2} = 0.18 \text{ eV}, \qquad k_\perp\rho_e = 2\frac{v_\perp}{c} ,$$

and, using Eq. (12),

$$\langle\Delta W\rangle \cong 1.4\underbrace{\left(\frac{v_\perp}{c}\right)^2}_{\sim 10^{-4}}\underbrace{\left(\frac{L}{\rho_e}\right)^{1/3}}_{\sim 10^4}\left(\frac{v_\perp}{v_z}\right)^{4/3} \sim 1.4\left(\frac{v_\perp}{v_z}\right)^{4/3} \text{ eV/bounce} , \quad (18)$$

where we have taken $v_\perp$ to be approximately equal to the thermal speed. Using the bounce frequency $\omega_B \cong 1.3 \times 10^7/s$ in Eq. (13) gives

$$\frac{\langle \Delta W \rangle}{\Delta t} \cong 1.8 \times 10^6 \left(\frac{v_\perp}{v_z}\right)^{4/3} \text{ eV/s} . \tag{19}$$

We turn now to the question raised in the introduction, namely, how can the second harmonic resonance play such a fundamental role in the formation of the annulus in view of the weakness of the interaction when $k_\perp \rho_e$ is small? To compare second harmonic and fundamental heating, it is necessary to investigate resonant heating when the resonant zone is not at the mirror midplane but is displaced toward the mirror throat. Taking the magnetic field strength as linearly increasing near the resonant zone, $\Omega(z) = \Omega_0[1 + (z/B)(dB/dz)]$, and using a stationary phase argument similar to that above, one obtains for the average energy gain per transit

$$\langle \Delta W \rangle = \frac{\pi e^2 |E_+|^2}{2m} \frac{J_\ell^2(k_\perp v_\perp/\Omega_0)}{(\ell + 1)\Omega_0 v_z \frac{1}{B}\frac{dB}{dz}} \tag{20}$$

Note that the energy gain is proportional to $[v_z(1/B)(\partial B/\partial z)]^{-1}$ (i.e., the time the particle spends in resonance). As the resonant zone moves closer to the midplane, $(1/B)(dB/dz)$ decreases. At the midplane, where the mod B contour is tangent to the field line, $(1/B)(dB/dz)$ vanishes and Eq. (20) becomes infinite. However, when (d^2B/dz^2) is properly included in the stationary phase procedure, only a modest enhancement in $\langle \Delta W \rangle$ is obtained at the midplane.

To obtain a rough comparison between fundamental and second harmonic heating we take $|E_+|^2$ to be constant in space, take $(1/B)(dB/dz) = (1/L)$, and compare Eq. (16) with $\ell = 1$ to Eq. (20) with $\ell = 0$,

$$\frac{\langle \Delta W \rangle_{\text{second harmonic}}}{\langle \Delta W \rangle_{\text{fundamental}}} \cong \frac{2A}{2^{2/3}} J_\ell^2(k_\perp \rho_e) \left(\frac{v_\perp}{v_z}\right)^{1/3} \left(\frac{L}{\rho_e}\right)^{1/3} \tag{21}$$

If we use the same plasma parameters as in the previous example, then $J_\ell^2(k_\perp \rho_e)(L/\rho_e)^{1/3} \sim 0.02$, so that for the bulk of the particles with $v_\perp/v_z \sim 1$, the second harmonic heating is negligible. Interestingly enough, experience with the Oak Ridge 2-D kinetic model has shown that it is necessary to artificially enhance the second harmonic heating by a factor of order 100 if the second harmonic resonance is to have a significant influence.

It is clear from Eqs. (18) and (19) that second harmonic heating is much increased for large pitch angle particles. Indeed, it is seen from Eq. (18) that for particles having $v_\perp/v_z \sim 10$ we have $\langle \Delta W \rangle \sim W$. It is also of interest to examine the width of the zone over which the interaction takes place. Most of the contribution to the phase integral comes from $G'''/3!t^3 \lesssim 1$, or

$$z \lesssim \Delta z \equiv \left(\frac{3\rho_e}{2\kappa}\frac{v_z}{v_\perp}\right)^{1/3}$$

For the parobolic well field model the particle turning point is $z_t = v_z/v_\perp\sqrt{\kappa}$, which gives

$$\frac{\Delta z}{z_t} = \left(\frac{v_\perp}{v_z}\right)^{2/3}\left(\frac{3}{2}\frac{\rho_e}{L}\right)^{1/3} \sim 0.1\left(\frac{v_\perp}{v_z}\right)^{2/3}$$

Therefore, for $v_\perp/v_z \sim 10$ the entire orbit is in the wave interaction region. Clearly, for particles with large pitch angle the conventional picture breaks down, in which successive transits through a thin interaction zone are independent and the energy gain in each transit does not significantly modify the particle's parallel motion. We should, therefore, consider the long-term coherent motion of resonant, large pitch angle particles.

The simplest possible example of this coherent interaction is a particle with $v_z = 0$, exactly at second harmonic resonance $2\Omega(t) = \omega =$ constant in a perpendicularly propagating, circularly polarized wave,

$$E_+(\underset{\sim}{x},t) = E_+^0 \exp\,[i(k_x x - \omega t)] \ .$$

Under these circumstances, the particle simply winds up in the rotating electric field. If we assume a solution of Eq. (5) of the form

$$x(t) = \frac{v_\perp(t)}{\Omega} \sin\,[\Omega t - \phi(t)] \ ,$$

where $v_\perp(t)$ and $\phi(t)$ are slowly varying functions [i.e., $(1/v_\perp)(dv_\perp/dt) \ll \Omega$] and average over one orbit, we get for the average rate of energy increase

$$\frac{d}{dt}\overline{W}_\perp = \frac{1}{2} J_\ell^2 \left[\frac{k_\perp}{\Omega} v_\perp(t)\right]\left[\frac{e|E_+|^2}{m} t + ev_\perp E_+^0 \cos\,(2\phi)\right] \ . \tag{22}$$

We now expand the Bessel functions and consider those particles for which $\phi = \pi/4$. Then only the secular term remains and Eq. (22) reduces to

$$\frac{d\overline{W}_\perp}{dt} = \alpha^2 \overline{W}_\perp t \ , \quad \overline{W}_\perp(t) = W_\perp^0 \exp\,(\alpha t)^2 \ , \tag{23}$$

where $\alpha = k_\perp e|E_+|/m\Omega_e$.

For this class of particles, admittedly of measure zero in velocity space, there is extremely rapid energy gain provided the particles can remain in resonance for a few times α^{-1}. For the parameters of the previous examples ($E_+ \sim 200$ V/cm, $f_\mu = 18$ GHz), we find $\alpha = 2 \times 10^7/s = f_\mu/800$. If the particles can remain in resonance for 50 ns, the energy e-folds. If the particles can remain in resonance for 150 ns, the energy increases by nearly four orders of magnitude.

In order to evaluate the importance of this coherent wave-particle interaction in more general circumstances, we have numerically integrated the relativistic equations of motion, Eq. (1), for a slightly more realistic mirror equilibrium field,

$$B_x(x,z) = -2\kappa B_0 xz$$

$$B_y(x,z) = 0 \tag{24}$$

$$B_z(x,z) = B_0[1 + \kappa(z^2 - x^2)] \ .$$

The wave was chosen to be circularly polarized and propagating in the y direction with unity index of refraction. The particles were initialized to ($v_\perp \cos\phi$, $v_\perp \sin\phi$, v_z) and [$x = -\gamma v_\perp/\Omega(0) \sin\phi$, $y = \gamma v_\perp/\Omega(0) \cos\phi$, $z = 0$]. Figure 4 shows the results of these calculations for parameters used in previous examples [$E_+ = 200$ V/cm, $f_\mu = 18$ GHz, $\Omega(0) = 9$ GHz, $\kappa = (1/20 \text{ cm})^2$] and with initial values of $v_\perp = 0.01c$, and $\phi = \pi/4$. Figures 4(a), 4(b), 4(c), and 4(d) have initial values of $v_z/c = 0.0$, $0.5 + 10^{-3}$, 1.0×10^{-3}, and 2.0×10^{-3}, respectively. The solid curve is particle energy vs time, and the dotted curve indicates the instantaneous z position of the particle normalized to its largest excursion. The time is measured in wave periods. In Figs. 4(a), 4(b), and 4(c) there is a rapid energy gain until the detuning effects of relativistic mass gain and increased Larmor radius cause the gyromotion of the particle to become out of phase with the driving field, at which point the energy drops. The net effect is a periodic energy sloshing. However, the energy excursion is over a factor of 20, taking particles initially at 25 eV to >500 eV in a time comparable to one mirror bounce time. It is also clear from the dotted curves in Figs. 4(b), 4(c), and 4(d) that the wave profoundly influences the parallel motion. For sufficiently large v_z, the particle does leave the resonant interaction region, returning with a random phase with respect to the wave. In this case, the energy gain does appear to be stochastic with large increments as the particle passes through resonance, $z = 0$.

These calculations demonstrate that for a finite region of velocity space near $v_z = 0$, the simple stochastic heating picture breaks down and the coherent long-term interaction of the particles with the waves needs to be considered. The rapid energy gain at the second harmonic resonance occurs because the interaction strength is proportional to $J_1^2(k_\perp \rho_e) \propto W_\perp$.

These considerations do not by any means constitute a theory, but they do suggest a mechanism by which a small group of particles could be rapidly accelerated to a large enough value of $k_\perp^2\rho_e^2$ that the linear electron cyclotron interaction is nonnegligible at the second harmonic.

REFERENCES

1. D. B. Batchelor and R. C. Goldfinger, *A Theoretical Study of Electron-Cyclotron Heating in ELMO Bumpy Torus*, ORNL/TM-6992, Oak Ridge, Tennessee (1979), submitted to Nucl. Fusion.
2. C. F. Kennell and F. Engelmann, Phys. Fluids 9, 2377 (1966).
3. O. Eldridge, Phys. Fluids 15, 676 (1972).

FIGURE CAPTIONS

Fig. 1. Location of first and second harmonic cyclotron resonance zones and the right-hand cutoff zones for 18-GHz extraordinary mode radiation in a model EBT-I equilibrium.

Fig. 2. Extraordinary mode propagation in EBT-I. Numbers by rays indicate fraction of power absorbed.

Fig. 3. Ordinary mode propagation in EBT-I. Numbers by rays indicate fraction of power absorbed.

Fig. 4. Particle energies (solid curves) and z positions (dotted curves) as a function of time (in wave periods) for initial v_z/c = (a) 0.0, (b) 0.5×10^{-3}, (c) 1.0×10^{-3}, and (d) 2.0×10^{-3}.

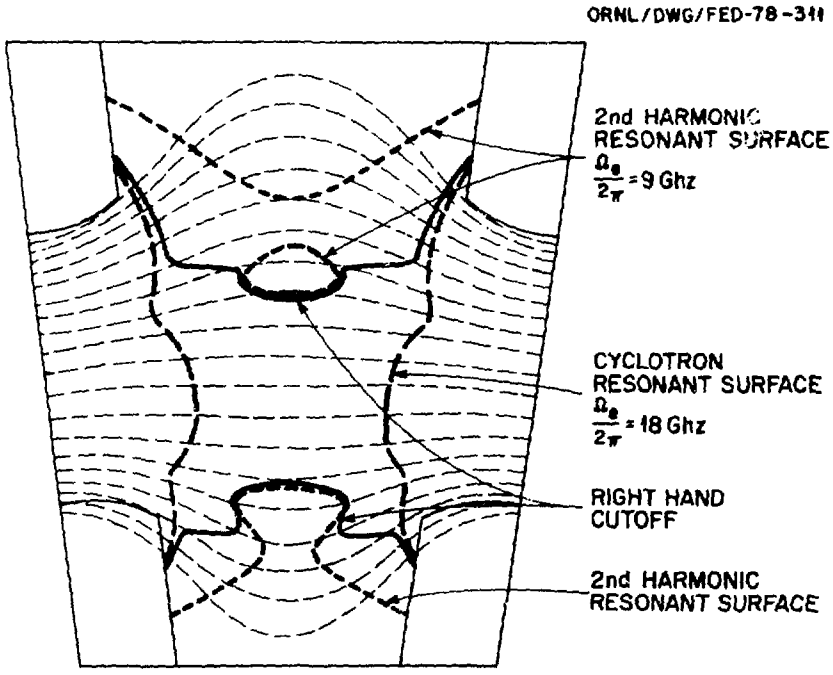
ORNL/DWG/FED-78-311
2nd HARMONIC
RESONANT SURFACE
$\frac{\Omega_e}{2\pi}$ = 9 Ghz
CYCLOTRON
RESONANT SURFACE
$\frac{\Omega_e}{2\pi}$ = 18 Ghz
RIGHT HAND
CUTOFF
2nd HARMONIC
RESONANT SURFACE

Fig. 1

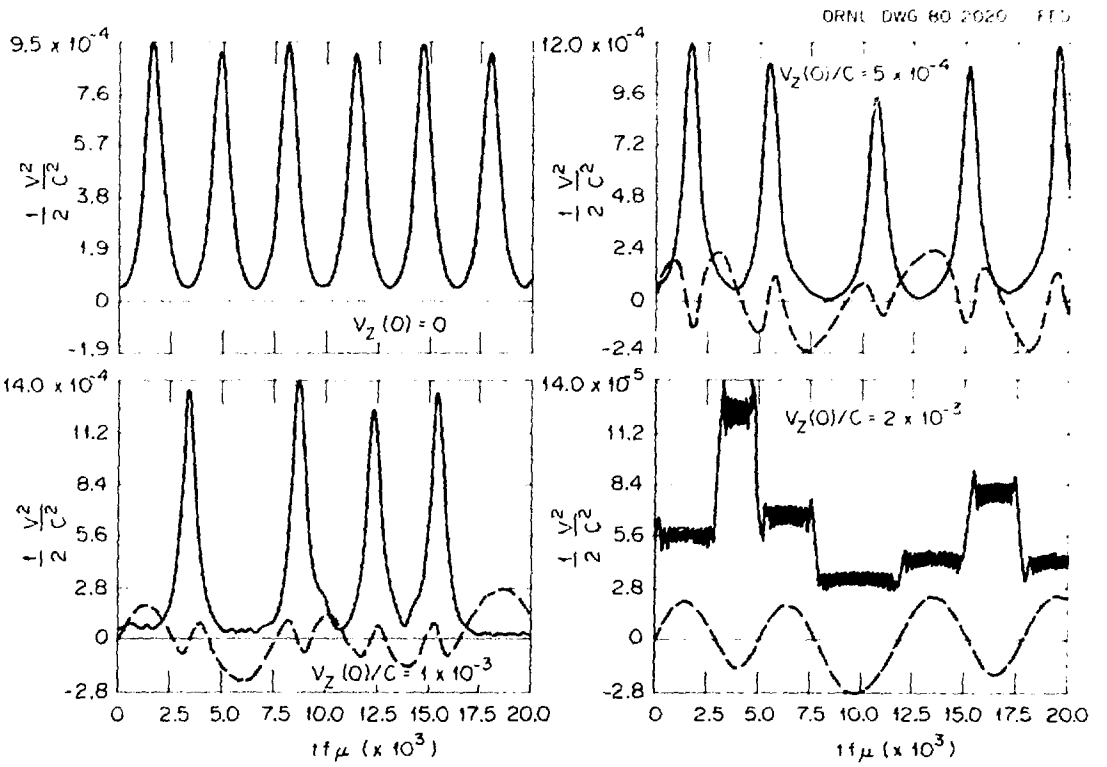
ORNL DWG 80 2020 FED
9.5 x 10^-4
7.6
5.7
3.8
1.9
0
-1.9
V_Z (0) = 0
12.0 x 10^-4
9.6
7.2
4.8
2.4
0
-2.4
V_Z(0)/C = 5 x 10^-4
14.0 x 10^-4
11.2
8.4
5.6
2.8
0
-2.8
V_Z (0)/C = 1 x 10^-3
14.0 x 10^-5
V_Z(0)/C = 2 x 10^-3
0 2.5 5.0 7.5 10.0 12.5 15.0 17.5 20.0
t f μ (x 10^3)

Fig. 2

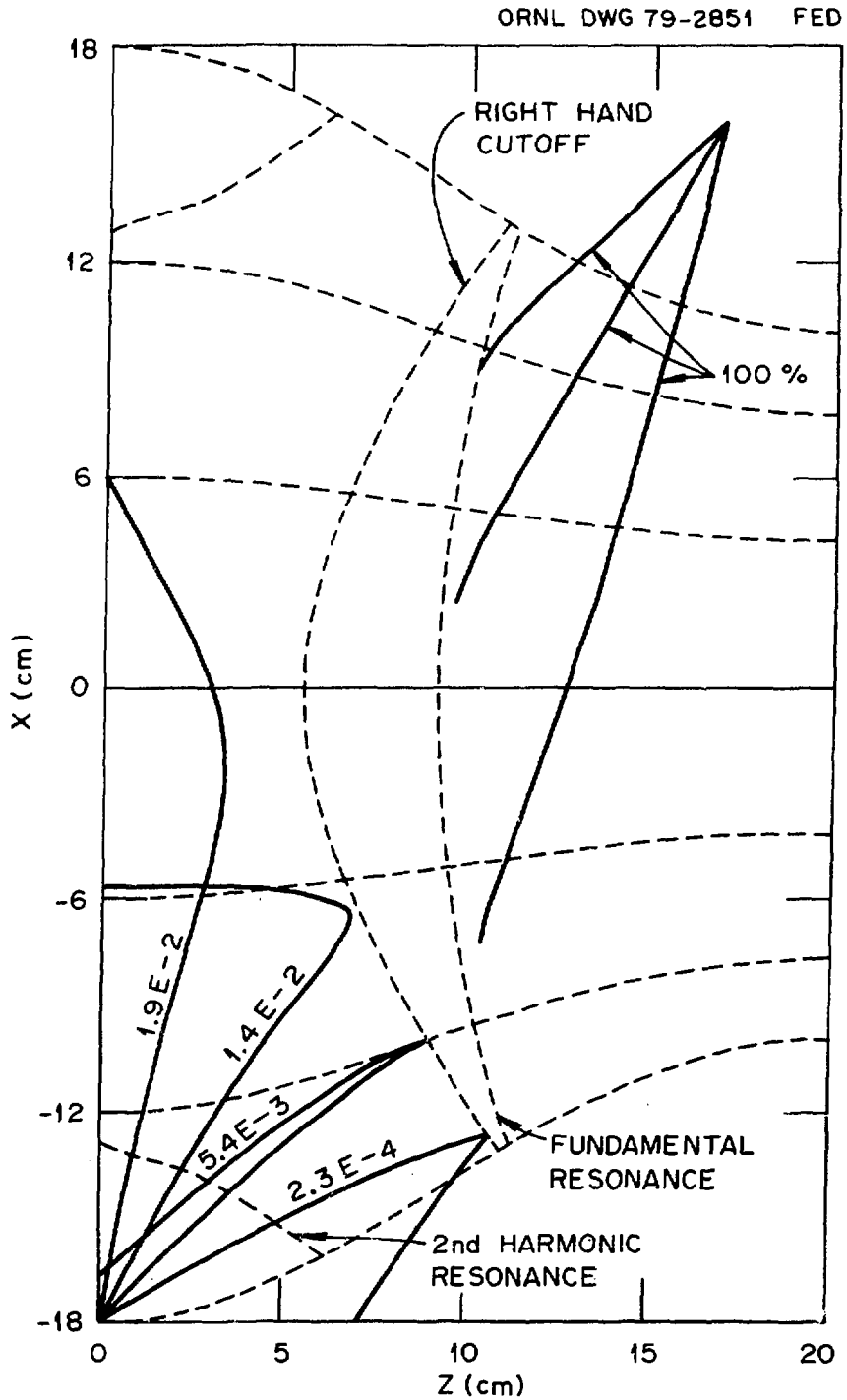
ORNL DWG 79-2851 FED
RIGHT HAND
CUTOFF
100 %
1.9E-2
1.4E-2
5.4E-3
2.3E-4
FUNDAMENTAL
RESONANCE
2nd HARMONIC
RESONANCE
X (cm)
Z (cm)
18
12
6
0
-6
-12
-18
0
5
10
15
20

Fig. 3

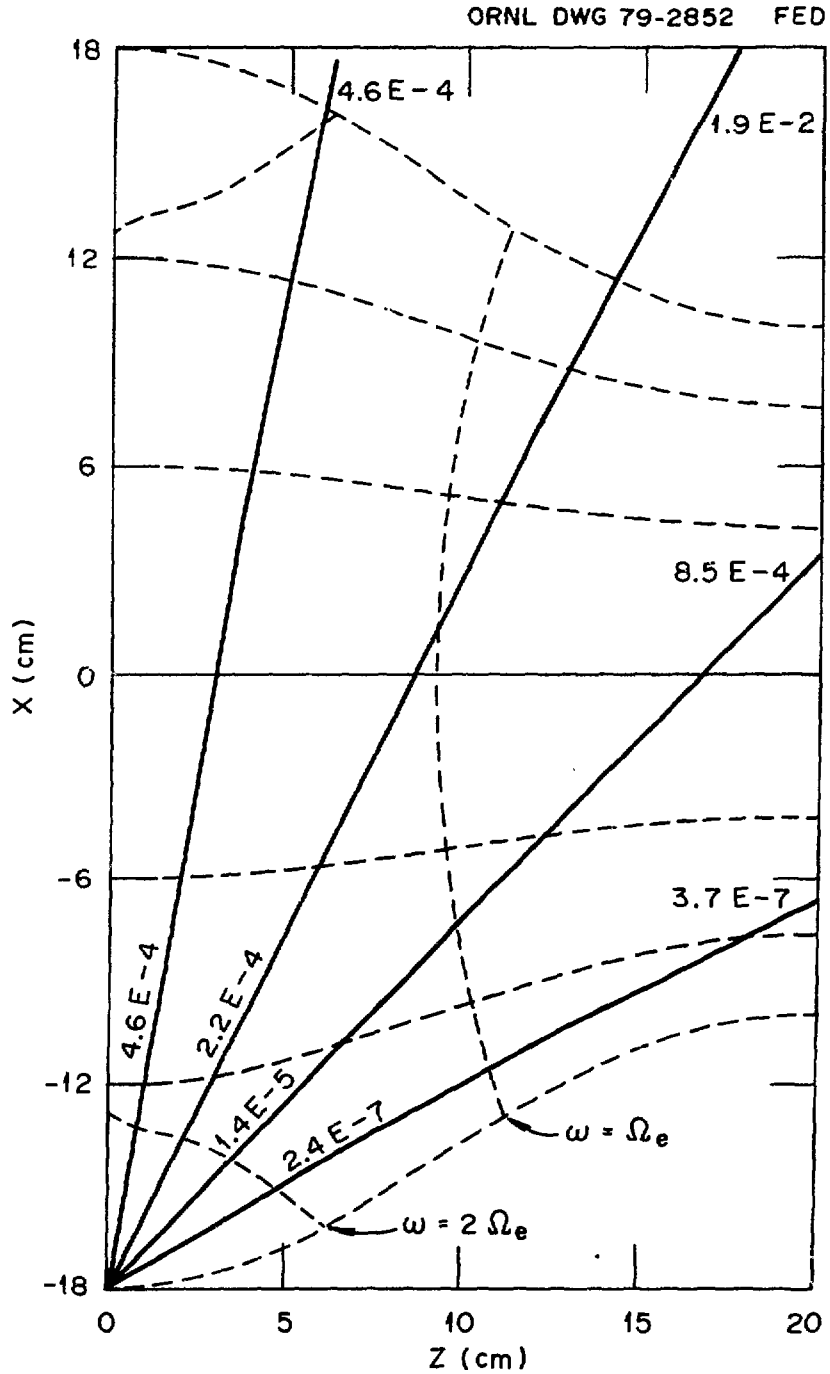
ORNL DWG 79-2852 FED
18
12
6
0
-6
-12
-18
X (cm)
0
5
10
15
20
Z (cm)
4.6 E-4
1.9 E-2
8.5 E-4
3.7 E-7
4.6 E-4
2.2 E-4
1.4 E-5
2.4 E-7
ω = Ωe
ω = 2 Ωe

Fig. 4

DISCUSSION

S. TAMOR: I agree that coherence effects are likely to be important, and to point out that the theory presented by D. Baxter in principle includes such effects. The bounce sum leads to a factor which can be interpreted as a decorrelation time. It should be noted that an upper limit on the decorrelation time is independent of electron dynamics, due to finite phase stability of the rf source and possibly due to multiple reflection in the cavity.

D. BATCHELOR: Baxter's quasilinear model may have the capability of including phase correlation between successive bounces, but I doubt if it includes the kind of nonlinear coherent wave-particle effects I talked about. I doubt that the phase stability of the microwave source limits the wave correlation time. For the example I discussed, only about 10^3 wave periods are necessary. The stability of the klystrons used in EBT-I is certainly much better than this and I anticipate the same will be true of the gyrotrons. It is not the overall band width of the microwaves but the frequency slow rate which is important. For example, if the frequency were modulated all due to 60-Hz power supply ripple, the time scale is 16 ms, which is five orders of magnitude slower than the required correlation time. The superposition of reflected waves seems much more likely to destroy the wave coherence.

A. BOOZER: The correlation time on the phase of a wave and hence the time a particle can interact with it is limited by the quality factor Q, with $\tau_{corr} \lesssim Q/\omega$.

D. BATCHELOR: No, I disagree with that.

MICROWAVE INTERACTION WITH HOT ELECTRON PLASMAS

M. Tanaka*, M, Fujiwara and H. Ikegami

Institute of Plasma Physics, Nagoya University,
Nagoya 464, Japan

INTRODUCTION

Microwave interaction with finite temperature plasmas is one of the most important problem from the view point of plasma production and heating In a bumpy torus , plasmas are produced by microwave at the fundamental cyclotron resonance zone, and hot electron rings, which contain and stabilize the toroidal core plasma, are formed at the second harmonic resonance zone through the interaction of second harmonic electron cyclotron resonance in each mirror section. So that, it is necessary to understand the basic characteristics of microwave propagation and heating for the study of a bumpy torus.

We present the numerical calculation of ray trajectories and cyclotron damping for toroidal plasmas using geometrical optics. In the absorption region, group velocity does not always coincide with the velocity of energy flow[1], therefore it should be careful to apply the geometrical optics to finite temperature plasmas.In our calculations, attention will be paid mainly to the finite temperature effect on ray tracing[2]. Some numerical results for ordinary waves are presented in Section 1.

Second, new cutoff and resonance appear in the plasmas with anisotropic electron temperature. This resonance frequency is shifted from the usual cyclotron resonance by an amount proportional to $T_{\parallel}/mc^2$, so that

---

Parmanent address:

* Institute for Applied Mechanics , Kyushu University, Fukuoka 812, Japan

we can determine $T_{\parallel}$ when this resonance frequency is measured. Simple discussion are given in Section 2.

In section 3, we present the results of recent density measurement on Nagoya Bumpy Torus obtained by interferometer system with different frequencies, 35 GHz and 55 GHz. The results are different each other in T-mode. The possible reasones of these difference are enumerated in this section.

1. RAY TRACING

The determination of ray trajectories and the estimation of power absorption of the electromagnetic waves launched from the outside of the plasma are practically important from the view point of plasma heating and generation of hot electron plasmas. Usually the wavelength is very short compared with the scale length of inhomogeneity of the plasma (1-3 cm in bumpy torus, 1-0.3 cm in tokamak), so that we can apply the geometrical optics to determine the ray trajectories, i.e.,

$$\frac{d\mathbf{x}}{dt} = -\frac{\partial G/\partial \mathbf{k}}{\partial G/\partial \omega} ,$$

$$\frac{d\mathbf{k}}{dt} = \frac{\partial G/\partial \mathbf{x}}{\partial G/\partial \omega} .$$

where G is the dispersion equation and $\mathbf{x}$, $\mathbf{k}$, ω are the position, wave number and wave frequency, respectively. The power absorption along the ray path is given by

$$P_{ab}/P_o = 1 - \exp[-2\int \mathbf{k}_1 \cdot d\mathbf{s}]$$

$$= 1 - \exp[-2 \int \frac{\mathrm{Im}[G(\mathbf{k}_o, \omega)]}{\partial G_o/\partial \omega} dt] ,$$

where P_{ab} and P_o are the absorbed power and initial power input, respec-

tively, and k_1 is the imaginary part of wave number, ds the line element along the ray path, and ImG is the imaginary part of dispersion equation with real k and ω (see Appendix I). As a dispersion equation, we use the general expression taken into ccount of finite temperature effect, which is given in Appendix II, eq.(A-II-1), and also use the Appleton-Hartree equation (cold plasma approximation) to investigate the finite temperature effect on ray tracing. Cylindrical plasma column with parabolic electron temperature and density is subject to study the wave propagation. The toroidicity is taken into account in the magnetic field intensity. Parameters used in calculations are as follows:

electron density:	$n_e(0) = 10^{13}$ cm^{-3}
electron temperature:	$T_e(0) = 1$ keV
toroidal magnetic field:	$B_t(0) = 12.5$ kG
wave frequency:	$f = 35$ GHz
$\omega_{pe}(0)/\omega_{ce}(0)$:	0.81

where $\omega_{pe}(0)$ and $\omega_{ce}(0)$ are the electron plasma frequency and electron cyclotron frequency at the center of the plasma column, respectively. Figure 1 shows the CMA diagram and the profile of plasma parameters. There exists upper hybrid resonance and cyclotron cutoff for extraordinary waves, while there is no singular region for ordinary waves in these parameter range. We consider the incidence from inside of the torus, and the results for ordinary waves are shown in Fig.2 (2(a): ray trajectory, 2(b): group velocity). The direction of magnetic field is along z-axis in Fig.2(a), and dashed curve in Fig.2(b) shows the results obtained by cold plasma approximation. In Fig.2(b), X axis is expressed by ω/ω_{ce}, where ω_{ce} is the electron cyclotron frequency at the center. Ordinary waves take a straight path and the wave energy is absorbed in the vicinity of electron cyclotron resonance region which is located at the center of the plasma column (open circles indicate every 10 % damping of initial wave energy).

The group velocity shows the singular behavior in the electron cyclotron resonance region in spite of good agreement with the results obtained by cold plasma approximation in the off-resonant, $\omega \neq \omega_{ce}$, region (peripheral region). The magnitude of group velocity exceeds the velocity of light in the electron cyclotron resonance region, which means that the group velocity loses its physical meaning as the velocity of energy flow in this region, where one of the assumption is already violated in deducing the group velocity, that is, the medium is no longer non-dissipative.

This singular behavior of group velocity qualitatively agrees with the results obtained by Brillouin[1] in a dispersive dielectric media. From the results shown in Fig.2(b), we must anticipate that the group velocity is no more the velocity of energy flow around the electron cyclotron resonance region. Therefore this must be taken into consideration in determining the ray trajectory which has never been treated properly.

Although the calculations presented here are not for bumpy geometry but for tokamak, the results show general feature, i.e., in the absorption region, the geometrical optics does not give the reliable calculations of ray tracing.[2] In a bumpy torus, there exists the strong absorption region (fundamental and second harmonic resonance region), so that we should be careful for investigating the ray trajectories and cyclotron damping. Unfortunately, for lack of the expression for the velocity of energy flow valid in the absorption region, the reliable calcultions have not been carried out yet, as far as authors' knowledge. This problem will be important in future devices, because the region where the group velocity loses its physical meaning increases with temperature.

2. NEW CUTOFF AND RESONANCE

In this section, we present new cutoff and resonance phenomena which come from the anisotropic electron temperature. These cutoff and resonance may give rise to new diagnostics to estimate the parallel component of the plasma beta value ($\beta_{\parallel}$). The refractive index for ordinary waves is given by

$$N^2 = \varepsilon_{33} , \qquad \theta \approx 90° \tag{5}$$

where ε_{33} is the element of dielectric tensor. For the plasma with anisotropic electron temperature, ε_{33} is written by

$$\varepsilon_{33} = 1 - \frac{\omega_{pe}^2}{\omega^2} \sum_{\ell=-\infty}^{\infty} \frac{\omega}{\omega - \ell\omega_{ce}} \left[1 - \frac{\ell\omega_{ce}}{\omega} \left(\frac{T_{\parallel}}{T_{\perp}} - 1\right)\right] e^{-a} I_{\ell}(a) , \tag{6}$$

where ω_{pe} is the plasma frequency, ω_{ce} cyclotron frequency, and a is $k_{\perp}^2\rho^2$ ($k_{\perp}$: perpendicular wave number, ρ_e: electron Larmor radius). When $a \ll 1$ is satisfied, we can expand the term $e^{-a}I_{\ell}(a)$ in power series of a and retain to the first order in a

$$\varepsilon_{33} = 1 - \frac{\omega_{pe}^2}{\omega^2}\{(1 - a) + \frac{\omega}{\omega - \omega_{ce}}[1 + \frac{\omega_{ce}}{\omega}(\frac{T_{\parallel}}{T_{\perp}} - 1)]\frac{a}{2}$$

$$+ \frac{\omega}{\omega + \omega_{ce}}[1 - \frac{\omega_{ce}}{\omega}(\frac{T_{\parallel}}{T_{\perp}} - 1)]\frac{a}{2}\}$$

$$= 1 - \frac{\omega_{pe}^2}{\omega^2} + (\frac{kc}{\omega})^2(\frac{T_{\parallel}}{mc^2})(\frac{\omega_{pe}}{\omega_{ce}})^2\{1 - \frac{\omega_{ce}^2}{\omega^2 - \omega_{ce}^2}\frac{T_{\parallel}}{T_{\perp}}\} \qquad (7)$$

Finally we obtain the refractive index for ordinary wave;

$$N^2 = \frac{1 - \frac{\omega_{pe}^2}{\omega^2}}{1 + (\frac{\omega_{pe}}{\omega_{ce}})^2(\frac{T_{\parallel}}{mc^2})\frac{\omega_{ce}^2}{\omega^2 - \omega_{ce}^2}} \qquad (8)$$

When the wave frequency ω approaches to ω_{ce} from the low frequency side, the denominator of this equation vanishes at the frequency,

$$\omega_1^2 = \omega_{ce}^2 - (\frac{T_{\parallel}}{mc^2})\,\omega_p^2\ , \qquad (9)$$

which gives the new-resonance shifted from the usual cyclotron resonance by an amount of $(\frac{T_{\parallel}}{mc^2})\omega_{pe}^2$ and then at the frequency $\omega = \omega_{ce}$, eq.(8) gives the cutoff (not resonance), as shown in Fig.3. If we can measure the resonance frequency, we can determine the $\beta_{\parallel}$ value from the equation (9), i.e.,

$$\beta_{\parallel} = (\frac{T_{\parallel}}{mc^2}) = \frac{\omega_{ce}^2 - \omega_1^2}{\omega_{pe}^2}\ .$$

This method may give the $\beta_{\parallel}$ of toroidal hot plasma in a bumpy torus.

3. DENSITY MEASUREMENT BY MICROWAVE INTERFEROMETER

Microwave interferometer system is one of the most reliable measurement system to determine electron density. But in mirror machine with hot electron plsmas, it is reported that the consistent determination of electron density is very difficult. We carried out the experiment of density measurement on NBT by microwave interferometer with different frequencies, 35 GHz and 55 GHz (Fig.4). As seen in this figure, the results of two interferometer show good agreement in the high pressure region (C-mode), but are different each other in the low pressure region (T-mode). This means that the density measurement on bumpy torus by microwave interferometer

loses its stand point to determine the C-T mode transition, which is usually determined by the starting point of density increase with decreasing the neutral gas pressure. It is necessary to cross-check the results of the interferometer with those obtianed by other density measurement system. We are now preparing for Li-neutral beam probing system.

The possible reasons for the difference of two interferometric measurement are considered as follows: (i) Hot electrons with mildly relativistic temperature change the dielectric coefficient from the usual value ($1- \omega^2/\omega_{pe}^2$), and then interferometric signal is not proportional to electron density. (ii) Anisotropic electron temperature also changes the dielectric coefficient as shown in section 2 (in this case, wave frequency corresponds to higher harmonic of electron cyclotron frequency). These effect must be investigated theoretically and experimentally furthermore.

REFERENCES

1) L. Brillouin: Wave Propagation and Group Velocity (Academic Press, 1960).

2) M. Tanaka, M. Fujiwara and H. Ikegami: Institute of Plasma Physics, Nagoya University Report, IPPJ-427 (1979).

APPENDIX I

The ratio of absorbed power to the wave power input is given by

$$P_{ab}/P_o = 1 - \exp[-2\int \mathbf{k}_1 \cdot d\mathbf{s}]$$
$$= 1 - \exp[-2\int \mathbf{k}_1 \cdot \mathbf{v}_g \, dt] \ , \qquad \text{(A-I-1)}$$

where P_{ab} is the absorbed power, P_o is the input power of wave energy, k_1 is the imaginary part of the wavenumber v_g is group velocity, and ds is line element along the ray path. The exponent of the eq.(9) is deduced from a warm plasma dispersion equation, that is, the dispersion equation is expanded in Taylor series around the real axis in the complex k plane with an assumption of weak absorption

$$G(\mathbf{k}, \omega) = G_o(\mathbf{k}_o, \omega) + i \frac{\partial G_o}{\partial \mathbf{k}} \mathbf{k}_1 + iG_1(\mathbf{k}_o, \omega) \ , \qquad \text{(A-I-2)}$$

where

$$G_o = \mathrm{Re}[G(k_o, \omega)] \ ,$$

$$G_1 = \mathrm{Im}[G(k_o, \omega)] \ ,$$

$$\mathbf{k} = \mathbf{k}_o + i\mathbf{k}_1 \ ,$$

$$\frac{|\mathbf{k}_1|}{|\mathbf{k}_o|} << 1 \ .$$

The real part gives dispersion equation in zeroth order of Imk

$$G_o(\mathbf{k}_o, \omega) = 0 \ , \qquad \text{(A-I-3)}$$

and the imaginary part gives

$$-\frac{\partial G_0}{\partial k}\mathbf{k}_1 = G_1(\mathbf{k}_0, \omega) = \mathrm{Im}[G(\mathbf{k}_0, \omega)] \qquad \text{(A-I-4)}$$

Deviding eq.(12) by $\partial G_0/\partial\omega$ and using eq.(7), we find

$$-\frac{\partial G_0/\partial k}{\partial G_0/\partial\omega}\cdot\mathbf{k}_1 = \mathbf{v}_g\cdot\mathbf{k}_1 = \frac{\mathrm{Im}[G(\mathbf{k}_0, \omega)]}{\partial G_0/\partial\omega} \quad . \qquad \text{(A-I-5)}$$

Thus eq.(9) is rewritten as follows

$$\frac{P_{abs}}{P_0} = 1 - \exp[-2\int \frac{\mathrm{Im}[G(k_0, \omega)]}{\partial G_0/\partial\omega}\, dt] \quad . \qquad \text{(A-I-6)}$$

This equation determines the power absorption along the ray path.

APPENDIX II

We use the following equations as a dispersion equation, i.e.,

$$G(k, \omega) = \mathrm{Det}\left|\frac{\omega^2}{c^2}(k_i k_j - \delta_{ij}) + \varepsilon_{ij}\right| \quad , \qquad \text{(A-II-1)}$$

where ε_{ij} is the dielectric constant of a plasma and given by

$$\varepsilon_{ij} = \delta_{ij} + \frac{\omega_{pe}^2}{\omega^2}\left[\sum_{\ell=-\infty}^{\infty} i\sqrt{\pi}\, z_0 W(z_\ell)\Pi_{ij}^{(\ell)} + 2z_0 b_i b_j\right] , \qquad \text{(A-II-2)}$$

$$z_\ell = \frac{\omega - \ell\omega_{ce}}{\sqrt{2}\, k_\parallel v_{th}} \quad .$$

$W(z_\ell)$ is a plasma dispersion function, b is the unit vector along the static magnetic field,

$$\Pi^{(\ell)} \equiv \begin{pmatrix} \frac{\ell^2}{a} A_\ell(a) , & i\ell A'_\ell(a) , & \sqrt{2/a}\ \ell z_\ell A_\ell(a) \\ -i\ell A'_\ell(a) , & \frac{\ell^2}{a} \cdot A_\ell(a) - 2aA'_\ell(a), & i\sqrt{2a}\ z_\ell A'_\ell(a) \\ \sqrt{2/a}\ \ell z_\ell A_\ell(a) , & i\sqrt{2a}\ zA'_\ell(a) , & 2z_\ell^2 A_\ell(a) \end{pmatrix} \qquad \text{(A-II-3)}$$

where

$$A_\ell(x) \equiv e^{-x} I_\ell(x) ,$$

$$A'_\ell(x) \equiv \frac{dA}{dx} ,$$

$$a \equiv k_\perp^2 \rho_e^2 ,$$

$$\mathrm{sgn}\sqrt{a} = -1 .$$

In the above equations, $k_\perp$ is a perpendicular wave number and ρ_e is the electron Larmor radius. We neglect the ion contribution and summation over ℓ is taken up to $\ell = 5$.

Figure Captions

Fig.1. CMA diagram and the profile of plasma parameters. C: cut-off for OR-wave, CR: electron cyclotron resonance, U: upper hybrid resonance, CC: cyclotron cut-off for EX-wave. The radius of plasma is 17 cm, and the toroidal magnetic field is given by $B_T = B_0/(1 + x/R_0)$, where B_0 is the magnetic field intensity at the center of the plasma, R_0 is 91 cm.

Fig.2. (a) Ray trajectory of OR-wave. Propagation angle is 80° at entrance. ----: cold plasma approximation.
(b) Group velocity of OR-wave normalized by velocity of light. ----: cold plasma approximation.

Fig.3. Schematic diagram of refractive index for OR-wave as a function of wave frequency. ω_1: resonance, ω_{ce}: cutoff.

Fig.4. Electron density as a function of neutral gas pressure measured by microwave interferometer with different two frequencies, 35 GHz and 55 GHz.

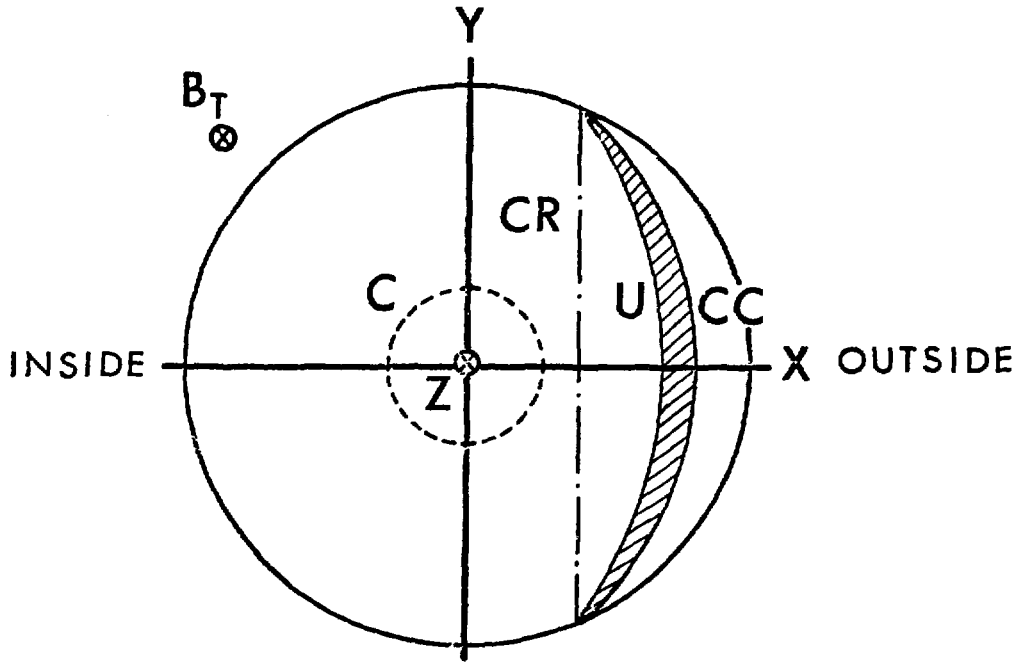
Y
B_T
CR
C
U
CC
INSIDE
X
OUTSIDE
Z

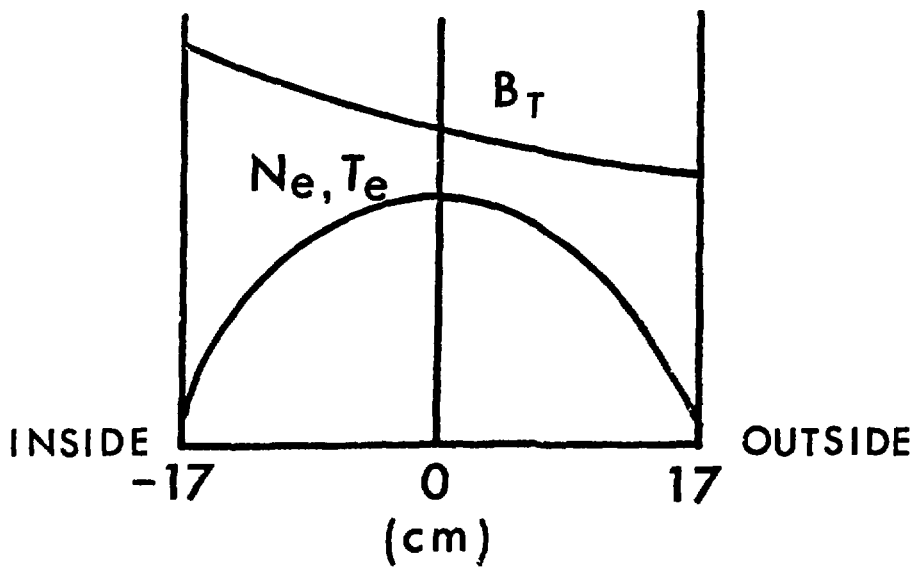
B_T
N_e, T_e
INSIDE
OUTSIDE
-17
0
17
(cm)

FIG. 1

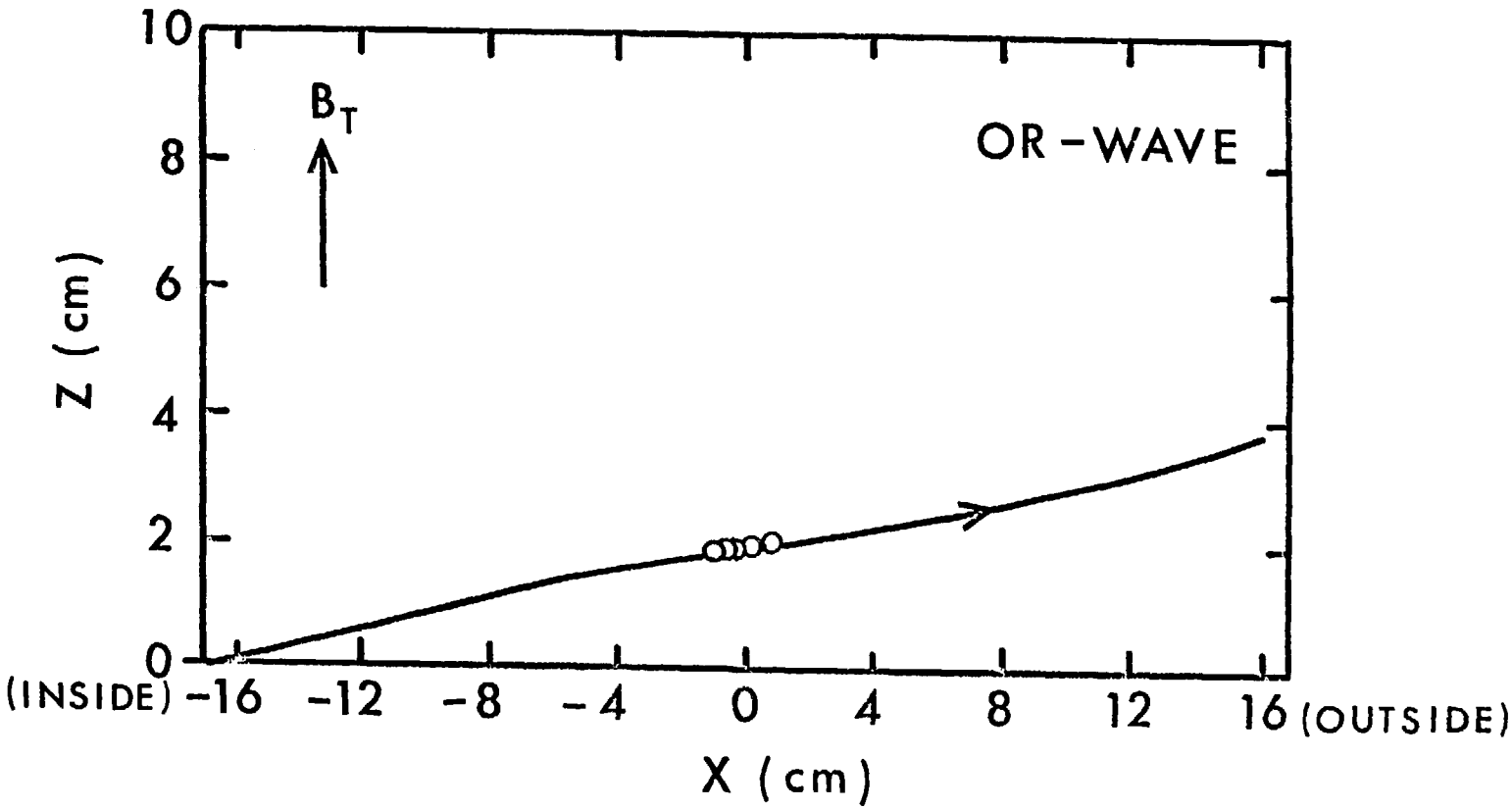

FIG.2-a

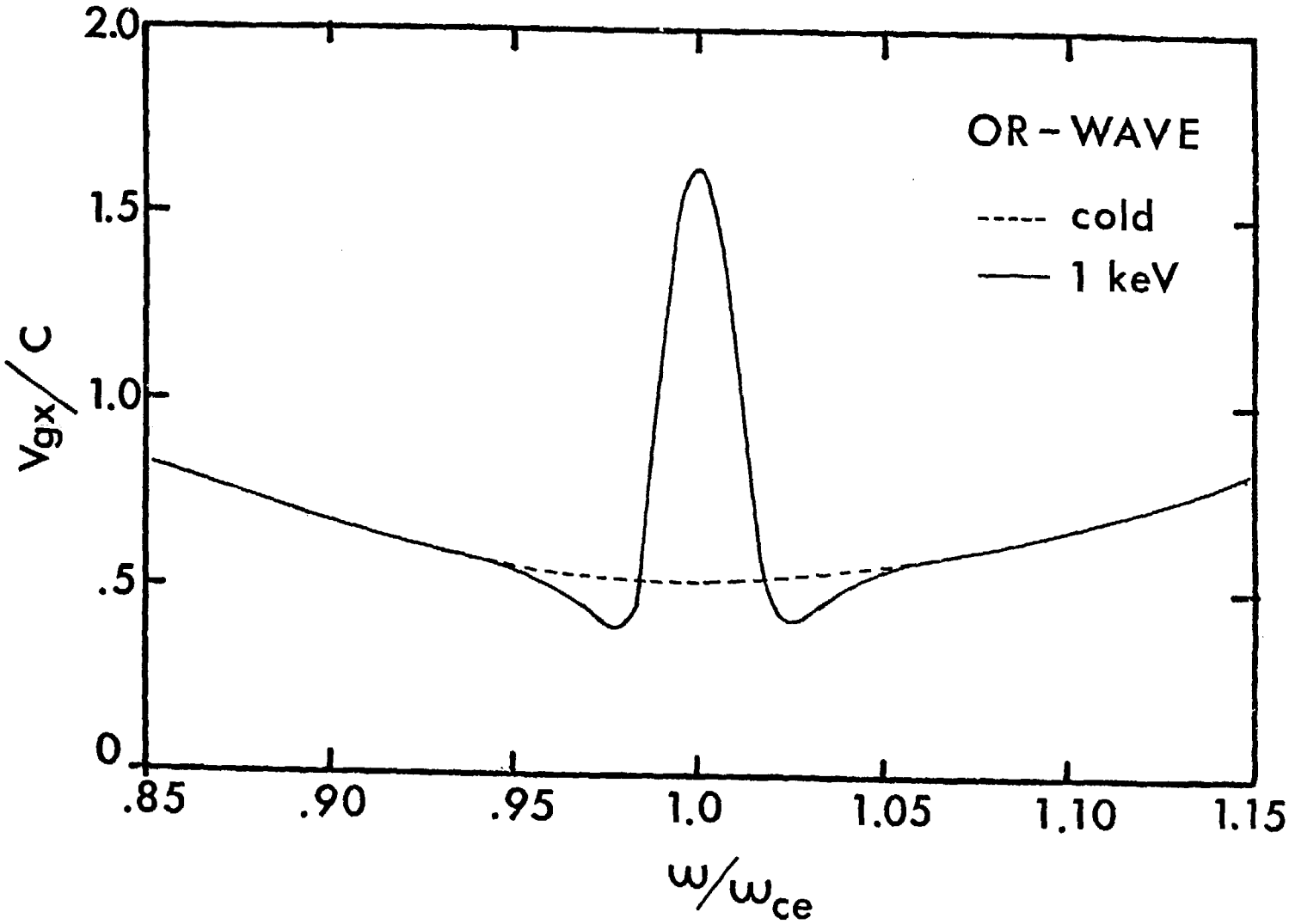
OR-WAVE
cold
1 keV
2.0
1.5
1.0
.5
0
V_{gx}/C
.85
.90
.95
1.0
1.05
1.10
1.15
ω/ω_{ce}

FIG. 2-b

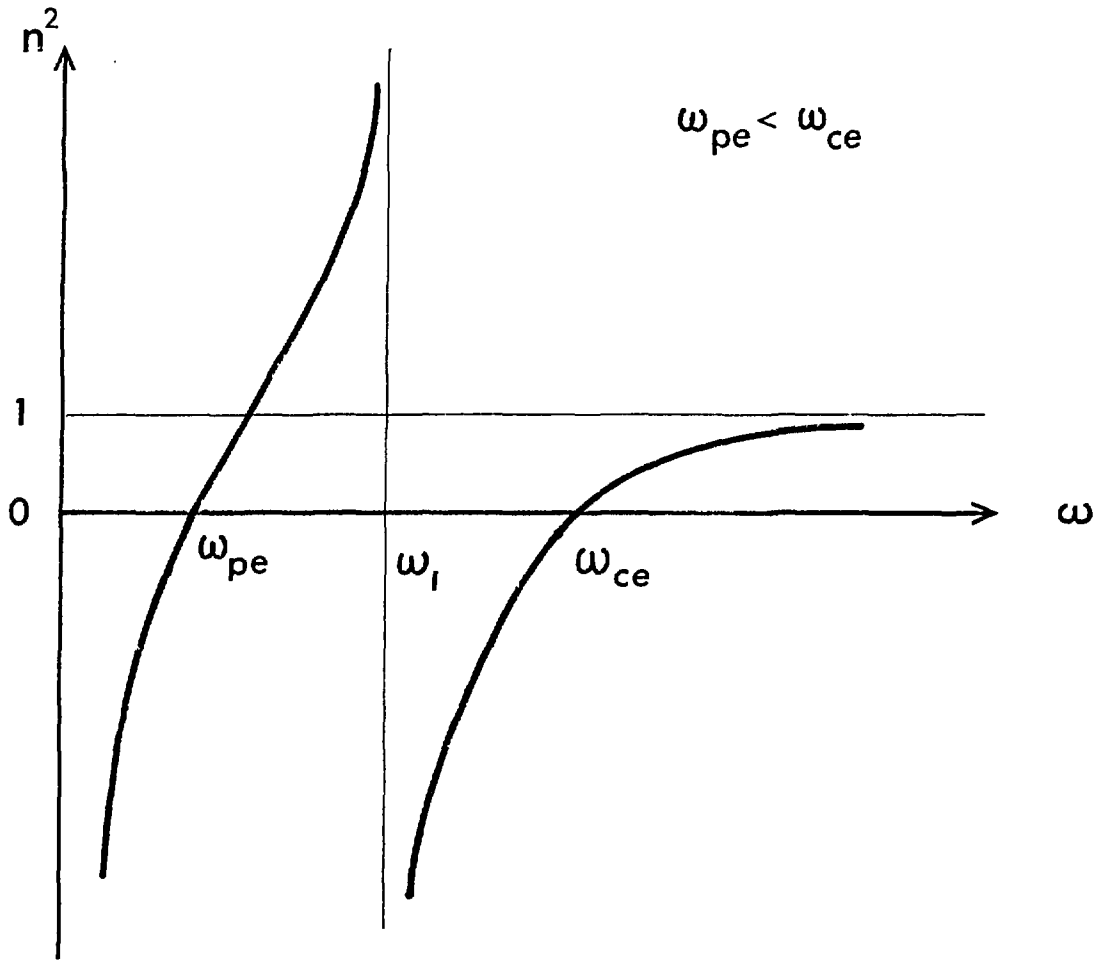

FIG. 3

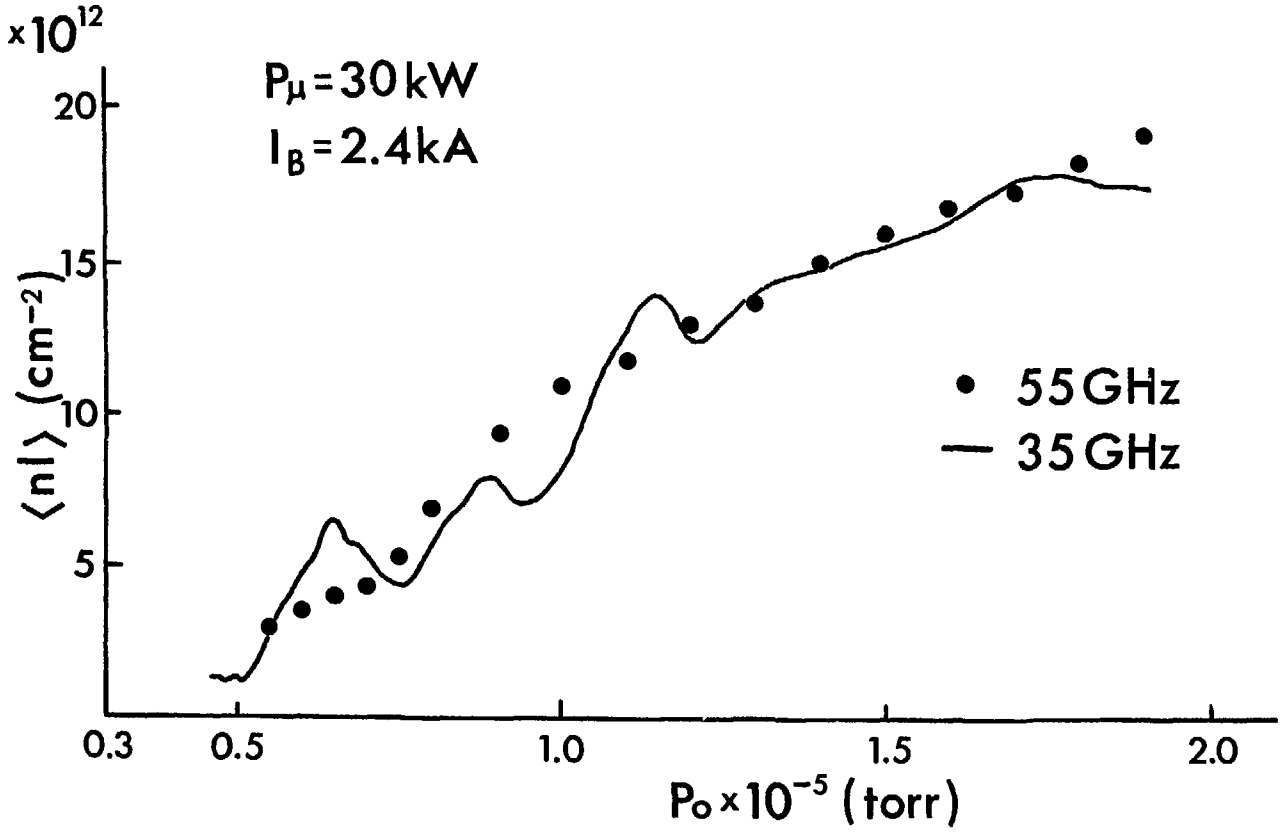
×10^12
20
15
10
5
⟨nl⟩ (cm^-2)
Pμ=30kW
IB=2.4kA
• 55GHz
— 35GHz
0.3
0.5
1.0
1.5
2.0
Po×10^-5 (torr)

Fig. 4

DISCUSSION

D. BATCHELOR: In your slide of v_g vs ω/Ω_e for ordinary mode what are k_i and k_i/k_r? Is relativistic resonance broadening included?

M. TONAKA: In our calculation code k_i is not only evaluated, but also the coupled form $\vec{k}_i \times \vec{v}_g$ is estimated from the damping of waves. In a typical condition the damping length is about 3.3 cm and the wave length is 0.8 cm, so that k_i is not small compared with k_r. As to the effect of the relativisitic resonance broadening, we consider it in the following way: The resonance condition is $\omega - \Omega_e' - k_\parallel v = 0$ (where Ω_e' is $eB\sqrt{1 - \beta^2}/m_0c$. If $\beta << 1$, the equation is expressed as $\omega - \Omega_e(1 - \beta^2/2) - k_\parallel v = 0$, where Ω_e is eB/m_0c.

The term $1/2\ \beta^2\Omega_e$, which comes from the relativistic effect, becomes dominant when the condition $n \cos\theta \leqslant \beta^2/2$ is satisfied, where θ is the propagation angle against the magnetic field line. With the parameters of our calculation ($\beta \sim 0.04$ and $n \sim 0.54$), the relativistic effect is dominant for $\theta \geqslant 88°$, but at the condition with $\theta \cong 72°$ the Doppler effect is still dominant.

Synchrotron Radiation from the Ring and Nonlinear Effects in Microwave Heating of EBT

V. K. Tripathi, E. Ott and C. S. Liu
Department of Physics and Astronomy
University of Maryland
College Park, Maryland 20742

Abstract

The possibility exists that measurements of synchrotron radiation from the EBT ring can be used to determine ring properties. In order to utilize such a diagnostic technique, theoretical models for radiation from the ring are needed.

We are developing a computer program, for the spectral distribution of synchrotron radiation, especially at higher harmonics, from the ring. Using the single particle emission coefficients as given by Bekefi, we have obtained the expressions for the intensity of radiation in the ordinary and extraordinary modes. The radiation is primarily coming from the hot electron ring with parameters: $n_h \sim 10^{11}$ cm^{-3}, $T_h \sim$ 0.2-2 Mev, radius $\sim$12-15 cm, width $\sim$5-7 cm, thickness $\sim$3-4 cm. We have assumed a gaussian profile for electron density and a consistent profile for magnetic field is deduced, using the pressure balance. The electron distribution function is taken to lie in the narrow pitch angle cone.

The interest is restricted to perpendicular radiation, where relativistic effects are pronounced.

On account of large electron temperature the frequency widths of higher harmonics are large and they strongly overlap over each other. The intensity of the ordinary mode is much smaller than the extraordinary mode (by a factor of $\psi_o^2 v_e^2/c^2$, ψ_o is the pitch angle of the cone).

We have also looked into the possibility of nonlinear effects in the microwave heating of the ring. It seems that the microwaves around the second cyclotron harmonic can effectively decay into two electron Bernstein waves and may account for the formation of the ring.

I. Introduction

The microwaves launched into the mirror mid planes of EBT by waveguide horns are substantially absorbed at the second cyclotron harmonic layer $\omega=2\omega_c$. The electrons attain large perpendicular energies; typically 10% electrons have energies of the order of 0.2 - 2 MeV. They also produce a large azimuthal current (due to $\underline{\nabla}$ p$\times\underline{B}$) and thus a hot electron annulus is formed. The azimuthal current perturbs the magnetic field; a dip in the magnetic field is produced at the $2\omega_c$ layer.

The ring (or annulus) must radiate efficiently at the harmonics of cyclotron frequency. Since the electrons possess very large energies ($v_e/c \gtrsim 0.5$), the radiated harmonics $n\omega_c$ would have large widths ($\Delta\omega \sim n\omega_c\ T/M_oc^2$) and the higher harmonics would strongly overlap over each other. This radiation could be effectively utilized for plasma diagnostics. In this paper we have obtained the expressions for the intensity of synchrotron radiation, using the Bekefi's expressions for single particle emission coefficients and assuming (a) a narrow pitch angle distribution function for electrons, (b) gaussian profile for electron density, (c) self consistent modification in the magnetic field and (d) neglecting the plasma effects. The neglect of plasma effects is justified because $\omega_p^2/\omega^2 < 0.1$ for $\omega \gtrsim 3\omega_c$ where ω_p is the background plasma frequency and our interest is essentially focused on higher harmonics ($n \gtrsim 3$).

We have also looked into the possibility of nonlinear effects on the microwave heating at second cyclotron harmonic. The most important nonlinearity is expected to be the parametric decay of the microwave into two Bernstein waves. This channel should have minimum threshold because the Bernstein waves propagate with small group velocity. We have obtained the expression for convective amplification of this decay by solving full Vlasov equation for electrons.

II. Synchrotron Radiation

For most part of this section we would confine ourselves to the radiation being emitted in the perpendicular direction with respect to the magnetic field. At the end we will mention the modifications at oblique angles. We refer the direction of static magnetic field (at the mirror mid plane) to be z axis and x axis normally outward. Taking ψ as the angle between electron momentum $\underline{p}$ and the z axis, the electron distribution function may be written as

$$f(\underline{p}) = A\, e^{-\varepsilon/T} \text{ for } \frac{\pi}{2} - \psi_o < \psi < \frac{\pi}{2} + \psi_o$$
$$= o \text{ otherwise} \qquad (1)$$

where

$$A = [\, 4\pi \sin\psi_o \int_o^\infty p^2\, dp\, \exp(-\varepsilon/T)]^{-1},$$

$2\,\psi_o$ is the pitch angle spread, ε is the electron energy and T is the temperature (of the ring). It must be added here that the microwaves at $\omega \sim 2\omega_c$ preferentially heat the electrons in the perpendicular direction. However, the electrons that are heated away from the mirror mid plane, when pass through the mid plane they attain parallel momentum. Consequently the pitch angle width ψ_o is larger for broader rings (larger z_o, z_o is the half width of the ring in the z direction). Also ψ_o is a function of z; ψ_o is maximum at z=0 (mirror mid plane) and zero at the ring edges.

The electron density of the ring is modelled as

$$n_h = n_1\, e^{-z^2/z_o^2 - (X-R)^2/X_o^2} \qquad (2)$$

where R is the radius of the ring and X_o is the half width of the ring in the X direction.

The self consistent modification in the magnetic field may be obtained from the pressure balance

$$P + B^2/8\pi = \text{const}$$

$$\Rightarrow \quad B \simeq B_o\,(1 - \beta_h\,(x,z)/2) \qquad (3)$$

where B_o is the initial field and β_h is the beta of the annulus. Using Eqs(2) and (3) the electron gyro frequency (at rest mass) may be written as

$$\omega_{co}\,(X,z) = \omega_{co}(0,0)\,[1 - \frac{\beta_h(0,0)}{2}\,e^{z^2/z_o^2} - (X - R)^2/X_o^2]$$
$$\cdot(1 - X/L_\perp)$$

$L_\perp$ is the scale length of magnetic field variation in the x direction in the absence of ring.

RADIATION

The coefficient of spontaneous emission i.e. the energy radiated per electron per unit solid angle per unit frequency interval per second is given by

$$\eta_\omega = \frac{e^2\omega^2}{8\pi^2 c}\,\frac{P_{||}^2}{m^2c^2}\,J_n^2(x)\,\delta(y) \qquad \text{ordinary mode} \qquad (5)$$

$$= \frac{e^2\omega^2}{8\pi^2 c}\,\frac{P_\perp^2}{m^2c^2}\,J_n'^2(x)\,\delta(y) \qquad \text{extraordinary mode} \qquad (6)$$

where $x = \frac{\omega}{\omega_{co}}\,\frac{P_\perp}{m_{oc}}$, $y = n\omega_c - \omega$

$$m = m_o(1+p^2/m_o^2c^2)^{1/2}$$

$$\varepsilon = (p^2c^2+m_o^2\,c^4)^{1/2}$$

and n is the number of cyclotron harmonic. In order to obtain the total emissivity at frequency ω, a summation over n must be carried out. The radiation emitted by the electrons per unit volume, per unit solid angle,

per unit frequency interval, per second can obtained as

$$j_\omega = \sum_n \eta_h \iint_{0\ \pi/2-\psi_o}^{\infty\ \ \pi/2+\psi_o} \eta_\omega\ f\ (\underline{p})\ p^2\ dp\ \mathrm{Sin}\ \psi\ d\psi \tag{7}$$

Using Eq. (1) and carrying out the p integration, we get

$$j_\omega = \sum_n \frac{n_h e^2}{4\pi c}\ n\ \omega_{co}\ p_o^3\ A\ e^{-\frac{n\omega_{co}}{\omega}\ \frac{m_{oc}^2}{T}}\ \Phi \tag{8}$$

$$\Phi = \int_{\frac{\pi}{2}-\psi_o}^{\frac{\pi}{2}+\psi_o} J_n^2\ (\beta\ \mathrm{Sin}\ \psi)\ \mathrm{Sin}\ \psi\ \mathrm{Cos}^2\ \psi\ d\ \psi \qquad \text{ordinary mode} \tag{9A}$$

$$= \qquad J_n'^2\ (\beta\ \mathrm{Sin}\ \psi)\ \mathrm{Sin}^3\ \psi\ d\ \psi \qquad \text{extraordinary mode} \tag{9B}$$

where $p_o = m_o c \left(\frac{n^2\omega_{co}^2}{\omega^2} - 1\right)^{1/2}$

$$\beta = \frac{\omega}{\omega_{co}} \left(\frac{\omega_{co}^2\ n^2}{\omega^2} - 1\right)^{1/2}$$

J_n' is the derivative of Bessel function with respect to its orgument.

The intensity of synchrotron radiation I is governed by

$$\frac{dI}{dx} = j_\omega \tag{10}$$

where the absorption and stimulated emission of radiation is neglected. Eq. (10) gives

$$I = \frac{A\ e^2}{4\pi\ c} \sum_n \int n_h\ \ n\omega_{co}\ p_o^3\ e^{-\frac{n\omega_{co}}{\omega}\ \frac{m_{oc}^2}{T}}$$

$$\cdot\ \Phi\ \ dX \tag{11}$$

Eq. (11) will be solved numerically on computer for EBT ring parameters.

In the special case of small pitch angle spread $\psi_o << \pi/2$, Eq. (11) simplifies to give

$$I = \sum_n \frac{A_1 e^2}{4_\pi c} \frac{2}{3} \psi_o^2 \int n_h \; n\omega_{co} \; p_o^3 \; J_n^2 (\beta)$$

$$e^{-\frac{n\omega_{co}}{\omega} \frac{m_o c^2}{T}} dx \qquad \text{ordinary mode} \qquad (12)$$

$$= \sum_n \frac{A_1 e^2}{4\pi c} \; 2 \psi_o \int n_h \; n\omega_{co} \; p_o^3 \; J_n'^2 (\beta)$$

$$e^{-\frac{n\omega_{co}}{\omega} \frac{m_o c^2}{T}} dx \qquad \text{extraordinary mode} \qquad (13)$$

where $$A_1 = [4\pi \int p^2 \, dp \; e^{-\varepsilon/T}]^{-1}$$

As ψ_o decreases the intensity of the extra ordinary mode tends to a constant value, where as the intensity of the ordinary mode goes to zero. As a matter of fact for all values of ψ_o, the intensity of ordinary mode would be smaller than that of the extraordinary mode as $J_n' (\beta) > J_n(\beta)$.

In the other limiting case of $m_o c^2 >> T$, the expression for the intensity of synchrotron radiation is again simplified.

OBLIQUE ANGLES

The single particle emissivitive for radiation at an angle θ, with respect to magnetic field is written as

$$\eta_\omega(\theta) = \frac{e^2 \omega^2}{8\pi^2 c} \left[\frac{\text{Cos}\theta - \beta_{11}}{\text{Sin}\theta}^{\;2} J_n^2 (x) + J_n'^2 (x) \; \beta_\perp^2 \right] \delta(y) \qquad (14)$$

where $$x = \frac{\omega}{\omega_{co}} \frac{p \text{ Sin } \psi \text{ Sin } \theta}{m_o c}, \quad \beta_{11} = \frac{p \text{ Cos } \psi}{mc}$$

$$y = n\omega_c - \omega(1 - \frac{p \text{ Cos } \theta \text{ Cos } \psi}{mc})$$

$$\beta_{\perp} = \frac{p \operatorname{Sin} \psi}{mc}$$

Using Eq. (14) in Eq. (7) and carrying out the p integration we obtain

$$j_{\omega} = \sum \frac{n_h e^2 \omega^2}{8\pi^2 c} A \; 2\pi \; \Psi \tag{15}$$

$$\Psi = \int_{\pi/2-\psi_o}^{\pi/2+\psi_o} p_o^2 \; e^{-\varepsilon(p_o)/T} \; \frac{\operatorname{Sin} \psi}{g(p_o)} \; d\psi$$

$$\cdot \left[J_n^2 (x_o) \; \frac{\{\operatorname{Cos}\theta - p_o \operatorname{Cos}\psi/m_o c \; (1 + p_o^2/m_o^2 c^2)^{1/2}\}^2}{\operatorname{Sin}^2\theta} \right.$$

$$\left. + \; J_n'^2(x_o) \; \frac{p_o^2 \operatorname{Sin}^2\psi}{m_o^2 c^2 \; (1 + p_o^2/m_o^2 c^2)} \right] \tag{16}$$

$$g(p_o) = (1 + p_o^2/m_o^2 c^2)^{-1} \; [(1 + p_o^2/m_o^2 c^2)^{1/2}$$

$$\cdot \frac{\omega}{m_o c} \operatorname{Cos}\theta \operatorname{Cos}\psi - \frac{p_o \omega}{m_o^2 c^2} \;] \; ,$$

$$p_o = \frac{m_o c}{1 - \operatorname{Cos}^2\theta \operatorname{Cos}^2\psi} \; \frac{n\omega_{co}}{\omega} \operatorname{Cos}\theta \operatorname{Cos}\psi$$

$$+ \; \{ \frac{n^2 \omega_{co}^2}{\omega^2} + \operatorname{Cos}^2\theta \operatorname{Cos}^2\psi - 1 \}^{1/2} \;] \; ,$$

$$x_o = \frac{\omega}{\omega_{co}} \frac{p_o}{m_o c} \operatorname{Sin}\theta \operatorname{Sin} \psi$$

In this case ψ integration is extremely complicated and the extraordinary and ordinary modes can not be separated out.

Using Eq. (15) one can obtain the intensity of synchrotron radiation.

We are developing a computer program to numerically obtain the intensity of synchrotron radiation from the EBT ring.

III. Convective Decay of the Microwave Pump into Two Bernstein Waves

A high power microwave propagating through the second harmonic cyclotron layer in EBT can decay into two Bernstein waves. We consider the microwave (ω_o, $\underline{k}_o || \hat{x}$) to propagate in the upper hybrid mode and the decay waves ($\omega, \underline{k}$), ($\omega_1, \underline{k}_1$; $\omega_1 = \omega - \omega_o$, $\underline{k}_1 = \underline{k} - \underline{k}_o$) to be flute type ($k_{\Pi} \simeq 0$) Bernstein modes,

$$k_o = \frac{\omega_o}{c} \left[1 - \frac{\omega_p^2}{\omega_o^2} \frac{\omega_o^2 - \omega_p^2}{\omega_o^2 - \omega_u^2}\right]^{1/2} \tag{17}$$

$$\omega = \omega_c \left[1 + \frac{\omega_c I_1 e^{-b}}{(1 - I_o e^{-b} + b\, \omega_c^2/\omega_p^2)}\right] \tag{18}$$

$$b = \frac{1}{2} k_\perp^2 v_e^2/\omega_c^2, \quad v_e = (2T/m)^{1/2}, \quad \omega_u^2 = \omega_p^2 + \omega_c^2 .$$

I's are the modified Bessel functions of argument b. Since we are interested in the decay process in the initial phase of microwave heating we have ignored the effects of the ring on the dispersion relations. The decay waves have $k\, v_e/\omega_c > 1$ hence we need to use full Vlasov equation to evaluate the coupling coefficients. We have solved the Vlasov equation in guiding center coordinates $\underline{x}_g$, magnetic moment $\mu = \frac{1}{2} m v_\perp^2/\omega_c$, gyrophase angle θ and parallel momentum p_z,

$$\frac{\partial f}{\partial t} + \dot{\underline{x}}_{g\perp} \cdot \frac{\partial f}{\partial \underline{x}_{g\perp}} + \dot{\mu} \frac{\partial f}{\partial \mu} + \frac{p_z}{m} \frac{\partial f}{\partial z} - e\, E_z \frac{\partial f}{\partial p_z} = 0 \tag{19}$$

Following Liu and Tripathi,[1] we have obtained the following nonlinear

dispersion relation for the decay waves

$$\varepsilon\ \varepsilon_1 = \mu \simeq \frac{\pi}{4} \left(\frac{\omega_p^2}{\omega_c^2}\right)^2 \frac{\omega_c^2}{k^2 \nu_e^2} \frac{u^2}{c^2} \tag{20}$$

where u is the oscillatory electron velocity due to the pump field, and $\varepsilon(\omega,\underline{k})$ and $\varepsilon_1(\omega_1,\underline{k}_1)$ are the linear dielectric functions for the decay waves. Assuming linear profile for electron density (with scale length L_n) the convective amplification[2] of the decay waves turns out to be

$$A \simeq \frac{\omega_c^2}{\nu_e^2} \frac{u^2}{c^2} \frac{L_n}{k_o}$$

$$\simeq 0.1\ p$$

at 200 ev when p is in kw/cm^2, The threshold power at 200 ev turns out to be $\sim$10 kw/cm^2 and at 20 ev it is 1 kw/cm^2. These thresholds can be reduced further if the decay waves are trapped in the region of interaction and the instability could become absolute. The presently employed power densities in EBT are a few times smaller than the convective threshold. Nevertheless a detailed study of this instability is warranted.

IV. Conclusions

The synchrotron radiation from EBT ring would provide information about the pitch angle spread of the distribution function and temperature, density and magnetic field profiles of the ring. The theoretical model presented here would be employed to infer these parameters from the experiments.

We also suggest that at power densities exceeding a few kilo $watt/cm^2$ the parametric decay of the microwave heating wave into two Bernstein waves is relevant in the initial phase of ring formation.

Acknowledgment

This work was supported by the Department of Energy.

References

1. C. S. Liu and V. K. Tripathi, Nuclear Fusion (Comm. 1979); V. K. Tripathi, C. S. Liu and C. Grebogi, Phys. Fluids 22, 301 (1979).
2. C. S. Liu, Adv. in Plasma Phys. 6, 83 (1976).

DISCUSSION

H. SANUKI: Have you considered the wave number mismatch effects in the parametric decay process, because at $\omega = 2\omega_{ce}$ the density decreases rapidly?

V. K. TRIPATHI: Yes. Due to the finite density and magnetic field gradients the decay instability is convective. We have obtained the convective threshold and convective amplification.

S. TAMOR: In the expression presented for emission the two terms do not represent extraordinary and ordinary waves except at 90°?

V. K. TRIPATHI: This is true. For perpendicular and near perpendicular propagation ($\theta - \pi/2 \ll \pi/2$), the ordinary and extraordinary modes are separated out.

6. POWER BALANCE

A. Favale, Session Chairman

RING POWER BALANCE*

S. K. Borowski,† N. A. Uckan, E. F. Jaeger, and T. Kammash†
Oak Ridge National Laboratory
Oak Ridge, Tennessee 37830

ABSTRACT

The ring power balance has provided valuable information concerning the relativistic electron rings in ELMO Bumpy Torus (EBT). In this paper, annulus microwave power scaling is reviewed and the importance of stability and ring/core coupling is discussed in connection with the proposed EBT-P device and a potential EBT fusion reactor.

1. INTRODUCTION

An essential feature of the ELMO Bumpy Torus (EBT) is the presence of a relativistic electron annulus in each of the toroidal mirror sectors. These high beta annuli are formed and sustained by microwave heating and are of sufficient density and temperature for diamagnetic currents to produce the necessary minimum in the magnetic field required for the MHD stability of the toroidal core plasma. The stability of the electron ring itself requires the presence of an appreciable cold electron density component, $n_{cold}/n_{hot} > 1$.[1]

Because electron rings play an important role in the confinement characteristics and performance of EBT, the tradeoff between the quality of the confinement afforded by the rings and the power required to sustain them represents an important physics question for EBT-P and for scaling the EBT to a reactor.

Recent studies of the ring power balance[2] in EBT-I have indicated that the energy transfer between relativistic annulus electrons and core

*Research sponsored by the Office of Fusion Energy, U.S. Department of Energy, under contract W-7405-eng-26 with the Union Carbide Corporation.

†Department of Nuclear Engineering, University of Michigan, Ann Arbor, Michigan.

electrons via Coulomb collisions (i.e., drag cooling) is the dominant loss mechanism. Experimental measurements of the annulus decay time[3] are within a factor of ~ 2 of the theoretical drag time, indicating the importance of this loss mechanism in the present EBT device.

In this paper we review the scaling used for estimating the microwave power required to sustain the rings against drag cooling and other classical loss mechanisms. The results of this scaling, covered in Sect. 2, emphasize the importance of both ring/core coupling and annulus volume. In Sect. 3 the scaling curves for EBT-P are presented. These curves enable us to estimate the annulus power requirements for operation at a given annulus beta and varying levels of ring/core coupling. Because the stability of the rings is essential to the overall stability of the EBT toroidal core plasma, ring stability requirements have also been integrated into our scaling projections for EBT-P. Finally, in Sect. 4 the power balance implications for a reactor are analyzed and possible steps toward optimizing the reactor Q value are discussed.

2. ANNULUS MICROWAVE POWER SCALING

Because the core-stabilizing electron annulus must be continuously driven by the microwave sources during steady-state operation, the question of power drain from the annulus is extremely important in scaling the microwave power requirements. In its most basic form the annulus power balance is given by

$$P_{\mu A} = P_{synch} + P_{brems} + P_{scatt} + P_{drag} , \tag{2.1}$$

where P_{synch} and P_{brems} represent the power lost by synchrotron and bremsstrahlung radiation, P_{scatt} is the 90° pitch-angle scattering of the ring electrons on the core plasma ions, P_{drag} represents the power lost from the relativistic electrons due to drag on the toroidal core electrons, and $P_{\mu A}$ is the microwave power required to sustain the annulus. In terms of plasma and machine parameters, Eq. (2.1) can be expressed as follows (mks units with T in keV; see Refs. 2, 4, and 5 for details):

$$P_{\mu A}(\mathrm{MW}) = \Bigg\{ \underbrace{6.2 \times 10^{-23} B_A^2 n_A T_A \left[1 + \frac{T_A}{2(511)}\right]}_{P_{synch}}$$

$$+ \underbrace{5.35 \times 10^{-43} n_A n_{ip} T_A^{1/2}}_{P_{brems}}$$

$$+ \underbrace{1.1 \times 10^{-38} \frac{n_A n_{ip} \ln \Lambda_{ei}}{T_A^{1/2}}}_{P_{scatt}}$$

$$+ \underbrace{2.5 \times 10^{-39} \frac{\gamma^{\alpha} \ln \Lambda_{\alpha}}{\sqrt{\gamma^2 - 1}} n_A n_{ep}}_{P_{drag}} \Bigg\} V_A \,, \qquad (2.2)$$

where $\gamma = 1 + T_A/511$; $\ln \Lambda_{ei} \cong 38 - \ln (\sqrt{n_A}/T_A)$; n_A, T_A, and B_A are the density, kinetic energy, and magnetic field strength at the annulus, respectively; $n_p \cong n_{ip} \cong n_{ep}$ is the toroidal core plasma (ion/electron) density in the vicinity of the annulus; V_A is the total annulus volume; $\alpha = 1$ or 2 depending on the assumed drag model chosen;[4,6] and $\ln \Lambda_{\alpha}$ is the Coulomb logarithm with slight differences in definition for $\alpha = 1$ or $\alpha = 2$ ($\ln \Lambda_1 \sim 20$-30; $\ln \Lambda_2 \sim 16$ for typical parameter ranges of annulus).

An evaluation of the individual loss mechanisms for various EBT experiments[2] and a possible reactor[7] has indicated that drag cooling is the dominant drain on annulus energy. Assuming that drag losses are classical ($\alpha = 1$), Eq. (2.2) can be expressed in the following simplified form:

$$P_{\mu A}(\mathrm{MW}) \cong \left(6.25 \times 10^{-38} \frac{\gamma}{\sqrt{\gamma^2 - 1}} n_A n_{ep}\right) V_A \ . \tag{2.3}$$

Because the relativistic term $\gamma/\sqrt{\gamma^2 - 1}$ will vary little ($\sim$1.15-1.06) in future EBT devices ($T_A \sim$ 500 keV-1 MeV), the annulus power will depend on essentially two terms: the density product $n_A n_{ep}$, which is basically a ring/core coupling term, and the ring volume.

The stability of hot electron rings requires an appreciable cold electron density component in the vicinity of the rings, $n_p/n_A > 1$.[1] An experimental examination of the annulus stability boundaries is planned for EBT-S and will help to establish the acceptable range for the ratio of cold-to-hot plasma density for ring stabilization. Defining the ring stability ratio as

$$f_R = \frac{n_{cold}}{n_{hot}} = \frac{n_p}{n_A} \ , \tag{2.4}$$

one can write the following expression for the annulus power density (in MW/m^3):

$$\frac{P_{\mu A}}{V_A} \cong 6.9 \times 10^{-38} \frac{n_{ep}^2}{f_R} \ . \tag{2.5}$$

For EBT-P with B_A (@ the second harmonic) $\cong$ 1 T, $n_{ep} = n_{cutoff}$ (@ B_A = 1 T) $\cong 10^{19}$ m^{-3}, and $T_A \sim$ 0.5 MeV, Eq. (2.5) reduces to

$$\frac{P_{\mu A}}{V_A}(\mathrm{MW/m^3}) = \begin{Bmatrix} 6.9 \\ 9.0 \end{Bmatrix} f_R^{-1} \begin{cases} \text{for } P_{\mu A} \cong P_{drag} & (2.6a) \\ \text{for } P_{\mu A} \cong P_{drag} + P_{scatt} + P_{synch} & (2.6b) \end{cases}$$

Bremsstrahlung radiation is smaller than the least of the other losses by more than two orders of magnitude and is therefore neglected in Eq. (2.6b). It should be noted that for $n_{ep} \cong 50\%\ n_{cutoff}$, one obtains $\sim$3.5 f_R^{-1} and $\sim$5.6 f_R^{-1} for Eqs. (2.6a) and (2.6b), respectively. In

going to a reactor, the fundamental heating frequency will be increased significantly to 110 GHz with B_A(@ 55 GHz) $\cong$ 2 T and $n_{ep} \cong 4 \times 10^{19}$ m^{-3}, assuming full cutoff. This implies a factor of 16 increase in the annulus power density as given by Eq. (2.6).

An accurate determination of $P_{\mu A}$ given by Eqs. (2.5) and (2.6) requires detailed knowledge of the ring stability requirements and accurate measurements of the volume V_A, which at present remains a vague quantity. Based on experimental measurements[3,8] and theoretical estimates, it appears that a range exists for the annulus thickness δ_A; this range varies between a minimum of the relativistic gyrodiameter and a maximum of $\sim$3-4 cm as measured on ELMO.[9] From these results one can write a general expression for the annulus volume:

$$V_A \cong 2\pi a_p \cdot \delta_A \cdot L_A \cong 2.15 \times 10^{-2} \frac{\sqrt{\gamma^2 - 1}}{B_A} a_p^2 N(f_E f_L) \ , \qquad (2.7)$$

where a_p is the core plasma radius, f_E is the thickness enhancement factor that allows for annuli thicknesses larger than the diameter of relativistic electron orbits, and $L_A = \ell_A N = f_L a_p N$ is the total length of the annulus (ℓ_A is the annulus length per sector and N is the number of sectors). In the EBT-I experiment,[3,8] indications are that $\ell_A \sim a_p$ (i.e., $f_L \cong 1$) and $f_E \cong 3$, giving an annulus thickness $\delta_A \cong 2.5$ cm and a ring/core volume ratio $V_A/V_p \sim 10\%$. If this scaling with relativistic gyrodiameters continues to hold for an EBT reactor (EBTR) with $a_p \cong 1.0$ m, N = 24 sectors, and $B_A \cong 2$ T, then Eq. (2.7) reduces to

$$V_A \sim 0.8\sqrt{\gamma^2 - 1}\ m^3 \ ; \qquad (2.8)$$

this indicates a broadening of ring thickness with annulus energy. Over the annulus energy range of interest ($T_A \sim$ 500 keV-1 MeV), annulus volumes of $\sim$1.5-2.5 m^3 are predicted. Comparing this to a reactor core volume of $\sim$600 m^3 ($R_T \sim$ 30 m, $a_p \sim$ 1 m),[10] the result is a reduction in the value of V_A/V_p by a factor of $\gtrsim$20 over that in EBT-I. The importance of this reduction will be discussed in more detail in Sect. 4.

3. SCALING PROJECTIONS FOR EBT-P

Reasonably good agreement between the experimental and theoretical estimates of $P_{\mu A}$ for EBT-I[2] provides a level of confidence in the predicted annulus power requirements for EBT-P. Such an assessment is necessary for EBT-P and future machines. In the near term, it can provide valuable sizing information pertaining to the fraction of the system power necessary to drive the microwave sources. Such information will benefit the ongoing development program for millimeter wavelength, continuous wave (cw) microwave sources by ensuring tube procurement at sufficiently high power levels. On the longer time scales envisioned for EBTR, the continuous microwave power required to sustain the annulus during steady-state operation may become the determining factor for overall reactor efficiency. This is to be expected because after ignition, the bulk heating (either ECH or neutral beam) will be terminated and the plasma temperature maintained by alpha particle heating and collisional energy gains from the annulus.

Because enhanced drag cooling is anticipated in EBT-P, scaling curves have been devised for initial EBT-P operation. For a given annulus volume these curves enable us to determine the microwave power levels required to sustain the rings at a given annular beta for increasing (or decreasing) levels of ring/core coupling. The constant power density curves shown in Fig. 1 are based on the annulus power balance given by Eq. (2.2) and assume the following parameters: $\alpha = 1$, $B_A = 1$ T for $f_\mu \cong 28$ GHz and $n_{ep} = n_{cutoff}$ (@ $B_A = 1$ T) $\cong 10^{19}$ m^{-3}. Because of the present uncertainty associated with annulus volume scaling, these projections do not include any assumptions regarding ring size.

The strong dependence of the annulus power density on f_R is apparent in Eq. (2.5) and indicates the importance of ring/core coupling. To analyze the sensitivity of microwave power to this parameter, f_R is plotted vs annulus energy for various microwave power levels. One can notice that as the coupling between the core and annulus densities becomes stronger (small f_R), increased drag losses require higher levels of microwave power to maintain a given value of annular beta.

These same characteristics were observed in earlier studies[2] of the EBT-I/S experiments, although in those cases the axes were reversed, i.e., n_A was fixed instead of n_{ep} as in Fig. 1.

Figure 1 also illustrates the correlation between values of annular beta and the various modes of EBT operation (C-, T-, and M-modes).[3] The C-mode corresponds to the noisy mode of operation in which insufficient microwave power is supplied to produce enough β_A. At $\beta_A \gtrsim \beta_{crit}$ ($\sim$10%) there is a transition from the C-mode to the quiet, macrostable T-mode, in which stable, steady-state operation of a toroidal core plasma occurs. For β_A values much larger than 50%, an abrupt transition into an M-mode occurs.

Over the range of annular beta values $\beta_A \sim$ 10-50%, the stability of the hot electron ring itself requires the presence of an appreciable cold electron density component.[1] Following the analysis of Ref. 1, stability curves have been superimposed on Fig. 1 for expected values of δ ($\delta = 1/kr_p$, $r_p^{-1} = n^{-1}dn/dr$). This shows possible stability regions for the hot electrons. Potential operating windows for the ring electrons are indicated in Fig. 1. The desired operating regions, bounded by the β_A curves from the sides (T-mode) and the appropriate δ curve from below, ensure stability of the EBT ring/core configuration.

Each of the constant power density curves shown in Fig. 1 also exhibits a minimum in f_R, corresponding to the maximum annulus density sustainable at a given annulus energy and microwave power level. This minimum is bounded by scattering and collisional drag from one side and synchrotron radiation from the other end of the annulus energy spectrum. Although both scattering and drag are important at very low energies, drag dominates over a significant portion of the energy range ($\lesssim$1 MeV), decreasing roughly as $\sim 1/v$ until a minimum is reached, at which point the electron kinetic energy is approximately equal to its rest mass.

Accelerated ring cooling occurs at high energies due to synchrotron radiation.[5] This mechanism can produce losses comparable to those resulting from drag, provided the magnetic fields are large and annulus temperatures are $\gtrsim$1 MeV. For a fixed input power level, supporting MeV ring energies require an appreciable decoupling of the ring/core densities

(large f_R) due to the deteriorating confinement in this energy regime. A ceiling on the maximum value of f_R is expected from ring stability considerations.

4. THE IMPLICATION OF RING DRAG ON EBTR PERFORMANCE

During the extrapolation of the EBT confinement concept to a commercial fusion power reactor design, features such as power production, engineering desirability, and technology were used as prime considerations in establishing reactor characteristics and operating parameters.[11] Recent studies of the annulus power balance[2] have indicated that drag cooling is the dominant loss mechanism for ring energies $\lesssim$1 MeV. These considerations have led to a reexamination of reactor operating parameters to determine the effect of ring power losses on potential reactor performance.[7]

In the EBT concept, the core-stabilizing electron annulus must be continuously driven by the microwave sources during steady-state operation. As a result, annulus power requirements represent a fundamental performance figure of merit directly impacting the energy multiplication capabilities of the system and the reactor Q value. In its simplest form the reactor Q value (i.e., $Q_{electric}$) can be defined as

$$Q_E \cong \eta_{th}\eta_\mu\eta_c(P_{th}/P_{\mu A}) \ , \tag{4.1}$$

where

$$P_{th}(MW) = 3.36 \times 10^{-18}\left(\frac{n_i^2\langle\sigma v\rangle_{DT}}{4}\right) V_p \tag{4.2}$$

is the total thermal fusion power corresponding to ∿21-MeV fusion reaction in a D-T plasma with tritium breeding. Here, $\langle\sigma v\rangle_{DT}$ is the Maxwellian-averaged fusion reaction probability, n_i is the toroidal core ion density, V_p is the toroidal plasma volume, η_{th} and η_μ are the thermal conversion and microwave conversion efficiencies, respectively, and η_c is the coupling efficiency of the microwave power to the annulus. The annulus microwave power $P_{\mu A}$ is given by Eq. (2.3).

Because drag losses dominate the ring power balance for energies $\lesssim$1 MeV, Eq. (4.1) can be written as

$$Q_E \cong \eta_{th}\eta_\mu\eta_c \left[1.34 \times 10^{19} \frac{\langle\sigma v\rangle_{DT}}{(\gamma/\sqrt{\gamma^2 - 1})} \left(\frac{n_i}{n_{ep}}\right)^2 f_R\right] \frac{V_P}{V_A} . \tag{4.3}$$

Assuming $\eta_{th} \cong 35\%$, $\eta_\mu \cong 50\%$, $\eta_c \cong 100\%$, $T_A \sim 500$ keV-1 MeV ($\gamma/\sqrt{\gamma^2 - 1} \sim 1.1$) and $T_i \sim 20$-30 keV [$\langle\sigma v\rangle_{DT} \sim 4.3$-$6.6 \times 10^{-22}$ m^3/s], one obtains:

$$Q_E \cong 1.0\text{-}1.5 \times 10^{-3} \left(\frac{n_i}{n_{ep}}\right)^2 f_R \cdot \frac{V_P}{V_A} . \tag{4.4}$$

Desirable values of Q_E are 8-10 in order to ensure increased maintainability (lower recirculating power) and favorable economics. For $Q_E \sim 10$, Eq. (4.4) reduces to

$$10^4 \sim \left(\frac{n_i}{n_{ep}}\right)^2 f_R \cdot \frac{V_P}{V_A} . \tag{4.5}$$

For a ratio of annulus/core volume of $\lesssim$1% and $n_i \sim 3\, n_{ep}$, Eq. (4.5) requires that $f_R \gtrsim 10$. It becomes quite apparent, therefore, that the ring/core coupling term is at least as important as the volume ratio in obtaining a favorable energy multiplication. Insight into possible directions for optimizing Q can be obtained by inserting Eqs. (2.3) and (2.7) into Eq. (4.1); this gives the following expression:

$$Q_E \cong 2.15 \times 10^{21} \frac{\langle\sigma v\rangle_{DT}}{\gamma} \left[\frac{(n_i/n_{ep})^2 f_R}{f_E f_L}\right] \frac{RB_A}{N} . \tag{4.6}$$

The quantity RB_A/N is approximately fixed for a given mirror ratio ($\sim$2 in EBT for optimum operation[3]) and modular construction. If one can maintain annulus temperatures between 0.5-1 MeV, which minimizes ring

losses, a reactor with $R \cong 30$ m, $N = 24$, and $B_A \cong 2$ T would have a

$$Q \cong \begin{Bmatrix} 0.73 \\ 1.79 \end{Bmatrix} \left[\frac{(n_i/n_{ep})^2 f_R}{f_E f_L}\right] \quad \begin{cases} \text{for } T_i \cong 15 \text{ keV} \\ \text{for } T_i \cong 30 \text{ keV} \end{cases}, \tag{4.7}$$

where $(n_i/n_{ep})^2 f_R$ represents the ring/core coupling and $f_E f_L$ are the geometry form factors. Equation (4.7) indicates that a factor of $\sim$2.5 can be gained by increasing the ion temperature; additional gains can be obtained by minimizing the thickness f_E and length f_L of the annulus. The significant power multiplication, however, is associated with the ring/core coupling term. Experimental observations[3,8] and stability considerations[1] indicate $n_i \sim 2\text{-}3\ n_{ep}$, $f_R \sim 5\text{-}20$, $f_E \sim 3$, and $f_L \sim 0.5\text{-}1$. Covering the range of values, this leads to a factor of 20-180 for the coupling term and 1.5-3 for the annulus form factor.

The above calculations indicate the possibility of attractive Q values provided the scaling trends observed for density profiles, stability, and ring volume remain favorable. A more definitive statement cannot be made at this time because of the uncertainties associated with postulating the simultaneous existence of thin rings, steep density gradients, and acceptable bulk plasma transport. Furthermore, the modest parameter range accessible in present EBT experiments does little to reduce these uncertainties or to allow for credible straightforward extrapolation to an EBT reactor.

The planned EBT-P device is expected to bridge this gap between existing experiments and reactor-grade plasmas. The proposed EBT-P device has the capability of operating with frequencies in the range of $\sim$28-90 GHz, which correspond to $B_{resonance} \sim 1\text{-}3.1$ T ($B_A \sim 0.5\text{-}1.5$ T). With this capability and with the flexibility given by various possible improvements in the area of microwave feeding and separate control of the annulus, it should be possible to accomplish the objective of establishing the ring power balance scaling.

REFERENCES

1. R. R. Dominguez and H. L. Berk, Phys. Fluids 21, 827 (1978); D. B. Nelson and C. L. Hedrick, Nucl. Fusion 19, 283 (1979).
2. S. K. Borowski, N. A. Uckan, E. F. Jaeger, and T. Kammash, Oak Ridge National Laboratory Report ORNL/TM-6910, Oak Ridge, Tennessee (1979); also to be published in Nucl. Fusion.
3. R. A. Dandl et al., Oak Ridge National Laboratory Report ORNL/TM-6457, Oak Ridge, Tennessee (1978).
4. J. D. Jackson, *Classical Electrodynamics*, 2nd ed., p. 618, John Wiley and Sons, New York, 1975.
5. D. J. Rose and M. Clark, Jr., *Plasmas and Controlled Fusion*, pp. 165 and 251, Massachusetts Institute of Technology Press, Cambridge, 1961.
6. T. Kammash and D. L. Galbraith, Nucl. Fusion 13, 464 (1973).
7. N. A. Uckan, S. K. Borowski, D. B. Batchelor, C. L. Hedrick, and E. F. Jaeger, *Proc. 8th Symp. on Engineering Problems of Fusion Research* (1979), to be published.
8. R. A. Dandl et al., Oak Ridge National Laboratory Report ORNL/TM-3694, Oak Ridge, Tennessee (1971).
9. R. A. Dandl et al., *Plasma Physics and Controlled Nuclear Fusion Research 1968*, Vol. II, p. 435 (1969).
10. N. A. Uckan et al., *Plasma Physics and Controlled Nuclear Fusion Research 1978*, Vol. III, p. 343 (1979).
11. D. G. McAlees et al., Oak Ridge National Laboratory Report ORNL/TM-5669, Oak Ridge, Tennessee (1976).

ORNL-DWG 79-3732 FED

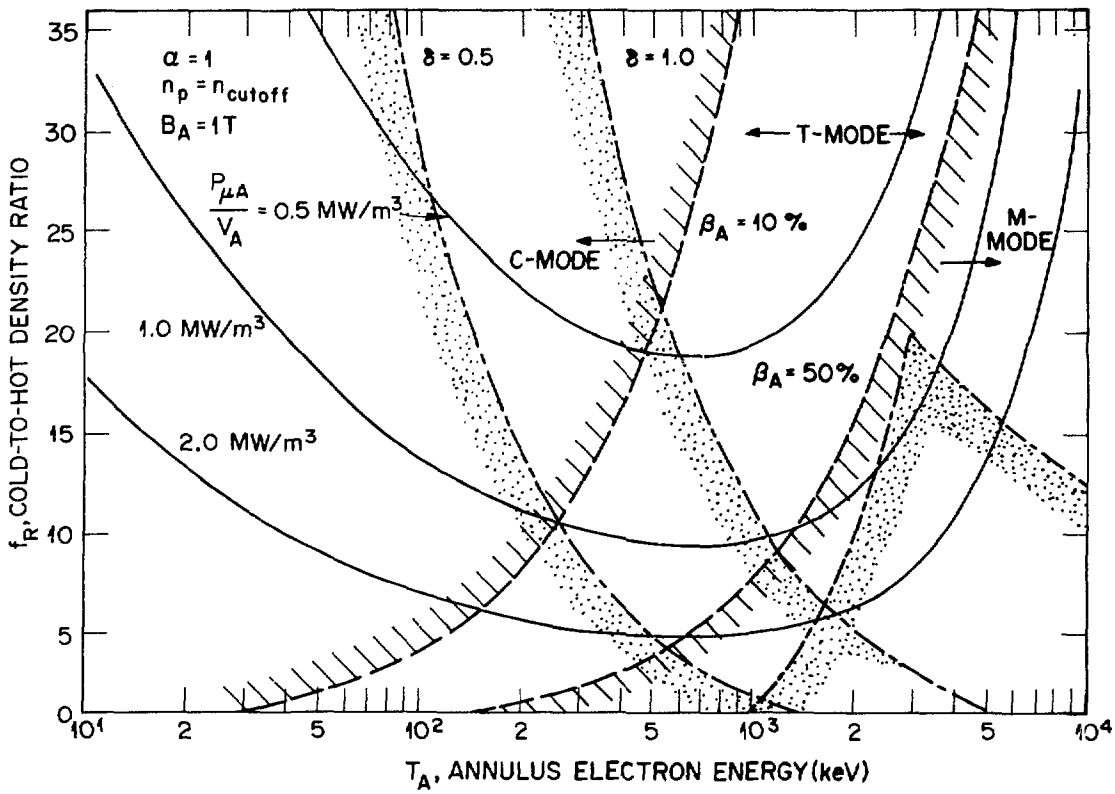

Fig. 1. The fraction of cold-to-hot electron $f_R = n_{cold}/n_{hot} = n_p/n_A$ vs annulus electron energy T_A for $P_{\mu A}/V_A$ = 0.5, 1.0, and 2.0 MW/m³.

DISCUSSION

W. H. MINER: In your power balance calculations, you mentioned an enhancement factor in the drag term of γ^{α}, where α was an unknown factor. What value of α did you use in your calculations and did you find your results sensitive to this number?

S. K. BOROWSKI: The general term for drag losses P_{drag} given in Eq. (2.2) shows a dependence on the relitivistic term as $\gamma^{\alpha}\ \ell n\ \Lambda_{\alpha}/\sqrt{\gamma^2 - 1}$, where γ is the relativistic mass ratio, $\alpha = 1$ or 2, and $\ell n\ \Lambda_{\alpha}$ is the Coulomb logarithm with slight differences in definition for $\alpha = 1$ or 2 (i.e., $\ell n\ \Lambda_1 \sim 20$-30 and $\ell n\ \Lambda_2 \sim 16$ for typical parameter ranges). For the case of classical drag cooling ($\alpha = 1$), P_{drag} decreases as $\sim 1/v_A$ until v_A approaches c ($v_A = c\sqrt{\gamma^2 - 1}/\gamma$, velocity of the annulus electrons). The binary collision model ($\alpha = 2$), on the other hand, indicates a stronger γ dependence at high energies. However, the difference of the effect of the two assumed drag models on the <u>total</u> power loss is small ($\sim$10-20%).

Some of the examples I showed here have assumed both $\alpha = 1$ and $\alpha = 2$ to indicate differences, but specifics were given for $\alpha = 1$. If $\alpha = 2$ is chosen, drag power loss itself becomes much more severe for ring energies above 1 MeV. However, this severity is somewhat masked at higher energies (>1 MeV) due to synchotron losses that begin to dominate the annulus power balance.

A. BOOZER: You gave the annulus thickness as a few hot electron gyroradii. This is roughly an ion gyroradius in the bulk plasma. Since much of the pressure drop in the bulk plasma must occur across the annulus, such a thin ring would give unacceptably high bulk plasma transport. The finite drift orbits due to toroidal effects limit the rings' thinness as well.

S. K. BOROWSKI: Using a particle-orbit argument, one would anticipate the minimum thickness of the rings to be a relativistic electron gyro-diameter (i.e., $2\rho_{eA}$). Experimental measurements made on ELMO and EBT-I indicate, however, that the radial extent of the rings is approximately a factor of 3 larger than this, and $\delta_A \cong 6\rho_{eA}$ is used in this

study. Neglecting any deterioration in the ion temperature near the vicinity of the rings, the ratio of δ_A/ion gyrodiameter (i.e., $\delta_A/2\rho_i$) is still greater than one in going from EBT-I ($\delta_A/2\rho_i > 5$) to an EBTR ($\delta_A/2\rho_i > 1$). The potential for increased bulk plasma transport due to thin rings does remain a possibility; however, an experiment like EBT-P is needed to address this question.

V. K. TRIPATHI: Could Whistler instability be significant in the power balance? Have you studied this instability to see the effect of it in a reactor?

N. A. UCKAN: The Whistler mode was observed in TPM, which was reported by H. Ikegami in his talk (see Sects. 1 and 2). This instability, as indicated by Ikegami, is very important. It seems to destroy the rings and is believed to be responsible for the M-mode. Theoretical investigations of this mode were carried out in the past, but to answer your question, we have not reexamined it for a reactor. The high energy component of the hot electrons ($\gtrsim$100 keV) appears unaffected by the instability; namely, it is stable against this mode. That is to say, a relativistic spread in the electron cyclotron frequency leads to high energy resonant particles that contribute to damping rather than growth. The expected ring energies in a reactor would be much higher than 500 keV, and it can be expected that the effect of this instability in the quiescent T-mode would not be degrading. Of course, the real answer awaits the detailed theoretical studies and experimental observations from NBT, EBT-S, and EBT-P. Perhaps H. Ikegami can comment on this further.

H. IKEGAMI: I do not have much to add, but I would like to point out that rings are most susceptible to Whistler instabilities that destroy the ring at low pressure levels. They are experimentally studied in detail on the TPM mirror machine at the Institute of Plasma Physics, Nagoya. Theoretical studies including the instability itself and the enhanced loss associated with the instability are also made and compared with the experiments around 1968.

ANNULUS POWER LOSSES IN EBT *

R. J. Kashuba and W. B. Ard
McDonnell Douglas Research Laboratories
St. Louis, MO 63141

The power input required to sustain the hot electron annulus can be very important in the EBT-P device and in scaling EBT to a reactor. In order to estimate the annulus power requirements we calculate the energy losses by classical processes in the annulus. If the annulus can be stabilized against drift instabilities, as is the case in simple mirrors and EBT-I, the classical losses should dominate the power requirements. The classical loss processes are averaged over a two-dimensional relativistic distribution with temperatures characteristic of x-ray bremsstrahlung measurements. The loss rate is found to have a minimum as a function of annulus temperature and density. In addition the power balance of an ion annulus for EBT is examined. The power balance is shown to be favorable for a reactor and a meaningful experiment will be considered for EBT-P.

*Research performed under subcontract no. 22Y21040V with McDonnell Douglas Corporation under Union Carbide Corporation Nuclear Division contract W-7405-ENG-26 with the U.S. Department of Energy and under McDonnell Douglas Corporation IRAD Program.

ANNULUS POWER BALANCE

The power input required to sustain the high energy annulus is very important for the EBT-P device and in scaling the EBT to a reactor. In the first part of this appendix the electron annulus power requirements are obtained. In the second part some considerations for high beta ion rings in EBT are discussed.

PART I: ELECTRON ANNULUS

In order to estimate the annulus power requirements we calculate the energy losses by classical processes in the annulus. If the annulus can be stabilized against drift instabilities, as is the case in simple mirrors and EBT-I, the classical losses should dominate the power requirements.

The main classical loss processes are drag due to energy loss to the background cool electrons, particle loss from the annulus due to scattering into the mirror loss cone and emission of radiation by synchrotron and bremsstrahlung processes. These processes have been treated theoretically in considerable detail and the theoretical results have been verified experimentally over a wide range of electron energy.

The energy range appropriate to hot electron annuli requires that the energy losses be calculated relativistically. The dependence of the energy loss processes on the electron energy will be given in terms of γ, where $\gamma = 1 + K/mc^2$. K is the kinetic energy of the fast electrons.

The energy lost per unit distance by a fast electron traversing matter, including a plasma, is

$$\frac{dE}{dx} = \frac{4\pi e^4 n_e}{mv^2}\left[\ln(B) - \frac{v^2}{c^2}\right], \qquad \text{(B-1)}$$

where m is the rest mass of the electron and enters the process because of the mass of the background electrons (with density n_e) not the fast electrons, and v is the speed of the fast electrons. B is essentially the ratio of the maximum energy the electron can lose in a collision to the minimum energy; in a plasma the minimum energy is determined by the Debye length.

The energy lost per unit time is just

$$\left.\frac{dE}{dt}\right)_D = \frac{4\pi e^4 n_e}{mv}\left[\ln(B) - \frac{v^2}{c^2}\right].$$

Using the relation $v = \frac{c\sqrt{\gamma^2-1}}{\gamma}$ and $\beta = \frac{v}{c}$ the energy loss per second is

$$\left.\frac{dE}{dt}\right)_D = \frac{4\pi e^4 n_e}{mc} \frac{\gamma}{\sqrt{\gamma^2-1}} [\ln(B) - \beta^2].$$

Although B increases as the electron energy increases and is proportional to γ at high energy, we will ignore its energy dependence since it enters as the logarithm. At the energies of interest, $[\ln(B) - \beta^2] \approx 20$, and we have

$$\left.\frac{dE}{dt}\right)_D \approx 5 \times 10^{-26}\, n_e \frac{\gamma}{\sqrt{\gamma^2-1}} \text{ watts}. \tag{B-2}$$

The energy loss due to scattering out the mirror is the electron kinetic energy, $(\gamma-1)\, mc^2$, times the mirror loss rate which is about $\frac{\nu_{90}}{2}$ in a 2:1 mirror. ν_{90} is the coulomb 90^0 scattering rate, mostly due to collisions with the more massive ions,

$$\nu_{90} = \frac{32\, e^4 n_i}{\pi p^2 v} \ln(\lambda), \tag{B-3}$$

p is the fast electron momentum, γmv, v is again the fast electron velocity, λ is similar to B in the drag equation, and n_i is the ion density. We will again neglect the energy dependence of $\ln \lambda$. Making the substitution for p and v we have

$$\left.\frac{dE}{dt}\right)_c = \frac{\nu_{90}}{2} (\gamma-1)\, mc^2 = \frac{16\, e^4 n_i}{\pi\, mc} \frac{\gamma(\gamma-1)}{(\gamma^2-1)^{3/2}} \ln \lambda .$$

With $\ln \lambda \approx 25$ we have

$$\left.\frac{dE}{dt}\right)_c \approx 2.5 \times 10^{-26}\, n_i \frac{\gamma(\gamma-1)}{(\gamma^2-1)^{3/2}} \text{ watts}. \tag{B-4}$$

The energy loss due to bremsstrahlung also depends on the background ion energy and is given by

$$\left.\frac{dE}{dt}\right)_B = v n_i \gamma mc^2\, \phi_{rad}. \tag{B-5}$$

Here, as in the coulomb scattering, we assume that the ions have a z of 1.

ϕ_{rad}, the radiation cross-section, is a very complicated function of the electron energy, however it is a slowly varying function. In the non-relativistic (N.R.) limit it is

$$\phi_{rad} = \frac{16}{3}\bar{\phi}, \qquad \text{N.R.}$$

and in the extreme relativistic (E.R.) limit it is

$$\phi_{rad} = 4\left(\ln 2\gamma - \frac{1}{3}\right)\bar{\phi}, \qquad \text{E.R.}$$

where

$$\bar{\phi} = \frac{r_o^2}{137} = \frac{e^4}{137\, m^2 c^4}.$$

We take, as an average over the range of energies 0 to 5 MeV,

$$\phi_{rad} = 7.5\,\bar{\phi},$$

$$\left.\frac{dE}{dt}\right)_B \approx 7.5\, v n_i \gamma m c^2\, \bar{\phi} \approx 8 \times 10^{-30}\, n_i \sqrt{\gamma^2 - 1} \text{ watts}. \qquad \text{(B-6)}$$

Unlike the above loss processes, the energy loss from synchotron radiation does not depend on the background density. It depends only on the magnetic field strength and the electron energy. We assume that in the annulus the electrons have $v_\perp^2 \gg v_\parallel^2$, that is they are confined near the midplane of the magnetic field. The energy radiated by an electron is then given by

$$\left.\frac{dE}{dt}\right)_s = \frac{2}{3}\,\frac{e^2 \gamma^2 \omega^2 p^2}{m^2 c^3} \qquad \text{(B-7)}$$

where ω is the actual electron frequency, $\omega = \frac{eB}{\gamma mc}$. This expression reduces to

$$\left.\frac{dE}{dt}\right)_s = \frac{2}{3}\,\frac{e^4 B^2 (\gamma^2 - 1)}{m^2 c^3} = 1.6 \times 10^{-14}\, B^2 (\gamma^2 - 1) \text{ watts} \qquad \text{(B-8)}$$

The total energy loss rate for an annulus electron is the sum of the losses discussed above, Eqs (B-2), (B-4), (B-6), (B-8),

$$\frac{dE}{dt} = \left.\frac{dE}{dt}\right)_D + \left.\frac{dE}{dt}\right)_C + \left.\frac{dE}{dt}\right)_B + \left.\frac{dE}{dt}\right)_S \qquad \text{(B-9)}$$

The first three terms depend on the background plasma density. Although the scattering and bremsstrahlung loss depend on the total ion density, the annulus electron density is usually considerably less than the background plasma density so little error should be introduced by making the assumption that $n_i = n_e = n_p$, where n_p is the density of the core plasma at the annulus. With this assumption we can relate the local background plasma density to the local magnetic field by expressing it as a fraction, f, of the microwave cut-off density, n_c, i.e., the density at which the plasma frequency is equal to the gyro-frequency. Therefore, we have at the annulus

$$n_p = f n_c ,$$

where

$$n_c = 1 \times 10^{13} B^2 ,$$

so that

$$n_p = 1 \times 10^{13} f B^2 .$$

With this substitution all four of the loss processes will have the same dependence on the magnetic field and we can write the loss rate as

$$\frac{dE}{dt} = B^2 \left[5 \times 10^{-13} f \left(\frac{\gamma}{\sqrt{\gamma^2-1}} + \frac{.5\gamma\,(\gamma-1)}{(\gamma^2-1)^{3/2}} + 1.6 \times 10^{-4} \sqrt{\gamma^2-1} \right) + 1.6 \times 10^{-14} (\gamma^2-1) \right] . \tag{B-10}$$

Although the third term in the energy loss expression, due to bremmsstrahlung, increases with γ, it is always negligible since at low electron energies it is much less than the drag loss and at high energies it is much less than the synchotron loss. Neglecting this term we have

$$\frac{dE}{dt} = 5 \times 10^{-13} B^2 \left[\frac{f\gamma}{\sqrt{\gamma^2-1}} \left(1 + \frac{1}{2\,(\gamma+1)}\right) + 3.2 \times 10^{-2} (\gamma^2-1) \right] \tag{B-11}$$

The total power lost by the annulus is

$$P = n_a V_a \frac{dE}{dt} \tag{B-12}$$

where n_a and V_a are the annulus electron density and volume respectively. The annulus density is determined by the beta required to maintain the MHD stability of the core plasma. Therefore the minimum annulus electron density in an EBT is given by

$$n_a kT = \frac{\beta_c B^2}{8\pi}$$

and

$$n_a = \frac{\beta_c B^2}{8\pi kT} = \frac{\beta_c B^2}{8\pi T} mc^2 = \frac{5 \times 10^{12}\ \beta_c B^2}{T} \tag{B-13}$$

where T is in units of mc^2.

With this substitution we have the power loss per cm^3

$$\tilde{P} = \frac{P}{V_a} = \frac{2.5\ \beta_c B^4}{T} \left[\frac{f\gamma}{(\sqrt{\gamma^2-1})} \left(1 + \frac{1}{2\ (\gamma+1)}\right) + 3.2 \times 10^{-2}\ (\gamma^2-1) \right] \text{watts cm}^{-3}. \tag{B-14}$$

The term in brackets represents the energy loss by an electron with a given γ from drag, mirror loss and synchoton radiation. This term should be averaged over the annulus electron energy distribution to arrive at the power loss for the annulus. As an example we assume a distribution function characteristic of a relativistic two dimensional "maxwellian" gas since experiments on mirrors and EBT-I show that the axial extent of the annulus is small, indicating that the electron energy is mostly perpendicular to the magnetic field and that the electron energy distribution as determined from x-ray bremsstrahlung measurements decreases exponentially at higher energies. This distribution function is

$$f(\gamma) = \alpha\gamma e^{-\gamma/T}. \tag{B-15}$$

The parameter T that characterizes the distribution is the temperature of the gas in the sense that the relativistic kinetic pressure computed from this function is nkT.

Averaging over this distribution function we find

$$\tilde{P}_{(D+C)} = \frac{2.5\ \beta_c B^4}{T}\ f \left[\frac{\int_1^\infty \frac{\gamma^2}{\sqrt{\gamma^2-1}} \left(1 + \frac{1}{2(\gamma+1)}\right) e^{-\frac{\gamma}{T}}\, d\gamma}{\int_1^\infty \gamma e^{-\frac{\gamma}{T}}\, d\gamma} \right], \tag{B-16}$$

and

$$\tilde{P}_{(S)} = \frac{8 \times 10^{-2}\, \beta_c B^4}{T} \left[\frac{\int_1^\infty \gamma(\gamma^2 - 1)\, e^{-\frac{\gamma}{T}}\, d\gamma}{\int_1^\infty \gamma e^{-\frac{\gamma}{T}}\, d\gamma} \right]. \tag{B-17}$$

The second expression can be integrated directly to give

$$\tilde{P}_{(S)} = \frac{8 \times 10^{-2}\, \beta_c B^4}{T} \left(6T^2 + \frac{3T + 1}{T + 1} - 1 \right). \tag{B-18}$$

The expression for $\tilde{P}_{(D+C)}$ has been integrated numerically and is given in Table 1 along with $P_{(S)}$ and the total energy loss for f = 1 and .5 for different values of T, the annulus "temperature" The power loss as a function of T is plotted in Figure 1.

ANNULUS POWER LOSS DEPENDENCE ON ELECTRON TEMPERATURE

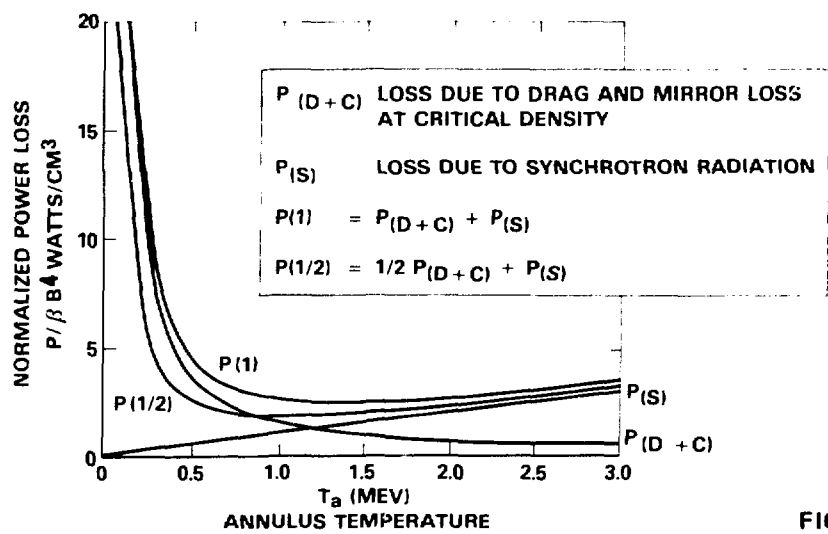

FIGURE 1

Since the drag and scattering loss decrease with T while the synchotron loss increases with T there is a T that results in a minimum power loss. The T for minimum loss depends on f, the ratio of the background plasma density at the annulus to the microwave cut-off density. For f = 1 the minimum is near T = 3, 1.5 MeV, and is $\tilde{P} = 2.4\, \beta_c B^4$ watts/cm^3.

TABLE 1

K (MeV)	T	$P_{(D+C)}$	$P_{(S)}$	$P_{(f=1)}$	$P_{(f=.5)}$
.1	.2	38.8	.23	39.0	19.6
.2	.4	13.9	.31	14.2	7.27
.3	.6	7.76	.39	8.14	4.27
.4	.8	5.18	.47	5.65	3.06
.5	1.0	3.82	.56	4.38	2.47
.6	1.2	2.99	.65	3.64	2.14
.7	1.4	2.44	.74	3.18	1.96
.8	1.6	2.06	.83	2.89	1.86
.9	1.8	1.78	.92	2.70	1.80
1.0	2.0	1.56	1.01	2.57	1.79
1.2	2.4	1.24	1.20	2.45	1.82
1.4	2.8	1.04	1.38	2.42	1.90
1.6	3.2	.89	1.57	2.46	2.02
1.8	3.6	.77	1.76	2.54	2.15
2.0	4.0	.69	1.95	2.64	2.30
2.5	5.0	.54	2.43	2.96	2.69
3.0	6.0	.44	2.90	3.34	3.12

(B-19)

For f = .5 the minimum loss is for T = 2, 1 MeV, with

$$\tilde{P} = 1.8\ \beta_c B^4 \text{ watts/cm}^3. \tag{B-20}$$

These results are valid for essentially all conditions of interest for EBT's. The only limitation is that the calculation of the drag loss assumes that the annulus temperature is much higher than the core plasma temperature. In the case of high core temperature and low annulus temperature the drag power loss should be multiplied by the factor $\frac{T_a - T_c}{T_a}$. The neglect of the logarithmic dependence of the drag and scattering losses on γ introduces some error in these terms at large γ. However, these losses are small relative to the synchotron loss at large γ so that the total

power loss is hardly affected by the neglect of the log γ dependence.

As an example of the application of these results we estimate the power required to sustain the annulus in the EBT-I experiment. The annulus temperature in EBT-I is estimated from the slope of the bremsstrahlung spectra to be about 200 keV. With the magnetic field at the annulus (0.32 tesla) and the background plasma density 0.5×10^{11} cm^{-3} (f = .5) the power lost at an annulus beta of 0.3 is 2.3×10^{-2} watts/cm^3. The total power lost in the estimated annulus volume of 6×10^4 cm^3 is 1.4 kW. This result is consistent with the input power in EBT-I.

The microwave power required to sustain the annulus in EBT-I is modest. However, the power required for an EBT-P is very significant. We assume an EBT-P with 2 times the EBT-I minor radius and 36 sectors with a field at the annulus of 1 tesla. If the annulus temperature and f remain the same, 200 keV and .5, the power lost per cm^3 is 2.2 watts at a beta of 0.3. If the annulus volume increases in the same ratio as the total plasma volume the total power required to sustain the EBT-P annulus is 1.6 MW. This power could be reduced to 400 kW if an annulus temperature of 1 MeV could be obtained. We note from Eqs. (B-12) and (B-13) that the annulus power requirements scale at least as B^2 even if the core density were constant. However, as the magnetic field is increased the core density should also increase and we have the B^4 scaling exhibited in Eq. (B-14).

It is obvious from the data in Figure 1 that the annulus temperature is critical to the performance of an EBT reactor. The specific power loss in a typical reactor (f = .5, β_c = .5, B = 2 tesla) with an annulus temperature of 1 MeV is about 15 watts/cm^3. Since the net electrical power output from the reactor would be about 2 or 3 watts/cm^3, the annulus volume can be only a small fraction of the total reactor volume if the reactor is to be economically feasible. There is not much advantage to be gained by considering different magnetic field strengths since both the thermonuclear power output and annulus loss scale with B^4.

The directions for optimizing reactor performance are to minimize the thickness and length of the annulus, locate it at as large a radius as possible, that is, locate it in as low a field and in as low core density as possible, and obtain as large a fraction as possible of the annulus beta with ion temperature. This must be done within the constraint that the annulus beta and geometry satisfy stability requirements.

PART II: SOME CONSIDERATIONS REGARDING HIGH BETA IONS IN EBT

Consideration for a Reactor

The electrical power required to maintain high beta electron rings in an EBT reactor could result in a circulating power fraction large enough to seriously affect the economics of the reactor. It might be possible to reduce the ring power requirements by providing most of the required ring beta with energetic ions. Although there are no experimental results on the stability of high beta ion rings, there is theoretical evidence that they can be stabilized by a background plasma as the electron rings apparently are.[4]

The energy loss processes applicable to ion rings are different from those for energetic electrons and conditions might be obtainable for a high beta ion ring with a more favorable power balance. In general energy losses decrease as the particle energies increase. However particle energies are limited. The limit on electron temperature results from the fast increase in synchotron radiation with electron energy. Ion energies are ultimately limited by the size of the Larmor orbits. (For this discussion we limit the EBT to a toroidal system stabilized by high beta annuli as distinguished from toroidally linked reversed field mirrors.) The diameter of the ion orbit must be smaller than the thickness of the annulus. As we shall see this limits the ion energy in an EBT reactor to something less than 1 MeV.

The limiting ion temperature, T, is given by

$$T = 9.61 \times \frac{Z^2}{A} B^2 d^2 \text{ keV}, \tag{B-21}$$

where d is the maximum orbit radius consistant with the annulus thickness. This radius should probably not be more than 1/4 of the annulus thickness.

Present estimates of EBT reactor parameters give a magnetic field at the annulus of from 2 to 3 tesla and a plasma radius of 100 cm. The temperature of a D^+ annulus with a thickness of 20 cm in this reactor would be between 500 and 1000 keV, that is, a limiting Larmor radius of 5 cm.

The major energy loss mechanism for ring ions will be due to charge exchange, drag on the core electrons or drag on the core ions depending on the ring temperature. Charge exchange losses are difficult to estimate for a reactor because of the uncertainty of the neutral background density. In fact the neutral density near the

edge where the ring is located could be quite low with pellet injection fueling. We can get a very rough estimate of neutral density with edge feed fueling.

We assume the following reactor parameters:

$r_p = 100$ cm

$T_e = T_i = 20$ Kev

$n_e = 10^{14}/cm^3$

$B_A = 2T$

$\overline{n\tau} = 10^{15}\ cm^{-3}s$

$\bar{\tau} = 10$

$\beta_A = .5$

The edge neutral density is estimated from the flux required to sustain the plasma

$$F_o A = \frac{nV}{\tau}\ , \tag{B-22}$$

since

$$\frac{V}{A} = \frac{r_p}{2}\ ,$$

then

$$F_o = \frac{10^{14} \times 50}{10} = 5 \times 10^{14}/sec/cm^2$$

$$= \frac{n_o v_o}{4}\ ,$$

or

$$n_o = \frac{2 \times 10^{15}}{v_o}\ cm^{-3}\ .$$

At a neutral thermal speed of 2×10^5 cm/sec

$$n_o = 10^{10}\ cm^{-3}\ .$$

The power lost by the ring due to charge exchange is

$$P_{cx} = n_A T\ n_o (\sigma v)_{cx}\ ,$$

since

$$n_A T = \frac{\beta_A B^2}{8\pi} \tag{B-23}$$

then

$$P_{cx} = \frac{\beta_A B^2 n_o (\sigma v)_{cx}}{8\pi} \quad . \tag{B-24}$$

The fusion electric power produced by this reactor is 2 to 3 watts/cm^3. Therefore the power dissipated by the ring should not exceed say 5 watts/cm^3. This would require

$$(\sigma v)_{cx} < 6 \times 10^{-10} \text{ cm}^2/\text{sec} \tag{B-25}$$

The D^+ energy must be over 300 keV for an edge neutral density no larger than 10^{10}/cm^3. The actual neutral density in a reactor could be much larger and require a considerably larger ion energy to keep the power loss reasonable.

Since the annulus ions must have energies greater than 300 keV to make charge exchange tolerable, we look at other energy loss rates for ions in the energy range 300 to 1000 keV. The energy loss to electrons is given by

$$\frac{dE}{dt} = 5.4 \times 10^{-9} \frac{A^{1/2} n_e \ln\lambda \, T_i}{T_i^{3/2}} \frac{2}{\sqrt{\pi}} \int_o^x y^{1/2} e^{-y} dy \tag{B-26}$$

where X is the ratio v_i^2/v_e^2. This ratio can be written

$$X = \frac{m_e}{M_I} \frac{T_i}{T_e} = \frac{1}{1836\ A} \frac{T_i}{T_e}$$

For $X \geq 1$

$$\frac{2}{\sqrt{\pi}} \int_o^x y^{1/2} e^{-y} dy \rightarrow 1$$

For $X \ll 1$, $T_i \ll 1836\ AT_e$

$$\frac{2}{\sqrt{\pi}} \int_o^x y^{1/2} e^{-y} dy \rightarrow \frac{2}{\sqrt{\pi}} \int_o^x y^{1/2} dy = \frac{4}{3\sqrt{\pi}} X^{3/2}$$

$$= \frac{9.6 \times 10^{-6}}{A^{3/2}} \frac{T_i^{3/2}}{T_e^{3/2}}$$

and

$$\left.\frac{dE}{dt}\right)_{x<<1} = 5.1 \times 10^{-14} \frac{n_e \ln\lambda \; T_i}{A \; T_e^{3/2}} \tag{B-27}$$

For a deuterium annulus with temperatures between 300 and 1000 keV and a core electron temperature of 20 KeV and density of $5 \times 10^{13}/cm^3$

$$X = 4 \times 10^{-3} \text{ to } 1.4 \times 10^{-2},$$

and, with $\ln \lambda = 20$,

$$\frac{dE}{dt} = .29 \; T_i \; sec^{-1} \tag{B-28}$$

The energy lost per cm^3 in the annulus would be

$$P_e = .29 \frac{\beta B^2}{8\pi} \; sec^{-1} \tag{B-29}$$

at $\beta = .5$ in a field of 2T (20kG) the power lost per cm^3 is .23 watts. This is likely to be negligible compared with the power lost through charge exchange or the net power produced from fusion.

The power lost by this annulus due to drag on the core ions is

$$P_i = \frac{\beta B^2}{8\pi} \times 4 \times 10^{-12} \frac{n_e \ln \lambda}{T_i^{3/2}} \tag{B-30}$$

for T_i = 300 KeV this power is .62 watts/cm^3 and at 1000 KeV it is .1 watts/cm^3 for a total power loss from drag, $P_e + P_i$, of .33 to .85 watts/cm^3.

The power loss from scattering will be proportional to the ion drag loss and be about equal to the ion drag loss at lower annulus temperatures since ions scatter off the total ion density and, at the lower temperatures, the annulus density is about equal to the core density at the annulus.

It is apparent that all the loss processes decrease as the annulus temperature increases. Since the maximum temperature increases with the square of the maximum ion radius in the annulus, a fatter annulus could actually result in a lower total power loss from the annulus. Energy balance would also greatly favor a proton ring rather than a deuterium ring.

Consideration for EBT-P

The dependence of the ion annulus temperature on the maximum ion Larmor radius places severe restriction on an ion ring experiment in EBT-P. The maximum Larmor radius of a proton ring in EBT-P would be about 2 cm. At a 2 tesla field at the ring the temperature would be limited to about 150 KeV. $(\sigma v)_{cx}$ at this temperature is about 1×10^{-8} cm^3/sec. An 8 cm thick annulus in one sector would have a volume of about 1.3×10^4 cm^3. The total power lost by the ring in one sector due to charge exchange would be

$$P = \frac{\beta B^2}{8\pi} n_o (\sigma v)_{cx} V = 2 \times 10^{-4} \beta n_o \text{ watts} \tag{B-31}$$

The maximum ion heating power into a single sector probably should not exceed 200 kW. With a coupling efficiency of .5 this would limit the ring power loss to 100 kW. If a beta as large as .1 is required to carry out a reasonable experiment, the neutral density that can be tolerated is about $5 \times 10^9/cm^3$. This is considerably lower than that expected at the edge in EBT-P.

This consideration does not, however, rule out a significant ion ring experiment as part of the EBT-P program. The charge exchange loss can be reduced considerably by forming the ring well inside the core plasma and utilizing the neutral gas shielding provided by the dense core plasma. This would be equivalent to forming a second annulus inside the electron annulus as is done by the addition of profile heating power in EBT-I. This experiment could give considerable information on the physics of ion rings and their production.

References

1. Jackson, J. D., Classical Electrodynamics, 2nd ed., John Wiley & Sons, Inc., (1975).
2. Heitler, W., Quantum Theory of Radiation, 3rd ed., Oxford University Press, (1954).
3. Synge, J. L., The Relativistic Gas, North-Holland Publishing Co., (1957).
4. H. S. Uhm and R. C. Davidson, Phys. Fluids 22, 1329 (1979).

Appendix: The Drag Term as a Power Input to the Core Plasma

All of the terms considered are power loss terms for the annulus and all but the drag term is a loss to the EBT plasma. The drag loss goes into heating of the core plasma albeit in a rather unfavorable position. For equilibrium plasma calculations such as the radial 1-D code it is desirable to include this term as a power source term at the position of the annulus. Therefore, we want to obtain an expression for the drag loss which could be used in the 1-D code.

The power loss rate due to drag is given from above as

$$\frac{dP}{dt} = 5 \times 10^{-26}\, n_a n_e \frac{\gamma}{\sqrt{\gamma^2 - 1}},$$

where n_a, n_e are the density of the annulus and core electrons, respectively. The power is given in watts per cm^3. If this expression is averaged over the two-dimensional relativistic Maxwellian we obtain

$$\frac{dP}{dt} = (5 \times 10^{-6}\, n_a n_e) \times \frac{e^{mc^2/T}}{\left((T/mc^2) + 1\right)} \left\{ K_1\left(\frac{mc^2}{T}\right) + \frac{T}{mc^2} K_o\left(\frac{mc^2}{T}\right) \right\}.$$

In the above expression K_1, K_o are the McDonald functions of first and zeroth order, respectively.

An approximate polynomial fit to the above expression is given by

$$\frac{dP}{dt} = (5 \times 10^{-26}\, n_a n_e) \left\{ 1 + \frac{(.397)\, mc^2}{T} - (6.2 \times 10^{-3}) \left(\frac{mc^2}{T}\right)^2 - 4.3 \times 10^{-4} \left(\frac{mc^2}{T}\right)^3 \right\}.$$

DISCUSSION

J. T. WOO: What is the effect of the rapid scattering of electrons that converts $v_\perp$ to $v_\parallel$ on the power balance of the electron annuli?

R. KASHUBA: Scattering into the mirror loss cone has been included. Power loss due to scattering is not as much as drag and at high energies it isn't as large as synchrotron radiation. However, this scattering loss also takes away particles and thus keeps the distribution anisotropic.

A. BOOZER: Pitch angle scattering does not significantly affect the power balance in EBT rings if all the annular drift orbits are confined. Isotropic or anisotropic pressure does not make a large difference on the power needed to maintain a given field depression by the ring.

J. T. WOO: If you make use of the fusion α to create an ion ring, you should be able to eliminate the charge exchange loss and significantly improve the power balance.

R. KASHUBA: Yes, α particles would be best provided that the rings could be formed. However, we must have a stable plasma before we can reach ignition and that requires the rings.

V. K. TRIPATHI: Is there any evidence of ion annulus formation with ICRH?

R. KASHUBA: Well, not in EBT since no ICRH has been used yet. Studies indicate a tail should form on the ion distribution with second harmonic heating.

Optimization of EBT Annulus Power Drain with Respect to Core Properties*

M. C. Vella

Lawrence Berkeley Laboratory, University of California
Berkeley, California 94720

Reduction of EBT annulus power drain in comparison with core power density and energy transport is discussed for overdense core operation. Increasing $(\omega_{pe}/\Omega_{ce})_{core}$ is found to offer a scaling advantage for any technique which can be developed for ring generation and/or core heating at high core density. Development of microwave heating for operation with the core at cutoff density could significantly reduce the importance of annulus power drain, and the associated recirculating power fraction. Alternatively, development of either beam plasma electron heating or ion cyclotron core heating for core densities above cutoff offers the possibility of substantial improvement over present operation.

One result of current interest in EBT reactor studies is that the difficulty of scaling the hot electron annulus into the reactor regime has become apparent. At least two papers[1,2] have appeared which model the power drain of the annulus, and some rather severe limitations on annulus volume emerge if the pr-sent operating regime is extrapolated. Scaling relationships natural to EBT are pointed out which suggest that increasing $(\omega_{pe})_{core}/\Omega_{ce}$ has the effect of reducing annulus power drain in comparison with either core power density or energy transport. Although this study was originally

*Work supported by the Office of Fusion Energy of the U. S. Department of Energy, under Contract No. W-7405-ENG-48.

motivated by an interest in developing beam plasma electron heating, this conclusion applies to any heating technique which allows operation with the core near or above cutoff density. Since microwave heating is presently standard for EBT, all scaling is done in terms of the familiar cutoff density.

Reactor power production scales like $\sim(n_i^2)_{cr}$, where the subscript 'cr' is used to denote core parameters. Microwave cutoff density is given by the condition, $\omega_{pe} = \Omega_{ce}$, or,

$$n_c = 9.74 \times 10^4 B^2, \tag{1}$$

where all units used are cgs, except temperature (eV). If the ratio of core to cutoff density is defined as,

$$d = n_{cr}/n_c,$$

reactor power density scales like $\sim d^2 B^4$, multiplied by a core temperature form factor. Taking the usual definition, $\beta = (n_e T_e + n_i T_i)/(B^2/8\pi)$, the core temperature is fixed by,

$$(T_e + T_i)_{cr} \leq 256\ \beta_{cr/d}\ (\text{keV}), \tag{2}$$

where quasineutrality has been assumed. The choice of core operating temperature is dictated by a number of tradeoffs properly considered in a reactor design study. However, an obvious implication of Eq. (2) is that, for a given density ratio, d, (which is fixed by heating technology) $T_{cr} \propto \beta$. For example, at present, d = 0.5, which gives $\beta \approx 6\%$

for $(T_e + T_i)_{cr} = 30$ keV. Higher β operation at reasonable core temperature requires development of a technique to raise d. In addition, from (2), core temeperature form factors are now implicitly a function of β and d. In a reactor, thermonuclear power production is balanced by energy transport to the walls. At present, this is thought to be neoclassical, which also scales like n_{cr}^2, multiplied by a form factor. Thus, to lowest order, both power production and thermal transport scale like, $n_{cr}^2 \approx d^2B^4$.

Annulus power drain can have a significant impact on EBT reactor economics if it results in a high recirculating power fraction. Although the cited references[1,2] do not agree on the details, both find the dominant hot electron energy loss mechanisms to be drag due to core electrons, large angle classical scattering, and synchrotron radiation, written as,

$$P_a = P_{d+c} + P_s,$$

where subscript 'a' refers to the annulus, the drag and collision processes, P_{d+c}, scale like $n_{cr}n_a$, and the synchrotron term scales like n_aB^2. Since $n_a \propto \beta_aB^2/T_a$ and $n_{cr} \propto dB^2$, all dominant terms in annulus and core scaling are proportional to B^4, giving,

$$P_a/P_{cr} \approx \frac{\beta_a[C_{d+c}\, d\, g_{d+c}(T_a,T_{cr}) + C_s g_s(T_a)]}{C_{cr}d^2 g(T_{cr})} . \qquad (4)$$

From (2), T_{cr} may be viewed as a function of d, where equilibration is assumed, i.e., $(T_e)_{cr} \approx (T_i)_{cr}$. Neglecting the temperature form factors, Eq. (4) strongly suggests that P_a/P_{cr} can be reduced by

raising d. Although annulus properties implicitly affect the core power balance, e.g., via hot electron drag at a given operating point P_{cr} is not explicitly dependent on annulus parameters. This is also true of core energy transport. Thus, minimization of P_a with respect to T_a separates from minimization of P_a/P_{cr}. Conversely, in the reactor regime, core temperature has a weak effect on annulus drag and scattering losses, and, from (2), the effect of T_{cr} can be neglected in P_a. Wall loading represents an additional constraint which may limit both core temperature, $T_{cr} \lesssim 20$ keV, and power density, $P_{cr} \propto d^2B^4g(T_{cr}) \lesssim$ few watts/cm^3. This suggests the following strategy for annulus optimization: (i) adjust the magnetic field, B, to satisfy wall loading limits; (ii) minimize P_a with respect to T_a; and (iii) reduce P_a/P_{cr} by operating at the maximum density ratio, d, consistent with overall transport, stability and reactor economics considerations. Using Eq. (2), T_{cr} is now regarded as a function of d and B_{cr}.

Two simple examples are now considered in order to estimate the possible reduction in P_a/P_{cr} which might be achieved with high density operation. First, core power density is taken with a simple quadratic dependence on d. Following Ref. (2), annulus power drain per unit volume is assumed to be dominated by core electron drag, ion loss cone scattering, and synchrotron radiation,

$$P_a = P_{d+c} + P_s$$

$$\simeq \beta_a B^4[dI_{d+c}(t_a) + 0.08\, t_a^{-1}(6\, t_a^2 + \frac{3t_a+1}{t_a+1} - 1)], \quad (5)$$

where the annulus temperature has been normalized to the electron rest mass energy, $t_a = T_a(\mathrm{MeV})/0.511$ and a two-dimensional relativistic Maxwellian distribution has been assumed. The drag plus collision term has been integrated numerically,[2] and the tabulated result is reproduced here in Table 1. Neglecting temperature effects, the simplest model for core power production (or energy transport), is

$$P_{cr} \approx C_{cr}\, n_i^2 \approx C_{cr}\, d^2 B^4, \tag{6}$$

which gives,

$$P_a/P_{cr} \,\alpha\, \frac{\beta_\alpha[dI_{d+c}(t_a) + 0.08\, t_a^{-1}(6t_a^2 + \frac{3t_a+1}{t_a+1} - 1)]}{d^2}\,. \tag{7}$$

Equation (7) is plotted as a function of T_a, for fixed d, in Figure 1. Present microwave operation is represented by d = 0.5. The upper limit for microwave operation is assumed to be d = 1.0, which offers a reduction of P_a/P_{cr} by a factor of ~1/3. The region with the core above cutoff, $d = n_{cr}/n_c > 1$, is probably accessible only with new heating techniques. A potential reduction in P_a/P_{cr} of an order of magnitude, or more, is apparent for $d \geq 2$.

If electron thermal conductivity is assumed to dominate core energy transport, simple neoclassical collisionless scaling[3] gives,

$$P_e \approx \frac{C_e}{A^3}\frac{d^2B^4}{T_{cr}^{1/2}} = \frac{C_e'}{A^3}\beta_{cr}^{-1/2} d^{5/2} B^4, \tag{8}$$

where A represents the magnetic aspect ratio, and finite drift orbit and higher order collision effects have been neglected. This gives a somewhat stronger scaling,

$$P_a/P_e \propto \frac{\beta_a \beta_{cr}^{1/2}}{d^{5/2}}[dI_{d+c} + 0.08\ t_a^{-1}(6t_a^2 + \frac{3t_a+1}{t_a+1} -1)], \qquad (9)$$

which is illustrated in Figure 2.

For comparison with present microwave operation, both (7) and (9) have been normalized to P_a/P_{cr} and P_a/P_e, respectively, for d = 0.5 and T_a = 1.0 MeV (i.e., the minimum of P_a at d = 0.5). Since the reduction in P_a/P_{cr} is less optimistic than P_a/P_e, the former is discussed in more detail. From Figure 3, operation with core density near cutoff, d = 1, offers a possible reduction in P_a/P_{cr} by a factor of ~0.4. Development of alternative heating techniques could reduce P_a/P_{cr} by an order of magnitude over present microwave operation at d = 2. Comparison with "best possible" microwave operation is made by normalizing to d = 1 at T_a = 1.4 meV, the minimum of P_a. The results are plotted in Figure 4, where d = 4 is seen to be required for an order of magnitude reduction in P_a/P_{cr}.

Conclusions

The possibility of reducing the importance of EBT annulus power drain in the reactor regime has been explored by scaling in ω_{pe}/Ω_{ce}, or, equivalently, in $d = n_{cr}/n_c$. A natural scaling advantage at high d is pointed out by comparing the annulus power drain to the core power and energy transport per unit volume, P_a/P_{cr}. The results

obtained here indicate that, even with microwaves, a significant improvement over present operation, d = 0.5, may be possible. Development of an alternative technique for EBT operation, e.g., beam plasma electron heating[4] or ion cyclotron core heating, offers the possibility of a substantial reduction in the importance of annulus power drain in the reactor regime. Further investigation appears merited, using better models for core power and energy transport and folding in stability limitations. The present results suggest a strong motivation for developing techniques for overdense core operation.

The author gratefully acknowledges numerous suggestions which have come up in conversation with W. B. Ard, C. L. Hedrick, and N. A. Uckan.

References

1. S. K. Borowski, N. A. Uckan, E. F. Jaeger, and T. Kaminash, "A Simple Annulus Power Balance in EBT-I," ORNL/TM-6910 (197).
2. R. J. Kashuba and W. B. Ard, "Annulus Power Balance in EBT," McDonnell Douglas Research Laboratories (1979).
3. C. L. Hedrick, E. F. Jaeger, D. A. Spong, G. E. Guest, N. A. Krall, J. B. McBride, and G. W. Stuart, Nucl. Fusion 17, 1237 (1977).
4. W. B. Kunkel, M. C. Vella, and B. Feinberg, "Beam Generated Hot Electrons," Lawrence Berkeley Laboratory Proposal (1979).

TABLE I (Ref. 2)

T_a (MeV)	I_{d+c}
0.1	38.8
0.2	13.9
0.3	7.76
0.4	5.18
0.5	3.82
0.6	2.99
0.7	2.44
0.8	2.06
0.9	1.78
1.0	1.56
1.2	1.24
1.4	1.04
1.6	0.89
1.8	0.77
2.0	0.69
2.5	0.54
3.0	0.44

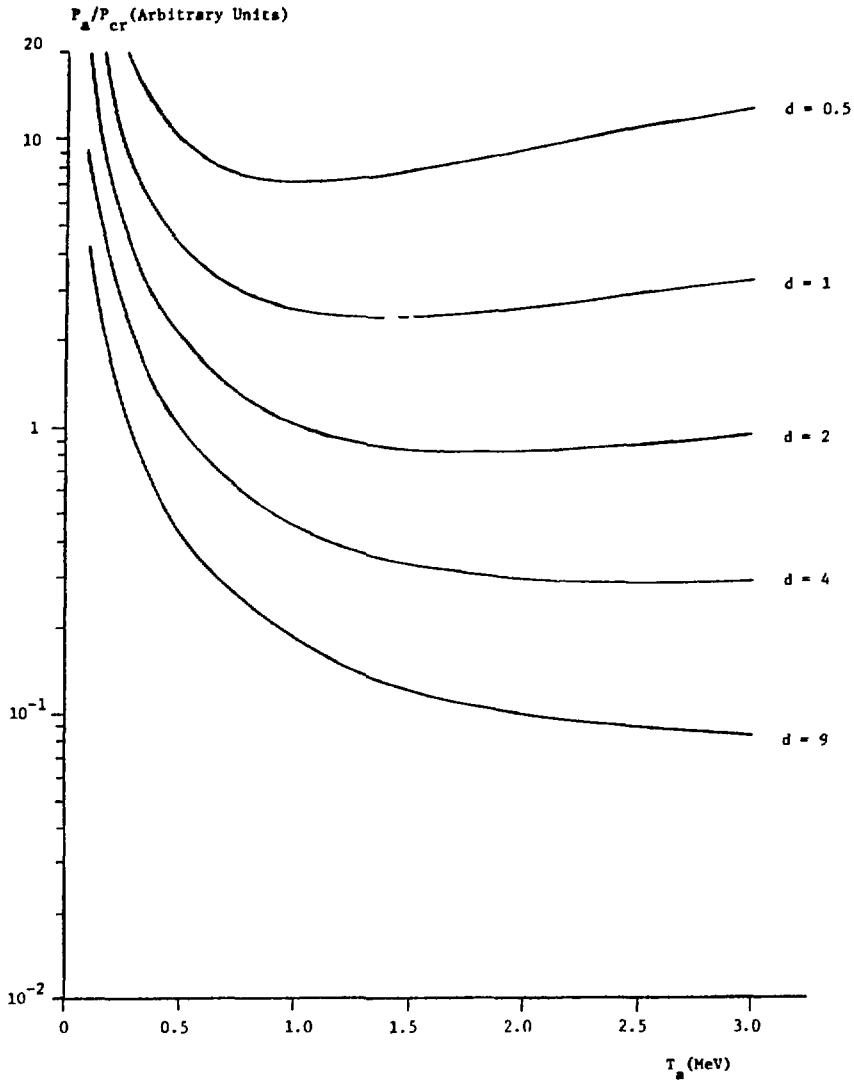

Figure 1. Comparison of hot electron power drain per unit volume, P_a, with core power production, P_{cr}, as a function of annulus temperature, T_a, and density ratio, d.

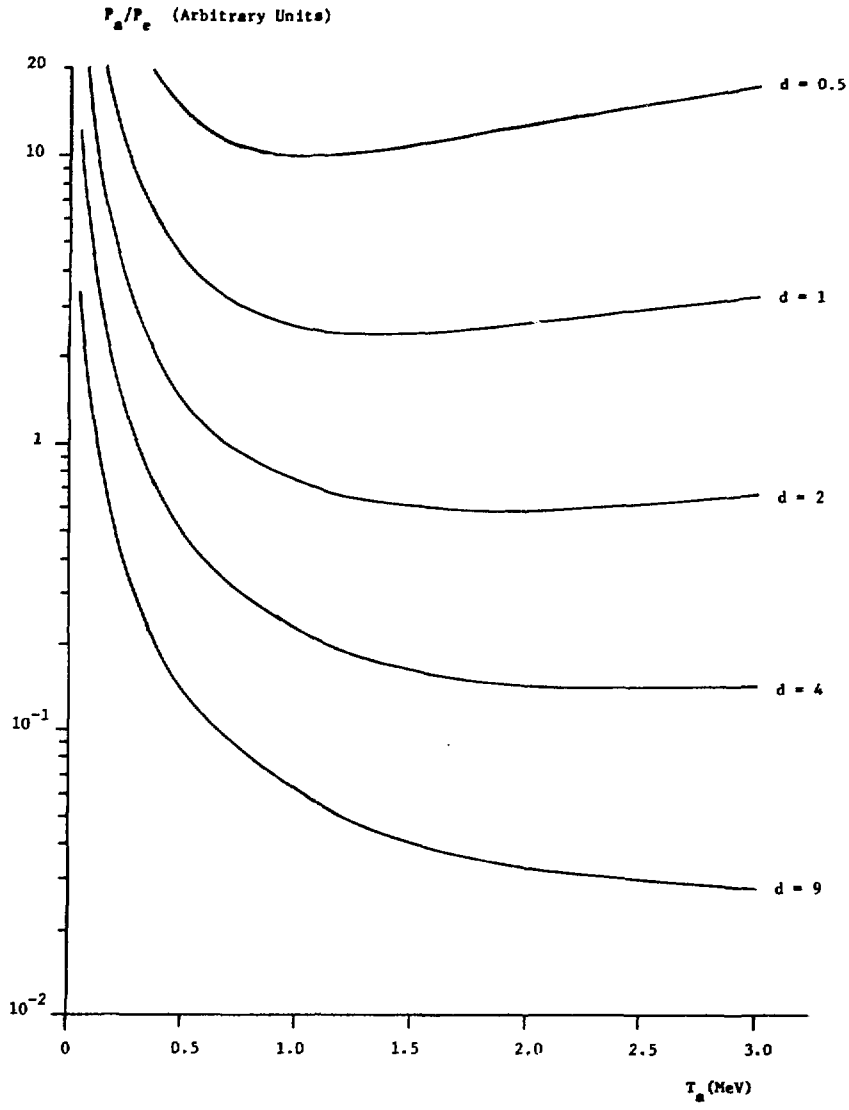

Figure 2. Comparison of hot electron power drain, P_a, with electron thermal conductivity, P_e.

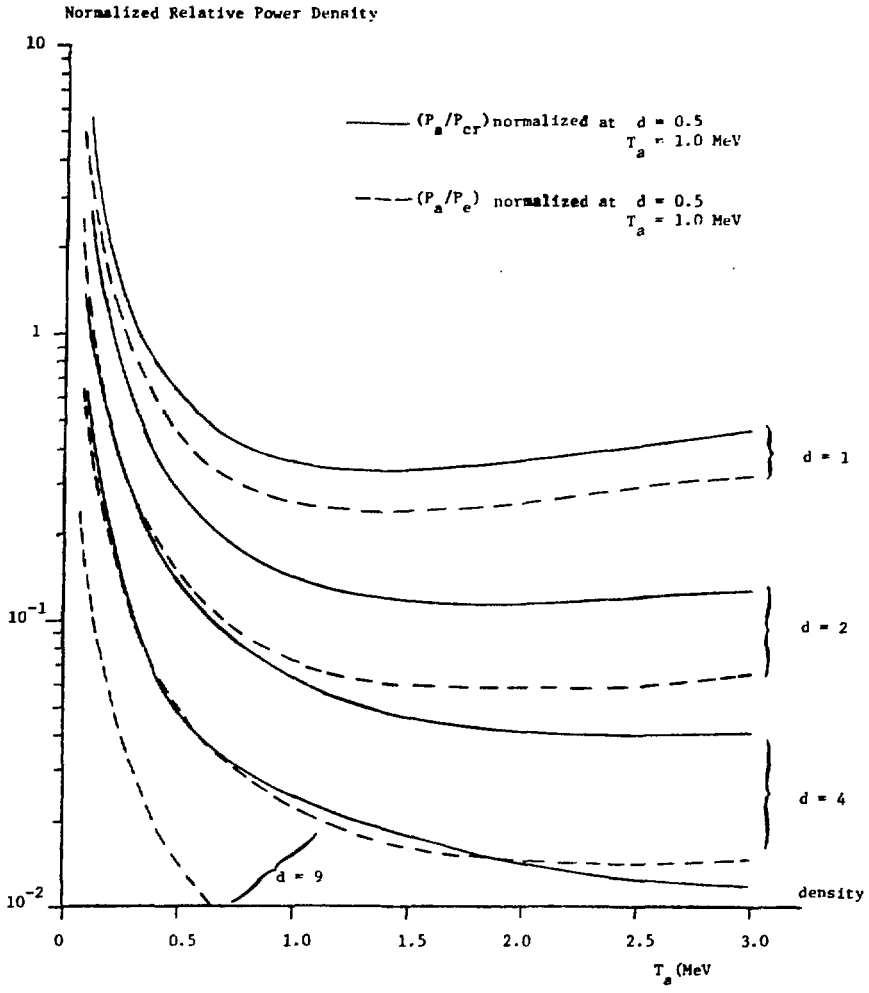

Figure 3. Comparison of annulus and core power densities, normalized to the present microwave operating regime, d = 0.5, at the minimum of P_a, $T_a \approx 1.0$ MeV.

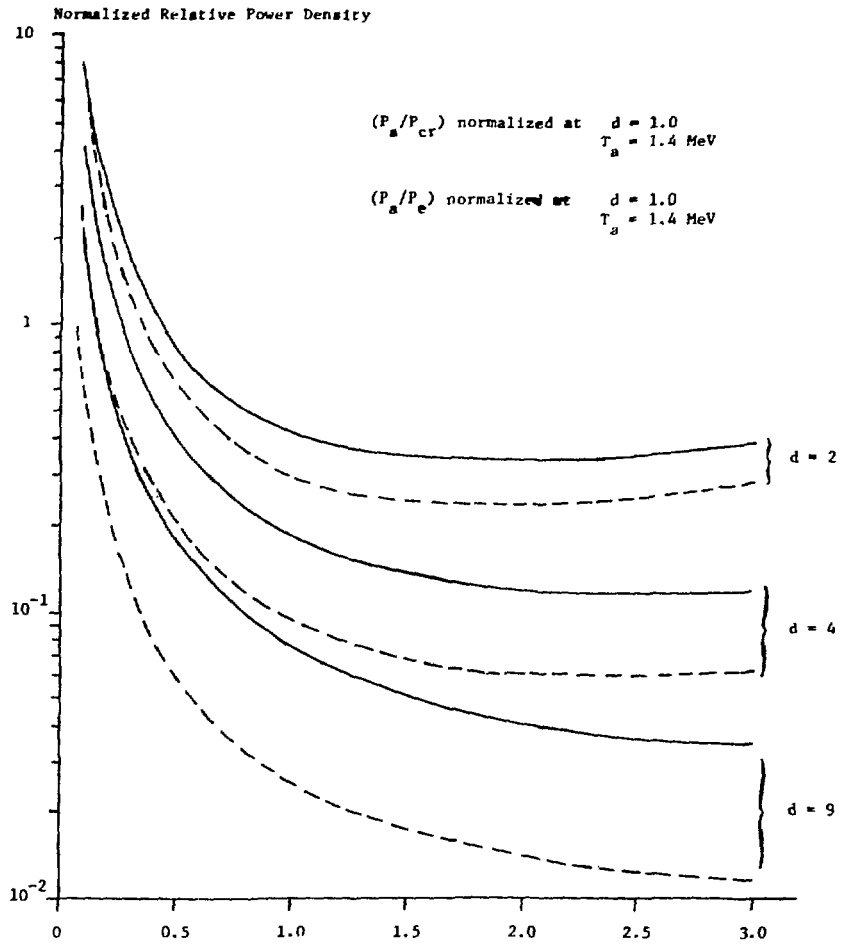

Figure 4. Comparison of annulus and core power densities, normalized to d = 1.0 at the minimum of P_a, T_a = 1.4 MeV.

DISCUSSION

C. BATHKE: What are the reactor implications of over-dense operation upon T and β?

M. VELLA: Core properties, T, β and d, are uniquely related by Eq. (2) for all types of EBT operation.

J. REECE ROTH: Can you estimate the recirculating power fraction associated with the hot electron rings in a characteristic reactor application?

M. VELLA: The recirculating power fraction for an over-dense EBT reactor can be estimated by using Fig. (3) or Fig. (4). For any given reference design, this estimate should include a guess at the relative volume of the annulus for the over-and under-dense cases, and a comparison of over-dense annulus heating efficiency with the present overall microwave efficiency.

STEADY-STATE MICROWAVE POWER REQUIREMENTS FOR EBTR ELECTRON RINGS

by

A. Andrade, R. A. Krakowski
and
C. G. Bathke

University of California
Los Alamos Scientific Laboratory
Los Alamos, New Mexico 87545

I. INTRODUCTION

Relativistic electron rings play an essential role in providing a minimum-B field topology for the toroidally-linked simple mirror configuration known as the ELMO Bumpy Torus (EBT). Generally, these electron rings are formed and sustained by microwave power applied at the midplane of each simple mirror and contain a level of perpendicular energy to render a high beta for an energetic electron density, n_R, that is considerably below the background (cold) electron density, n.

Recent calculations,[1] using a simplified Fokker-Planck model to estimate the electron ring distribution function, concluded that the entire thermal output of the proposed EBTR-48 4000-MWt unit[2] would be consumed in sustaining the rings against energy losses associated with collisional drag against the colder background electrons. The analysis given in Ref. 1 calculates hot electron ring distribution functions that are heavily weighted at energies near the toroidal background plasma energies. Since the Rutherford cross-section varies as the inverse square of the relative energy between interacting particles, for these distributions the ring energy is quickly dissipated against the thermal background distribution. Based on these results, a prohibitively large microwave power is predicted to be necessary to maintain the rings at high energy (100's keV). A more recent calculation[3] of energy losses from the electron rings in the EBT-I experiment concluded that collisional drag, rather than orbit effects associated with the toroidal mirror cant, could explain the observed electron ring energy losses. Losses associated with collisional drag scale as the product $n_R n = F_R n^2$, where F_R is defined as n_R/n, and the nearly two orders of magnitude increase in n expected

in projecting EBT-I to EBTR would project collisional drag a serious energy-loss mechanism for the reactor.

In this report it is shown that certain parameters, including the annular electron-ring beta, β_R, the ratio of ring electron density to toroidal background plasma density, F_R, and the ratio of toroidal volume, to electron-ring volume, ε_R, play a decisive role in determining whether a reactor based on bumpy torus confinement is feasible. Moreover, a general formalism is developed to estimate the power dissipation from the electron ring when the energy distribution is known. It is also shown that the power loss associated with collisional drag is not strongly dependent on the ring distribution function in the non-relativistic limit, but the dissipated power does diminish by a moderate percentage for electron energy distributions that are peaked at high energies. Except for the use of a non-relativistic formulation, the analysis presented herein is similar to that given in Ref. 3. The non-relativistic slowing-down equations were used in order to obtain analytic expressions for this estimate of electron-ring losses in a reactor-grade plasma. The formalism used to estimate collisional drag losses is developed in Sec. II: this formalism is then applied to a range of assumed electron ring energy distributions in Sec. III. A parametric analysis of the effects of the parameters β_R, F_R, and ε_R on reactor performance is given in Sec. IV. It is emphasized that this analysis is highly approximate, but the results indicate strongly the need for a more careful resolution of this problem for the EBT reactor embodiment.

II. COLLISIONAL POWER LOSS

In this section the methodology is developed for calculating the power loss from a distribution of electrons at high energies resulting from collisional drag against a background of thermalized (Maxwell-Boltzmann) plasma. Defining dP_R as the collisional power loss, per unit electron-ring volume, between the hot electrons with speed u and the background Maxwell-Boltzmann distribution of electrons

$$dP_R = -n_R f_R(u) \frac{\left[\frac{1}{2} m_e u^2\right] 4\pi u^2 du}{\tau_w(u)} \quad , \tag{1}$$

where $f_R(u)$ is the electron ring distribution function, $\tau_W(u)$ the energy exchange time, and n_R electron-ring density.

To obtain the total power loss per unit volume, P_R, Eq. (1) is integrated over the ring distribution of speeds. Before integrating, however, an explicit form of $\tau_W(u)$ is needed. By taking the second velocity moment of the Fokker-Planck equation[4], in which the background distributions of ions and electrons are assumed Maxwellian, and defining the characteristic energy exchange time as $\tau_W = -W/(dW/dt)$, the following expression results

$$1/\tau_W(u) = -\{2n\alpha u \frac{\partial}{\partial u}\left[(1+\frac{m}{m_e})\frac{\phi(x)}{u} + (1+\frac{m}{m_i})\frac{\phi(x\sqrt{\rho_m})}{u}\right]$$

$$+ n\alpha\left(\frac{2}{u}\frac{\partial}{\partial u} + \frac{\partial^2}{\partial u^2}\right)\left[\frac{e^{-x^2}}{\sqrt{a\pi}} + (1+2x^2)\frac{\phi(x)}{2au}\right. \tag{2}$$

$$\left. + \frac{e^{-x^2\rho_m}}{\sqrt{A\pi}} + (1+2x^2\rho_m)\frac{\phi(x\sqrt{\rho_m})}{2Au}\right]\}/u^2 \quad ,$$

where, $x = u\sqrt{a}$, $a = m_e/2kT$, $A = m_i/2kT$, $\rho_m = m_i/m_e$, $\alpha = 4\pi e^4 Z^2 \ln\Lambda/m_e^2$, $\phi(x)$ is the error function, and n is the background electron density.

If Eq. (1) is rewritten in the limit of large ρ_m, the following expression results

$$1/\tau_W(u) \simeq -\{2n\alpha u \frac{\partial}{\partial u}\left[\frac{2\phi(x)}{u} + \frac{1}{u}\right]$$

$$+ n\alpha\left(\frac{2}{u}\frac{\partial}{\partial u} + \frac{\partial^2}{\partial u^2}\right)\left(\frac{e^{-ax^2}}{\sqrt{a\pi}} + (1+2x^2)\frac{\phi(x)}{2au}\right. \tag{3}$$

$$\left. + (1+2x^2\rho_m)\frac{1}{2Au}\right)\}/u^2 \quad .$$

Taking derivatives in Eq. (3) and arranging the result into dimensionless form yields

$$\zeta \equiv \frac{x^2}{n\alpha\tau_W\, a^{3/2}} = 2\left[\frac{\mathrm{erf}(x)}{x} - \frac{4}{\sqrt{\pi}}\, e^{-x^2}\right] \quad . \tag{4}$$

If the relativistic form of the electron stopping power, (dW/dt) were used[3,5] then $\zeta^* = 2\left[\gamma^2/[(\gamma+1)/2]^{1/2}\mathrm{erf}(x)/x - (4/\sqrt{\pi})e^{-x^2}\right]$, and x^2 would equal $m_e c^2(\gamma-1)/kT$, where, here, $\gamma = (1-\beta^2)^{-1/2}$ and $\beta = u/c$. For the sake of analytic simplicity, the above relativistic correction is not applied.

It is noted that the above formulation for τ_W is identical to that given by Spitzer.[6] Additionally, Eq. (4) takes the appropriate values in the limiting cases of large and small x, as described by Montgomery[4]; that is, for large x

$$\tau_W \rightarrow u^3/2n\alpha \quad . \tag{5}$$

When x approaches unity (i.e., u approaches the thermal velocity of the background electrons)

$$1/\tau_W \rightarrow \alpha n u^3\left[\mathrm{erf}(1) - 4/e\sqrt{\pi}\right] \quad . \tag{7}$$

The total collisional power loss from the electron ring distribution to the background electron distribution is given by the integral of Eq. (1), using Eq. (4)

$$P_R = -nn_R m_e \frac{4\pi\alpha}{a} \int_1^{x_{max}} f_R(x)\; x^2\left[\frac{\mathrm{erf}(x)}{x} - \frac{4}{\sqrt{\pi}}\, e^{-x^2}\right] dx \quad . \tag{8}$$

III. EVALUATION OF P_R FOR A RANGE OF ASSUMED ELECTRON-RING SPECTRA

Evaluation of the expression for power loss, Eq. (8), requires that $f_R(x)$ be known. In this section the power loss is shown to be only weakly dependent on the assumed ring spectrum. For the sake of comparison only Maxwellian, delta-function and Gaussian distributions are evaluated. The Maxwellian and delta-function distributions may represent near extremes for EBT in that the Maxwellian can have a significant population near thermal energies, and the delta function would only occur if a thermal electron could be accelerated to ring energies in an infinitesimal time without losses being incurred during the acceleration process. The power loss from a Gaussian electron-ring distribution is also computed to examine an intermediate case.

A. Maxwellian Electron-Ring Distribution

A Maxwellian electron ring distribution with a temperature $T_R >> T$, where T is the background plasma temperature, is first assumed. Hence,*

$$f_R(x) = \left(\frac{b}{\pi}\right)^{3/2} \exp(-x^2\rho) \quad , \tag{9}$$

where $b = m_e/2kT_R$ and $\rho = T/T_R$. The ratio ρ is treated parametrically in this analysis.

Combining Eqs. (8) and (9) results in

$$P_R(W/m^3) = -n^2 F_R \ln\Lambda \frac{4.4(10)^{-32}}{T^{1/2}} \left\{ \frac{\rho^{1/2}\ (1-\rho)}{(1+\rho)^{3/2}} \right\} \quad , \tag{10}$$

where F_R equals n_R/n and $\alpha(m^6/s^4) = 8.06(10)^5 \ln\Lambda$.

---

*In the relativistic limit, $f_R(x) = 2(\rho/\xi)^{3/2}\ (\rho x^2+\xi)\sqrt{(\rho/\xi)x^2 + 2}\ \exp\left[-(\rho x^2+\xi)\right]/K_2(\xi)$, where $x^2 = m_e c^2(\gamma-1)/kT$, $\xi = m_e c^2/kT_R$, and $K_2(\xi)$ is a modified Bessel function of the second order.

For $\rho = 1$ $(T = T_R)$, $P_R = 0$, i.e., no net power loss occurs; for $\rho > 1$ $(T > T_R)$, $P_R > 0$, background electrons transfer energy to the rings: and for $\rho < 1$ $(T < T_R)$, $P_R < 0$, i.e., collisional energy loss from the rings to background electrons occurs.

For the following EBTR parameters: $n = (10)^{20}\ m^{-3}$, $\ln\Lambda = 20$, $T = 15$ kev, $T_R = 500$ keV, the energy loss from the ring distribution to the background distribution is given by

$$P_R(W/m^3) = -3.65(10)^8\ F_R \quad , \tag{11}$$

where in all cases power is expressed per unit electron-ring volume.

B. Delta-Function Electron-Ring Distribution

A delta-function electron-ring distribution, $f_R(u) = \delta(u-u')/4\pi u^2$, transforms into the following expression when the variable $x = u\sqrt{a}$ is used,

$$f_R(x) = \frac{a^{3/2}}{4\pi x^2}\,\delta(x-x') \quad , \tag{12}$$

where u' represents some maximum speed that a ring electron can achieve, as limited by radiative and collisional processes. The following expression for P_R results for this case

$$P_R(W/m^3) = -3.9(10)^{-32}\ F_R\ \frac{\ln\Lambda\ n^2}{T^{1/2}}\left[\frac{\mathrm{erf}(x')}{x'} - \frac{4}{\sqrt{\pi}}\,e^{-x'^2}\right] \quad . \tag{13}$$

For the same EBTR parameters used above

$$P_R(W/m^3) \simeq -3.48(10)^8\ F_R \quad . \tag{14}$$

The delta-function distribution gives a power loss that varies by 5% from that given for the case of a Maxwellian distribution in the $\rho = T/T_R$ range of practical interest.

C. Gaussian Electron-Ring Distribution

A calculation similar to those above is performed with a Gaussian distribution function, since it represents an intermediate distribution of speeds between the Maxwellian and the delta distribution functions. In this case the distribution function is given by

$$f_R(u) = \frac{1}{\sqrt{2\pi}\sigma} \exp - \frac{1}{2}\left[\frac{u - u_o}{\sigma}\right]^2 \tag{15}$$

where $\sigma = \sqrt{kT_R/m_e}$. The speed, u_o, characterizing the shift from $u = 0$, is defined here to equal $(2kT_R/m_e)^{1/2}$. Using the definitions of x $(= u\sqrt{a})$ and ρ $(= T/T_R)$, Eq. (15) can be written in the following form

$$f_R(x) = \left(\frac{a\rho}{\pi}\right)^{1/2} \exp - \left\{\rho x^2 - 2\sqrt{\rho}x + 1\right\} \quad . \tag{16}$$

In the one dimensional case, Eq. (8) can be written as

$$P_R = -n^2 F_R \alpha m_e \int f_R(x) \left[\frac{\mathrm{erf}(x)}{x} - \frac{4}{\sqrt{\pi}} e^{-x^2}\right] dx \quad . \tag{17}$$

Combining Eqs. (15) and (17) yields the following expression for $P_R(W/m^3)$

$$P_R = -8.12(10)^{-33} \frac{n^2 F_R \ln\Lambda \rho^{1/2}}{T^{1/2}} \int \exp(-\rho x^2 + 2\sqrt{\rho}x) \left[\frac{\mathrm{erf}(x)}{x} - \frac{4}{\sqrt{\pi}} e^{-x^2}\right] dx \ . \tag{18}$$

The integral in Eq. (18) must be performed numerically, and, if the same background and plasma parameters selected for the two previous cases are used, the resulting power loss is

$$P_R(W/m^3) = -3.08(10)^8 F_R \quad . \tag{19}$$

The power loss determined for three different ring spectra used an electron-ring "temperature" equal to 500 keV. Equations (10), (13), and (18) have been evaluated as a function of the temperature ratio, $\rho = T/T_R$, and is shown in Fig. 1 for a practical range of temperature ratios. Figure 1 shows that for the range of operating temperature ratios of interest, the power loss from the electron rings to the background plasma is only weakly dependent on the ring distribution function for the range of T/T_R considered.

IV. EBT PLASMA Q

The power loss resulting from collisional drag was shown to be nearly independent of the assumed ring spectrum for $T/T_R < 0.1$. To illustrate the importance of the parameter F_R and to point out the existence of others, the ring energy loss is evaluated relative to the total fusion power. To this end the ratio, Q, of fusion power, $P_F V_P$, to ring heating rate, $P_\mu V_R$, is defined as

$$Q = P_F V_P / V_R P_\mu \tag{20}$$

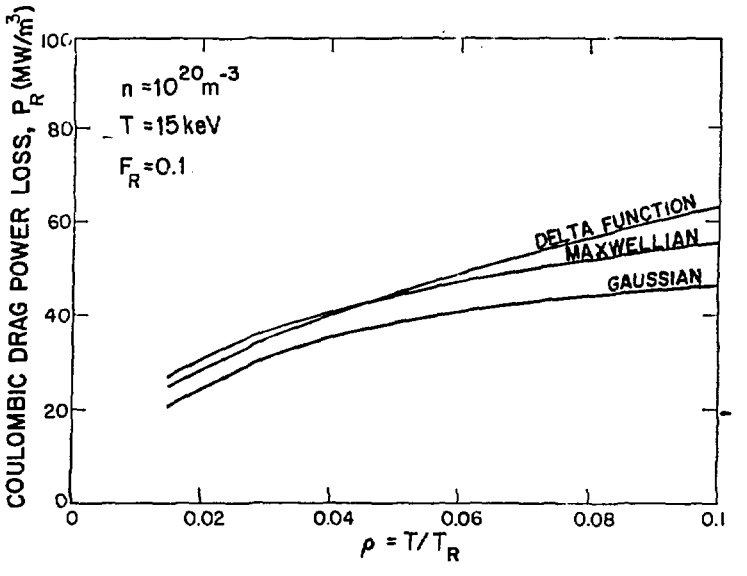

Fig. 1 Power loss dependence on the parameter $\rho = T/T_R$ for three different ring electron distribution functions. Background toroidal plasma parameters are held fixed at $n = 10^{20}\ m^{-3}$, $\ln\Lambda = 20$, and $T = 15$ keV.

where V_P is the toroidal plasma volume and V_R is the electron ring volume. The fusion power density is given by

$$P_F(W/m^3) = \frac{n^2}{4} \langle\sigma v\rangle E_F \quad , \tag{21}$$

and $P_\mu(W/m^3)$ corresponds to the microwave power density delivered to the ring volume.

In steady-state operation the microwave power must sustain the electron rings against coulombic drag and radiative losses. Consequently,

$$P_\mu = P_{CY} + P_{BR} + P_R \tag{22}$$

The Bremsstrahlung power, P_{BR}, is given by [7]

$$P_{BR}(W/m^3) \simeq 5.35(10)^{-37}\, n_R \sum_i (n_i Z^2)\, T_R^{1/2}, \tag{23}$$

and P_{CY} is approximated by[8]

$$P_{CY}(W/m^3) = 6.2(10)^{-17}\, B^2 n_R T_R \left(1 + \frac{T_R}{204}\right), \tag{24}$$

The coulombic drag power, P_R, for a Maxwellian ring spectrum is given by Eq. (10). As previously shown, the exact form of the ring energy spectrum does not appear to be crucial. Defining a ring beta

$$\beta_R = \frac{2\mu_o n_R\, kT_R(1+\lambda)}{B^2} \quad , \tag{25}$$

where $\lambda = T_i/T_R$, and using the definition for $F_R = n_R/n$, Eq. (22) becomes

$$P_\mu(W/m^2) = n^2 F_R \left\{2.5(10)^{-38} \frac{F_R T_R^{\,2}}{\beta_R}\left(1 + \frac{T_R}{204}\right) + \right.$$

$$\left. 5.35(10)^{-37} T_R^{\,1/2} + 4.4(10)^{-32} \frac{\ln\Lambda(.946)}{T_R^{\,1/2}}\right\} \tag{26}$$

The quantity $(1-\rho)/(1+\rho)^{3/2}$ appearing in Eq. (10) for the collisional drag power has been interpolated between T_R equal 500 and 1000 keV for $T = 15$ keV (i.e., .946). Furthermore, $\lambda = T_1/T_R$ has been taken to be small.

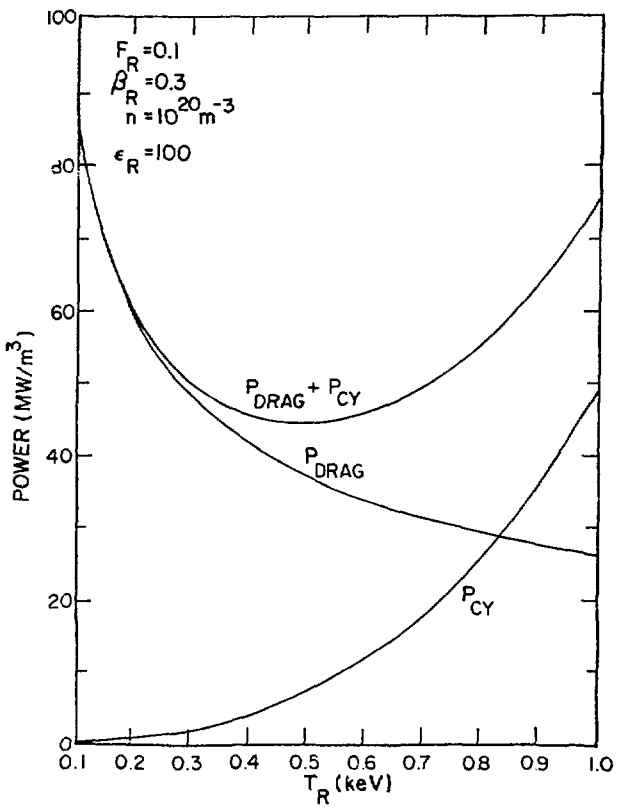

Fig. 2 Dependence of electron-ring losses, expressed per unit volume of electron ring, on the electron-ring temperature, T_R, for a Maxwellian energy distribution.

An optimum for which the microwave power is minimized is shown in Fig. 2 for a device with $F_R = .1$, $\beta_R = .3$, and $n = 10^{20} m^{-3}$. Bremsstrahlung radiation is negligible compared to collisional dissipation and cyclotron radiation at typical electron-ring temperatures. Also, the collisional drag dominates the cyclotron loss, in general for electron-ring temperatures below ~ 500 keV. These conclusions, however, must be tempered with the non-relativistic theory upon which this analysis is based.

Defining, the volume ratio $\varepsilon_R = V_P/V_R$, using the background plasma quantities $n = (10)^{20}\ m^{-3}$, $T = 15$ keV, $\langle\sigma v\rangle = 3.2(10)^{-22}\ m^3/s$,[7,8] and $\ln\Lambda = 20$ and taking the recoverable fusion energy, E_F, as 20 MeV/fusion, the plasma Q as defined by Eq. (20) becomes

$$Q = \frac{\varepsilon_R}{F_R\left\{2.08(10)^{-4}\frac{F_R T_R^2}{\beta_R}\left(1+\frac{T_R}{204}\right) + 2.23(10)^{-3}\,T_R^{1/2} + \frac{3.44(10)^3}{T_R^{1/2}}\right\}} \quad . \quad (27)$$

This expression is evaluated parametrically as a function of F_R, β_R, ε_R and T_R, to measure their relative importance and sensitivity in maximizing Q.

Figure 3 shows the sensitivity of Q to changes in F_R, with Q increasing rapidly for $F_R < 0.05$ when β_R and ε_R are held constant at the indicated values. This result was anticipated in Section III. If the ring beta is varied, the resultant effects on Q are in Fig. 4, for F_R and ε_R held constant. The dependence of Q on the volume ratio, ε_R, is shown in Fig. 5.

V. CONCLUSIONS

Collisional dissipation and radiative processes, which are expected to represent the dominant energy loss mechanisms operative in EBT electron rings, may not be so high as to discredit its attractiveness as a reactor, depending on whether certain parameters can be obtained for a high-Q operating point. The density ratio, F_R, appears to be a crucial variable, this preliminary estimate indicating values no greater than a few percent (or less if ε_R is closer to 10 than the value of 100 assumed in this analysis) may be allowed for high-Q reactor operation. A better quantification and optimization of key parameters defined in this study to minimize the recirculating power fraction

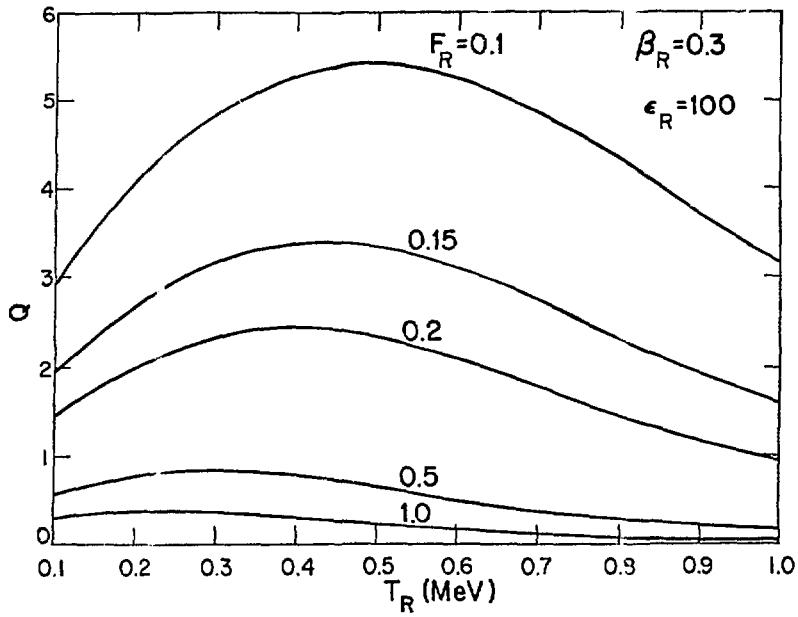

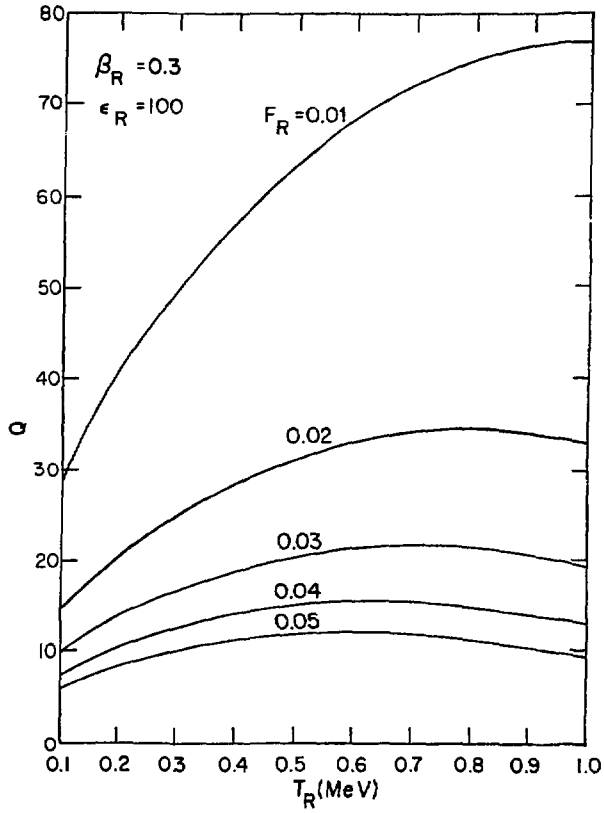

Fig. 3 Dependence of plasma Q-value (Eq. (20)) on ring-to-background electron density ratio, R_R, as a function of electron-ring-temperature, T_R.

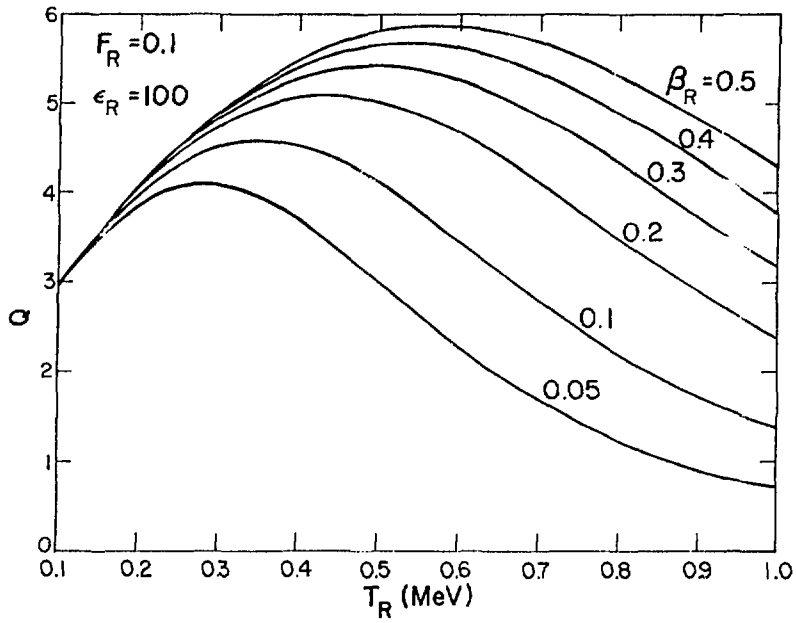

Fig. 4 Dependence of plasma Q-value (Eq. (20) on electron-ring beta, β_R, as a function of electron ring temperature, T_R.

should be the goal of a larger design effort that is based upon a better physics model for the electron ring.

It is noted that incorporation of relativistic effects will make the estimate of power loss by collisional drag considerably worse than the non-relativistic theory upon which this analysis is based. As previously noted, the relativistic counterparts to Eqs. (4) and (9) are

$$\zeta^*(x) = 2\left[\frac{\gamma^2}{\sqrt{(\gamma+1)/2}} \frac{\mathrm{erf}(x)}{x} - \frac{4}{\sqrt{\pi}} e^{-x^2} \right] \tag{28}$$

$$f_R^*(x) = \frac{2(\rho/\xi)^{3/2}}{K_2(\xi)} \left[\rho x^2 + \xi\right] \sqrt{(\rho/\xi)x^2 + 2}\; e^{-(\rho x^2 + \xi)} \quad , \tag{29}$$

where $\xi = m_e c^2/kT_R$, $x = m_e c^2(\gamma-1)/kT$, and $\gamma = 1/\sqrt{1-(u/c)^2}$. The quanitity $K_2(\xi)$

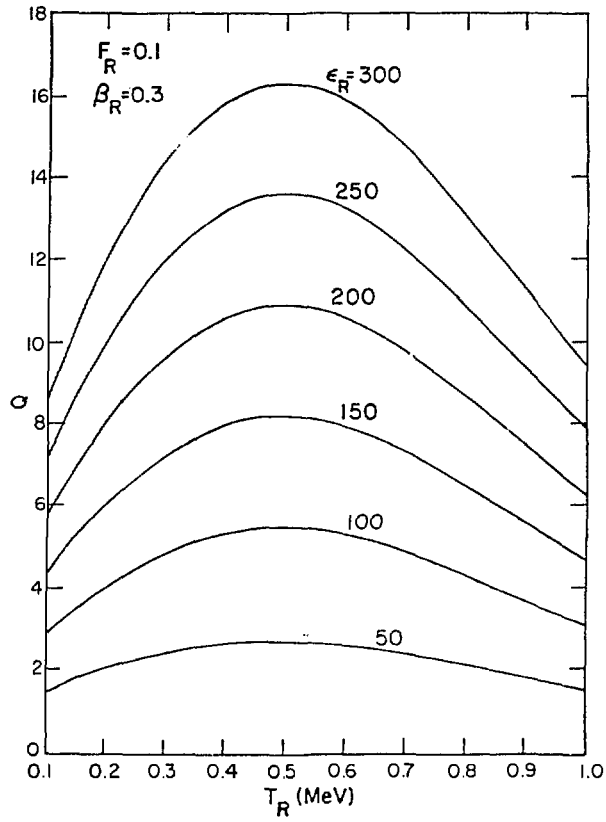

Fig. 5 Dependence of plasma Q-value (Eq. (20)) on background-to-ring volume ratio, E_R, as a function of electron-ring temperature, T_R.

is a modified Bessel function of second order. Using these expressions, Eq. (28), being accurate to order kT/m_ec^2, a relativity error measure can be formulated

$$P_R^*/P_R = \frac{\int \zeta^* f_R{}^* x^2 dx}{\int \zeta\ f_R x^2 dx} \quad , \tag{30}$$

where the unstarred quantities correspond to the non-relativistic limit, $\gamma \to 1$ (i.e., Eq. (10), for the Maxwellian distribution assumed here). Figure 6 shows the dependence of P_R^*/P_R on T_R for three values of T. From Fig. 6 it is seen that incorporation of relativistic effects predicts collisional drag losses

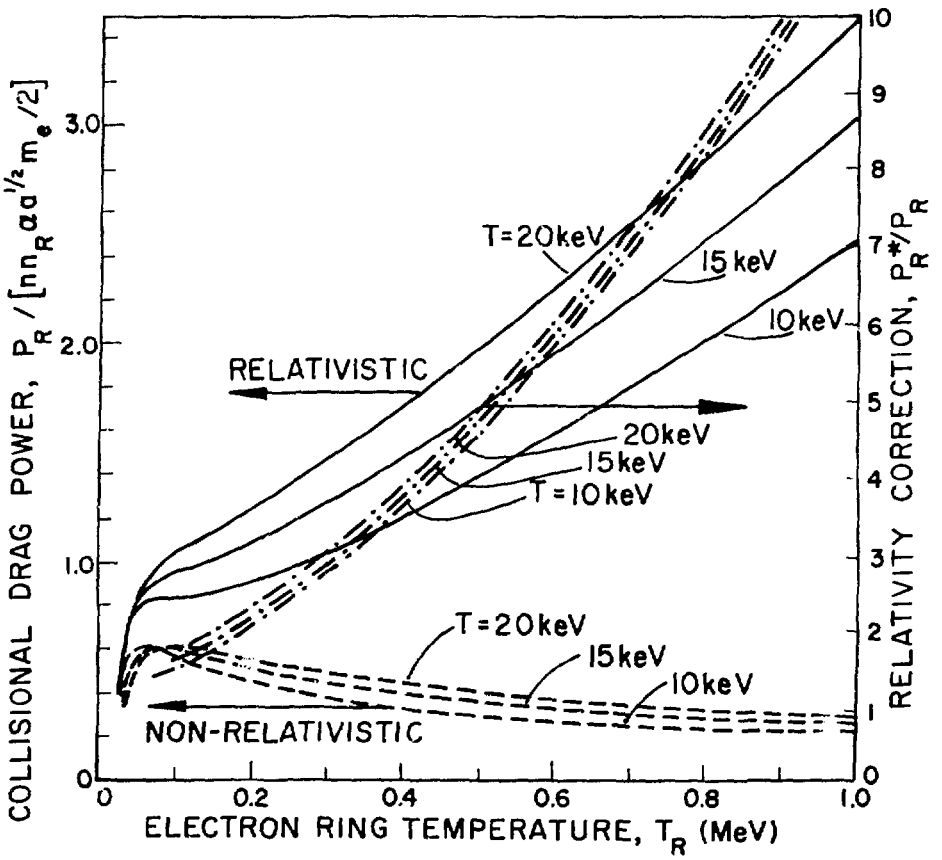

Fig. 6 Comparison of collisional drag power losses for a Maxwellian electron ring of temperature T_R with and without relativistic corrections applied.

that could be up to an order of magnitude greater than that predicted by non-relativistic expressions (Eq. (10)).

REFERENCES

1. G. W. Stuart, "Microwave Power Requirements for EBT," Science Applications, Inc., report (1979).

2. D. G. McAlees, et al, "The Elmo Bumpy Torus Reactor (EBTR) Reference Design," Oak Ridge National Laboratory ORNL/TM-5669, (November 1976).

3. S. K. Borowski, N. A. Uckan, E. F. Jaeger, and T. Kammash, "A Simple Annulus Power Balance in EBT-I," Oak Ridge National Laboratory report ORNL/TM-6910 (September, 1979).

4. D. C. Montgomery and D. A. Tidman, Plasma Kinetic Theory, McGraw-Hill (1964).

5. T. Kammash and D. L. Galbraith, "The Slowing Down of Relativistic Electrons in Plasma," Nucl. Fus., 13, 464 (1973).

6. L. Spitzer, Physics of Fully Ionized Gases, Interscience, (1956).

7. T. Kammash, Fusion Reactor Physics:Principles and Technology, Ann Arbor Science, (1976).

8. D. J. Rose and M. Clark, Plasmas and Controlled Fusion, MIT Press, (1961).

DISCUSSION

A. BOOZER: You indicated the ring volume needed to be less than 1% of the plasma volume due to the ring power requirements. How can such a small ring be consistent with the bulk plasma transport being small enough for a reactor?

C. BATHKE: It doesn't have to be in our study. The motivation of our study was to deduce target values of n_{ring}/n_{plasma}, V_{ring}/V_{plasma}, and β_{ring} necessary for attractive reactor operation, assuming ring energy balance considerations dominate. If our conclusion regarding such a small ring volume detracts from the bulk plasma, then one may either back off of V_{ring}/V_{plasma} or provide auxilliary heating if necessary. In either case, reactor performance will suffer. This effect and others must be included in analyses of whether attractive reactors are achievable.

7. STABILITY

G. E. Guest, Session Chairman

Rup

FLUTE-INTERCHANGE STABILITY IN A HOT ELECTRON PLASMA

R. R. Dominguez

General Atomic Company,
San Diego, California 92138

ABSTRACT

Several topics in the kinetic stability theory of flute-interchange modes in a hot electron plasma are discussed. The stability analysis of the hot-electron, curvature-driven flute-interchange mode, previously performed in a slab goemetry, is extended to a cylindrical plasma. The cold electron concentration necessary for stability differs substantially from previous criteria. The inclusion of a finite temperature background plasma in the stability analysis results in an ion curvature-driven flute-interchange mode which may be stabilized by either hot-electron diamagnetic effects, hot-electron plasma density, or finite (ion) Larmor radius effects.

Work supported by Department of Energy,
Contract DE-AT03-76-ET51011.

NOTICE

This report was prepared as an account of work sponsored by the United States Government. Neither the United States nor the Department of Energy, nor any of their employees, nor any of their contractors, subcontractors, or their employees, makes any warranty, express or implied, or assumes any legal liability or responsibility for the accuracy, completeness or usefulness of any information, apparatus, product or process disclosed, or represents that its use would not infringe privately owned rights.

I. INTRODUCTION

The stability of flute-interchange modes in a hot electron plasma has recently been considered by several authors.[1-5] The stability analyses have emphasized either the kinetic hot electron plasma[1-3] or the MHD bulk plasma.[4,5] The stability analyses of hot electron driven modes in the presence of a cold, bulk plasma background concluded that an interchange instability exists with "bad" magnetic field curvature for both small and large hot electron precessional frequency, and this instability is stabilized by a sufficient concentration of cold electrons. The MHD stability analysis,[4] performed assuming an unperturbable (rigid) hot electron plasma, also concludes that cold plasma will stabilize the interchange instability. The kinetic stability analyses have necessarily employed a simplified geometry and considered only localized (within the hot electron region) modes while the MHD analysis considered a more realistic geometry, but did not employ a self-consistent model for the hot electron plasma.

In this work, we extend the stability analysis of the hot electron curvature driven flute-interchange mode[3] to a cylindrical geometry. In addition, the synthesis of localized kinetic hot electron and bulk plasma modes is considered by performing a stability analysis of flute-interchange modes including the effects of finite ion Larmor radius and ion precessional drifts associated with the bulk plasma.

Employing a sharp boundary pressure profile in the cylindrical plasma model,[6] we perform in Sec. II a non-local stability analysis of the hot electron curvature driven flute-interchange mode. The amount of cold plasma necessary for stability is shown to differ substantially from the criteria obtained from the local stability analysis.[3]

Finite ion temperature effects of the bulk plasma are more difficult to include in a non-local stability analysis. Hence, in the present work we have simplified the analysis by considering finite ion temperature effects only in the local approximation. In Sec. III we use a slab geometry to show that, in addition to the hot electron curvature driven interchange mode, an additional hybrid mode results from the inclusion of finite ion temperatures. This mode was discussed by Nelson[5] in a more restricted stability analysis. Unlike the hot electron curvature driven mode, the self-field generated by the hot electrons may have a strong stabilizing effect. Additional stabilizing effects arise from either the hot electron density or the finite ion Larmor radius.[7,8]

The electromagnetic equations used to perform the stability analysis in Sec. II are derived from the variational method for a cylindrical plasma,[6] which obtains the correct set of Maxwell equations. Stability plots are presented and a comparison of the local and non-local criteria for cold electron stabilization is made.

In Sec. III, we employ the results of the variational method for a slab geometry[9] to obtain the local Maxwell equations used in the local stability analysis.

II. HOT ELECTRON FLUTE INTERCHANGE MODE

The variational method[9] employed to obtain the Vlasov-Maxwell integral equations in Fourier space for a slab geometry has recently been extended to a cylindrical geometry.[6] From the Fourier space integral form of the Maxwell equations approximate Maxwell differential equations may be obtained in the long wavelength limit $k_\perp a_s < 1$ (a_s is the Larmor radius of species s = electrons, ions). The resulting set of Maxwell differential equations is manifestly Hermitian for real eigenvalues ω when Landau resonances are neglected.

As an application of the results of the variational method in a cylindrical geometry, we analyse the stability of finite β long wavelength flute-interchange modes in a hot electron plasma which contains cold electron and ion components. We present the relevant results of Ref. 6 without derivation, and refer the reader to this reference for details.

In the cylindrical plasma model we shall assume a density variation in the radial direction, $N_s(r)$, and an unperturbed magnetic field $\underset{\sim}{B}_o = B_z(r)\hat{\underset{\sim}{z}}$. To simulate the curvature of $\underset{\sim}{B}_o$, we assume that the plasma is situated in an external species dependent gravitational field $\underset{\sim}{g}_s = \underset{\sim}{g}_s(r)\hat{\underset{\sim}{r}}$.

The plasma equilibrium is specified by the force balance and quasi-neutrality conditions

$$\frac{d}{dr}\left(N_h T + \frac{B_z^2}{8\pi}\right) = N_h m_e g \quad , \quad N_i = N_h + N_c \quad , \tag{1}$$

with the ion, cold electron and hot electron densities being given by $N_i = N(r)$, $N_e = (1 - \alpha)N(r)$, and $N_h = \alpha N(r)$. The magnitude of g is chosen as $g = (T/m_e R_c)(r/R_p)$ with T the hot electron temperature, R_c the radius of curvature of the external field, and R_p is a characteristic plasma scale length. To obtain analytically tractable results, we use an idealized model, the sharp boundary model, for the plasma density profile. We define the sharp boundary model by the equations

$$N(r) = \begin{cases} N_o & r < R \\ 0 & r \geq R \end{cases} , \tag{2a}$$

and

$$\alpha = \begin{cases} \alpha_o & R(1 - \varepsilon) \leq r < R \\ 0 & \text{otherwise} \end{cases} , \tag{2b}$$

where $\varepsilon << 1$. We restrict consideration to pure flute perturbations ($k_{\parallel} = 0$) generating the electric field

$$\underset{\sim}{E}(\underset{\sim}{r}) = - \nabla\phi(\underset{\sim}{r}) - \nabla x[a(\underset{\sim}{r})\hat{\underset{\sim}{z}}] \quad , \tag{3}$$

where $\phi(\underset{\sim}{r}) = \phi_\ell(r)\exp i(\ell\psi - \omega t)$, ..., with ψ being the azimuthal angle and $\ell = 1, 2, \ldots$.

The Vlasov charge density and current response to the perturbation in Eq. (3) are the source terms in the Poisson equation and Ampère's Law. The

resulting Maxwell differential equations[6] for long wavelength flute-interchange modes are

$$B'\phi_\ell(r) = \hat{\varepsilon}_{11}\phi_\ell(r) - i\hat{\varepsilon}_{12}a_\ell(r) \quad , \tag{4a}$$

$$B'\left(B' + \frac{\omega^2}{c^2}\right)a_\ell(r) = \frac{\omega^2}{c^2}[i\hat{\varepsilon}_{12}\phi_\ell(r) + \hat{\varepsilon}_{22}a_\ell(r)] \quad , \tag{4b}$$

where $B' = (1/r)(d/dr)[r(d/dr)] - \ell^2/r^2$ and $\hat{\varepsilon}_{\alpha\beta}$ are differential operators defined by

$$\hat{\varepsilon}_{11}\phi_\ell = \sum_s \frac{4\pi}{\omega}\int d\underset{\sim}{v}\left(\phi_\ell\left\{\left(1 - k_r^2\frac{a_s^2}{4}\right)\left[-\omega q_s^2\frac{\partial f_o^{(s)}}{\partial H}\right.\right.\right.$$

$$\left.\left. + \frac{D^{(s)}(\omega - k_\parallel v_\parallel)^2}{\tilde{\omega}}\right] + \frac{\ell}{r}\frac{d}{dr}\left[\frac{a_s^2}{2}D^{(s)}(\omega - k_\parallel v_\parallel)\frac{\tilde{\omega}\Omega_s}{\tilde{\omega}^2 - \Omega_s^2}\right]\right\}$$

$$\left. - \left(B'\phi_\ell + \frac{d\phi_\ell}{dr}\frac{d}{dr}\right)\left[\frac{a_s^2}{2}\frac{D^{(s)}(\omega - k_\parallel v_\parallel)^2}{\tilde{\omega}}\frac{\Omega_s^2}{\tilde{\omega}^2 - \Omega_s^2}\right]\right) \quad , \tag{5a}$$

$$\hat{\varepsilon}_{12}a = \sum_s \frac{4\pi}{\omega} \int d\underset{\sim}{v} \left\{ \frac{\ell}{r} a_\ell \frac{d}{dr} \left[\frac{v_\perp^2}{2\Omega_s} D^{(s)} (\omega - k_\parallel v_\parallel) \frac{\Omega_s}{\tilde{\omega}^2 - \Omega_s^2} \right] \right.$$

$$- \left(B' a_\ell + \frac{da_\ell}{dr} \frac{d}{dr} \right) \left(\frac{v_\perp^2}{2\Omega_s} D^{(s)} \frac{\omega - k_\parallel v_\parallel}{\tilde{\omega}} \frac{\Omega_s^2}{\tilde{\omega}^2 - \Omega_s^2} \right)$$

$$\left. - \frac{da_\ell}{dr} \frac{d}{dr} \left[\frac{v_\perp^2}{2\Omega_s} \left(D^{(s)} \frac{\omega_d}{\tilde{\omega}} + \frac{q_s^2}{M_s} \frac{\ell}{\omega \Omega_s r} \frac{\partial f_o^{(s)}}{\partial r} \right) \right] \right\} , \tag{5b}$$

$$\hat{\varepsilon}_{22} a_\ell = \sum_s \frac{4\pi}{\omega} \int d\underset{\sim}{v} \left[B' \left(\frac{v_\perp^2 a_s^2}{4\tilde{\omega}} D^{(s)} B' a_\ell \right) + a_\ell \frac{\ell}{r} \frac{d}{dr} \left(\frac{v_\perp^2}{2} D^{(s)} \frac{\Omega_s}{\tilde{\omega}^2 - \Omega_s^2} \right) \right.$$

$$\left. - \left(B' a_\ell + \frac{da_\ell}{dr} \frac{d}{dr} \right) \left(\frac{v_\perp^2}{2} D^{(s)} \frac{\tilde{\omega}}{\tilde{\omega}^2 - \Omega_s^2} \right) \right] , \tag{5c}$$

with $\tilde{\omega} = \omega - \omega_d - k_\parallel v_\parallel$, $\omega_d = (\ell/r) v_d$, $v_d = (v_\perp^2/2\Omega_s)(d\ell og\ B_z/dr) - (g_s/\Omega_s)$, $\Omega_s = q_s B_z / M_s c$, and g_s is the magnitude of the species dependent gravitational field (in the present case $g_i = 0$). For the flute mode analysis $k = 0$ in Eq. (5).

The cold species response may be derived either from fluid equations or from Eq. (4) by choosing a distribution

$$f_{e,i}^{(c)} = F_{e,i}(H, R_G, v_\parallel) \quad ,$$

such that $\int d\underset{\sim}{v}\, v_\perp^2\, F_{e,i} = 0$. For the hot electrons, we choose the delta function distribution

$$f_h = \frac{\alpha}{2\pi v_o^2} N(R_G)\,\delta\left(\frac{\mathcal{H} - m_e v^2/2}{\mathcal{H}_o} - 1\right) F(v_\parallel) \quad ; \tag{6}$$

$$N_h = \int d\underset{\sim}{v}\, f_h \quad , \quad \mathcal{H}_o = T = m_e v_o^2/2 \quad , \quad \int d\underset{\sim}{v}\; F(v_\parallel) = 1 \quad ,$$

in order to readily evaluate the hot electron resonant denominators in Eq. (4).

Using $f_{e,i}^{(c)}$ and f_h in Eq. (4) and performing some straightforward manipulations, we obtain the coupled differential equations

$$\left\{\left(1 + \frac{\omega_{pi}^2}{\Omega_i^2 - \omega^2}\right) B'\phi_\ell + \frac{d}{dr}\left(1 + \frac{\omega_{pi}^2}{\Omega_i^2 - \omega^2}\right)\frac{d\phi_\ell}{dr}\right.$$

$$\left. - \frac{\ell}{r}\phi_\ell \frac{d}{dr}\left[\frac{\Omega_i}{\omega}\frac{\omega_{pi}^2}{\Omega_i^2 - \omega^2} - \frac{(1-\alpha)\omega_{pi}^2}{\omega\Omega_i}\right] - \frac{\alpha}{\lambda_e^2}\phi_\ell \frac{\omega_e}{\tilde{\omega}}\left(1 + \frac{\beta}{2}\frac{\omega - \omega_g}{\tilde{\omega}}\right)\right\}$$

$$- i\left(\frac{\omega_{pi}^2}{\omega\Omega_i}\left\{\alpha\left[\frac{\omega_e}{\tilde{\omega}}\left(1 + \frac{\beta}{2}\frac{\omega - \omega_g}{\tilde{\omega}}\right) - \frac{\omega_b}{\omega}\right] - \frac{\omega^2}{\omega^2 - \Omega_i^2}\right\} B' a_\ell\right.$$

$$\left. + \frac{\ell}{r} a_\ell \frac{d}{dr}\left(\frac{\omega_{pi}^2}{\omega^2 - \Omega_i^2}\right) - \frac{d}{dr}\left(\frac{\omega_{pi}^2}{\omega^2 - \Omega_i^2}\frac{\omega}{\Omega_i}\right)\frac{da_\ell}{dr}\right) = 0 \quad , \tag{7a}$$

$$i\left(\frac{\omega_{pi}^2}{\omega\Omega_i}\left\{\alpha\left[\frac{\omega_e}{\tilde{\omega}}\left(1+\frac{\beta}{2}\frac{\omega-\omega_g}{\tilde{\omega}}\right)-\frac{\omega_b}{\tilde{\omega}}\right]-\frac{\omega^2}{\omega^2-\Omega_i^2}\right\}B'\phi_\ell\right.$$

$$\left.+\frac{\ell}{r}\phi_\ell\frac{d}{dr}\left(\frac{\omega_{pi}^2}{\omega^2-\Omega_i^2}\right)-\frac{d}{dr}\left(\frac{\omega_{pi}^2}{\omega^2-\Omega_i^2}\frac{\omega}{\Omega_i}\right)\frac{d\phi_\ell}{dr}\right)$$

$$+\frac{c^2}{\omega^2}B'\left(\left\{1+\frac{\beta}{2}\left[\frac{2(\omega-\omega_g)}{\tilde{\omega}}-\frac{\omega_e}{\tilde{\omega}}\left(1+\frac{\beta}{2}\frac{\omega-\omega_g}{\tilde{\omega}}\right)\right]\right\}B'a_\ell\right)=0 \quad , \tag{7b}$$

with $\omega_e = (\ell/r)(T/m_e\Omega_e)[d\ell og\ N_h(r)]/dr$; $\omega_b = (\ell/r)(T/m_e\Omega_e)(d\ell og\ B_z)/dr$; $\omega_g = -(\ell/r)(g/\Omega_e)$; $\tilde{\omega} = \omega - \omega_d$; $\omega_d = \omega_b + \omega_g$; $T = m_e v_o^2/2$; and $\beta = 8\pi N_h T/B_z^2$. It is readily verified that Eq. (7) reduces to the hot electron dispersion relation of Dominguez and Berk[3] (with $\ell/r \to k_y$) when spatial derivatives of ϕ_ℓ and a_ℓ are neglected.

The eigenvalues, ω, for the sharp boundary model are obtained by integrating the coupled differential equations, Eq. (7), across the discontinuity at $r = R$. The detailed manipulations involve combining terms in Eq. (7) to obtain total derivatives and subsequently integrating by parts several times. Deleting these straightforward details, we find upon integrating Eq. (7) from $R_- = (1-\varepsilon)R$ to $R_+ = (1+\varepsilon)R$ ($\varepsilon \ll 1$) and using the continuity of ϕ_ℓ and a_ℓ, the system of algebraic equations

$$\left(\frac{\omega}{\omega+\Omega_i}+\frac{\alpha_o\omega_g}{\omega-\omega_g}\right)\phi_\ell(R)+i\frac{\omega}{\omega+\Omega_i}a_\ell(R)=0 \quad , \tag{8a}$$

$$i \frac{\omega}{\Omega_i} \frac{\omega}{\omega + \Omega_i} \phi_\ell(R) + 2 \frac{\ell^2}{R^2} \frac{c^2}{\omega_{pi}^2} (1 + \beta) a_\ell(R) = 0 \quad , \tag{8b}$$

where $\omega_{pi}^2 = 4\pi N_o e^2/M_i$, $\Omega_i = eB_o/M_i c$ ($B_z = B_o$ for $r < R$), and $\omega_g = (\ell T/M_i \Omega_i)(1/R_c R)$ (R_p is replaced by R). In obtaining Eq. (8), we have employed the approximate form for the eigenfunctions $\phi_\ell(r)$, $a_\ell(r)$

$$\phi_\ell(r),\ a_\ell(r) = (\phi_o, a_o) \begin{cases} (r/R)^\ell & r < R \\ (r/R)^{-\ell} & r \geq R \end{cases} \quad . \tag{9}$$

It is readily verified that Eq. (9) is a solution of Eq. (7) for N(r) = const. The dispersion relation is obtained from Eq. (7) by requiring that the determinant of the coefficients of $\phi_\ell(R)$ and $a_\ell(R)$ vanish. We obtain the result

$$X(X - q) + \alpha_o\, q(X + 1) + \frac{\delta}{q} \frac{X^3(X - q)}{X + 1} = 0 \tag{10}$$

where $X = \omega/\Omega_i$, $\delta = (1/4\alpha_o \ell)(R/R_c)[\beta/(1 + \beta)]$, $q = (\ell T/M_i \Omega_i^2)(1/R_c R)$, $b_e = (1/2)k^2 a_e^2 = k^2 T/m_e \Omega_e^2$, and $k = \ell/R$.

The finite β correction term in Eq. (10) may be shown to yield corrections or order $\alpha_o \delta$ compared to unity. Neglecting this term, Eq. (10) is readily solved to obtain the root

$$X = \frac{q(1 - \alpha_o)}{2} \pm \sqrt{\left[\frac{q}{2}(1 - \alpha_o)\right]^2 - \alpha_o q} \quad . \tag{11}$$

In the presence of "bad" curvature, $q > 0$, an interchange instability is possible at both small and large precessional frequency. Cold electrons are stabilizing and stability results for $(1 - \alpha_o)^2 > 4\alpha_o/q$. Unlike finite ion Larmor radius stabilization of the low frequency flute-interchange mode, there is no cancellation of the cold electron stabilizing term for the lowest order $\ell = 1$ mode. We also note that Eq. (11) is precisely the result that would be obtained from a simple electrostatic theory.

From Eq. (11), we obtain the marginal stability condition

$$\frac{N_c}{N_h} = \frac{2}{q}\left(1 + \sqrt{1 + q}\right) \quad , \quad q = \frac{\ell T}{M_i \Omega_i^2} \frac{1}{RR_c} \equiv \ell q_o \tag{12}$$

Observe that, unlike the local criteria, there is no β dependence in Eq. (12). For $N_c/N_h > 2q^{-1}(1 + \sqrt{1 + q})$, we have stability. In Fig. 1 we plot the fraction of cold to hot electrons, $N_c/N_h = (1 - \alpha_o)/\alpha_o$, at marginal stability as a function of the parameter q_o for several poloidal mode numbers $\ell = 1$, 10, and 25. In the plots the regions above the curves are stable while those below are unstable. Clearly, the $\ell = 1$ mode requires the largest cold electron concentration for stability.

In Fig. 2 we plot the fraction N_c/N_h at marginal stability, obtained from the local stability analysis and Eq. (12), as a function of q_o for $\beta = 0.1$, $\ell = 10$, and $R_c/R = 20$. At small precessional frequency, $q \ll 1$, the critical fraction $N_c/N_h \approx 4/q$ is substantially larger than the result of the local stability analysis $N_c/N_h \simeq 4/\ell q$ for $\ell > 1$. At large precessional frequency, $q \gg 1$, the critical fraction for stability $N_c/N_h \approx 2\, q^{-1/2}$. By

comparison, the local stability analysis obtains the critical fraction $N_c/N_h \approx 2/\beta$ for $q \approx \ell > 1$ and for larger q, $q \gg \ell > 1$, $N_c/N_h \approx 2(q/\ell)^{-1/2}$. Hence, the critical fraction of cold to hot electrons for stability of high frequency modes may be substantially smaller than local theory indicates.

III. FINITE ION TEMPERATURE FLUTE-INTERCHANGE MODE

The stability of localized flute-interchange modes in a hot electron plasma has previously been considered for the case of a cold electron-ion background plasma.[3] In this section, we extend the analysis to include finite ion temperature effects; finite electron temperature effects of the background plasma are negligible.

To perform the analysis, we use a slab geometry with density and magnetic field gradients in the x direction, an unperturbed magnetic field $\underset{\sim}{B}_o = B_z(x)\hat{\underset{\sim}{z}}$, and a species dependent gravitational field $\underset{\sim}{g}_s = - g_s \hat{\underset{\sim}{x}}$ that simulates the curvature of $\underset{\sim}{B}_o$ as seen by the hot electrons and ions.

The plasma equilibrium satisfies conditions analogous to Eq. (1)

$$\frac{d}{dx}\left(N_h T_h + N_i T_i + \frac{B_z^2}{8\pi}\right) = - N_h m_e g_e - N_h M_i g_i \quad , \tag{13a}$$

$$N_i = N_h + N_c \quad , \tag{13b}$$

where $N_i = N_o(x)$, $N_c = (1 - \alpha)N_o(x)$, and $N_h = \alpha N_o(x)$. The magnitude of $\underset{\sim}{g}_s$ is chosen as $g_s = T_s/M_s R_c$, R_c being the radius of curvature of the external field and T_s being the temperature of species s (s = hot electrons, ions). Perturbations of the equilibrium are of the form of Eq. (3) with $\phi(\underset{\sim}{r})$ replaced by $\phi(\underset{\sim}{x}) = \phi(x)\exp i(ky - \omega t)$, ... , where $\underset{\sim}{k} = k\hat{y}$.

To obtain the set of local Maxwell equations, we use the results of Ref. 9. In the local approximation, one assumes that

$$k^{-1}\,\frac{d\ell og\ \phi}{dx} \quad , \quad k^{-1}\,\frac{d\ell og\ a}{dx} << 1$$

and hence we obtain the system of algebraic equations

$$(1 + \varepsilon_{11})\phi - i\varepsilon_{12}a = 0 \quad , \tag{14a}$$

$$i\varepsilon_{12}\phi + \left(1 - \frac{k^2c^2}{\omega^2} + \varepsilon_{22}\right)a = 0 \quad , \tag{14b}$$

where

$$\varepsilon_{11} = \frac{4\pi}{k^2\omega}\sum_s \frac{q_s^2}{M_s}\int d\underset{\sim}{v}\left[- M_s\omega\,\frac{\partial f_s}{\partial H} + D^{(s)}\sum_N \frac{\omega^2 J_N^2}{\tilde{\omega}_s - N\Omega_s}\right.$$

$$\left. + \frac{1}{k}\,\frac{d}{dx}\left(D^{(s)}\sum_N \frac{N^2\ \omega\Omega_s\ J_N^2}{\tilde{\omega}_s - N\Omega_s}\right)\right] \quad , \tag{15a}$$

$$\varepsilon_{12} = \frac{4\pi}{k^2\omega}\sum_s \frac{q_s^2}{M_s}\int d\underset{\sim}{v}\left[D^{(s)}\sum_N \frac{\omega z_s\ \Omega_s\ J_N\ J_N'}{\tilde{\omega}_s - N\Omega_s}\right.$$

$$\left. + \frac{1}{k}\,\frac{d}{dx}\left(D^{(s)}\sum_N \frac{N z_s\ \omega\Omega_s\ J_N J_N'}{\tilde{\omega}_s - N\Omega_s}\right)\right] \quad , \tag{15b}$$

$$\varepsilon_{22} = \frac{4\pi}{k^2\omega}\sum_s \frac{q_s^2}{M_s}\int d\underset{\sim}{v}\left[D^{(s)}\sum_N \frac{z_s^2\,\Omega_s^2\,J_N'^2}{\tilde{\omega}_s - N\Omega_s}\right.$$

$$\left. + \frac{1}{k}\frac{d}{dx}\left(D^{(s)}\sum_N \frac{N\,z_s^2\,\Omega_s^2\,J_N'^2}{\tilde{\omega}_s - N\Omega_s}\right)\right] \quad , \tag{15c}$$

in which $D^{(s)} = M_s\,\partial f_s/\partial H + (k/\omega\Omega_s)\partial f_s/\partial x$, $f_s = f_s(H_s,x,v_\parallel)$, $z_s = kv_\perp/\Omega_s$, $J_N = J_N(z_s)$, $J_N' = dJ_N/dz_s$, $\tilde{\omega}_s = \omega - \omega_{d_s}$, $\omega_{d_s} = (kv_\perp^2/2\Omega_s)(d\ell og\ B_z/dx) + (kg_s/\Omega_s)$, and $H_s = M_s v^2/2 + M_s g_s x$. [In Eq. (15), the summation over species includes the hot electrons, ions, and cold electrons.] The local dispersion relation results from the condition that Eq. (14) have a non-trivial solution.

The hot electron matrix elements in Eq. (15) typically contain the resonant denominators $\tilde{\omega}_e = \omega - \omega_{d_e}$. To readily evaluate these terms, we choose a delta function distribution for the hot electrons

$$f_h(H_h,x,v_\parallel) = \frac{\alpha\,N_o(x)\,\delta}{2\pi\,v_{oh}}\left(\frac{H_h - m_e v^2/2}{H_{oh}} - 1\right)F_h(v_\parallel) \quad , \tag{16}$$

where $H_{oh} = m_e v_{oh}^2/2 = T_h$ and $\int dv\,F_h(v_\parallel) = 1$. The ion matrix elements in Eq. (15) may be evaluated similiarly. For frequencies large compared to the

ion precessional frequency, $\omega >> \omega_{d_i}$, the $v_\parallel$ dependence of f_i is not crucial. Hence, we choose for the ion distribution

$$f_i(\mathcal{H}_i,x,v_\parallel) = \frac{N_o(x)}{2\pi\, v_{oi}^2}\, \delta\left(\frac{\mathcal{H}_i - M_i v_\parallel^2/2}{\mathcal{H}_{oi}} - 1\right) F_i(v_\parallel) \quad , \tag{17}$$

with $\mathcal{H}_{oi} = M_i v_{oi}^2/2 = T_i$ and $\int dv_\parallel F_i(v_\parallel)$. We note that in the present calculation, the results are independent of the form of $F_{h,i}(v_\parallel)$ in Eqs. (16) and (17). The cold electron response may be obtained from Eq. (15) by choosing a distribution $f_e = F_e(\mathcal{H}_e,x,v_\parallel)$ such that $\int d\underset{\sim}{v}\, v_\perp^2 F_e = 0$.

Using Eqs. (16) and (17) in Eq. (15), we obtain from Eq. (14) the local dispersion relation for waves $\omega << \Omega_i$

$$D_{es}\, D_{em} + (CT)^2 = 0 \quad , \tag{18}$$

where

$$D_{es} = \frac{\omega_{pi}^2}{\Omega_i^2}\left[1 - \frac{\omega_i}{\tilde{\omega}_i}(1+\beta) + \frac{\omega_{b_i}^2}{\tilde{\omega}_i^2}\right] + \frac{\delta\omega_{pi}^2}{\tilde{\omega}_i\Omega_i}\left(1 + \frac{\beta}{2}\frac{\omega - \omega_{g_i}}{\tilde{\omega}_i}\right)$$

$$- \frac{(1-\alpha)\delta\omega_{pi}^2}{\omega\Omega_i}\left(1 + \frac{\beta}{2}\right) + \frac{\alpha}{k^2\lambda_e^2}\frac{\omega_e}{\tilde{\omega}_e}\left(1 + \frac{\beta}{2}\frac{\omega - \omega_{g_e}}{\tilde{\omega}_e}\right) \quad , \tag{19a}$$

$$D_{em} = 1 + \frac{\beta_h}{2}\left[\frac{2(\omega - \omega_{g_e}) - \omega_e}{\tilde{\omega}_e} + \frac{\omega_{b_e}(\omega - \omega_{g_e})}{\tilde{\omega}_e^2}\right]$$

$$+ \frac{\beta_i}{2}\left[\frac{2(\omega - \omega_{g_i}) - \omega_i}{\tilde{\omega}_i} + \frac{\omega_{b_i}(\omega - \omega_{g_i})}{\omega_i^2}\right] \quad , \tag{19b}$$

$$CT = \left(\frac{\beta_h}{2k^2\lambda_e^2}\right)^{1/2}\left[\frac{\omega_e}{\tilde{\omega}_e}\left(1 + \frac{\beta}{2}\frac{\omega - \omega_{g_e}}{\tilde{\omega}_e}\right) - \frac{\omega_{b_e}}{\tilde{\omega}_e}\right]$$

$$- \left(\frac{\beta_i}{2k^2\lambda_i^2}\right)^{1/2}\left[\frac{\omega_i}{\tilde{\omega}_i}\left(1 + \frac{\beta}{2}\frac{\omega - \omega_{g_i}}{\tilde{\omega}_i}\right) - \frac{\omega_{b_i}}{\tilde{\omega}_i}\right] \quad , \tag{19c}$$

with $\omega_s = (kT_s/M_s\Omega_s)(d\ell og\ N_o/dx)$, $\omega_{b_s} = (kT_s/M_s\Omega_s)(d\ell og\ B_z/dx)$, $\delta = (kR_p^{-1})$, $\tilde{\omega}_s = \omega - \omega_{d_s}$, $\omega_{d_s} = \omega_{b_s} + \omega_{g_s}$, $\omega_{g_s} = (kg_s/\Omega_s)$, $\beta = \beta_h + \beta_i$, $\beta_h = 8\pi\alpha N_o T_h/B_z^2$, $\beta_i = 8\pi N_o T_i/B_z^2$, and $\lambda_s = (4\pi N_o e^2/T_s)^{-1/2}$. For higher frequency modes, $\omega \gtrsim \Omega_i$, the finite ion temperature modifications are negligible and the results of Ref. 3 are obtained.

The low-frequency dispersion relation is simplified by the assumption $\omega \gg \omega_{d_i}$. Further simplification, with no qualitative change in the results, is obtained by considering the moderate β regime $1 > \beta_h > \beta_i$. Employing these simplifications, we obtain the dispersion relation

$$(\omega - \omega_{g_e})(\omega - \omega_i) - \alpha\delta\Omega_i\omega_{g_e} + \delta\Omega_i\omega_{g_i}\frac{\tilde{\omega}_e}{\omega} = 0 \quad . \tag{20}$$

In the limit $\omega \approx \omega_{d_e} >> \omega_i$, Eq. (20) reduces to the results of Ref. 3. In the opposite limit (though not appropriate for localized modes in hot electron plasmas) $\omega \approx \omega_i >> \omega_{d_e}$, Eq. (20) yields the result of Pearlstein and Krall.[8]

Solutions of Eq. (20) may also be found in the frequency range $\omega_{d_e} >> \omega, \omega_i$. In this case, we obtain the root

$$\omega = \frac{\delta\Omega_i(b_i - \alpha)}{2} \pm \sqrt{\left[\frac{\delta\Omega_i(b_i - \alpha)}{2}\right]^2 + \delta\Omega_i \frac{T_i}{T_h} \omega_{d_e}} \quad , \tag{21}$$

where $b_i = k^2 T_i / M_i \Omega_i^2$. In the presence of "bad" curvature $R_p/R_c > 0$, instability may result. However, the hot-electron self-field terms do not cancel; the hot-electron ∇B_z drift in the drifing term may reverse the sign of ω_{d_e} and stabilize the mode. The character of the additional stabilizing term in Eq. (21) depends upon the relative magnitude of α and b_i. Note that the hot-electron stabilizing effect, obtained for $\alpha > b_i$, may be offset by a corresponding loss of cold-plasma stabilization of the hot-electron curvature-driven flute-interchange mode.

Finally, we point out that the "rigid" hot electron approximation, investigated by Nelson[5] in connection with Eq. (21) and employed in the MHD stability analysis of Nelson and Hedrick,[4] may lead to substantially more optimistic stability criteria than the full stability analysis would indicate.

In kinetic theory, the "rigid" hot electron model sets $\alpha = 0$ but retains finite β_h. Hence, in this approximation Eq. (21) is replaced by

$$\omega = \frac{\delta\Omega_i b_i}{2} \pm \sqrt{\left(\frac{\delta\Omega_i b_i}{2}\right)^2 + \delta\Omega_i \frac{T_i}{T_h} \omega_{d_e}} \quad . \tag{22}$$

Comparing Eqs. (21) and (22), we observe that for $b_i - \alpha < b_i$ the "rigid" hot electron model may yield overly optimistic stability criteria. The "rigid" hot electron approximation is not generally a good approximation of the complete analysis.[10]

ACKNOWLEDGMENT

This work was supported by Department of Energy, Contract DE-AT03-76ET51011.

REFERENCES

1. G. E. Guest, C. L. Hedrick, and D. B. Nelson, Phys. Fluids *18*, 871 (1975).

2. H. L. Berk, Phys. Fluids *19*, 1255 (1976).

3. R. R. Dominguez and H. L. Berk, Phys. Fluids *21*, 827 (1978).

4. D. B. Nelson and C. L. Hedrick, Nucl. Fusion *19*, 283 (1979).

5. D. B. Nelson, "Effect of Hot Electrons on Magnetohydrodynamic Modes in EBT," Oak Ridge National Laboratory Report ORNL/TM-6824 (1979).

6. R. R. Dominguez, Ph. D. thesis, University of California, Berkeley (1978).

7. M. N. Rosenbluth, N. A. Krall, and N. Rostoker, Nucl. Fusion Suppl. *Part I*, 143 (1962).

8. L. D. Pearlstein and N. A. Krall, Phys. Fluids *9*, 2231 (1966).

9. H. L. Berk and R. R. Dominguez, J. Plasma Phys. *18*, 31 (1977).

10. R. L. Miller, R. R. Dominguez, G. E. Guest, and T. Ohkawa, EBT Workshop, paper F-2, Oak Ridge, TN, 1979.

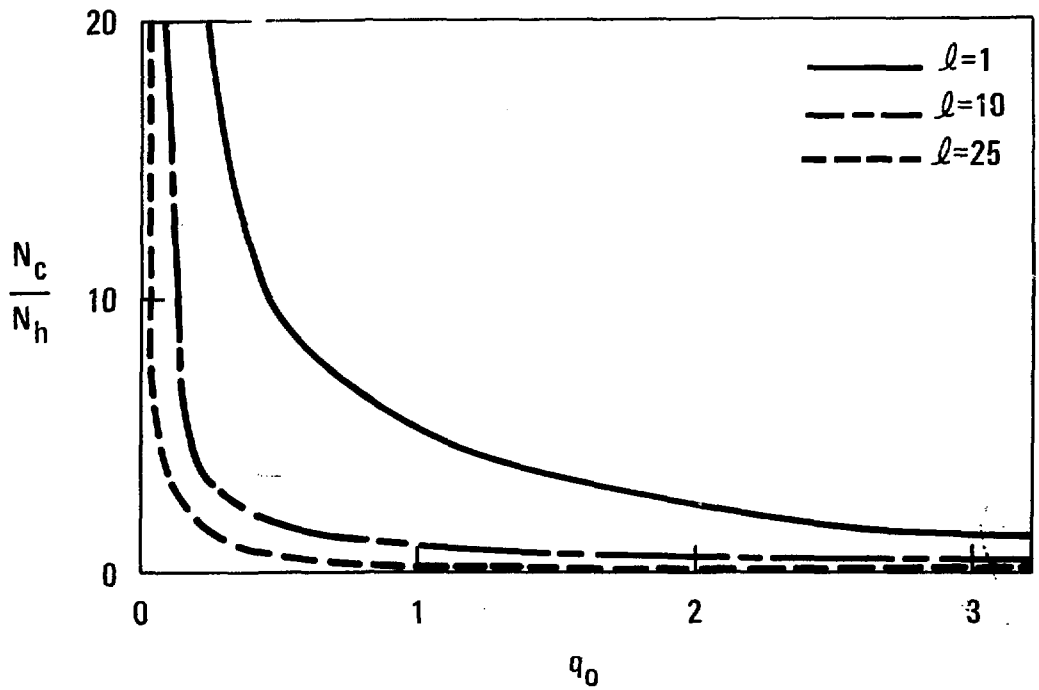

1. The critical value of the relative cold-electron density predicted by the non-local theory vs. the ratio of hot-electron precession frequency to the ion gyrofrequency for ℓ = 1, 10, and 25.

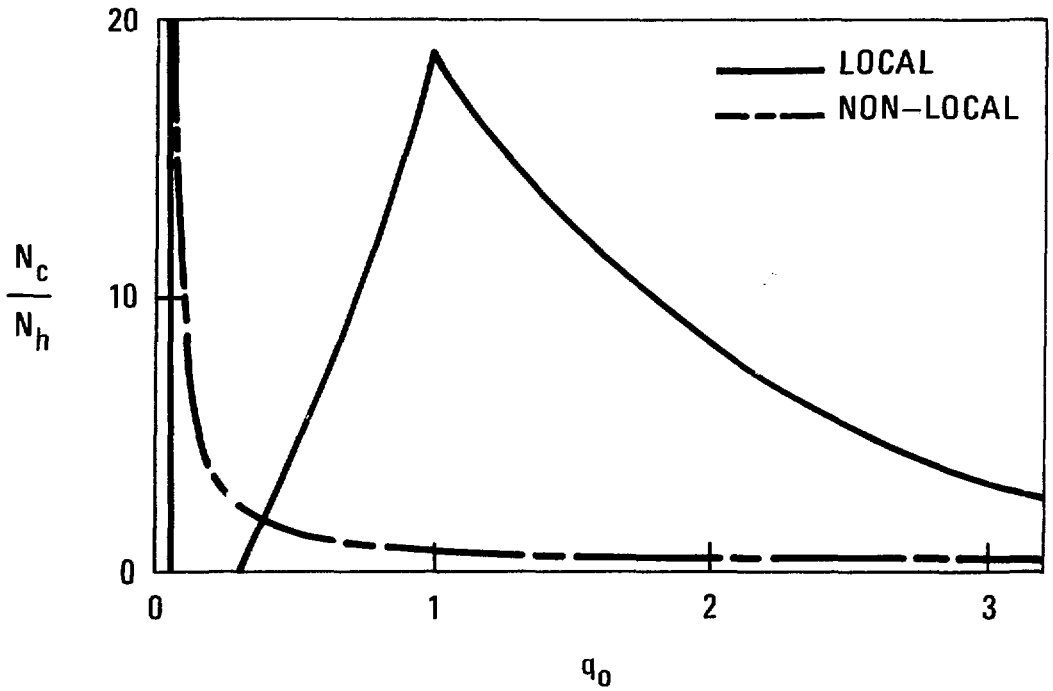

2. A comparison of the critical cold-electron density predicted by the localized theory and the corresponding values from the non-local theory.

DISCUSSION

V. K. TRIPATHI: How do the cold electrons stabilize the instability in the cylindrical model? What is the physics?

R. DOMINGUEZ: The flute-interchange mode is essentially electrostatic. Hence, the cold electron stabilization may be interpreted as a phase shift between the perturbed electrostatic potential and the electron density response; regions where local charge accumulation reinforce the electrostatic potential in the absence of cold electrons are effectively "shorted."

A. BOOZER: Could you summarize the dependence of your theory on dimensionless parameters like the electron precession to the ion cyclotron frequency?

R. DOMINGUEZ: For eigenmodes localized within the hot electron annular region, the amount of cold electron plasma necessary to stabilize the hot electron flute-interchange mode is a decreasing function of the hot electron precessional frequency when the precessional frequency is less than the ion cyclotron frequency. If the precessional frequency is comparable to or larger than the ion cyclotron frequency, the critical cold electron concentration has a more complicated nonmonotonic dependence on the precessional frequency (see Dominguez and Berk, Phys. Fluids paper).

Radially nonlocalized eigenmodes obtain simpler stability criteria. The sharp boundary cylindrical model predicts that the critical cold electron concentration for stability is a monotonically decreasing function of the hot electron precessional frequency.

H. SANUKI: Have you considered the case of diffused boundary condition for density? If you take into account a relativistic effect on hot electrons, what does the marginal curve look like?

R. DOMINGUEZ: The stability of the hot electron flute-interchange mode for the diffuse boundary model may be analyzed by use of the WKB method.

One finds that the localization of the eigenmode is possible for large poloidal mode numbers. The resulting dispersion relation is given by the local dispersion relation of Dominguez and Berk.

The relativistic effects of the hot electrons are minimal. The reason is that instability of the hot electron flute-interchange mode is driven solely by "bed" curvature and is independent of kinematics. The dominant relativistic effects, associated with the relativistic mass, are corrections of less than 5% in the stability boundaries.

N. A. UCKAN: As you indicated, while comparing slab and cylindrical models, the slab model overestimates n_{cold}/n_{hot} for large q_o values (i.e., for large ω_{de}/ω_{ci}). However, for small q_o values ($q_o \lesssim 0.5$ probably $q_o \sim 0.1$), which is expected to be valid for future devices, the slab model underestimates stability boundary for n_{cold}/n_{hot}. Is this a right observation and what are your comments about the q_o range for future experiments and a reactor?

R. DOMINGUEZ: In the cylindrical sharp boundary model, cold plasma stabilization of the hot electron flute-interchange mode results for relative cold electron concentrations

$$\frac{n_c}{n_h} = \frac{n_{cold}}{n_{hot}} > \frac{2}{mq_o}\left[1 + (1 + mq_o)^{1/2}\right]$$

where m is the poloidal mode number. For $mq_o \ll 1$, the critical fraction for stability $n_c/n_h \approx 4/mq_o$ may substantially exceed the slab model result $n_c/n_h \approx 4/m^2q_o$ for higher order modes.

MACROSCOPIC STABILITY OF THE HOT ELECTRON ANNULUS IN EBT*

R. L. Miller, R. R. Dominguez, G. E. Guest, and T. Ohkawa

General Atomic Company
San Diego, California 92138

ABSTRACT

One stability question concerning the ELMO Bumpy Torus (EBT) which has received little attention is the macroscopic stability of the hot electron annulus. Previous macroscopic stability studies have concentrated on localized modes. Kinetic theory may be used to determine how "hard" (rigid) or "soft" (perturbable) the rings are for idealized perturbations in a slab geometry. However in this macroscopic analysis, we employ a realistic geometry, a "bumpy" cylinder with a 2:1 magnetic mirror ratio, and we make the pessimistic assumption that the rings are "soft." We use guiding center theory (with $p_\perp >> p_\parallel$) and study the second variation in the plasma energy (δW) using a finite element representation to identify the least stable mode for the hot electron ring. Stability boundaries will be established by considering a wide range of anisotropic high-β equilibrium models of the ELMO rings.

*Work supported by Department of Energy, Contract DE-AT03-76ET-51011.

The hot electron ring is observed to be stable in present EBT experiments with sufficient ambient gas pressure but this stability is not fully understood. A more complete understanding is desirable to provide confidence of similar stable behavior in EBT-P and reactor-size devices. The ring stability problem has been explored theoretically using kinetic theory, two fluid models and guiding center theory (see reviews of G. E. Guest and D. Spong at this workshop). Perhaps the most successful approaches have been those which stress the stabilization due to cold plasma[1,2]. However, these calculations have been performed only in slab geometry or in an idealized cylindrical geometry and therefore are expected to accurately apply only for short wavelength modes. It is therefore of interest to examine the guiding center theory where it is possible to provide a correct treatment of the geometry and to study long wavelength modes($m \sim 1$).

In the present study, we use guiding center theory and perform a numerical 2-D macroscopic analysis of ring stability for all poloidal mode numbers. Past fluid studies of ring stability have focused upon short wavelength interchange or ballooning modes where a one-dimensional analysis is sufficient. Major shortcomings of this guiding center model are the neglect of two-fluid effects (cold plasma stabilization), and the neglect of kinetic effects (e.g., finite Larmor radius stabilization). Thus we see that none of these approaches (kinetic, two fluid, guiding center theory) can include enough of the relevant physical effects to provide a complete stability picture,

but each can provide insight not easy to attain (and in some cases not possible to attain) from the other two approaches.

The approach used here is quite analagous to the isotropic fluid stability studies now routinely performed in the tokamak program using the stability codes PEST, ERATO, and GATO. In fact, much of the computer coding used in this study was obtained quite painlessly through modification of the GA stability code, GATO.

Briefly, we begin by calculating an axisymmetric numerical equilibrium in a "bumpy" cylinder with a 2:1 magnetic mirror ratio. The equilibrium solution, which is defined on an r-z mesh (see viewgraph 2) is then mapped on to an orthogonal ψ-χ mesh where ψ labels a field line and χ measures the distance along a field line. In this coordinate system, the second variation of the plasma and field energy (δW), as derived by Kruskal and Oberman[3], is evaluated in terms of finite elements used to represent the plasma displacement. Eigenvalues and eigenvectors can then be determined numerically.

The equilibrium problem is discussed in viewgraph 2, where a comparison is made between the tokamak and the EBT equilibrium formulation. In viewgraphs 3 through 8 a representative equilibrium solution is presented. The pressure model is one used by Guest, Hedrick, and Nelson[4]. The geometry is that of EBT-I with the z dimension between mirror coils equal to 40 cm and a mirror ratio of 2. The hot electron ring is approximately 6 cm wide and 10 cm long. In viewgraph 4, the magnetic field lines are shown in the r-z plane, while in viewgraph 5 the constant $|B|$ contours show the minimum B configuration created by the ring. Viewgraph 6 shows a radial plot in the

midplane of $p_\perp$ (Δ) and $p_\parallel$ (o); both are zero outside of the ring. Viewgraph 7 is another radial plot in the midplane which shows the dipole current required for pressure balance, while viewgraph 8 shows the strong minimum B configuration created by this dipole current. The other curve in viewgraph 8 (□) shows the magnetic field when no hot electron ring is present.

The stability of equilibria such as the one just shown may be assessed using the energy principle derived by Kruskal and Oberman[3] which is shown in viewgraph 9. A Fourier analysis has been performed in the θ direction and hence the integration is only over ψ and χ and a poloidal mode number, m, has appeared. The most unstable or least stable perturbation in guiding center theory requires $\vec{\xi} \cdot \vec{B} = 0$, so ξ_χ does not appear in δW. The first two terms in the equation for δW with coefficient σ are the components of $Q_\perp^2$, the perturbed magnetic field perpendicular to $\vec{B}$, while the third term with coefficient τ [$= (1/\mu_0) + (1/B)(\partial p_\perp/\partial B)$] is $Q_\parallel^2$, the perturbed magnetic field parallel to $\vec{B}$. δW_k is a small stabilizing kinetic term involving the distribution function and will henceforth be ignored. Thus we evaluate a sufficient but not necessary criteria for stability. In viewgraph 10, the expression for δW is rewritten by completing a square so that each term has a definite sign. Then in viewgraph 11, each of the potentially destabilizing terms is examined for both the inner and outer regions of the ring. Numerically it is found that the primary destabilizing term is the curvature term in the outer part of the ring.

We now show numerical results of the stability analysis beginning with viewgraph 12 where the finite elements are displayed. Effectively, the values of X and Y at the center of each rectangle are determined by

the minimization. Viewgraphs 13 through 19 present the most unstable $m = 1$ eigenmode and the most unstable $m = 5$ eigenmode for the $\beta_\perp = .37$ equilibrium displayed in viewgraphs 3 through 8. Viewgraph 13 shows the eigenvector of the $m = 1$ mode in the r-z plane. It is evident that the displacement is largest in the region of the ring and that $\vec{\xi} \cdot \vec{B} = 0$. The same mode is shown in the r-θ plane at the midplane in viewgraph 14. Here the $m = 1$ character of the mode is obvious and a large poloidal rotation is observed. This poloidal rotation can be partially understood by referring back to the equation for δW in viewgraph 9. The curvature term is negative only in the outer portion of the ring and stabilizing elsewhere. Hence the mode will tend to have a large X only in the outer ring. However, a conducting wall is assumed at the plasma boundary and therefore $X = 0$ at the edge of the plasma; also X should be small in the inner region of the ring where the curvature term is stabilizing. These two conditions imply a large $(\partial X/\partial\psi)$ in the ring region which is verified numerically in viewgraph 16 for the $m = 1$ mode and in viewgraph 17 for the $m = 5$ mode. As mentioned earlier, $Q_{\parallel} \propto [(\partial X/\partial\psi) + (mY)]$ so Y must tend to compensate for $(\partial X/\partial\psi)$ to avoid a large stabilizing force due to field line distortion, $Q_{\parallel}^2$. This compensating ξ_θ (Y) creates the poloidal rotation seen in viewgraph 14. The same effect can also be seen for the $m = 5$ mode (viewgraph 15), but here ξ_χ (X) is larger relative to ξ_θ as would be expected from the $Q_{\parallel} \sim 0$ argument since m is now larger.

Viewgraphs 16 and 17 show ξ_ψ versus ψ at the midplane for $m = 1$ and $m = 5$ respectively, and a comparison of the two shows that ξ_ψ is more localized in the $m = 5$ case. Viewgraphs 18 and 19 show ξ_ψ versus χ on a

field line passing through the ring for m = 1 and m = 5 respectively. Here ξ_ψ is strongly localized in both cases and little difference can be discerned between the two.

Viewgraph 20 displays X versus χ (m = 5 mode) for a series of equilibria with increasing $\beta_\perp$. For a pure interchange mode $Q_\perp = 0$, and hence $(\partial X/\partial \chi) = 0$. Thus the variation of X with respect to χ shown in viewgraph 20 illustrates the deviation of these modes from pure interchange through a ballooning effect which increases with increasing $\beta_\perp$.

Viewgraph 21 summarizes the stability results obtained in this study to date. (γ^2/ω_A^2) is plotted versus $\beta_\perp$ for m = 1, 5, 10, and 100. ω_A is the Alfven frequency defined by $\omega_A = (v_A/40\ \text{cm})$, and the magnetic field strength is taken to be the value on axis at the midplane. Growth rates do not continue to increase appreciably as m exceeds 100.

Conclusions of the study are presented in viewgraph 22. The scope of this work could be extended by considering variations on the length and width of the ring, different anisotropic pressure profiles, finite background pressure, etc. but it is not anticipated that the basic conclusions presented here would be altered by such extensions.

REFERENCES

1. Guest, G. E. and Harris, E. G., Phys. Rev. Lett. *27*, 1500 (1971).

2. Dominguez, R. R. and H. L. Berk, Phys. Fluids *21*, 827 (1978).

3. Kruskal, M. D. and Oberman, D. R., Phys. Fluids *1*, 275 (1958).

4. Hedrick, C. L., Guest, G. E., and Nelson, D. B., ORNL-TM-4076 (1972).

- MOTIVATION
  - TREAT GEOMETRY CORRECTLY
  - STUDY GLOBAL MODES ($m \sim 1$)
  - ESTABLISHES WHAT STABILIZATION IS REQUIRED FROM TWO-FLUID AND/OR KINETIC EFFECTS

- APPROACH (STRONG ANALOGY WITH TOKAMAK PROGRAM)
  - NUMERICAL EQUILIBRIA (AXISYMMETRIC)
  - MAP TO ORTHOGONAL COORDINATES (ψ, χ, ϕ)
  - USE FINITE ELEMENT REPRESENTATION TO EVALUATE $E^{(2)}$ (δW)

1. Macroscopic stability of the hot electron annulus in EBT guiding center theory ($P_\perp >> P_\parallel$) -- motivation and approach.

	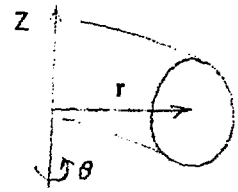
SYMMETRIC IN θ	SYMMETRIC IN θ
$\vec{B} = \nabla\psi \times \nabla\theta$	$\vec{B} = f\nabla\theta + \nabla\psi \times \nabla\theta$
ψ LABELS FIELD LINE	ψ LABELS POLOIDAL FIELD LINE
$2\pi\psi$ IS Z FLUX	$2\pi\psi$ IS POLOIDAL FLUX
$\vec{J} \times \vec{B} = \nabla \cdot \overleftrightarrow{P}$	$\vec{J} \times \vec{B} = \nabla P$
$\Delta^*\psi = -\mu_0 r J_\theta$	$\Delta^*\psi = -\mu_0 r J_\theta$
$\mu_0 r J_\theta = \sigma^{-1}\left[\nabla\sigma\cdot\nabla\psi + r^2 \frac{\partial P_\parallel}{\partial\psi}\right]$ $\sigma = \frac{1}{\mu_0} + \frac{P_\perp - P_\parallel}{B^2}$	$\mu_0 r J_\theta = r^2 \mu_0 \frac{\partial P}{\partial\psi} + f \frac{f}{\partial\psi}$
$J \cdot B = 0$	$J \cdot B \sim J_\theta f/r$
$P_\parallel(B,\psi)$, $P_\perp(B,\psi)$, $P(\psi)$	$P(\psi)$, $f(\psi)$
ELLIPTIC IF $\sigma\left(\frac{1}{\mu_0} + B^{-1}\frac{\partial P_\perp}{\partial B}\right) > 0$	ALWAYS ELLIPTIC

2. Analogy between the tokamak and EBT equilibrium formulation.

MAGNETIC FIELD (TESLA)

$B = 1.4/0.7$

MIRROR RATIO = 2

BETA

$$\beta_{\perp} = \frac{2\mu_0 P_{\perp,MAX}}{B^2_{MIDPLANE}} = .37$$

$$\beta_{PLASMA} = 0$$

CURRENT (AMPERES)

COIL CURRENT	$= 3.5 \times 10^5$
TOTAL e^- RING CURRENT	$= -2.3 \times 10^3$
POSITIVE e^- RING CURRENT	$= 1.3 \times 10^4$
NEGATIVE e^- RING CURRENT	$= -1.56 \times 10^4$

PRESSURE MODEL[1]

$$P_{\perp}(\psi,B) = \frac{s}{2}\, g(\psi)\, (B_c^2 - B^2)$$

$$P_{\parallel}(\psi,B) = \frac{s}{2}\, g(\psi)\, (B - B_c)^2$$

3. Representative equilibrium solution.

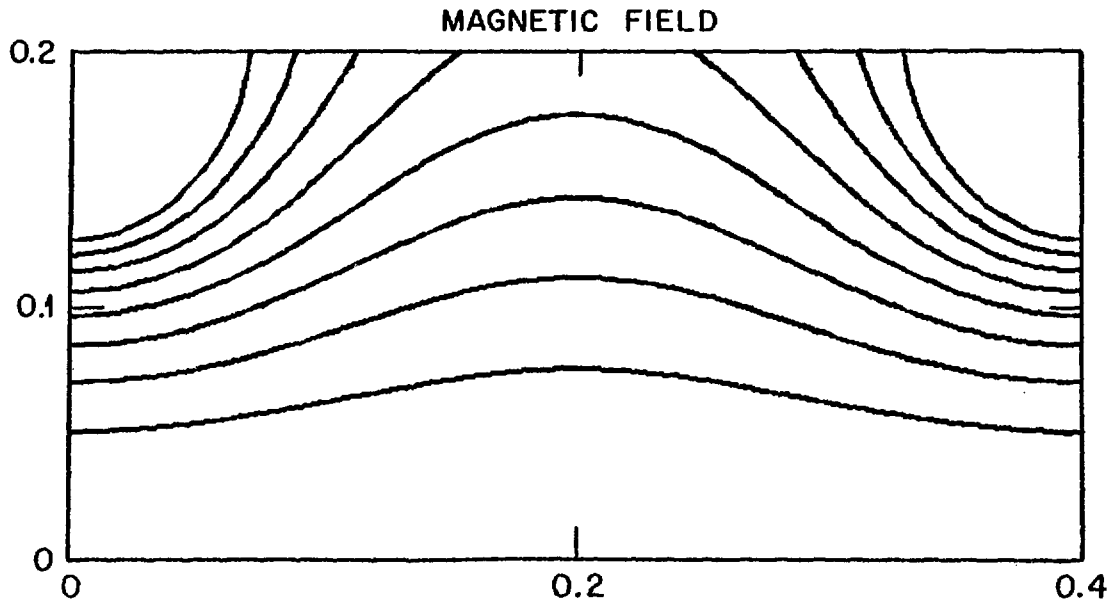

4. Magnetic field lines in (r-z) plane for EBT-I geometry.

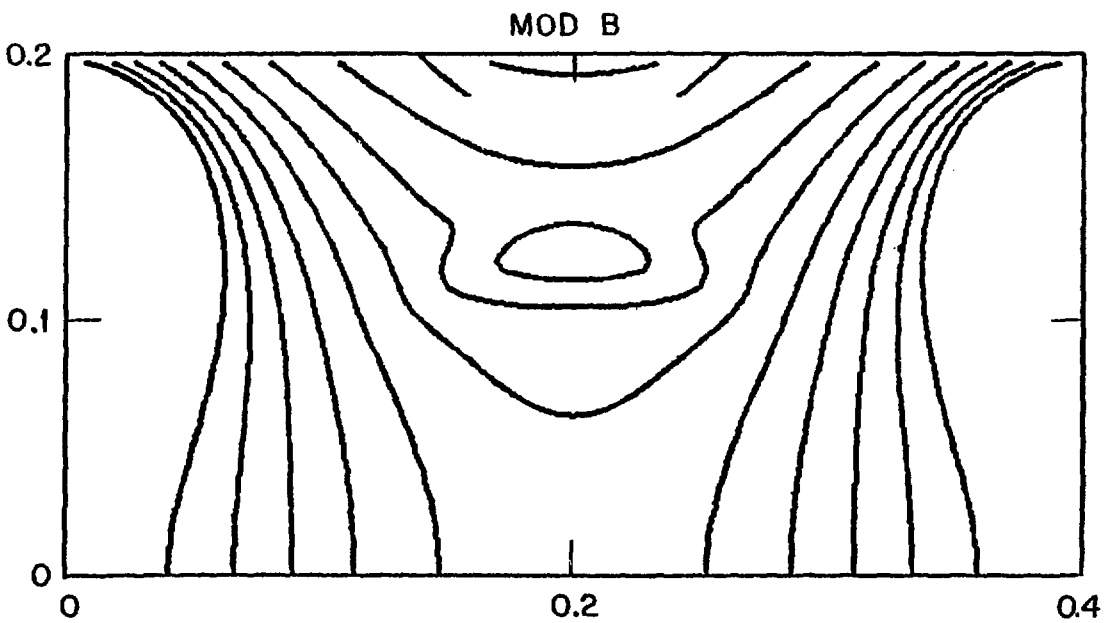

5. Constant |B| contours (of Figure/Viewgraph 4) show the minimum B configuration created by the ring.

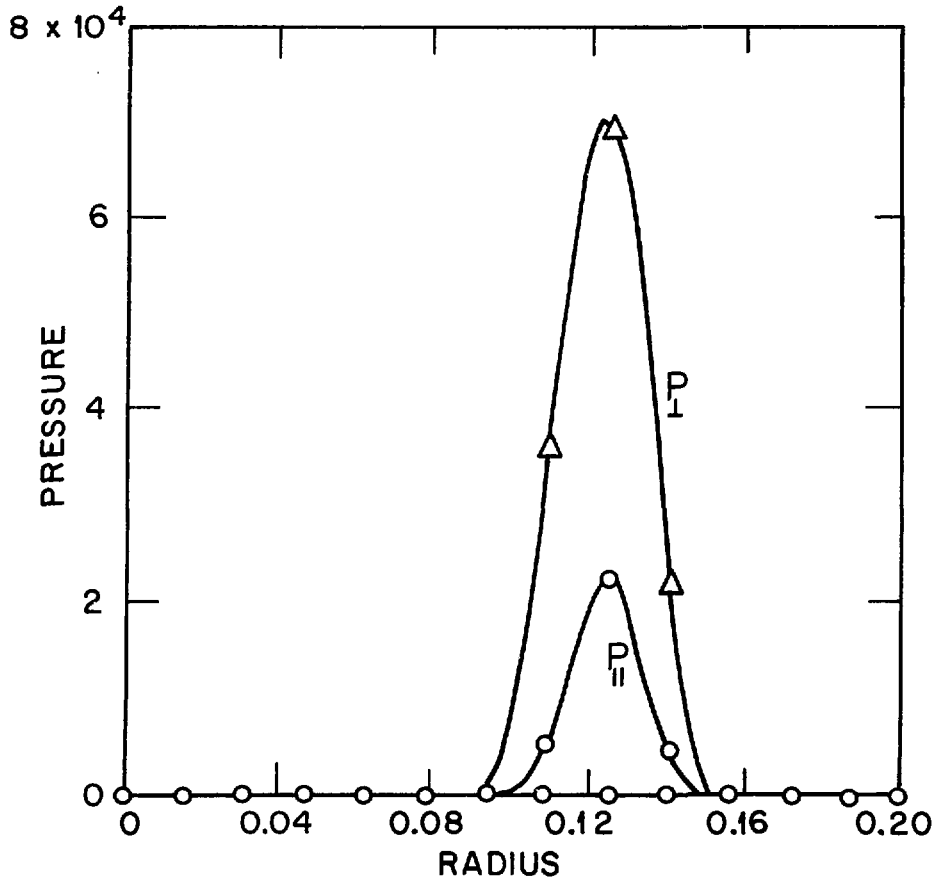

6. Radial variation of $P_{\perp}$ and $P_{\parallel}$ in the midplane.

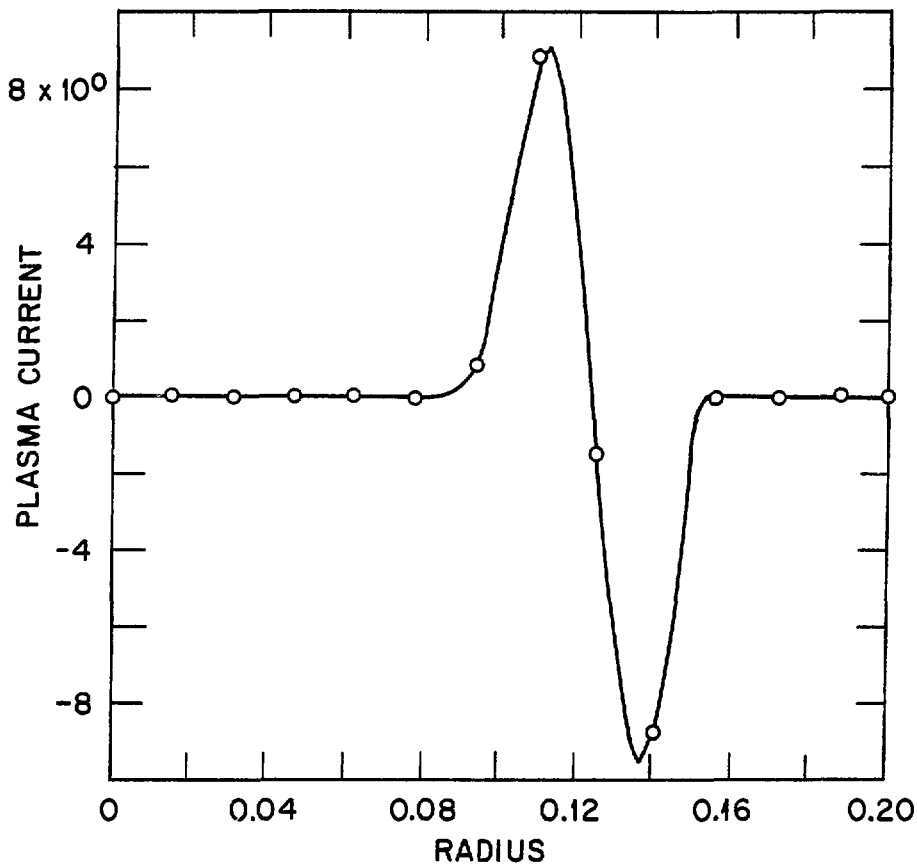

7. Radial variation of the dipole current required for pressure balance in the midplane.

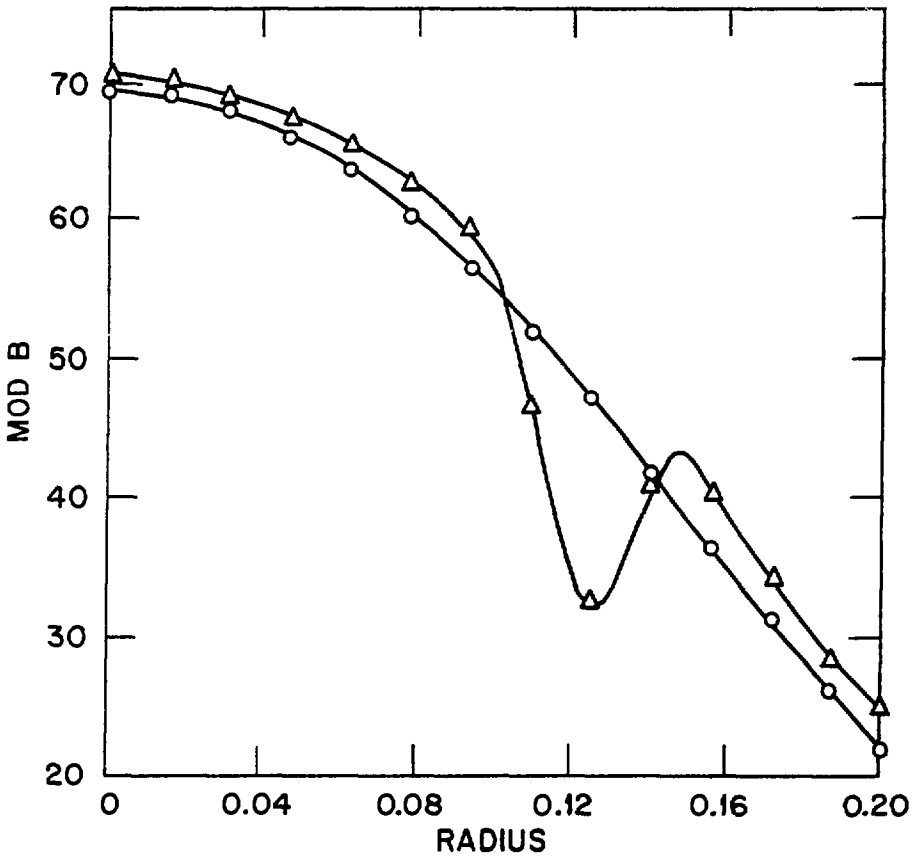

8. Radial variation of magnetic field in the midplane with (Δ) and without (0) hot electron ring.

$$\delta W = \frac{\pi}{2}\int \mathcal{J}\, d\psi\, dx \left\{ \sigma\left[\frac{1}{rB\mathcal{J}}\frac{\partial X}{\partial x}\right]^2 + \sigma\left[\frac{r}{\mathcal{J}}\frac{\partial Y}{\partial x}\right]^2 + \tau B^2\left[\frac{\partial X}{\partial \psi} + mY\right]^2 + 2\left[\frac{\partial X}{\partial \psi} + mY\right] X\,\frac{P_\perp}{\psi} - \left[\frac{\kappa}{rB}\frac{\partial P_\parallel}{\partial \psi} + \frac{\partial \ln B}{\partial \psi}\frac{\partial P_\perp}{\partial \psi}\right] X^2 \right\} + \delta W_\kappa$$

$\mathcal{J}$ IS JACOBIAN

x IS VARIABLE ALONG THE FIELD LINE

$$\xi_\psi = \frac{X}{rB}\cos m\theta$$

$$\xi_\theta = rY \sin m\theta$$

$$\kappa = \text{CURVATURE} = -rB\left[\frac{\partial \ln B}{\partial \psi} + \frac{\partial \ln \mathcal{J}}{\psi}\right]$$

<u>NOTE</u>:

$$\vec{\xi}\cdot\vec{B} = 0 \quad \text{AND} \quad \vec{J}\cdot\vec{B} = 0$$

9. Energy principle derived by Kruskal and Oberman.[3]

$$\delta W = \frac{\pi}{2}\int \mathcal{J}\, d\psi\, dx \left\{ \sigma\left[\frac{1}{rB\mathcal{J}}\ \frac{X}{\psi}\right]^2 + \sigma\left[\frac{r}{\mathcal{J}}\ \frac{\partial Y}{\partial x}\right]^2 \right.$$

$$+ \left[\left(\frac{\partial X}{\partial \psi} + mY\right) + \frac{X}{\tau B^2}\ \frac{P_\perp}{\psi}\right]^2 \tau B^2$$

$$\left. - \left[\frac{\kappa}{rB}\ \frac{\partial P_\parallel}{\partial \psi} + \frac{\partial \ln B}{\partial \psi}\ \frac{\partial P_\perp}{\partial \psi} + \frac{1}{\tau B^2}\left(\frac{\partial P_\perp}{\partial \psi}\right)^2\right] X^2 \right\}$$

10. Rewritten expression for δW in terms of squared quantities.

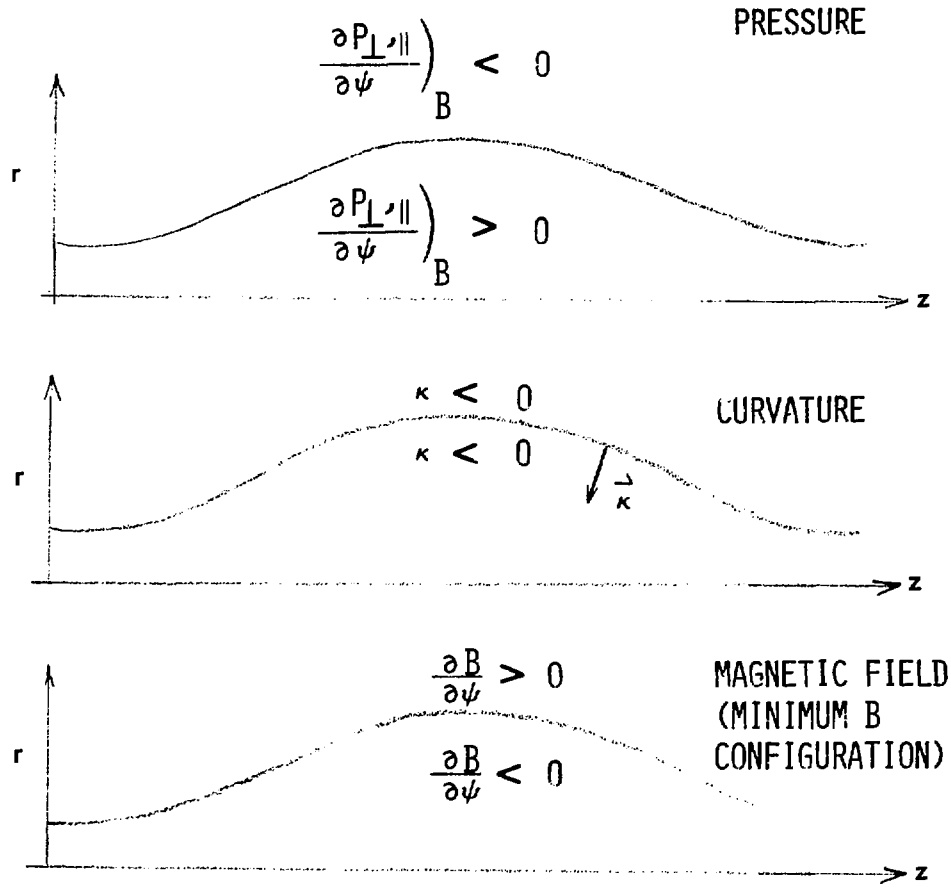

	OUTER RING	INNER RING
$-\frac{\kappa}{rB}\left.\frac{\partial P_{\parallel}}{\partial \psi}\right)_B$	DESTAB.	STAB.
$-\frac{\partial \ln B}{\partial \psi}\left.\frac{\partial P_{\perp}}{\partial \psi}\right)_B$	STAB.	STAB.
$-\frac{1}{\tau B^2}\left.\frac{P_{\perp}}{\partial \psi}\right)_B^2$	DESTAB.	DESTAB.

11. Potential destabilizing terms for both the inner and outer regions of the ring.

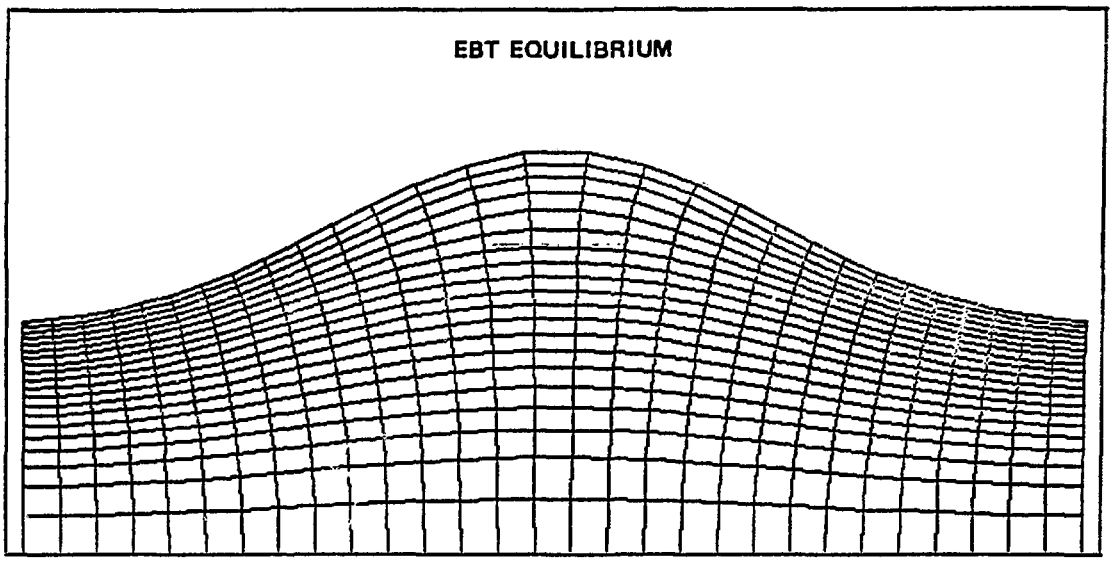

12. Numerical EBT equilibrium in orthogonalized (X,Y) space.

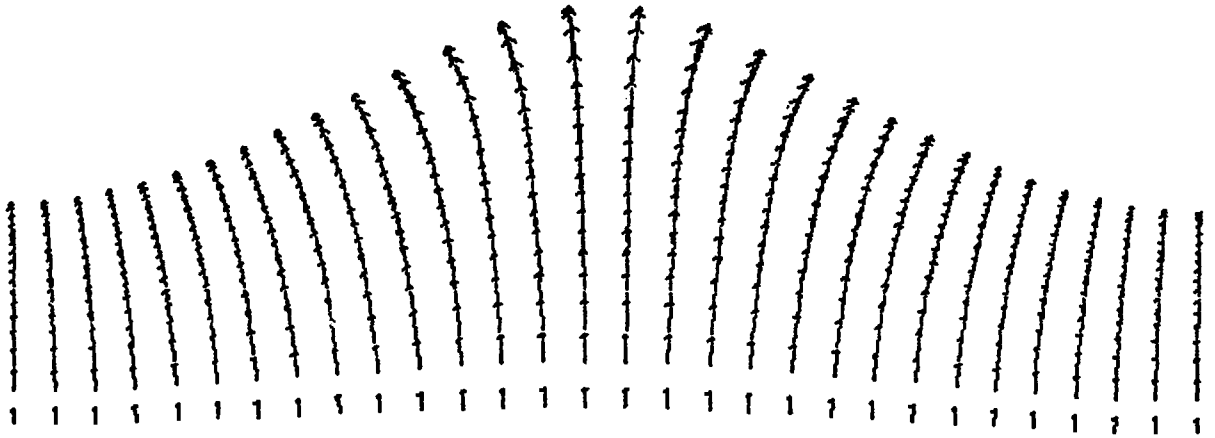

13. Eigenvector of the m=1 mode in r-z plane.

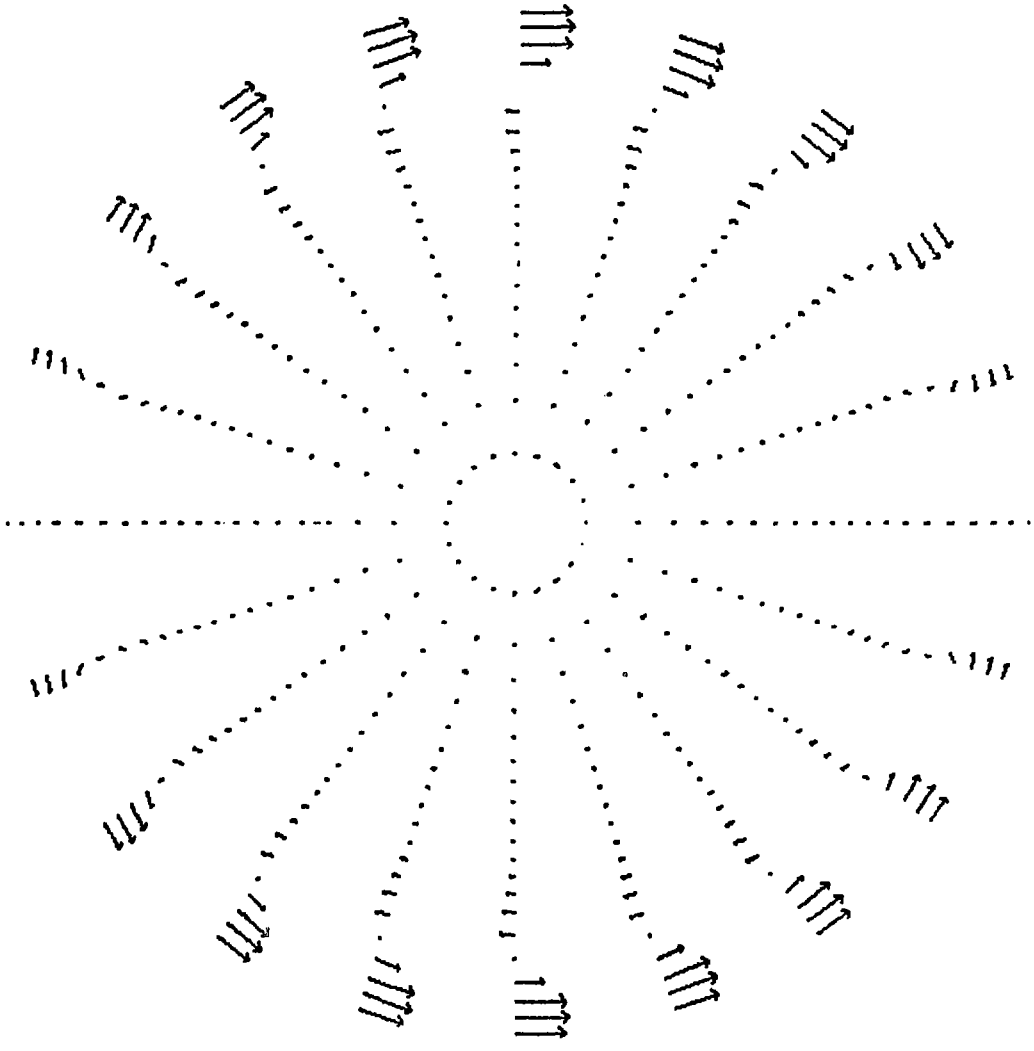

14. Eigenvector of the m=1 mode in r-θ plane at the midplane.

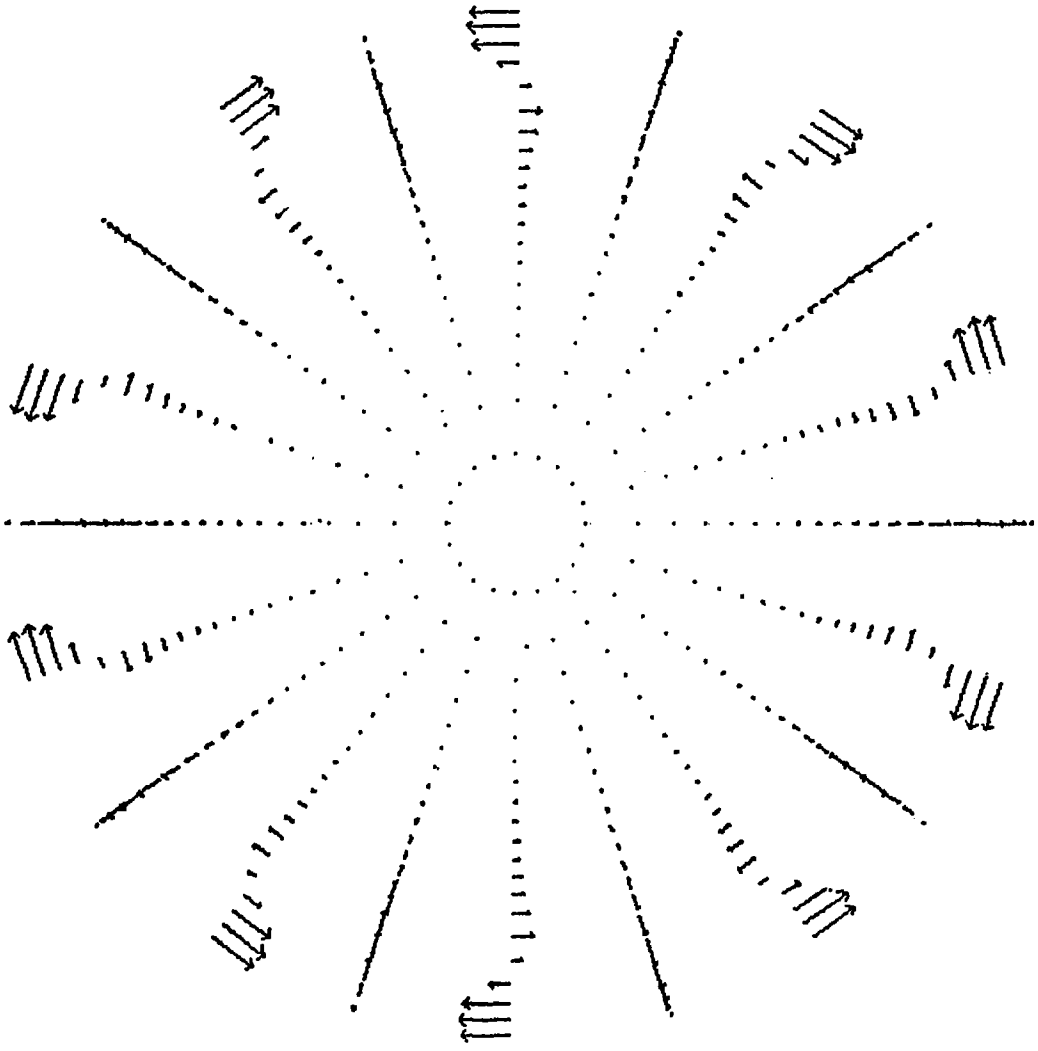

15. Eigenvector of the m=5 mode in r-θ plane at the midplane.

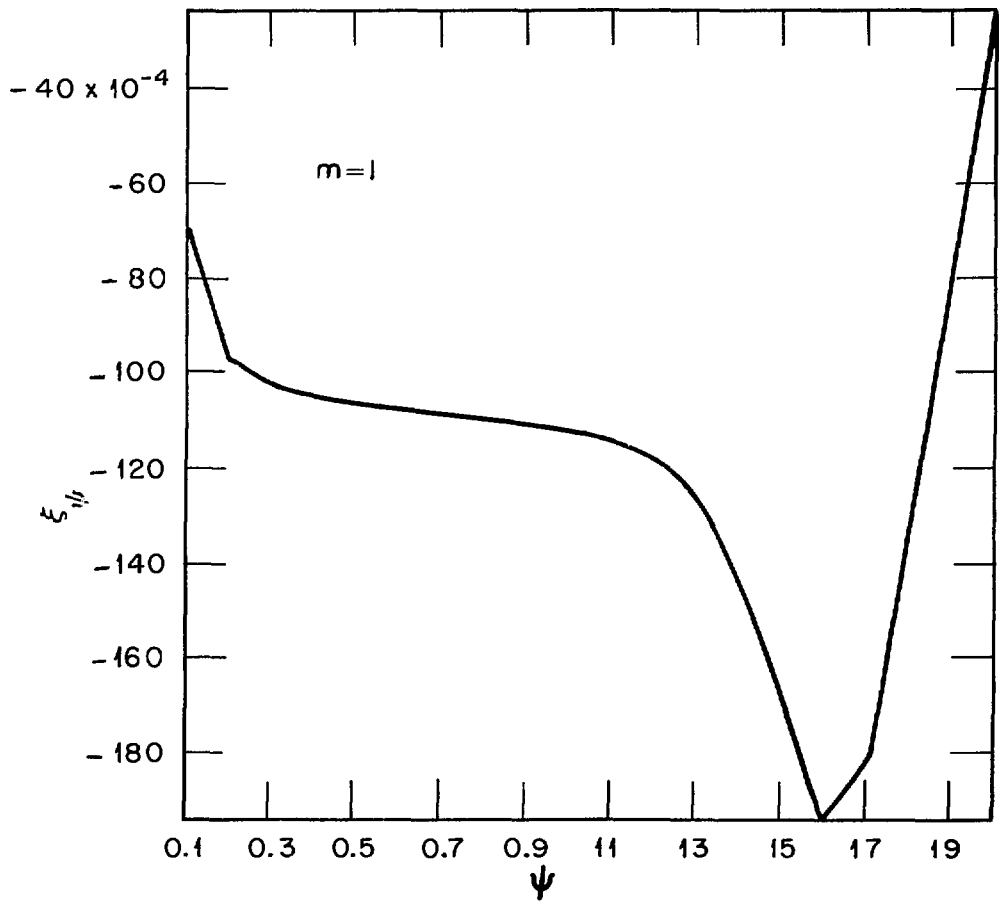

16. ξ_ψ versus ψ at the midplane for m=1.

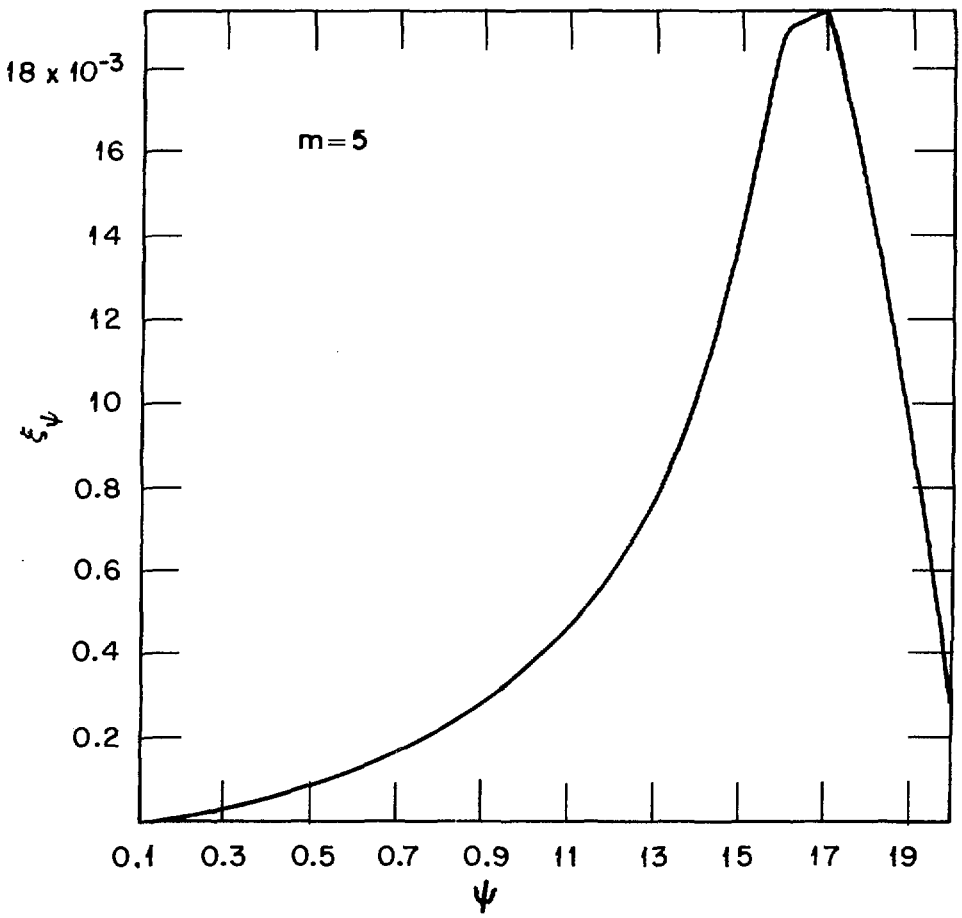

17. ξ_ψ versus ψ at the midplane for m=5.

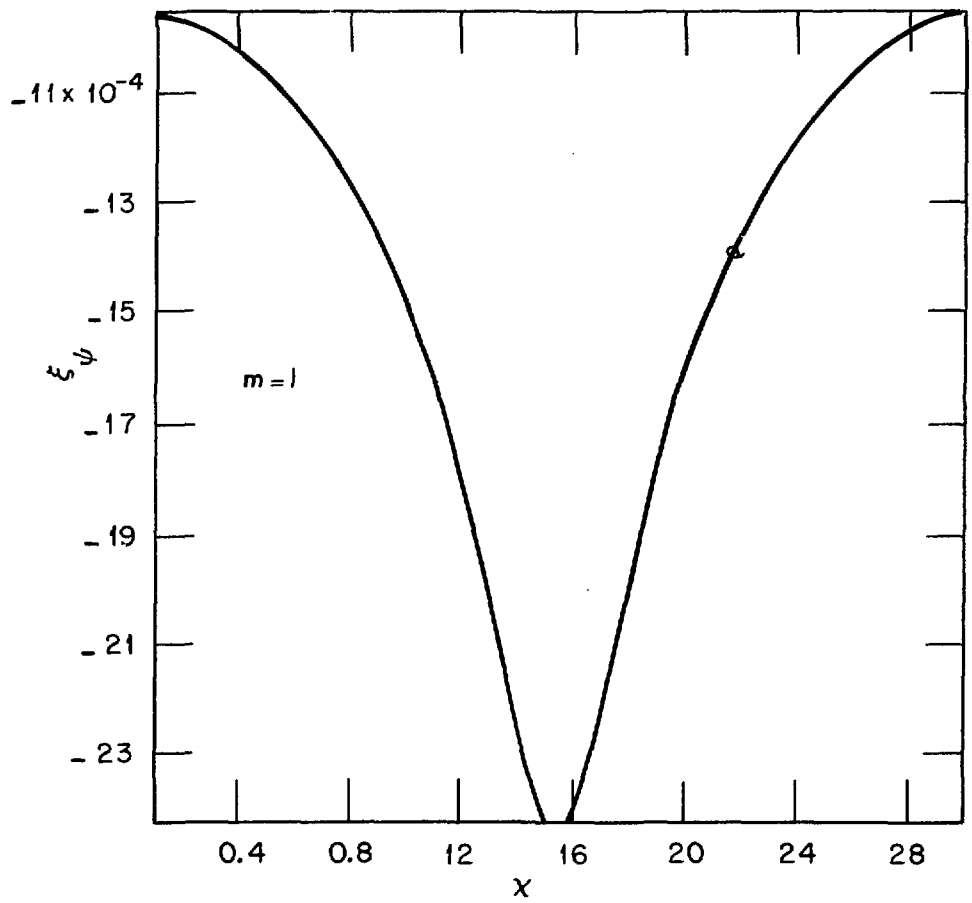

18. ξ_ψ versus X on a field line passing through the ring for m=1.

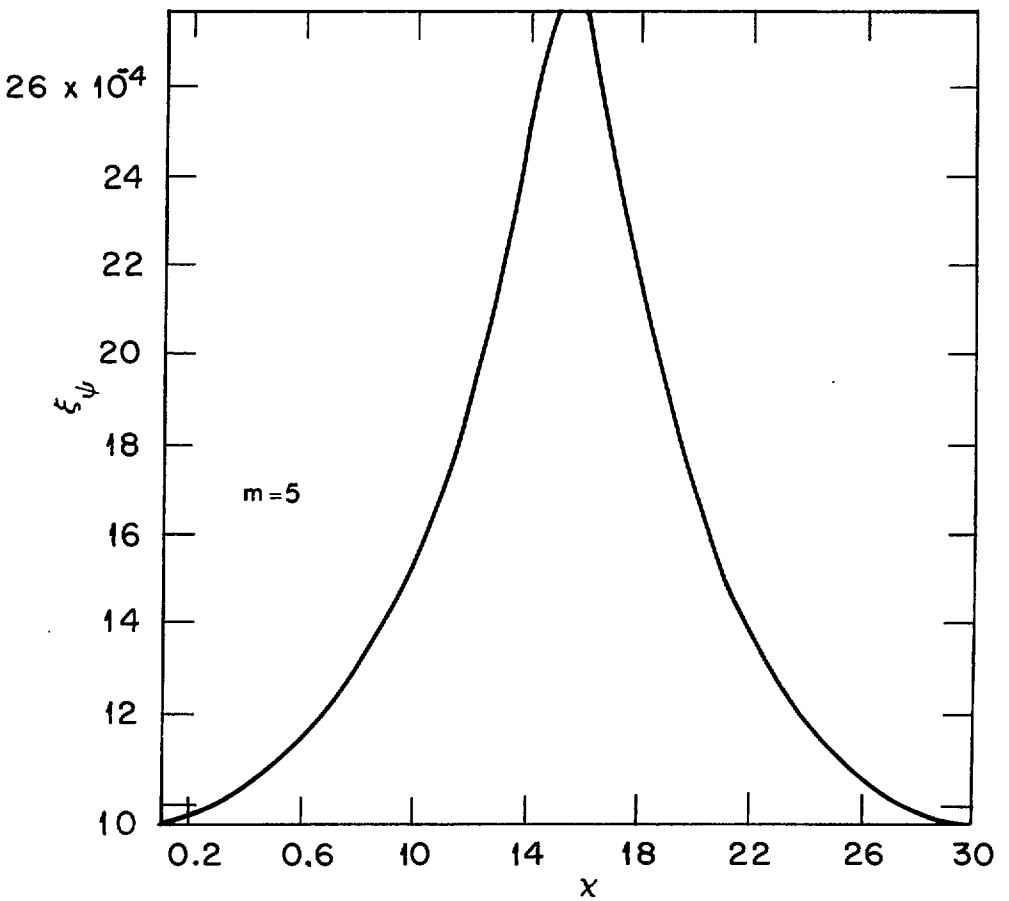

19. ξ_ψ versus χ on a field line passing through the ring for m=5.

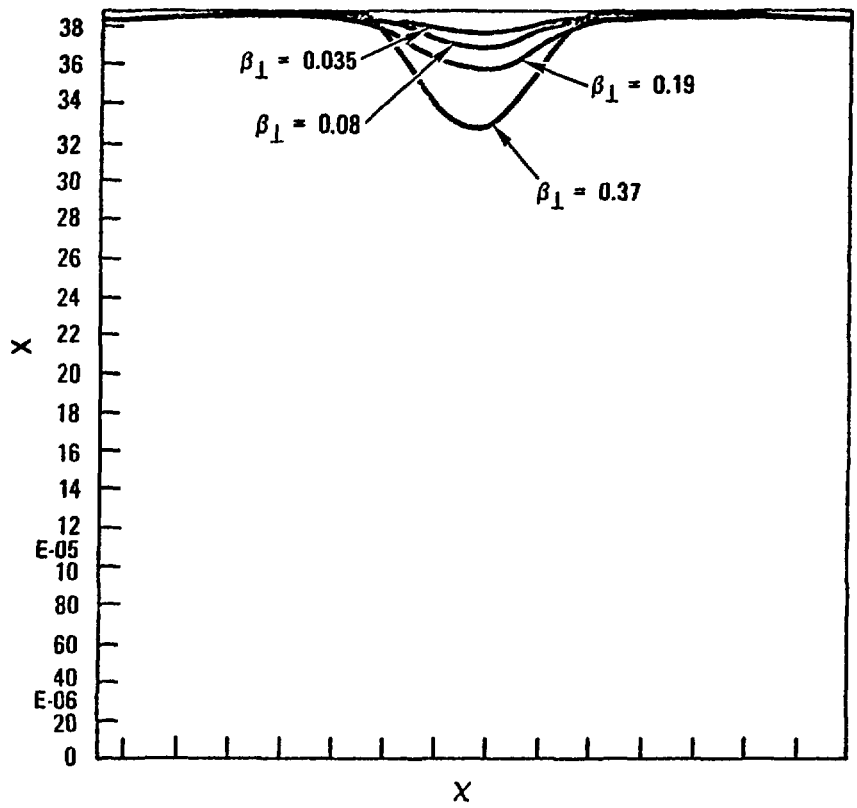

20. X versus χ (for m=5 mode) for a series of equilibria with changing $\beta_\perp$.

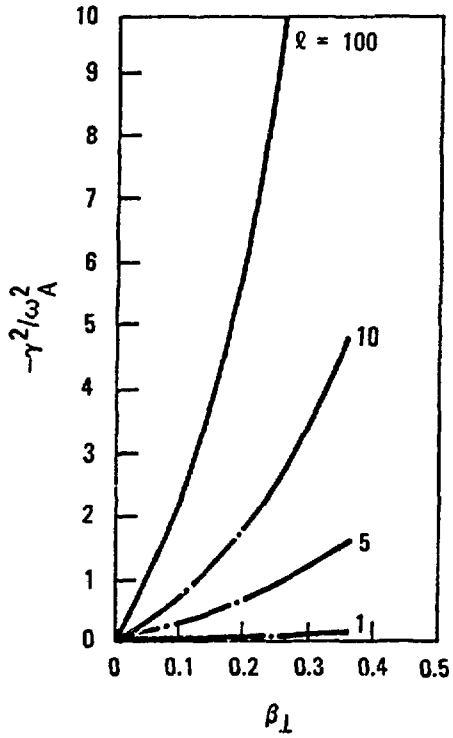

21. Growth rate (γ^2/ω_A^2) versus $\beta_\perp$ for various modes.

(GUIDING CENTER MODEL)

- PLASMA UNSTABLE TO $m = 1$ MODE EVEN WITH A CONDUCTING WALL AT THE PLASMA BOUNDARY
- γ INCREASES WITH $\beta_\perp$ AND WITH m
- AT LOW $\beta_\perp$ MODES ARE ESSENTIALLY INTERCHANGE MODES
- AT LARGER $\beta_\perp$, STRONG BALLOONING EFFECTS ARISE
- TWO-FLUID AND/OR KINETIC EFFECTS REQUIRED TO STABILIZE ALL FLUID MODES

22. Conclusions.

Dup

A TWO-POINT MODEL FOR ELECTRON TRANSPORT IN EBT

S. C. Chiu and G. E. Guest

General Atomic Company,
San Diego, California 92138

ABSTRACT

The electron transport in EBT is simulated by a two-point model corresponding to the central plasma and the edge. The central plasma is assumed to obey neoclassical collisionless transport. The edge plasma is assumed turbulent and modeled by Bohm diffusion. The steady-state temperatures and densities in both regions are obtained as functions of neutral influx and microwave power. It is found that as the neutral influx decreases and power increases, the edge density decreases while the core density increases. We conclude that if ring instability is responsible for the T-M mode transition, and if stability is correlated with the cold electron density at the edge, it will depend sensitively on ambient gas pressure and microwave power.

Work supported by Department of Energy,
Contract DE-AT03-76ET51011.

NOTICE

This report was prepared as an account of work sponsored by the United States Government. Neither the United States nor the Department of Energy, nor any of their employees, nor any of their contractors, subcontractors, or their employees, makes any warranty, express or implied, or assumes any legal liability or responsibility for the accuracy, completeness or usefulness of any information, apparatus, product or process disclosed, or represents that its use would not infringe privately owned rights.

Plasma turbulence at the surface of the quiescent central plasma in the ELMO Bumpy Torus (EBT) can have a significant influence on the overall stability of the plasma through its effect on the rate of creation and relative concentration of cold electrons. The nature of the dominant effects can be seen from an elementary model in which the plasma is divided into two regions: (a) a stable central region which obeys neoclassical transport; (b) a turbulent edge region extending from the outer part of the annulus to the container wall, which we assume to obey Bohm diffusion.

In an open-ended system, it is appropriate to consider a slab model for the edge in which a steady neutral flux passes through the slab of width, a, and the increase in density due to ionization is balanced by Bohm diffusion loss. We arrive at the equation

$$1 - e^{-N_c} = \frac{N_e}{N_o} \quad , \tag{1}$$

where $N_e = \bar{n}_e \langle\overline{\sigma v}\rangle_{ioniz}\, a/v_o$, $N_o = n_o \langle\overline{\sigma v}\rangle a^2/D_{Be}$, and bar denotes averages over the slab, v_o being the thermal velocity of the neutrals of density n_o. Figure 1 plots N_e versus N_o in Eq. (1). We note that as $N_o \to 1$, $N_e \to 0$, so that at this critical neutral density, the edge region is suddenly deficient of cold electrons. If we take $T_e \sim 50$ eV, $B \sim 5$ kG, $a \sim 5$ cm, and $\langle\sigma v\rangle_{ioniz}$ 2.5×10^{-8} cm^3/5, the critical neutral density $n_{o\ crit} \sim 10^{11}/\text{cm}^3$.

In a toroidal device such as EBT, one should, in principle, consider the particle and energy balance of both the electrons and ions in the presence of a self-consistent ambipolar field. However, we note that the ions in EBT-I and EBT-P are mainly in the plateau region where the diffusion coefficient varies exponentially with the ambipolar field $[D_i \propto \exp(eB\Phi'/kT_i B')]$. We therefore expect that the ambipolar field contrains the ion transport so that $e\Phi/kT_i$ is roughly constant (or logarithmically). The main energy exchange between the electrons and ions is due to Coulomb collisions which is usually only a small fraction of the total microwave power input. One may then expect a reasonably good description of the electron power balance by neglecting electron-ion energy exchange, and replacing $e\phi/kT_e$ by a constant (we have used unity) in the electron transport equations.

The edge plasma is unstable and a plausible transport model is Bohm diffusion ($D_{Be} = ckT_e/16\ eB$). The relation between the particle diffusion coefficient and heat conductivity is unknown, however, and we assume a relation $K_{Be} = \beta_T\ kn_e/D_{Be}$ where β_T is an adjustable constant.

The continuity equations for particle and energy are

$$\frac{\partial n_e}{\partial t} + \frac{1}{r}\frac{\partial(r\Gamma_e)}{\partial r} = n_e\langle\sigma v\rangle_i\, n_o \quad , \tag{2}$$

$$\frac{\partial}{\partial t}\left(\frac{3}{2} n_e kT_e\right) + \frac{1}{r}\frac{\partial(rQ_e)}{\partial r} - e\Gamma_e E_r = - E_I\langle\sigma v\rangle_i\, n_e n_o + P_\mu \quad , \tag{3}$$

where Γ_e and Q_e are the particle and energy fluxes, E_r is the ambipolar field field; n_o, P_μ, E_I, and $\langle\sigma v\rangle_i$ are respectively the neutral density, microwave power, ionization energy, and ionization rate.

We assume a neutral density radial dependence given by

$$n_o(r) = n_o \frac{r_2}{r} \exp\left(-\int_r^{r_2} n_e \frac{\langle\sigma v\rangle_i}{v_o} dr\right) \quad , \tag{4}$$

where r_1, r_2 are the radii of the bulk and edge region, and v_o is a mean neutral velocity. Although this profile is singular at $r = 0$, it gives a finite flux for all r. If the plasma line density, na, is not too high, as is the case in EBT-I, the integral in Eq. (4) is approximated in each region by

$$\int_r^{r_2} \frac{n_e \langle\sigma v\rangle_i}{v_o} dr$$

$$\approx \begin{cases} \dfrac{\bar{n}_{e_2} \langle\overline{\sigma v}\rangle_{i2}}{v_o} (r_2 - r) & \text{in edge (region 2)} \\ \dfrac{\bar{n}_{e_2} \langle\overline{\sigma v}\rangle_{i2}}{v_o} \Delta r + \dfrac{\bar{n}_{e_1} \langle\overline{\sigma v}\rangle_{i1}}{v_o} (r_1 - r) & \text{in bulk (region 1)} \end{cases} \tag{5}$$

where $\Delta r = r_2 - r_1$ is the thickness of the edge, and the bar and subscript denote average values in each region.

On integrating over the volumes of the two regions separately, we get point model transport equations for each region. The fluxes Γ_e, Q_e in region 1 are given by Kvriznykh.[1] We restrict ourselves to collisionless regime and replace the factor $\nu/(\nu^2 + \Omega_p^2)$ by ν/Ω_p^2 in the diffusion coefficients. By replacing the densities and temperatures by averages in each region, we arrive at the point model for region 1:

$$\frac{d\,\bar{n}_{e_1}}{dt} = -\frac{4(1+\eta_1)\,D_{ne_1}\,\bar{n}_{e_1}}{r_1\,L_{n_1}} + \frac{2\,r_2}{r_1^2}\,n_o v_o\left(1 - e^{-N_{e_1}}\right)$$

$$\times \exp - \left(\frac{\Delta r}{r^2}\,N_{e_2}\right) \quad , \tag{6}$$

$$\frac{d}{dt}\left(\frac{3}{2}\,\bar{n}_{e_1} k\bar{T}_1\right) = -\left[7 + 101\,\eta_1 - \frac{2\,r_1}{L_{n_1}}\,(1+\eta_1)\right] D_{ne_1}\,\frac{\bar{n}_{e_1} k\bar{T}_1}{r_1\,L_{n_1}}$$

$$-\frac{2\,r_2}{r_1^2}\,E_{I1}\,n_o v_o\left(1 - e^{-N_{e_1}}\right)$$

$$\times \exp - \left(\frac{\Delta r}{r_2}\,N_{e_2}\right) + P_{\mu_1} \quad , \tag{7}$$

where L_{n_1} is the density gradient scale length, η_1 is the ratio of logarithmic derivatives of temperature and density; D_{ne_1} is the Kvriznykh diffusion which in the collisionless limit is given by the expression

$$D_{ne_1} \approx \frac{1}{6}\left(\frac{r_1 R_c}{R_T}\right)^2 \frac{1}{\tau_{ei}} \quad , \tag{8}$$

$$\tau_{ei} = \frac{3}{4}\sqrt{\frac{m_e}{2\pi}}\,\frac{(k\bar{T}_1)^{3/2}}{e^4\,\bar{n}_{e_1}\,\ell n\Lambda} \quad , \tag{9}$$

where R_c and R_T are the mean magnetic radius of curvature and the toroidal radius. We have replaced all $e\,Er/k\bar{T}_1$ by $1/L_{n_1}$ in Eqs. (6) and (7), and defined the quantities N_{ej}, $j = 1, 2$:

$$N_{ej} = \frac{\bar{n}_{ej}\langle\sigma v\rangle_{ij}\, r_j}{v_o} \quad . \tag{10}$$

The ambipolar field in the edge region is difficult to treat and we neglect it (or rather absorb its effects in the definition of density gradient length). We arrive at the equations:

$$\frac{d\,\bar{n}_{e_2}}{dt} = -\frac{2\,D_{Be}}{r_2\,L_{n_2}}\,\bar{n}_{e_2} + \frac{2\,n_o v_o}{r_2}\left[1 - \exp - \left(N_{e_1} + \frac{\Delta r}{r^2}\,N_{e_2}\right)\right] \quad , \tag{11}$$

$$\frac{d}{dt}\left(\frac{3}{2}\bar{n}_{e_2}k\bar{T}_2\right) = -2\,\beta_T\,\frac{D_{Be}}{r_2\,L_{n_2}}\,\bar{n}_{e_2}k\bar{T}_2 - \frac{2\,E_{I2}n_o v_o}{r_2}\left(1 - e^{-\Delta r\,N_{e_2}/r_2}\right)$$

$$+\frac{1}{r_2}\left(P_{\mu_1}r_1 + \frac{r_2^2 - r_1^2}{r_2}\,P_{\mu_2}\right) \tag{12}$$

We note that in assuming two distinct diffusion mechanisms in the central and edge regions, we are neglecting the inevitable transition region which hopefully do not affect the overall particle, energy balance. Also we have not considered the annulus in the transport equations. Furthermore, we have neglected charge exchange, but when solving Eqs. (6), (7), (11), and (12) numerically, we add an *ad hoc* amount to the ionization energy E_I in each region to partially take this effect into account. A simple, and yet useful, understanding of the steady state can be obtained in the limit when the edge is thin and the center is thick, (i.e., $N_{e_2} << 1$, $N_{e_1} >> 1$ which is appropriate for EBT-P parameters). Equation (6) becomes

$$2(1 + \eta_1)D_{ne_1}\frac{\bar{n}_{e_1}}{L_{n_1}} = \frac{r_2}{r_1}\,n_o v_o \tag{13}$$

and Eq. (7) becomes

$$\left[7 + 101\,\eta_1 - \frac{2\,r_1}{L_{n_1}}\,(1 + \eta_1)\right]D_{ne_1}\,\frac{\bar{n}_{e_1}k\bar{T}_1}{L_{n_1}} = P_{\mu_1}r_1 \tag{14}$$

Dividing Eq. (14) by Eq. (13), we immediately get

$$\bar{T}_1 \propto \frac{P_{\mu_1}}{n_o} \quad , \tag{15}$$

and from Eq. (13),

$$\bar{n}_{e_1} \propto \frac{P_{\mu_1}^{3/4}}{n_o^{1/4}} \quad . \tag{16}$$

Similarly, for the edge region,

$$\bar{T}_2 \propto \frac{P_\mu}{n_o} \quad , \tag{17}$$

$$\bar{n}_2 \propto \frac{n_o^2}{P_\mu} \quad , \tag{18}$$

where $P_\mu = P_{\mu_1} + 1 - (r_1^2/r_2^2)\, P_{\mu_2}$.

Equations (11), (12), (6), and (7) have been solved numerically at EBT-I parameters and the results are shown in Figs. 2 and 3. If we write $n_{e_j} = n_o^{\alpha_j} P_{\mu_1}^{\beta_j}$, $T_{e_j} = n_o^{\alpha_j} P_{\mu_1}^{\beta_j}$, then $\alpha_1 = -0.30$, $\alpha_2 = 2.10$, $\beta_1 = 0.76$, $\beta_2 = -0.62$, $\gamma_1 = -1.09$, $\gamma_2 = -1.05$, $\delta_1 = 0.90$, $\delta_2 = 0.76$. The neutral density

dependence is seen to be quite close to the limiting values previously obtained. The dependence on the microwave power is off somewhat partly because the center is not thick, and partly because δ_2, β_2 are in terms of P_{μ_1} in the numerical study rather than P_μ in Eqs. (17)–(18).

The nonsteady solution [Fig. (4)] seems to be always stable as in the one-point model.

Experimentally, T-M mode occurs as the microwave power P_μ is increased or n_o is decreased. An interesting effect in the present model is that such variations of P and n_o cause $\bar{n}_{e_1}$, $\bar{T}_1$, and $\bar{T}_2$ to increase, but $\bar{n}_{e_2}$ to decrease. Various theories have predicted that the stability of the annulus requires cold-hot electron density ratio, n_c/n_h, to be above certain thresholds. For example, in the absence of line tying, Dominguez and Berk[2] showed that (when $\omega_g/\Omega_i \ll 1$)

$$\frac{n_c}{n_h} \gtrsim \frac{4\left(1 + \frac{\beta_h}{2}\right)\Omega_i}{\omega_g} - 1 \quad .$$

Although, due to the simplifying assumptions of the theory, the absolute magnitude may not closely correspond to actual values under experimental conditions, they underline the vital role transport, which controls n_c, may have on ring stability. If the onset of ring instability corresponds to T-M mode transition in EBT, we can draw conclusions from the present result as to whether the core density or the cold edge density is the plasma variable which is responsible for T-M mode transition. Specifically, as one

decreases n_o, the central density increases, and n_h should not increase, so that core density varies in a more stabilizing direction. However, the edge electron density decreases quickly so that one has to conclude that the lack of cold edge electrons is responsible for the T-M mode transition. It thus seems worthwhile to experimentally correlate the edge plasma parameters with ring parameters.

ACKNOWLEDGMENT

This work was supported by Department of Energy, Contract DE-AT03-76ET51011.

REFERENCES

1. L. M. Kovriznykh, Sov. Phys.–JETP *29*, 475 (1969).

2. R. R. Dominguez and H. L. Berk, Phys. Fluids *21*, 827 (1978).

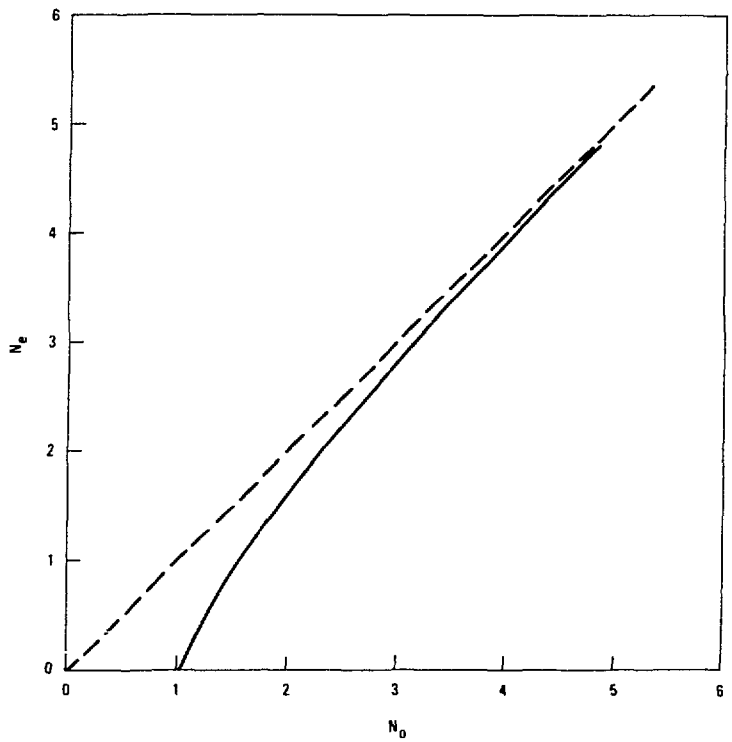

1. N_e vs N_o for Eq. (1).

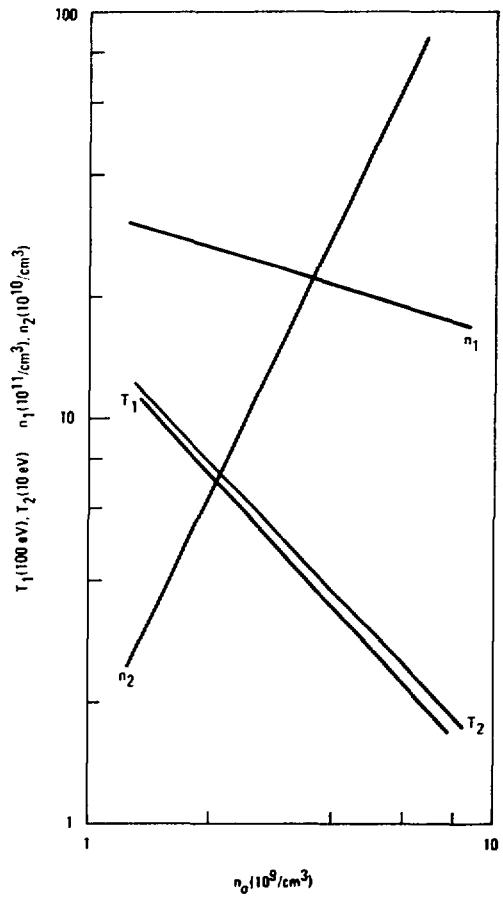

2. Steady-state solutions of Eqs. (11), (12), (6), and (7) as a function of n_o, with $P_{\mu_1} = 20\ kW/m^3$, $P_{\mu_2} = 2\ kW/m^3$. Parameters used are those of EBT-I: $r_1 = 10$ cm, $r_2 = 15$ cm, $B_o = 6.5$ kG, $L_{n_1} = 5$ cm, $L_{n_2} = 6.7$ cm, $\eta_1 = 0.03$, $R_T = 156$ cm, $rR_c = 150\ cm^2$, and $\beta_T = 8$.

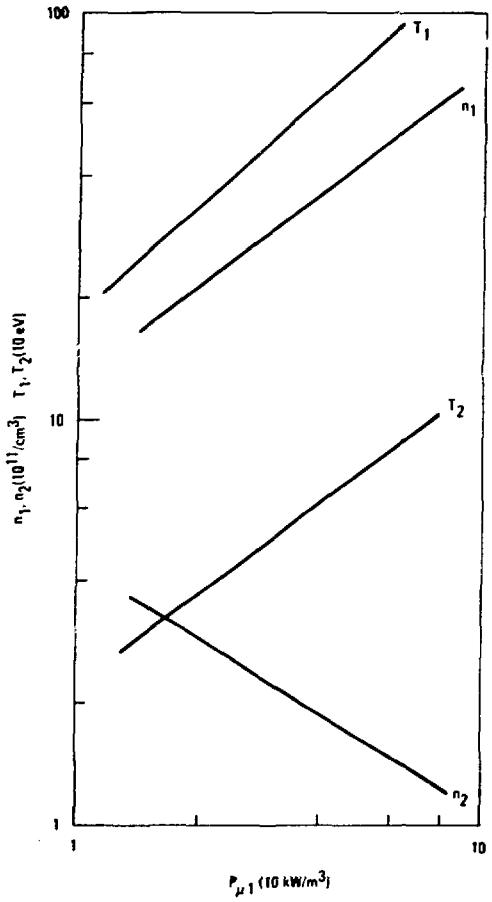

3. Steady-state solutions of Eqs. (11), (12), (6), and (7) as a function of P_{μ_1} with $P_{\mu_2} = 2$ kW/m^3, $n_o = 4 \times 10^9/cm^3$. Parameters are the same as in Fig. 2.

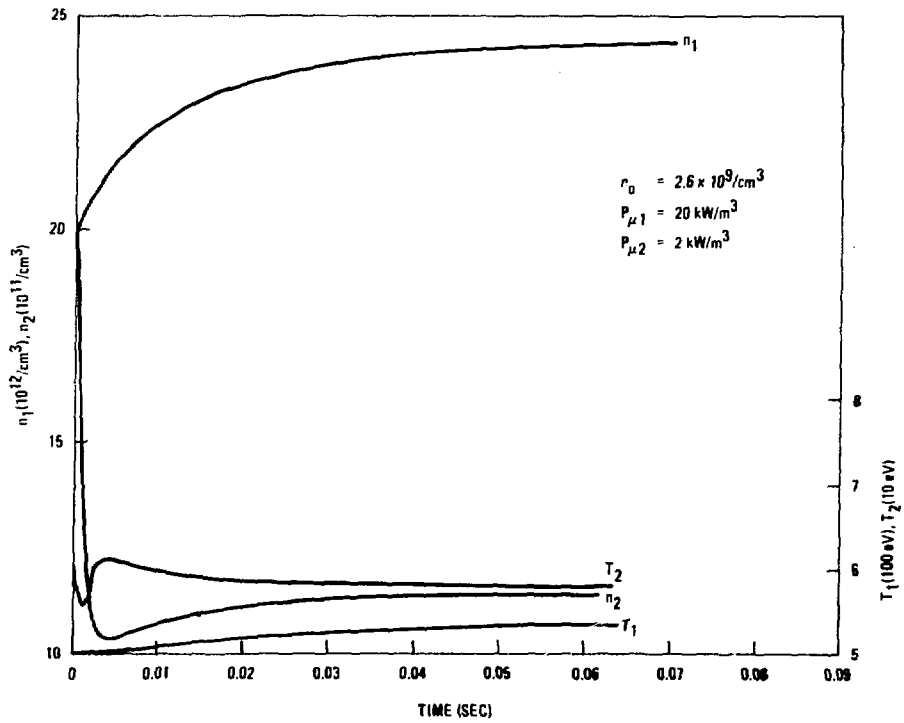

4. Transient solution of Eqs. (11), (12), (6), and (7). Parameters are the same as in Fig. 2.

STABILITY OF A TOROIDAL PLASMA BY HOT ELECTRON ANNULUS IN A BUMPY TORUS

H. Sanuki and M. Fujiwara

Nagoya University
Nagoya 464, Japan

ABSTRACT

An analytical study of the ballooning instability is presented in a bumpy configuration using a relatively simple fluid model of an inhomogeneous slab plasma with grativational field simultating the bad curvature effect and the grad-B effect due to hot electron annulus. Mathieu type equation is derived to investigate a linear analysis. Stability boundary giving the maximum stable β_p (beta value of bulk plasma) as a function of β_h and the threshold for β_h (beta value of hot electron annulus) are studied for Nagoya Bumpy Torus (NBT) parameters. The relevance of our theoretical analysis is discussed in a comparison with the previous results.

1. INTRODUCTION

Recently there has been considerable interest in the ballooning instability in ELMO Bumpy Torus[1-3] as it appears to set a limiting achievable β (the ratio of plasma to magnetic pressure). It has also been shown that in the purely fluid model of the bulk plasma, the magnetohydrodynamic (MHD) ballooning and interchange modes can be stabilized by the hot electrons if we assume the latter to be a rigid, noninteracting external current[1]. In general, the bumpy torus theory is necessarily rather complicated because of the many degrees of freedom in the actual geometry of EBT and NBT.

In this paper we present an analytical study of the balooning mode in a bumpy configuration using a simple model. Because the ballooning mode is essentially the finite β-interchange[4] instability localized along the magnetic field line in the region of bad curvature we use a simple fluid model of an inhomogeneous slab plasma with gravitational field simulating the bad curvature effects. Also included are effects of grad-B drift due to hot electrons and finite Larmor radius on the electromagnetic perturbation of the shear Alfvén wave. In section 2, we derive our model equation. Section 3 presents a linear stability calculation and the stability limit that results from it.

2. DERIVATION OF MODEL EQUATION

The present configuration is shown conceptually in Fig.1, and this corresponds to one sector of the equivalent bumpy cylinder. The hot electron annulus, formed by electron cyclotron resonance heating, is mirror-confined and threaded in a region between each pair of throats.

The magnetic field B(x) is shown in Fig.2 as a function of radius. The hot electrons are located at $x = x_0$ with the width δ along x direction (x_0 corresponds to the location of second harmonic electron cyclotron resonance) and also at $z = 0$ with ℓ_h along the field line. As indicated in Fig.2, ∇B is positive near the outer edge of the hot electron annulus, so that in this region a bulk plasma can be stably contained.

The model used is similar to that employed in Ref.[5]: slab geometry with density and magnetic gradients in the x direction, an equilibrium magnetic field $B = B(x)\hat{z}$. The plasma equilibrium is composed of three species: warm ions, warm electrons and hot electrons. For finite but small $\beta << 1$, we may neglect the compressional component of the magnetic perturbation and introduce the two potentials ϕ and ψ such that $E_\perp = -\nabla_\perp\phi$, $E_\parallel = -\frac{\partial\psi}{\partial z} = 0$. The parallel E field is zero since we do not consider the region of coupling to the electrostatic drift wave. From Maxwell's equations

$$\frac{4\pi}{c} J_\parallel = (\nabla \times \vec{B})_\parallel \ , \tag{1}$$

$$\frac{1}{c}\frac{\partial B_\perp}{\partial t} = -\nabla \times \vec{E}_\perp \ , \tag{2}$$

we obtain

$$\frac{\partial J_\parallel}{\partial t} = \frac{c^2}{4\pi}\frac{\partial}{\partial z}\Delta_\perp\phi \ . \tag{3}$$

From the continuity equation and quasineutrality condition we obtain

$$\frac{\partial J_\parallel}{\partial z} = -\, e\nabla_\perp\cdot[n(\vec{v}_{\perp i} - \vec{v}_{\perp e})] \ . \tag{4}$$

From the fluid equation of motion, we obtain the velocity perpendicular to the unperturbed magnetic field:

$$\vec{v}_\perp = \vec{v}_o + \vec{v}_p + \frac{c}{qB_o}\,\frac{\hat{z} \times \nabla(nT)}{n} + \frac{c}{qn}\,\hat{z} \times \nabla\pi + \vec{v}_g \ , \tag{5}$$

with

$$\vec{v}_o = \frac{c}{B_o}\,\hat{z} \times \nabla_\perp\phi + \frac{v_\parallel}{B_o}\,\vec{B}_\perp \ , \tag{6a}$$

$$\vec{v}_p = -\frac{m}{q}\frac{c}{B_o}\frac{\partial}{\partial t}\nabla_\perp\phi + (\vec{v}\cdot\nabla)\,\nabla_\perp\phi \ , \tag{6b}$$

$$\vec{v}_d = \frac{c}{qB_o n_o}\frac{d}{dx}(n_o T)\hat{y} \ , \tag{6c}$$

$$\vec{v}_g = \left(\frac{g_o}{\Omega}\cos\frac{2\pi z}{L} - \frac{g_1}{\Omega}\right)\hat{y} \ , \tag{6d}$$

where $\vec{v}_p$ is the polarization drift, $\vec{v}_d$ the diamagnetic drift, π is the stress tensor, and $\vec{v}_g$ is the gravitational drift velocity. In Eq.(6d), g_o, g_1 are given respectively by (see Appendix),

$$g_o = \frac{1}{R_c}\left[\frac{v_\perp^2}{2}\left(\alpha - \frac{R_c}{\pi\delta}\,\beta_h \sin\frac{\ell_h\pi}{L}\right) + v_\parallel^2\right] \ , \tag{7a}$$

$$g_1 = \frac{1}{2\delta}\left[\frac{\ell_h}{L}\,\beta_h - \frac{\delta}{R_c}\,\varepsilon\right] \ , \tag{7b}$$

where $\alpha = (M + 1)^2/4M$, $\varepsilon = (M^2 - 1)/(2\pi M)$, M is the mirror ratio and R_c is the local radius of magnetic curvature. Since the third term on the right hand side of (5) will not contribute when inserted into (2) we obtain, dropping the electron polarization and gravitational drifts

$$\frac{\partial J_\parallel}{\partial z} = -e\vec{v}_{gi}\cdot\nabla n + e\nabla_\perp\cdot\left(n_o\,\frac{\vec{v}_{\parallel e} - \vec{v}_{\parallel i}}{B_o}\,B_\perp\right) - en_o\nabla\cdot\vec{v}_{pi}$$

$$- \frac{e^2}{T_i}\,n_o\eta\Delta_\perp^2\phi \ , \tag{8}$$

where $\eta = 0.075\nu_{ii}\rho_i^4$, ρ_i is the ion Larmor radius and ν_{ii} is the ion-ion collision frequency. We now write $e/B_0\ \nabla_\perp\cdot[n_0(\vec{v}_{\parallel e} - \vec{v}_{\parallel i})B_\perp] = \frac{1}{B_0}\nabla_\perp(J_\parallel B_\perp)$. From (3) and $1/c\ \partial B_\perp/\partial t = \nabla \times \nabla_\perp\phi$ we find by writing $\partial/\partial t = -i\Omega(t)$ and $\partial/\partial z = ik_\parallel$,

$$\frac{1}{B_0}\nabla_\perp(J_\parallel B_\perp) = -\frac{c^3}{4\pi B_0}\frac{k_\parallel^2}{\Omega^2}[(\nabla_\perp\phi \times \hat{z})\cdot\nabla_\perp]\ \nabla_\perp\phi\ . \tag{9}$$

In order to express the density perturbation of ions n in the potential we use the quasineutrality condition and the electron equation of motion. If $v_{te} > v_A$, i.e., $\beta > (m_e/m_i)$, the electrons will thermalize along the field lines and we obtain

$$\frac{n_e}{n_0} = \frac{e\phi}{T_e}\frac{\omega_{*e}}{\omega}\ ,$$

where $\omega_{*e} = k_y v_{De}$. From (3), (8) and (9) we now obtain a nonlinear wave equation for Alfvén modes propagating along the field line in a gravitational field

$$\left[\frac{\partial^2}{\partial t^2} - v_A^2\frac{\partial^2}{\partial z^2} - v_T\cdot\nabla\frac{\partial}{\partial t} - \mu\Delta_\perp\frac{\partial}{\partial t}\right]\Delta_\perp\phi$$

$$-\kappa\left[g_0\cos\frac{2\pi}{L}z - g_1\right]\frac{\partial^2\phi}{\partial y^2}$$

$$= \frac{c}{B_0}\left(1 - \frac{k_\parallel^2 v_A^2}{\Omega^2}\right)\frac{\partial}{\partial t}[(\nabla_\perp\phi \times \hat{z})\cdot\nabla_\perp]\ \Delta_\perp\phi\ , \tag{10}$$

where $\kappa = -\ d/dx(\ln n_0)$, $\mu = (e/T_i)B_0\omega_{ci}/c$ and $\vec{v}_T = \vec{v}_{Di} + \vec{v}_{gi}$. Equation (10) is our model equation describing drift Alfvén waves propagating along the field line shown in Fig.1 under a gravitational force due to hot electron annulus.

3. LINEAR STABILITY ANALYSIS

We now restrict ourselves to considering the linear stability of bulk

plasma by hot electron annulus on the basis of (10). For simplicity we neglect the nonlinear effects and also the gravitational drift compared to the diamagnetic drift in v_T term. If we write the potential as

$$\phi\ (r,\ t) = \overline{\phi}(z)\ e^{i(k_x x + k_y y - \omega t)} \quad ,$$

and introduce a new variable, $\xi = 2\pi z/L$, and neglect the viscosity term, Eq.(10) can be converted into

$$\left(\frac{\partial^2}{\partial \xi^2} + A + B\ \cos\xi\right)\overline{\phi}(\xi) = 0 \ , \tag{11}$$

with the definitions of

$$A = \left(\frac{L}{2\pi}\right)^2 \frac{1}{v_A^2}\left(\omega^2 + \omega v_{Di} k_y - \kappa g_1 \frac{k_y^2}{k_\perp^2}\right) \ , \tag{12}$$

$$B = \left(\frac{L}{2\pi}\right)^2 \frac{1}{v_A^2}\ \kappa g_0 \frac{k_y^2}{k_\perp^2} \quad , \tag{13}$$

where $k_\perp^2 = k_x^2 + k_y^2$ and Eq.(11) is of the standard Mathieu form. We can regard (11) as the equation describing the pendulum problem. The stability condition for (11) in the case of negative value of A is given by

$$-2A \leq B^2 \quad . \tag{14}$$

In order to investigate the stability boundary of (11), we assume $\omega = 0$ and $v_\perp \simeq v_\parallel \simeq c_s$ in (12) and (13) and substitute them into (14), we obtain

$$\beta_p \leq \frac{16\pi^2}{9}\frac{r_p}{\delta}\frac{R_c^2}{L^2}\left(\frac{k_\perp^2}{k_y^2}\right)\frac{1}{\alpha}\frac{\ell_h}{L}\ \frac{\left(\beta_h - \frac{L}{\ell_h}\frac{\delta}{R_c}\varepsilon\right)}{\left[1 - \frac{4}{3\pi}\frac{1}{\alpha}\frac{R_c}{\delta}\beta_h \sin\left(\frac{\ell_h}{L}\pi\right)\right]} \quad . \tag{15}$$

This gives the stability boundary giving the maximum stable β_p as a function of β_h for given parameters.

In Fig.3 we plot the stability boundary for β_p as a function of β_h for different values of ℓ_h, which correspond to the short and long annuli, respectively. For the parameters r_p, δ, R_c, L and M, we used values available in NBT experiment. The effect of a long hot electron annulus is more efficient than a shorter annulus in point of the stability of a toroidal plasma. The stability analyses for ballooning modes have been developed for a diffused boundary by Nelson and Hedrick and for a sharp boundary by Miller using the energy principle in a bumpy cylinder configuration. Nelson also studied the stability boundary for electromagnetic modes based on the kinetic equation in a slab geometry including the hot electron component. Their results are also shown in Fig.3. While we can not compare exactly our results with those in Refs.[1]-[3] because the definition of long or short annulus is not clear in their calculation and the parameters in EBT is slightly different from those in NBT, the effect of a short vs. long annulus is similar to that in Ref.[1]. It turns out from (15) that there is a threshold for β_h and the stability is achieved for

$$\beta_h \geq \beta_{hc} = \frac{L}{\ell_h}\frac{\delta}{R_c}\varepsilon \quad . \tag{16}$$

For the parameters in NBT experiment $\beta_{hc} \simeq 0.06$ for a long annulus ($\ell_h/L = 1/2$), 0.18 for a short annulus ($\ell_h/L = 1/6$).

The present analysis is based on the assumption of "rigid" hot electrons, which contribute to only the force balance. We did not discuss the stability of hot electron ring. As was shown in Fig.3, however, the present results obtained using the very simple analysis are in good qualitative agreement with the previous results[1-3]. This analysis can be extended to the problems in the actual toroidal geometries of NBT and EBT.

ACKNOWLEDGEMENTS

We are grateful to Professor H. Ikegami, Dr. C. L. Hedrick, and the members of NBT group of Institute of Plasma Physics, Nagoya University for their useful discussions. We would also like to acknowledge Professor Y. H. Ichikawa for his interest in this work. One of the authors (H.S.) would like to thank Dr. J. Weiland for contributing to the derivation of model equation.

APPENDIX

Derivation of Equation (6d)

In general, the gravitational drift velocity $\vec{v}_g$, which consists of the curvature and grad-B drifts, is given by

$$\vec{v}_g = \frac{1}{\Omega}\left[-\frac{v_\perp^2}{2}\frac{\nabla B}{B_o} + \frac{v_\parallel^2}{R_c}\right]\hat{y} \ . \tag{A1}$$

We now consider the grad-B drifts including the effect due to hot electron annulus. From the pressure balance equation:

$$p_h + \frac{B^2}{8\pi} = \frac{B_o^2}{8\pi} \ , \tag{A2}$$

we obtain approximately the magnetic field in the region of hot electron annulus,

$$B(x) \simeq B_o(x)\left(1 - \frac{\beta_h}{2}\right) \ , \tag{A3}$$

where $\beta_h = p_h/(B_o^2/8\pi) < 1$. From the present configuration shown in Fig.2, we obtain using (A3)

$$B(x) \simeq B(x_o) + \frac{B(x_o + \frac{\delta}{2}) - B(x_o)}{\frac{1}{2}\delta}(x - x_o) \ ,$$

which yields

$$\frac{\nabla_x B}{B_o} \simeq \frac{1}{\delta}\left(\beta_h + \delta\frac{\nabla_x B_o}{B_o}\right) \ . \tag{A4}$$

The first term in (A4) is the effect of hot electrons and the second term is the grad-B effect of bulk plasma. We first consider the grad-B drift of bulk plasma, which is given by

$$(v_{\nabla B})_{bulk} \simeq \frac{mc}{q}\frac{v_\perp^2}{2}\frac{\nabla_x B_o}{B_o^2(z)} \simeq \frac{mc}{q}\frac{v_\perp^2}{2}\left|\frac{1}{R_c B_o(z)}\right| . \tag{A5}$$

We should note that the direction of grad-B drift is positive in the midplane and negative in the mirror throat. If we assume the magnetic field,

$$B_o(x, z) = B_o(1 - \frac{M-1}{M+1}\cos\frac{2\pi}{L}z) ,$$

We can express approximately $1/R_c B_o(z)$ by

$$-\frac{1}{R_c B_o(z)} = \begin{cases} \frac{1}{R_c B_{oMAX}}\cos\frac{2\pi}{L}z , & -\frac{L}{2} < z < -\frac{L}{4} \\ \frac{1}{R_c B_{oMIN}}\cos\frac{2\pi}{L}z , & -\frac{L}{4} < z < \frac{L}{4} \\ \frac{1}{R_c B_{oMAX}}\cos\frac{2\pi}{L}z , & \frac{L}{4} < z < \frac{L}{2} , \end{cases} \tag{A6}$$

where $B_{oMAX} = B_o M/(M+1)$, $B_{oMIN} = B_o 2/(M+1)$. If we expand the function (A6) using Fourier expansion method, we obtain

$$\frac{1}{R_c B_o(z)} \simeq -\frac{1}{R_c B_o}(\varepsilon + \alpha\cos\frac{2\pi}{L}z + \cdots) , \tag{A7}$$

where $\alpha = (M+1)^2/4M$, $\varepsilon = (M^2 - 1)/(2\pi M)$.

We next consider the grad-B drift due to hot electron annulus. Since β_h is assumed to be constant in the region, $-\ell_h/2 < z < \ell_h/2$, the z-dependence of $B_o(z)$ in $(v_{\nabla B})_{hot}$ may be neglected.

Using Fourier expansion method, we can expand β_h by

$$\beta_h\Big|_{[-\frac{\ell_h}{2} \sim \frac{\ell_h}{2}]} \simeq \frac{\ell_h}{L}\beta_h + \frac{\beta_h}{\pi}\sin\left(\frac{\ell_h}{L}\pi\right)\cos\frac{2\pi}{L}z + \cdots . \qquad \text{(A8)}$$

Substitution of (A4), (A5), (A7) and (A8) into (A1) yields Eq.(6d).

REFERENCES

[1] D. B. Nelson and C. L. Hedrick, Nuclear Fusion 19, 283 (1979).

[2] D. B. Nelson, Oak Ridge National Laboratory Report, ORNL/TM-6829 (1979).

[3] G. Miller, LA-7618-MS (1979).

[4] K. V. Roberts and J. B. Taylor, Phys. Fluids 8, 315 (1965).

[5] J. Weiland, H. Sanuki and C. S. Liu, Institute for Electromagnetic Field Theory Report, CTH-IEFT/PP-1979-12 (Chalmers Univ. of Technology, Göteborg, Sweden).

FIGURE CAPTIONS

Fig.1. Geometry of bumpy cylinder. The hot electron annulus is denoted by the shaded region. The distance between mirror throats is L and the length of hot electron annulus is ℓ_h.

Fig.2. Magnetic field B and the radial profile of hot electron annulus are plotted as functions of radius in midplane. The electron annulus is denoted by the shaded region.

Fig.3. Stability boundary of the main plasma as a function of β_p and β_h from Eq.(15) for R_c = 20 cm, L = 40 cm, δ = 3 cm, r_p = 3 cm and M = 1.8. Results for long annulus with $\frac{\ell_h}{L} = \frac{1}{2}$, S-F (Long) and short annulus with $\frac{\ell_h}{L} = \frac{1}{6}$, S-F (Short), are denoted by the solid lines (——). Results by Nelson and Hedrick, N-H (Long) and N-H (Short)(-·-·-), and by Nelson (---) with the notation $\delta = n_h/n_c$ are also illustrated. Results by Miller, M (Long) with $\frac{\ell_h}{L} = \frac{1}{3}$ and M (Short) with $\frac{\ell_h}{L} = \frac{1}{10}$ (-··-) are also shown for the mode number m = 30.

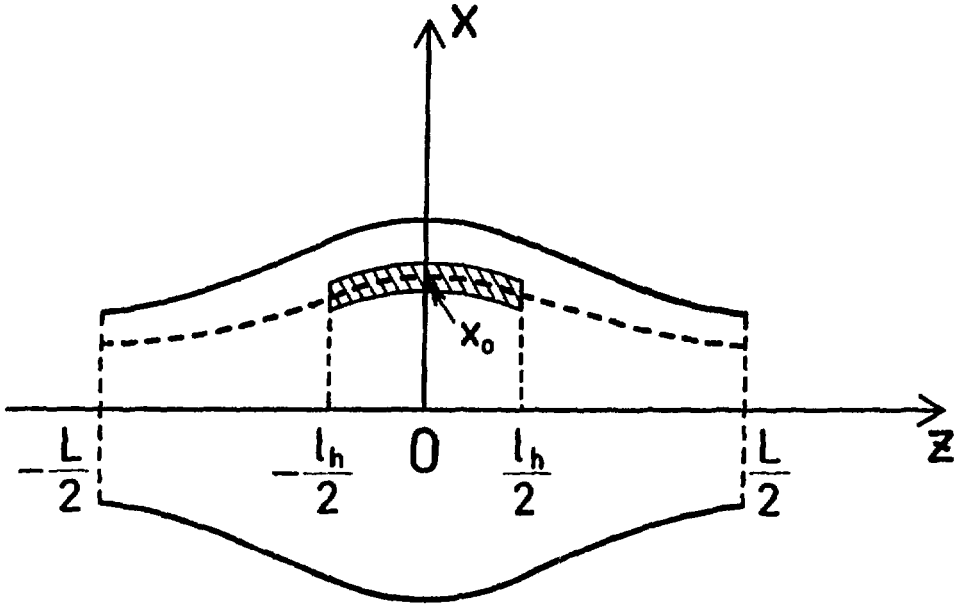

Fig.1

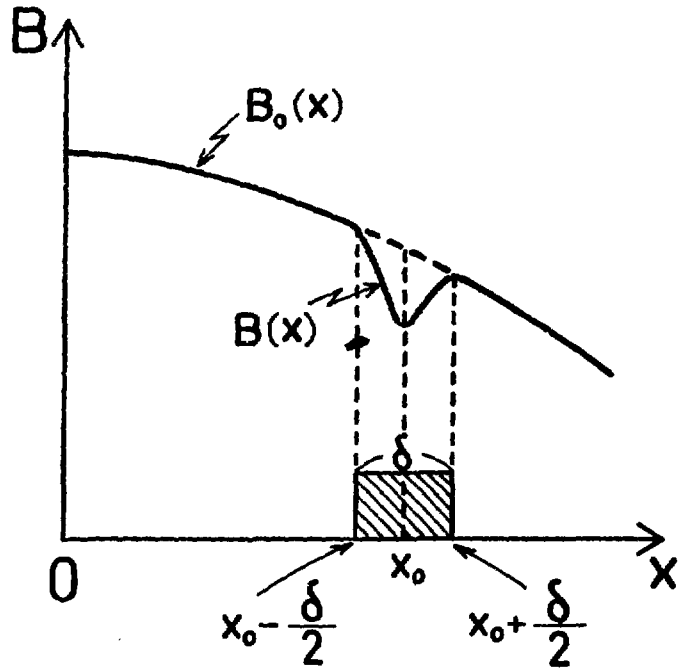

Fig. 2

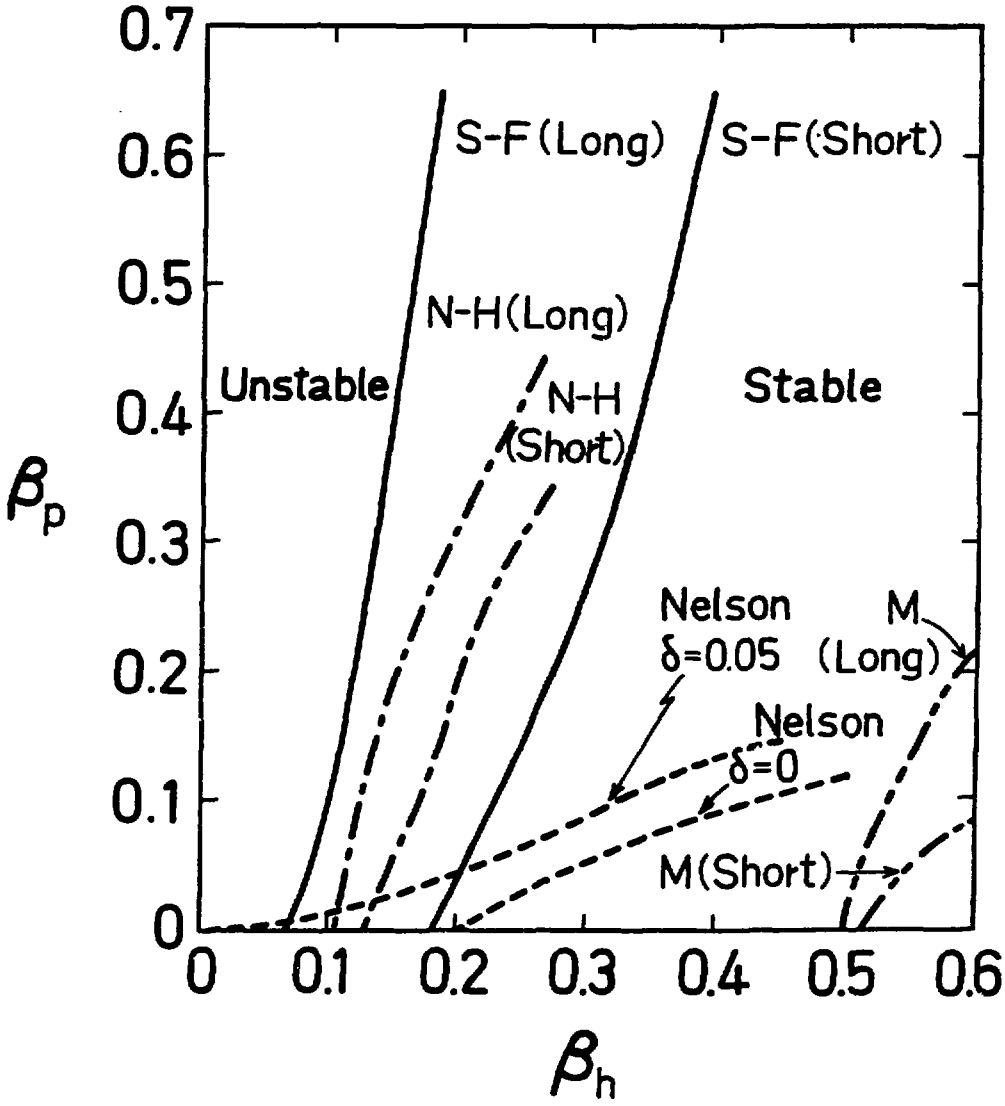
0.7
0.6
0.5
0.4
0.3
0.2
0.1
0
β_p
S-F (Long)
S-F (Short)
N-H (Long)
Unstable
N-H
(Short)
Stable
Nelson
δ=0.05
M
(Long)
Nelson
δ=0
M (Short)
0
0.1
0.2
0.3
0.4
0.5
0.6
β_h

Fig.3

DISCUSSION

V. K. TRIPATHI: Is the mode localized inside the ring in z and x directions?

H. SANUKI: Yes, the mode may be localized near the bad curvature region under the linear approximation. When the nonlinear effects are taken into account, however, we obtain several possibilities for this mode to be localized along the field line (z) and also x directions. This is associated with the formation of the convective mode at the unfavorable region.

STABILITY ANALYSIS OF A HOT ELECTRON EBT PLASMA

J. W. Van Dam and Y. C. Lee*
Institute for Advanced Study, Princeton, New Jersey 08540

ABSTRACT

Previous theoretical studies have predicted that an EBT-confined plasma will have a stable equilibrium for beta values of the toroidal core plasma comparable to the beta value for the hot electron annulus. We show that, when the ring is allowed to be perturbed, there is a new physical effect, enhanced compression of the core plasma; that in the limit of negligible β_{core}, the interchange mode is stable for β_{ring} greater than about 20%, as was found before; but that when the core pressure is increased, the plasma goes unstable again at values of β_{core} significantly smaller than the value for β_{ring}.

*Also, Department of Physics & Astronomy, University of Maryland, College Park, MD 20742.

1. INTRODUCTION

One proof-of-principle objective for the proposed EBT-P device is to demonstrate bulk plasma stability at high values for the plasma temperature and beta: specifically, for $T_i > 1$ keV and $\beta_i > 1\%$. The reason for this interest is that theory has predicted that, at high β, an EBT plasma can have a stable equilibrium for beta values of the toroidal core plasma comparable to the beta value for the hot electron annulus and on the order of 20-40%. Such a feature would make an EBT confinement device very attractive from the reactor scaling point of view.

This theoretical result was obtained from two somewhat differing approaches. Nelson and Hedrick [1] used a modified MHD approach, treating the hot electron annulus as a rigid non-interacting current ring and modeling the EBT as a bumpy cylinder. Nelson [2] used a slab-model kinetic approach and allowed the hot electron component to be perturbed.

In this paper, we also use low-frequency kinetic theory and include the perturbation behavior of the hot electron ring, as well as that of the warm core plasma. The model we study is that of a bumpyless torus. We find that the response of the hot electron species leads to a marked enhancement of the compression of the core plasma. This is a new physical effect, overlooked in the analysis of Ref. 2. In the limit of

negligible core beta, the plasma is found to be interchange stable when the annulus beta value exceeds 20% (or approximately four times the ratio of the annulus width to the local radius of curvature). This is the same result as before, although we will show that it comes from slightly different physics. Our most significant result is that as the core pressure is increased, the plasma will again become interchange unstable, at values for the core plasma beta which are substantially smaller than that for the ring beta, in contrast to earlier predictions.

2. PHYSICAL BEHAVIOR OF PLASMA AND RINGS

In the EBT device, macrostability is provided by the hot electron rings, created through microwave heating. These have a large dipolar diamagnetic current and produce a local magnetic well, which can lead to average minimum-B stability. The experimentally observed transition from the cold, noisy C-mode of operation to the relatively quiet T-mode which occurs when the ring beta is increased beyond a value of 10-15% is generally associated with this stability mechanism. Previous theories [1,2] calculated this beta threshold to be 10-20%, in good agreement. The other theoretical prediction, that the plasma is still stable for the core beta comparable to the ring beta above threshold, is difficult to check since current EBT experiments cannot achieve core beta values above 0.5-1.0%.

Ideally, the bulk plasma profile in EBT is nearly flat topped, with the magnetic well due to the annulus located where the pressure falls off [cf. Fig. 4 of Ref. 1]. In the region of interest, defined as the region where the radial gradient of the magnetic field strength is non-negative, we will make the crude simplifying assumption that the hot electrons and the warm core plasma have the same density profile. (The spatial dependence of their temperatures will be ignored, also for simplicity.) For later reference, we note that the density scale length (or ring half width), r_p, divided by the radius of curvature, R_c, is considered to be about 0.05 in current EBT experiments. The hot electron to core plasma temperature ratio is $T_h/T_i \simeq 10^3$; the density ratio, $\delta = N_h/N_i$, is about 0.1 or smaller.

The toroidal core plasma behaves like a warm fluid, for which the diamagnetic frequency, $\omega_* = -i(v_{th}^2/\Omega)(\hat{\underset{\sim}{b}} \times \underset{\sim}{\nabla} \ell n N)\cdot \underset{\sim}{\nabla}_\perp$, and the magnetic drift frequency, $\omega_d = -i\,\Omega^{-1}\left[v_\parallel^2(\hat{\underset{\sim}{b}}\times\hat{\underset{\sim}{b}}\cdot\underset{\sim}{\nabla}\hat{\underset{\sim}{b}}) + \tfrac{1}{2}v_\perp^2(\hat{\underset{\sim}{b}}\times\underset{\sim}{\nabla}\ell n B)\right]\cdot\underset{\sim}{\nabla}_\perp$, may be taken to be smaller than the fluctuation frequencies, ω, of interest here. The core plasma basically responds to $E \times B$ motion. Hence, its pressure perturbation (for an isotropic distribution) is given by the MHD expression

$$\tilde{p} = -\underset{\sim}{\xi}_\perp\cdot\underset{\sim}{\nabla} p + \frac{\gamma P}{B^2}\left[\underset{\sim}{\xi}_\perp\cdot(\underset{\sim}{B}\cdot\underset{\sim}{\nabla}\underset{\sim}{B}) + \underset{\sim}{\xi}_\perp\cdot\underset{\sim}{\nabla}(\tfrac{1}{2}B^2) + \underset{\sim}{B}\cdot\tilde{\underset{\sim}{B}}\right] . \qquad (1)$$

Perturbed quantities are denoted by a tilde. Kinetic theory, for $\omega >> \omega_*, \omega_d$, yields an equivalent expression:

$$\tilde{p} = -eN_i(\omega_{*i}/\omega)(1+\tau)\tilde{\Phi} + eN_i(\omega_{di}/\omega)(1+\tau)\tilde{\Phi} + (\beta/4\pi)B\tilde{B}_{\parallel} , \qquad (2)$$

with $\tau = T_e/T_i$. The first term in either Eq. (1) or (2) is the convective pressure change; the remaining terms represent the change in pressure due to compression. Now recall the quasi-static condition for transverse perturbed pressure balance,

$$B\tilde{B}_{\parallel} + 4\pi\tilde{p}_{\perp} = 0 , \qquad (3)$$

which is generally valid for low frequency modes whose perpendicular wavelength is much smaller than its parallel wavelength or any equilibrium scale length. The condition (3) may be interpreted as eliminating the fast Alfvén wave from consideration. Taken together with either Eq. (1) or (2), it implies that the longitudinal magnetic field perturbation is proportional to the electrostatic part of the pressure fluctuation divided by $1 + \beta$. This is the usual MHD finite-beta effect.

The hot electrons in the annulus, on the other hand, due to their large perpendicular energy, respond poorly to $E \times B$

drifts and basically exhibit adiabatic behavior, i.e., $\omega \ll \omega_{*h}$, ω_{dh} . Their drift motion follows the field lines

$$\underset{\sim}{v}_{dh} \cdot \underset{\sim}{\nabla} \tilde{p}_{\perp h} + \tilde{\underset{\sim}{v}}_{dh} \cdot \underset{\sim}{\nabla} p_{\perp h} = 0 \ . \tag{4}$$

If the magnetic field is perturbed, the hot electrons will have their trajectories deformed accordingly. Thus, the ring current satisfies $\underset{\sim}{\nabla} \cdot \tilde{\underset{\sim}{J}}_{\perp h} \cong 0$, since it is mostly due to the perturbed ∇B-drift. Furthermore, because the surfaces of constant pressure are the same as the const-B contours in the adiabatic limit, we may express the hot electron pressure perturbation as

$$\tilde{p}_{\perp h} \cong \left(\frac{\partial p_{\perp h}}{\partial B}\right) \tilde{B}_{\parallel} = \tfrac{1}{2} \beta_h \left(\frac{\omega_{*h}}{\omega_{bh}}\right) B \, \tilde{B}_{\parallel} \ , \tag{5}$$

with ω_{bh} the velocity-averaged ∇B-drift frequency for the hot electrons. The expression in Eq. (5) is consistent with the statement of Eq. (4) since we may assume $T_{\perp h} \gg T_{\parallel h}$ from anisotropic heating.

Equations (2) and (5) combined with the quasi-static condition (3) now yield the longitudinal field perturbation as

$$B\tilde{B}_{\parallel} = -4\pi \tilde{p}_{\perp}^{\,e.s.} / [1 + \beta_c + \tfrac{1}{2} \beta_h (\omega_{*h}/\omega_{bh})] \ . \tag{6}$$

Here, $\beta_c = \beta_i + \beta_e$ is the total core beta, and $\tilde{p}_\perp^{e.s.}$ is the electrostatic part of the total perpendicular pressure fluctuation. If, for example, we use the slab equilibrium pressure balance relation to write $\omega_{*h}/\omega_{bh} \cong \omega_{*i}/\omega_{bi} = -2/\beta$ (since there is no curvature in the slab model), we find a near cancellation between the first and last terms in the denominator of Eq. (6). More precisely, we have

$$D \equiv 1+\beta_c + \tfrac{1}{2}\beta_h\left(\frac{\omega_{*h}}{\omega_{bh}}\right) \rightarrow \frac{\beta_c}{\beta}(1+\beta) \ , \qquad (7)$$

which for current EBT parameters is very small compared to unity. Clearly, the magnetic field perturbation is greatly enhanced by the behavior of the hot electron population. This interesting new physical effect does not occur in a rigid-ring analysis, nor was it noticed in Ref. 2. Its significance is that it produces a considerable enhancement of the bulk plasma compression. (specifically, the inductive part), which will be shown to influence the stability analysis.

3. DISCUSSION OF STABILITY ($\delta = 0$)

We confine our attention to low-frequency ($\omega \ll \Omega_i$) flute interchange modes. These are described by the equation

$$\frac{c^2}{c_A^2}(\omega-\omega_{*i})\ \nabla_\perp^2 \tilde{\Phi} - \left(\frac{4\pi i c}{B}\right)[\hat{\underset{\sim}{b}}\times(\hat{\underset{\sim}{b}}\cdot\underset{\sim}{\nabla}\hat{\underset{\sim}{b}})]\cdot\underset{\sim}{\nabla}_\perp(\tilde{p}_M + \tilde{p}_\perp) = 0 \ , \qquad (8)$$

which is equivalent to charge quasi-neutrality and is valid in general geometry for modes with small transverse wavelength. Equation (8) may be readily derived, for instance, from the

zeroth moment of the drift-kinetic equation with magnetic moment $\mu = Mv_\perp^2/2B$ and longitudinal invariant $J = v_\parallel R$ as constants of the motion [3]. The first term in Eq. (8) arises from the ion polarization drift and the finite gyroradius remnant of the ion E×B drift, the third term from the field line curvature drift of all species.

In order to discuss as simply as possible how the annulus stabilizes the bulk plasma, we will consider the hot electron density fraction $\delta = N_h/N_i$ to be vanishingly small even though its beta value is still finite. For current EBT parameters, this is not an unreasonable approximation. Also, we will employ a large-poloidal-mode-number local approximation, ignoring azimuthal variation in the equilibrium quantities. The enhanced compression effect described in Sec. 2 implies that $\tilde{p}_\perp = \tilde{p}_{\perp c} + \tilde{p}_{\perp h} = \tilde{p}_{\perp c}/D$. Then, take an isotropic, convective pressure perturbation for the warm core plasma: $\tilde{p}_{\parallel c} = \tilde{p}_{\perp c} = -eN_i(\omega_{*i}/\omega)(1+\tau)\tilde{\phi}$. Under these assumptions, Eq. (8) turns into a local dispersion relation,

$$\omega(\omega - \omega_{*i})\, k_\perp^2 \rho_i^2 = -\omega_{\kappa i}\omega_{*i}(1+\tau)(1+\frac{1}{D}) \quad , \tag{9}$$

with $\omega_{\kappa i}$ the velocity-averaged ion curvature-drift frequency. We will analyze Eq. (9) in various limits.

First, suppose that the core beta is negligibly small. When the hot electron ring is absent ($\beta_h = 0$), we have $D \simeq 1$ and immediately obtain the usual interchange instability with $\omega^2 = c_s^2/r_p R_c$, purely growing if we neglect finite Larmor radius stabilization (i.e., $\omega \gg \omega_{*i}$) . In this case, the driving term

in Eq. (9) involves pure curvature only, which merely shows that the bulk plasma cannot be stabilized by its own diamagnetic well.

However, with the annulus present, we have $D \cong \omega_{\kappa i}/\omega_{bi}$, if we temporarily overlook the detail of anisotropy. Then one obtains $\omega^2 = -\omega_{\kappa i}\omega_{*i}(1+\tau)[1+\omega_{bi}/\omega_{\kappa i}] = -\omega_{*i}\,\omega_{di}(1+\tau)$, and the mode becomes stable when the magnetic drift frequency ω_{di} changes sign relative to ω_{*i}. This requires a local minimum in the field strength such that the gradient is of order $|\nabla B/B| \simeq 1/R_c$, which in turn implies that, for stability, the ring beta must be at least as large as the threshold value

$$\beta_h = 4(r_p/R_c) \cong 20\% \ . \qquad (10)$$

This result is the same as that obtained by using a rigid-ring analysis[1]. The reason is that the hot electron species is incompressible in the limit $N_h/N_i \to 0$ and, as long as $\beta_c \ll \beta_h$, therefore enters the problem only through the equilibrium pressure balance.

For satisfactory reactor performance, it is desirable to boost the core plasma pressure and also to have a narrow annulus (i.e., reduce the ring power input). Under these conditions, it is possible to have $\frac{1}{2}\beta_c|\nabla p/p| > 1/R_c$, which means that curvature may be ignored in the equilibrium pressure relation (as in a slab model). Then one finds that interchange modes are no longer stable, even though mod-B may still have a local minimum.

A slightly more detailed explanation for this transition back to instability follows from the observation that, generally speaking, the enhanced compressional terms (enhancement factor = 1/D) can contribute to stability only when D is negative. Such is indeed the case when $\beta_c = 0$. But, as β_c increases in value, the sign of D can become positive. This can be seen from writing

$$D \cong \omega_{Ki}/\omega_{bi} + \beta_c(1-\omega_{*i}/2\omega_{bi})$$

$$\propto (\varepsilon-\tfrac{1}{2}\beta_c)(1+\beta_c) - \tfrac{1}{2}\beta_c\beta_h \ , \tag{11}$$

with $\varepsilon = r_p/R_c$. Equation (11) yields an upper limit on β_c for stability against interchange:

$$\beta_c \le 2\varepsilon/(1+\beta_h) \ . \tag{12}$$

For β_h in the 20-40% range, this limit requires $\beta_c \le$ 7-8% .

Figure 1 displays the regime of values for β_i and β_h (shown shaded) within which the enhanced compression terms can contribute to stabilization. (Setting $T_e/T_i = 0$ does not materially affect the net result.) The upper boundary of this region corresponds to where $D = 0$, the left-hand boundary to where $\omega_{di} = 0$. For purposes of comparison, we also plot in Fig. 1 the three curves labeled $\delta = 0$, 0.05, and 0.10 . These are the marginal stability curves derived by Nelson [2]: interchange modes are claimed to be "stable" for all values of β_i below a given such curve. Qualitatively similar curves were obtained by Nelson and Hedrick [1], with annulus elongation instead of δ as the parameter. Both of these theories predicted

substantially higher values of β_i to be stably attainable than does our theory. The difference becomes quite clear (for $\delta = 0$) when β_h is larger than 35% and β_i is greater than about 7%. We contend that the diminished stable region obtained in our theory follows from properly taking into account the adiabatic response of the annular hot electrons.

4. STABILITY ANALYSIS FOR FINITE δ

In what follows, we will retain space-charge effects associated with finite $\delta = N_h/N_i$. Also, we will not begin from Eq. (8), but will instead use a different though equivalent approach in order to compare directly with the analysis of Ref. 2.

For flute modes, only the electrostatic potential $\tilde{\Phi}$ and the parallel component $\tilde{B}_{\parallel}$ are needed to describe the perturbed electromagnetic fields. These two field quantities are related by the condition of quasi-neutrality, $\sum q\tilde{n} = 0$ (with the summation being over all species), and by the quasi-static condition, Eq.(3). The partial charge density is given by

$$q\tilde{n} = -\frac{k_D^2}{4\pi}\left[\tilde{\Phi} - (\omega-\omega_*)\left\langle\frac{1}{\omega-\omega_d}\left(1-\frac{k_\perp^2 v_\perp^2}{2\Omega^2}\right)\left(\tilde{\Phi}+\frac{v_\perp^2}{2\Omega}\tilde{B}_{\parallel}\right)\right\rangle\right] , \tag{13}$$

and the total transverse pressure perturbation by

$$\tilde{p}_\perp = \sum \left(\frac{qMN}{T}\right)(\omega-\omega_*)\left\langle\frac{v_\perp^2/2}{\omega-\omega_d}\left(1-\frac{k_\perp^2 v_\perp^2}{2\Omega^2}\right)\left(\tilde{\Phi}+\frac{v_\perp^2}{2\Omega}\tilde{B}_{\parallel}\right)\right\rangle . \tag{14}$$

If, as before, we assume $\omega >> \omega_{*i,e}, \omega_{di,e}$, for the bulk plasma ions and electrons and reverse the inequality for the hot electrons, we can easily derive a local dispersion relation: $a\omega^2 + b\omega + c = 0$. The coefficients of the quadratic equation are:

$$a = (k_\perp \rho_i)^2 + \delta^2 \left(\frac{\beta_i}{2D}\right)\left(1 - \frac{\omega_{*h}}{\omega_{bh}}\right)^2 \tag{15}$$

$$b = \delta\left[\omega_{*i} - \omega_{di} - \left(\frac{\beta_c}{D}\right)\left(1 - \frac{\omega_{*h}}{\omega_{bh}}\right)(\omega_{*i} - \omega_{di} - \omega_{bi})\right] , \tag{16}$$

$$c = \left[(\omega_{*i} - \omega_{di})\ \omega_{di} - \omega_{bi}{}^2 + \left(\frac{\beta_c}{2D}\right)(\omega_{*i} - \omega_{di} - \omega_{bi})^2\right](1+\tau) , \tag{17}$$

with $\beta_c = \beta_i + \beta_e$ and $\tau = (1-\delta)(T_e/T_i)$. The implicit neglect of hot electron gyroradius effects and the rather cavalier handling of temperature anisotropy in this derivation may be suspect. However, with Eqs. (15)-(17), the local dispersion relation has the same form as that derived in Ref. 2. For simplicity, we will again take $T_e = 0$.

We now analyze this local dispersion relation using two different models. The first such is the <u>slab model</u>, referred to previously and also used exclusively in the work of Ref. 2. In this model, we have $D \propto \beta_i$ from Eq. (7). A curious consequence is that then β_i and β_h no longer appear separately in

the dispersion relation, rather only in combination as the total beta $\beta = \beta_i + \beta_h$. The other free parameter is δ . The condition for stability, namely, $b^2-4ac \geq 0$, is never satisfied when $\delta = 0$. In Fig. 2 is plotted the density fraction required for marginal stability (with $k_\perp \rho_i = 0.1$). At high beta values, δ must be greater than roughly 5% to have stability. The result shown in Fig. 2 is what a slab-model treatment, such as that of Ref. 2, should find. A stability plot like that of Fig. 1 cannot be obtained in this model.

However, because the effect of the curvature cannot be ignored, we will adopt instead a <u>local model</u> such that $\omega_{*i}/\omega_{bi} = -(2/\beta)(1-\omega_{\kappa i}/\omega_{bi})$, with the curvature and various gradients replaced by their local values, e.g., $|\omega_\kappa| \propto 1/R_c$. A marginal stability analysis then yields β_i as a function of β_h , as in Fig. 1 earlier. The complete results (for $k_\perp \rho_i = 0.1$) are shown in Fig. 3

We see that for finite values of δ , there are now <u>two</u> stability regions. The lower one is nearly the same as the fundamental stability region for $\delta = 0$ (shown shaded) which was discussed previously. The only difference is that the threshold for β_h, when β_i is zero, is shifted from 20% down to 10% as δ increases from zero. For $\delta \geq 0.05$, the left-hand boundary of this lower region approximates the diagonal line beyond which $|B|$ no longer has a minimum. The upper boundary is still determined by the strong effect at $D = 0$. The rather singular behavior when $D \to 0$ appears to indicate conversion to a new electromagnetic mode carried by the hot electrons.

The upper stability region shown in Fig. 3 allows larger values for β_i but is probably unrealistic unless the ion temperature can be dramatically increased. To appreciate this, consider that the ratio of ring and ion plasma pressures is given by

$$\beta_h/\beta_i = \delta(T_h/T_i) \ . \tag{18}$$

For current EBT parameters, this ratio is about 100; even for the proposed EBT-P device, it is still an order of magnitude. Furthermore, if one tries to decrease the hot density fraction, the upper stability region disappears.

Thus, the relevant stability region is the lower one. We should append the qualification that in the vicinity of the vertical axis in Fig. 3, the stability results are probably not creditable since $\beta_h \simeq 0$, $\delta \neq 0$ implies an unphysical cold but yet adiabatic response for the annulus electrons.

Nevertheless, our overall conclusion remains essentially unchanged: viz., that the maximum value for the toroidal core pressure allowed for stability against interchange modes is rather less than the annulus pressure and substantially smaller than predicted in other theories. Whether this somewhat pessimistic result for EBT stability will be confirmed by a non-local calculation in a realistic geometry and with a proper equilibrium remains to be seen.

ACKNOWLEDGMENTS

Valuable discussions with Professor M. N. Rosenbluth and useful information received from Dr. J. L. Johnson are gratefully acknowledged. This work was partially supported by the U. S. Department of Energy under Contract EY-76-S-02-3237.

NOTED ADDED IN PROOF: Curves similar to those of Fig. 3, with two stability regions, were recently obtained also at Oak Ridge National Laboratory by D. A. Spong (private communication).

REFERENCES

[1] D. B. Nelson and C. L. Hedrick, Nucl. Fusion 19, 283 (1979).

[2] D. B. Nelson, "Effect of Hot Electrons on Magnetohydrodynamic Modes in EBT" (Oak Ridge National Laboratory Report ORNL/TM-6824, June, 1979).

[3] M. N. Rosenbluth, private communication.

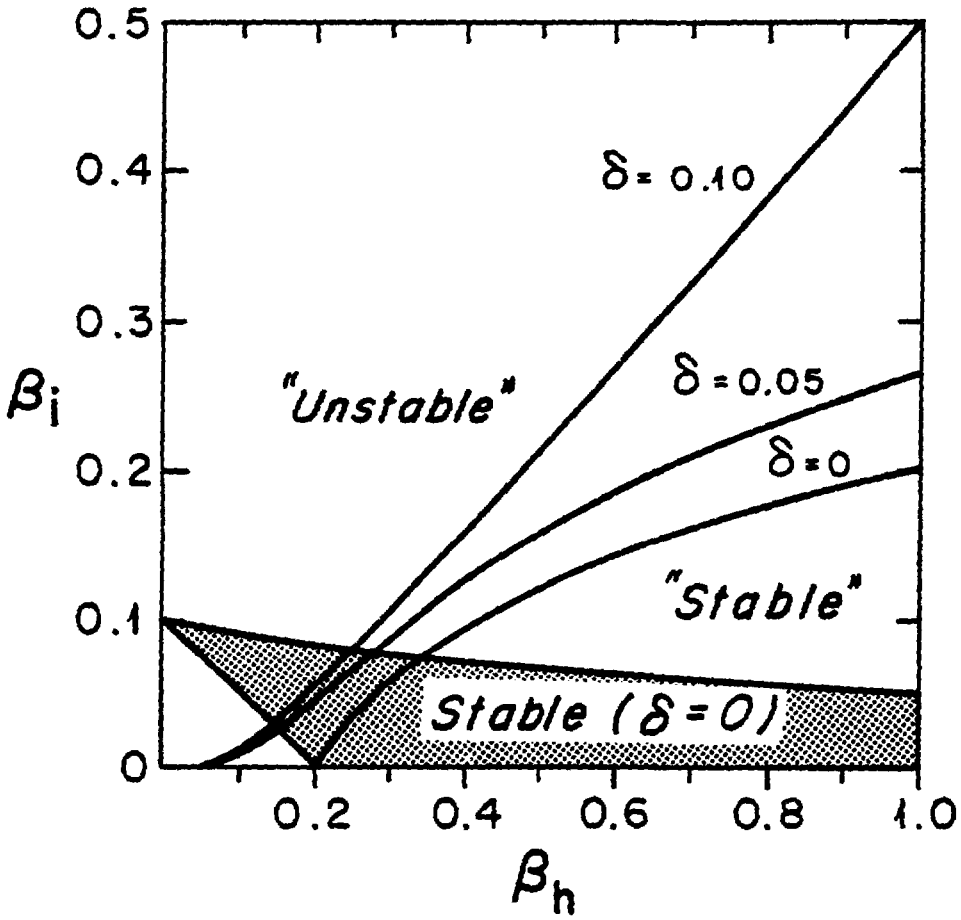

FIGURE 1. Toroidal core plasma and annulus pressures, β_i and β_h, for interchange stability when $\delta = 0$, as derived in our theory (shaded region). Reference #2 predicted "stability" below and "instability" above the marginal curves ($\delta = 0$, 0.05, 0.10), shown here for comparison.

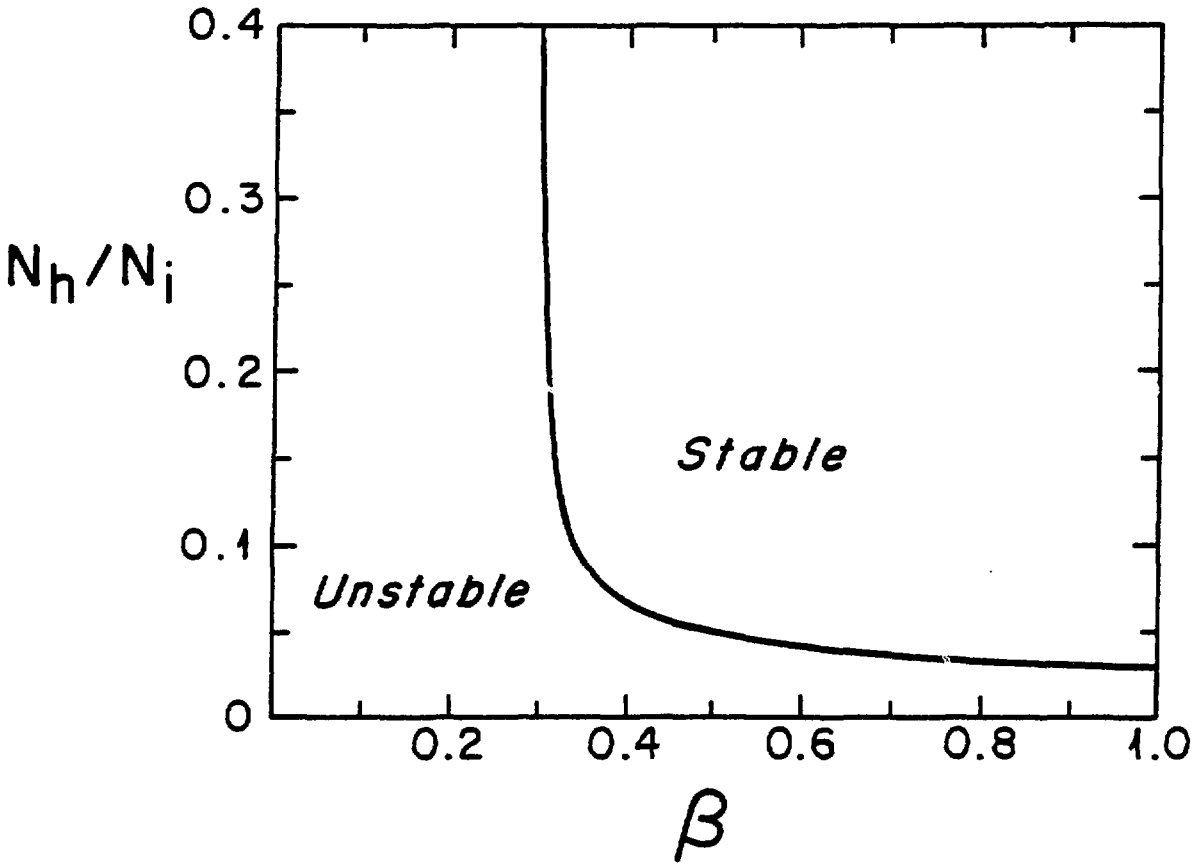

FIGURE 2. Hot electron density fraction, $\delta = N_h/N_i$, required for marginal stability for a given total beta, $\beta = \beta_i + \beta_h$, in a slab model (no curvature); $k_\perp \rho_i = 0.1$.

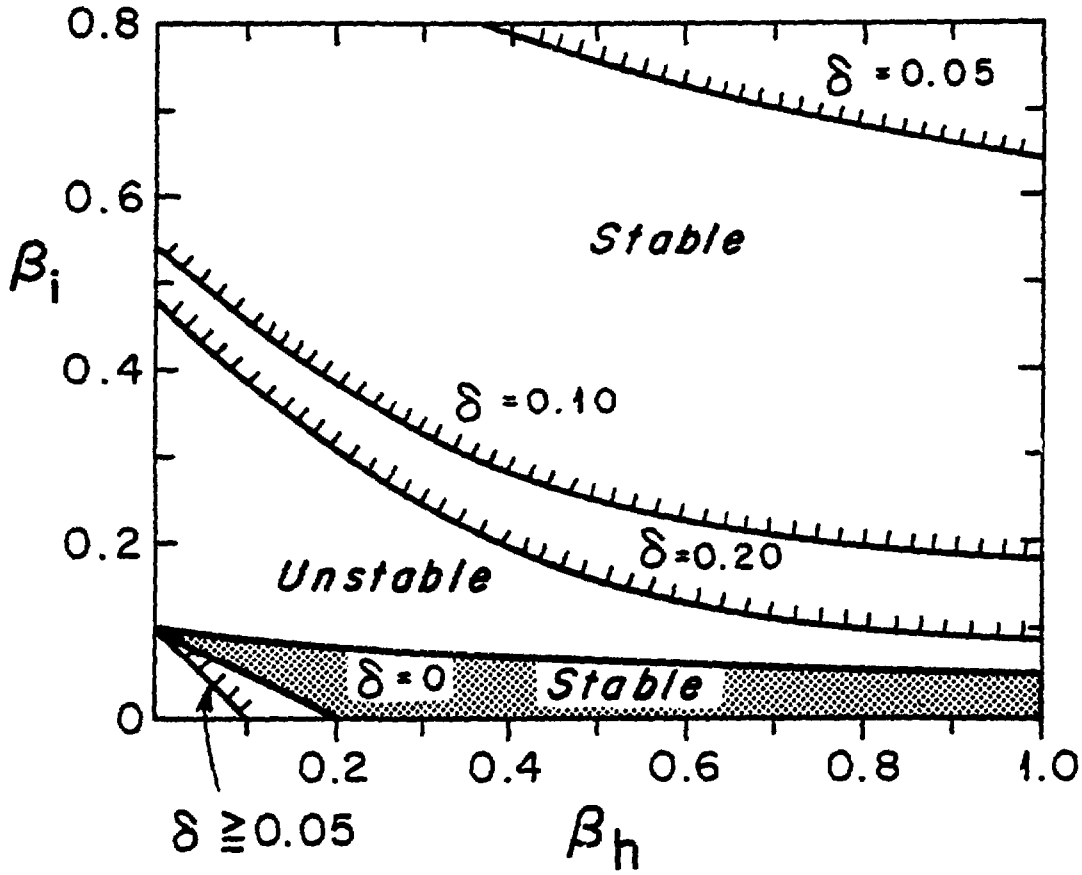

FIGURE 3. Marginal stability boundaries for β_i vs. β_h, with δ as parameter and $k_\perp \rho_i = 0.1$. Interchange stable both below the common lower boundary (top of the fundamental region for $\delta = 0$, shown shaded) and also above the upper curve (labeled by the appropriate δ value).

DISCUSSION

D. SPONG: Do you have any idea how the effects of realistic geometry and profiles may change the stability boundaries obtained in the slab model?

J. VAN DAM: We would like to calculate realistic equilibria and to develop a genuine toroidal geometry treatment. A three-dimensional approach will obviously allow ballooning instabilities, in addition to the flute variety discussed here. I have heard the comment from Dr. J. L. Johnson that a Helmholtz shear-type instability may become possible if one does not assume similar radial density profiles for the hot electrons and the core plasma.

J. T. WOO: At low β_{ring}, your results are less stringent for toroidal stability than Nelson's. Can you comment on the reason for the difference?

J. VAN DAM: The physical reason is not clear. What can be said is that at least for small toroidal beta values, stability is still mostly determined by the magnitude of the total beta. This would imply that the marginal stability threshold value for the ring beta is then slightly decreased from its value for the case of zero core beta.

G. HASTE: The present experiment can't reach β_{core} comparable with the ring β. However, it appears that at zero β_{core} the value of β_{ring} at which the stabilization takes place appears to be different in your theory and in others (say Nelson's). Could this fact be used to distinguish between them?

J. VAN DAM: This may be interesting, although I cannot comment on the experimental capabilities. Both in Nelson's results and in ours, the threshold ring beta value at zero core beta depends on the value of the hot electron density fraction $\delta = n_h/n_i$; that is, it decreases from the value of about 20% with increasing δ (due to space-charge stabilization). However, threshold is not sharply defined for finite δ in Nelson's results. Also, our theory indicates that the ring beta threshold will be no smaller than 10% (for the parameters used in both studies) since, below this value, the magnetic field gradient is no longer reversed.

8. OPEN SESSION DISCUSSIONS

Panel Members:

N. A. Uckan, W. B. Ard, G. E. Guest, R. A. Dandl, A. Favale, G. R. Haste, C. L. Hedrick, H. Ikegami

8.1 INSTABILITIES IN HOT ELECTRON PLASMAS

INSTABILITIES IN HOT ELECTRON PLASMAS: SUMMARY OF THE OPEN SESSION

M. C. Vella
Lawrence Berkeley Laboratory
Berkeley, California 94720

Twenty years of experimental and theoretical investigation of instabilities in hot electron plasmas were surveyed. Attention focused on phenomena occurring in simple mirror experiments and their possible relevance to the T-M transition presently observed in EBT and NBT.

The session began with a review by Bill Ard of the properties of instabilities observed in PTF, a simple mirror experiment that ran in the mid-1960s. Microwave heating was at the fundamental electron cyclotron resonance, with the second-harmonic zone in the hot electron confinement region. X-ray evidence indicated the possibility of weak ring formation. Plasma β was limited to $\lesssim$10% by instability, of which two distinct types were observed. In Mode 1, most of the stored particle energy was lost along field lines in $\lesssim$1 μs. This correlated with a burst of intense, narrow-band microwave radiation at $\omega_\mu/2$. Mode 2 was observed to have a flute-like structure, an azimuthal phase velocity approximately equal to the electron ∇B drift velocity, and an overall time scale of $\sim$10-100 μs. Ard felt that Mode 1 was driven by β and that Mode 2 was associated with inadequate cold electron stabilization. However, he noted that these are difficult to distinguish because, at fixed microwave power, lower pressure and/or lower cold plasma density is accompanied by a rise in β.

Experimental results from the TPM simple mirror at Nagoya in late 1960s were presented by Hideo Ikegami. Like the PTF, this device has bulk heating at the fundamental with the second-harmonic zone in the confinement region. Strong electromagnetic instabilities at one-third harmonics of the fundamental have been observed to dump a large fraction of the stored energy in $\sim$1 μs. From x-ray measurements, the high energy component (>100 keV) appears unaffected by the instability, which was identified as a Whistler mode from the polarization of radiation. This instability has been triggered during the afterglow plasma both by

pulsing the microwave power and by extracting cold electrons with a positively driven probe. Ard felt that this may be similar to the Mode 1 instability seen in PTF.

Ray Dandl summarized the hot electron instabilities seen in ELMO, a variable ratio mirror that operated from approximately 1964 to 1973. Three microwave heating sources (10.6 GHz, 35 GHz, and 55 GHz) were available for use in various combinations of fundamental resonance and upper and lower off-resonant heating. With microwave heating only at the fundamental (10.6 GHz), low power experiments exhibited narrow-band instabilities near $\omega_\mu/2$ with only a fractional decrease of perpendicular energy from an instability. High power experiments had broad-band instabilities from ∿3-12 GHz. These instabilities were absent when a small fraction (∿10% of resonant) of upper off-resonant (35-GHz) power was added. In fact, only with both microwave sources could high ring β (∿0.5-1) be achieved. Strong ring formation was first observed in ELMO under these circumstances, and later Ikegami pointed out the significance of second-harmonic heating. These high-β plasmas were observed to be unstable at low gas pressure, where each event resulted in rapid loss of the energetic plasmas. Dandl felt that attempts at detailed studies of these high-β instabilities had only limited success because of failure to initiate the instability by external means. However, subsequent associated wall radioactivity suggested that the electron loss was sufficiently fast for the resulting charge imbalance to produce 0.5-MeV protons. These high-β instabilities could not be stimulated by either pulsed rf or pulsed extraction of cold electrons in cw operation.

The theoretical perspective on hot electron instabilities in simple mirrors was summarized by Gareth Guest and Lew Hedrick. Guest felt that upper off-resonant heating in ELMO produced a more stable plasma, both by the reduction of the temperature anisotropy of the hot electrons and by the relativistic broadening of the particle cyclotron spectrum. Flute modes observed in PTF and ELMO were thought to be electrostatic in character and, therefore, susceptible to cold plasma stabilization. In general, Guest felt that linear theory had been successful in identifying critical conditions for the onset of instability, but that theoretical understanding of nonlinear evolution was less successful. Hedrick

pointed out that the theoretical perspective on instabilities in simple mirrors was well summarized in an Oak Ridge National Laboratory Report (ORNL-4688, 1971), although some phenomena in the canted mirror facility were not fully understood at shutdown.

Underlying the discussion of simple mirror instabilities is an interest in the onset and the nature of the T-M transition observed in present bumpy torus experiments, since this affects present reactor scaling. Dandl pointed out that detailed experimental study has not yet been possible, partially because of the high priority assigned to the investigation of other phenomena, e.g., transport. However, experimental difficulties associated with wall sputtering during unstable operation are also a concern. Of particular interest are the deterioration of subsequent machine performance caused by aluminum impurities and the deposition of aluminum on diagnostics. He also pointed out that the half-harmonic (fundamental) microwave emission common in ELMO is not observed at present in the M-mode. Ikegami believes that M-mode instabilities are electromagnetic, but this has not yet been confirmed by experiment. The general consensus was that transition to the M-mode is inhibited by cold plasma and neutrals. Ard pointed out that neither the critical densities nor the instability mechanisms have as yet been identified. Glenn Haste and Lew Hedrick suggested the possibility that the T-M transition may be associated with the thermal runaway of the core plasma. When the electron energy confinement time exceeds the neutral particle replacement time, a positive feedback between electron heating and decreasing ionization cross section can occur. This conjecture is based on both simulation and the experimental observation that the onset of the T-M transition is affected by wall conditioning. In addition, Haste noted that passing from the T-mode into the M-mode by lowering pressure was accompanied by a rise in stored energy and higher peak stored energy in the unstable M-mode.

Gareth Guest and Rene Dominguez discussed the continuing theoretical study of plasma instability mechanisms in bumpy torus geometry. Investigation is presently concerned with the effect on stability of cold plasma, local variations in the space potential, and finite length collisionless mixing. Guest expressed the opinion that improved theoretical techniques

developed in recent years allow better treatment of real geometries. Significant progress may be possible in the future.

In conclusion, experimental and theoretical investigation of the T-M transition is in a relatively early stage of development. At present, information available from EBT and NBT is insufficient to identify observed instabilities with known simple mirror phenomena, which might be studied more easily. Effects of the intrinsic physical differences between open and closed geometry have not been isolated, although an awareness of simple mirror results has provided useful guidance. General agreement was evident that cold plasma and neutrals have a stabilizing effect in the bumpy torus experiments.

INSTABILITIES IN MIRROR CONFINED HOT ELECTRON PLASMAS

W. B. Ard

McDonnell Douglas Corporation
St. Louis, Missouri 63166

Early experiments on ECRH plasmas in simple mirrors showed that under some operating conditions rapid losses of a considerable fraction of the plasma energy could occur. Further observations allowed the identification of two distinct modes of instability. These experiments were carried out in the PTF device at ORNL about 1965-1966. The PTF device was a simple mirror machine heated with up to 4 kW of ECRH power at a frequency of 10.6 GHz. The plasma radius in the midplane was about 10 cm.

Stable plasmas could be produced with electron temperature in the range 50-100 keV and densities of a few x 10^{11} cm^{-3}. The average beta was from .05 to .1. The energy density was approximately constant over the plasma although it did have a maximum near the outer edge of the plasma (Ref. 1).

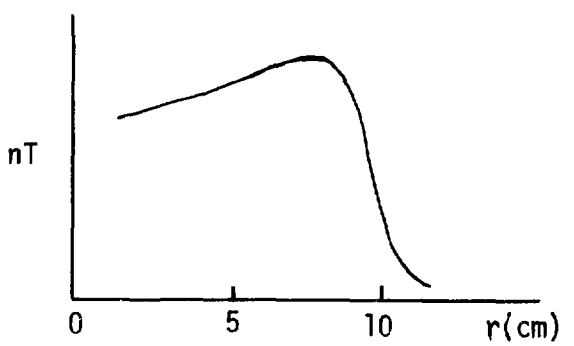

Although there was no apparent hot electron ring, there was evidence of a thin shell of very hot electrons near the outer edge of the plasma. It was not determined whether the location of the hot electron shell was at the position of the 2nd harmonic resonance; however, it may well have been.

The general behavior of the plasma was the increasing the ECRH power input increased the stored energy at constant background pressure,

and, at constant ECRH power, the stored energy increased with decreasing background pressure. However, at some point, further power increases or pressure decreases resulted in fast dumps of stored energy. These limits of pressure and power levels for stable operation were dependent on the magnetic field, or location of the resonance heating zone. Although the behavior of the plasma at a given pressure, power level, and magnetic field was very reproducible, the nature of the stability boundaries was confusing until it was discovered that the hot electrons lost during an energy dump were lost either radially across the field lines, or along the field to the ends, but never both ways in a given energy dump. Once it was discovered that two completely different instabilities were involved, the stability boundaries for each instability could be determined.

The instability that dumped hot electrons out along field lines (mode 1) was only indirectly dependent on power and pressure. This instability developed when the stored energy reached a particular value. The limiting stored energy increased as the magnetic field was lowered, moving the resonance zone further from the midplane toward the mirror throats (Ref. 2).

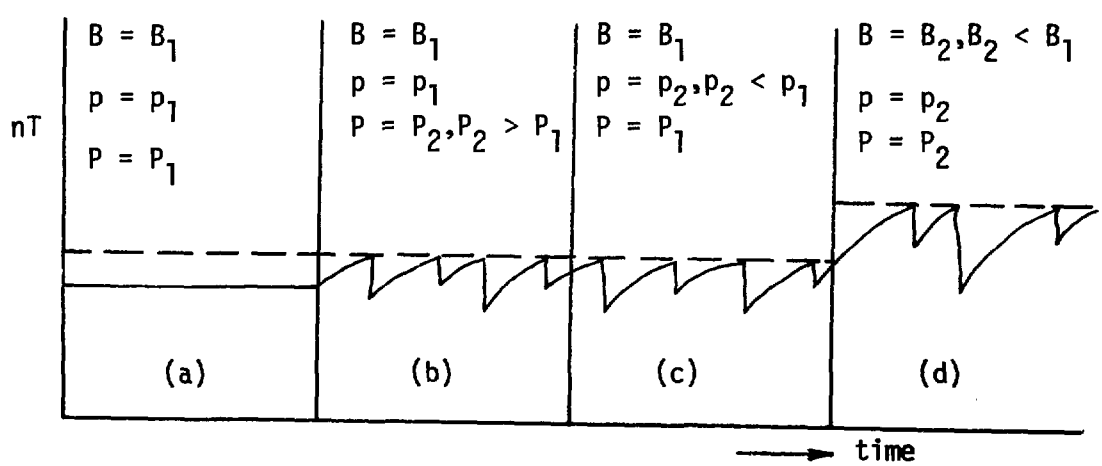

The behavior illustrated above was observed provided the external neutral pressure, p, was larger than some threshold pressure, p_0. If the external pressure were near p_0, gross behavior similar to that shown above was observed; however, the energy lost in the dumps was lost

across the magnetic field lines (mode 2). The onset of the instability occurred at a pressure p_0 and p_0 was only a very weak function of the stored energy.

The reason for the initial confusion about the stability boundaries was that the standard operating procedure was to set the magnetic field and heating power level and to reduce the pressure after formation of the plasma in order to increase the plasma energy. The result was that the plasma became unstable to whichever instability had the highest pressure threshold at the particular field and power settings.

The high beta, or high stored energy (mode 1), instability was identified with the mirror instability, or loss of equilibrium, when

$$\beta > \frac{v_{\parallel}}{v_{\perp}} \quad .$$

The beta at the onset of the instability was consistent with this condition if it was assumed that the hot electron turning points lay inside the resonant mod B surface. During this instability fast electrons were lost out the mirror. Measurements of the loss as a function of radius showed that the loss rate during the event was essentially independent of radius. During an event as much as 10-15% of the total plasma energy could be lost in about 1-2 μsec. During the event microwave radiation was detected at a frequency near one-half the heating frequency, near 5.3 GHz. The microwave E field was perpendicular to the static B field.

The instability that developed because of low background neutral pressure, mode 2, was identified as a flute mode (Ref. 3). The surface of the plasma developed azimuthal perturbations that propagated around the surface in the direction of the electron grad B drift with a phase velocity consistant with the hot electron grad B drift velocity. The modes most often seen were

$$4 \leq m \leq 10 \quad .$$

The radial transport velocity was about 10^5 cm/sec. This was estimated from the observation that about one-tenth of the total energy in a plasma with a radius of about 10 cm would be scraped off by the radial

limiter in about 10 μsec. The same instability could develop after turn-off of the microwave heating power. At turn-off, the mode would appear after the cold background plasma had decayed, about 1 msec after turn-off of the power. The mode would continue for 100-200 μsec and dump essentially all the hot electron plasma.

These two instabilities were the only unstable modes observed in the PTF plasma. It is possible that fine grained turbulence in the hot plasma could have degraded confinement in the device without being detected in the experiments. However, any observed limit in the performance of the PTF plasma appeared to be associated with the onset of one or the other of the two modes described above.

References

1. W. B. Ard and R. A. Dandl, Proc. of VI Intern. Conf. on Ionization Phenomena in Gases, Paris, Vol. 4, pp. 75-78 (July 1963).
2. W. B. Ard, R. A. Dandl and R. F. Stetson, Phys. Fluids 9, 1498 (1966).
3. E. H. Christi, Ph.D. thesis, Tulane University (1966).

8.2 POWER BALANCE IMPLICATIONS FOR A REACTOR

POWER BALANCE IMPLICATIONS FOR A REACTOR: SUMMARY OF THE OPEN SESSION

W. B. Ard
McDonnell Douglas Corporation
St. Louis, Missouri 63166

The consensus from the open session discussions on ring power balance was that the identified energy loss processes (drag, scattering, and synchrotron radiation) and the estimates of energy loss as a function of hot electron temperature, magnetic field, and plasma parameters are probably correct. The microwave power required to sustain the rings in EBT-I, NBT, and recently in EBT-S is modest and reasonably well estimated by the theoretical models. There was, however, a considerable amount of discussion about how the total power to sustain the rings would scale to a reactor.

The question here was how the ring volume will scale with magnetic field, core plasma radius, magnetic field gradients, etc. The modest parameter range accessible in the past mirror and EBT/NBT experiments, which all had similar device and plasma parameters, is not sufficiently broad to make a credible extrapolation to future larger devices, especially to a reactor. When scaled up from EBT-I/S, the ring power requirements for a reactor can become favorable or unfavorable depending on the scaling assumptions made for the volume as well as the completeness and/or self-consistency of the models used (i.e., stability, ring-core interaction, etc.). There was also concern that rings sufficiently thin to allow a favorable power balance in a reactor would require the radial density gradients in the core plasma to be unrealistically steep. However, transport models predict rather steep density profiles. Of course the validity of the models requires that the scale lengths of the

density gradients be at least several gyroradii. Because the ring electrons and core ions near the surface have comparable gyroradii (i.e., relativistic electron gyroradius $\sim$ ion gyroradius near the rings), minimum ring thickness (of a few gyrodiameters) and minimum core density scale lengths are not incompatible.

Another possible limitation on the thinness of the ring could result from stability requirements on the ring or on the minimum ring dimensions required for core stability. Stability calculations are presently under way to determine the limits of the ring thickness. On the other hand, a number of ring instabilities (Whistlers, mirror modes, etc.) are avoided through isotropization. Since the ring length is related to the size of $T_{\parallel}/T_{\perp}$, such requirements may lead to a lower bound on the finite ring length.

RING POWER BALANCE IMPLICATIONS FOR A REACTOR*

Nermin A. Uckan
Oak Ridge National Laboratory
Oak Ridge, Tennessee 37830

1. INTRODUCTION

The high-beta (β), hot electron rings (annuli) are an essential part of the EBT concept and play an important role in confinement and operating characteristics. If the plasma in a reactor were to be heated to ignition, the toroidal plasma heating would be turned off; the ring heating will, however, have to be sustained throughout the steady-state operation. Therefore, the power required to sustain the rings defines the figure of merit (recirculating power fraction) for a reactor and affects the economic performance.[1]

Self-consistent treatment of the problem requires consideration of the following:

- particle orbits,
- heating and formation,
- equilibrium and stability requirements,
- ring-core interaction,
- scaling, and
- power balance.

Each of the more than two dozen papers (experimental and theoretical) presented at this workshop covered one or more of these areas and treated them in different ways by emphasizing their relative importance. Specifically, four papers concerning the ring power balance were presented in the Power Balance session[2] (see Sect. 6). While disagreement is seen in details, the models developed in these and earlier papers[2-4] are in qualitative agreement, predicting the dominant loss mechanisms to be

- drag cooling,
- scattering, and
- synchrotron radiation.

*Research sponsored by the Office of Fusion Energy, U.S. Department of Energy, under contract W-7405-26 with the Union Carbide Corporation.

The modeling of the microwave power necessary to sustain the ring at high β against these losses has been based on the experimental observations in ELMO and EBT-I/NBT. These studies[1-4] indicate that the drag losses (the energy transfer between the relativistic ring electrons and the toroidal plasma electrons via Coulomb collisions) dominate a significant range of the ring energy and that power requirements are reasonably well estimated in the present experiments (EBT-I/S). When scaled up from the existing experiments, the ring power requirements for a reactor can become favorable or unfavorable depending on the scaling assumptions made and on the completeness and/or self-consistency of the models used. Here, simple formalisms will be used for the fusion power and ring power densities to indicate the effects of the various parameters and assumptions on the reactor Q value ($Q_{ELECTRIC}$ or Q_E).

2. REACTOR Q_E VALUE

A simple reactor power flow diagram is shown in Fig. 1. The reactor Q_E value can be defined as

$$Q_E = \frac{P_{net}}{P_m} = \frac{P_e - P_m}{P_m} , \tag{1}$$

where

P_{net} = net electrical power,

P_e = gross electrical power produced, and

P_m = input maintenance power.

In terms of reactor parameters,

$$P_e = \eta_{th}(P_{th} + P_\mu) \tag{2}$$

and

$$P_m = \frac{P_\mu}{\eta_\mu} + P_{aux} , \tag{3}$$

where η_{th} and η_μ are the thermal conversion efficiency and the microwave conversion efficiency, respectively; P_{aux} is the power required for auxiliary loads (refrigeration, pumping, etc.); P_{th} is total "thermal" fusion power; and P_μ is the microwave power necessary to sustain the rings. The details of P_{th} and P_μ will be discussed in the next sections. Thus, Q_E may be expressed as

$$Q_E = \frac{\eta_{th}(P_{th} + P_\mu) - (P_{aux} + P_\mu/\eta_\mu)}{P_{aux} + P_\mu/\eta_\mu} . \tag{4}$$

Assuming $P_{aux} < P_\mu/\eta_\mu$, then

$$Q_E = \eta_{th}\eta_\mu \frac{P_{th}}{P_\mu} - (1 - \eta_{th}\eta_\mu) . \tag{5}$$

A large value of Q implies a lower recirculating power fraction and a higher overall reactor efficiency. For small Q, the reactor cost/kW(e) rises sharply, but for higher values of Q, the unit cost [$/kW(e)] decreases and is relatively flat for Q > 15.[5] Economic considerations indicate that Q ∿ (8-12) is within the compatible unit cost range of other fusion reactors (i.e., tokamaks).[5,6]

3. FUSION POWER DENSITY

The total thermal fusion power density (corresponding to 21 MeV per fusion event in a D-T plasma) in mks units (with temperatures in keV) is given by

$$\frac{P_{th}}{V_p} (MW/m^3) \cong 8.5 \times 10^{-19} n_i^2 \langle\sigma v\rangle_{DT} , \tag{6}$$

where

n_i = toroidal plasma ion density,

$\langle\sigma v\rangle_{DT}$ = D-T fusion reaction rate probability,

V_p = toroidal plasma volume, $[(2\pi R)(\pi a^2)$, with average plasma radius a and major radius R].

In terms of *toroidal* plasma β and magnetic field strength B, Eq. (6) can also be written as

$$\frac{P_{th}}{V_p}\ (\mathrm{MW/m^3}) \cong 1.33 \times 10^{24}\ \frac{\langle\sigma v\rangle_{DT}}{T^2}\ \beta^2 B^4\ . \tag{7}$$

Here $T \cong T_e \cong T_i$ has been assumed and $n_i^2 \cong 1.56 \times 10^{42}\beta^2 B^4 T^{-2}$ has been used.

4. RING POWER BALANCE

If the annulus can be stabilized against drift instabilities (see Sects. 1, 2, 3, and 7), as is the case in simple mirrors and EBT/NBT, classical losses should dominate the power requirements. In its most basic form the annulus power balance is given by

$$P_{\mu A} = P_{synch} + P_{brems} + P_{scatt} + P_{drag}\ , \tag{8}$$

where P_{synch} and P_{brems} represent power lost by synchrotron and bremsstrahlung radiation, P_{scatt} is the 90° pitch angle scattering of the ring electrons on the core plasma ions, P_{drag} represents the power lost from the relativistic electrons due to drag on the toroidal core electrons, and $P_{\mu A}$ is the microwave power required to sustain the annulus. In terms of plasma and machine parameters, Eq. (8) can be expressed in mks units with T in keV as follows (see Refs. 1-4 for details):

$$\frac{P_{\mu A}}{V_A}\,(\mathrm{MW/m^3}) \cong \underbrace{3.2 \times 10^{-20} B_A^2 n_A (\gamma - 1)[1 + 0.5(\gamma - 1)]}_{P_{synch}}$$

$$+ \underbrace{8 \times 10^{-42}\; n_A n_{ep} \sqrt{\gamma^2 - 1}}_{P_{brems}}$$

$$+ \underbrace{1.0 \times 10^{-39}\; n_A n_{ip} \frac{\gamma(\gamma - 1)}{(\gamma^2 - 1)^{3/2}}\, \ln \Lambda_{ei}}_{P_{scatt}}$$

$$+ \underbrace{2.5 \times 10^{-39}\; n_A n_{ep} \frac{\gamma \ln \Lambda}{\sqrt{\gamma^2 - 1}}}_{P_{drag}}, \qquad (9)$$

where

$$\gamma = 1 + T_A/511 \;;$$

$$\ln \Lambda_{ei} \cong 38 - \ln (\sqrt{n_A}/T_A) \cong 20\text{-}25 \;;$$

n_A, T_A, and B_A are the density, kinetic energy, and magnetic field strength at the annulus, respectively; $n_p \cong n_{ip} \cong n_{ep}$ is the toroidal core plasma (ion/electron) density *near the vicinity of the annulus*; $\ln \Lambda$ is the Coulomb logarithm ($\cong$20); and V_A is the total annulus volume, namely,

$$V_A \cong 2\pi a \cdot \delta_A \cdot L_A \,,$$

with annulus thicknes δ_A and annulus total length L_A($= \ell_A N$, where ℓ_A is the annulus length per sector and N is the number of sectors). Simplifying Eq. (9) further yields

$$\frac{P_{\mu A}}{V_A} \cong 3.2 \times 10^{-20} n_A \left\{ B_A^2(\gamma - 1)[1 + 0.5(\gamma - 1)] \right.$$

$$\left. + 1.56 \times 10^{-18} n_p \frac{\gamma}{\sqrt{\gamma^2 - 1}} \left(1 + \frac{0.5}{\gamma + 1}\right) \right\} . \quad (10)$$

Bremsstrahlung radiation is smaller than the least of the other losses by better than two orders of magnitude and is therefore neglected in Eq. (10).

One can also express the microwave power loss from the annulus in terms of magnetic field at the annulus B_A and annulus beta β_A. The cutoff for microwave propagation (electron plasma frequency $\omega_{pe} \lesssim$ electron cyclotron frequency ω_{ce}) imposes an upper limit on core density n_p near the annulus; this scales as the square of the magnetic field. Defining a fraction f_c of the microwave cutoff as

$$n_p = f_c \, n_{cutoff} = f_c n_c ,$$

where

$$n_c \cong 10^{19} B_A^2 ,$$

and defining annulus density n_A in terms of β_A and B_A as

$$n_A \cong \frac{2.5 \times 10^{21} \, \beta_A B_A^2}{T_A} \cong \frac{5 \times 10^{18} \, \beta_A B_A^2}{(T_A/511)} ,$$

Eq. (10) can be rewritten as

$$\frac{P_{\mu A}}{V_A} (\mathrm{MW/m^3}) \cong 3.2 \times 10^{-20} \, n_A B_A^2 \left\{ (\gamma - 1)[1 + 0.5(\gamma - 1)] \right.$$

$$\left. + 15.6 \, f_c \frac{\gamma}{\sqrt{\gamma^2 - 1}} \left(1 + \frac{0.5}{\gamma + 1}\right) \right\} \quad (11)$$

$$\cong 3.2 \times 10^{-20}\ n_A B_A^2 F_c(\gamma, f_c) \tag{12}$$

or

$$\frac{P_{\mu A}}{V_A}\ (\mathrm{MW/m^3}) \cong \frac{0.16\beta_A B_A^4}{(T_A/511)} F_c(\gamma, f_c) \tag{13a}$$

$$\cong 2.5\ f_c \frac{\gamma}{\sqrt{\gamma^2 - 1}} \frac{\beta_A B_A^4}{(T_A/511)} \quad \text{for} \quad T_A < 1\ \mathrm{MeV}\ , \tag{13b}$$

where

$$F_c(\gamma, f_c) = (\gamma - 1)[1 + 0.5(\gamma - 1)] + 15.6\ f_c \frac{\gamma}{\sqrt{\gamma^2 - 1}} \left(1 + \frac{0.5}{\gamma + 1}\right)$$

$$\cong 16 f_c \frac{\gamma}{\sqrt{\gamma^2 - 1}} \quad \text{for} \quad T_A < 1\ \mathrm{MeV}\ . \tag{14}$$

The stability of hot electron rings requires an appreciable cold electron density component near the vicinity of the rings:[7,8] $n_p/n_A > 1$. Defining the ring stability ratio as

$$f_R = \frac{n_{cold}}{n_{hot}} = \frac{n_{ep}}{n_A} = \frac{n_p}{n_A}\ ,$$

one can rewrite Eq. (10) as

$$\frac{P_{\mu A}}{V_A}\ (\mathrm{MW/m^3}) \cong 3.2 \times 10^{-20}\ B_A^2 n_A (\gamma - 1)[1 + 0.5(\gamma - 1)]$$

$$+ 5 \times 10^{-38} f_R n_A^2 \frac{\gamma}{\sqrt{\gamma^2 - 1}} \left(1 + \frac{0.5}{\gamma + 1}\right) \tag{15a}$$

$$\cong 1.2 f_R \frac{\gamma}{\sqrt{\gamma^2 - 1}} \frac{\beta_A^2 B_A^4}{(T_A/511)^2} \quad \text{for} \quad T_A < 1 \text{ MeV} \tag{15b}$$

or

$$\cong 1.2 \frac{1}{f_R} \frac{\gamma}{\sqrt{\gamma^2 - 1}} \frac{\beta_{ep}^2 B_A^4}{(T_{ep}/511)^2} , \tag{15c}$$

where $\beta_{ep}(\propto n_{ep} T_{ep}/B_A^2)$ is the *toroidal core electron plasma beta near the vicinity of the annulus* and T_{ep} is the corresponding plasma electron temperature.

As indicated before and as is apparent from Eqs. (13) and (15), drag losses dominate a significant range of the ring energy and are large for small energies, decreasing as $T_A^{-1/2}$. At high ring energies $T_A > 2$ MeV, accelerated ring cooling occurs due to the synchrotron radiation. Hence, the resulting total loss rate has a broad minimum that is bounded by these loss mechanisms.[1-4] As can be seen from the above equations, the parameters important for the total power loss are: the ring beta β_A, the ratio of cold-to-hot plasma density f_R required for ring stability, the magnetic field strength near the vicinity of the rings B_A, the fraction of the microwave cutoff f_c, and the ring volume V_A. An accurate determination of this power loss ($P_{\mu A}$) requires detailed knowledge of all of the above-mentioned ring and ring-core interface parameters.

The microwave power required to sustain the rings in EBT-I and EBT-S is modest and reasonably well estimated by the theoretical models discussed.[2-4] Good agreement between the experimental measurements and theoretical estimates of $P_{\mu A}$ for the past (ELMO) and present experiments (EBT-I/S, NBT) provides a level of confidence in the identified energy loss processes (drag, scattering, and synchrotron radiation) and the estimates of energy loss as a function of ring and toroidal plasma parameters. The modest parameter range accessible in these experiments, however, cannot be considered sufficiently broad to allow a straightforward extrapolation to a reactor. Nevertheless, it is possible by parametric analyses to determine the influence of various scaling

parameters on the boundaries of possible operating space while maintaining the self-consistency. One such scaling curve for a reactor is shown in Fig. 2. Plotted in Fig. 2 is f_R versus annulus energy for various microwave power densities (MW/m^3), which are based on the annular power balance given by Eq. (10) [or Eq. (11) or Eq. (15a)]. It assumes that the field at the second harmonic[1,9] $B_A \cong 2$ T, which is resonant at $\sim$55 GHz (fundamental frequency $\sim$ 110 GHz) and is normalized to f_c = 1(= n_p/n_c, $n_c \cong 4 \times 10^{19}$ m^{-3} @ the second harmonic).

Also shown in Fig. 2 is the correlation between values of β_A and the various modes of EBT operation (C-, T-, and M-modes).[10] The C-mode corresponds to the noisy operation when insufficient microwave power is supplied to produce enough β_A ($\lesssim$10%). At $\beta_A \gtrsim \beta_{crit}$ ($\sim$10%)[10,11] there is a transition from the C-mode to the quiet, macrostable T-mode, where the stable steady-state operation occurs. For β_A values much larger than $\sim$50%, abrupt transition into an M-mode occurs.[10]

For a range of β_A values of 10-50%, the stability of the hot electron ring itself requires the presence of an appreciable cold electron density component.[7,8] The stability curve derived by Dominguez in his recent study[8] is also superimposed on Fig. 2 to show a possible stable operating regime for the hot electrons. For this stable operating regime, it is clearly shown in Fig. 2 that the microwave power required to sustain rings is in the range of 3-7 MW/m^3 with corresponding $f_R \gtrsim 20$.

5. RING VOLUME SCALING

Because of the uncertainty associated with the annulus volume, our scaling projections thus far have not included any assumptions regarding ring size. Based on experimental measurements and theoretical estimates, it appears that a range exists for the annulus thickness which varies between a minimum of the relativistic gyrodiameter and a maximum value of $\sim$(3-4) cm as measured on ELMO. It appears that the annulus length in those experiments is comparable to the plasma size, but all are within the $\sim$10-cm range. It is also true that the maximum length of the ring can only extend to the first harmonic zone. In general, the length of the rings is associated with $T_{\parallel}/T_{\perp}$ (anisotropy) and $W_{\perp}/W$, which in turn

is associated with their stability boundaries and drift surface characteristics. All the experiments during the past two decades in mirrors and EBTs (NBT as well) had similar device and plasma parameters; it is difficult to make a definitive estimate for the ring volume scaling. However, some projections can be made that are shown to fit past and present experiments.

A general expression for the ring volume is given by

$$V_A = 2\pi a \cdot \delta_A \cdot \ell_A N \ . \tag{16}$$

All the quantities in Eq. (16) have been defined previously. One can make the following assumptions:

(A) the ring thickness $\delta_A \cong$ a few times the annulus electron (relativistic) gyroradii ρ_{eA}, and the ring length ℓ_A (per sector) $\lesssim$ plasma radius a or

(B) relative dimensionless ring and core parameters remain constant (i.e., δ_A/a, ℓ_A/a) from device to device.

It should be noted that these two assumptions fairly well represent the existing experiments. Let us look at these two cases closely.

Case A

Since a relativistic electron in the annulus has a gyroradius given by

$$\rho_{eA}(m) \cong 1.7 \times 10^{-3} \frac{\sqrt{\gamma^2 - 1}}{B_A} \ , \tag{17}$$

one can rewrite Eq. (16) for the annulus volume as

$$V_A \cong 1.07 \times 10^{-2} \frac{\sqrt{\gamma^2 - 1}}{B_A} f_E \cdot f_L \cdot a^2 \cdot N \ , \tag{18}$$

where f_E is the annulus thickness enhancement factor ($\delta_A = f_E \cdot \rho_{eA}$) and f_L is the annulus length enhancement factor ($\ell_A = f_L \cdot a$). From the experiments, $f_E \sim (4\text{-}6)$ and $f_L \sim (0.5\text{-}1.0)$.

Case B

Ratio of the ring-to-toroidal core plasma volume is written as

$$\frac{V_A}{V_p} = \frac{2\pi a \cdot \delta_A \cdot \ell_A N}{\pi a^2 \cdot 2\pi R} = \frac{\delta_A}{a} \cdot \frac{\ell_A}{a} \cdot \frac{a}{R} \cdot \frac{N}{\pi} . \tag{19}$$

In EBT-I:[10]

$$\begin{aligned} &\frac{\delta_A}{a} \sim (0.1\text{-}0.2) \quad [\text{corresponds to } (3\text{-}6)\ \rho_{eA}] , \\ &\frac{\ell_A}{a} \lesssim 1.0, \\ &\frac{a}{R} \sim 0.1, \text{ and} \\ &\frac{N}{\pi} \sim 8. \end{aligned} \tag{20}$$

This gives $V_A/V_p \sim (0.1\text{-}0.15)$.

Similar assumptions for a reactor plasma,[9] that is,

$$\begin{aligned} &\frac{\delta_A}{a} \sim 0.1 \ [\text{corresponds to } \sim(40\text{-}60)\rho_{eA}] , \\ &\frac{\ell_A}{a} < 1.0 , \\ &\frac{a}{R} \sim 0.03 , \text{ and} \\ &\frac{N}{\pi} \sim 8 , \end{aligned} \tag{21}$$

yield $V_A/V_p \lesssim 0.025$. It is clear from Eq. (21) that the assumption of $\delta_A/a \sim 0.1$ corresponds to $\sim(40\text{-}60)\rho_{eA}$ in a reactor of a = 1.0 m plasma[9] in comparison with $\sim(3\text{-}6)\rho_{eA}$ in the present experiments. Reduction in ring thickness from $(40\text{-}60)\rho_{eA}$ to a reasonable value of $\sim(10\text{-}20)\rho_{eA}$ will further reduce the volume ratios V_A/V_p by a factor of more than 3.

It should be pointed out that the tradeoff between the ring thickness and the toroidal core stability and transport properties should be considered in a self-consistent way. Although minimum core density scale lengths (of few ion gyrodiameters) and minimum ring thickness (of few electron gyrodiameters) are compatible (i.e., *relativistic* ring electron gyroradius $\sim$ toroidal core ion gyroradius near the rings), the stability limits are unclear and presently under investigation.

6. DISCUSSION

In terms of plasma and machine parameters, Q_E of the reactor can be calculated by using Eqs. (6) [or (7)] and (10) [or (11), (13), or (15)] in Eq. (5). Because the drag losses dominate the ring power balance for ring energies in the range of interest ($\sim$300-1000 keV), Eqs. (13b) or (15b,c) will be used here for simplicity. Assuming $\eta_{th} \cong 0.35$ and $\eta_\mu \cong 0.5$, one can write

$$Q_E \cong \eta_{th}\eta_\mu \frac{P_{th}}{P_{\mu A}}$$

$$\cong 3 \times 10^{18} \frac{V_p}{V_A} \cdot \frac{n_i^2}{n_A n_p} \cdot \langle\sigma v\rangle_{DT} \cdot \frac{\sqrt{\gamma^2 - 1}}{\gamma} \tag{22}$$

or

$$Q_E \cong 7.5 \times 10^{17} \frac{V_p}{V_A} \cdot f_R \cdot \left(\frac{\beta}{\beta_{ep}}\right)^2 \cdot \left(\frac{T_{ep}}{T}\right)^2 \cdot \left(\frac{B}{B_A}\right)^4 \cdot \langle\sigma v\rangle_{DT} \cdot \frac{\sqrt{\gamma^2 - 1}}{\gamma} . \tag{23}$$

Equations (22) and (23) are equivalent [namely, $n_i \cong (B/B_A)^2 n_p = f_R(B/B_A)^2 n_A$, assuming that the fraction of microwave cutoff is the same for fundamental ($n_i \sim f_c B^2$) and second harmonic ($n_p \sim f_c B_A^2$); $\beta \sim n_i(T_e + T_i)/B^2 \sim 2f_c T$ for $T_e \sim T_i \sim T$; and $\beta_{ep} \sim n_{ep}T_{ep}/B_A^2 \sim f_c T_{ep}$] and, simply,

$$Q_E \cong 3 \times 10^{18} \frac{V_p}{V_A} f_R \left(\frac{B}{B_A}\right)^4 \langle\sigma v\rangle_{DT} \frac{\sqrt{\gamma^2 - 1}}{\gamma}$$

$$\cong 4.8 \times 10^{19} \frac{V_p}{V_A} f_R \langle\sigma v\rangle_{DT} \frac{\sqrt{\gamma^2 - 1}}{\gamma} . \tag{24}$$

For toroidal plasma temperatures of $T_e \sim T_i \sim$ (15-25) keV, $\langle\sigma v\rangle_{DT} \sim (3\text{-}6) \times 10^{-22}$, and for ring energies of $T_A \sim$ (700-1500) keV, $\sqrt{\gamma^2 - 1}/\gamma \sim 0.9\text{-}0.97 \sim O(1)$, leading to

$$Q_E \cong (1.4\text{-}2.8) \times 10^{-2} \cdot f_R \cdot \frac{V_p}{V_A} . \tag{25}$$

From Fig. 2, $f_R \gtrsim f_R$ (threshold) ~ 20 for stability gives

$$Q_E \gtrsim (0.3\text{-}0.6) \cdot \frac{V_p}{V_A} . \tag{26}$$

For the volume ratio V_p/V_A, either the assumption A or B can be used.

For Case A,

$$\frac{V_p}{V_A} \cong 1.85 \times 10^3 \frac{RB_A}{N} \cdot \frac{1}{f_E f_L} \frac{1}{\sqrt{\gamma^2 - 1}} > 100 , \tag{27}$$

for $T_A \sim$ (700-1500) keV, $f_E \gtrsim 10$, $f_L \sim 1.0$, $R \sim 30$ m, $N = 24$, and $B_A \cong 2$ T. Thus,

$$Q_E > 30 . \tag{28}$$

For Case B,

$$\frac{V_P}{V_A} > 40 \tag{29}$$

[see Eqs. (19) and (21)], and with this volume ratio, Eq. (26) reads

$$Q_E > 10 \ . \tag{30}$$

It should be pointed out once more that analyses given here are intended to demonstrate the effects of various parameters and assumptions on the reactor performance (i.e., Q_E) and to determine boundaries of possible stable operating space.

An experimental examination of the annulus stability boundaries is planned for EBT-S and will help to establish the acceptable range for the ratio of cold-to-hot plasma density for ring stabilization as well as to determine ring characteristics. EBT-S is presently operating with ∿50 kW of 28 GHz and is expected to reach power levels of ∿100 kW shortly. The scale up in magnetic field and microwave frequency from EBT-I (28 GHz, resonant field $B_r \cong 1.0$ T) has resulted in significantly improved ring parameters and performance.

Optimization of ring behavior and power losses through separate control of the ring electrons is possible; however, present and past experiments are not capable of giving this information. On the other hand, EBT-P[12] is expected to bridge this gap. One of the physics objectives of EBT-P is the study of hot electron rings. The proposed EBT-P device has the capability to operate with frequencies in the range of ∿28-90 GHz, which correspond to $B_{resonance} \sim (1\text{-}3.1)$ T [$B_A \sim (0.5\text{-}1.5)$ T]. With this capability and with the flexibility given by various possible improvements in the area of microwave feeding and separate control of the annulus, it should be possible to accomplish the objective of establishing the ring power balance scaling.

REFERENCES

1. N. A. Uckan et al., "Ring Power Balance Optimization in an EBT Fusion Reactor," in *Proc. 8th Symp. on Engineering Problems of Fusion Research* (to be published).
2. In Sect. 6 of these proceedings, see S. K. Borowski et al., R. J. Kashuba et al., M. C. Vella, and A. Andrade et al.
3. S. K. Borowski et al., Oak Ridge National Laboratory Report ORNL/TM-6910 (1979); also to be published in Nucl. Fusion.
4. For example, see Appendix A.3 in Oak Ridge National Laboratory Report ORNL/TM-7066 (1979); Appendix B in McDonnell-Douglas Astronautics Company Report MDC-E2160 (1979); and Appendix 1 in Oak Ridge National Laboratory Report ORNL/TM-7191 (1980).
5. J. T. Woo, N. A. Uckan, and L. M. Lidsky, *Proc. 7th Symp. on Engineering Problems of Fusion Research*, Vol. I, p. 681 (1977).
6. R. L. Reid and D. Steiner, *Proc. 7th Symp. on Engineering Problems of Fusion Research*, Vol. I, p. 675 (1977).
7. R. R. Dominguez and H. L. Berk, Phys. Fluids 21, 827 (1978); H. L. Berk, Phys. Fluids 19, 1255 (1976).
8. In Sect. 7 of these proceedings, see R. R. Dominguez; S. C. Chiu and G. E. Guest; and R. L. Miller et al. Also see Sects. 1 and 2 for experimental confirmations.
9. N. A. Uckan et al., *Plasma Physics and Controlled Nuclear Fusion Research 1978*, Vol. III, p. 343 (1979).
10. R. A. Dandl et al., Oak Ridge National Laboratory Report ORNL/TM-6457 (1978); Oak Ridge National Laboratory Report ORNL-TM-4941 (1975); and Oak Ridge National Laboratory Report ORNL-TM-3694 (1971).
11. D. B. Nelson and C. L. Hedrick, Nucl. Fusion 19, 283 (1979).
12. EBT Group, Oak Ridge National Laboratory Report ORNL/TM-7191 (1980).

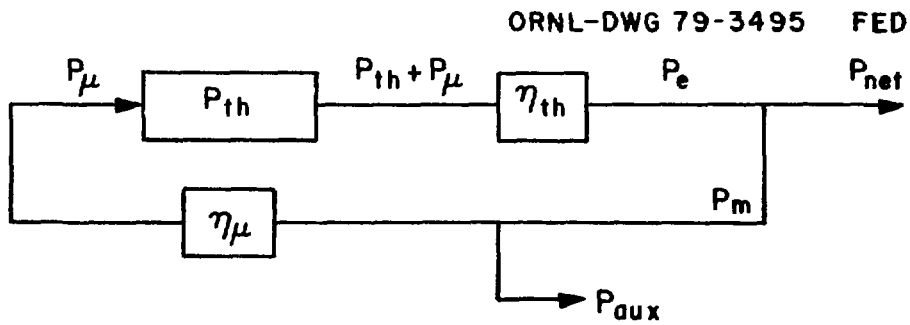

Fig. 1. Simple power flow diagram.

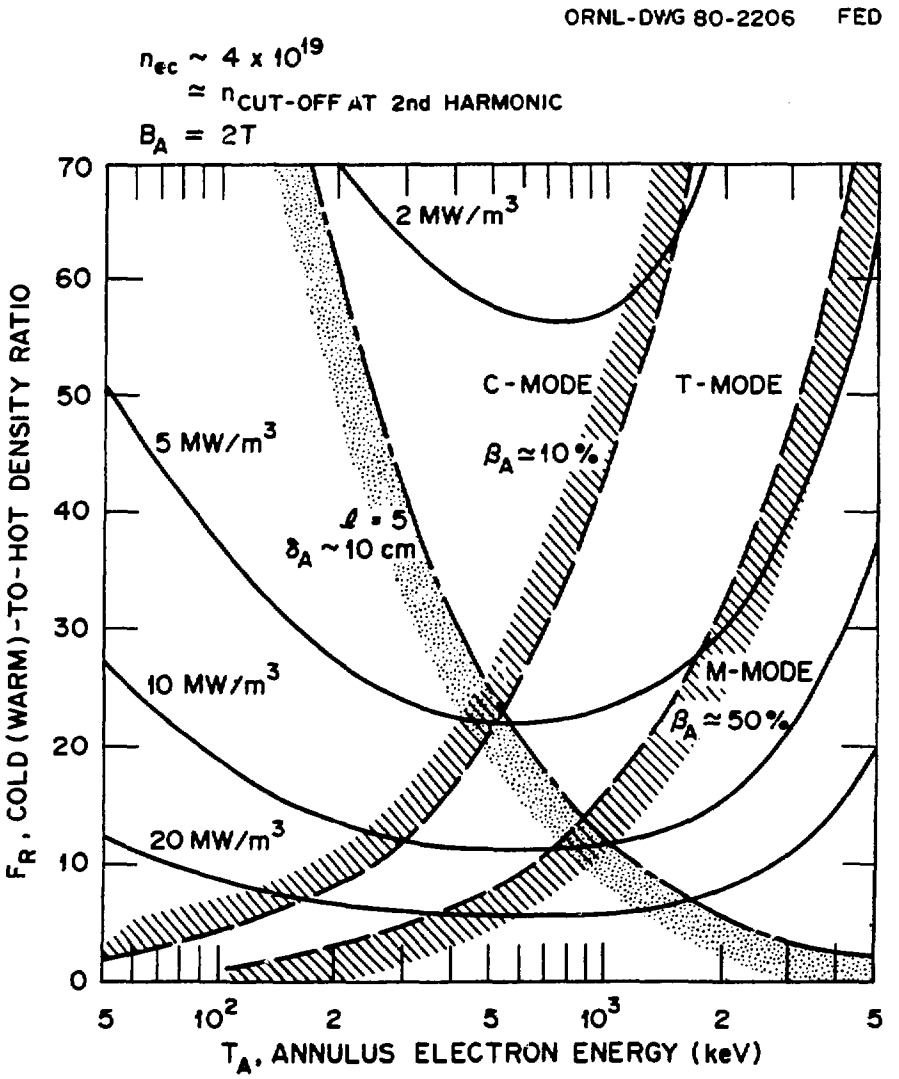

Fig. 2. The fraction of cold-to-hot electrons $f_R = n_{cold}/n_{hot} = n_P/n_A$ vs annulus electron energy T_A for $P_{\mu A}/V_A$ = 2, 5, 10, and 20 MW/m³. The fraction of microwave cutoff $f_c = 1$ (i.e., $n_P = n_{cutoff}$ @ second harmonic) and B_A = 2 T. The C-, T-, M-mode boundaries are indicated with $\beta_A \cong 10\%$ and 50% curves. The marginal stability curve (from Ref. 8) for $\delta_A \cong 10$ cm (ring thickness) and $\ell = 5$ (poloidal mode number) is also shown as an example. Stable operating regimes for ring electrons are bounded by the β_A curves from the sides (T-mode) and the marginal stability curve from below.

8.3 DIAGNOSTICS

DIAGNOSTICS: SUMMARY OF THE OPEN SESSION

G. R. Haste

Oak Ridge National Laboratory
Oak Ridge, Tennessee

In the EBT area, a list was presented of the present diagnostics which are applicable to the ring measurements. Also presented was a list of possible future diagnostics which will give some information on the ring. These lists are summarized in Table 1.

M. Fujiwara presented a sequence of measurements which had been performed on the NBT. Diamagnetic loops of 3 different diameters have been used to determine the stored energy in the electron rings. These diameters were 40, 50, and 100 cm. It was observed that the signals obtained with each of these loops were of the same order. This observation provoked a great deal of discussion. It was pointed out that each of these loops measures the flux from more than just to the cavity which it surrounds. The NBT staff members indicated that the equality of the signals on the various loops indicated that the electron rings were quite long, that is, that they must be longer than 10 cm. They also pointed out that a measurement of the radial magnetic field produced by these rings indicates that the Z extent of the energetic rings becomes longer as the rings become more intense.

Hideo Ikegami presented a list of measurements which were required for the energetic electrons. Included in this list were:

- potential measurements,
- the confinement time of the energetic particles,
- the stability of the rings,
- the structure of the rings, and
- information about the cause of the T-M transition (is this, for example, a Whistler instability?)

Ikegami also pointed out that there is a toroidal energetic electron ring and that measurements on this population are urgently needed.

Table 1. EBT Ring Diagnostics

Present

- Diamagnetic Loops
  - Large — $W_\perp$
  - Small — geometry
- Skimmer/Ionization Chamber Probe
  - Geometry, energy distribution
- Heavy Ion Beam Probe
  - Potential, T_e near rings, geometry, fluctuations, β?
- Bremsstrahlung
  - Energy distribution (T_e) density

Future

- Synchrotron Radiation
  - Geometry r,L
  - Temperature
  - Density
- Barium Ion Beam
  - Density
  - Local magnetic field (β)
- Faraday Rotation
  - Local magnetic field (β)

MEASUREMENTS OF THE STORED RING ENERGY IN EBT-I

R. J. Colchin
Oak Ridge National Laboratory
Oak Ridge, Tennessee 37830

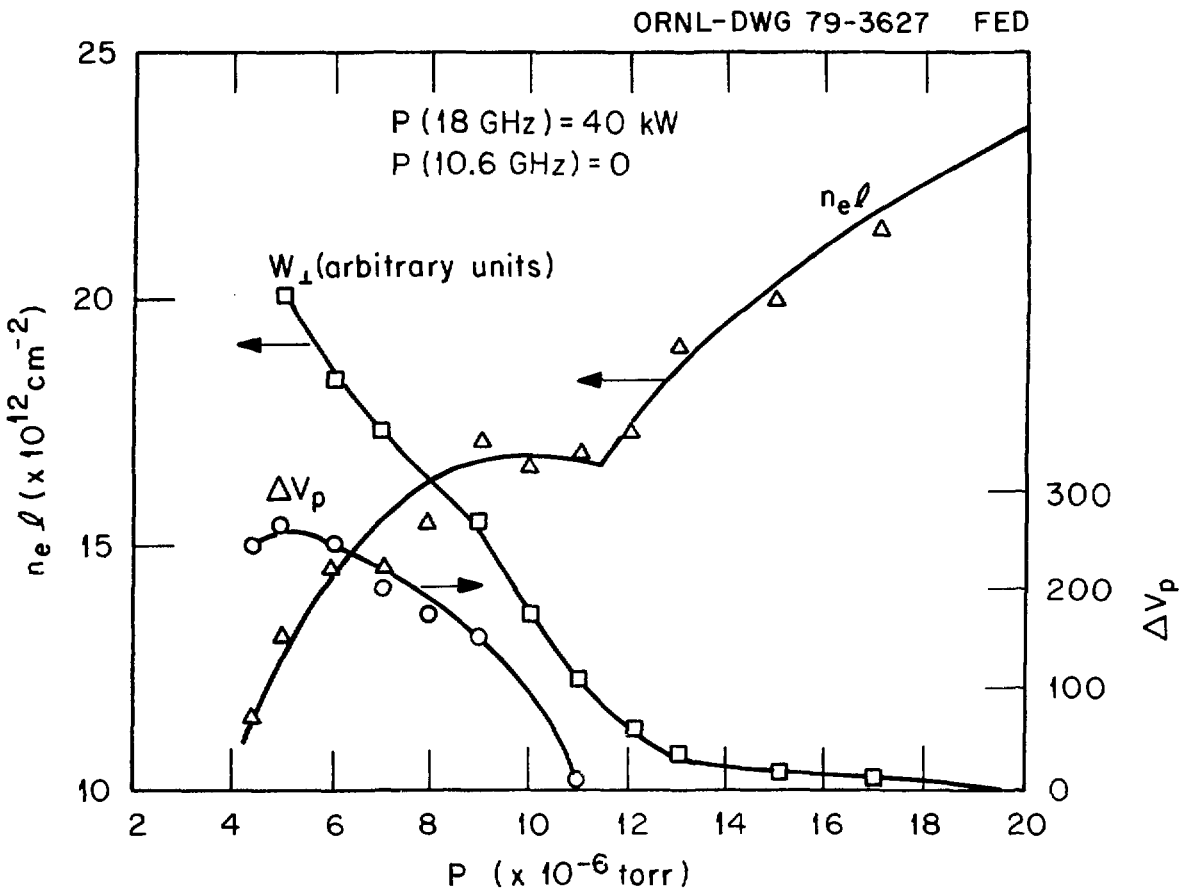

Variations in the stored energy, $n_e\ell$, and potential well depth as a function of power. In the T-mode, $W_\perp$ rises as the pressure decreases.

ORNL-DWG 79-3628 FED

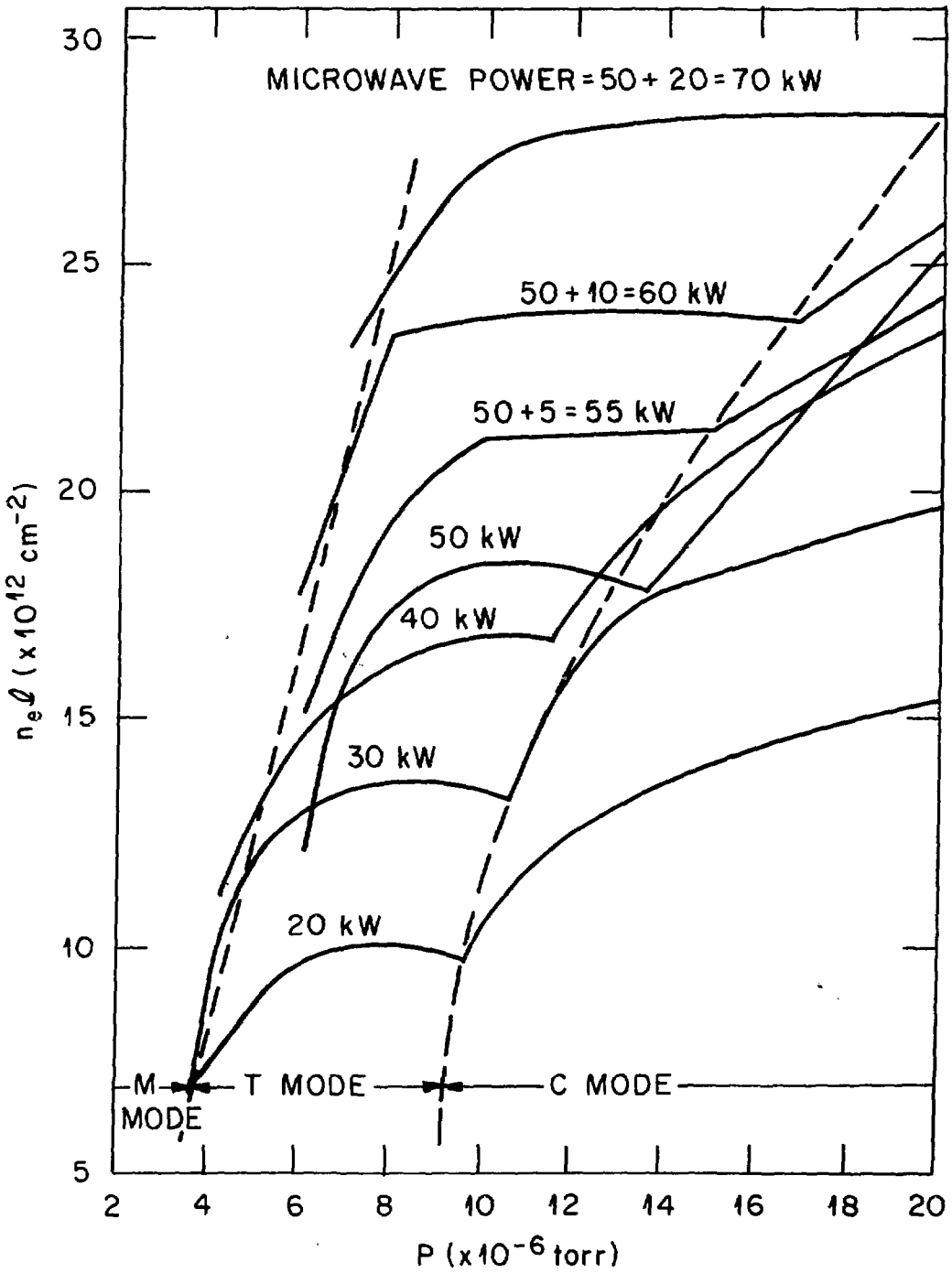

Various operating regimes are indicated as a function of microwave power and pressure.

ORNL-DWG 79-3728 FED

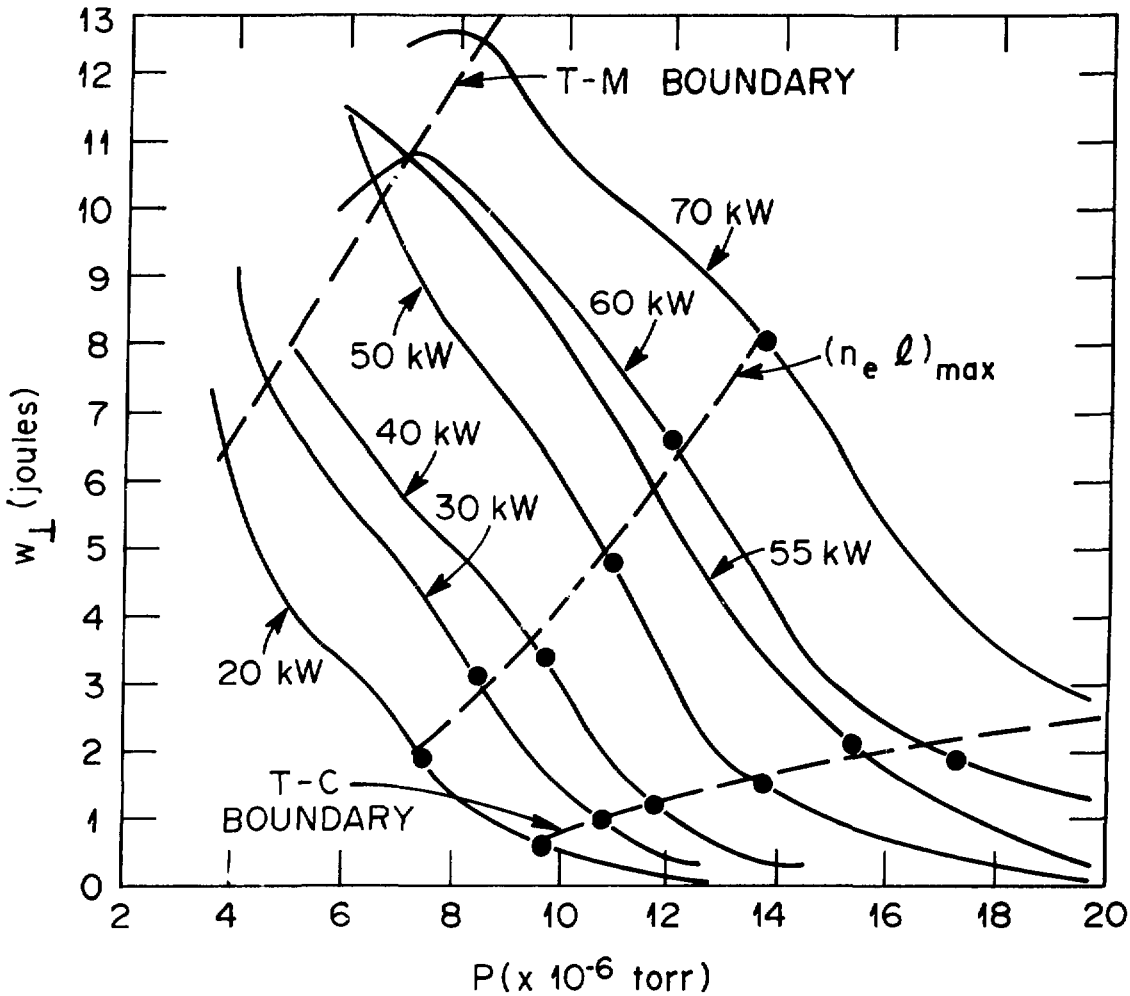

The stored energy for each of the power levels shown in the last figure is plotted. A computer code, discussed in paper by K. H. Carpenter, was used to generate the values of $W_\perp$ from diamagnetic loop signals. Approximate mode boundaries and T-mode "peak" values of $n_e \ell$ (which must be obtained from the raw data in some cases) are also indicated.

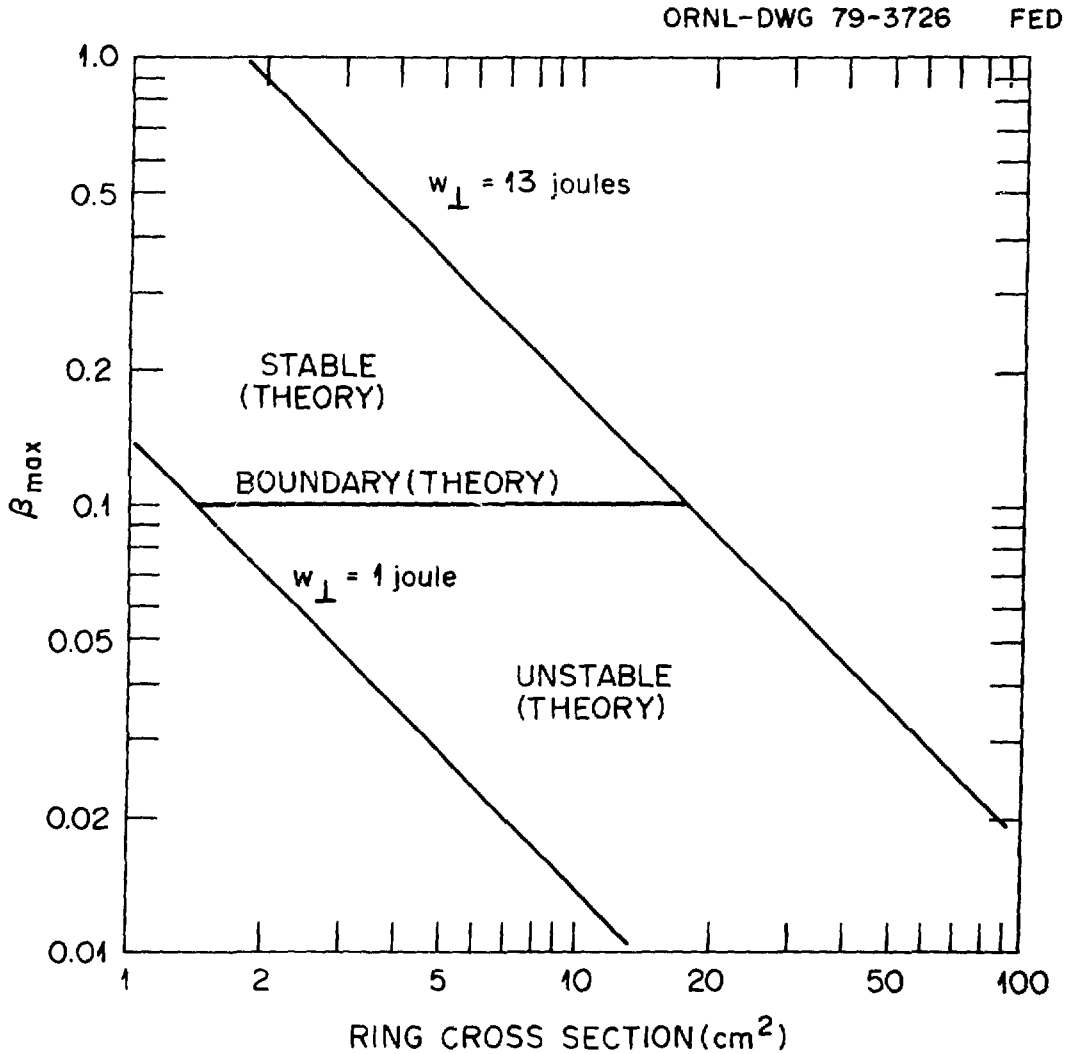

Ring cross-sectional area is plotted versus β. Diagonal lines indicate limits of the stored energy in the T-mode, as taken from data in the previous figure. MHD stable and unstable regimes are indicated between these lines assuming a theoretical stability boundary of β = 10%.

AUTHOR INDEX

A. Andrade, 363
W. B. Ard, 1, 333, 499, 505
D. B. Batchelor, 261
C. G. Bathke, 363
D. C. Baxter, 221
I. B. Bernstein, 221
A. H. Boozer, 253
S. K. Borowski, 319
K. H. Carpenter, 143
S. C. Chiu, 437
R. J. Colchin, 529
R. A. Dandl, 1, 31
R. R. Dominguez, 383, 409
A. Favale, 1
M. Fujiwara, 123, 289, 453
G. E. Guest, 1, 97, 409, 437
S. Hamasaki, 233
G. R. Haste, 1, 163, 527
C. L. Hedrick, 1, 175, 193
M. Hosokawa, 59, 123
H. Iguchi, 123
H. Ikegami, 1, 59, 123, 289
E. F. Jaeger, 175, 193, 319
T. Kammash, 319
R. J. Kashuba, 333
H. H. Klein, 233
N. A. Krall, 233
R. A. Krakowski, 363
Y. C. Lee, 471
C. S. Liu, 305
J. B. McBride, 233
R. L. Miller, 409
T. Ohkawa, 409
E. Ott, 305
L. W. Owen, 175
J. F. Pipkins, withdrawn
H. Sanuki, 123, 453
T. Shoji, 123
J. L. Sperling, 233
D. A. Spong, 75
M. Tanaka, 123, 289
J. S. Tolliver, 193
V. K. Tripathi, 305
N. A. Uckan, 1, 319, 491, 507
J. W. Van Dam, 471
M. C. Vella, 349, 495

ATTENDANCE LIST

EBT RING PHYSICS WORKSHOP

December 3-5, 1979

Oak Ridge, Tennessee

William B. Ard
McDonnell Douglas
Bldg. 81, P. O. Box 516
St. Louis, MO 63166

F. W. Baity
Oak Ridge National Laboratory
P. O. Box Y
Oak Ridge, TN 37830

D. B. Batchelor
Oak Ridge National Laboratory
P. O. Box Y
Oak Ridge, TN 37830

C. G. Bathke
Los Alamos Scientific Laboratory
MS-641
Los Alamos, NM 87544

D. C. Baxter
Science Applications, Inc.
P. O. Box 2351
La Jolla, CA 92037

L. A. Berry
Oak Ridge National Laboratory
P. O. Box Y
Oak Ridge, TN 37830

F. M. Bieniosek
Rensselaer Polytechnic Institute
1304 Chipwood Rd.
Knoxville, TN 37922

Allen H. Boozer
Princeton Plasma Physics Laboratory
P. O. Box 451
Princeton, NJ 08544

S. K. Borowski
Oak Ridge National Laboratory
P. O. Box Y
Oak Ridge, TN 37830

K. C. Carpenter
Department of Electrical Eng.
University of Missouri-Rolla
Rolla, MO 65401

Christine M. Celata
Dartmouth College
Physics Department
Hanover, NH 03755

Shi-Chu Chiu
General Atomic Company
P. O. Box 81608
San Diego, CA 92138

R. J. Colchin
Oak Ridge National Laboratory
P. O. Box Y
Oak Ridge, TN 37830

R. L. Copeland
Oak Ridge National Laboratory
P. O. Box Y
Oak Ridge, TN 37830

R. A. Dandl
TRW
1 Space Park
Redondo Beach, CA 90278

William A. Davis
Oak Ridge National Laboratory
P. O. Box Y
Oak Ridge, TN 37830

S. O. Dean
Science Applications, Inc.
2 Professional Dr., Suite 249
Gaithersburg, MD 20767

W. F. DiVergilio
TRW
1 Space Park
Redondo Beach, CA 90278

R. R. Dominguez
General Atomic Company
P. O. Box 81608
San Diego, CA 92138

R. A. Dory
Oak Ridge National Laboratory
P. O. Box Y
Oak Ridge, TN 37830

A. T. Favale
Grumman Aerospace Corp.
Research Dept., A01-26
Bethpage, NY 11714

M. E. Fenstermacher
Westinghouse
214 W. 9th Avenue
Pittsburgh, PA 15236

Masami Fujiwara
Institute of Plasma Physics
Nagoya University
464 Nagoya City, Japan

Gordon Gibson
Westinghouse
Fusion Power Systems Department
Box 10864
Pittsburgh, PA 15236

J. C. Glowienka
Oak Ridge National Laboratory
P. O. Box Y
Oak Ridge, TN 37830

R. C. Goldfinger
Oak Ridge National Laboratory
P. O. Box Y
Oak Ridge, TN 37830

G. E. Guest
General Atomic Company
P. O. Box 81608
San Diego, CA 92138

Seishi Hamasaki
JAYCOR
1401 Camino Del Mar
Del Mar, CA 92075

G. R. Haste
Oak Ridge National Laboratory
P. O. Box Y
Oak Ridge, TN 37830

C. L. Hedrick, Jr.
Oak Ridge National Laboratory
P. O. Box Y
Oak Ridge, TN 37830

D. L. Hillis
Oak Ridge National Laboratory
P. O. Box Y
Oak Ridge, TN 37830

Minoru Hosokawa
Institute of Plasma Physics
Nagoya University
Nagoya 464, Japan

B. H. Hui
Naval Research Laboratory
Code 6790
Washington, DC 20375

Harukazu Iguchi
Institute of Plasma Physics
Nagoya University
Nagoya 464, Japan

Hideo Ikegami
Institute of Plasma Physics
Nagoya University
Nagoya 464, Japan

E. F. Jaeger
Oak Ridge National Laboratory
P. O. Box Y
Oak Ridge, TN 37830

A. Kadish
Office of Fusion Energy
Department of Energy
MS G-234
Washington, DC 20545

R. J. Kashuba
McDonnell Douglas
Bldg. 81, P. O. Box 516
St. Louis, MO 63141

Akio Komori
Oak Ridge National Laboratory
P. O. Box Y
Oak Ridge, TN 37830

T. J. Kurey
General Electric Company
1 River Road
Bldg. 23, Rm. 289
Schenectady, NY 12345

Lang L. Lao
Oak Ridge National Laboratory
P. O. Box Y
Oak Ridge, TN 37830

John B. McBride
JAYCOR
1401 Camino Del Mar
Del Mar, CA 92014

Robert L. Miller
General Atomic Company
P. O. Box 81608
San Diego, CA 92138

O. B. Morgan
Oak Ridge National Laboratory
P. O. Box Y
Oak Ridge, TN 37830

W. H. Muner
Science Applications, Inc.
7406 Northrop Rd.
Alexandria, VA 22306

James F. Pipkins
General Atomic Company
P. O. Box 81608
San Diego, CA 92138

Bill H. Quon
TRW, 1 Space Park
Redondo Beach, CA 90278

M. E. Rensink
Lawrence Livermore Laboratory
P. O. Box 808, L-437
Livermore, CA 94550

R. K. Richards
Oak Ridge National Laboratory
P. O. Box Y
Oak Ridge, TN 37830

J. Reece Roth
University of Tennessee
Dept. of Electrical Engineering
Knoxville, TN 37916

T. K. Samec
TRW
1 Space Park, R1/1078
Redondo Beach, CA 90278

Heiji Sanuki
Institute of Plasma Physics
Nagoya University
Nagoya 464, Japan

J. Sheffield
Oak Ridge National Laboratory
P. O. Box Y
Oak Ridge, TN 37830

Tatsui Shoji
Institute of Plasma Physics
Nagoya University
Nagoya 464, Japan

D. J. Sigmar
Oak Ridge National Laboratory
P. O. Box Y
Oak Ridge, TN 37830

D. A. Spong
Oak Ridge National Laboratory
P. O. Box Y
Oak Ridge, TN 37830

Barry W. Stallard
Lawrence Livermore Laboratory
P. O. Box 808, L-437
Livermore, CA 94550

Stephen Tamor
Science Applications, Inc.
P. O. Box 2351
La Jolla, CA 92037

Masayoshi Tanaka
Institute of Plasma Physics
Nagoya University
Nagoya 464, Japan

J. S. Tolliver
Oak Ridge National Laboratory
P. O. Box Y
Oak Ridge, TN 37830

V. K. Tripathi
University of Maryland
Dept. of Physics & Astronomy
College Park, MD 20742

G. D. Tsakiris
University of Maryland
Dept. of Physics & Astronomy
College Park, MD 20742

K. T. Tsang
Oak Ridge National Laboratory
P. O. Box Y
Oak Ridge, TN 37830

James M. Turner
Office of Fusion Energy
Department of Energy
MS G-234
Washington, DC 20545

N. A. Uckan
Oak Ridge National Laboratory
P. O. Box Y
Oak Ridge, TN 37830

T. Uckan
Oak Ridge National Laboratory
P. O. Box Y
Oak Ridge, TN 37830

James W. Van Dam
Institute for Advanced Study
Bldg. E-102
Princeton, NJ 08540

Michael C. Vella
Lawrence Berkeley Laboratory
Bldg. 9
Berkeley, CA 94720

James T. Woo
Renssalaer Polytechnic Institute
Troy, NY 12181

EBT RING PHYSICS WORKSHOP

December 3-5, 1979

Holiday Inn
Oak Ridge, Tennessee

Sponsored by

OAK RIDGE NATIONAL LABORATORY
Oak Ridge, Tennessee

AGENDA

Monday, December 3, 1979

9:00		L. A. Berry: Welcome
9:10		N. A. Uckan: Opening Remarks
9:20		Session A: Overview N. A. Uckan, Chairman
	A.1	R. A. Dandl, "Review of Ring Experiments"
	A.2	H. Ikegami and M. Hosokawa, "Characteristics of Hot Electrons in a Simple Magnetic Mirror Field"
	A.3	D. A. Spong, "Review of EBT Electron Ring Stability"
	A.4	G. E. Guest, "A Brief Review of ELMO Ring Stability Theory"
12:00		LUNCH
1:00		Session B: Experiments W. B. Ard, Chairman
	B.1	M. Fujiwara, M. Hosokawa, H. Iguchi, T. Shoji, M. Tanaka and H. Ikegami, "The Ring Formation in Nagoya Bumpy Torus"
	B.2	K. H. Carpenter, "Diamagnetic Measurements for Experimental Determination of EBT Ring Parameters"
	B.3	G. R. Haste, "Comparison of Energetic Electron Formation in EBT and in Minimum-B Configurations"
2:45		COFFEE BREAK
3:00		Session C: Ring/Core Modeling C. L. Hedrick, Chairman
	C.1	L. Owen, "Hot Electron Ring Equilibria and Effects on EBT Transport"
	C.2	J. Tolliver, "Numerical Calculation of the Electron Distribution Function for EBT Ring Electrons"
	C.3	D. C. Baxter, "A Model Equation for Electron Cyclotron Heating of EBT Rings"
	C.4	S. Hamasaki, H. H. Klein, N. A. Krall, J. B. McBride and J. L. Sperling, "A Model for Electron Ring Formation in EBT"
	C.5	A. H. Boozer, "Anisotropy of the EBT Ring Electrons"
6:00		*RECEPTION, Reactor Room, Holiday Inn (Cash Bar)*

Tuesday, December 4, 1979

9:00		Session D: Microwave Heating and Radiation G. R. Haste, Chairman
	D.1	D. B. Batchelor, "Microwave Absorption by the Annulus in EBT"
	D.2	M. Tanaka, M. Fujiwara and H. Ikegami, "Microwave Interaction with Hot Electron Plasmas"
	D.3	V. K. Tripathi, E. Ott and C. S. Liu, "Synchrotron Radiation from the Ring and Nonlinear Effects in Microwave Heating of EBT"
	D.4	J. F. Pipkins, "Finite k and Relativistic Effects on Resonance Abosrption in Non-Uniform Magnetic Fields"
10:30		COFFEE BREAK
10:45		Session E: Power Balance A. Favale, Chairman
	E.1	S. K. Borowski and N. A. Uckan, "Ring Power Balance"
	E.2	R. J. Kashuba and W. B. Ard, "Annulus Power Losses in EBT"
	E.3	M. C. Vella, "Beam Electron Heating for High Density EBT Operation"
	E.4	A. Andrade and R. A. Krakowski, "Steady-State Microwave Power Requirements for EBTR Electron Rings"
12:15		LUNCH
1:15		Session F: Stability G. E. Guest, Chairman
	F.1	R. R. Dominguez, "Interchange Stability of Hot Electron Rings in a Warm Plasma"
	F.2	R. L. Miller, R. R. Dominguez, G. E. Guest, and T. Ohkawa, "Macroscopic Stability of the Hot Electron Annulus in EBT"
	F.3	S. C. Chiu, "A Two-Point Model for EBT Transport"
	F.4	H. Sanuki and M. Fujiwara, "Stability of a Toroidal Plasma by Hot Electron Annulus in a Bumpy Torus"
	F.5	J. W. Van Dam and Y. C. Lee, "Stability Analysis of a Hot Electron EBT Plasma"
3:30		COFFEE BREAK
3:45		Session O: Open Forum Panel: N. A. Uckan, W. B. Ard, G. E. Guest, R. A. Dandl, G. R. Haste, L. C. Hedrick, H. Ikegami, M. C. Vella

Wednesday, December 5, 1979

9:00	Session O: Open Forum (continued)
10:30	COFFEE BREAK
10:45	Session S: Summaries by Session Chairmen
12:00	END OF WORKSHOP
1:30	TOUR OF FED (optional)

☆U.S. GOVERNMENT PRINTING OFFICE: 1980-640-245-457